Consultative Committee for Space Data Systems

REPORT OF THE PROCEEDINGS OF THE

RF AND MODULATION

SUBPANEL 1E MEETING
AT THE
GERMAN SPACE OPERATIONS CENTRE
SEPTEMBER 20-24, 1993

TIEN M. NGUYEN, EDITOR

CCSDS B20.0-Y-1

YELLOW BOOK

FEBRUARY 1994

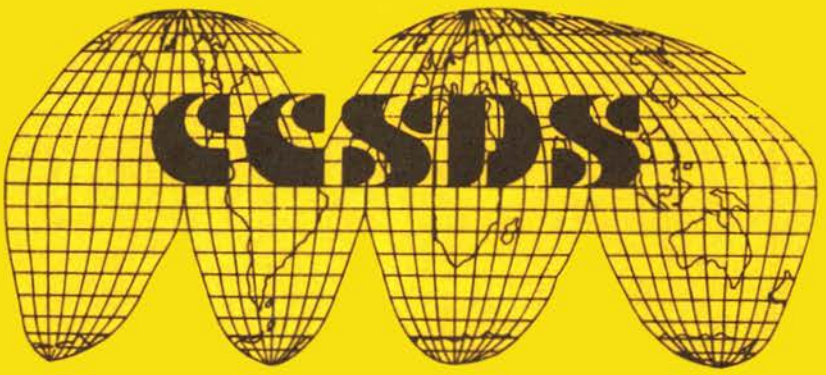

Consultative Committee for Space Data Systems

REPORT OF THE PROCEEDINGS
OF THE

RF AND MODULATION

SUBPANEL 1E MEETING
AT THE
GERMAN SPACE OPERATIONS CENTRE
SEPTEMBER 20-24, 1993

TIEN M. NGUYEN, EDITOR

CCSDS B20.0-Y-1

YELLOW BOOK

FEBRUARY 1994

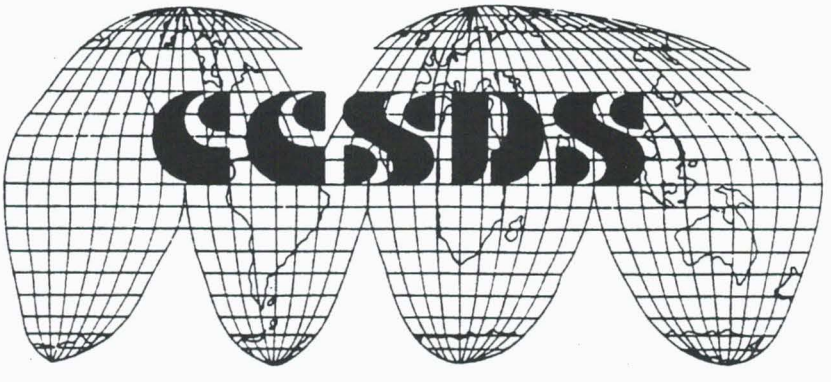

PREFACE

The Consultative Committee for Space Data Systems (CCSDS) is an organization officially established by nine member space agencies and fourteen observer agencies. The nine member agencies, which make up the core of the CCSDS, are: the British National Space Centre (BNSC)/ United Kingdom, Canadian Space Agency (CSA)/Canada, Centre National d'Etudes Spatiales (CNES)/France, Deutsche Forschungsanstalt fuer Luft- und Raumfahrt e.V (DLR)/Germany, European Space Agency (ESA)/Europe, Indian Space Research Organization (ISRO)/India, Institutode Pesquisas Espaciais (INPE)/Brazil, National Aeronautics and Space Administration (NASA)/USA, and National Space Development Agency of Japan (NASDA)/ Japan. The fourteen observer agencies, which concur in the technical recommendations made by the core member agencies, are: the China Astronautics Standards Institute (CASI)/People's Republic of China, Chinese Academy of Space Technology (CAST)/People's Republic of China, Central Research Institute of Physics (CRIP)/Hungary, Communication Research Laboratory, (CRL)/Japan, Council for Science and Industrial Research (CSIR)/South Africa, Centro Tecnico Aerospacial (CTA)/Brazil, Department of Communications, Communications Research Centre (DOC-CRC)/Canada, Danish Space Research Institute (DSRI)/Denmark, European Organization for the Exploitation of Meteorological Satellites (EUMETSAT)/Germany, Institute of Space Research (IKI)/Russia, Institute of Space and Astronautical Science (ISAS)/Japan, National Oceanic and Atmospheric Administration (NOAA)/USA, Swedish Space Corporation (SSC)/Sweden, and Central Soviet Research Institute for Machine Building (TsNIIMash)/Russia.

The committee convenes periodically to discuss space data systems issues that are common to all member space agencies. While the major concern of the CCSDS is the standardization of space data structures, one subpanel, the Radio Frequency and Modulation Subpanel, is concerned with standardizing the physical transport layer. The primary objective of this Subpanel is to promote sufficient compatibility in transport systems to allow cross-support among member agencies.

This year, the Radio Frequency and Modulation Subpanel 1E meeting took place on September 20-24, 1993, at the German Space Operations Centre, Oberpfaffenhofen, Germany. There were more than twenty-one position papers presented at this meeting by the investigators of member space agencies. The purpose of these position papers is twofold: (1) to stimulate technical discussions on radio frequency and modulation subjects and (2) to promote uniform solutions to specified problems. These uniform solutions will ensure compatibility among the CCSDS space agencies' RF and modulation systems.

Seven sessions were formed, each manned by experts from member space agencies. The seven sessions were (1) Advanced Modulation Techniques and Related Topics, (2) Synchronization, (3) Navigation, (4) Required Bandwidth, Spurious Emission, and Interference Susceptibility, (5) Spacecraft Transponder, (6) Modulation and Coding, and (7) K_A-Band Experiment and Weather Models. All sessions were chaired by Mr. W. L. Martin.

This document begins with Session 1, Advanced Modulation Techniques and Related Topics. Five papers were submitted in this session. These position papers discussed the performance of PCM/PM communications systems in non-ideal channels, cross-talk in QPSK systems and effects of bit asymmetry on BPSK systems.

Only one paper was submitted to the Synchronization Session (Session 2). This position paper dealt with the effect of transition density on the performance of the digital data transition tracking loop.

The technical characteristics and accuracy capabilities of delta differential one-way ranging as a spacecraft navigation tool were discussed in the Navigation Session (Session 3).

Session 4 investigated required vs. occupied bandwidth; spurious emission; and interference susceptibility for both residual and suppressed carrier modulation systems. The impact of filtering on bit error rate performance for the PCM/PSK/PM and PCM/PM/Bi-phase modulation schemes was also discussed. A total of five papers were submitted in this session.

Session 5 was devoted to the spacecraft transponder. Three position papers were presented in this session, one from ESA and two from NASA. ESA's position paper presented the activities of ESA/ESTEC on the development of the deep space transponder. On the other hand, the two NASA papers dealt with the preliminary design and implementation and the turnaround frequency ratios for future deep space transponders.

Advanced modulation coding schemes and bandwidth-efficient modulation methods were the main themes for Session 6. Six position papers presented in this session provided many key experimental and theoretical results regarding the performance of Trellis Coded Modulation (TCM) systems and other bandwidth-efficient coding systems. The advantages and the impact of the advanced coding schemes (e.g., rate 1/4 and 1/6 convolutional coding), and the impact of the periodic data frame on the RF carrier performance were also examined in this session.

Finally, Session 7 discussed the K_A-Band link experiment and the CCSDS link budget weather related losses. A total of two papers were submitted in this session.

Special thanks belong to Mr. Warren L. Martin, the CCSDS Subpanel 1E Chairman, for programmatic support and encouragement during the preparation of this document, and to Dr. John Koukos for his technical contributions and his generous assistance in putting this proceedings together.

Finally, I want to express my gratitude to Drs. Joe Yuen and Sami Hinedi for their constant support during the preparation and publication of this proceedings, and L. Anderson for her assistance in preparing the proceedings.

Tien M. Nguyen
Pasadena, California

INTRODUCTION TO SUBPANEL 1E PROCEEDINGS

MUNICH MEETING

The Consultative Committee for Space Data Systems (CCSDS) comprises nine member space agencies and was formed to investigate issues and to adopt Recommendations for space data system standards. Fourteen observer space agencies may also concur with the technical Recommendations made by the CCSDS. While the primary effort of the CCSDS is the standardization of data structures, one group, Radio Frequency and Modulation, Subpanel 1E, is concerned with standardizing the physical layer. The objective of this subpanel is to promote sufficient compatibility in transport systems to permit one agency's spacecraft to be supported by another agency's communications network.

Subpanel 1E achieves its objectives by studying problems pertaining to: (1) Earth-to-space and space-to-Earth RF links, (2) Earth stations and spacecraft data systems, and (3) radio metric systems. Uniform solutions to problems are sought to ensure compatibility among the several CCSDS space agencies' RF and modulation systems. When adopted by the CCSDS, these solutions are published as Recommendations in the CCSDS RF and Modulation Blue Book (CCSDS 401.0-B-1). Presently, Subpanel 1E has several Recommendations at Blue Book, Red Book, and White Book stages.

New concepts are introduced by position papers. This proceedings contains those papers submitted at the most recent Subpanel 1E meeting, held 20-24 September 1993, at the German Space Operations Centre in Oberpfaffenhofen, Germany. This document is intended to serve as a record of the technical work, which forms the basis for future Recommendations.

Studies of PCM/PM modulation techniques continued at the most recent meeting. Three position papers dealing with this topic were submitted. These papers explored the effects of non-ideal channels on the performance of PCM/PM receivers and formed the core of the Advanced Modulation Techniques Session. Other issues, such as cross-talk between QPSK channels and the effect of data asymmetry on BPSK systems, were also considered.

Last year, Subpanel 1E was asked to investigate required bandwidth, spurious emissions and interference susceptibility for various modulation schemes such as: PCM/PM/NRZ, PCM/PM/Bi-ϕ, PCM/PSK/PM-Sinewave, PCPM/PSK/PM-Square, BPSK/NRZ, BPSK/Bi-ϕ, QPSK, MSK and GMSK. Five position papers exploring these topics were presented in this meeting. Two years ago, Subpanel 1E identified the need for advanced digital techniques for future spacecraft transponders. Two papers concerned with this topic, together with a paper on the selection of the turnaround frequency ratios for K_A-band, were also submitted for this session.

Besides the Advanced Modulation Techniques, Spectrum Bandwidth and Spacecraft Transponder sessions, four other subject areas were discussed during this meeting. They were: Synchronization, Navigation, Modulation and Coding, and K_A-band Experiment and Weather Models. These sessions explored issues concerning the standardization of: (1) future modulation

and coding techniques, (2) cross-talk level in QPSK systems, (3) the acceptable amount of data asymmetry in BPSK systems, (4) the minimum transition density for the Earth-to-space link, (5) future navigation techniques, and (6) future spacecraft transponders.

This volume contains a large number of excellent submissions. My special thanks to all of you who contributed papers to the meeting and especially to Dr. Tien M. Nguyen, who compiled the papers and assembled this book. This is the first proceedings to be issued since the April 1989 meeting at the Ames Research Center. Each of you can be justifiably proud of your work in our Subpanel.

Warren L. Martin
Chairman, CCSDS
Subpanel 1E,
RF and Modulation

TABLE OF CONTENTS

Session 4
Required Bandwidth, Spurious Emission, and Interference Susceptibility

Session 5
Spacecraft Transponder

Session 6
Modulation and Coding

Session 7
K_A-Band Experiment and Weather Models

SESSION 1

ADVANCED MODULATION TECHNIQUES

AND RELATED TOPICS

THE BEHAVIOR OF PCM/PM RECEIVERS IN NON-IDEAL CHANNELS

Part I: The Separate Effects of Imperfect Data Streams and Band-limiting Channels on Performance[1]

Tien Manh Nguyen
National Aeronautics and Space Administration
Jet Propulsion Laboratory
California Institute of Technology
4800 Oak Grove Drive
Pasadena, CA 91109

ABSTRACT

The performance of residual carrier communication systems that are used for space telemetry signals and that employ a PCM/PM modulation technique with an imperfect NRZ or Bi-ϕ data format and band-limited channels is investigated in this paper. In this particular modulation scheme, the data (either Non-Return-to-Zero, NRZ, or Bi-ϕ) is directly modulated on the RF residual carrier. Undesired spectral components caused by the imperfect data stream (e.g., data asymmetry due to rising and falling voltage transitions or an imbalance between +1's and -1's in the data stream) can degrade the carrier tracking and symbol synchronization performances. Only the effects of imperfect carrier tracking due to an imperfect data stream are considered. The Symbol Error Rate (SER) performance degradation due to the presence of an imperfect data stream is evaluated for both NRZ and Bi-ϕ data formats, and these evaluations are compared. Furthermore, the SER performance for both PCM/PM/NRZ and PCM/PM/Bi-ϕ is analyzed for the presence of a band-limited channel. The effects of the InterSymbol Interference (ISI) created by a band-limited channel on system performance are evaluated for an ideal low-pass filter.

[1] The work described in this paper was carried out at the Jet Propulsion Laboratory, California Institute of Technology, under contract with the National Aeronautics and Space Administration.

1. Introduction

There are considerable interests among international space agencies to search for a bandwidth-efficient modulation scheme that can be used for future space missions without major modifications to their ground stations. The Consultative Committee for Space Data Systems (CCSDS) (established by nine international space agencies and eight observer agencies [1]) has undertaken the task to investigate a modulation scheme that offers both of these features (bandwidth efficiency and no major hardware modifications to the current systems.)

Currently, the space telemetry systems employ residual carrier modulation with the subcarriers which are used to separate the data from the RF residual carrier [1]. The CCSDS has recommended that squarewaves and sinewaves are used for the deep space and near earth missions, respectively. This modulation scheme is called PCM/PSK/PM and it was developed at a time when weak signals and low data rates dominated [2]. As the technology in antenna, transmitters and signal processing improved, a significant increase in the available signal power can provide much higher telemetry bit rate. For high telemetry bit rate, the use of the subcarrier causes the occupied bandwidth to increase significantly [3]. This is prohibitive because the space telemetry systems often operate under imposed bandwidth constraints. A natural solution is to use the residual carrier modulation without the subcarriers. This modulation scheme is referred to as PCM/PM. Because this modulation technique requires a minimum hardware modification to the current systems and, at the same time, the bandwidth efficiency can be achieved. Recently, [4] has compared the performance of PCM/PM and PCM/PSK/PM modulation techniques for space telemetry applications. The results presented in [4] show that, for certain operating conditions, the performance of PCM/PM/NRZ will be as good as PCM/PM/Bi-ϕ or PCM/PSK/PM. Furthermore, [5] also shows that PCM/PM/NRZ provides smaller occupied bandwidth as compared to PCM/PSK/PM and PCM/PM/Bi-ϕ. However, the results shown in [4-5] were derived based on perfect operating conditions, e.g., perfect data stream with balanced +1's and -1's and unlimited bandwidth channel.

In the recent past, [6-8] have investigated only the effects of data asymmetry and bandlimiting channel on the performance of space telemetry systems. However, [6] only considers the effects of NRZ data asymmetry on PCM/PSK/PM systems with squarewave subcarriers, and [7] only investigates the effects of data asymmetry of a perfectly balanced Bi-ϕ data stream on the carrier tracking performance and the consequent effect upon the probability of error. On the other hand, [7] only analyzes the effects of data asymmetry and bandlimiting channel on the performance of suppressed carrier systems. Furthermore, when analyzing the effects of bandlimiting, [7] has assumed that (1) the amount of data asymmetry is known so that an optimum sampling time can be set for the sample detector, and (2) the carrier tracking is perfect.

The goal of this paper is to investigate and assess the impacts of imperfect data stream and bandlimiting channel conditions on the performance degradation of the space telemetry receivers in the presence of the PCM/PM signals. Separate effects of data asymmetry, unbalanced data stream and ISI caused by band-limited channel on

performances of PCM/PM/NRZ and PCM/PM/Bi-ϕ receivers are analyzed. This extends previously reported work that assumed ideal operating conditions [4-8].

This paper is organized in the following manner. Section 2 introduces the space telemetry system models employing PCM/PM modulation technique. Section 3 investigates the effects of data asymmetry on the system performance. The effects of imbalance between +1's and -1's in the data streams are analyzed in Section 4. Section 5 presents the analysis for band-limited channel. Numerical results and discussions are shown in Section 6. Finally, Section 7 presents the main conclusion of the paper.

2. Space Telemetry System Models

Figure 1 illustrates a space telemetry system model in which the data stream can be either NRZ or Bi-ϕ (Bi-phase or Manchester) data stream with a transition density, p_t, which is less than or equal to 1/2. In this model the transmitted telemetry signal is given by

$$S_T(t) = \sqrt{2P}\cos(\omega_c t + m_T d(t)) \tag{1}$$

where P is the transmitted power, $\omega_c = 2\pi f_c$ is the angular carrier center frequency in rad/sec, m_T is the telemetry modulation index in rads which is less than $\pi/2$, and d(t) is NRZ data Sequence (PCM/PM/NRZ) or the Manchester data waveform generated by the binary (± 1) NRZ data sequence (PCM/PM/Bi-ϕ). Figures 2(a) and 2(b) show the plots of the power spectral densities of $S_T(t)$ for PCM/PM/Bi-ϕ and PCM/PM/NRZ, respectively.

The received signal $S_r(t)$ is corrupted by additive white Gaussian noise n(t) with one-sided noise spectral density N_o and data asymmetry or unbalanced data stream. Expanding the received signal we have

$$S_r(t) = \sqrt{2P}\left[\cos(m_T)\cos(\omega_c t+\theta_o) - d(t)\sin(m_T)\sin(\omega_c t+\theta_o)\right] + n(t) \tag{2}$$

where ω_o is the initial phase offset caused by the transmission medium. The first and second terms of Eqn (2) are the residual carrier and data components, respectively.

The data asymmetry and/or the imbalance between +1's and -1's in the data stream will produce undesired spectral components at the carrier frequency creating an imperfect carrier reference that will degrade the telemetry system performance. In addition, the ISI created by the band-limited channel can cause further disturbance to the carrier reference.

If we let $\hat{\theta}$ denote the carrier loop estimate of θ_o, the phase error θ_e due to the thermal noise and the interference caused by the data asymmetry/or unbalanced data stream is defined as

$$\theta_e = \theta_o - \hat{\theta} \tag{3}$$

The carrier loop tracks the residual carrier component in Eqn (2) to provide an imperfect reference for the modulation given by

$$r(t) = \sqrt{2}\cos(\omega_c t + \hat{\theta}) \tag{4}$$

Assuming the symbol sync clock C(t) as shown in Figures 3(a) and 3(b) for NRZ and Bi-ϕ respectively, and using the imperfect carrier reference in (4), one can show that the signal output of the integrate-and-dump at time $t = T_s$ is given by

$$Z(T_s) = \sqrt{P}\sin(m_T)\cos(\theta_e)\int_0^{T_s} d(t)C(t)\,dt + n(T_s) \tag{5}$$

Here one has assumed that the phase error process θ_e of Eqn (3) is essentially constant during the symbol interval T_s, and that the corrupting noise process $n(T_s)$ is a zero-mean Gaussian random variable with a variance $N_o T_s/2$.

The test statistic $Z(T_s)$ of Eqn (5) represents the observed data at the receiver. This test statistic is needed to determine the SER performance. Using this test statistic, the performance of the telemetry system shown in Figure 1 has been evaluated in [4] for both NRZ and Bi-ϕ data formats. The results of [4] are presented here for the sake of completeness. The average probability of error is given by

$$P_e = \int_{\theta_e} P_e(\theta_e)P(\theta_e)d\theta_e \tag{6}$$

where $P_e(\theta_e)$ is the conditional probability of error and $P(\theta_e)$ is the probability density function (pdf) for θ_e. For perfect data stream and ideal channel, this conditional probability of error is:

$$P_e(\theta_e) = (1/2)\,\mathrm{erfc}\{\sqrt{E_s/N_o}\cos(\theta_e)\} \tag{7}$$

where E_s denotes the symbol energy, i.e., $E_s = (PT_s)\sin^2(m_T)$. In this paper, one postulates a Tikhonov pdf for θ_e, which is entirely characterized by the variance σ^2 of the carrier tracking phase error. When the loop signal-to-noise ratio is high the Tikhonov pdf can be approximated by

$$P(\theta_e) \approx \exp(-\theta_e^2/2\sigma^2)/[2\pi\sigma^2]^{-1/2},\ -\infty < \theta_e < \infty \tag{8}$$

For perfect data streams and high-data-rate case ($B_L/R_s << 0.1$, where B_L and R_s denote the one-sided loop bandwidth and the symbol rate, respectively), the variance of the carrier tracking phase error has been found in [4]. For perfect NRZ data format, it is found to be

$$\sigma^2 = (1/\rho_o) + (B_L/R_s)\tan^2(m_T) \tag{9}$$

and, for perfect Bi-ϕ data format σ^2 becomes

$$\sigma^2 = (1/\rho_o) + (I/C)\tan^2(m_T) \tag{10}$$

where

$$\rho_o = \frac{(E_s/N_o)}{(B_L/R_s)\tan^2(m_T)}, \tag{11}$$

$$\begin{aligned} I/C = {} & (1/2) + (9/16)(B_L/R_s)^{-1} \\ & - (3/4)(B_L/R_s)^{-1}\exp\{-(2/3)(B_L/R_s)\}[\cos\{(2/3)(B_L/R_s)\} + 3\sin\{(2/3)(B_L/R_s)\}] \\ & + (3/16)(B_L/R_s)^{-1}\exp\{-(4/3)(B_L/R_s)\}[\cos\{(4/3)(B_L/R_s)\} + 3\sin\{(4/3)(B_L/R_s)\}] \end{aligned} \tag{12}$$

In the following sections, one will determine the conditional error probability and the carrier tracking phase error when the data stream is disturbed by the data asymmetry or when there exists an unbalanced between +1's and -1's in the transmitting data stream. Moreover, the effects of a band-limited channel on the performance of the PCM/PM receivers are also investigated.

3. The Effects of Data Asymmetry

The telemetry data asymmetry due to rising and falling voltage transitions can cause undesired spectral components at the output of the spacecraft's transmitter. The effects of these spectral components on the performance degradation of the space telemetry receivers have been investigated in [6, 8]. As mentioned earlier, [6] and [8] investigate the PCM/PSK/PM with squarewave subcarriers and PCM/PM/Bi-ϕ modulation systems with balanced data streams, respectively. Whenever it is applicable, the results presented in these references will be used in the following analyses.

Figures 4(a) and 4(b) show the data asymmetry models that will be considered in the following sections. For NRZ data stream, +1 NRZ symbols are elongated by $\Delta T_s/2$ (relative to their nominal value of T_s seconds) when a negative-going data transition occurs and -1 symbols are shortened by the same amount when a positive-going data transition occurs, and the symbols maintain their nominal T_s seconds when no transitions occur. Similarly, For Bi-ϕ data stream, +1 Bi-ϕ symbols are elongated by $\Delta T_s/4$ (relative to their nominal value of $T_s/2$ seconds) when a negative-going data transition occurs and -1 symbols are shortened by the same amount when a positive-going data transition occurs, and the symbols maintain their nominal $T_s/2$ seconds when no transitions occur.

3.1 The Effects of Data Asymmetry on PCM/PM/NRZ System Performance

The impact of NRZ data asymmetry on the performance of a space telemetry system that employed PCM/PSK/PM modulation has been investigated in [6]. Since PCM/PSK/PM uses the subcarrier to separate the data from the RF residual carrier, the interference from the data to the carrier tracking is neglected in [6]. This section will extend the results presented in [6] to include PCM/PM/NRZ signal format.

For the data asymmetry model shown in Figure 4(a) and for a purely random and equiprobable NRZ data (i.e., perfectly balanced NRZ data stream), the conditional average probability of error associated with hard decision made on the in-phase integrate-and-dump output of the symbol synchronizer can be shown to have the following form (using Eqn. (5) and similar technique presented in [7])

$$P_e(\theta_e) = (5/16)\ \mathrm{erfc}\{\sqrt{E_s/N_o}\cos(\theta_e)\} +$$

$$(1/8)\ \mathrm{erfc}\{\sqrt{E_s/N_o}(1-\xi)\cos(\theta_e)\} + (1/16)\ \mathrm{erfc}\{\sqrt{E_s/N_o}(1-2\xi)\cos(\theta_e)\} \qquad (13)$$

where ξ denotes the data asymmetry. Here, one has assumed that the carrier tracking is imperfect and the symbol synchronizer operates perfectly.

In order to calculate the average probability of error in Eqn. (6), the variance of the tracking phase error σ^2 must be found. Using the linear model for the carrier tracking loop, the variance σ^2 is given by [2]

$$\sigma^2 = 2B_L N/(2P_c) \qquad (14)$$

where N is the modified noise spectral density resulting from the thermal noise and NRZ data asymmetry, $2B_L$ is the two-sided loop bandwidth, and P_c is the carrier power equal to $P\cos^2(m_T)$.

If we let $H(j2\pi f)$ denote the carrier loop transfer function, the two-sided loop bandwidth and the modified noise spectral density can be written, respectively, as

$$2B_L = \int_{-\infty}^{\infty} |\ H(2\pi f)\ |^2\, df \qquad (15)$$

$$N = (1/2B_L) \int_{-\infty}^{\infty} |\ H(2\pi f)\ |^2\, [N_o + S_I(f)]df \qquad (16)$$

where $S_I(f)$ is the data spectrum that causes the interference to the carrier tracking. In general, for $2B_L << R_s$, the interference data spectrum $S_I(f)$ can be written as

$$S_I(f) = P\sin^2(m_T)[S_{dc}(f) + S_c(f)] \qquad (17)$$

where $S_{dc}(f)$ is the dc component (or the harmonic components) caused by the imperfect

data stream that falls on the RF residual carrier, and $S_c(f)$ is the continuous data spectrum that falls within the carrier tracking loop bandwidth.

Substituting Eqn (16) into Eqn (14) we obtain the variance of the carrier tracking phase error. Assuming $|H(0)|^2 = 1$, we get

$$\sigma^2 = 1/\rho_o + (\alpha/2)\tan^2(m_T) + (1/2)(I/C) \tag{18}$$

where ρ_o is defined as before, and

$$\alpha = \text{interference due to continuous spectrum} = \int_{-\infty}^{\infty} |H(2\pi f)|^2 S_c(f)df \tag{19}$$

I/C = Interference caused by dc component-to-carrier-power ratio

$$= \tan^2(m_T)\int_{-\infty}^{\infty} S_{dc}(f)\, df \tag{20}$$

[6] has derived the power spectral density for the asymmetric NRZ data stream illustrated in Figure 4(a). The dc and continuous spectral components for equiprobable symbols are given by [6]

$$S_{dc}(f) = (1/4)\xi^2\,\delta(f) \tag{21}$$

$$S_c(f) = (T_s/8)[\sin^2(\pi fT_s)/(\pi fT_s)^2][3 + 5\cos^2(\pi fT_s\xi)]$$

$$+ (T_s/8)[\sin^2(2\pi fT_s\xi)/(\pi fT_s)^2][3\cos^2(\pi fT_s) + \cos^2(2\pi fT_s\xi)] \tag{22}$$

For this case, we have

$$I/C = (1/4)\xi^2\tan^2(m_T) \tag{23}$$

and the interference due to continuous spectrum can be computed by substituting Eqn (22) into Eqn (19). Having I/C and α we can calculate the variance of the tracking phase error, and hence the pdf of the tracking phase error is completely characterized. Using the resultant pdf together with Eqn (13), the average error probability can be calculated using Eqn (6). The numerical results are plotted in Figures 5a and 5b for the second order Phase-Locked Loop (PLL) with the loop transfer function given by [9]

$$|H(j2\pi f)|^2 = [1 + 2(f/f_n)]/[1 + (f/f_n)] \tag{24}$$

The loop transfer function given in Eqn. (24) is for a particular case when the damping factor β is equal to 0.707. The loop natural frequency f_n for this case is related to the two-sided loop bandwidth $2B_L$ through

$$2B_L = 2\pi f_n[\beta + 1/(4\beta)]. \tag{25}$$

A typical value for modulation index (m_T) of 1.25 rad are used in the computation of the effective carrier loop SNR and average SER shown in Figures 5a and 5b, respectively. The two-sided loop bandwidth-to-symbol rate ratio ($2B_L/R_s$) of 0.001 is chosen in this computation because it has been shown in [4] that the performance of PCM/PM/NRZ will approach ideal BPSK when $2B_L/R_s \leq 0.001$. Figure 5a illustrates the effective carrier loop SNR as a function of symbol SNR for various values of data asymmetry. When plotting Figure 5a one assumes that the carrier loop operates in the linear region so that the loop SNR is inversely proportional to the variance of the tracking phase error. Figure 5b shows that the symbol SNR degradation for PCM/PM/NRZ is between 0.2 dB to 0.25 dB for $10^{-5} \leq SER \leq 10^{-7}$, and data asymmetry ($\xi$) of 6% and about 0.1 dB or less when $\xi = 2$ %.

3.2 The Effects of Data Asymmetry on PCM/PM/Bi-ϕ System Performance

[8] has analyzed the effects of Bi-ϕ data asymmetry on the space telemetry performance degradation. The average probability of error conditioned on the carrier phase error is found to be [8]

$$P_e(\theta_e) = (1/4)[\text{erfc}\{\sqrt{E_s/N_o}(1-\xi)\cos(\theta_e)\} + \text{erfc}\{\sqrt{E_s/N_o}(1-\xi/2)\cos(\theta_e)\}] \quad (26)$$

Based on the data asymmetry model shown in Figure 4(b), the power spectral density for a balanced Bi-ϕ data stream has been derived in [8], and consequently, we can show that the interference caused by dc component-to-carrier-power ratio and the continuous spectral component are given by, respectively

$$I/C = (9/4)\xi^2\tan^2(m_T) \quad (27)$$

$$\begin{aligned} S_c(f) = {} & T_s(\pi fT_s/2)^{-2}C_6(\xi)\sin^2[\pi fT_s(1+\xi)/2] \\ & + T_s(\pi fT_s/2)^{-2}C_7(\xi)\sin^2[\pi fT_s(1-\xi)/2] + T_s(\pi fT_s)^{-2}\sin^4[\pi fT_s/2] \\ & - T_s(\pi fT_s/2)^{-2}[C_1(\xi) + C_2(\xi) + C_3(\xi)]\sin^2[\pi fT_s\xi] \\ & - T_s(\pi fT_s/2)^{-2}C_4(\xi)\sin^2[\pi fT_s\xi/2] - T_s(\pi fT_s/2)^{-2}C_5(\xi)\sin^2[\pi fT_s\xi/2] \end{aligned} \quad (28)$$

The parameters $C_1(\xi)$-$C_7(\xi)$ found in Eqn (28) are defined as follows:

$$C_1(\xi) = (1/4)\sin^2[\pi fT_s(1+\xi)/2]\{\sin^2[\pi fT_s(1-\xi)/2] + \cos(\pi\xi fT_s)\} \quad (29)$$

$$C_2(\xi) = (1/8)\cos^2[\pi fT_s\xi]\{2\sin^2[\pi fT_s(1-\xi)/2] - \sin^2(\pi\xi fT_s/2)\} \quad (30)$$

$$C_3(\xi) = (1/8)[1 - 4\cos(\pi fT_s/4)] \quad (31)$$

$$C_4(\xi) = (1/8)\sin[\pi fT_s\xi]\sin[\pi fT_s\xi/2] + \sin[5\pi\xi fT_s/2]\sin[\pi fT_s\xi]\{1-\cos(\pi fT_s)\cos(\pi fT_s\xi)\} \quad (32)$$

$$C_5(\xi) = -(3/8)\sin[\pi f T_s/4]\sin[\pi f T_s \xi/4] + (1/8)\{2\cos[3\pi\xi f T_s] + \cos[2\pi\xi f T_s]\} \quad (33)$$

$$C_6(\xi) = (1/8)\{\sin^2[\pi f T_s(1 - \xi)/2] - (3/2)\sin^2[\pi f T_s(1 + \xi)/2]\} \quad (34)$$

$$C_7(\xi) = (3/16)\sin^2[\pi f T_s(1 - \xi)/2] + (1/4)\sin^2[\pi f T_s \xi/2]\cos(\pi\xi f T_s)\} \quad (35)$$

The interference due to continuous spectrum, α, can be calculated by substituting Eqn. (28) into Eqn. (19). Again, after calculating I/C and α we can obtain the variance of the tracking phase error and hence the average probability, using Eqns. (18), (8), (26) and (6). The numerical results are plotted in Figures 6a and 6b for the second order PLL with the transfer function given by Eqn (24). Figure 6a plots the effective carrier loop SNR as a function of symbol SNR with data asymmetry as a parameter. Figure 6b shows the SER as a function of symbol SNR for various values of data asymmetry and modulation index of 1.25 rad, $2B_L/R_s = 0.001$. The symbol SNR degradation for PCM/PM/Bi-ϕ obtained from this figure is between 0.67 dB to 0.87 dB for $10^{-5} \leq$ SER $\leq 10^{-7}$, and data asymmetry of 6%. Note that in order to compare the results presented in Figure 6b with those in Figure 5b for NRZ data, use equal amounts of asymmetry as measured by the actual time displacement of both waveforms transitions. For a fair comparison, one replaces ξ (data asymmetry) in Figure 6b by 2ξ when compared with Figure 5b. As an example, the SER curve for PCM/PM/NRZ operating at 2 % data asymmetry shown in Figure 5b corresponds to the 4 % data asymmetry curve for PCM/PM/Bi-ϕ shown in Figure 6b.

4. The Effects of Unbalanced Data Stream

As in the case for the data asymmetry, the imbalances between +1's and -1's in the data stream can also cause undesired spectral components at the output of the spacecraft's transmitter. These undesired components can potentially degrade the performance of the space telemetry system. Sections 4.1 and 4.2 will analyze the effects of unbalanced data stream on the performance degradation of PCM/PM systems with NRZ and Bi-ϕ data formats, respectively.

4.1 The Effects of Unbalanced Data Stream on PCM/PM/NRZ System Performance

Recall from the previous sections that in order to calculate the average probability of error (Eqn (6)) one needs to determine the conditional probability of error $P_e(\theta_e)$ and the tracking variance σ^2. This is because one postulates a Gaussian density for the tracking phase error (Eqn (8)). Using Eqn (5) one can show that the conditional probability of error is the same as Eqn (7) for the case of ideal data stream. Therefore, the problem remains is to evaluate the tracking variance.

The tracking variance for this case can also be calculated using Eqn (18). To evaluate this equation one needs to have the power spectral density for the unbalanced NRZ data stream. The dc and continuous components for unbalanced NRZ data stream are found to be [2]

$$S_{dc}(f) = (1 - 2p)^2\, \delta(f) \quad (36)$$

$$S_c(f) = 4T_s p(1 - p)[\sin^2(\pi f T_s)/(\pi f T_s)^2] \quad (37)$$

where p is the probability of transmitting a +1 pulse or probability of mark. For unbalanced data stream, $p \neq 1/2$. Note that for purely random NRZ data source, the transition density p_t can easily be verified to be $2p(1 - p)$.

Using Eqns (19) and (20) one can show that the interferences due to continuous spectrum and dc component have the following forms:

$$I/C = (1 - 2p)^2 \tan^2(m_T) \quad (38)$$

$$\alpha = 4T_s p(1 - p) \int_{-\infty}^{\infty} | H(2\pi f) |^2 [\sin^2(\pi f T_s)/(\pi f T_s)^2] \quad (39)$$

Substituting Eqns (38) and (39) into Eqn (18) one obtains the tracking variance for this case and hence the pdf for the tracking phase error $P(\theta_e)$ is completely characterized. Substituting the resultant pdf and Eqn (7) into Eqn (6) one obtains an expression for the average probability of error for an unbalanced NRZ data stream. This average error probability is calculated as a function of symbol SNR for various values of p and modulation index m_t, and the results are plotted in Figures 7a, 7b and 8, respectively. Figure 7a plots the effective carrier loop SNR as a function of symbol SNR for various values of p. Figure 7b shows that the symbol SNR degrades seriously when $p \leq 0.4$ for $m_T = 1.25$ rad and $2B_L/R_s = 0.001$. As we decrease the modulation index the SER performance improves because more power is allocated to the carrier and less to the dc component created by the unbalanced between +1's and -1's. This improvement is evident from Figure 8.

4.2 The Effects of Unbalanced Data Stream on PCM/PM/Bi-ϕ System Performance

As in Section 4.1, the conditional probability of error can be shown to have the same form as in Eqn (7) for the case of ideal data stream, and the task is to determine the tracking variance. If one assumes $2B_L << R_s$ then the dc and continuous components for unbalanced Bi-ϕ data stream can be shown to be [2]

$$S_{dc}(f) = 0 \quad (40)$$

$$S_c(f) = 4T_s p(1 - p)[\sin^4(\pi f T_s/2)/(\pi f T_s/2)^2] \quad (41)$$

Therefore, the parameters I/C and α become

$$I/C = 0 \quad (42)$$

$$\alpha = 4T_s p(1 - p) \int_{-\infty}^{\infty} | H(2\pi f) |^2 [\sin^4(\pi f T_s/2)/(\pi f T_s/2)^2] \quad (43)$$

Again, substituting Eqns (42) and (43) into Eqn (18) we obtain the tracking variance for this case and hence the pdf for the tracking phase error $P(\theta_e)$. Substituting the resultant pdf and Eqn (7) into Eqn (6) one gets an expression for the average probability of error for an unbalanced Bi-ϕ data stream. The numerical results for the effective carrier loop SNR and the average probability of error are plotted in Figures 9a and 9b, respectively. Both Figure 9a and 9b show that the performance of the PCM/PM/Bi-ϕ receiver is not susceptible to the unbalanced data stream.

5. Behavior of PCM/PM Receivers in the Presence of Band-Limited Channels

When the RF filter bandwidth becomes less than the main spectrum hump of the modulated carrier, the information-bearing pulses are spread out in time. Each pulse is overlaid with the tails of previous pulses and the precursors of the subsequent ones, and this so-called Intersymbol Interference (ISI) behaves like an additional random noise. This additional random noise can cause potential degradation to the receiver. In addition, excessive filtering of the pulse can also cause a loss of bit energy during the bit time. This section will analyze the performance of the PCM/PM receiver in the presence of ISI.

Let P(t) denote the pulse shape of the data and h(t) denote the impulse response of the equivalent low-pass filter of the RF bandpass filter with bandwidth B. The received data can be expressed in term of P(t) and h(t) as follow

$$d(t) = \sum_{k=-\infty}^{\infty} d_k \, g(t - kT_s) \tag{44}$$

where $d_k = \pm 1$ with $Pr\{d_k = +1\} = Pr\{d_k = -1\} = 1/2$, and g(t) is given by

$$g(t) = P(t) * h(t) \tag{45}$$

where * denotes the convolution.

For this case the symbol energy becomes

$$E_s = P\sin^2(m_T)\int_0^T | g(t) |^2 \, dt \tag{46}$$

Using Eqn (5) one can show that the output of the integrate-and-dump filter in the presence of the band-limited channel have the following form

$$Z(T_s) = E_s[1 + \sum_{k=-\infty}^{\infty}{}' d_k \lambda_k]\cos\theta_e + n(T_s) \tag{47}$$

where the prime in the sum indicates the omission of the term k = 0, and

$$\lambda_k = \frac{\int_0^{T_s} g(t)g(t+kT_s)dt}{\int_0^{T_s} |g(t)|^2 dt} \tag{48}$$

Note that in Eqn (47) one has assumed $d_o = +1$. Therefore, the conditional probability $P_e(\theta_e)$ of error is then the probability that $Z(T_s) < 0$ when $d_0 = +1$,

$$P_e(\theta_e) = Pr\{Z(T_s) < 0/\theta_e, d_0 = +1\} \tag{49}$$

Calculating $P_e(\theta_e)$ exactly is very difficult, because one has to take all possible combinations of the digits $d_k = \pm 1$ into account, $1 \leq |k| \leq \infty$. Here one will assume that only a finite number M of pulses before and after d_0, i.e., one considers only the ISI effects of the M preceding and M subsequent bits on the bit under detection. In order to calculate $P_e(\theta_e)$ exactly for M pulses before and after d_0 one needs to account for 2^{2M} combinations. Since, for accuracy, the value of M selected typically depends on the time-bandwidth product BT_s and the value of M becomes very large when $BT_s << 1$; the length of the computation grows exponentially with M. To avoid the complexity associated with this technique for large M, Helstrom [10] has shown that this conditional error probability $P_e(\theta_e)$ can be evaluated by numerical quadrature of a Laplace inversion integral along a contour in the complex plane passing through a saddlepoint of the integrand. For finite M, the amount of computation associated with this technique only increases linearly with M.

For $BT_s \geq 1$, the value of $1 \leq M \leq 2$ is sufficient. When M is small, direct computation of the conditional error probability $P_e(\theta_e)$ is feasible through the following equation

$$P_e(\theta_e) = (1/2)[(1/2^{2M}) \sum_{\substack{k=2^{2M} \\ \text{combinations}}} \text{erfc}\{\sqrt{E_s/N_o}[1 + \Sigma' d_k \lambda_k]\cos\theta_e\} \tag{50}$$

As an example, for M = 1, Eqn (50) becomes

$$P_e(\theta_e) = (1/2)[(1/4)\text{erfc}\{\sqrt{E_s/N_o}(1+\lambda_{-1}+\lambda_{+1})\cos\theta_e\} + (1/4)\text{erfc}\{\sqrt{E_s/N_o}(1+\lambda_{-1}-\lambda_{+1})\cos\theta_e\}$$
$$+ (1/4)\text{erfc}\{\sqrt{E_s/N_o}(1-\lambda_{-1}+\lambda_{+1})\cos\theta_e\} + (1/4)\text{erfc}\{\sqrt{E_s/N_o}(1-\lambda_{-1}-\lambda_{+1})\cos\theta_e\}] \tag{51}$$

To simplify the computation one will assume ideal bandpass filter so that the transfer function for the equivalent low-pass filter is given by

$$H(f) = \begin{cases} 1, & -B < f < B \\ 0, & \text{elsewhere} \end{cases} \tag{52}$$

The impulse response h(t) is found to be

$$h(t) = 2B\ \mathrm{sinc}(2Bt) \tag{53}$$

where $\mathrm{sinc}(x) = \sin(\pi x)/(\pi x)$.

Thus, for ideal lowpass filter and perfect data stream, the ouput of the filter g(t) can be obtained by substituting Eqn (53) into (45). For NRZ data format, $g_{NRZ}(t+kT_s)$ can be shown to be

$$g_{NRZ}(t+kT_s) = \frac{1}{\pi}[\mathrm{si}\{2\pi B(t+T_s(k+1/2))\} - \mathrm{si}\{2\pi B(t+T_s(k-1/2))\}] \tag{54}$$

For Bi-ϕ data format one gets

$$g_{Bi\text{-}\phi}(t+kT_s) = \frac{1}{\pi}[\mathrm{si}\{2\pi B(t+T_s(k+1/2))\} + \mathrm{si}\{2\pi B(t+T_s(k-1/2))\} - 2\mathrm{si}(2\pi B(t+kT_s)] \tag{55}$$

where

$$\mathrm{si}(x) = \int_0^x [\sin(u)/u]du \tag{56}$$

Substituting Eqns (54) and (55) into Eqn (48) one can calculate λ_k for NRZ and Bi-ϕ data formats, respectively. Therefore, for $1 \leq M \leq 2$, one can obtain the average error probability P_e by substituting Eqns (8) and (50) into Eqn (6) and performing the numerical integration in a digital computer. Note that the variances of the carrier tracking phase error used in these calculations are given by Eqns (9) and (10) for NRZ and Bi-ϕ data formats, respectively. The numerical results are plotted in Figures 10 and 11 for PCM/PM/NRZ and PCM/PM/Bi-ϕ, respectively. Again, the results shown in these figures are for $m_T = 1.25$ rad and $2B_L/R_s = 0.001$. As expected, these numerical results show that the PCM/PM/NRZ outperforms PCM/PM/Bi-ϕ in the presence of ISI caused by band-limited channel.

6. Numerical Results and Discussions

Figures 12-14 show the performance comparison between PCM/PM/NRZ and PCM/PM/Bi-ϕ in the presence of data asymmetry, unbalanced data stream and bandlimiting channel, respectively. Figure 12 shows that for fixed modulation index, $2B_L/R_s$ and data asymmetry, the symbol error probability for PCM/PM/NRZ is superior than that of PCM/PM/Bi-ϕ. This phenomenon can be explained as follow. As shown in Figure 1, the

Bi-ϕ data stream is derived from the NRZ data stream, hence the amount of data asymmetry inherent in the Bi-ϕ data stream will be twice that of NRZ. This is because the transition in Bi-ϕ data stream is effectively twice that of NRZ. The numerical results show that, for data asymmetry less than or equal to 2 %, the symbol SNR degradation is at the order of 0.1 dB or less for both systems when they operate at typical operating conditions (m_T = 1.25 rad and $2B_L/R_s$ = 0.001).

Figure 13 compares the performance of PCM/PM/NRZ and PCM/PM/Bi-ϕ in the presence of unbalanced data streams. As the probability of transmitting a +1 pulse, p, deviates from 1/2, the performance of PCM/PM/NRZ degrades seriously, and that the degradation becomes unacceptable when $p < 0.45$. This is due to the presence of a strong dc component (caused by the unbalanced NRZ data stream) at the carrier. On the other hand, due to the absence of the dc component at the carrier frequency for the unbalanced bi-ϕ data, the performance of PCM/PM/Bi-ϕ is insensitive to the amount of unbalanced between +1's and -1's. The symbol SNR degradation for PCM/PM/Bi-ϕ is about 0.3 dB for $p < 0.4$, m_T = 1.25 rad and $2B_L/R_s$ = 0.001, and it is expected to be less than 0.3 dB when $m_T < 1.25$ rad.

Figure 14 illustrates the performances of PCM/PM/NRZ and PCM/PM/Bi-ϕ when they operate under bandwidth constraint. For $10^{-5} \leq SER \leq 10^{-7}$, m_T = 1.25 rad and $2B_L/R_s$ = 0.001, the symbol SNR degradation of PCM/PM/NRZ is at the order of 1-1.2 dB for BT_s = 1, and less than 0.3 dB for BT_s = 2. Under the same operating conditions, the performance degradation of the PCM/PM/Bi-ϕ is unacceptable for BT_s = 1, and more than 0.6 dB for BT_s = 2. Therefore, the performance of PCM/PM/Bi-ϕ is more susceptible to bandlimiting channels than PCM/PM/NRZ.

7. Conclusion

This paper has analyzed and explained the separate effects of data asymmetry, unbalanced data and ISI on the performances of both PCM/PM/NRZ and PCM/PM/Bi-ϕ systems. In the presence of imperfect carrier tracking due to imperfect data stream, it was found that the PCM/PM/Bi-ϕ is sensitive to ISI and data asymmetry. On the other hand, the PCM/PM/NRZ is sensitive to the unbalanced data stream.

Numerical results also indicate that, for typical operating conditions (m_T = 1.25 rad, $2B_L/R_s$ = 0.001) PCM/PM/NRZ outperforms PCM/PM/Bi-ϕ system in bandlimiting channel as well as in the presence of data asymmetry. In addition, the PCM/PM/Bi-ϕ system is found to be superior than PCM/PM/NRZ when operating under unbalanced data condition, and results also show that the performance degradation of PCM/PM/NRZ becomes unacceptable when the probability of transmitting a +1 pulse becomes smaller than 0.45. The combined effects of both imperfect data stream and bandlimiting channels on the performance of the PCM/PM receivers will be investigated in Part II of this paper.

Acknowledgement

The work described in this paper was carried out at the Jet Propulsion Laboratory, California Institute of Technology, under contract with the National Aeronautics and Space Administration.

References

[1] Consultative Committee for Space Data Systems, Recommendations for Space Data System Standards, Radio Frequency and Modulation Systems, Part I, Earth Stations and Spacecraft, CCSDS 401.0-B, Blue Book, CCSDS Secretariat, Communications and Data systems Division, (Code OS), NASA, Washington D.C.

[2] Joe Yuen, editor, Deep Space Telecommunications Systems Engineering, Plenum Press, New York, 1983.

[3] Tien M. Nguyen, "Closed Form Expressions for Computing the Occupied Bandwidth of PCM/PSK/PM Signals," 1991 IEEE International Symposium on EMC Proceedings, September 1991, Cherry Hills, New Jersey.

[4] Mazen M. Shihabi, Tien M. Nguyen, Sami M. Hinedi, "On the Use of Subcarriers in Future DSN Missions," the Telecommunications and Data Acquisition Progress Report 42-111, November 15, 1992, NASA, Jet Propulsion Laboratory, Pasadena, California.

[5] Tien M. Nguyen, "Occupied Bandwidths for PCM/PSK/PM and PCM/PM Signals-A Comparative Study," presented to the International Consultative Committee for Space Data Systems, Subpanel 1E, RF and Modulation, Salzburg, Austria, May 1992.

[6] Tien M. Nguyen, "The Impact of NRZ Data Asymmetry on the Performance of a Space Telemetry System," IEEE Transactions on EMC, Vol. 33, No. 4, November 1991.

[7] W. K. Alem, G. K. Huth, M. K. Simon, "Integrated Source and Channel Encoded Digital Communication System Design Study," Final Report (R7803-7) under Contract NAS 9-15240, Mar. 31, 1978, Axiomatix, Marina del Rey, CA.

[8] Tien M. Nguyen, "Space Telemetry Degradation due to Manchester Data Asymmetry Induced Carrier Tracking Phase Error," IEEE Transactions on EMC, Vol. 33, No. 3, August 1991.

[9] J. K. Holmes, Coherent Spread Spectrum Systems, New York: Wiley-Interscience, 1982, Chapter 4.

[10] C. W. Helstrom, "Calculating Error Probabilities for Intersymbol and Cochannel Interference," IEEE Transactions on Communication, Vol.COM-34, No.5, May 1986.

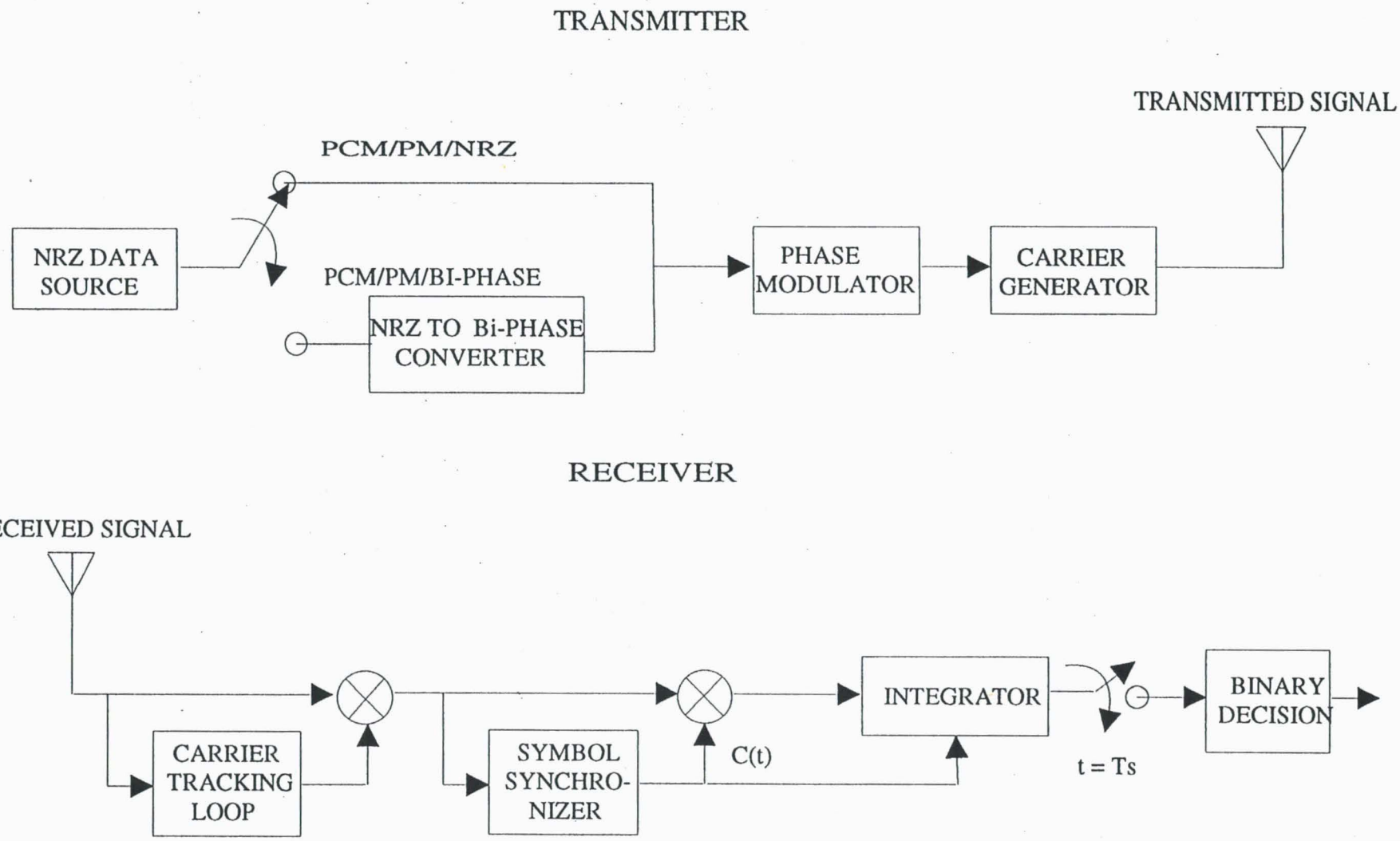

FIGURE 1. SPACE TELEMETRY SYSTEM MODEL

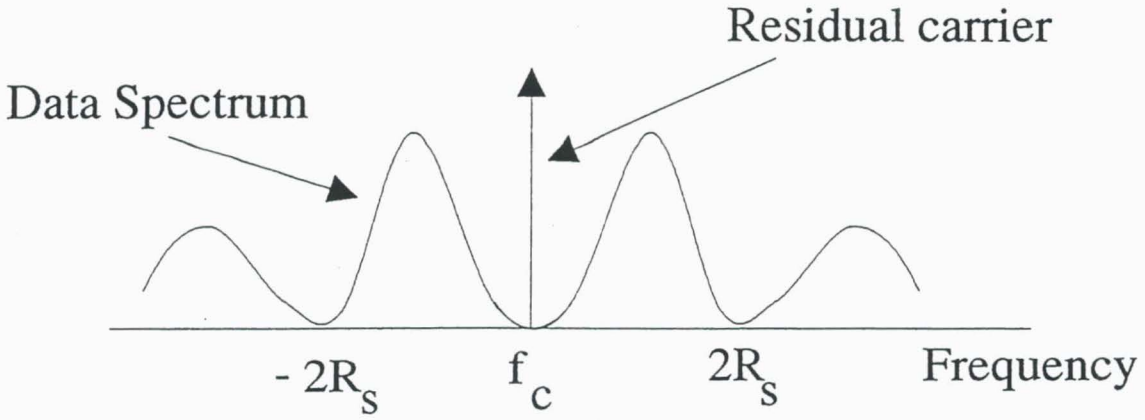

2(a) Power Spectrum of PCM/PM/Bi-Phase Signal

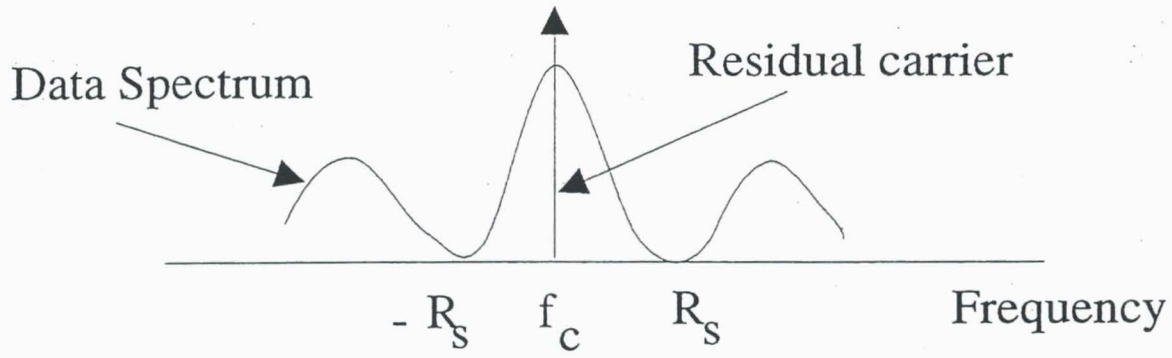

2(b) Power Spectrum of PCM/PM/NRZ Signal

FIGURE 2 POWER SPECTRUM OF PCM/PM SIGNAL

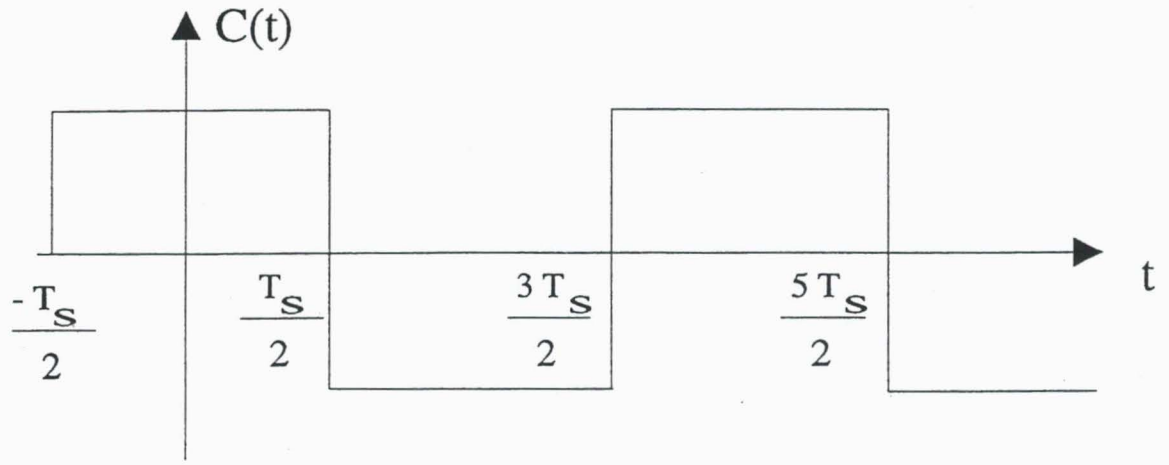

(a) Symbol Sync Clock for NRZ Data

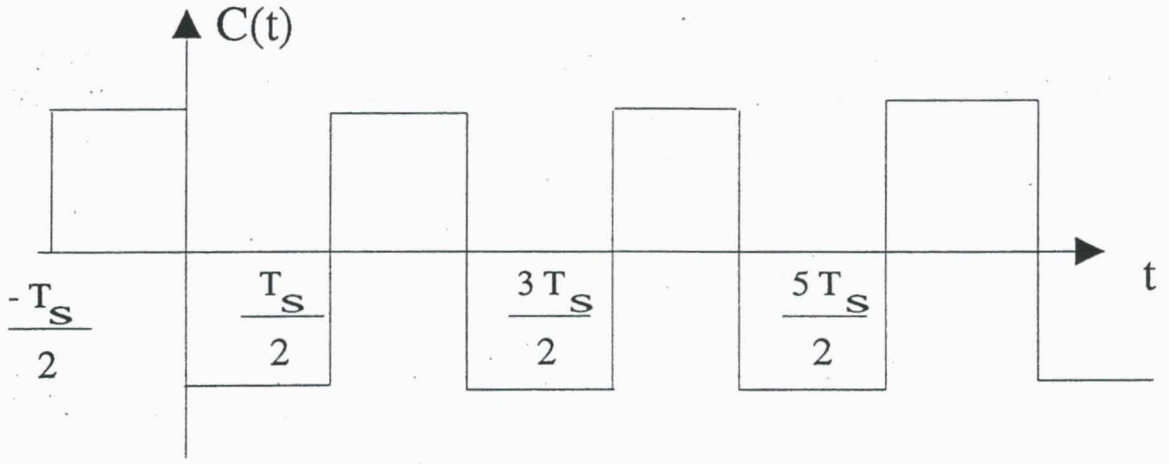

(b) Symbol Sync Clock for Bi-Phase Data

Figure 3. Symbol Sync Clock C(t)

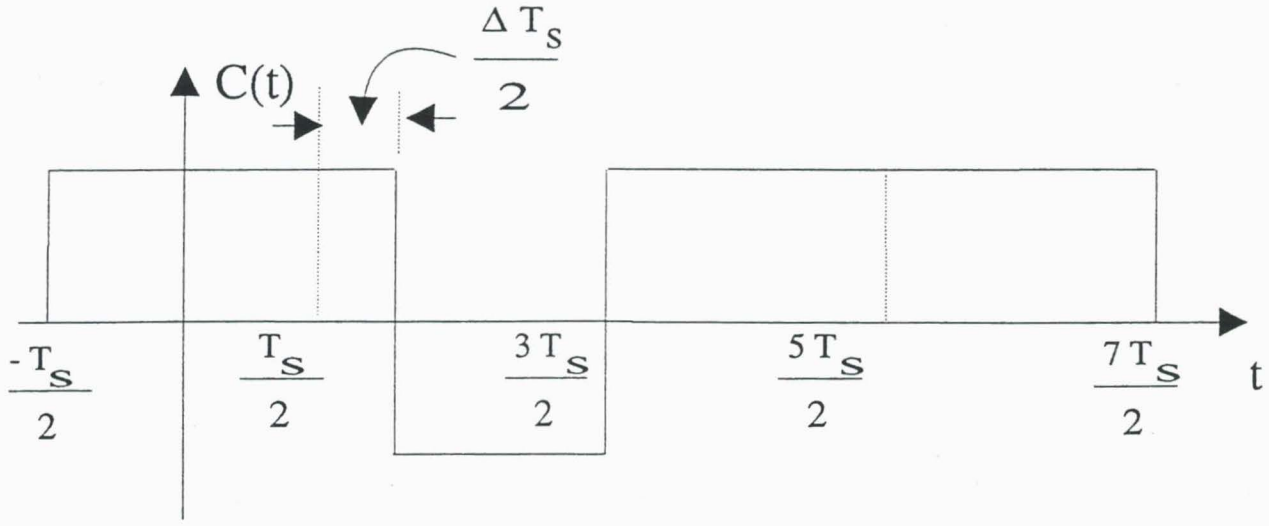

(a) Asymmetry Model for NRZ Data Stream

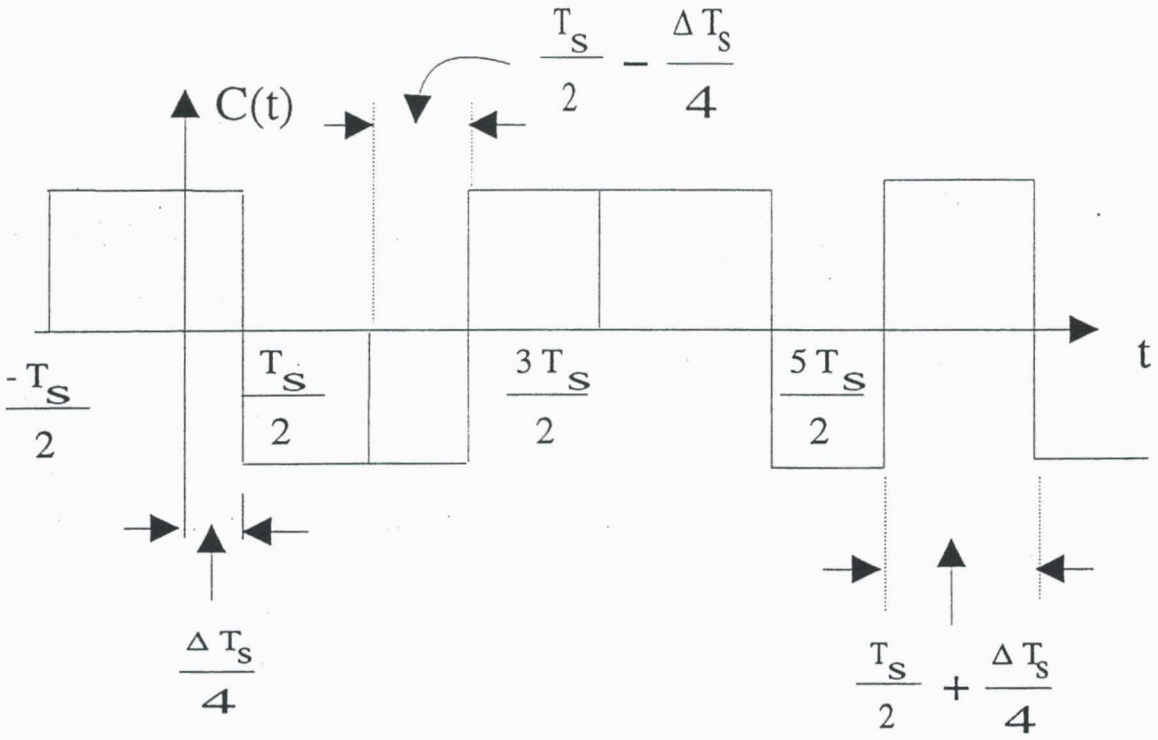

(b) Asymmetry Model for Bi-Phase Data Stream

Figure 4. Asymmetry Models for NRZ and Bi-Phase

Figure 5a. Carrier Loop SNR vs Symbol SNR for Data Asymmetry

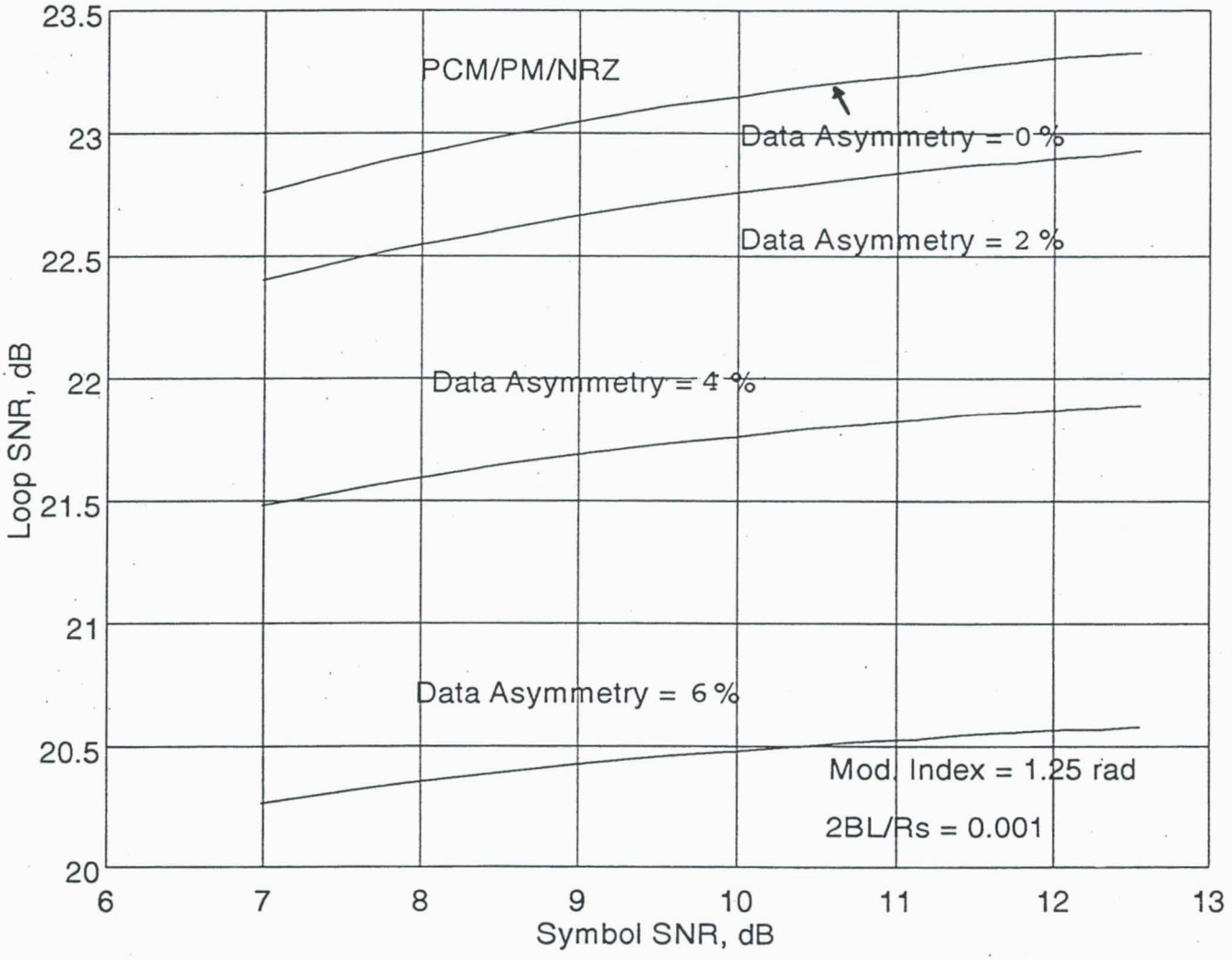

Figure 5b. Performance of PCM/PM/NRZ for Data Asymmetry

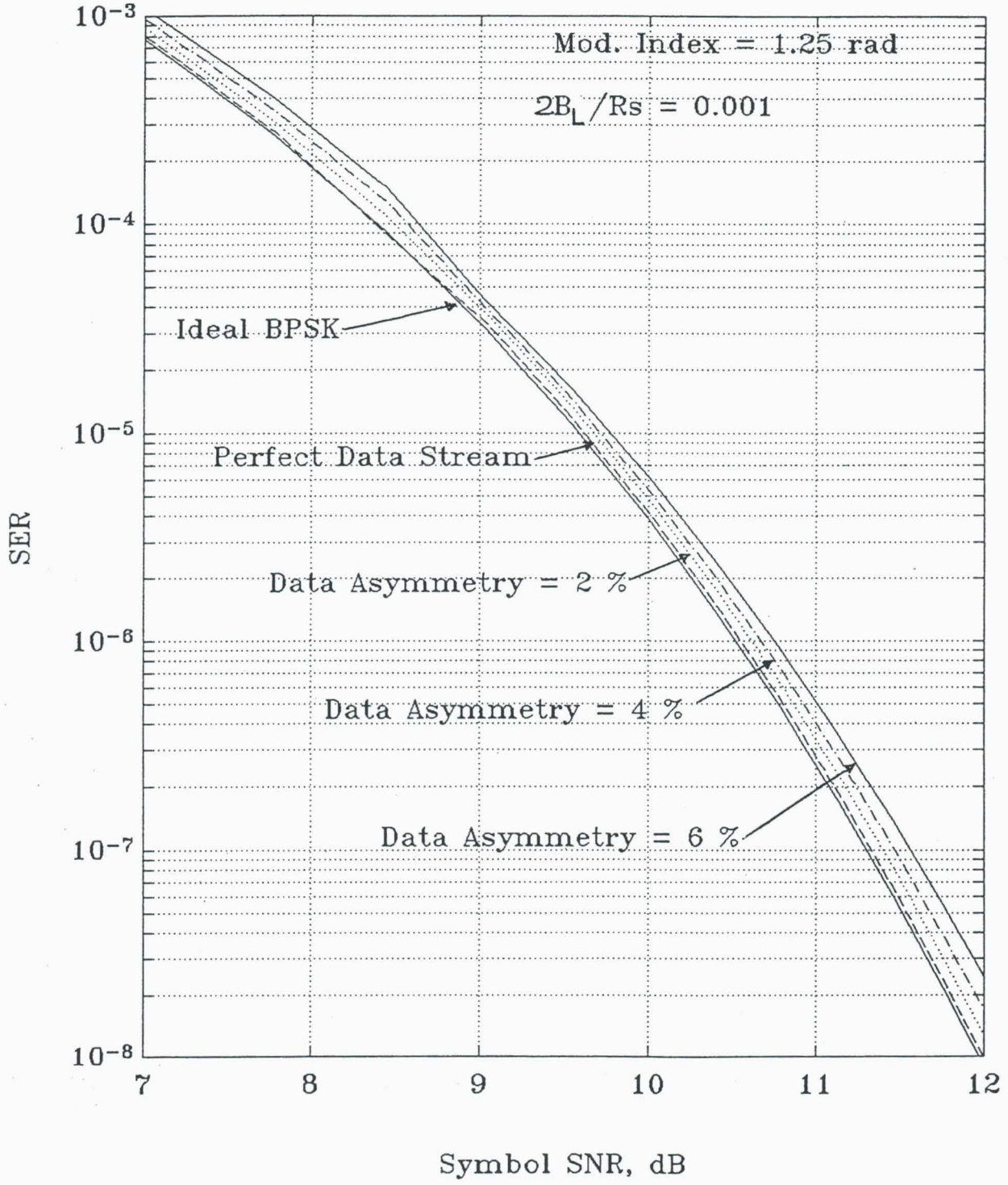

Figure 6a. Carrier Loop SNR vs Symbol SNR for Data Asymmetry

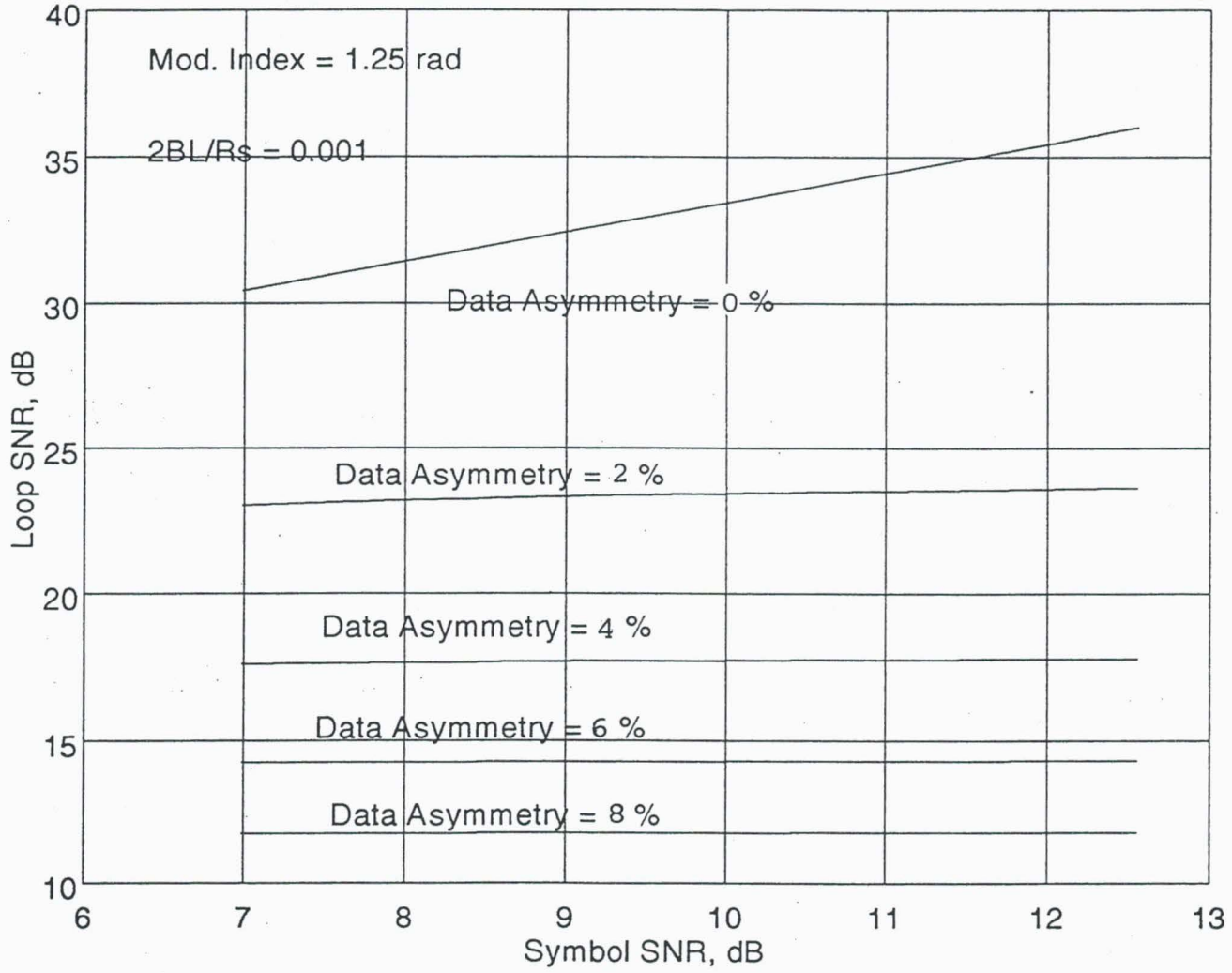

Figure 6b.PCM/PM/Bi-Phase With Data Asymmetry

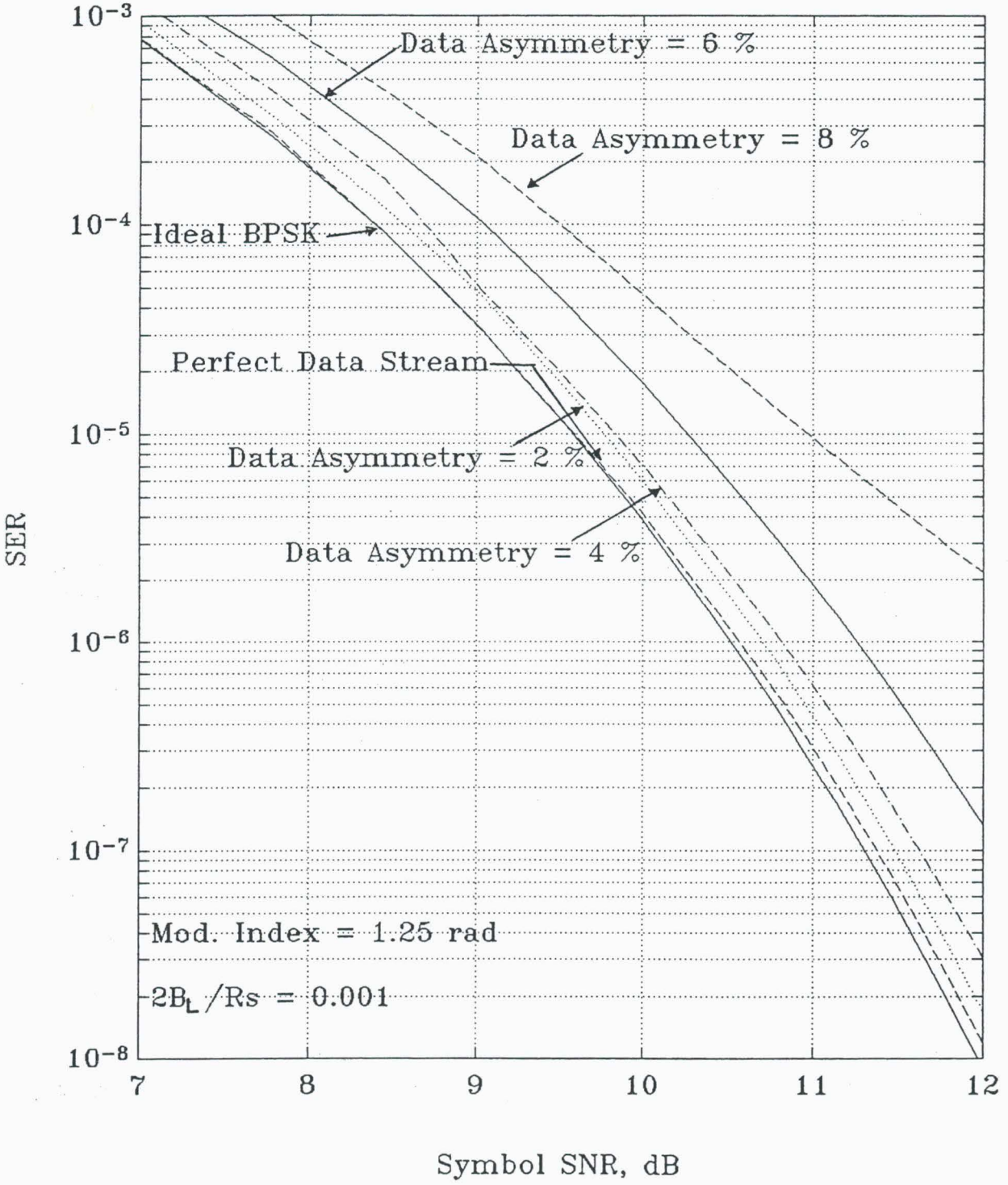

Figure 7a. Carrier Loop SNR vs Symbol SNR for Unbalanced Data

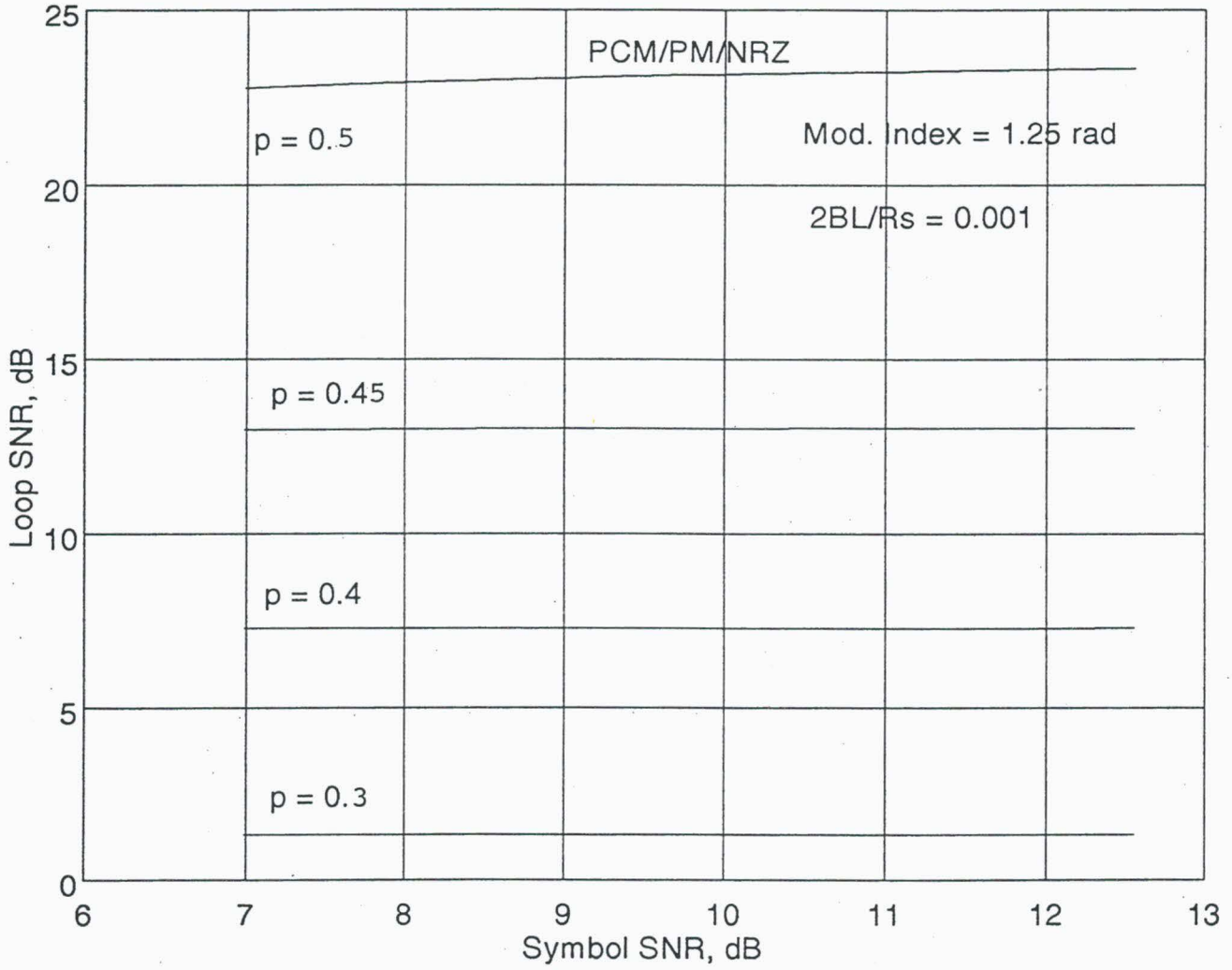

Figure 7b, Performance of PCM/PM/NRZ for Unbalanced Data

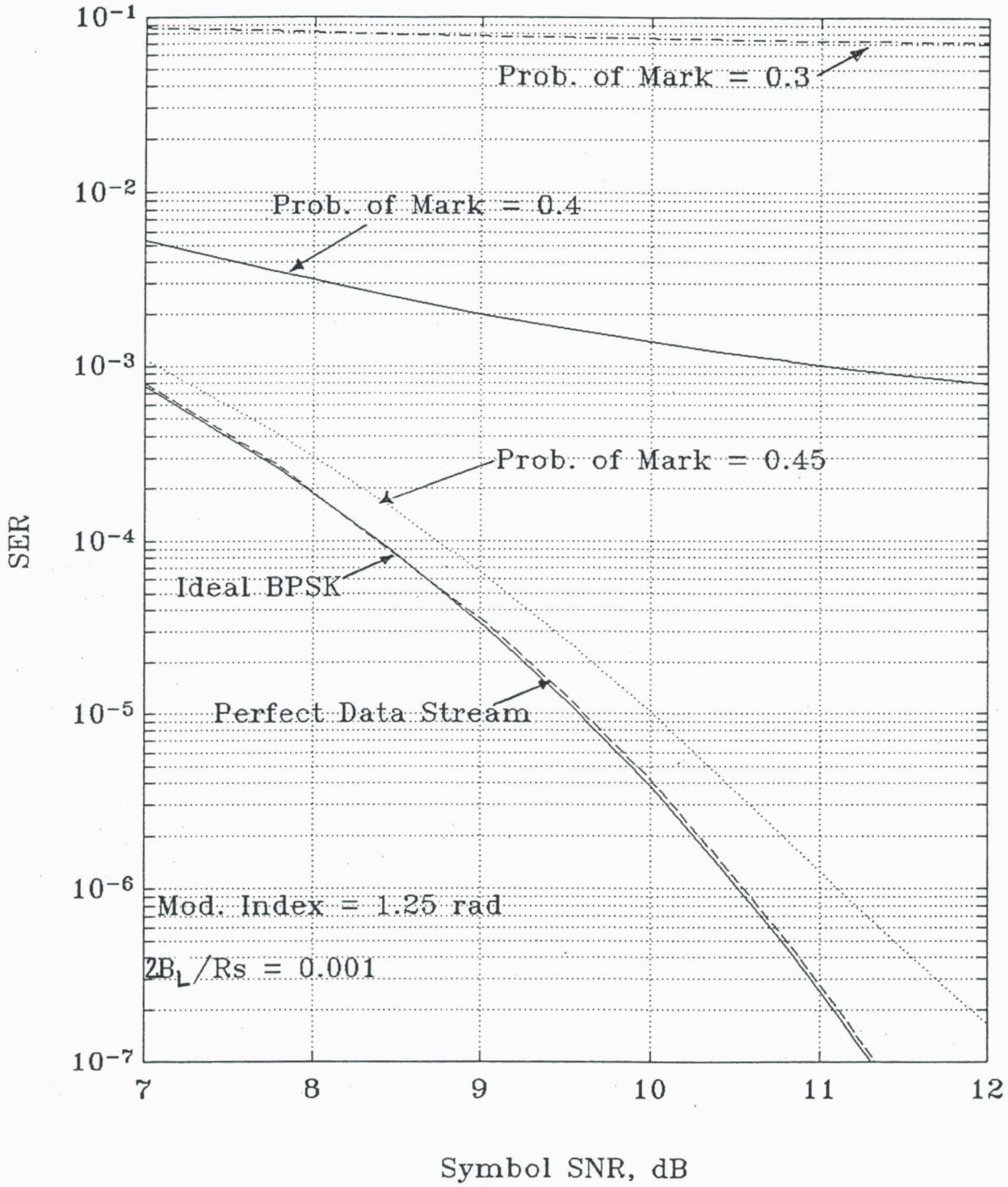

Figure 8. PCM/PM/NRZ With Unbalanced Data

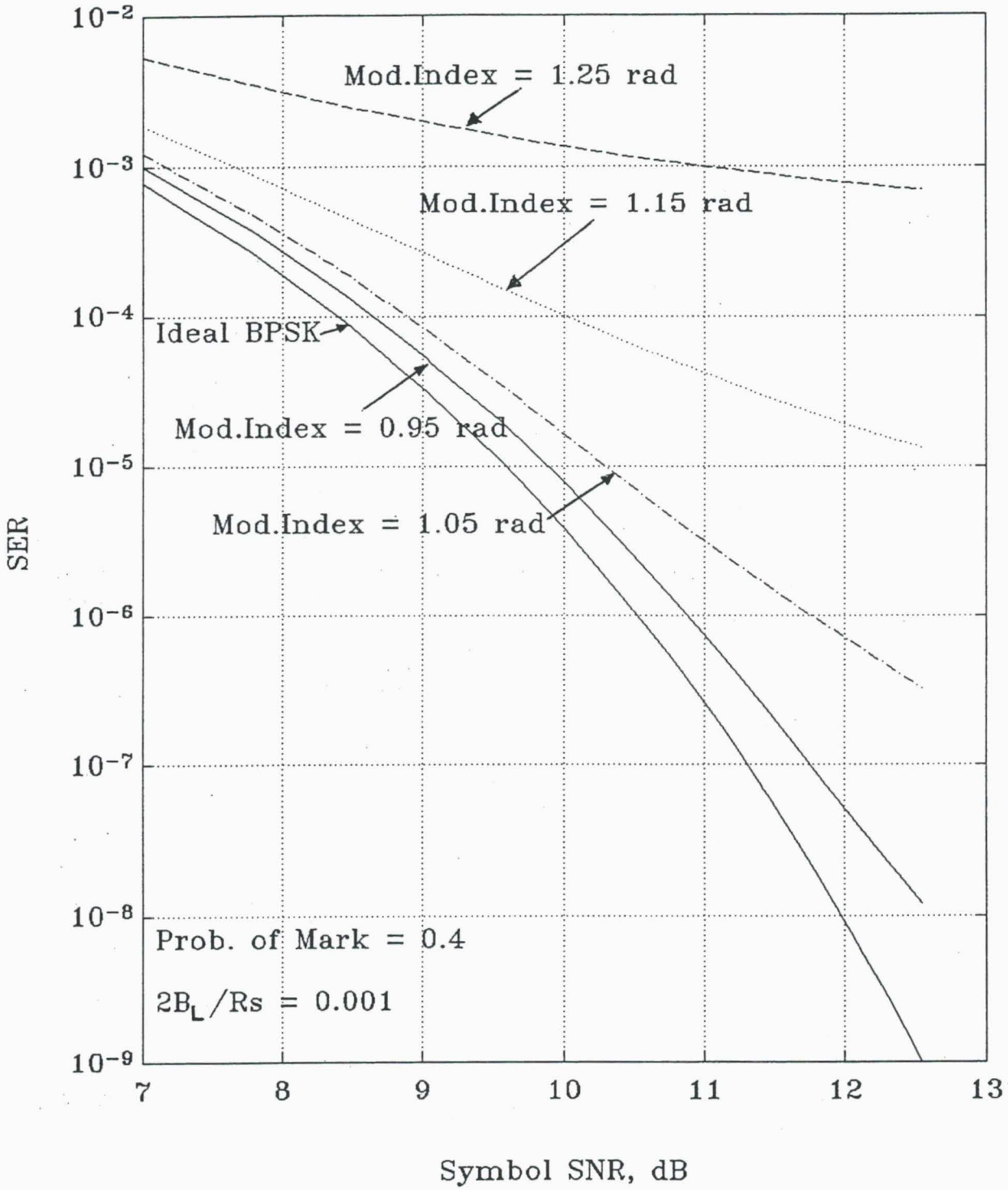

Figure 9a. Carrier Loop SNR vs Symbol SNR for Unbalanced Data

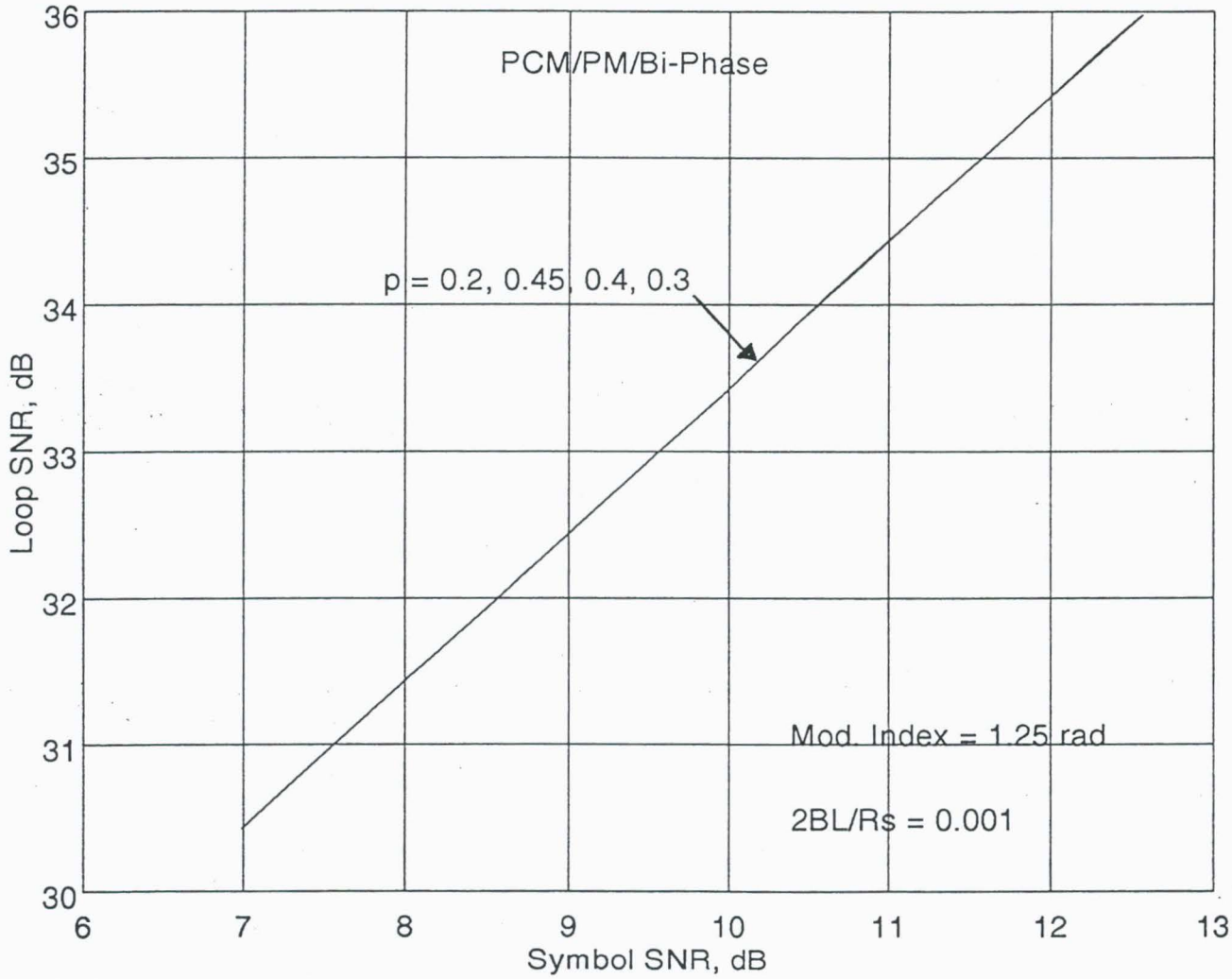

Figure 9b.PCM/PM/Bi-Phase With Unbalanced Data

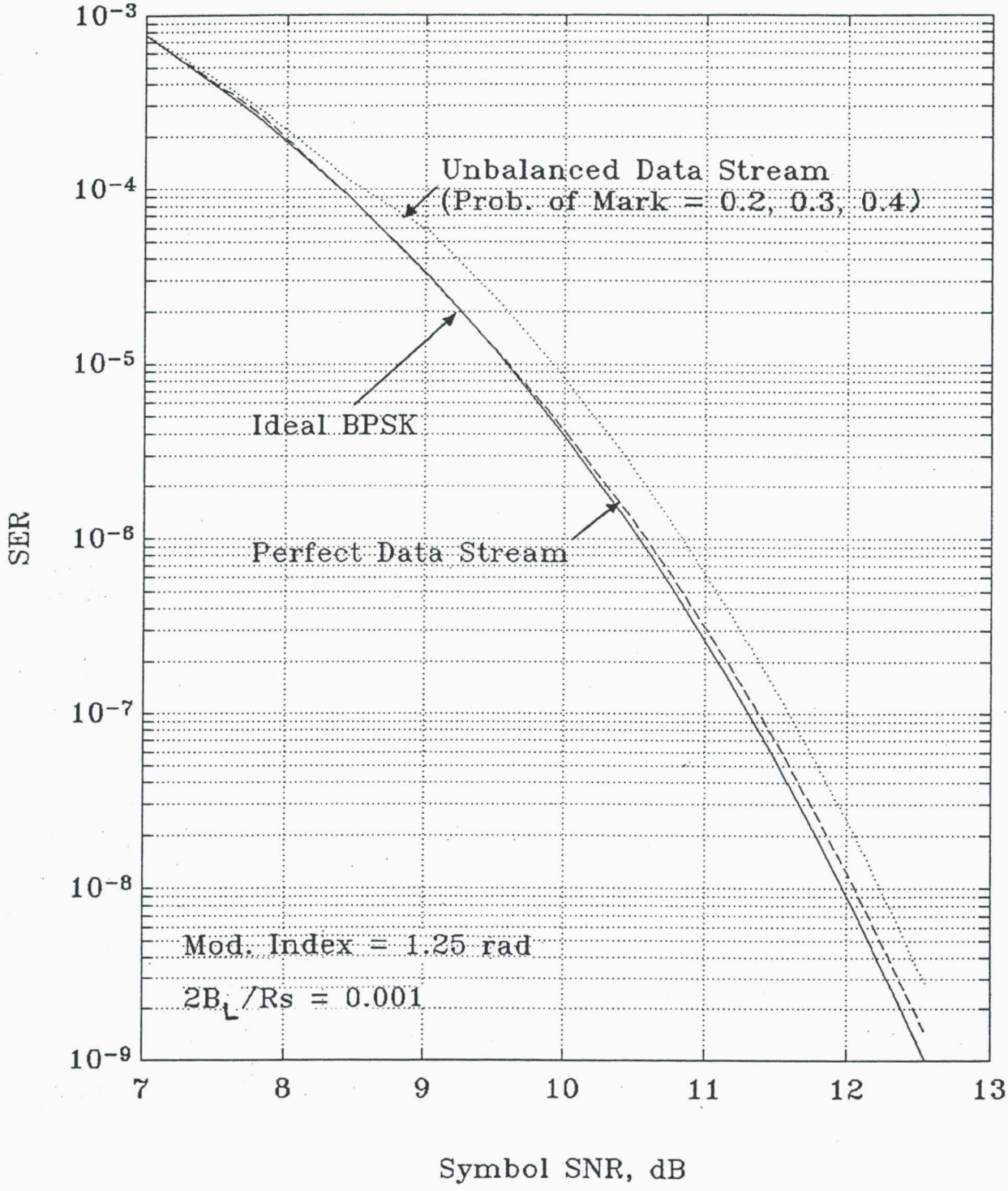

Figure 10. PCM/PM/NRZ With Band-Limited Channel

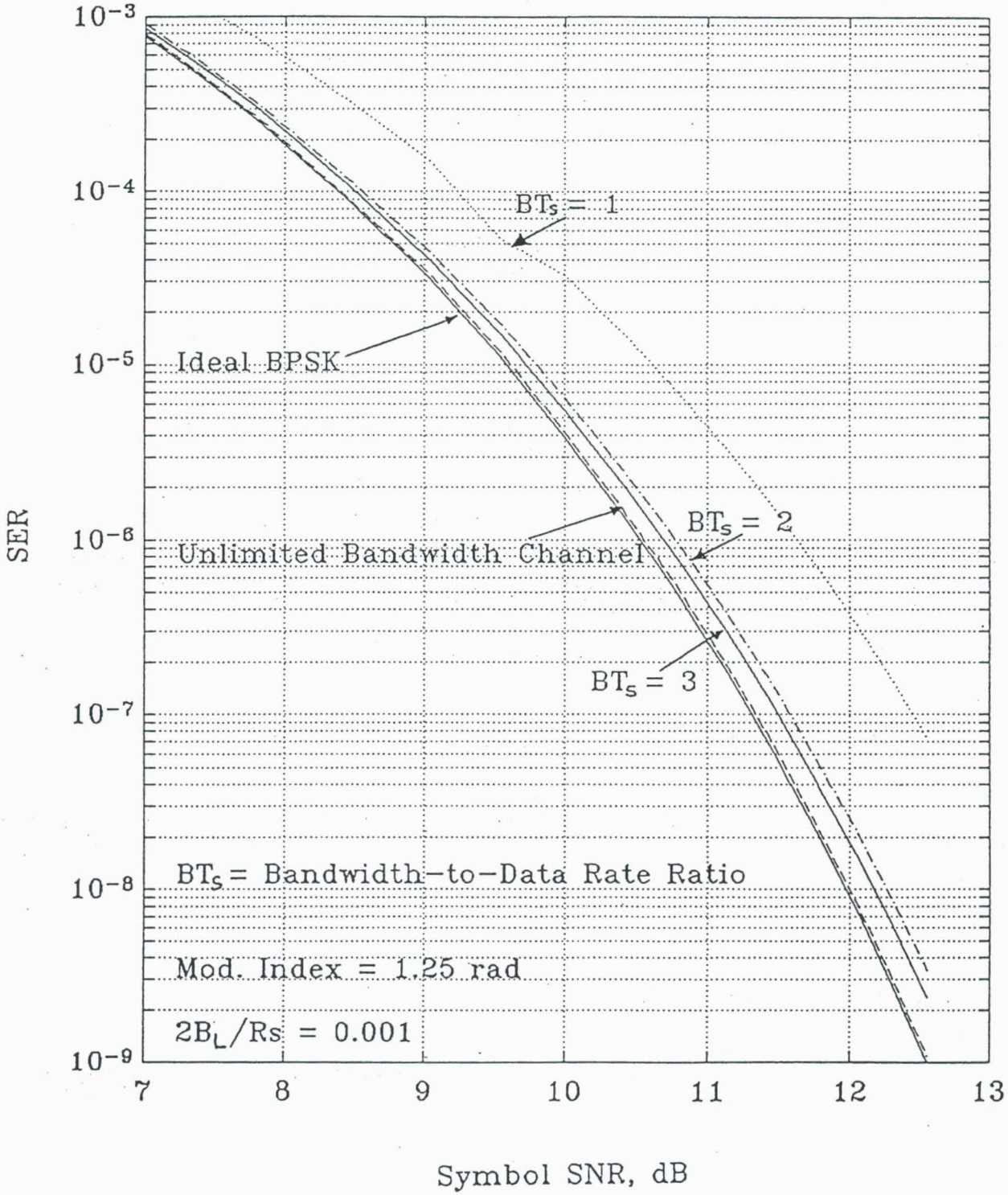

Figure 11. PCM/PM/Bi-Phase With Band-Limited Channel

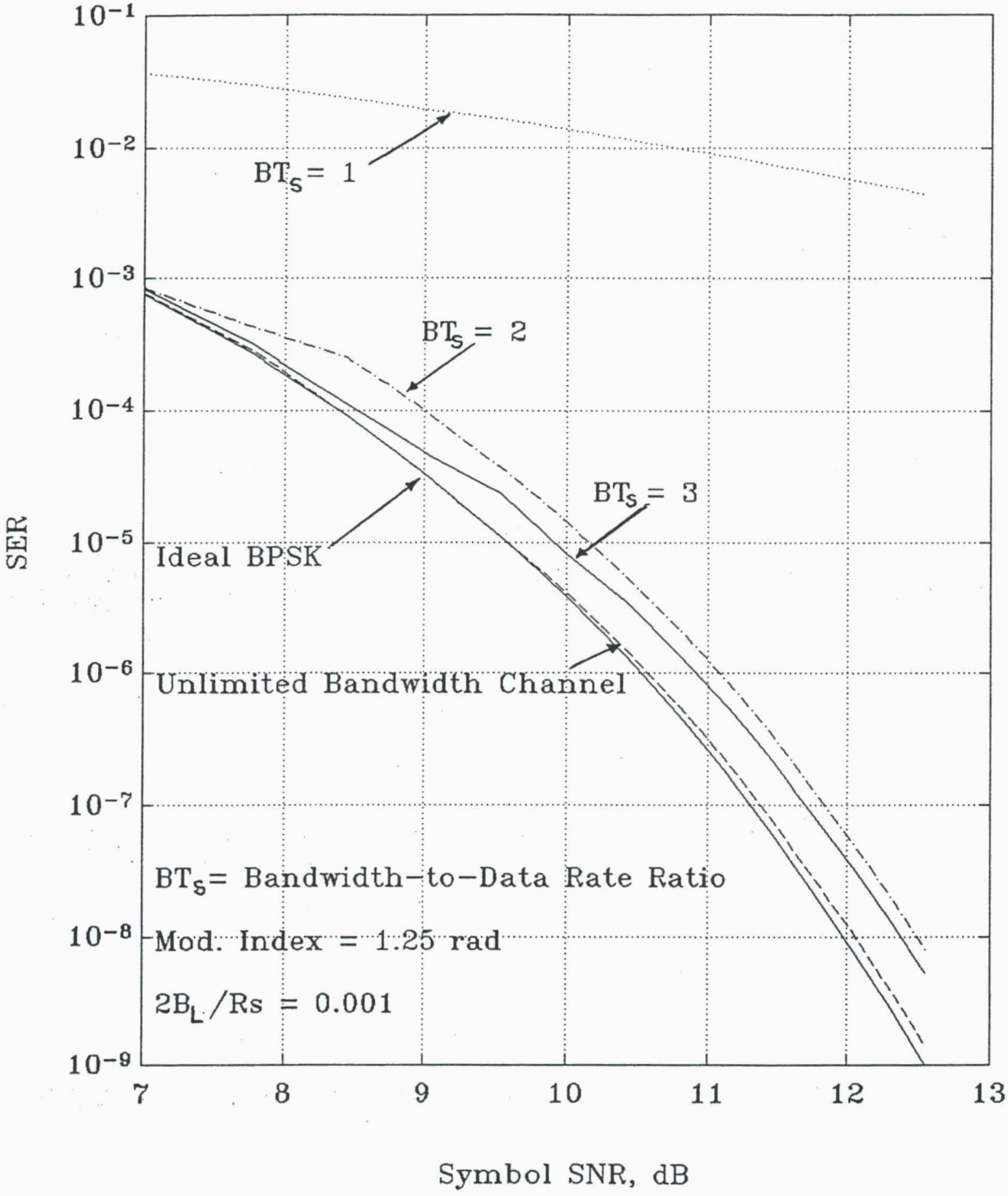

Figure 12. Performance Comparison for Data Asymmetry

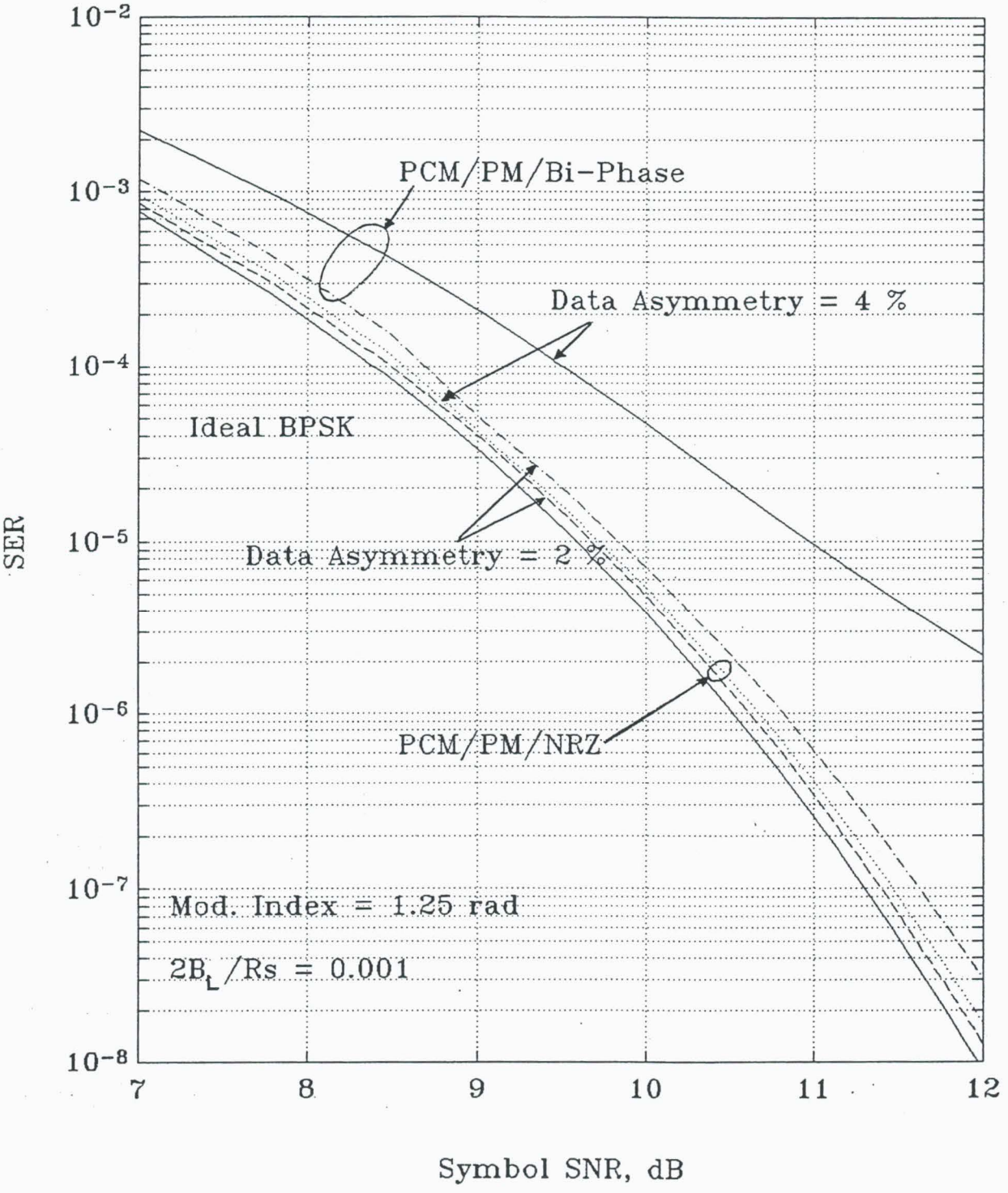

Figure 13. Performance Comparison for Unbalanced Data

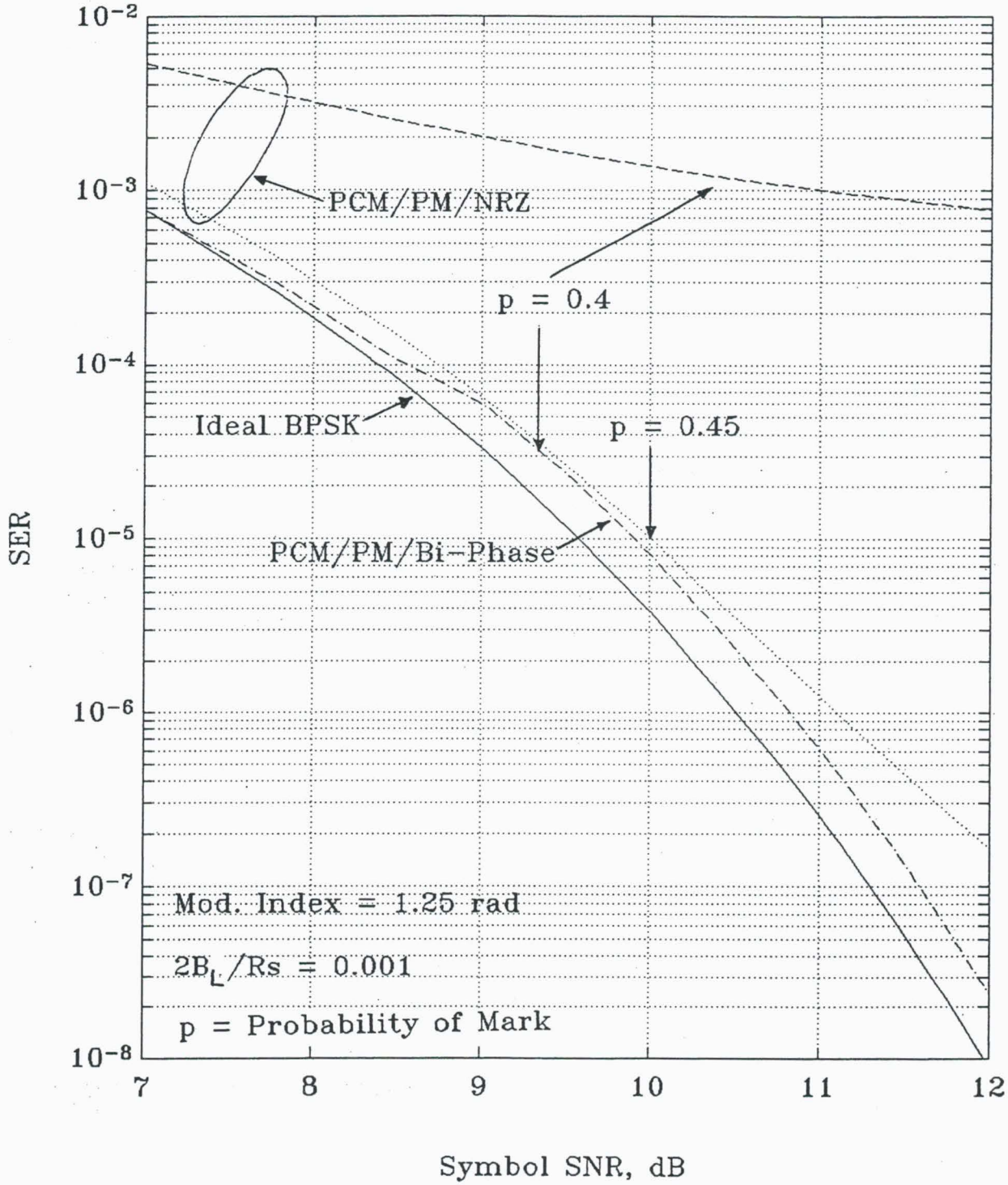

Figure 14. Performance Comparison for ISI Channel

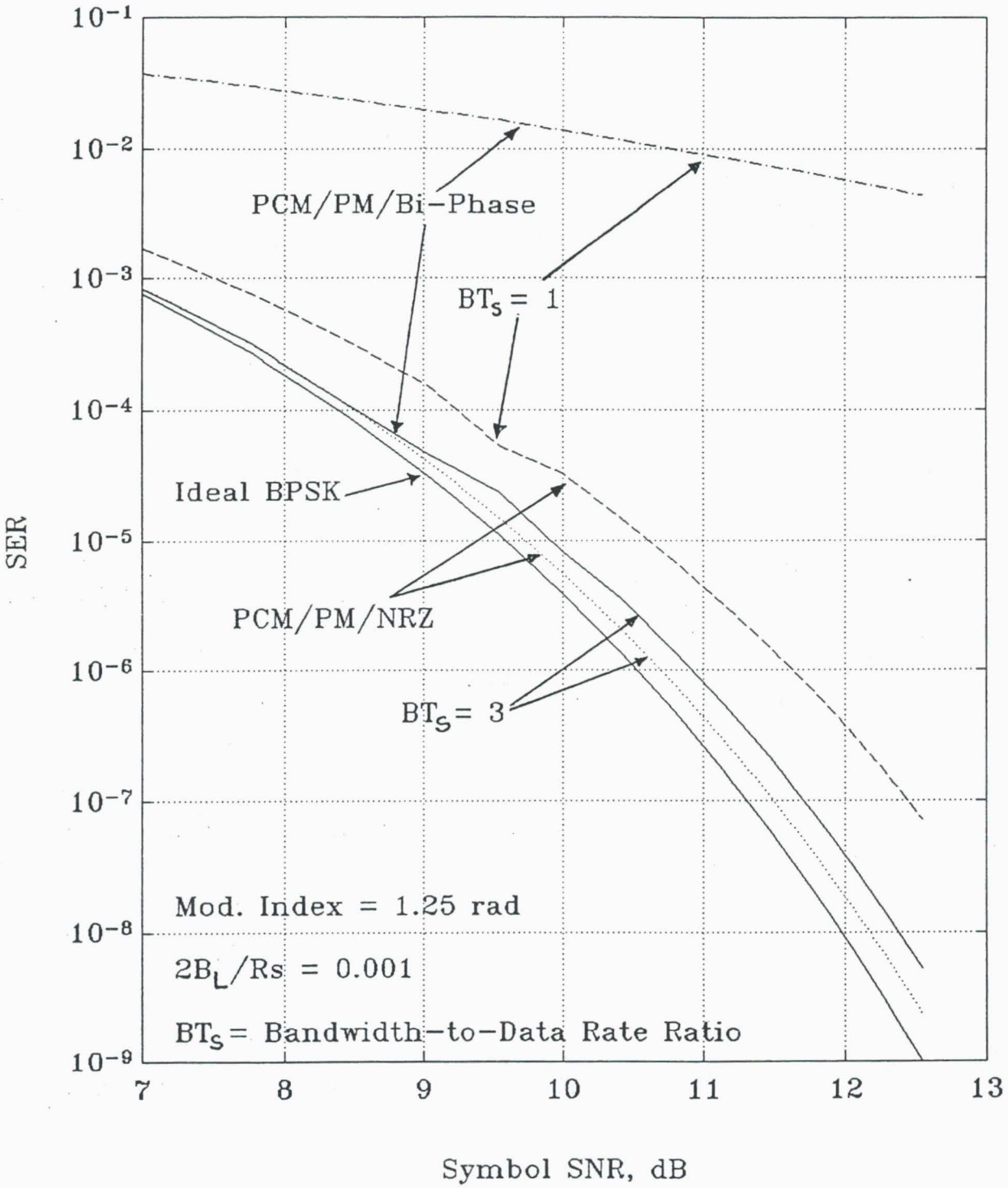

THE BEHAVIOR OF PCM/PM RECEIVERS IN NON-IDEAL CHANNELS

Part II: The Combined Effect of Imperfect Data Streams and Band-limiting Channels on Performance[1]

Tien Manh Nguyen
National Aeronautics and Space Administration
Jet Propulsion Laboratory
California Institute of Technology
4800 Oak Grove Drive
Pasadena, CA 91109

ABSTRACT

This paper presents a performance evaluation of residual carrier communication systems that employ a PCM/PM modulation technique operating over non-ideal channels. The non-ideal channels under investigation include data asymmetry, an unbalanced data stream (i.e., transition density deviates from 0.5) and InterSymbol Interference (ISI). In this particular modulation scheme, the data (either NRZ or Bi-ϕ) is directly modulated on the RF residual carrier. The combined effect of both an imperfect data stream (e.g., data asymmetry and an unbalanced data stream) and ISI on the average Symbol Error Rate (SER) is determined for NRZ and Bi-ϕ data formats, and the results are compared. The performance degradations for uncoded and coded systems are evaluated and compared. For coded systems, the performance degradation is evaluated for convolutional code with rate 1/2 and constraint length 7.

[1] The work described in this paper was carried out at the Jet Propulsion Laboratory, California Institute of Technology, under contract with the National Aeronautics and Space Administration.

1. Introduction

In part I of this paper [1], the separate effects of data asymmetry, unbalanced data stream and bandlimiting data channels on the performance degradations of the space telemetry systems that employed PCM/PM modulation scheme have been investigated. [1] studied in detailed the effects of each of the undesired sources such as data asymmetry, unbalanced data and ISI caused by bandlimiting channel on the Symbol Error Rate (SER) performance of the PCM/PM receivers. Moreover, the performance of the PCM/PM with NRZ data format (PCM/PM/NRZ) has also been compared with PCM/PM/Bi-ϕ in [1].

Since in reality, the practical PCM/PM receivers operate in the presence of both data imperfections and bandlimiting channel. Note that the term "imperfect data stream" considered in this paper includes the effects of both data asymmetry and imbalance between +1's and -1's in the data stream (namely unbalanced data stream). Theoretical predictions for the total symbol SNR degradation of the receivers due to the presence of these three undesired sources are not the algebraic sum of each symbol SNR degradation due to a single source of degradation found in [1]. Therefore, it is necessary to study the combined effects of these three sources on the error probability performance. In this paper, mathematical models to evaluate the SER performances of the PCM/PM/NRZ and PCM/PM/Bi-ϕ receivers in the presence of both imperfect data stream and bandlimiting channel will be derived.

In the past, [3] has analyzed the combined effects of both data asymmetry and bandlimiting channel on the performance of the suppressed carrier systems where the carrier tracking is not disturbed by the data interferences. Furthermore, when analyzed the combined effects of data asymmetry and ISI caused by bandlimiting channel, [3] assumed that the amount of data asymmetry is known so that an optimum sampling time can be set for the sample detector.

The aim of this paper is to investigate and assess the impacts of the combined effects of unbalanced data stream, data asymmetry and ISI on the performance degradation of the PCM/PM receivers. Both data formats, NRZ and Bi-ϕ, are considered. This extends previously reported work [3] to include PCM/PM modulation schemes and the presence of unbalanced data stream on the transmitting signal.

This paper is organized as follows: Section 2 introduces briefly the space telemetry system models employing PCM/PM modulation technique and SER performance for ideal operating conditions. Section 3 derives a mathematical model to evaluate the combined effects of unbalanced data stream, data asymmetry and ISI on the PCM/PM/NRZ system performance. The combined effects of both imperfect data stream and bandlimitting data channel on PCM/PM/Bi-ϕ are analyzed in Section 4. Performance comparisons for PCM/PM/NRZ and PCM/PM/Bi-ϕ of both uncoded and coded systems are presented in Section 5. Finally, Section 6 presents the main conclusion of the paper.

2. Space Telemetry System Models

A typical space telemetry system model shown in Figure 1 of [1] will be considered in this paper. Again, In this model, the data stream can be either NRZ or Bi-ϕ (Manchester or Bi-phase) data stream with ξ% data asymmetry and a transition density, p_t, which is less than 1/2. The data symmetry models for NRZ and Bi-ϕ data streams use in the following analyses will be the same as shown in Figures 4(a) and 4(b) of [1], respectively. The mathematical model the transmitted telemetry signal is given by

$$S_T(t) = \sqrt{2P}\cos(\omega_c t + m_T d(t)) \tag{1}$$

where P is the transmitted power, $\omega_c = 2\pi f_c$ is the angular carrier center frequency in rad/sec, m_T is the telemetry modulation index in rads which is less than $\pi/2$, and d(t) is NRZ data Sequence (PCM/PM/NRZ) or the Manchester data waveform generated by the binary (± 1) NRZ data sequence (PCM/PM/Bi-ϕ).

The received signal $S_r(t)$ is corrupted by additive white Gaussian noise n(t) with one-sided noise spectral density N_o, data asymmetry, unbalanced data and ISI. Expanding the received signal we have

$$S_r(t) = \sqrt{2P}\left[\cos(m_T)\cos(\omega_c t+\theta_o)-d(t)\sin(m_T)\sin(\omega_c t+\theta_o)\right] + n(t) \tag{2}$$

where ω_o is the initial phase offset caused by the transmission medium. The first and second terms of Equation (2) are the residual carrier and data components, respectively.

As explained previously in [1, 2 and 4], the data asymmetry and imbalance between +1's and -1's in the data stream will produce undesired spectral components at the carrier frequency creating an imperfect carrier reference which will in turn degrade the telemetry system performance. In addition, the presence of ISI created by the band-limited channel can cause further disturbance to the carrier reference.

Let θ_e be the phase error due to the thermal noise and the interference caused by the data asymmetry and unbalanced data stream then one can show that the signal output of the integrate-and-dump at time $t = T_s$ (where T_s denotes the symbol period) is given by [1]

$$Z(T_s) = \sqrt{P}\sin(m_T)\cos(\theta_e)\int_0^{T_s} d(t)C(t)\,dt + n(T_s) \tag{3}$$

where C(t) is the symbol sync clock shown in Figures 3(a) and 3(b) of [1] for NRZ and Bi-ϕ, respectively. Eqn (3) assumes that the phase error process θ_e is essentially constant during the symbol interval T_s, and that the corrupting noise process $n(T_s)$ is a zero-mean Gaussian random variable with a variance $N_o T_s/2$.

The test statistic $Z(T_s)$ of Eqn (3) represents the observed data at the receiver. This test statistic is needed to determine the SER performance. Based on this test statistic, the performance of the telemetry system shown in Figure 1 has been evaluated in [1] for separate undesired sources of degradation (e.g., data asymmetry, unbalanced data and ISI). On the other hand, [5] has derived the SER for perfect data stream and unlimited bandwidth channel. The results are presented here for the purpose of comparison.

The average probability of error is given by [1]

$$P_e = \int_{\theta_e} P_e(\theta_e)P(\theta_e)d\theta_e \tag{4}$$

where $P_e(\theta_e)$ is the conditional probability of error and $P(\theta_e)$ is the probability density function (pdf) for θ_e. For perfect data stream and ideal channel, this conditional probability of error is given by [5]:

$$P_e(\theta_e) = (1/2)\ \mathrm{erfc}\{\sqrt{E_s/N_o}\cos(\theta_e)\} \tag{5}$$

where E_s denotes the symbol energy, i.e., $E_s = (PT_s)\sin^2(m_T)$. In this paper, one also postulates a Tikhonov pdf for θ_e, which is entirely characterized by the variance σ^2 of the carrier tracking phase error. When the loop signal-to-noise ratio is high the Tikhonov pdf can be approximated by

$$P(\theta_e) \approx \exp(-\theta_e^2/2\sigma^2)/[2\pi\sigma^2]^{-1/2},\ -\infty < \theta_e < \infty \tag{6}$$

For perfect data stream and high-data-rate case ($B_L/R_s << 0.1$, where B_L and R_s denote the one-sided loop bandwidth and the symbol rate, respectively), the variance of the carrier tracking phase error, σ^2, has been found in [5]. For perfect NRZ data format, it is given by

$$\sigma^2 = (1/\rho_o) + (B_L/R_s)\tan^2(m_T) \tag{7}$$

and, for perfect Bi-ϕ data format, σ^2 becomes

$$\sigma^2 = (1/\rho_o) + (I/C)\tan^2(m_T) \tag{8}$$

where

$$\rho_o = \frac{(E_s/N_o)}{(B_L/R_s)\tan^2(m_T)}, \tag{9}$$

$$I/C = (1/2) + (9/16)(B_L/R_s)^{-1}$$

$$- (3/4)(B_L/R_s)^{-1}\exp\{-(2/3)(B_L/R_s)\}[\cos\{(2/3)(B_L/R_s)\} + 3\sin\{(2/3)(B_L/R_s)\}]$$

$$+ (3/16)(B_L/R_s)^{-1}\exp\{-(4/3)(B_L/R_s)\}[\cos\{(4/3)(B_L/R_s)\}$$

$$+ 3\sin\{(4/3)(B_L/R_s)\}] \quad (10)$$

In the following sections one will determine the conditional error probability and the carrier tracking phase error when the data stream is disturbed by the data asymmetry, unbalanced data stream and ISI caused by bandlimiting channel.

3. Combined Effects on PCM/PM/NRZ Receivers

To determine the average SER in the presence of data asymmetry, unbalanced data stream and bandlimiting channel one will use the same approach presented in [1], i.e., we will find the probability of error conditioned on the carrier tracking phase error and the distribution of the phase error. Here the distribution of the phase error will be determined first.

Since one postulates a Tikhonov distribution for the phase error θ_e, the variance of θ_e completely characterizes the pdf of the carrier tracking phase error. Again using the linear model for the carrier tracking loop one can evaluate modified noise spectral density, N, resulting from the thermal noise, data asymmetry and unbalanced data [1, Eqn (16)].

To evaluate N one must derive the data power spectrum of an unbalanced and asymmetric NRZ data stream. Based on the asymmetric and unbalanced data stream shown in Figure 4(a), [2] has derived the power spectral density for the asymmetric NRZ data stream generated by a purely random source with a transition density P_t less than 1/2 (i.e. unbalanced data stream). The continuous spectrum component ($S_c(f)$, the dc ($S_{dc}(f)$) and harmonics ($S_h(f)$) components of the asymmetric and unbalanced NRZ data stream are given by [2]

$$S_{cNRZ}(f) = T_s[\sin(\pi fT_s)/(\pi fT_s)]^2[a_1(p_t) + a_2(p,p_t,\xi)] + T_s a_3(p_t,\xi)[\sin(\pi fT_s\xi)/(\pi fT_s)]^2$$

$$+ T_s[\sin(2\pi fT_s)/(\pi fT_s)^2][a_4(p,p_t,\xi) - a_5(p,p_t)] \quad (11)$$

$$S_{dcNRZ}(f) = [2p - (1 - 2\xi p_t)]^2\delta(f) \quad (12)$$

$$S_{hNRZ}(f) = 2(P_t/\pi)^2 \sum_{m=1}^{\infty} (1/m^2)c(m,p,\xi)\delta(f - mR_s) \quad (13)$$

where

$$a_1(p_t) = p_t(1 - p_t)[1 + 2(1 - p_t)] - p_t^3 \quad (14)$$

$$a_2(p,p_t,\xi) = \{3p_t^3 + p_t(1 - p_t)[1 + 2(1 - 2p)]\}\cos^2(pfT_s\xi) \quad (15)$$

$$a_3(p_t,\xi) = p_t(1 + p_t^2 - p_t)\cos^2(\pi fT_s) + p_t^3\cos(2\pi fT_s\xi) \quad (16)$$

$$a_4(p,p_t,\xi) = p_t(1 - p_t)(1 - 2p)[0.5\cos(2\pi fT_s\xi) - p\sin(2\pi fT_s\xi)] \quad (17)$$

$$a_5(p,p_t) = 0.5p_t(1 - p_t)(1 - 2p) \tag{18}$$

$$c(m,p,\xi) = \sin^2(m\pi\xi)[\cos^2(m\pi\xi) - (1 - 2p)^2\sin^2(m\pi\xi)] \tag{19}$$

Where p and p_t are defined as the probability of transmitting a +1 pulse and transition density, respectively. For a purely random data source, the transition density is given by

$$P_t = 2p(1 - p) \tag{20}$$

Note that when $p = p_t = 1/2$, i.e., the data stream is balanced, Eqns (11)-(13) reduce to Eqns (21)-(22) of [1]; and when $p = p_t = 1/2$ and $\xi = 0$, i.e., perfect data stream, Eqns (11)-(13) reduce to the well-known result for a perfect NRZ random data stream [6].

From Eqns (19) and (20) of [1] and Eqns (11)-(12) above, one obtains the interference due to continuous spectrum component, α, and interference caused by dc component-to-carrier power ratio I/C, respectively. Consequently, the variance of the carrier tracking phase error can be obtained by using Eqn (18) of [1]. It is found to be

$$\sigma^2 = 1/\rho_o + (\alpha/2)\tan^2(m_T) + (1/2)[2p - (1 - 2\xi p_t)]^2\tan^2(m_t) \tag{21}$$

where

$$\alpha = \int_{-\infty}^{\infty} | H(2\pi f) |^2 S_{cNRZ}(f)df \tag{22}$$

The harmonic components caused by the asymmetry do not interfere with carrier tracking because we have assumed that $2B_L << R_s$. Having determined the distribution of the carrier tracking phase error, the error probability conditioned on the phase error, $P_e(\theta_e)$ can be determined. When a sample detector shown in Figure 1 operates in the presence of data asymmetry and bandlimiting channel, the combined effects of these two sources of degradation have been investigated in [3]. However, the approach used in [3] is not applicable here because it is assumed that the amount of data is known and the optimum sampling time is not T_s. Here we are interested in the performance degradation of the receiver when the sampling time is T_s and the amount of data asymmetry is unknown.

This paper uses slightly different approach than [3] by assuming that the optimum sampling time is T_s. Based on the data asymmetry model presented in Figure 4(a)] of [1], one has a set of signals contain four different symbols, namely, $\{P_{iNRZ}(t), i = 1, 2, 3, 4\}$, with associated probability $\{p_i; i = 1, 2, 3, 4\}$. We have

$$P_{1NRZ}(t) = \begin{cases} +1 & -(T_s/2) < t \leq (T_s/2)(1 + \Delta) \\ 0 & \text{elsewhere} \end{cases} \tag{23}$$

$$P_{2NRZ}(t) = \begin{cases} -1 & -(T_s/2) < t \leq (T_s/2)(1 - \Delta) \\ 0 & \text{elsewhere} \end{cases} \tag{24}$$

$$P_{3NRZ}(t) = \begin{cases} +1 & -(T_s/2) < t \leq (T_s/2) \\ 0 & \text{elsewhere} \end{cases} \tag{25}$$

$$P_{4NRZ}(t) = \begin{cases} -1 & -(T_s/2) < t \leq (T_s/2) \\ 0 & \text{elsewhere} \end{cases} \tag{26}$$

$$p_1 = Pr\{g_{iNRz}(t) = g_{1NRZ}(t)\} = pp_t \tag{27}$$

$$p_2 = Pr\{g_{iNRZ}(t) = g_{2NRZ}(t)\} = (1 - p)p_t \tag{28}$$

$$p_3 = Pr\{g_{iNRZ}(t) = g_{3NRZ}(t)\} = p(1 - p_t) \tag{29}$$

$$p_4 = Pr\{g_{iNRZ}(t) = g_{4NRZ}(t)\} = (1 - p)(1- p_t) \tag{30}$$

where the data asymmetry is defined as

$$\xi = \Delta/2 \tag{31}$$

For ideal bandpass filter (Eqn (53), [1]) with imperfect data stream, the output of the filter $g_{iNRZ}(t)$ corresponding to the input $P_{iNRZ}(t)$ can be obtained by substituting Eqn (53) into Eqn (45) of [1] with P(t) is replaced by $P_{iNRZ}(t)$. For NRZ data format, $g_{iNRZ}(t+kT_s)$, for i = 1, 2, 3, 4, can be shown to be

$$g_{1NRZ}(t+kT_s) = \frac{1}{\pi}[si\{2\pi B(t+T_s(k+1/2))\} - si\{2\pi B(t+T_s(k-1/2-\xi))\}] \tag{32}$$

$$g_{2NRZ}(t+kT_s) = -\frac{1}{\pi}[si\{2\pi B(t+T_s(k+1/2))\} - si\{2\pi B(t+T_s(k-1/2+\xi))\}] \tag{33}$$

$$g_{3NRZ}(t+kT_s) = \frac{1}{\pi}[si\{2\pi B(t+T_s(k+1/2))\} - si\{2\pi B(t+T_s(k-1/2))\}] \tag{34}$$

$$g_{4NRZ}(t+kT_s) = - g_{3NRZ}(t+kT_s) \tag{35}$$

Note that the symbols $g_{iNRZ}(t)$, i = 1, 2, 3, 4, are independent because d_k's are independent.

Using the test statistic shown in Eqn (3) one can show that the conditional error probability of the PCM/PM/NRZ receiver in the presence of the bandlimiting channel and imperfect data channel is

$$P_e(\theta_e) = p\Pr\{Z(T_s) < 0/\theta_e,\ d_0 = +1\} + q\Pr\{Z(T_s) > 0/\theta_e,\ d_0 = -1\} \tag{36}$$

where $q = (1 - p)$, and the overbar denotes statistical averaging over the joint distribution of the doubly infinite data sequence d_k and the test statistic $Z(T_s)$ for this particular case becomes:

$$Z(T_s) = E_s[\pm 1 + \sum_{k=-\infty}^{\infty}{}' d_k\lambda_k(i)]\cos\theta_e + n(T_s) \tag{37}$$

where ± 1 corresponds to $d_0 = \pm 1$, and the prime in the sum indicates the omission of the term $k = 0$, and the parameter $\lambda_k(i)$ is defined as

$$\lambda_k(i) = \frac{\int_0^{T_s} g_{NRZ}(t)g_{iNRZ}(t+kT_s)dt}{\int_0^{T_s} |\, g_{NRZ}(t)\,|^2\, dt}, \quad i = 1, 2, 3, 4 \tag{38}$$

where $g_{iNRZ}(t)$ is defined in Eqns (32)-(35) for $i = 1, 2, 3, 4$, respectively and $g_{NRZ}(t)$ is the output of the ideal filter for perfect data stream which is given by [Eqn (54), 1]. Note that in this case we do not have the symmetry of the signals (because the data under consideration is imperfect) hence we must take all possible combinations into account when computing Eqn (36). In order to illustrate the use of Eqn (36), an example will be provided for the case $M = 1$. For $M = 1$, Eqn (36) becomes

$$\begin{aligned}
P_e(\theta_e) = {} & p[p_3p_3\mathrm{erfc}\{\sqrt{E_s/N_o}(1 + \lambda_{-1}(3) + \lambda_{+1}(3))\cos\theta_e\} \\
& + p_3p_1\mathrm{erfc}\{\sqrt{E_s/N_o}(1 + \lambda_{-1}(3) - \lambda_{+1}(1))\cos\theta_e\} \\
& + p_2p_3\mathrm{erfc}\{\sqrt{E_s/N_o}(1 - \lambda_{-1}(2) + \lambda_{+1}(3))\cos\theta_e\} \\
& + p_2p_1\mathrm{erfc}\{\sqrt{E_s/N_o}(1 - \lambda_{-1}(2) - \lambda_{+1}(1))\cos\theta_e\}] \\
& + q[p_1p_2\mathrm{erfc}\{\sqrt{E_s/N_o}(1 - \lambda_{-1}(2) - \lambda_{+1}(2))\cos\theta_e\} \\
& + p_1p_4\mathrm{erfc}\{\sqrt{E_s/N_o}(1 - \lambda_{-1}(1) + \lambda_{+1}(4))\cos\theta_e\} \\
& + p_4p_2\mathrm{erfc}\{\sqrt{E_s/N_o}(1 + \lambda_{-1}(4) - \lambda_{+1}(2))\cos\theta_e\} \\
& + p_4p_4\mathrm{erfc}\{\sqrt{E_s/N_o}(1 + \lambda_{-1}(4) + \lambda_{+1}(4))\cos\theta_e\}]
\end{aligned} \tag{39}$$

The conditional error probability for M = 2 is shown in the appendix. The average probability of error can be found by substituting Eqn (36) and the pdf for the phase error just found above into Eqn (4) and performing the numerical integration in digital computer. The results of the calculations are shown in Figures 1-3 for the second order Phased-Locked Loop (PLL) with the transfer function given by Eqn (24) of [1].

Figure 1 plots the SER as a function of symbol SNR in dB for fixed data asymmetry ξ of 2 % and $BT_s = 3$ with p, probability of mark, is a parameter. This figure indicates that, for $m_T = 1.25$ rad, $2B_L/R_s = 0.001$, the SER degrades seriously as p deviates from 0.45. As mentioned in [1], the typical values for $m_T = 1.25$ rad and $2B_L/R_s = 0.001$ are chosen because the performance of PCM/PM approaches the ideal BPSK.

Figure 2 shows the SER performance for various values of data asymmetry with $BT_s = 3$ and p = 0.45. The symbol SNR degradation is less than 0.5 dB for ξ = 6 %. Furthermore, this figure shows that PCM/PM/NRZ is not sensitive to data asymmetry, because the symbol SNR degradation is between 0.1-0.2 dB when ξ varies between 2-6 %.

Figure 3 illustrates the SER performance in the presence of bandlimiting channel. The figure plots SER as a function of symbol SNR for ξ = 2 %, p = 0.45 with BT_s is a parameter. The results show that, for $BT_s = 3$, the symbol SNR degradation is at the order of 0.4 dB or less when the SER is between 10^{-4}-10^{-7}.

4. Combined Effects on PCM/PM/Bi-ϕ Receivers

Using the same approach as shown in Section 3, one proceeds with the derivation of the power spectral density for the asymmetric Bi-ϕ data stream generated by a purely random NRZ source with a transition density P_t less than 1/2. Based on the model of asymmetric and unbalanced data stream shown in Figure 4(b) of [1] one has a set of signals contain four different symbols, namely, $\{P_{iBi\text{-}\phi}(t), i = 1, 2, 3, 4\}$, with associated probability $\{p'_i; i = 1, 2, 3, 4\}$. One has

$$P_{1Bi\text{-}\phi}(t) = \begin{cases} +1 & -(T_s/2) \le t \le (\Delta T_s/4) \\ -1 & (\Delta T_s/4) < t \le (T_s/2)(1 + \Delta/2) \\ 0 & \text{elsewhere} \end{cases} \tag{40}$$

$$P_{2Bi\text{-}\phi}(t) = \begin{cases} -1 & -(T_s/2) \le t \le -(\Delta T_s/4) \\ +1 & -(\Delta T_s/4) < t \le (T_s/2)(1 - \Delta/2) \\ 0 & \text{elsewhere} \end{cases} \tag{41}$$

$$P_{3Bi\text{-}\phi}(t) = \begin{cases} +1 & -(T_s/2) \le t \le (\Delta T_s/4) \\ -1 & (\Delta T_s/2) < t \le (T_s/2) \\ 0 & \text{elsewhere} \end{cases} \tag{42}$$

$$P_{4Bi\text{-}\phi}(t) = \begin{cases} -1 & -(T_s/2) \le t \le -(\Delta T_s/4) \\ +1 & -(\Delta T_s/4) < t \le (T_s/2) \\ 0 & \text{elsewhere} \end{cases} \tag{43}$$

$$p'_1 = \Pr\{g_{iBi\text{-}\phi}(t) = g_{1Bi\text{-}\phi}(t)\} = pp_t \tag{44}$$

$$p'_2 = \Pr\{g_{iBi\text{-}\phi}(t) = g_{2Bi\text{-}\phi}(t)\} = (1 - p)p_t \tag{45}$$

$$p'_3 = \Pr\{g_{iBi\text{-}\phi}(t) = g_{3Bi\text{-}\phi}(t)\} = p(1 - p_t) \tag{46}$$

$$p'_4 = \Pr\{g_{iBi\text{-}\phi}(t) = g_{4Bi\text{-}\phi}(t)\} = (1 - p)(1 - p_t) \tag{47}$$

where the data asymmetry for Bi-ϕ is defined as

$$\xi = \Delta/4 \tag{48}$$

It should be mentioned that the power spectral density for a purely random Bi-ϕ data with perfectly balanced data stream has been derived in [4]. Using the same technique presented in [4] and together with Eqns (40)-(47) we can show that the power spectral density for an asymmetric and unbalanced data stream illustrated in [Figure 4(b), 1] have the following form

$$S_{Bi\text{-}\phi}(f) = S_{cBi\text{-}\phi}(f) + S_{dcBi\text{-}\phi}(f) + S_{hBi\text{-}\phi}(f) \tag{49}$$

where $S_{cBi\text{-}\phi}(f)$, $S_{dcBi\text{-}\phi}(f)$ and $S_{hBi\text{-}\phi}$ are the continuous spectrum, dc and harmonic components of the imperfect Bi-ϕ data stream, respectively. They are given by

$$\begin{aligned} S_{cBi\text{-}\phi}(f) = {} & T_s p_t(1 - p_t)[\sin^2(\pi f T_s/2)/(\pi f T_s/2)]^2 \\ & - T_s[c_1(p_t,\xi) + c_2(p_t,\xi) + c_3(p_t)][\sin(\pi \xi f T_s)/(\pi f T_s/2)]^2 \\ & - T_s[c_4(p,p_t,\xi) + c_5(p_t,\xi)][\sin(\pi \xi f T_s/2)]^2 \\ & - T_s c_6(p,p_t,\xi)[\sin(\pi \xi f T_s/2)/(\pi f T_s/2)]^2 \\ & + T_s c_7(p,p_t,\xi)[\sin(\pi f T_s\{1 + \xi\}/2)/(\pi f T_s/2)]^2 \\ & + T_s c_8(p,p_t,\xi)[\sin(\pi f T_s\{1 - \xi\}/2)/(\pi f T_s/2)]^2 \end{aligned} \tag{50}$$

$$S_{dcBi\text{-}\phi}(f) = \xi^2(2 - p_t)^2\,\delta(f) \tag{51}$$

$$S_{hBi\text{-}\phi}(f) = (2/\pi)^2 \sum_{m=1}^{\infty} (1/m^2)[H_1(m,p,p_t,\xi)+H_2(m,p,p_t,\xi)+H_3(m,p,p_t,\xi)]\delta(f - mR_s) \tag{52}$$

where

$$c_1(p_t,\xi) = 2p_t^2\sin^2[\pi fT_s(1 + \xi)/2][p_t\sin^2[\pi fT_s(1 - \xi)/2] + (1-p_t)\cos(\pi\xi fT_s)] \tag{53}$$

$$c_2(p_t,\xi) = p_t^2(1 - p_t)\cos(\pi\xi fT_s)[2\sin^2[\pi fT_s(1 - \xi)/2] - \sin^2(\pi\xi fT_s/2)] \tag{54}$$

$$c_3(p_t) = p_t(1 - p_t)[1 - p_t + (2p_t - 3)\cos(\pi fT_s/4)] \tag{55}$$

$$c_4(p,p_t,\xi) = 2pp_t(1 - p_t)(1 - 2p)\sin^2[\pi fT_s/2]\sin[3\pi fT_s\xi/2] \tag{56}$$

$$\begin{aligned} c_5(p_t,\xi) = {} & p_t^2[(1 - p_t)\sin(\pi fT_s\xi)\sin[\pi fT_s\xi/2] \\ & + \sin(\pi\xi fT_s)\sin(5\pi fT_s\xi/2)\{1 - \cos(\pi fT_s)\cos(\pi fT_s\xi)\}] \end{aligned} \tag{57}$$

$$\begin{aligned} c_6(p,p_t,\xi) = {} & - p_t[(1 - p)(1 - p_t) + 1/2p_t^2]\cos[\pi fT_s(1 - \xi)/4] \\ & - pp_t(1 - pp_t)\cos[\pi fT_s(1 + \xi)/4] \\ & + p_t^2[\cos(3\pi\xi fT_s) + (1 - p_t)\cos(2\pi\xi fT_s)] \end{aligned} \tag{58}$$

$$\begin{aligned} c_7(p,p_t,\xi) = {} & p_t[p_t^2\sin^2[\pi fT_s(1 - \xi)/2] - 2(1 - p_t)(p^2 - 0.5p_t)\sin^2(\pi fT_s/2)\cos(\pi fT_s\xi) \\ & + p(1 - pp_t)\sin^2[\pi fT_s(1 + \xi)/2] \end{aligned} \tag{59}$$

$$\begin{aligned} c_8(p,p_t,\xi) = {} & p_t[p(1 - pp_t) + (1 - p_t)(1 - 2p)]\sin^2[\pi fT_s(1 - \xi)/2] \\ & + 2p_t(1 - p)(1 - p_t)\sin^2(\pi fT_s/2)\cos(\pi fT_s\xi) \end{aligned} \tag{60}$$

$$H_1(m,p,p_t,\xi) = p_t^2[\sin^2(m\pi\xi)[1+2h_1(m,\xi)]^2+(1-2p)^2\cos^2(m\pi\xi)[1-2h_1(m,\xi)]^2] \tag{61}$$

$$H_2(m,p,p_t,\xi) = \sin^2(2m\pi\xi) + (1 - 2p)^2h_2^2(m,p_t,\xi) \tag{62}$$

$$\begin{aligned} H_3(m,p,p_t,\xi) = {} & 2p_t[2\sin^2(m\pi\xi)\cos(m\pi\xi)[1 + 2h_1(m,\xi)] \\ & + (1 - 2p)^2\cos(m\pi\xi)[1 - 2h_1(m,\xi)]h_2(m,p_t,\xi)] \end{aligned} \tag{63}$$

where the parameters $h_1(m,\xi)$ and $h_2(m,p_t,\xi)$ in Eqns (61)-(63) are defined as

$$h_1(m,\xi) = \begin{cases} \cos^2(m\pi\xi/2), \text{ m odd} \\ \sin^2(m\pi\xi/2), \text{ m even} \end{cases} \quad (64)$$

$$h_2(m,p_t,\xi) = (1 - p_t)(-1)^m - \cos(2m\pi\xi) \quad (65)$$

If we let $p = p_t = 1/2$, then Eqns (50)-(52) reduce to the results for balanced data stream (or data stream with equiprobable symbols) presented in [4]. Furthermore, if we let $p = p_t = 1/2$ and $\xi = 0$, then Eqns (50)-(52) reduce to the well-known result for a perfect Bi-ϕ data stream [6].

Since $2B_L/R_s << 1$, the harmonic components in Eqn (97) do not cause interference to the carrier tracking and the variance of the carrier tracking phase error in the presence of unbalanced and asymmetric Bi-ϕ data stream becomes

$$\sigma^2 = 1/\rho_o + (\alpha/2)\tan^2(m_T) + (1/2)(2 - p_t)^2\xi^2\tan^2(m_t) \quad (66)$$

where

$$\alpha = \int_{-\infty}^{\infty} | H(2\pi f) |^2 S_{cBi\text{-}\phi}(f)df \quad (67)$$

The conditional probability of error for this case is the same as Eqns (36) and (39) except that the parameter $\lambda_k(i)$ is replaced by

$$\lambda_k(i) = \frac{\int_0^{T_s} g_{Bi\text{-}\phi}(t)g_{iBi\text{-}\phi}(t+kT_s)dt}{\int_0^{T_s} | g_{Bi\text{-}\phi}(t) |^2 dt}, \quad i = 1, 2, 3, 4 \quad (68)$$

where $g_{iBi\text{-}\phi}(t)$ is the output of an ideal bandpass filter corresponding to the input $P_{iBi\text{-}\phi}(t)$, for i = 1, 2, 3, 4, and $g_{Bi\text{-}\phi}(t)$ is the output of the ideal filter for a perfect data stream which is given by [Eqn (55), 1]. The output response $g_{iBi\text{-}\phi}(t+kT_s)$, for i = 1, 2, 3, 4, can easily be shown to be

$$g_{1Bi\text{-}\phi}(t+kT_s) = \frac{1}{\pi}[\text{si}\{2\pi B(t + T_s(k + 1/2))\} - 2\text{si}\{2\pi B(t + T_s(k-\xi))\} + \text{si}\{2\pi B(t+T_s(k-1/2-\xi))\}] \quad (69)$$

$$g_{2Bi\text{-}\phi}(t+kT_s) = -\frac{1}{\pi}[si\{2\pi B(t+T_s(k+1/2))\} - 2si\{2\pi B(t+T_s(k+\xi))\}$$

$$+ si\{2\pi B(t+T_s(k-1/2+\xi))\}] \quad (70)$$

$$g_{3Bi\text{-}\phi}(t+kT_s) = \frac{1}{\pi}[si\{2\pi B(t+T_s(k+1/2))\} - 2si\{2\pi B(t+T_s(k-\xi))\}$$

$$+ si\{2\pi B(t+T_s(k-1/2))\}] \quad (71)$$

$$g_{4Bi\text{-}\phi}(t+kT_s) = -\frac{1}{\pi}[si\{2\pi B(t+T_s(k+1/2))\} - 2si\{2\pi B(t+T_s(k+\xi))\}$$

$$+ si\{2\pi B(t+T_s(k-1/2))\}] \quad (72)$$

Using the variance found in Eqn (66) and the parameter $\lambda_k(i)$ found in Eqn (68) the average error probability can be calculated as before and the results for the second order PLL [Eqn (24), 1] are shown in Figures 4-6. These figures plot the SER as a function of symbol SNR for $m_T = 1.25$ rad and $2B_L/R_s = 0.001$.

Figure 4 presents the SER performance for fixed BT_s of 3 and $\xi = 2$ % with p is a parameter. This figure shows that the performance of PCM/PM/Bi-Phase is also sensitive to unbalanced data when there exists data asymmetry. The symbol SNR degradation is more than 1.2 dB when p deviates from 0.45.

Figure 5 shows the behavior of PCM/PM/Bi-Phase in the presence of data asymmetry. For fixed values of $BT_s = 3$, $p = 0.45$, the results shows that the SER performance is quite sensitive to data asymmetry. In [1] we have pointed out that in order to compare the results presented in Figure 5 with those in Figure 2 for NRZ data, use equal amounts of asymmetry as measured by the actual time displacement of both waveforms transitions. For a fair comparison, we replace ξ in Figure 5 by 2ξ when compared with Figure 2. As an example, the SER curve for PCM/PM/NRZ operating at 2 % data asymmetry shown in Figure 2 corresponds to the 4 % data asymmetry curve for PCM/PM/Bi-ϕ shown in Figure 5.

Figure 6 depicts the SER performance for PCM/PM/Bi-Phase for bandlimiting channel. Numerical results show that the performance is susceptible to bandlimiting channel. For $\xi = 2$ % and $p = 0.45$, The degradation is unacceptable for $BT_s = 1$, and is about 0.5 dB or more when $BT_s = 3$.

5. Numerical Results and Discussions

Performance comparisons between PCM/PM/NRZ and PCM/PM/Bi-ϕ are illustrated in Figures 7-9 for uncoded systems. These figures plot the SER performance as a function of symbol SNR for $m_T = 1.25$ rad and $2B_L/R_s = 0.001$. Figure 7 compares the performance of PCM/PM/NRZ and PCM/PM/Bi-ϕ in the presence unbalanced data. For a fixed data asymmetry of 2 %, this figure shows that both PCM/PM/NRZ and PCM/PM/Bi-ϕ experience unacceptable degradations when the probability of transmitting a +1 pulse deviates from 0.5, and that PCM/PM/NRZ is more sensitive to unbalanced data than PCM/PM/Bi-ϕ.

Figure 8 shows the performance comparison for both systems with data asymmetry as a parameter. As the data asymmetry increases from 0 to 2 % the SER performance of PCM/PM/Bi-ϕ degrades seriously. For $p = 0.45$, $BT_s = 3$, $\xi = 2$ % and SER $\leq 10^{-4}$, the degradation in symbol SNR for PCM/PM/Bi-ϕ is about 1.5 dB or more, and less than 0.5 dB for PCM/PM/NRZ.

Figure 9 compares the SER performance for both systems for fixed data asymmetry of 2 % and $p = 0.45$ with BT_s (bandwidth-to-data rate ratio) as a parameter. For $BT_s = 1$, the symbol SNR degradation for PCM/PM/Bi-ϕ is unacceptable. On the other hand, under the same operating conditions, the symbol SNR degradation for PCM/PM/NRZ is less than 1 dB for SER $\leq 10^{-4}$. For $BT_s = 3$, the symbol SNR degradations for PCM/PM/NRZ and PCM/PM/Bi-ϕ are at the order of 0.2 dB and 0.8 dB or less for SER $\geq 10^{-6}$, respectively. This figure also shows that PCM/PM/Bi-ϕ is more susceptible to bandwidth constraint than PCM/PM/NRZ.

Since the international Consultative Committee for Space Data System (CCSDS) recommends the convolutional coding scheme with rate 1/2 constraint length 7 for space telemetry signal, we are interested to determine the symbol SNR degradation for coded PCM/PM/NRZ and PCM/PM/Bi-ϕ systems due to the presence of both imperfect data stream and ISI. As mentioned earlier in [3], an exact analysis for coded systems is not possible. [3] suggested that the symbol SNR degradation due to imperfect data stream and ISI can be estimated from the decoder bit error performance curve and the results shown Figures 1-6 and the ideal bit error performance curve by assuming that the coding is transparent to the imperfect data stream and ISI and using the uncoded energy-to-noise density ratios corresponding to the coded bit energy-to-noise density ratios at the desired bit error rates. Tables 1 and 2 show the symbol energy-to-noise density ratio (E_s/N_o) degradations in dB for PCM/PM/NRZ and PCM/PM/Bi-ϕ, respectively. The numerical results presented in these tables are for $m_T = 1.25$ rad, $2B_L/R_s = 0.001$, $\xi = 2$ % and $p = 0.45$. The selected values of E_s/N_o presented in these tables are 0.8, 1.5 and 1.95 dB. The selected values correspond to bit energy-to-noise density ratios $E_b/N_o = 3.8$, 4.5, and 4.95 dB which correspond to Viterbi decoder bit error probabilities $P_b = 10^{-4}$, 10^{-5} and 10^{-6}, for rate 1/2 and constraint length 7, respectively.

Table 1. Degradation Due to Imperfect Data and ISI for Rate 1/2 Convolutionally Encoded Random NRZ Data, m_T = 1.25 rad, $2B_L/R_s$ = 0.001, p = 0.45, ξ = 2 %.

SER	E_s/N_o, dB	Symbol SNR Degradation, Δ(dB)		
		BT_s = 1	BT_s = 2	BT_s = 3
10^{-4}	0.80	0.30	0.05	0.01
10^{-5}	1.50	0.37	0.08	0.06
10^{-6}	1.95	0.47	0.10	0.07

Table 2. Degradation Due to Imperfect Data and ISI for Rate 1/2 Convolutionally Encoded Random Bi-ϕ Data, m_T = 1.25 rad, $2B_L/R_s$ = 0.001, p = 0.45, ξ = 2 %.

SER	E_s/N_o, dB	Symbol SNR Degradation, Δ(dB)		
		BT_s = 1	BT_s = 2	BT_s = 3
10^{-4}	0.80	2.53	0.4	0.25
10^{-5}	1.50	2.95	0.8	0.55
10^{-6}	1.95	3.33	0.9	0.63

6. Conclusion

Combined effects of the imperfect data stream and ISI caused by the bandlimiting channel on the performance of PCM/PM communications systems are investigated in this paper. Analytical models to predict the SER performance for both uncoded PCM/PM/NRZ and PCM/PM/Bi-ϕ systems were derived. In addition, the symbol SNR degradations for rate 1/2 constraint length 7 convolutional coded systems are also evaluated.

Numerical results show that theoretical predictions for the total symbol SNR degradation of the receivers due to the presence of both imperfect data and ISI are not the algebraic sum of each symbol SNR degradation due to a single source of degradation found in [1]. The results also show that, for 2 % data asymmetry, both PCM/PM/NRZ and PCM/PM/Bi-ϕ are susceptible to unbalanced data stream, and that PCM/PM/NRZ is more sensitive to unbalanced data than PCM/PM/Bi-ϕ. On the other hand, PCM/PM/Bi-ϕ is more susceptible to data asymmetry while PCM/PM/NRZ is not.

Furthermore, the results show that, for $BT_s = 3$, the SER performance of PCM/PM/NRZ is acceptable for both near earth and deep space missions. However, for PCM/PM/Bi-ϕ, the SER performance is found to be unacceptable for deep space missions and may be acceptable for near earth missions.

Acknowledgement

The work described in this paper was carried out at the Jet Propulsion Laboratory, California Institute of Technology, under contract with the National Aeronautics and Space Administration.

References

[1] Tien M. Nguyen, "Behavior of PCM/PM Receivers in Non-Ideal Channels, Part I: Separate Effects of Imperfect Data Streams and Bandlimitting Channels on Performances," to be published.

[2] Tien M. Nguyen, "The Impact of NRZ Data Asymmetry on the Performance of a Space Telemetry System," IEEE Transactions on EMC, Vol. 33, No. 4, November 1991.

[3] W. K. Alem, G. K. Huth, M. K. Simon, "Integrated Source and Channel Encoded Digital Communication System Design Study," Final Report (R7803-7) under Contract NAS 9-15240, Mar. 31, 1978, Axiomatix, Marina del Rey, CA.

[4] Tien M. Nguyen, "Space Telemetry Degradation due to Manchester Data Asymmetry Induced Carrier Tracking Phase Error," IEEE Transactions on EMC, Vol. 33, No. 3, August 1991.

[5] Mazen M. Shihabi, Tien M. Nguyen, Sami M. Hinedi, "On the Use of Subcarriers in Future DSN MIssions," the Telecommunications and Data Acquisition Progress Report 42-111, November 15, 1992, NASA, Jet Propulsion Laboratory, Pasadena, California.

[6] Joe Yuen, editor, Deep Space Telecommunications Systems Engineering, Plenum Press, New York, 1983.

Appendix

The conditional probability of error for M = 2

$$
\begin{aligned}
P_e(\theta_e) = {} & p[p_3p_3p_3p_3\mathrm{erfc}\{\sqrt{E_s/N_o}(1 + \lambda_{-2}(3) + \lambda_{-1}(3) + \lambda_1(3) + \lambda_2(3))\cos\theta_e\} \\
& + p_4p_2p_1p_4\mathrm{erfc}\{\sqrt{E_s/N_o}(1 - \lambda_{-2}(4) - \lambda_{-1}(2) - \lambda_1(1) - \lambda_2(4))\cos\theta_e\} \\
& + p_2p_3p_3p_1\mathrm{erfc}\{\sqrt{E_s/N_o}(1 - \lambda_{-2}(2) + \lambda_{-1}(3) + \lambda_1(3) - \lambda_2(1))\cos\theta_e\} \\
& + p_4p_2p_3p_1\mathrm{erfc}\{\sqrt{E_s/N_o}(1 - \lambda_{-2}(4) - \lambda_{-1}(2) + \lambda_1(3) - \lambda_2(1))\cos\theta_e\} \\
& + p_3p_3p_3p_1\mathrm{erfc}\{\sqrt{E_s/N_o}(1 + \lambda_{-2}(3) + \lambda_{-1}(3) + \lambda_1(3) - \lambda_2(1))\cos\theta_e\} \\
& + p_3p_3p_1p_2\mathrm{erfc}\{\sqrt{E_s/N_o}(1 + \lambda_{-2}(3) + \lambda_{-1}(3) - \lambda_1(1) + \lambda_2(2))\cos\theta_e\} \\
& + p_1p_2p_3p_3\mathrm{erfc}\{\sqrt{E_s/N_o}(1 + \lambda_{-2}(2) - \lambda_{-1}(3) + \lambda_1(3) + \lambda_2(1))\cos\theta_e\} \\
& + p_2p_3p_3p_3\mathrm{erfc}\{\sqrt{E_s/N_o}(1 - \lambda_{-2}(2) + \lambda_{-1}(3) + \lambda_1(3) + \lambda_2(3))\cos\theta_e\} \\
& + p_3p_3p_1p_4\mathrm{erfc}\{\sqrt{E_s/N_o}(1 + \lambda_{-2}(3) + \lambda_{-1}(3) - \lambda_1(1) - \lambda_2(4))\cos\theta_e\} \\
& + p_1p_2p_1p_2\mathrm{erfc}\{\sqrt{E_s/N_o}(1 + \lambda_{-2}(1) - \lambda_{-1}(2) - \lambda_1(1) + \lambda_2(2))\cos\theta_e\} \\
& + p_1p_2p_3p_1\mathrm{erfc}\{\sqrt{E_s/N_o}(1 + \lambda_{-2}(1) - \lambda_{-1}(2) + \lambda_1(3) - \lambda_2(1))\cos\theta_e\} \\
& + p_4p_2p_3p_3\mathrm{erfc}\{\sqrt{E_s/N_o}(1 - \lambda_{-2}(4) - \lambda_{-1}(2) + \lambda_1(3) + \lambda_2(3))\cos\theta_e\} \\
& + p_2p_3p_1p_2\mathrm{erfc}\{\sqrt{E_s/N_o}(1 - \lambda_{-2}(2) + \lambda_{-1}(3) - \lambda_1(1) + \lambda_2(2))\cos\theta_e\} \\
& + p_1p_2p_1p_4\mathrm{erfc}\{\sqrt{E_s/N_o}(1 + \lambda_{-2}(1) - \lambda_{-1}(2) - \lambda_1(1) - \lambda_2(4))\cos\theta_e\} \\
& + p_2p_3p_1p_4\mathrm{erfc}\{\sqrt{E_s/N_o}(1 - \lambda_{-2}(2) + \lambda_{-1}(3) - \lambda_1(1) - \lambda_2(4))\cos\theta_e\} \\
& + p_4p_2p_1p_2\mathrm{erfc}\{\sqrt{E_s/N_o}(1 - \lambda_{-2}(4) - \lambda_{-1}(2) - \lambda_1(1) + \lambda_2(2))\cos\theta_e\}] \\
& + q[p_3p_1p_2p_3\mathrm{erfc}\{\sqrt{E_s/N_o}(1 - \lambda_{-2}(3) - \lambda_{-1}(1) - \lambda_1(2) - \lambda_2(3))\cos\theta_e\} \\
& + p_4p_4p_4p_4\mathrm{erfc}\{\sqrt{E_s/N_o}(1 + \lambda_{-2}(4) + \lambda_{-1}(4) + \lambda_1(4) + \lambda_2(4))\cos\theta_e\}
\end{aligned}
$$

$$+ p_2p_1p_2p_1\text{erfc}\{\sqrt{E_s/N_o}(1 + \lambda_{-2}(2) - \lambda_{-1}(1) - \lambda_1(2) + \lambda_2(1))\cos\theta_e\}$$

$$+ p_4p_4p_2p_1\text{erfc}\{\sqrt{E_s/N_o}(1 + \lambda_{-2}(4) + \lambda_{-1}(4) - \lambda_1(2) + \lambda_2(1))\cos\theta_e\}$$

$$+ p_3p_1p_2p_1\text{erfc}\{\sqrt{E_s/N_o}(1 - \lambda_{-2}(3) - \lambda_{-1}(1) - \lambda_1(2) + \lambda_2(1))\cos\theta_e\}$$

$$+ p_3p_1p_4p_2\text{erfc}\{\sqrt{E_s/N_o}(1 - \lambda_{-2}(3) - \lambda_{-1}(1) + \lambda_1(4) - \lambda_2(2))\cos\theta_e\}$$

$$+ p_1p_4p_2p_3\text{erfc}\{\sqrt{E_s/N_o}(1 - \lambda_{-2}(2) + \lambda_{-1}(4) - \lambda_1(2) - \lambda_2(1))\cos\theta_e\}$$

$$+ p_2p_1p_2p_3\text{erfc}\{\sqrt{E_s/N_o}(1 + \lambda_{-2}(2) - \lambda_{-1}(1) - \lambda_1(2) - \lambda_2(3))\cos\theta_e\}$$

$$+ p_3p_1p_4p_4\text{erfc}\{\sqrt{E_s/N_o}(1 - \lambda_{-2}(3) - \lambda_{-1}(1) + \lambda_1(4) + \lambda_2(4))\cos\theta_e\}$$

$$+ p_1p_4p_4p_2\text{erfc}\{\sqrt{E_s/N_o}(1 - \lambda_{-2}(1) + \lambda_{-1}(4) + \lambda_1(4) - \lambda_2(2))\cos\theta_e\}$$

$$+ p_1p_4p_2p_1\text{erfc}\{\sqrt{E_s/N_o}(1 - \lambda_{-2}(1) + \lambda_{-1}(4) - \lambda_1(2) + \lambda_2(1))\cos\theta_e\}$$

$$+ p_4p_4p_2p_3\text{erfc}\{\sqrt{E_s/N_o}(1 + \lambda_{-2}(4) + \lambda_{-1}(4) - \lambda_1(2) - \lambda_2(3))\cos\theta_e\}$$

$$+ p_2p_1p_4p_2\text{erfc}\{\sqrt{E_s/N_o}(1 + \lambda_{-2}(2) - \lambda_{-1}(1) + \lambda_1(4) - \lambda_2(2))\cos\theta_e\}$$

$$+ p_1p_4p_4p_4\text{erfc}\{\sqrt{E_s/N_o}(1 - \lambda_{-2}(1) + \lambda_{-1}(4) + \lambda_1(4) + \lambda_2(4))\cos\theta_e\}$$

$$+ p_2p_1p_4p_4\text{erfc}\{\sqrt{E_s/N_o}(1 + \lambda_{-2}(2) - \lambda_{-1}(1) + \lambda_1(4) + \lambda_2(4))\cos\theta_e\}$$

$$+ p_4p_4p_4p_2\text{erfc}\{\sqrt{E_s/N_o}(1 + \lambda_{-2}(4) + \lambda_{-1}(4) + \lambda_1(4) - \lambda_2(2))\cos\theta_e\}]$$

Figure 1. SER for Various Probabilities of Mark

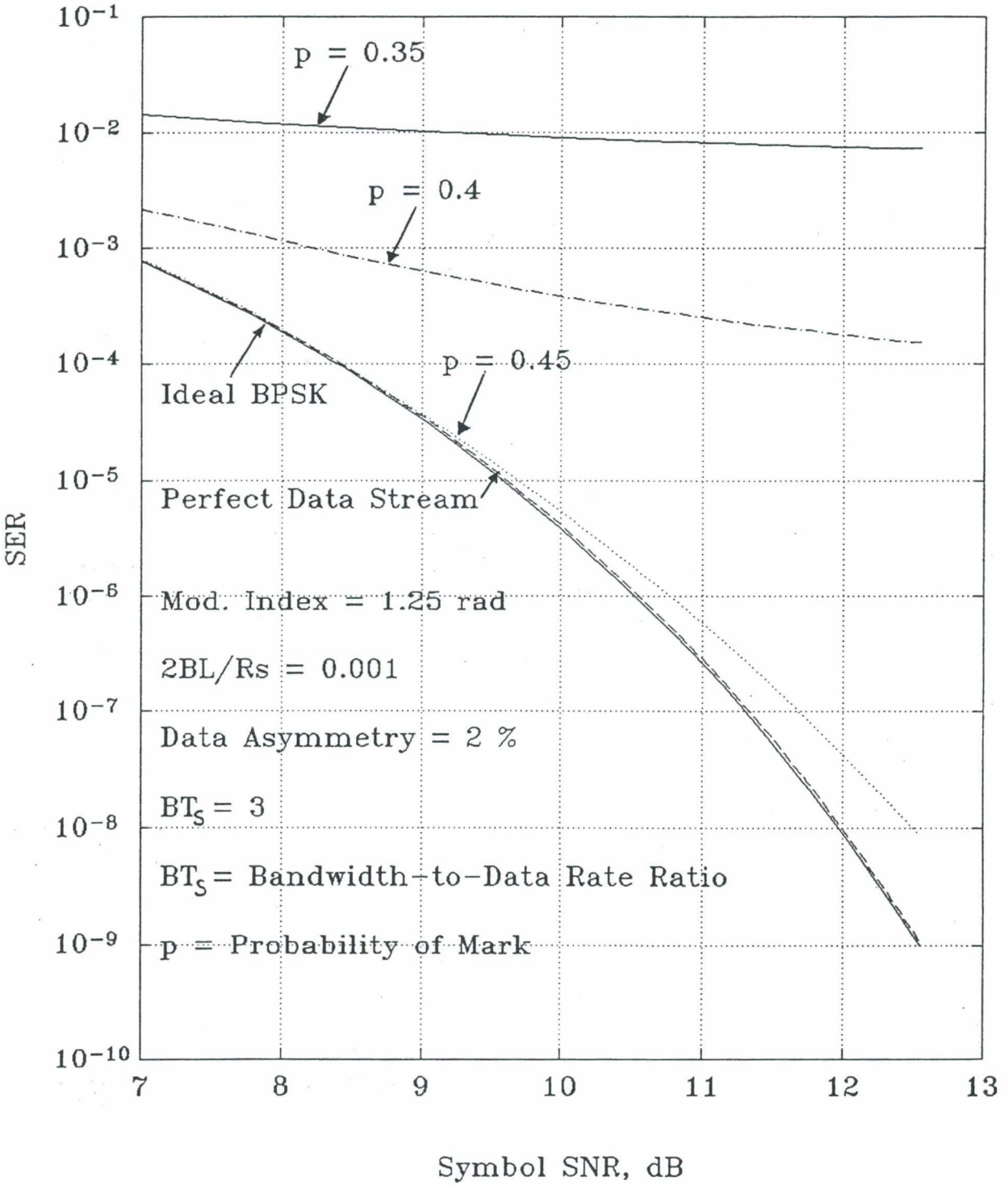

Figure 2. SER for Various Values of Data Asymmetry

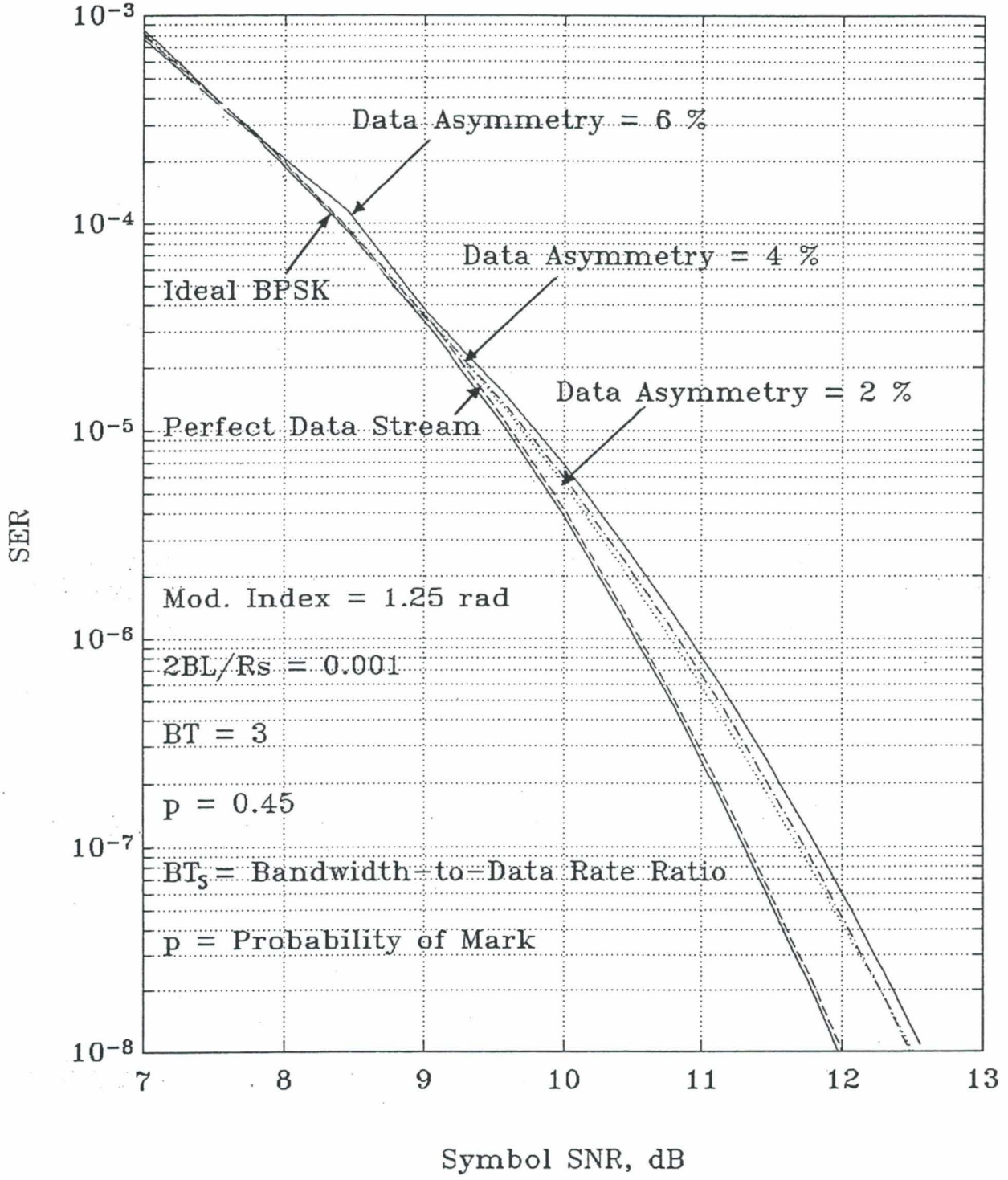

Figure 3. PCM/PM/NRZ-SER for Various Values of BT

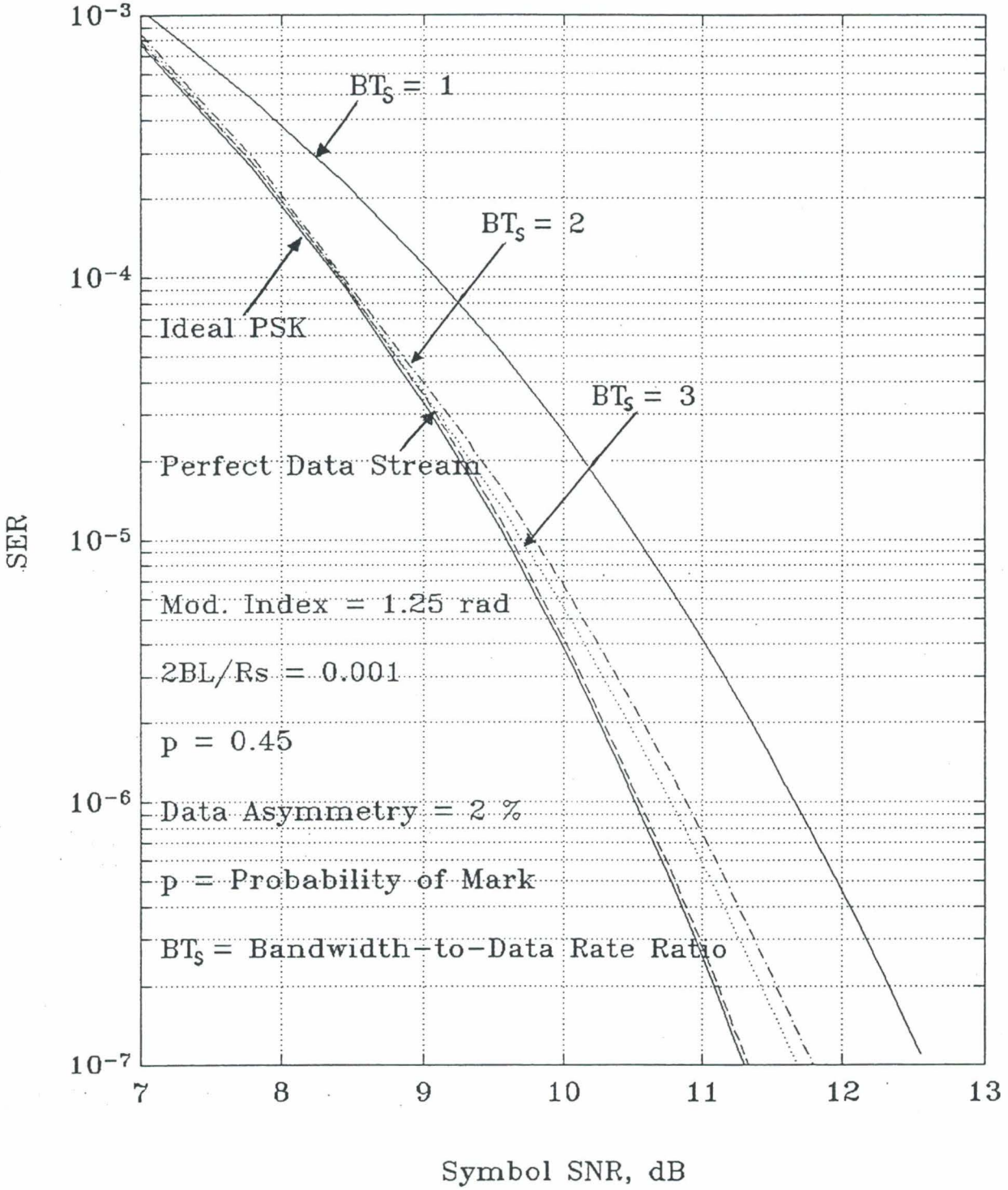

Figure 4. Bi-Phase-SER for Various Values of p

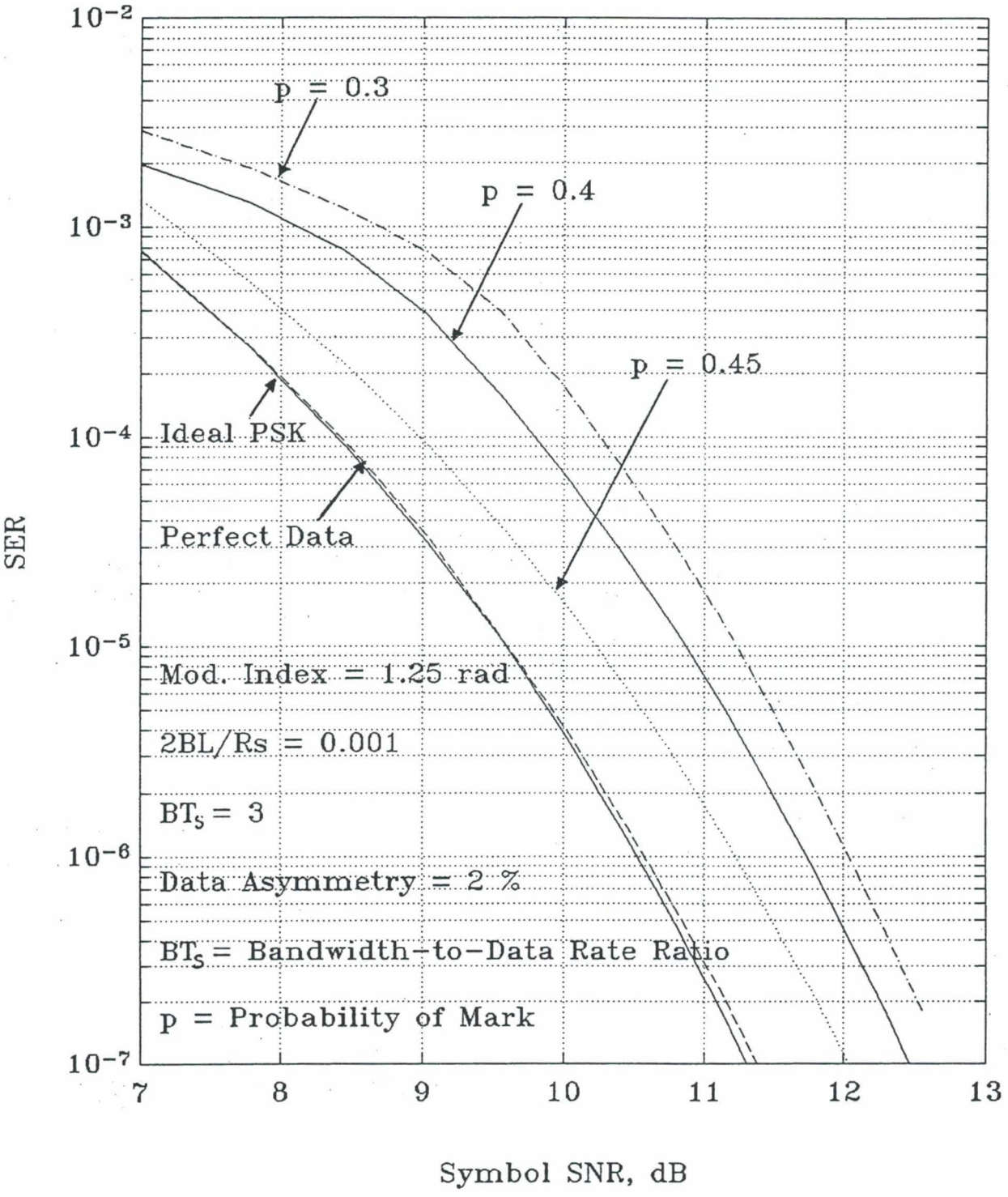

Figure 5. Bi-Phase-SER With Data Asymmetry

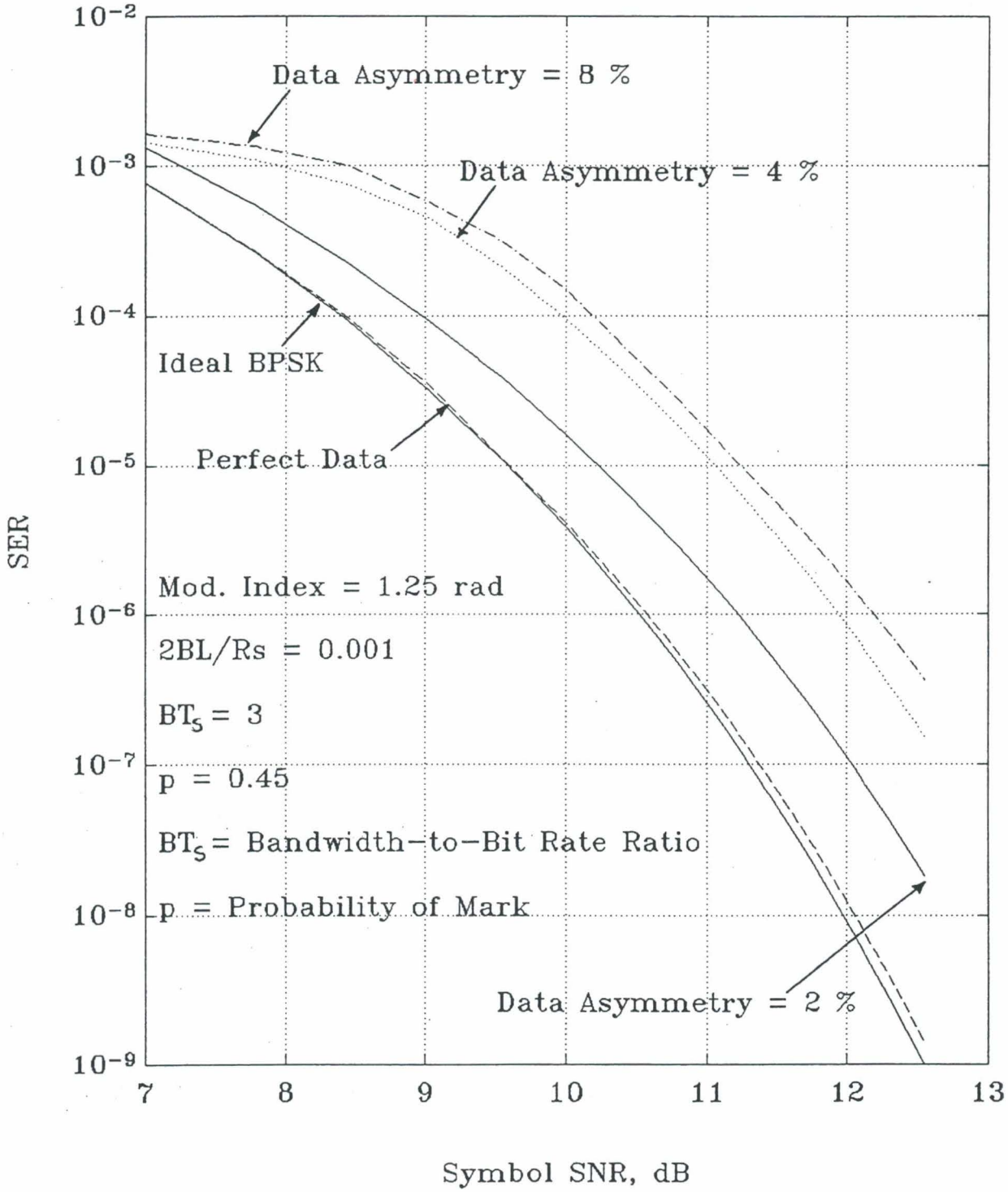

Figure 6. Bi-Phase-SER for Various Values of BT

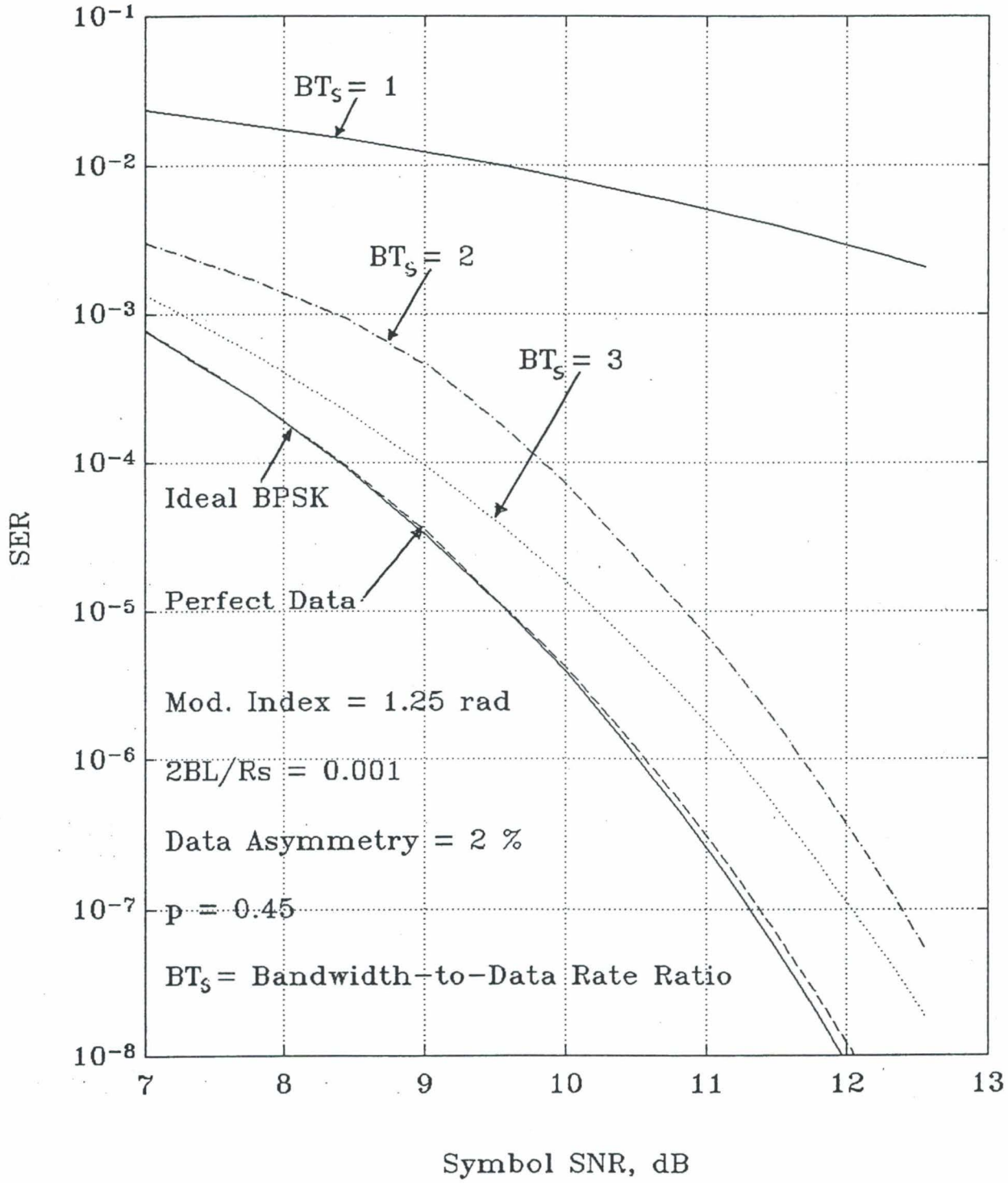

Figure 7. Performance Comparison for Unbalanced Data

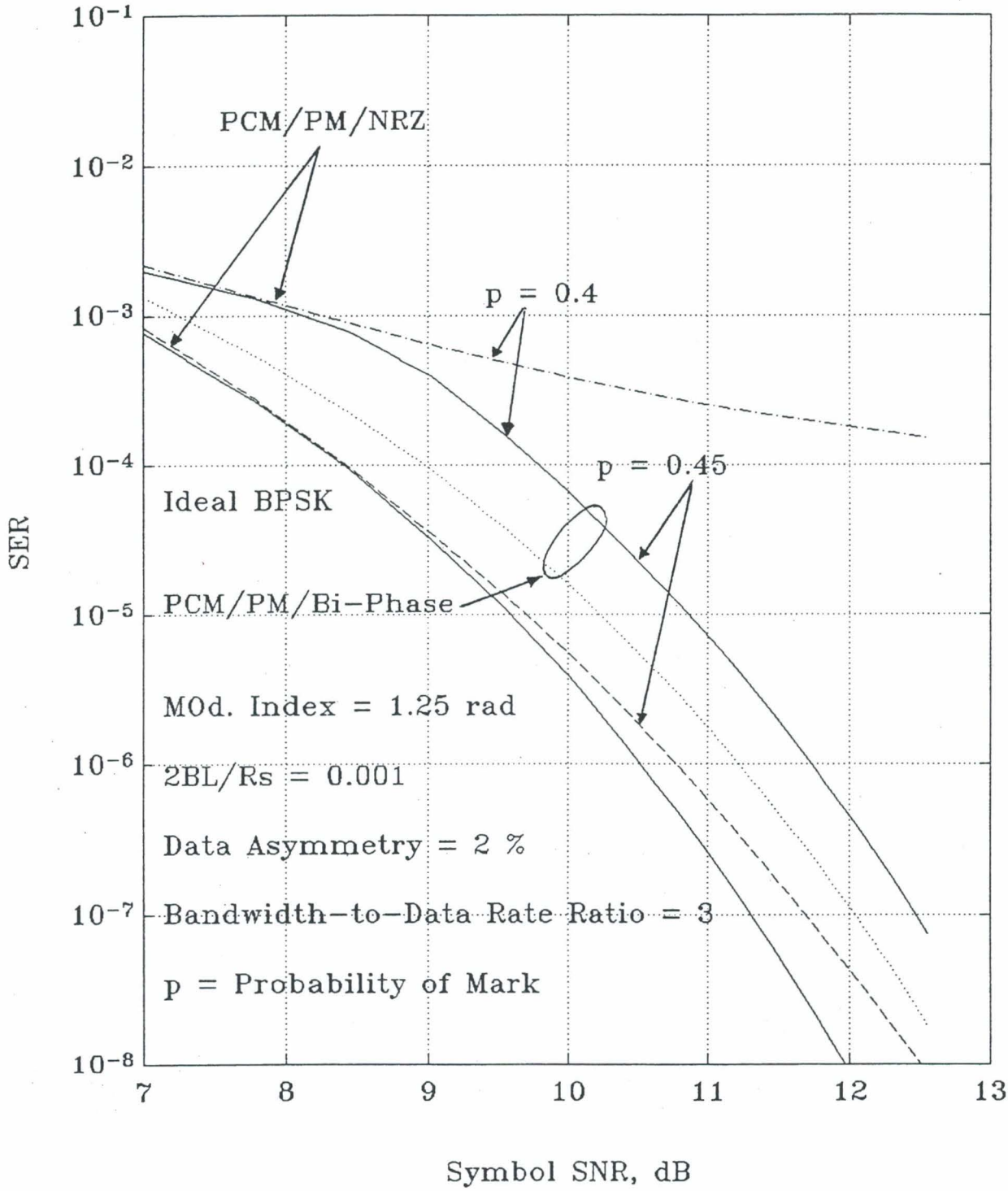

Figure 8. Performance Comparison for Data Asymmetry

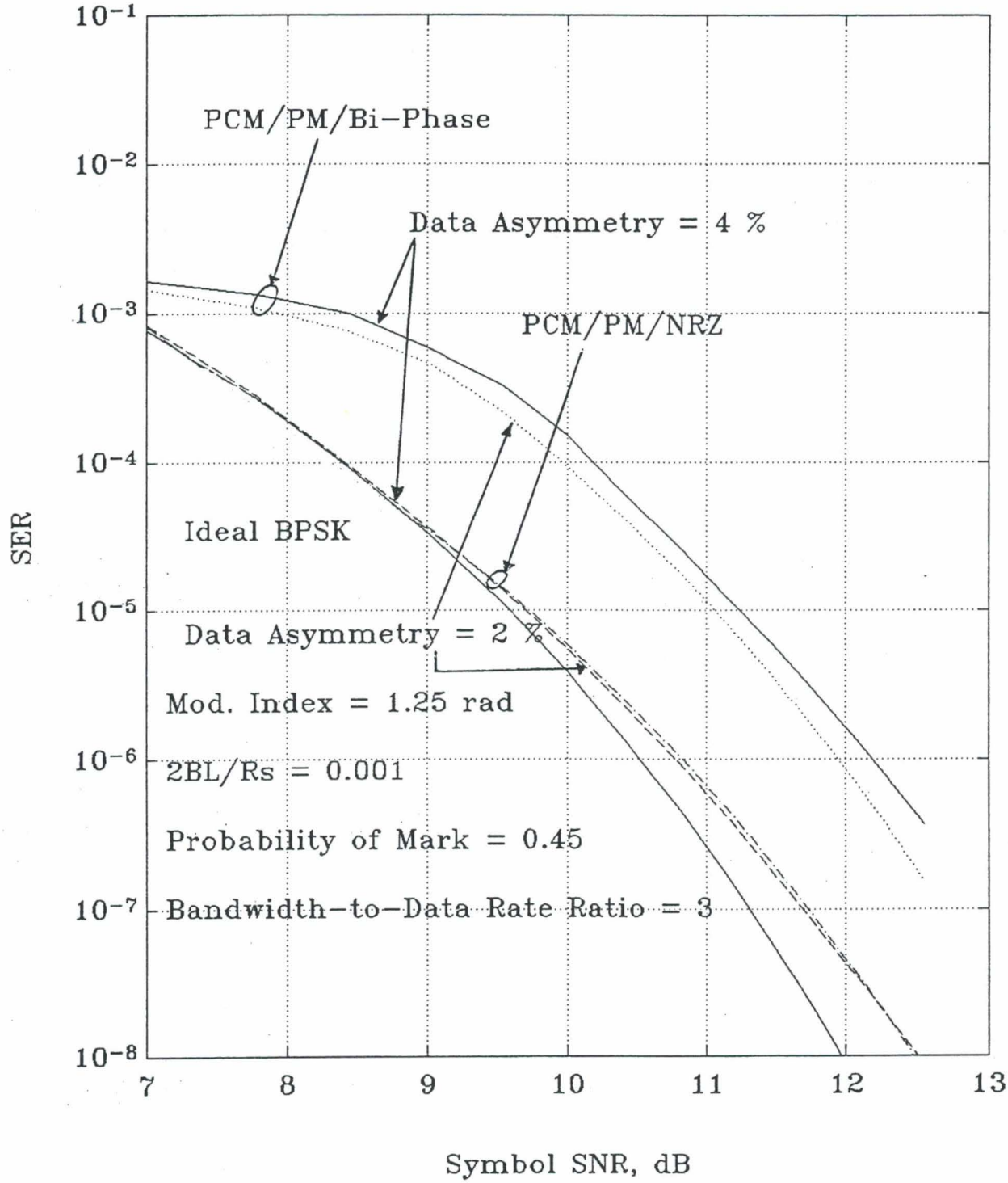

Figure 9. Performance Comparison for Bandlimiting Channel

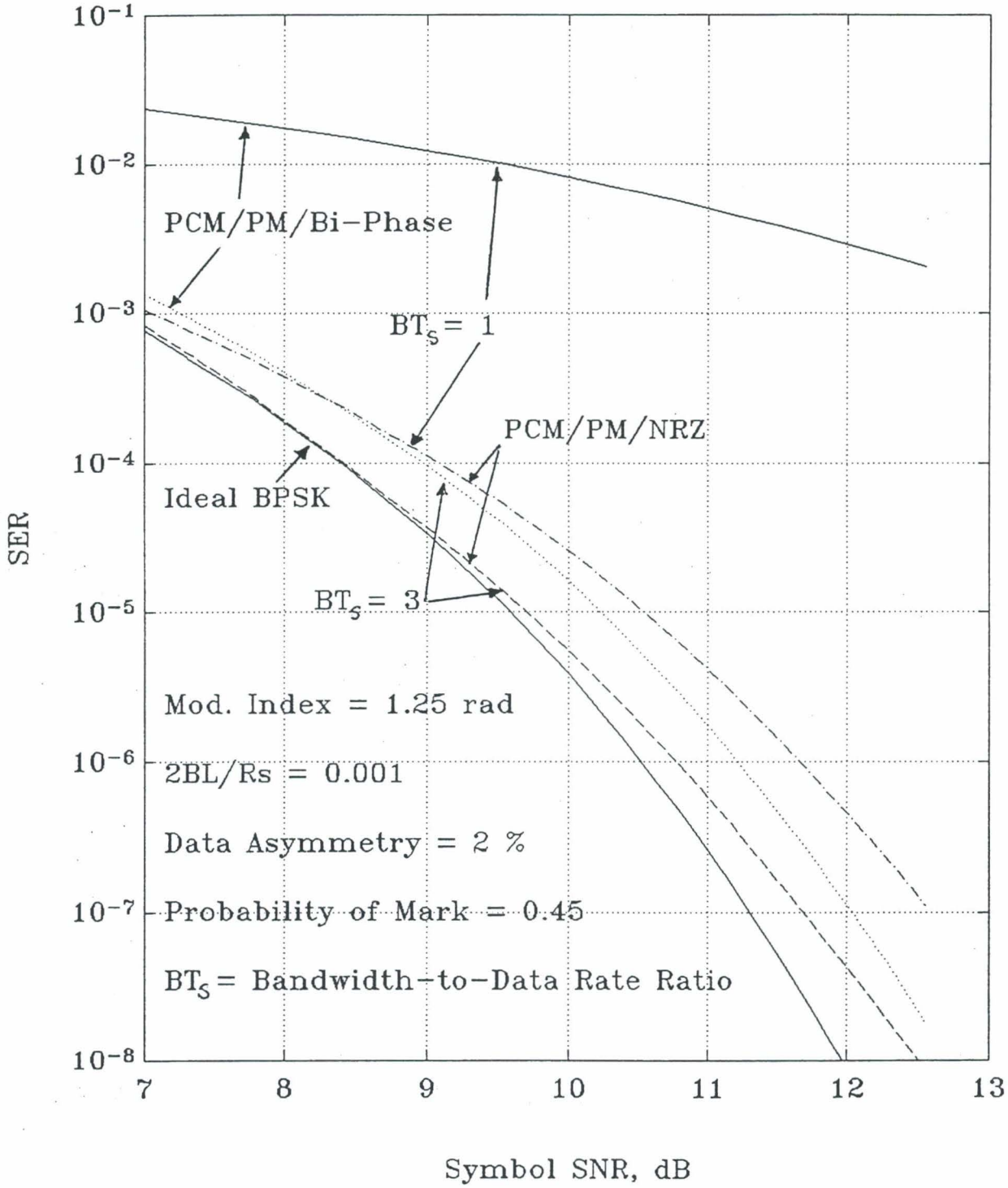

COMDISCO SIMULATION RESULTS FOR PCM/PM RECEIVERS IN NON-IDEAL CHANNELS[1]

Aseel Anabtawi, Tien M. Nguyen, Sami M. Hinedi, and Samson Million
National Aeronautics and Space Administration
Jet Propulsion Laboratory
California Institute of Technology
4800 Oak Grove Dr.
Pasadena, California 91109

ABSTRACT

This paper studies, by computer simulations, the performance of a PCM/PM/NRZ receiver in the presence of two separate effects, namely, an unbalanced data stream and a band-limited channel. The results obtained are then compared to the theoretical results presented in a previous report.

[1] The work described in this paper was carried out at the Jet Propulsion Laboratory, California Institute of Technology, under contract with the National Aeronautics and Space Administration.

1 Introduction

A previous report, [1], was written to study the behavior of PCM/PM receivers in non-ideal channels. This paper verifies, by simulation and measurement, the theoretical results presented in [1].

The presence of an imperfect data stream produces undesirable spectral components which degrade the performance of the system. The objective of this paper is to study the separate effects of unbalanced data and InterSymbol Interference (ISI) caused by bandlimited channel on the performance of PCM/PM/NRZ receivers.

The Signal Processing Worksystem (SPW) was used for developing, testing and simulating the system. The Symbol Error Rate (SER) was measured for perfect and imperfect data streams, and the results obtained were compared to the theory presented in [1].

The organization of this paper is as follows: Section 2 describes perfect, unbalanced and bandlimited data streams for PCM/PM/NRZ. Section 3 gives a brief description of the PCM/PM receiver blocks which were used to build the system in SPW, section 4 shows and discusses the simulation results and compares them to theory, and finally, section 5 presents the conclusion of this paper.

2 Description of PCM/PM Data Streams

The deep space received telemetry signal, in the absence of a subcarrier, is given by:

$$s_r(t) = \sqrt{2P}\left\{\cos(m_T)\cos(\omega_c t + \theta_c) - d(t)\sin(m_T)\sin(\omega_c t + \theta_c)\right\} + n(t) \tag{1}$$

where P is the transmitted power, m_T is the telemetry modulation index in rad, $\omega_c = 2\pi f_c$ is the angular carrier center frequency in rad/sec, θ_c is the carrier phase, $n(t)$ is an additive white Gaussian noise (AWGN), and $d(t)$ is the data stream (NRZ) with transition density, P_t, less or equal to 0.5 and is defined by

$$d(t) = \sum_{k=-\infty}^{\infty} d_k p(t + kT) \tag{2}$$

where $d_k = \pm 1$ and $p(t)$ is the baseband pulse. The first and second terms of Eq. (1) are the residual carrier and data components, respectively.

2.1 Perfect Data Stream

In a perfect data stream, the probability of transmitting a $+1$ pulse, p, is equal to the probability of transmitting a -1, q, with transition density, P_t, equal to 0.5 and given by

$$P_t = 2pq \tag{3}$$

where $q = 1 - p$.

When the data is balanced ($p = 0.5$), the carrier term of Eq. (1) generates a spike at f_c with power, P_c, given by

$$P_c = P\cos^2(m_T) \tag{4}$$

and the spectrum generated by the data component has power

$$P_D = P\sin^2(m_T) \tag{5}$$

Combining the carrier and data terms, the power spectrum of a PCM/PM/NRZ perfect data stream is shown in Fig 1.a. and is given by:

$$S(f) = S_D(f) + S_c(f) \tag{6}$$

2.2 Unbalanced Data Stream

The imbalance between $+1$'s and -1's in the data stream causes an additional corruption to the received signal in (1) generating undesirable spectral components which degrade the performance of the telemetry system. When p is not equal to 0.5 (and therefore, $P_t < 0.5$), the data component in (1) will be affected and the data spectrum can be written as

$$S_D(f) = P\sin^2(m_T)\{S_{dc}(f) + S_{con't}(f)\} \tag{7}$$

where $S_{dc}(f)$ is the dc (or harmonic) component caused by the imperfect data stream that falls on the RF carrier, and $S_{con't}(f)$ is the continuous data spectrum.

For PCM/PM/NRZ unbalanced data stream, the dc and continuous power spectral density components are found to be [1]

$$S_{dc}(f) = (1-2p)^2\delta(f) \tag{8}$$

$$S_{con't}(f) = 4Tp(1-p)\left\{\frac{\sin^2(\pi fT)}{(\pi fT)^2}\right\} \tag{9}$$

Therefore, in addition to the tone generated at f_c by the carrier component in (1) with power given by (4), the spectrum of the unbalanced NRZ data stream will have another tone at f_c generated by the imbalance between $+1$'s and -1's with power given by

$$P_{dc} = (1-2p)^2 P\sin^2(m_T) \tag{10}$$

and the continuous data spectrum will have power given by

$$P_{con't} = 4p(2-p)P\sin^2(m_T) \tag{11}$$

where

$$P_D = P_{dc} + P_{con't} \tag{12}$$

The spectrum of an unbalanced NRZ data stream is shown in Fig. 1.b for $p = 0.4$.

2.3 Bandlimited Channel

An additional impairment that contributes to the degradation of the overall performance of the system is the InterSymbol Interference (ISI) caused by the bandlimited channel. Bandlimiting causes interference between successive pulses producing the ISI effect which behaves like an additional random noise.

If we let $p(t)$ denote the pulse shape of the data and $h(t)$ denote the impulse response of the equivalent low-pass filter of the RF bandpass filter with bandwidth B, the received data can be expressed as [1]

$$d(t) = \sum_{k=-\infty}^{\infty} d_k g(t + kT_s) \tag{13}$$

where $d_k = \pm 1$ with $p = q = 0.5$, and $g(t)$ is given by

$$g(t) = p(t) * h(t) \tag{14}$$

where $*$ denotes convolution.

The impulse response of an ideal channel $h(t)$ is given by the inverse Fourier transform of the transfer function $H(f)$

$$H(f) = \begin{cases} 1 & \text{-B < f < B} \\ 0 & \text{otherwise} \end{cases} \tag{15}$$

resulting in

$$h(t) = 2B \sin(2\pi Bt)/(2\pi Bt) \tag{16}$$

For an ideal filter and a perfect data stream, g_{NRZ} can be found to be [1]

$$g_{NRZ}(t + kT) = \frac{1}{\pi} \{Si\{2\pi B(t + T(k + 1/2))\} - Si\{2\pi B(t + T(k - 1/2))\}\} \tag{17}$$

where

$$Si(x) = \int_0^x \frac{\sin(u)}{u} du \tag{18}$$

Fig. 2 shows a plot of the output response of the ideal filter to NRZ pulse ($g_{NRZ}(t/T)$ vs. t/T) for various values of time-bandwidth product BT. Note that the shape of the output is dependent on BT. For $BT >> 1$, the filtering is nonexistent and the output signal is the same as the input. As BT gets closer to 1, the rise and fall times of the output are significant when compared to the input, and the output signal is more spread in time.

3 Description of PCM/PM Receiver Blocks

Fig. 3 shows the block diagram of a PCM/PM receiver. This receiver consists of the TSG (Test Signal Generator), the ARX (Advanced Receiver), and the Error Counter. The TSG, shown in Fig. 4, generates the deep-space spacecraft signal at an intermediate frequency (IF). The TSG's Random Data block controls the parameter p (probability of +1). The TSG parameters are:

sampling rate f_s:	500×10^3 Hz
carrier frequency f_c:	100×10^3 Hz
initial carrier phase θ_c:	0 deg
symbol rate R_s:	10×10^3 Hz
modulation index m_T:	71.619725 deg (corresponding to 1.25 rad)

and the power-to-noise ratio P/N_0 is calculated using

$$P/N_0 = \frac{E_s}{N_0} - 10\log_{10}(\sin^2 m_T) + 10\log_{10} R_s - 10\log_{10}(4p(1-p)) \tag{19}$$

where E_s/N_0 is the Symbol SNR in dB. The last term in Eq. (19) is a factor generated by the unbalanced data stream and is equal to 0 dB when $p = 0.5$. This factor shows a reduction in the transmitting power when the data stream is unbalanced.
The ARX block, shown in Fig. 5, consists of the Carrier PLL (Phase Lock Loop) block which estimates the carrier phase, the Digital DTTL (Data Transition Tracking Loop) block which generates the symbol timing reference, the Sum Dump Hold Symbol block which outputs the soft symbols, and a Butterworth Lowpass Filter. Finally, the Error Counter block compares the soft symbols of the ARX to the transmitted symbols and outputs the number of errors N.

4 Discussion and simulation results

Using SPW, simulations were performed at 7, 8, 9 and 10 dB Symbol SNR, E_s/N_0, and the corresponding P/N_0 was calculated. The result of each simulation was the number of errors N (produced by the Error Counter as a result of comparing the soft symbols to the transmitted ones). The average error probability P_e was then calculated using

$$P_e = \frac{N}{\text{Number of Iterations}/(f_s/R_s)} \tag{20}$$

where f_s is the sampling frequency in Hz, the fraction $\frac{f_s}{R_s}$ is the number of samples per symbol, and

$$\text{Number of Iterations} = \frac{100}{SER}\frac{f_s}{R_s} \tag{21}$$

where SER is the Symbol Error Rate as given by the theory. Finally, P_e was plotted vs. Symbol SNR and the results were compared to the theory presented in [1].

4.1 Unbalanced Data

To verify the performance of the receiver in the presence of an unbalanced data stream, simulations were performed for $p = 0.5$, 0.45 and 0.4.

For PCM/PM/NRZ, the simulation results are shown in Table 1 and Fig. 6. When p is equal to 0.5 (balanced data stream), the simulation results are worse than, but close to the theoretical results (less than 0.125 dB difference). When p deviates from 0.5 (unbalanced data case), the simulation results were different than the theoretical results, and the difference ranged between 0.13 dB and 1 dB, except for p=0.4 and symbol SNR $>$ 9 dB where the simulation results are better than the theoretical.

The discrepancy between the theory and simulation may be explained by:

- It was assumed in the theory that the phase of the tone caused by the unbalanced data is coherent with the carrier phase. In reality, the phase of the tone may not.

- It was assumed in [1] that the pdf of the carrier tracking phase error has Tikhonov distribution with modified variance. This assumption may breakdown for certain values of interference-to-signal power ratios, loop bandwidth and loop SNR.

4.2 Bandlimited Channel

In order to test the effect of the bandlimited channel on the overall performance of the system, simulations were performed for different values of time-bandwidth product (BT): 1, 2 and 3. As expected, the higher the value of the product BT, the better the performance of the system. The simulation results are shown in Table 2 and Fig. 7.

The theoretical and simulation results are in good agreement. However, the simulation results are a little worse than the theoretical results. This is because the theoretical results were obtained for the case when the ISI is caused by two adjacent pulses, that is, two pulses before and two pulses after the current pulse are considered in the SER calculation.

5 Conclusion

This report studied, by simulations, the separate effects of unbalanced data and bandlimited channel of the performance of a PCM/PM/NRZ receiver. The simulation results were in agreement with the theoretical results for the balanced data stream and bandlimited channel

cases. However, there are some discrepancies between the theory and simulation for the unbalanced data stream case. It is recommended that the loop SNR and Symbol SNR are verified with the theoretical values for that case.

Similar testing as the one described in this report is currently being performed for PCM/PM/Bi-ϕ receivers. The Bi-ϕ data stream is generated by multiplying the NRZ data with a squarewave subcarrier with the subcarrier frequency being identical to the NRZ symbol rate. In addition, both PCM/PM/NRZ and PCM/PM/Bi-ϕ receivers' performances will be tested under the effect of data asymmetry which is due to rising and falling voltage transitions. It is recommended that the testing be continued to verify all the above mentioned cases for future work.

ACKNOWLEDGMENTS

The work described in this paper was carried out at the Jet Propulsion Laboratory, California Institute of Technology, under contract with the National Aeronautics and Space Administration.

REFERENCE

1. T. M. Nguyen, "The Behavior of PCM/PM Receivers in Non-Ideal Channels. Part I: The Separate Effects of Imperfect Data Streams and Band-limiting Channels on Performance," Consultative Committee for Space Data Systems, Report of the Proceedings of the RF and Modulation Subpanel 1E meeting at the German Space Operations Centre, September 20-24, 1993, CCSDS B20.0-Y-1, February 1994.

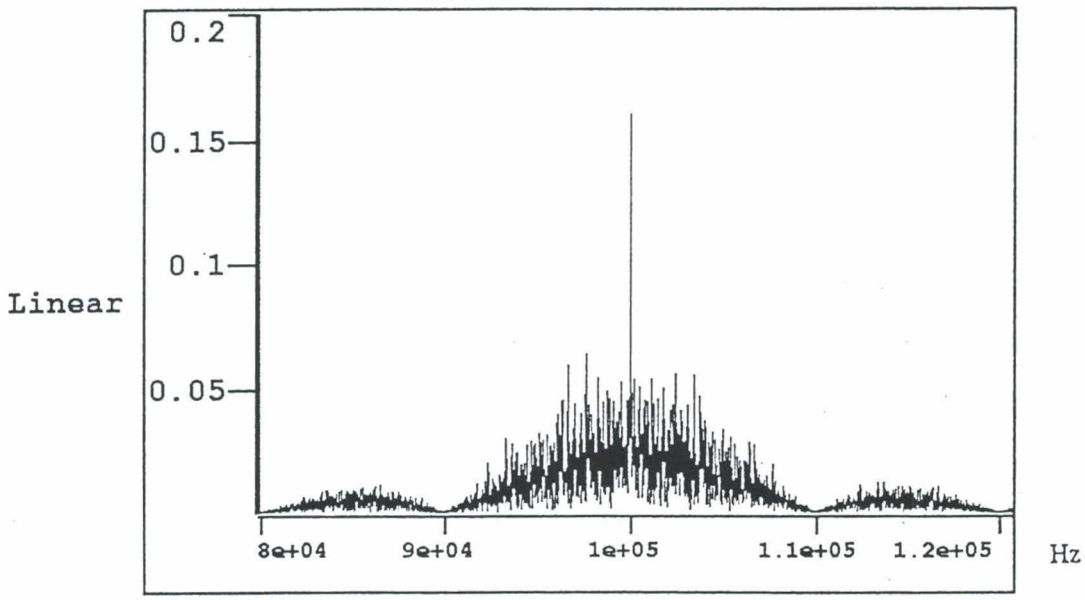

(a) p = 0.5 (Balanced data stream)

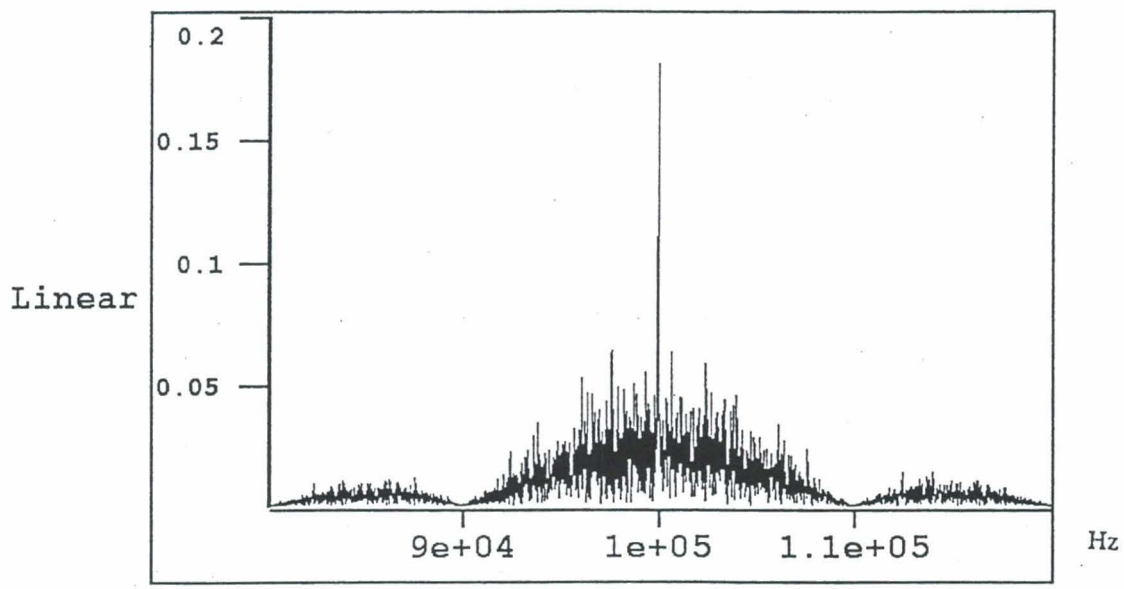

(b) p = 0.4 (Unbalanced data stream)

FIGURE 1

Spectrum of PCM/PM/NRZ for Different Values of p

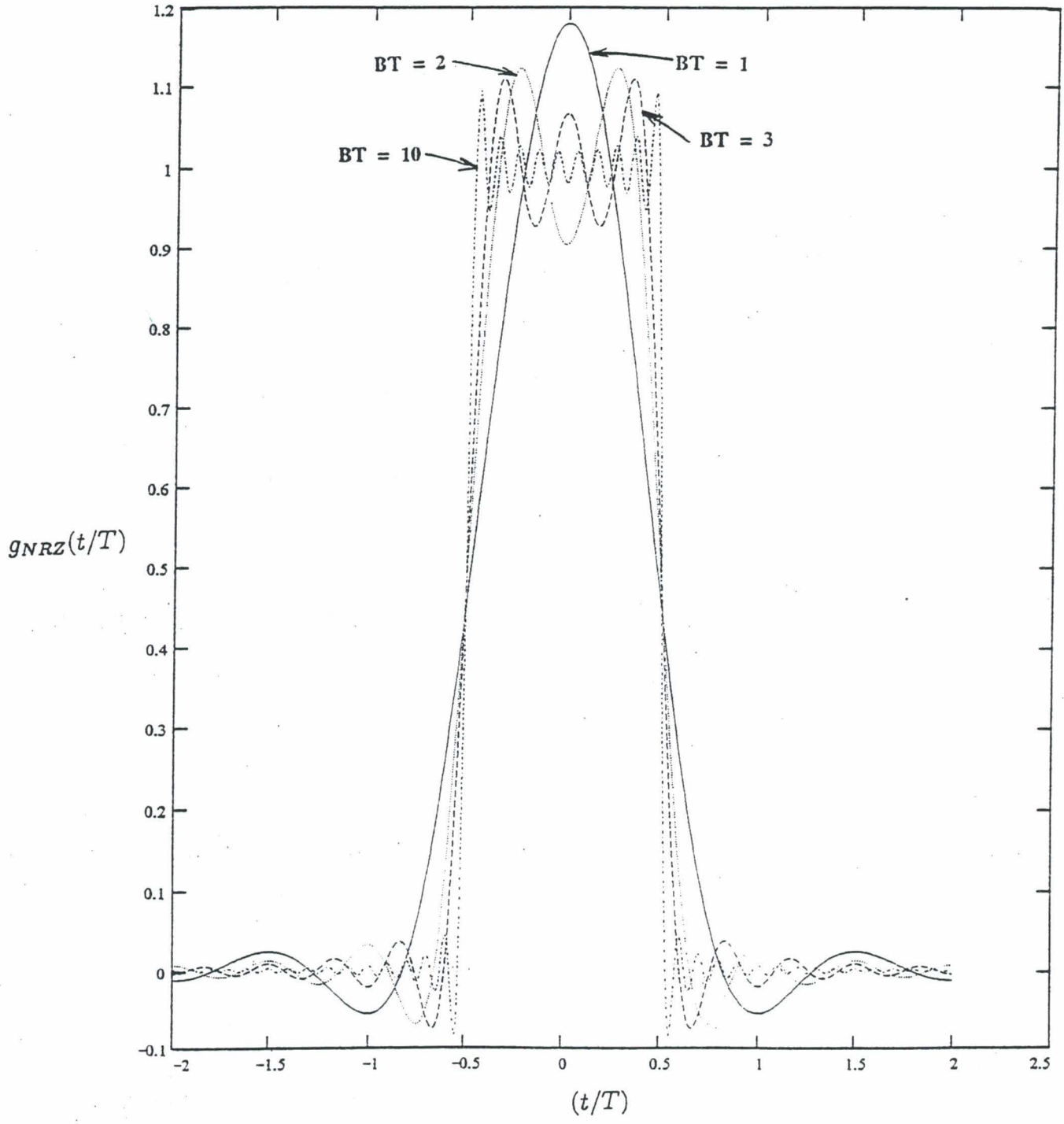

FIGURE 2

Output Response of the Ideal Filter to NRZ Pulse for various values of BT

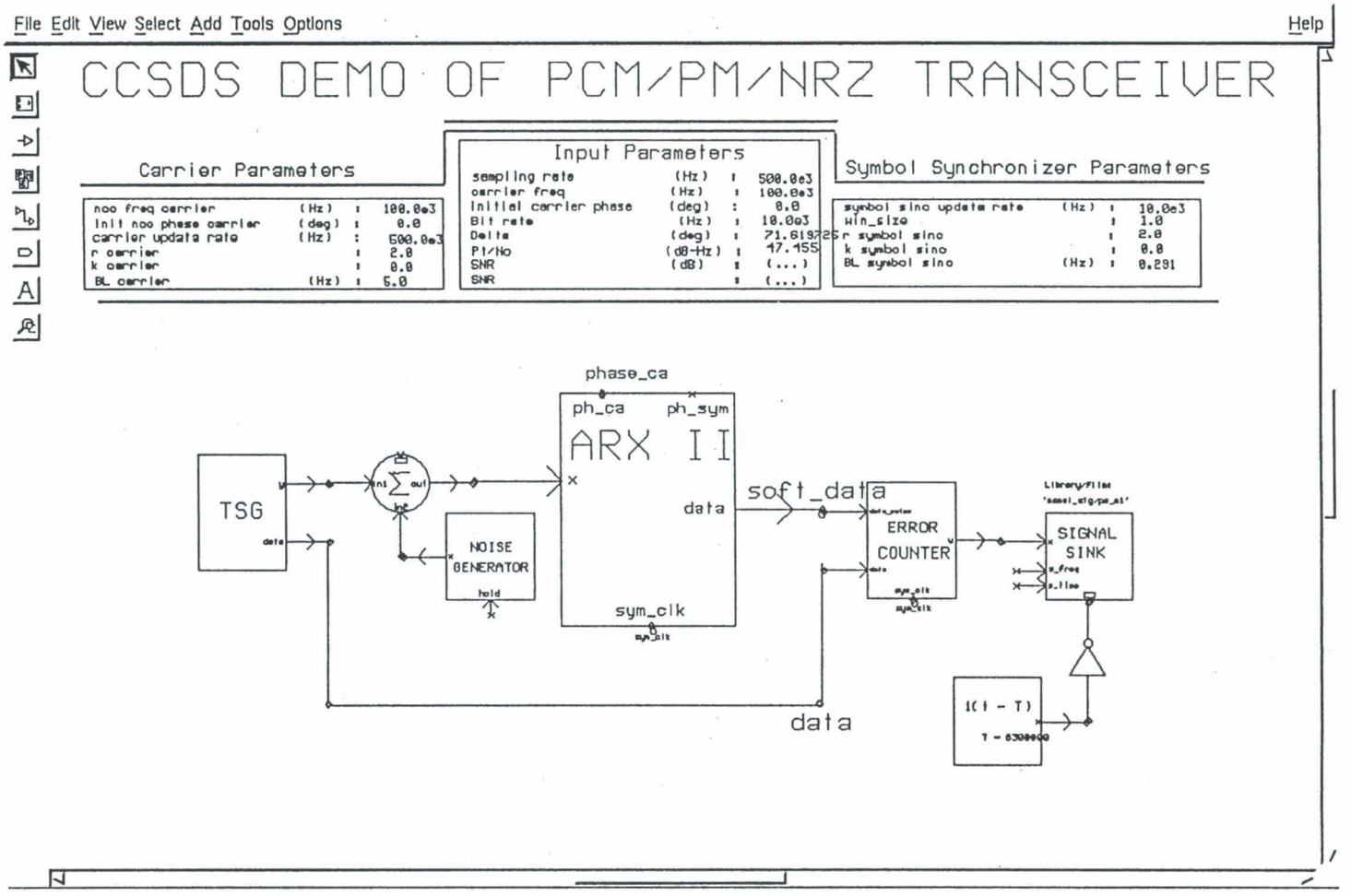

FIGURE 3

Block Diagram of PCM/PM/NRZ Receiver

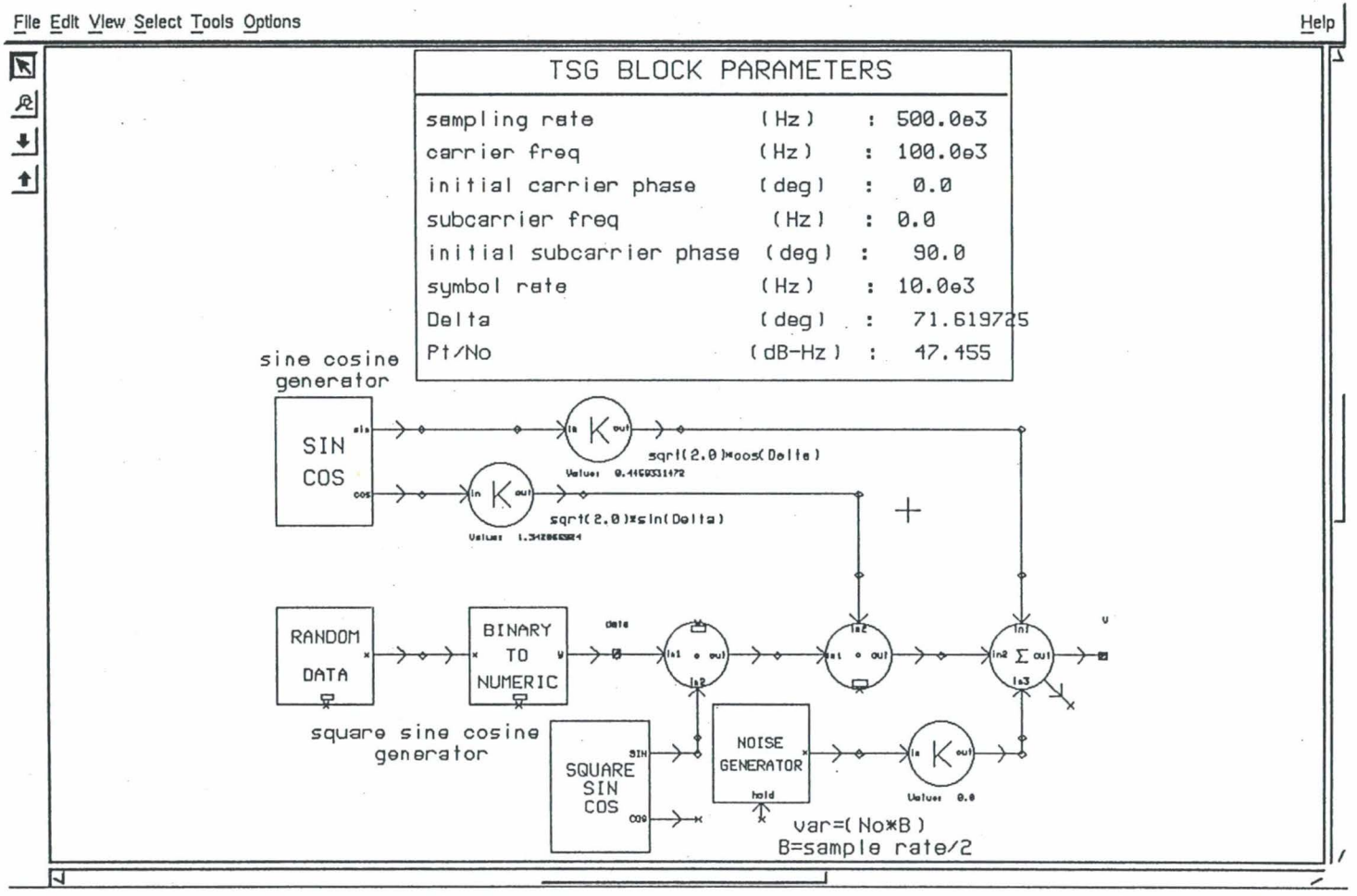

FIGURE 4

Test Signal Generator (TSG) Block Diagram

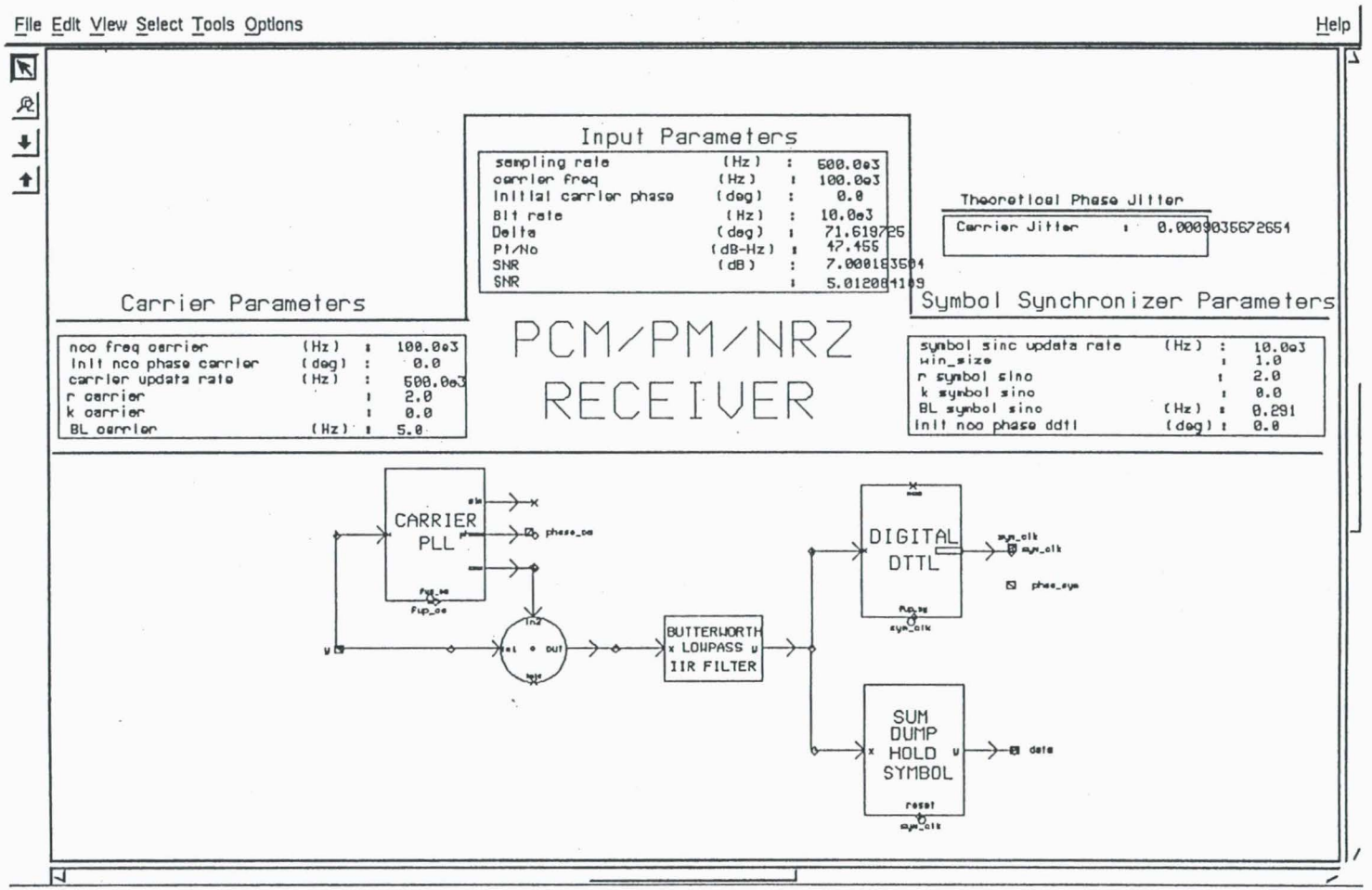

FIGURE 5

Advanced Receiver (ARX) Block Diagram

PCM/PM/NRZ

Unbalanced Data

(m=1.25 rad, Rs=10000 Hz, fs=500000 Hz, BL=5 Hz, 2.BL/Rs=0.001)

Prob. of Mark	Eb/No	Pt/No	# of Iterations	Nbar	Pe	Pe theory
0.5	7	47.455	6,600,000	119.333333	9.040E-04	7.727E-04
0.5	8	48.455	28,200,000	127	2.252E-04	1.909E-04
0.5	9	49.455	150,000,000	133.666667	4.456E-05	3.363E-05
0.5	10	50.455	1,300,000,000	132	5.077E-06	3.872E-05
0.45	7	47.498	6,600,000	292	2.212E-03	1.100E-03
0.45	8	48.498	25,200,000	427	8.472E-04	3.100E-04
0.45	9	49.498	80,200,000	440	2.743E-04	6.600E-05
0.45	10	50.498	500,200,000	605	6.048E-05	1.100E-05
0.4	7	47.632	6,600,000	1.27E+03	9.621E-03	5.400E-03
0.4	8	48.632	10,000,000	1.02E+03	5.100E-03	3.250E-03
0.4	9	49.632	15,000,000	625	2.083E-03	2.000E-03
0.4	10	50.632	25,000,000	404	8.080E-04	1.500E-03

TABLE 1

Simulation Data and Results for PCM/PM/NRZ Unbalanced Data

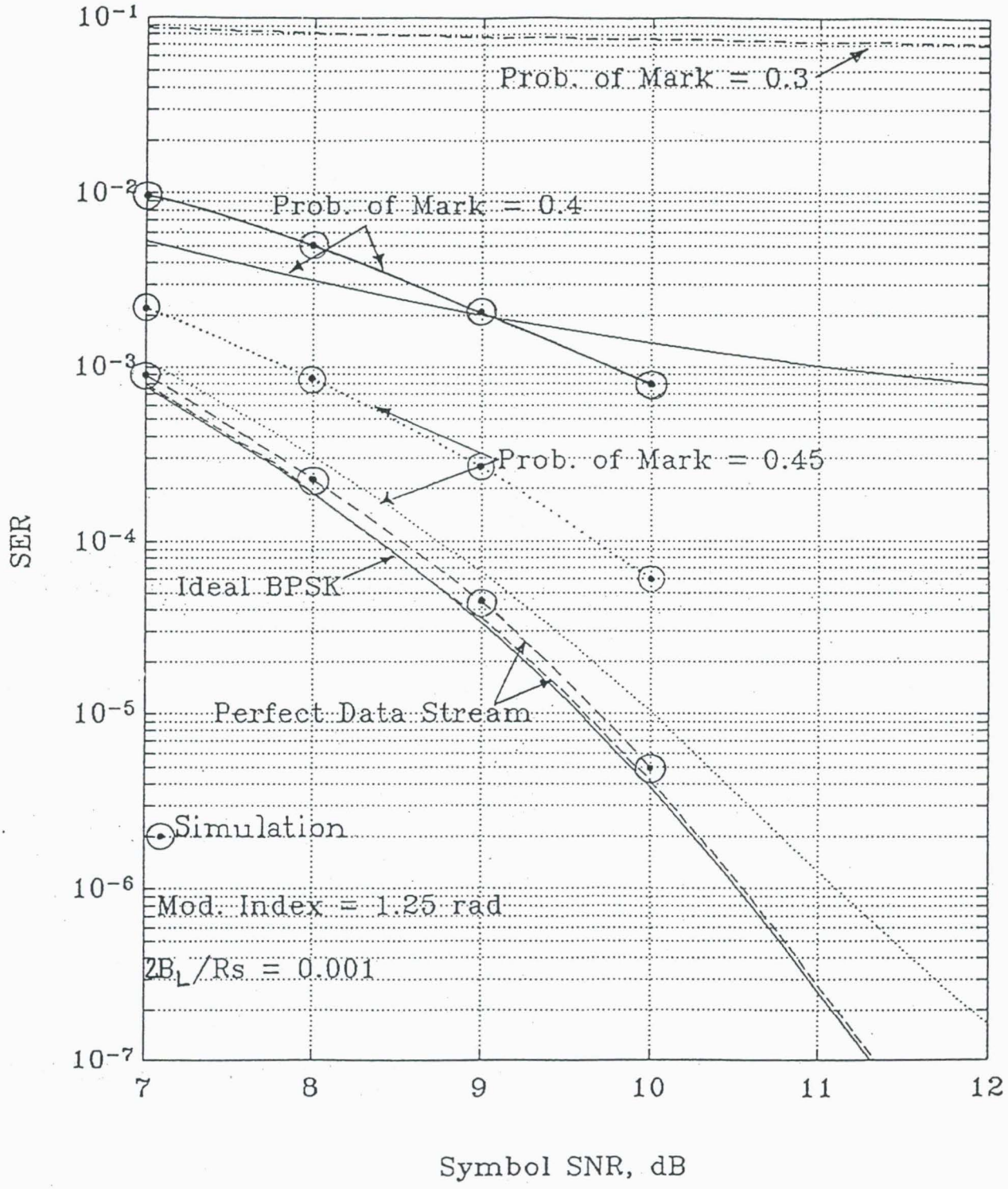

FIGURE 6

Theory and Simulation SER vs. Symbol SNR for PCM/PM/NRZ Unbalanced Data

PCM/PM/NRZ

Band-Limited Channel

(m=1.25 rad, Probability of Mark=0.5, Rs=10000 Hz, fs=500000 Hz, BL=5 Hz, 2.BL/Rs=0.001)

BT	Eb/No	Pt/No	# of Iterations	Nbar	Pe	Pe theory
1	7	47.455	6,600,000	387	2.932E-03	1.800E-03
1	8	48.455	11,000,000	206.333333	9.379E-04	5.800E-04
1	9	49.455	30,000,000	126.5	2.108E-04	1.700E-04
1	10	50.455	160,000,000	104.5	3.266E-05	3.300E-05
2	7	47.455	6,600,000	172.333333	1.306E-03	9.200E-04
2	8	48.455	21,000,000	146.5	3.488E-04	2.500E-04
2	9	49.455	105,000,000	157	7.476E-05	4.830E-05
2	10	50.455	800,000,000	137	8.563E-06	6.500E-06
3	7	47.455	6,600,000	146.333333	1.109E-03	8.600E-04
3	8	48.455	22,600,000	131	2.898E-04	2.300E-04
3	9	49.455	114,000,000	138	6.053E-05	4.400E-05
3	10	50.455	800,000,000	106	6.625E-06	5.600E-06

TABLE 2

Simulation Data and Results for PCM/PM/NRZ Band-Limited Channel

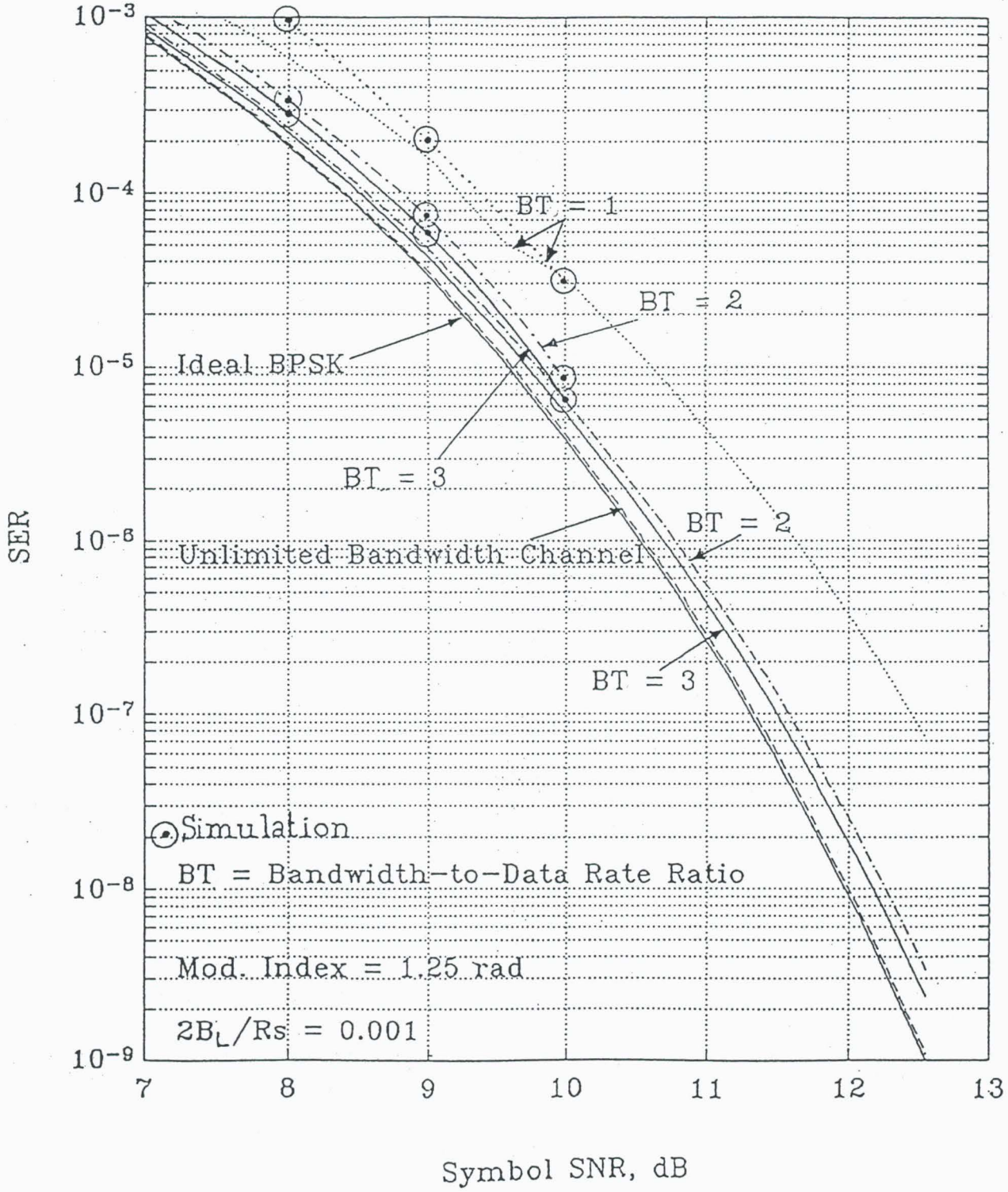

FIGURE 7

Theory and Simulation SER vs. Symbol SNR for PCM/PM/NRZ Bandlimited Channel

CROSS-TALK IN QPSK COMMUNICATION SYSTEMS[1]

Tien Manh Nguyen and Yvette Owens
National Aeronautics and Space Administration
Jet Propulsion Laboratory
California Institute of Technology
4800 Oak Grove Drive
Pasadena, CA 91109

ABSTRACT

This paper investigates the effects of cross-talk on the Bit Error Rate (BER) performance of QPSK communication systems. There are four different sources that can cause cross-talk in QPSK systems, namely, a band-limited channel, asymmetry in filters, phase imbalance between the channels, and imperfect carrier tracking. This paper emphasizes the last two problems (where either phase imbalance in the local VCOs or imperfect carrier tracking exists). The BER is derived as a function of phase imbalance (or phase error caused by imperfect carrier tracking) for both QPSK and Unbalanced QPSK (UQPSK). However, numerical results for QPSK only are presented. Numerical results are presented by a set of curves that can be used to: (1) write a specification for an acceptable phase imbalance between the In-phase (I) and Quadrature (Q) channels; and (2) specify the maximum allowable phase jitter produced by the carrier tracking loop.

[1] The work described in this paper was carried out at the Jet Propulsion Laboratory, California Institute of Technology, under contract with the National Aeronautics and Space Administration.

1. Introduction

The topic on cross-talk in QPSK communications systems has been treated by various authors [1-4]. Cross-talk can cause serious performance degradation in QPSK communications systems. There are four different sources that cause cross-talk to occur in QPSK systems. They are:

(1) Bandlimitted Channel: It is well-known that unfiltered QPSK signals have constant-amplitude envelope versus time characteristics. In ideal conditions, e.g., ideal limiting amplifier and unlimiting bandwidth channel, the system performance is the same as if the prelimiter filter and the limiting amplifier were absent. However, as the prelimiter bandwidth becomes narrower to the stage where significant signal energy is filtered away, the I and Q waveforms become seriously distorted and the signals acquire Amplitude Modulation (AM). The limiting amplifier removes the AM acquired during filtering, and in doing so further distorts the I and Q waveforms. As a result of this process, cross-talk between the waveforms occurs [1].

(2) Asymmetry in Filters: If the response of the filters (prelimiting filter or low pass filter, etc) are not symmetric about the center frequencies, a pure cosine (or sine) input signal will produce both sine and cosine terms at the output. As a result of this asymmetry, cross-talk between the I and Q channels has occurred [2].

(3) Phase Imbalanced Between the Channels: when the phase between the I and Q channels is not the same, the signal in the I channel can leak into the Q channel or vice versa. This process causes cross-talk between the channels.

(3) Imperfect Carrier Tracking: for QPSK systems, the imperfect carrier tracking can cause degradation from two sources. Firstly, it can cause degradation in the desired data signal by cos[F(t)] (where F(t) denotes the carrier tracking phase jitter) and secondly, it can cause crosstalk so that both the desired data and the opposite data channel appear in the desired data matched filter (where it can add or substract to the filter output)[3-4].

This paper investigates the last two cases, i.e., phase imbalanced between the local VCOs and imperfect carrier tracking. Probability of error for both QPSK and QPSK will be derived. However, numerical results are presented only for QPSK for future recommendations to the CCSDS.

2. Cross-talk Due to the Phase Imbalanced between the Channels

The phase imbalanced between the channels occurs When the phase shifter at the receiver is no longer operated in linear region due to aging or heating (see Figure 1). Due to the phase imbalanced between the channels, the signal in the I-channel leaks into the Q-channel causing potential performance degradation in that channel. In this section we will consider the case when the signal in the Q-channel leaks into the I-channel, and that the data rate on the I-channel is n times the data rate on the Q-channel.

Let's assume that the received signal plus noise is modeled as

$$x(t) = \sqrt{2P_I}d_I(t)\sin(\omega_C t) + \sqrt{2P_Q}d_Q(t)\cos(\omega_C t) + n(t) \quad (1)$$

where n(t) is the AGWN with one-sided power spectral density N_0, P_I and P_Q are the I and Q channel power, $d_I(t)$ and $d_Q(t)$ are data sequences with symbol duration of T_I and T_Q sec, respectively.
To simplify the analysis as well as the hardware for practical implementation, we will consider the case that

$$\frac{T_I}{T_Q} = \frac{R_Q}{R_I} \quad n,\ n\ an\ interger \quad (2)$$

where R_Q and R_I are respective data rate of each channel. If we assume that the signal in the Q-channel leaks into the I-channel and no signal in the I-channel gets into the Q-channel. Let f be the phase imbalanced between the I and Q channels. Using References 3 and 4, the conditional bit error probability in the I-channel can be shown to have the following form

$$P(E_I/\phi) = \frac{1}{2^n}\Sigma_{i=0}^{n}\binom{n}{i}Q\left[\sqrt{\frac{2E_{bI}}{N_0}}\cos(\phi) - \left(\frac{n-2i}{n}\right)\sqrt{\frac{2nE_{bQ}}{N_0}}\sin(\phi)\right] \quad (3)$$

where

$$\frac{E_{bI}}{N_0} = \frac{P_I T_I}{N_0} \quad Bit\ SNR\ in\ I\text{-}Channel \quad (4)$$

$$\frac{E_{bQ}}{N_0} = \frac{P_Q T_Q}{N_0} \quad Bit\ SNR\ in\ Q\text{-}Chann \quad (5)$$

Note that Eqn (3) was derived based on the assumption that the data formats for both channels are NRZ and that the symbol synchronization is perfect. Furthermore, the binomial coefficient appeared in Eqn (3) because there are n symbols of T_Q during T_I seconds, and there are i negative symbols with n-i positive symbols so that the matched filter output of the cross-product ($d_I(t)d_Q(t)$) is equal to (n-2i)/n. This value occurs with a probability

The conditional bit error probability in the Q channel can be shown to be

$$P(E_Q/\phi) = Q\left[\sqrt{\frac{2E_{bQ}}{N_0}}\right] \tag{6}$$

If we assume that the signal in the I-channel leaks into the Q-channel and no signal in the Q-channel gets into the I-channel, then we can show that the conditional bit error probability in the Q-channel is given by

$$P(E_Q/\phi) = \frac{1}{2}\left(Q\left[\sqrt{\frac{2E_{bQ}}{N_0}}\cos(\phi) - \sqrt{\frac{2nE_{bQ}}{N_0}}\sin(\phi)\right] + Q\left[\sqrt{\frac{2E_{bQ}}{N_0}}\cos(\phi) + \sqrt{\frac{2nE_{bQ}}{N_0}}\sin(\phi)\right]\right) \tag{7}$$

The conditional bit error probability in the I-channel becomes

$$P(E_I/\phi) = Q\left[\sqrt{\frac{2E_{bI}}{N_0}}\right] \tag{8}$$

Note that the Q(.) function is defined as

$$Q(x) = \frac{1}{\sqrt{2\pi}}\int_x^\infty e^{-\frac{t^2}{2}}dt \tag{9}$$

The relationship between the Q(.) funtion and the erfc(.) is given as

$$Q(x) = \frac{1}{2}erfc\left(\frac{x}{\sqrt{2}}\right) \tag{10}$$

For balanced power among the channels and equal data rate, i.e., QPSK (as contrast to Unbalanced QPSK, UQPSK), the conditional bit error probability in the I-channel, assuming the signal in the Q-channel leaks into the I-channel and no signal in the I-channel gets into the Q-channel, becomes

$$P(E_I/\phi) = \frac{1}{2}\left(Q\left[\sqrt{\frac{2E_b}{N_0}}\cos(\phi) - \sqrt{\frac{2E_b}{N_0}}\sin(\phi)\right] + Q\left[\sqrt{\frac{2E_b}{N_0}}\cos(\phi) + \sqrt{\frac{2E_b}{N_0}}\sin(\phi)\right]\right) \tag{11}$$

Similarly, the conditional bit error probability for the other case can be derived by setting n = 1, $E_{bQ}/N_0 = E_{bI}/N_0 = E_b/N_0$, and the result is identical to EQn (11).

3. Cross-talk Due to Imperfect Carrier Tracking

This case has been investigated in detail in [3-4]. AS mentioned earlier, imperfect carrier tracking can cause degradation from two sources, namely, the phase error degrades the desired data signal and the phase error also causes interchannel interference. If we assume perfect bit synchronization and NRZ data formats for both channels, the conditional probability of error in the I-channel for UQPSK is given by [3-4]

$$P(E_I/(\Phi(t) \equiv \phi)) = \frac{1}{2^n}\Sigma_{i=0}^{n}\binom{n}{i}Q\left[\sqrt{\frac{2E_{bI}}{N_0}}\cos(\phi) - \left(\frac{n-2i}{n}\right)\sqrt{\frac{2nE_{bQ}}{N_0}}\sin(\phi)\right] \tag{12}$$

and the conditional probability of bit error in the Q-channel for UQPSK is found to be [3-4]

$$P(E_Q/\Phi(t) \equiv \phi) = \frac{1}{2}\left(Q\left[\sqrt{\frac{2E_{bQ}}{N_0}}\cos(\phi) - \sqrt{\frac{2nE_{bQ}}{N_0}}\sin(\phi)\right] + Q\left[\sqrt{\frac{2E_{bQ}}{N_0}}\cos(\phi) + \sqrt{\frac{2nE_{bQ}}{N_0}}\sin(\phi)\right]\right) \tag{13}$$

For QPSK, the conditional bit error probability for I-channel becomes identical to the Q-channel and it is given by

$$P(E/\Phi(t) \equiv \phi) = \frac{1}{2}\left(Q\left[\sqrt{\frac{2E_b}{N_0}}\cos(\phi) - \sqrt{\frac{2E_b}{N_0}}\sin(\phi)\right] + Q\left[\sqrt{\frac{2E_b}{N_0}}\cos(\phi) + \sqrt{\frac{2E_b}{N_0}}\sin(\phi)\right]\right) \tag{14}$$

4. Numerical Results

Due to common interest in the CCSDS community, numerical results for QPSK are presented in this section. For this particular case the conditional bit error probability for phase imbalanced is identical for imperfect carrier tracking. However, for phase imbalanced case, only one channel is affected by the phase imbalanced depending on which channel is off as compared to the other channel. Since we are concerned with bit error rate degradation, hence Eqn (14) is important in the investigation of the effect of crosstalk in QPSK systems. Plot of Eqn (14) is shown in Figure 2. This figure plot the Bit Error Rate (BER) as a function of bit SNR with the phase imbalanced (or phase jitter) as a parameter. The numerical results show that as the phase imbalanced (or phase jitter) increases, the BER performance degradation also increases. Table 1

summarizes the results for various values of phase imbalanced and BERs.

5. Conclusions and Recommendations

Based on the numerical results presented in Figure 1 and Table 1, it is clear that when the phase imbalanced or phase jitter greater than 2 degrees, the bit SNR degradation is greater than or equal to 0.1 dB for BER $\leq 10^{-3}$. Therefore, in order to keep the bit SNR degradation due to the phase imbalanced less than 0.1 dB, the phase imbalanced between the I and Q channels should be kept less than or equal to 2 degrees.

Table 1: Bit SNR Degradation for Various Values of Phase Imbalanced or Phase Jitter

Phase Imbalanced (Degree)	Bit SNR Degradation		
	BER=10^{-3}	BER=10^{-4}	BER=10^{-5}
2	0.10 dB	0.10 dB	0.11 dB
4	0.25 dB	0.30 dB	0.35 dB
6	0.50 dB	0.62 dB	0.70 dB
8	0.85 dB	0.95 dB	1.07 dB

References

[1] K. Feher, Digital Communications, Satellite/Earth Station Engineering, Prentice-Hall, Englewood Cliffs, New Jersey, 1983

[2] L. B. Milstein, Digital Communications Systems, unpublished note, University of California San Diego, La Jolla, CA, 1981.

[3] Osborne, H. C., "Effects of Noisy Reference on Coherent Detection of Unbalanced Signals", Proceedings NTC 1978, Birmingham, Ala., December 3-5, 1978.

[4] J. K. Holmes, Coherent Communications Systems, John Wiley & Son, New York, 1982.

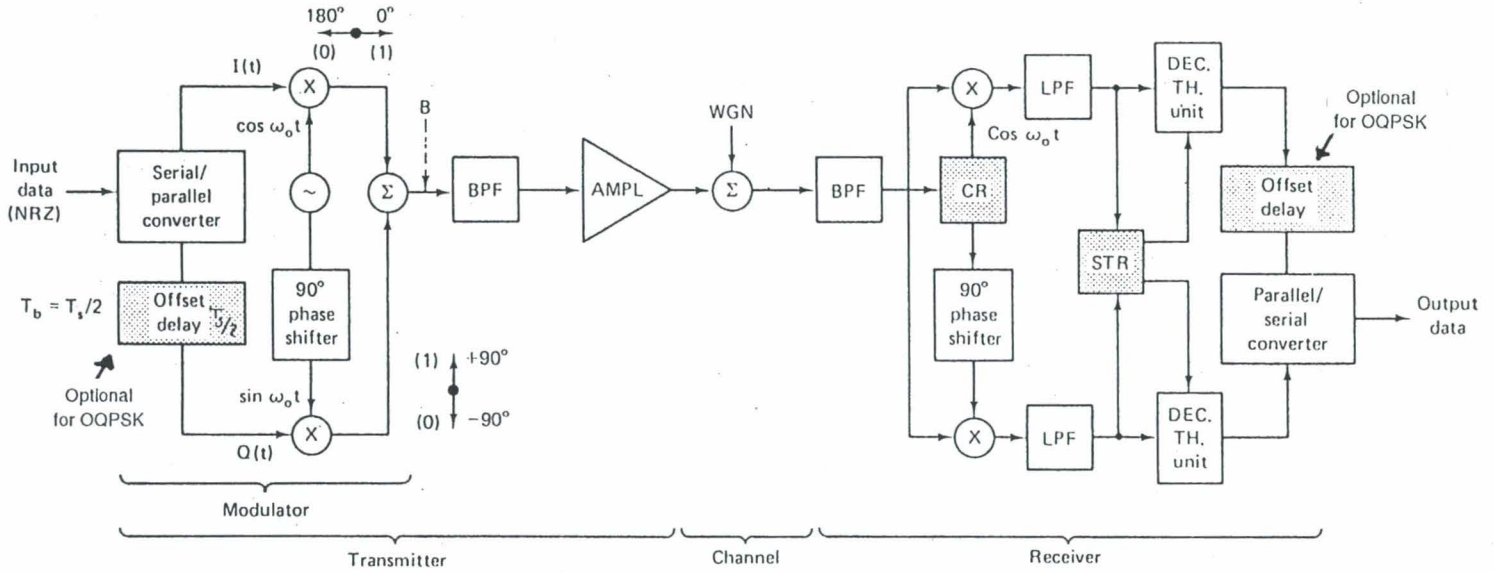

Figure 1. Typical QPSK Communications Modem-The Delay is Optional for Offset QPSK Systems

FIGURE 2. BIT ERROR RATE PROBABILITY VS Eb/N0 FOR VARIOUS VALUES OF PHASE IMBALANCED BETWEEN THE CHANNELS

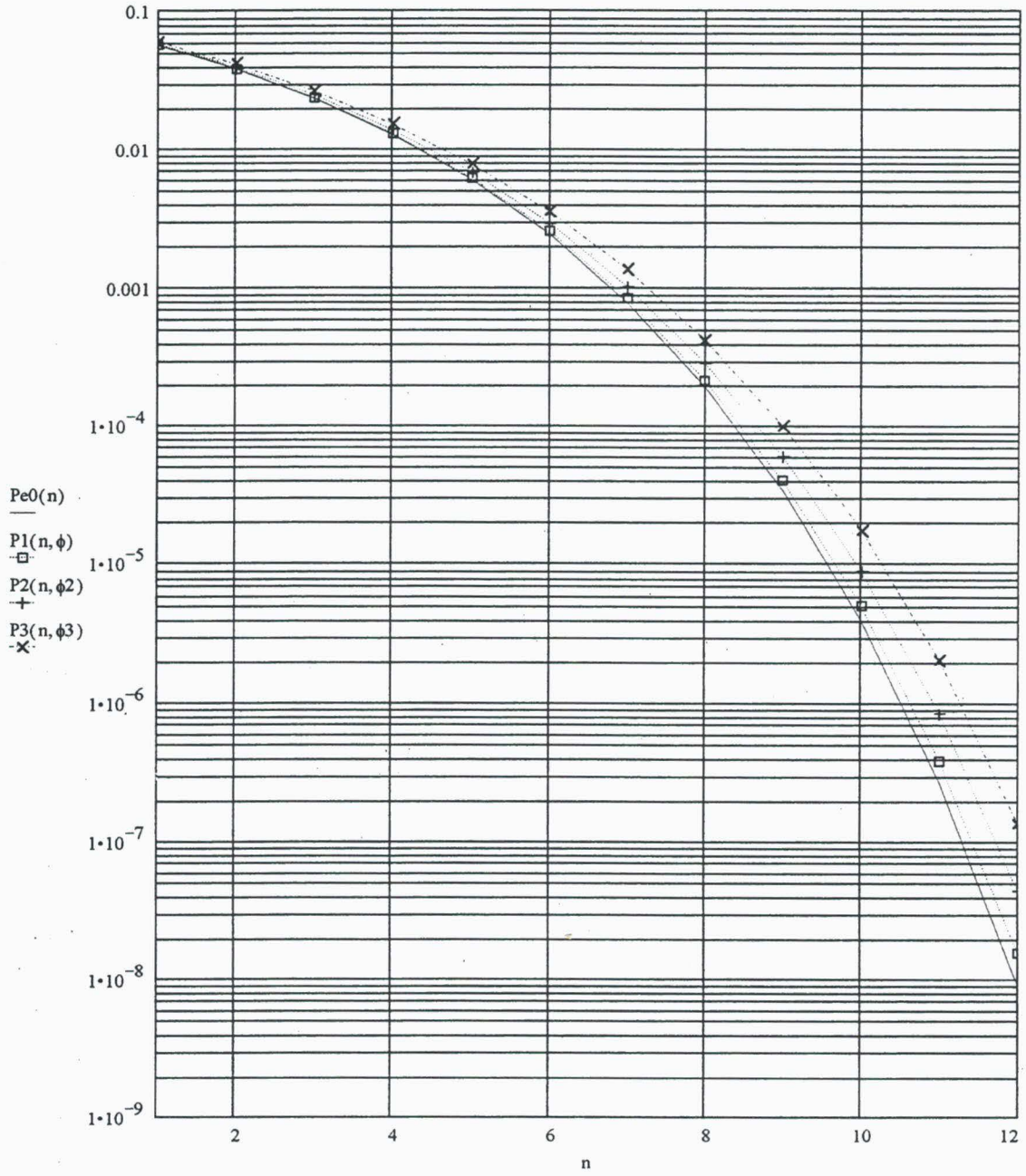

LEGEND:

Pe0(n) = BER for Ideal Case

P1(n,ϕ1) = BER at 2 Deg Phase imbalanced;

P2(n,ϕ2.) = BER at 4 Deg Phase imbalanced;

P3(n,ϕ3) = BER at 6 Deg Phase imbalanced

n = Bit SNR in dB

Figure 3. Average Bit Error Rate Probability vs Eb/No for Various Values of RMS Phase Jitter

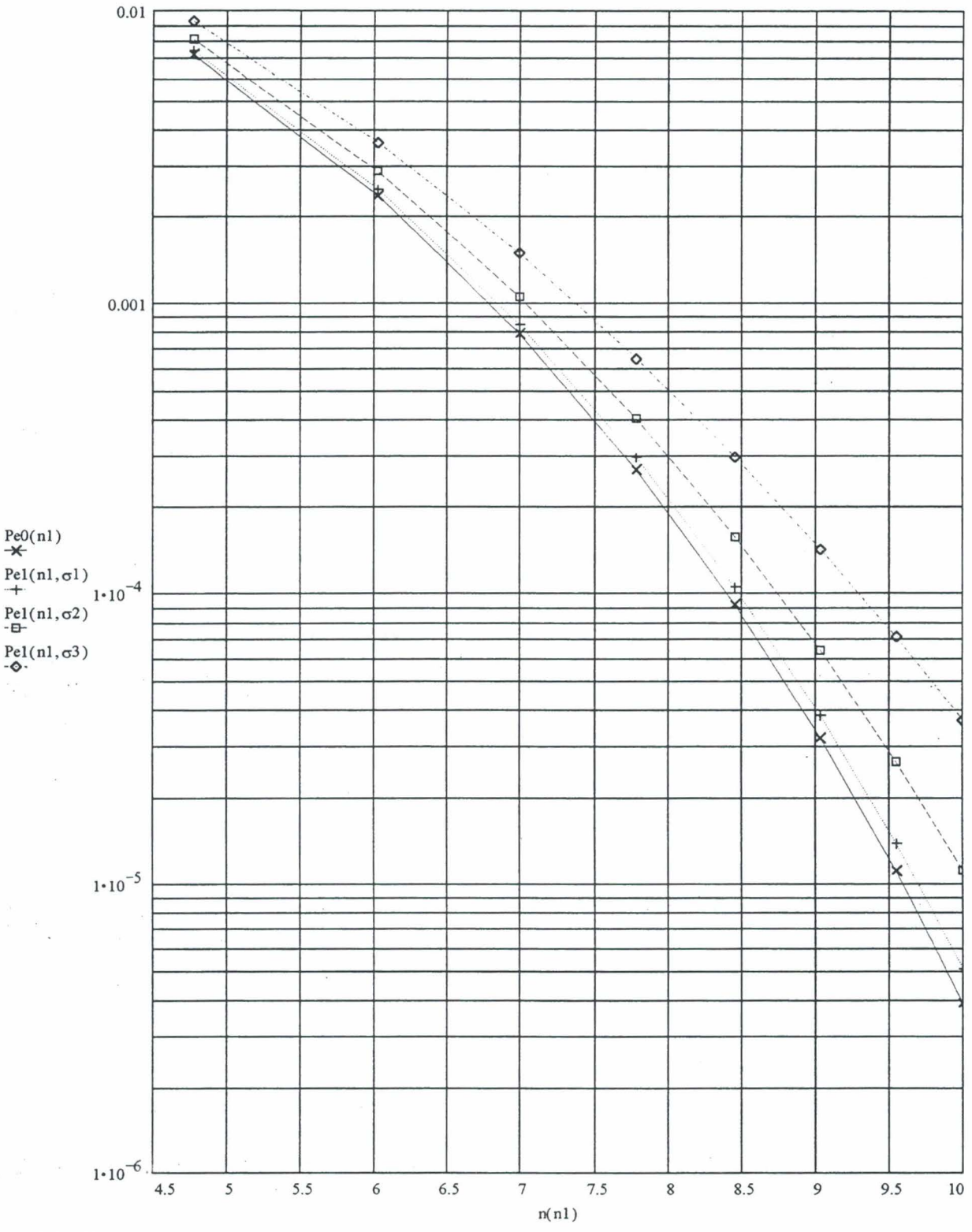

LEGEND:

Pe0(n1) = BER for Ideal Case

Pe1(n1,σ1) = Average BER at 2 Deg RMS Phase Jitter

Pe1(n1,σ2) = Average BER at 4 Deg RMS Phase Jitter

Pe1(n1,σ3) = Average BER at 6 Deg RMS Phase Jitter

n(n1) = Bit SNR in dB

THE EFFECT ON A BPSK SIGNAL SPECTRUM OF BIT ASYMMETRY OF THE MODULATION DATA STREAM

Jean-Luc Gerner
European Space Agency
European Space Research and Technology Centre
2200 AG Noordwijk, The Netherlands

ABSTRACT

In the crowded environment of the TT & C bands, which includes the 2-GHz band, Binary Phase Shift Key (BPSK) modulation is an attractive scheme for transmission at medium to high data rates, provided that the imperfections of the modulation process do not have a detrimental effect on the natural compactness of the spectrum. One of the most pernicious causes of bandwidth expansion for BPSK is the mark-to-space imbalance of the data stream when it is input to the modulator. This paper computes the level of spurious emission in the BPSK spectrum resulting from bit asymmetry. It shows that good engineering practice allows one to design transmitters with a bit asymmetry low enough to avoid interference with other users. The exception is in the 2-GHz band, where, it is explained, due to the vicinity of the near earth and deep space bands, full protection of deep space ground receivers cannot be ensured in most cases, and coordination between near earth and deep space services is necessary.

2. INTRODUCTION

BPSK is probably one of the most popular modulation schemes for space telecommunications where medium to high data transmission rates are required. Being a 'suppressed carrier' type of modulation scheme, it offers the best performances in terms of data throughput by allowing all the available power to the data transmission. Both modulator and demodulator are easy to implement and the spectral compactness is good provided that adequate filtering is applied. Bandwidth compactness is essential to an efficient sharing of the available bandwidth between space communications users. Therefore, BPSK is a promising modulation scheme. However, there may exist within the modulator chain factors of expansion of the occupied bandwidth. A good engineering approach shall consider these factors and investigate ways to reduce as much as possible their detrimental effect to the spectral bandwidth of the transmitted signal. The major contributors to bandwidth expansion are:

- *Non-linearities in the transmit chain.* AM/PM or AM/AM or both in the high power amplifier create an expansion of the BPSK continuous spectrum by the raising of distant sidelobes. This effect is dealt with by an increase of the amplifier back-off (at the expense of power efficiency) and/or with proper filtering of these distant lobes at the output of the power amplifier.

- *Mark-to-Space Imbalance of the data.* Imbalance between the duration of the 'ones' and of the 'zeros' of the data stream create a spike in the BPSK spectrum at the carrier frequency (carrier regeneration, due to the DC offset on the input data) as well interlobes spikes which envelope is much wider than the actual useful spectrum. The better 'ones' and 'zeros' are balanced, the lower these spikes are. It has been show in the past (Eureca), that such spikes occurring in a transmitter operating in the space-earth band 2.2-2.29 GHz may expand into the deep space band 2.29-2.30 GHz and severely interfere with communications in that band.

In the course of the coming paragraphs, we will analyze how this bit asymmetry on the NRZ encoded data can generate spikes in the BPSK modulated spectrum.

3. SPECTRUM OF A BPSK SIGNAL WITH DATA BIT ASYMMETRY

3.1 GENERAL FORMULA

BPSK modulation is the product of a pure carrier with a stream of NRZ encoded data that we will consider random for the purpose of this study. The modulated signal can be expressed as:

$$s(t) = d(t) \times \sin \omega_0 t$$

where $d(t) = \pm 1$ pseudo random

This modulation process is equivalent to a translation to the frequency ω_0 of the baseband spectrum of d(t). Therefore, we can perform the whole computation on the baseband signal without any loss of generality.

The asymmetrical data signal can be considered as the sum of an ideally balanced signal and of a stream of pulses as show on the picture below.

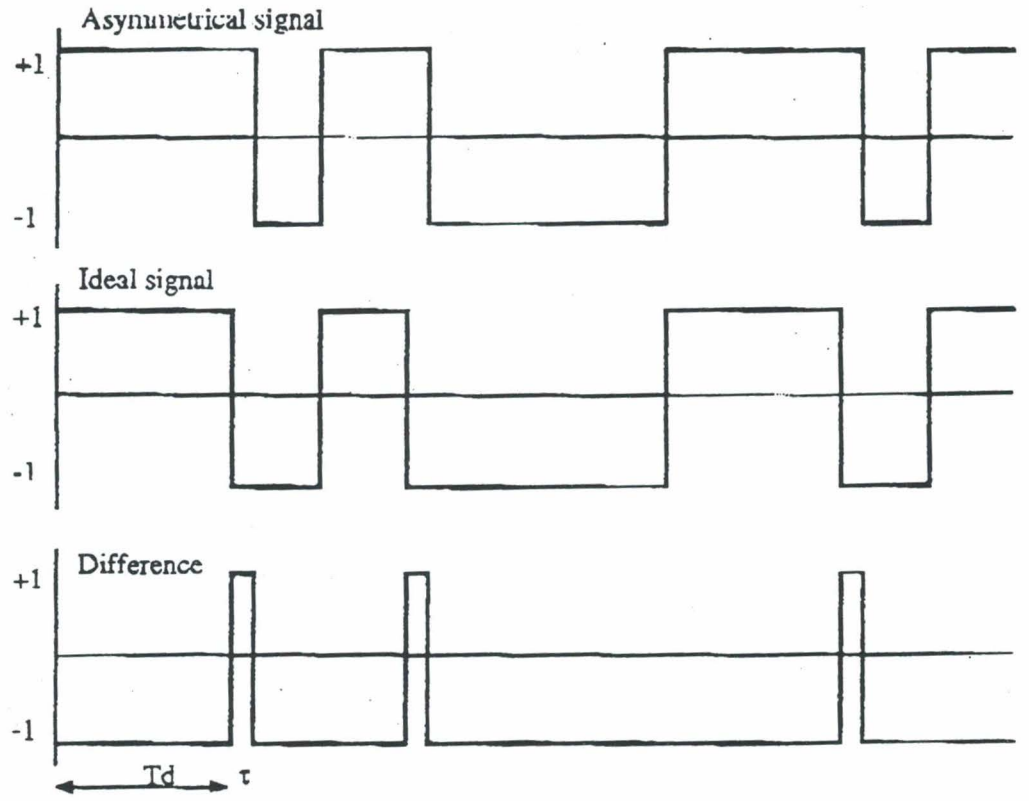

Synchronizing the data bits rising edges, the difference between ideal signal and actual asymmetrical signal is a series of pulses of width τ.

The durations of 'mark' and of 'space' being respectively T_1 and T_2, the data stream asymmetry can be defined as:

$$\alpha = 2 \times |T_1 - T_2| / (T_1 + T_2) = |T_1 - T_2| / T_d$$

and

$$\tau = (T_1 - T_d) - (T_d - T_2)$$

thus the bit asymmetry α can be expressed in function of the difference pulse width τ and the average bit duration T_d as:

$$\alpha = 2\tau/T_d$$

The asymmetrical signal is the sum of an 'ideal signal' and a 'difference signal'. The data bits being assumed pseudo-random, the spectrum of the ideal signal does not include discrete spectral lines. It will be referred to as $G_{BPSK}(f)$ in the rest of this analysis.

For the 'difference signal', a pulse occurs at every transition of the data bits from +1 to -1. The average occurrence of such a transition is 1/4. In other words, there are an average of $F_d/4$ pulses per second, where F_d is the data rate.

The 'difference signal' is composed of two states:

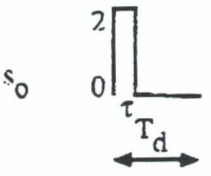

probability $p_0 = 0.25$

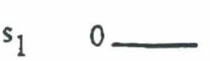

probability $p_1 = 0.75$

The spectrum $S_1(f)$ of s_1 is null.

The spectrum $G_m(f)$ of the 'difference signal' can be expressed as ([1], page 252, 10.10):

$$G_m(f) = \frac{1}{T_d}(p_0 |S_0(f)|^2) - \frac{1}{T_d}|p_0 S_0(f)|^2 + \frac{1}{T_d^2}|p_0 S_0(f)|^2 \sum_{k=-\infty}^{k=+\infty} \delta(f - \frac{k}{T_d}) \qquad (1)$$

$S_o(f)$ can be easily computed as:

$$|S_o(f)| = 2\frac{\sin \pi f \tau}{\pi f} \qquad (2)$$

and (1) can be rearranged as:

$$G_m(f) = \frac{1}{T_d}(p_o - p_o^2)\,|S_o(f)|^2 + \frac{p_o^2}{T_d^2}\sum_{k=-\infty}^{k=+\infty} S_o^2\left(\frac{k}{T_d}\right)\delta\left(f - \frac{k}{T_d}\right) \qquad (3)$$

$$G_m(f) = \quad A(f) \quad + \quad B(f)$$

The 'difference signal' spectrum $G_m(f)$ is the 'spurious spectrum' due to data bits asymmetry, superimposed to the spectrum of the ideal BPSK signal. Like the well know RZ signal, the 'difference signal' is a combination of random and of periodic components, which explains that the spectrum $G_m(f)$ is composed of a continuous component A(f) and of a discrete component B(f) (series of spectral lines).

3.2. CONTINUOUS COMPONENT OF THE 'SPURIOUS SPECTRUM'

The spectrum A(f) is of the form sinx/x, with the first zeros at a frequency $\pm 1/\tau$ from the carrier. From (2) and (3), A(f) can be rearranged as:

$$A(f) = (4/T_d)\,(p_o - p_o^2)\,\tau^2\,(\sin \pi\tau f/\pi\tau f)^2 \qquad (4)$$

Let P_A be the total power contained in A(f). We have:

$$P_A = \int_{-\infty}^{+\infty} A(f)\,df$$

$$= \frac{4}{T_d}(p_o - p_o^2)\,\tau^2 \int_{-\infty}^{+\infty} \left(\frac{\sin \pi\tau f}{\pi\tau f}\right)^2 df$$

$$= 4\,(p_o - p_o^2)\,\frac{\tau}{T_d}$$

The total power contained in A(f) versus the bit asymmetry is thus:

$$P_A = 2\,(p_o - p_o^2)\,\alpha = 0.375\,\alpha \qquad (5)$$

For a bit asymmetry of 1%, P_A represents less than 0.4% of the total power (less than 0.02 dB loss on the useful signal power).

A(f) close to the carrier frequency

The power density of A(f) at the top of the main lobe is:

$$A(0) = (4/T_d)(p_0 - p_0^2)\tau^2 = 0.75 \times \tau^2/T_d \qquad (6)$$

since $p_0 = 0.25$

We will now evaluate the contribution of the 'spurious' A(f) with regard to the spectrum of the ideal BPSK signal $G_{BPSK}(f)$.

We know that:

$$G_{BPSK}(f) = T_d (\sin\pi T_d f/\pi T_d f)^2 \qquad (7)$$

and

$$G_{BPSK}(0) = T_d$$

The relative level of A(f) with regard to $G_{BPSK}(f)$ is, at the center frequency:

$$a_{dB} = A(0)/G_{BPSK}(0) = -7.2 + 20 \text{ Log } (\alpha) \qquad (8)$$

α being the data bit asymmetry as defined before: $\alpha = 2\tau/T_d$

The plot of a_{dB} versus bit asymmetry α is shown on figure 1. It can be seen that, for example, a bit asymmetry α = 1% will generate a continuous spectrum with a main lobe 47 dB below the main lobe of the useful spectrum. This level is low enough to guarantee that no significant degradation is to be expected in the carrier recovery loop of the receiver.

A(f) far from the carrier frequency

To evaluate the potential interference due to the 'continuous' spectrum A(f) to adjacent channels, we will evaluate the relative power density of A(f) with regard to $G_{BPSK}(f)$ far from the carrier. A simple way to do it, and still accurate enough, is to compare the envelopes of the two spectra.

Let [A(f)] be the envelope of A(f). From (4), we obtain:

$$[A(f)] = \frac{4(p_0 - p_0^2)}{\pi^2 T_d} \frac{1}{f^2} \qquad (9)$$

Similarly, we compute the envelope equation of the useful signal spectrum $G_{BPSK}(f)$ from (7):

$$[G_{BPSK}(f)] = \frac{1}{\pi^2 T_d} \frac{1}{f^2} \qquad (10)$$

The peak power density of A(f) sidelobes far from the center frequency, relative to $G_{BPSK}(f)$ sidelobes peak power density, at a given frequency is expressed by the ratio of the envelopes of the two spectra:

$$\frac{[A(f)]}{[G_{BPSK}(f)]} = 4 (p_o - p_o^2) \; --1.25dB \qquad (11)$$

The power density maxima of A(f) far from the center frequency remain always below those of the useful signal by 1.25 dB, regardless of the data bit asymmetry. Therefore, we can assess that the generation of **the continuous spectrum A(f) due to data bit asymmetry is not a cause of interference into adjacent channels.**

3.3. DISCRETE COMPONENT OF THE 'SPURIOUS SPECTRUM'

The component B(f) of $G_m(f)$ is a series of spectral lines spaced every F_d. From (2) and (3), we can write:

$$B(f) = \frac{P_o^2}{T_d^2} \sum_{k=-\infty}^{+\infty} \tau^2 \cdot \frac{(\sin \pi \tau \frac{k}{T_d})^2}{(\pi \tau \frac{k}{T_d})^2} \delta(f - \frac{k}{T_d})$$

The envelope is, like with A(f), determined by $S_o(f)$, thus in the form sinx/x, with the first zeros $1/\tau$ away from the carrier.

B(f) at the carrier frequency

The highest spectral line is at the center frequency (k=0). Its level is:

$$B(0) = 4 p_o^2 / T_d^2 \; S_o^2(0) = 4 p_o^2 \tau^2 / T_d^2 \qquad (9)$$

$$B(0) = -12 + 20 \text{ Log } \alpha \quad \text{dB} \qquad (10)$$

B(0) represents the level, with regard to the unmodulated carrier, of the spurious line at the center frequency due to bit asymmetry. For example, a bit asymmetry $\alpha = 1\%$ will regenerate the carrier at a level of -52 dBc.

Figure 2 plots the variations of B(0) with the bit asymmetry.

For what concerns the impact on link performances of this spectral line B(0) at the carrier frequency, the reader can refer to references [2] and [3].

B(f) far from the carrier frequency

As already demonstrated above, the envelope of the spectral lines of B(f) is a sinx/x function which main lobe width is $\pm 1/\tau$, τ being small as compared with the data bit duration T_d, for all values of the bit asymmetry α below 10%, we can consider all spectral lines of B(f) within the band to be analyzed as constant and equal to B(0). According to the equation:

$$1/\tau = (2/\alpha) F_d$$

the first null of B(f) is at:

$$1/\tau = 400 F_d \quad \text{for } \alpha = 0.5\,\%$$

$$1/\tau = 20 F_d \quad \text{for } \alpha = 10\%$$

4. POTENTIAL INTERFERENCE PROBLEMS DUE TO DATA BIT ASYMMETRY

4.1. POWER FLUX DENSITY ON EARTH SURFACE (IN-BAND)

The power density of $G_{BPSK}(f)$ around the center frequency is:

$$[G_{BPSK}(f)]_{\Delta f} = T_d \Delta f \qquad \text{integrated over a band } \Delta f << F_d$$

Radio Regulations define the maximum acceptable power flux density within a certain reference bandwidth Δf that can be radiated from space on the Earth surface. For instance, in the 2 GHz band, the reference bandwidth is Δf = 4kHz. This criterion is one of the dimensioning factors in the design of spacecraft telemetry transmissions to ground. Therefore, it is essential that the telemetry transmitter using BPSK modulation be designed in such a way that the level of the remnant carrier B(0) due to bit asymmetry does not become the driving factor. In other words:

$$B(0) < T_d \Delta f$$

In the case of S-Band (2 GHz), the usual highest bit rate is about F_d = 6 Mb/s. Hence.

$$B(0) < -32 \text{ dBc}$$

From fig. 2, we can see that this can be achieved for $\alpha < 10\%$, or $\tau < 0.05\ T_d$, which leads to $\tau < 9$ ns, easily achievable with today's technology.

In the case of Ku-Band (13 - 15 GHz), F_d may be as high as 200 Mb/s, whereas the Radio Regulations still make use of a reference bandwidth of Δf = 4 kHz.

In the Ku-Band case:

$$B(0) < -47 \text{ dBc}$$

From fig. 2, we can see that this requires that $\alpha < 15\%$, or $\tau < 0.0075\ T_d$, which leads to $\tau <$ 37.5 ps (picoseconds). This challenging requirement cannot be achieved with present technology.

4.2 OUT-OF-BAND EMISSIONS

CCSDS Recommendation 3.2.2 "Maximum permissible out-of-band spurious emissions for Category A Spacecraft Transmitters in the 2 GHz and 8 GHz Bands" was recently raised to 'red' level and is presently under Agengy revue. It recommends that these emissions do not exceed -60 dBc over the band 10 MHz - 10000 MHz. This requirement can be met in the case of bit asymmetry without special RF filtering provided that:

$$B(0) < -60\ dBc$$

or, according to (10):

$$\alpha < 0.4\ \%$$

It has been shown on existing hardware that, provided that resynchronization is performed into the transmitter on the data stream before entering the modulator, a mark-to-space unbalance of no more than 3ns can be achieved without excessive complexity. From the equation:

$$F_d = \alpha/2\tau$$

It comes that, with τ=3ns, no filtering is needed for data rates up to

$$F_d = 650\ kb/s$$

and at the maximum rate of F_d = 6 Mb/s, a 20 dB attenuation on the modulated spectrum is necessary to comply with CCSDS Rec. 3.2.2.

4.3. A SPECIFIC PROBLEM: PROTECTION OF THE DEEP SPACE BANDS

One typical example is the interference into the Deep Space ground stations receivers, operating in the 2.29 - 2.30 GHz band, from near Earth spacecraft which operate in the adjacent band 2.20 - 2.29 GHz.

Radio Regulations stipulate (AP28, Table II) that the spurious power at the input to the receiver of a Deep Space ground station should not exceed -222 dBw/Hz in the 2.29 - 2.30 GHz band. Taking the most critical case of a Deep Space ground station with an antenna diameter of 70 m, this translates into a **maximum power flux density at the Deep Space station antenna of -258dBw/m^2/Hz.**

A near earth orbiting spacecraft is required not to exceed a power flux density (PFD) of -154dBw/m^2/4kHz at the earth surface. When addressing discrete lines, this can be translated into -190dBw/m^2/Hz.

Let us take the practical case of a near earth spacecraft transmitting in BPSK at a rate of 3 Mb/s.

Let us assume that the transmit power P_t is such that the radiated PFD on the earth surface reaches the regulatory limit of -190 dBw/m^2/Hz. The power spectral density PSD at the output of the transmitter is:

$$PSD = P_t - 65 \text{ dBw/Hz} \qquad \text{for a PFD} = -190\text{dBw/m}^2\text{/Hz}$$

With a mark-to-space ratio τ of 3ns, the asymmetry α is 1.8% and, according to (10), the level of discrete lines is:

$$B(0) = P_t - 47 \text{ dBw}$$

According to CCSDS Rec 3.2.2, the out-of-band spikes will be at a level of P_t - 60 dbw, generating a PFD of -185dBw/m^2/Hz. 73dB above the limit derived from Radio Regs AP28. The additional protection can only be provided by the means of a band-reject filter. However, since at 2 GHz near earth and deep space bands are adjacent, such a filter is not feasible in many cases, especially for near earth transmissions in the upper part of the allocated band, and only part of the required attenuation can be ensured. In that case, coordination procedures need to be set up to avoid interference to deep space communications.

5. CONCLUSION

NRZ data asymmetry for BPSK modulation should be minimized in order to restrict as much as possible the level of unwanted interlobes spikes. A good engineering design allows in general to meet requirements for interference avoidance except when it comes to the protection of Deep Space bands. In that context, a case-by-case analysis is generally necessary and coordination may have to be considered.

6. REFERENCES

[1] Theorie de la Communication, J. Dupraz, Eyrolles 1973

[2] The Impact of NRZ Data Asymmetry on the Performance of a Space Telemetry System, Tien Manh Nguyen, JPL, CCSDS Working Paper 1990

[3] Note on CCSDS Recommendation Concerning Symmetry Required for Squarewave Modulating Waveforms, Rev.1, W. Schwarz, DLR, CCSDS Working Paper, Sept 1990

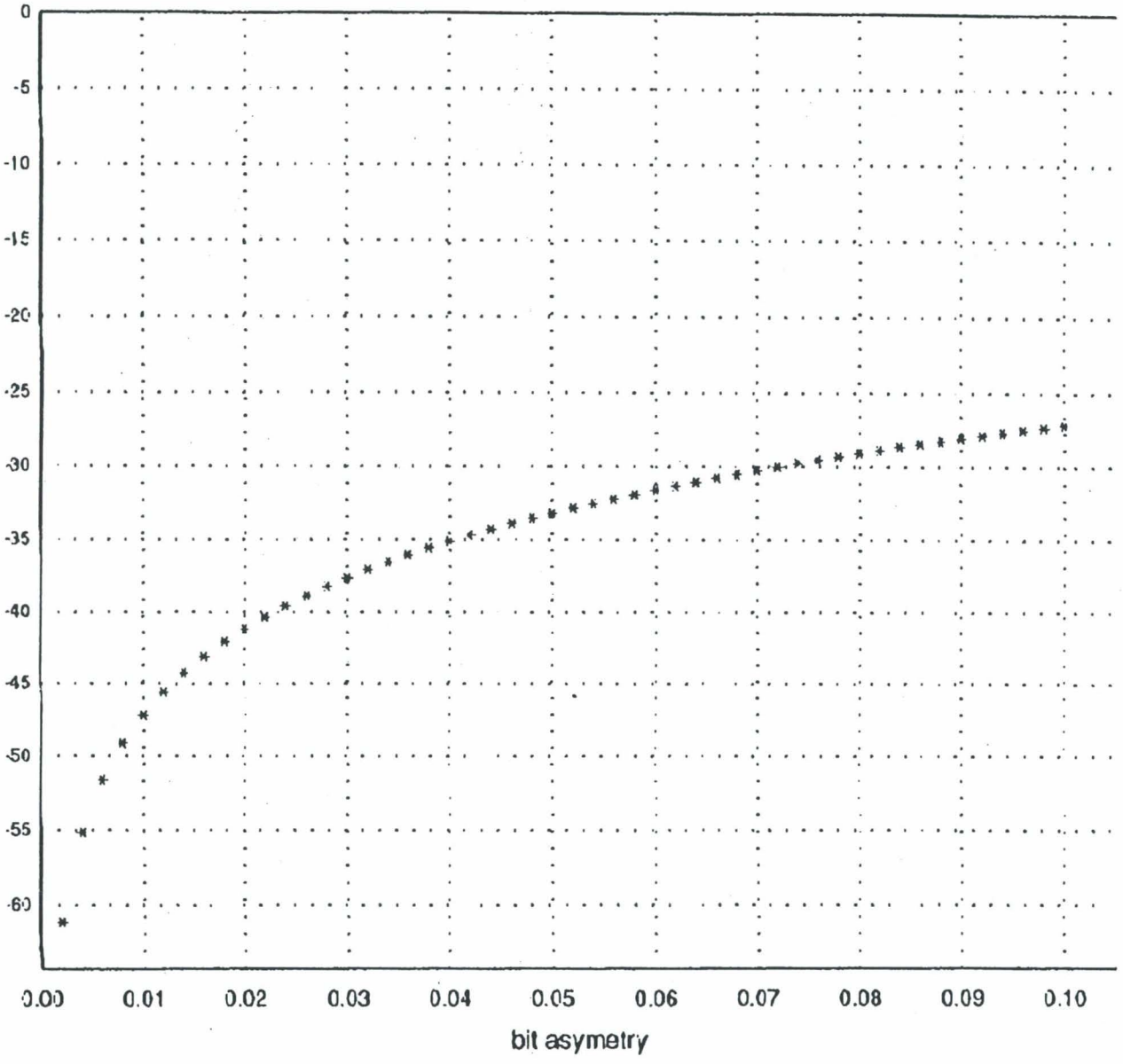

Fig. 1 : Variation of a(dB) with bit asymmetry

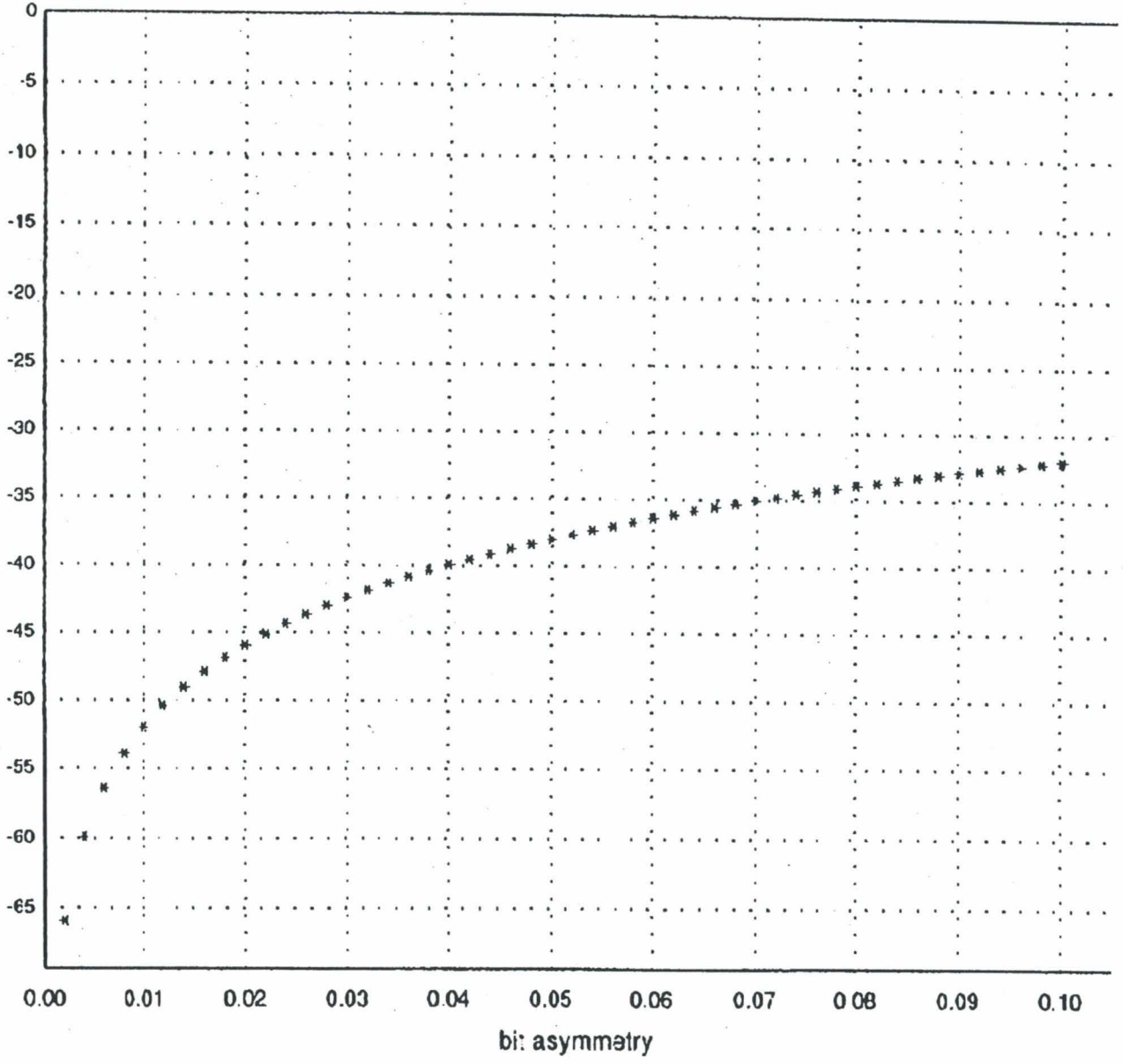

Fig. 2 : Variation of B(0) with bit asymmetry

SESSION 2

SYNCHRONIZATION

Minimum Symbol Transition Density on Earth-to-Space Links

S. Hinedi, T. Nguyen, and A. Anabtawi
National Aeronautics and Space Administration
Jet Propulsion Laboratory
California Institute of Technology
4800 Oak Grove Dr.
Pasadena, CA 91109

Abstract

This paper summarizes key results on the minimum modulated symbol transition density on Earth-to-Space links required by existing Command Detection Units (CDU's). The results are verified using computer simulations.

1 Introduction

Earth-to-Space links are typically characterized by high symbol signal-to-noise ratio (SNR) and low data rates ($7 - 500$ symbols per second). The uplink is uncoded and as a result, symbols and bits are identical. Existing transponders employ the Data Transition Tracking Loop (DTTL) in the Command Detection Unit (CDU) to perform symbol synchronization. The latter loop, depicted in Fig. 1, relies on an inphase and a midphase integrator to provide an error signal that is independent of the data polarity. The inphase integrator integrates over a symbol followed by a hard decision on the symbol polarity. By subtracting two successive decisions, a transition detection detector is used to determine whether a no transition (0), a $+1$ to -1 transition or a -1 to $+1$ transition occured. In the other arm, an integrator offset by half a symbol duration (thus the nomenclature, midphase integrator) produces an

estimate of the error in phase (or timing) modulated by the data polarity. Mulltiplying that output by the transition detector output wipes out the polarity and produces an error signal that is filtered by the loop filter and then, used to advance or delay the phase of the local symbol clock. In this paper, let P_t denote the transition probability and p denote the probability of $+1$. It is well known that $P_t = 2pq$, where $q = 1 - p$ is the probability of -1.

2 Performance of the DTTL when $P_t = 1/2$

The performance of the DTTL for random data (that is, $P_t = 1/2$) has been analysed in [1] where it is shown that the variance of the phase error (in units of cycle^2) is given by

$$\sigma_\lambda^2 = \frac{wB_{L0}T}{2R_s \text{erf}(\sqrt{R_s})} \tag{1}$$

where λ denotes the phase error (in cycles), w the midphase window with $w \leq 1$ (unitless), T the symbol duration (in sec), B_L the loop bandwidth (in Hz), R_s the symbol SNR (unitless) and $\text{erf}(x)$ is the error function of x. For $R_s > 6$ dB, $\text{erf}(\sqrt{R_s}) \simeq 1$ and (1) can be approximated by

$$\sigma_\lambda^2 \simeq \frac{wB_LT}{2R_s} \tag{2}$$

Note that the loop SNR (denoted by ρ) is related to σ_λ^2 through

$$\rho = \frac{1}{4\pi^2\sigma_\lambda^2} \tag{3}$$

As an example at 500 sym/sec, $R_s = 10$ dB, and $w = 1$, the minimum operating loop bandwidth required to maintain a 15 dB loop SNR is about xxx Hz.

3 Performance of the DTTL when $P_t \neq 1/2$

The performance of the DTTL for an arbitrary transition density was worked out in [2] assuming that the noise spectrum at the output of the loop phase detector is independent of the transition density. A technique was presented to select the minimum transition density

to achieve a specified degradation in the symbol error rate. More recently, the change in noise spectrum was accounted for in [3], assuning "high" R_s and $w = 1$. In addition, data asymmetry which accounts for unequal rise and fall times in the baseband pulse was included in the analysis. For the purpose of this report, we ignore data asymmetry and focus and transition density. It is shown in [3] that

$$\sigma_\lambda^2 = \frac{h(0)B_L T}{2R_s g_n'(0)} \tag{4}$$

where $g_n'(0)$ denotes the derivative of the S-curve evaluated at $\lambda = 0$ and is given by

$$g_n'(0) = 2P_t \text{erf}(\sqrt{R_s}) \tag{5}$$

and $h(0)$ denotes the normalized noise spectrum and is given by

$$h(0) = p^2 + q - \text{erf}^2(\sqrt{R_s})\left\{p^4 + q^2 - 2pq + p^2q(p+1) + 2pqR_s\right\} + pq(1 + 2R_s) \tag{6}$$

For "high" values of R_s, it can shown that $h(0) \simeq 2P_t$ and as a result, (4) reduces to

$$\sigma_\lambda^2 \simeq \frac{B_L T}{2R_s} \quad \text{independent of } P_t! \tag{7}$$

At first glance, this result might seem surprising and to a certain extent, erroneous. But a closer look at the response of the DTTL indicates that the transition density affects three different fundamental parameters of the loop in opposing ways and the various affects pull the loop in opposite diretions and end up cancelling each other. First as the transition density deviates from 50%, the loop bandwidth is reduced by $2P_t$. As an example if the loop was designed to operate with 5 Hz bandwidth with 50% transitions, the operating loop bandwidth with 3% transition would be $5 \times 2 \times 0.03 = .3$ Hz. It is important that the operating bandwidth remains large enough to accomodate the effects of nonideal oscillators such as clock drift and phase noise. To a first order approximation, the loop perturbation effect is independent of the SNR or the window size and is depicted in Fig. 2. In Fig. 2.a, the slopes for 40%, 20% and 3.1% transition probabilities are depicted in normalized form

(divided by the slope assuming 50% transition) versus symbol SNR. These curves in effect reflect the change in operating loop bandwidths as a function of P_t. In Fig. 2.b, similar results are presented with the normalization performed with respect to the 20% transition density. In this case, the operating bandwidth is the design bandwidth for a 20% transition and deviates (becomes larger or smaller) from that for different transition probabilities.

The second effect to be discussed is the change in signal power in the loop. Since the slope of the S-curve has changed, the signal power in the loop drops by the square of the slope. Hence, the signal power drops by $(2P_t)^2$.

Third, the noise spectral level in the loop also drops by $2P_t$ since $h(0) \rightarrow 2P_t$ at high symbol SNRs. Note that the noise enters the loop mainly through the midphase detector. As the number of transitions decreases, the midphase output is multiplied by more zeros from the transition detector, assuming the latter operates with few errors (which is the case at "high" symbol SNRs). Figure 3 depicts the normalized noise spectral level (normalized to 50% transition in Fig. 3.a and to 20% in Fig. 3.b). Finally, Fig. 4.a depicts the ratio of the tracking variance (with $w = 1$) for various transition densities normalized by the tracking variance for a 50% transition. The tracking variance for a 50% transition density is depicted in Fig. 4.b. Figure 5 (a and b) depict similar results with $w = 1/4$. The performance is verified through computer simulations which confirm the fact that the variance does not vary with the transition density at "high" SNR.

4 Conclusion

The goal of this study is to draft a recommendation for minimum transition densities required for Earth-to-Space links. The performance of the DTTL as a function of the transition density is understood for "high" symbol SNR and with window equal to unity. In this case, the tracking jitter (and thus, the degradation on telemetry) of the DTTL is unaffected by the transition density. However, the loop bandwidth varies with the transition density and

it is important to guarantee that the operating bandwidth at all times is adequate to handle the nonideal effects of the oscillators found in practice. Equally important is the effect of the transition density on the acquisition performance of the DTTL, which is not quantified in the literature to the best of the authors knowledge. It is suggested that further studies be performed by extending the results in [2] and [3] before any recommendation is drafted. Specifically,

the jitter should be characterized as a function of the transition density for "low" symbol SNR's and various windows, as future systems might have coded uplinks,

the acquisition of the DTTL should be characterized as a function of the symbol transition density,

the results should be verified through simulations and measurements with the Advanced Receiver,

ACKNOWLEDGEMENT

The work described in this paper was carried out at the Jet Propulsion Laboratory, California Institute of Technology, under contract with the National Aeronautics and Space Administration.

REFERENCES

1. M. K. Simon, "An Analysis of the Steady State Phase Noise Performance of A Digital Data-Transition Tracking Loop," SPS37-55, vol. III, *Jet Propulsion Laboratory*, Pasadena, CA, February 1969, pp. 54-62.

2. T. M. Nguyen and S. Hinedi, "Effect of the Transition Density on the Performance of Data-Derived Symbol Synchronizer," ESA/ESTEC, Noordjwik, The Netherlands, Session 4, pp. 35–51.

3. C. Tsang and C. M. Chie, "Effect of Signal Transition Variation on Bit Synchronizer Performance," *IEEE Transactions on Communications*, vol. 41, no. 5, May 1993, pp. 673–677.

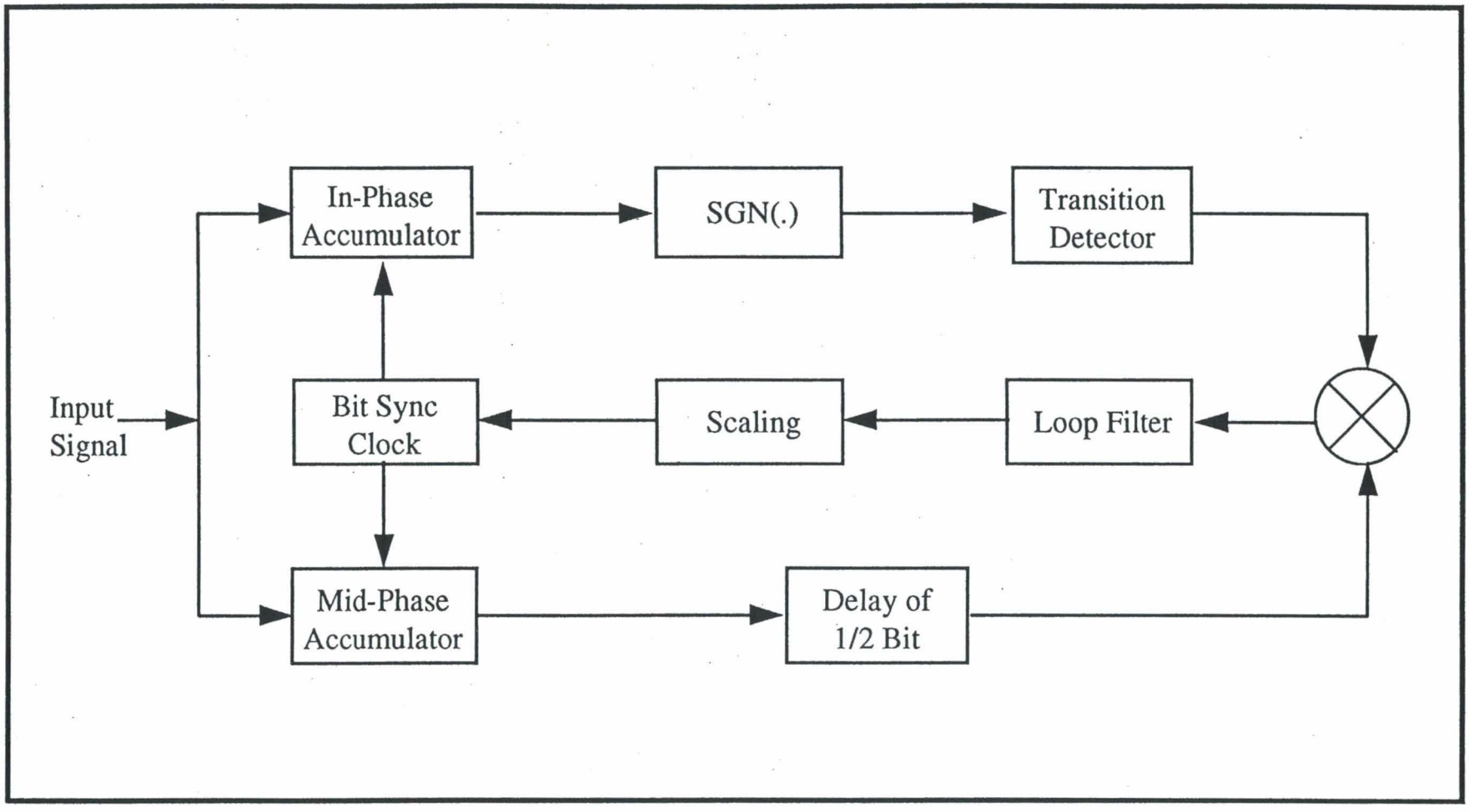

Figure 1 Block Diagram for the Digital Data Transition Tracking Loop (DTTL)

(a) $P_t = 50\%$

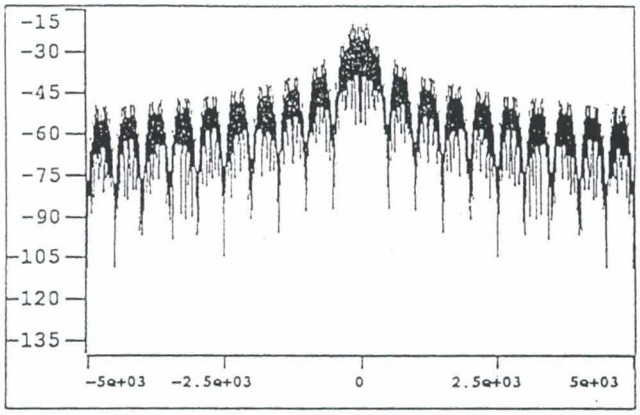

(b) $P_t = 40\%$

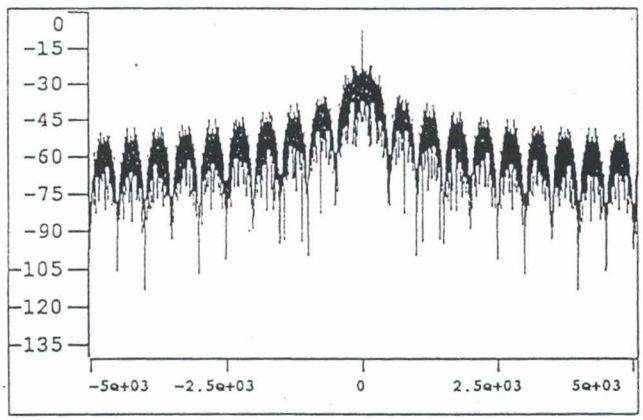

(c) $P_t = 20\%$

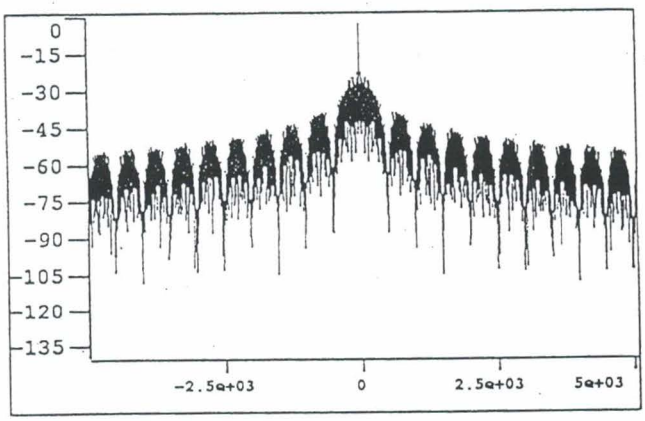

(d) $P_t = 3.1\%$

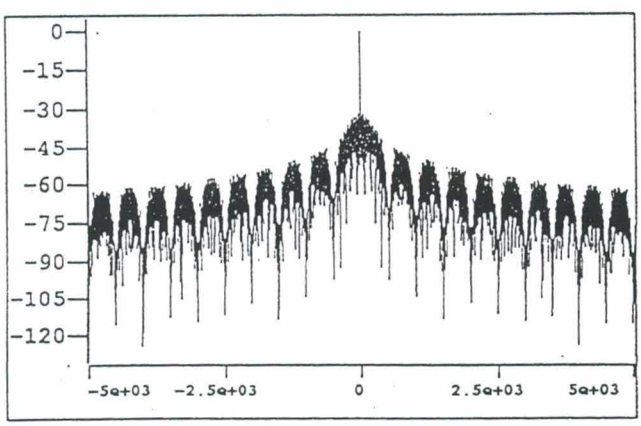

Figure 2 Data Spectrum for Various Transition Densities

Figure 3a g'(0) / g'(0)@Pt=50% vs Symbol SNR

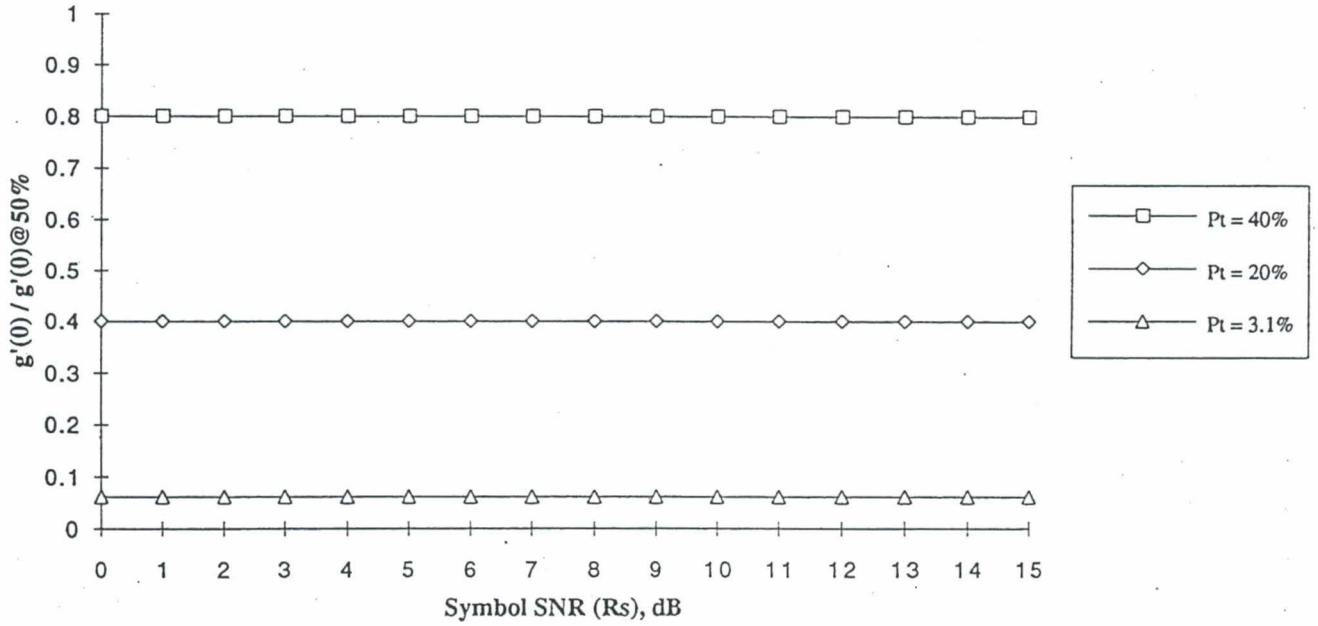

Figure 3b g'(0) / g'(0)@Pt=20% vs Symbol SNR

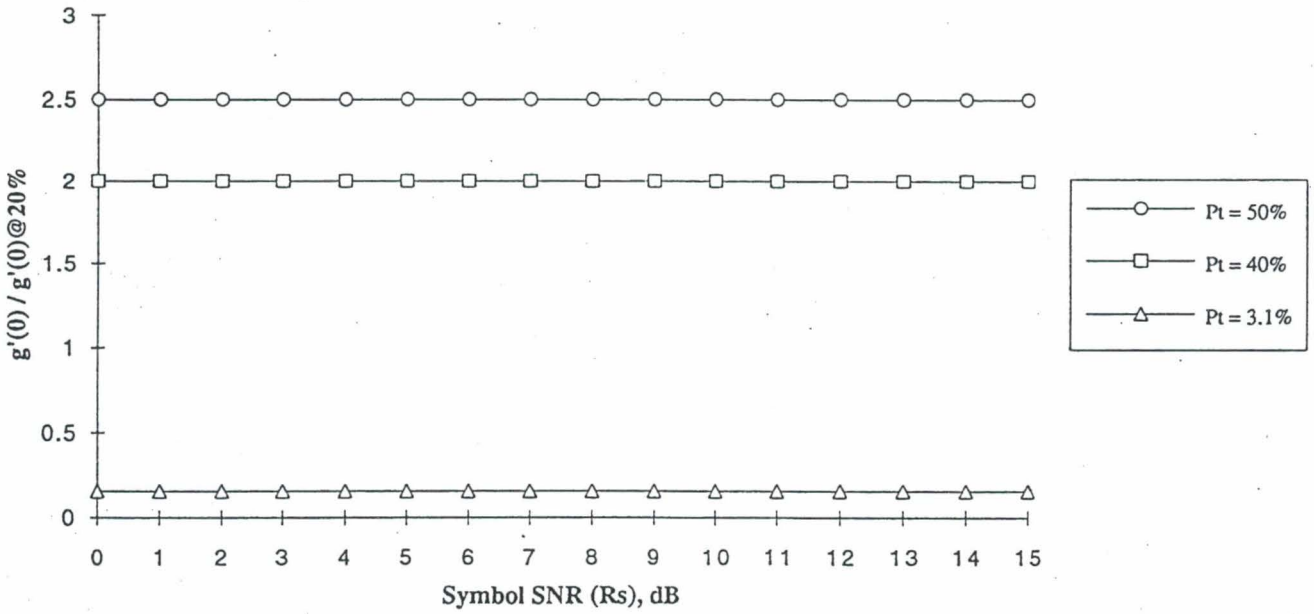

Figure 4a h(0) / h(0)@Pt=50% vs Symbol SNR

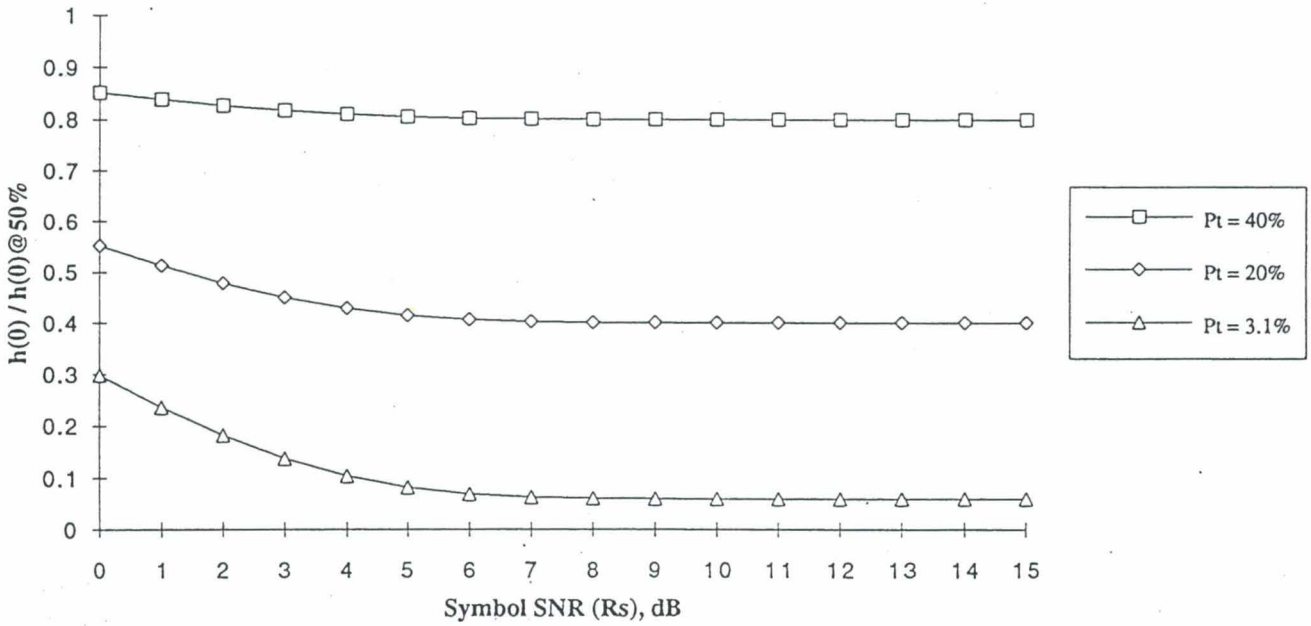

Figure 4b h(0) / h(0)@Pt=20% vs Symbol SNR

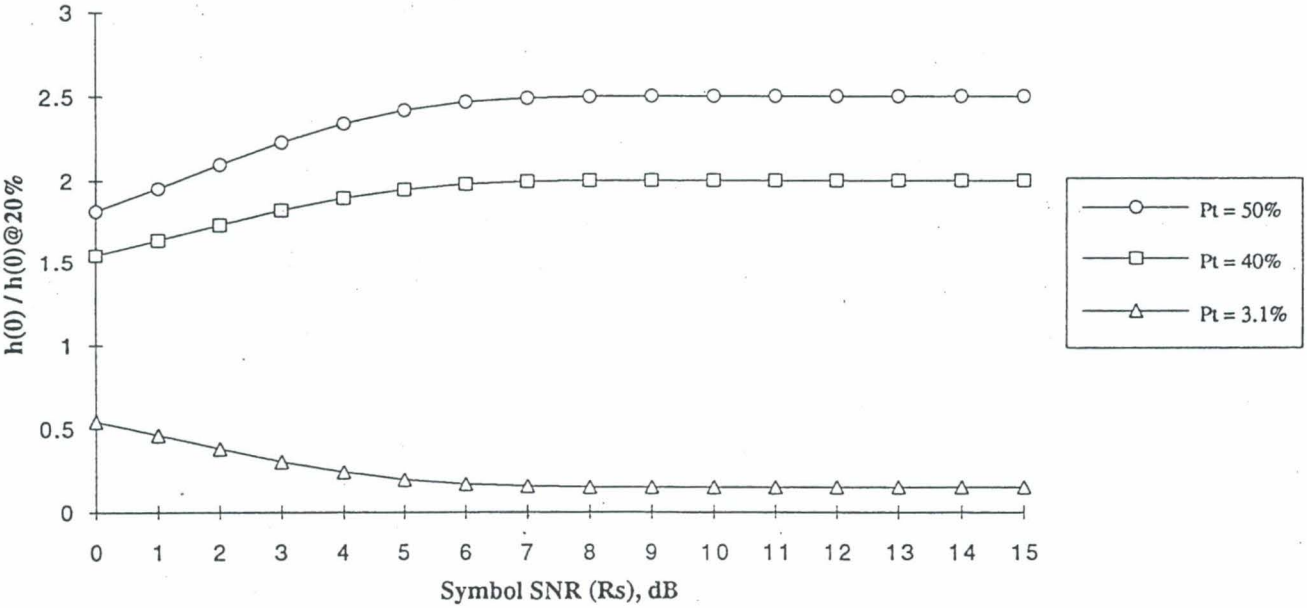

Figure 5a $\sigma_\lambda^2 / \sigma_\lambda^2$@50% vs Symbol SNR for w=1

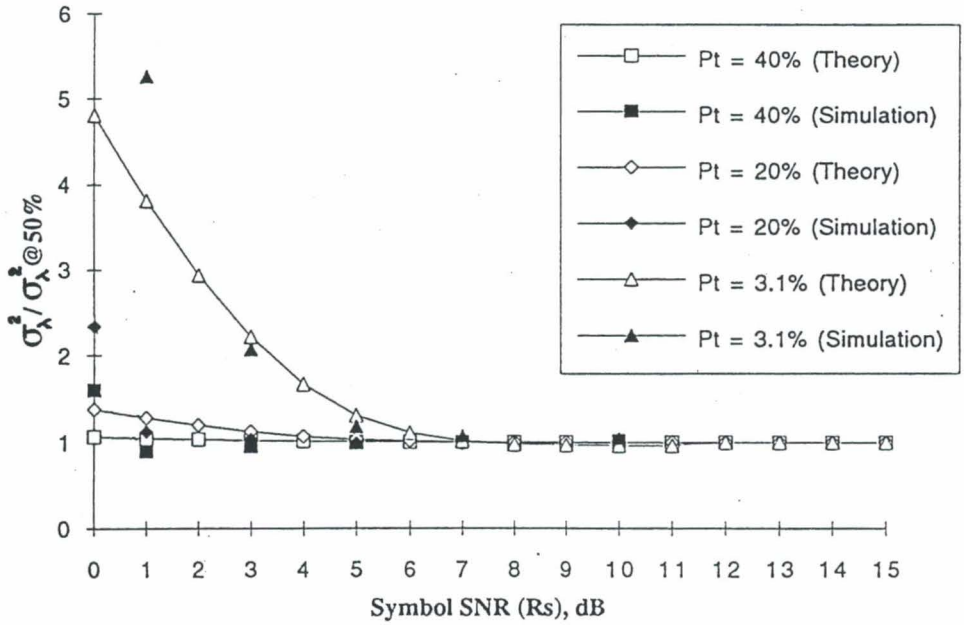

Figure 5b σ_λ^2 vs Symbol SNR for Pt=50% and w=1

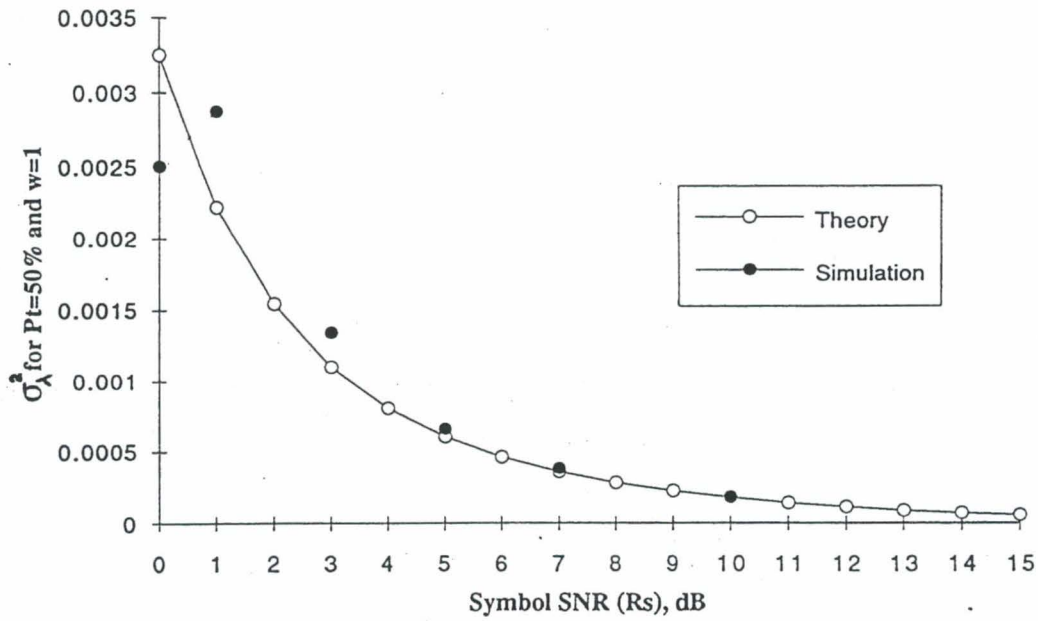

Figure 6a Simulation $\sigma_\lambda^2 / \sigma_\lambda^2$ @50% vs Symbol SNR for w=0.25

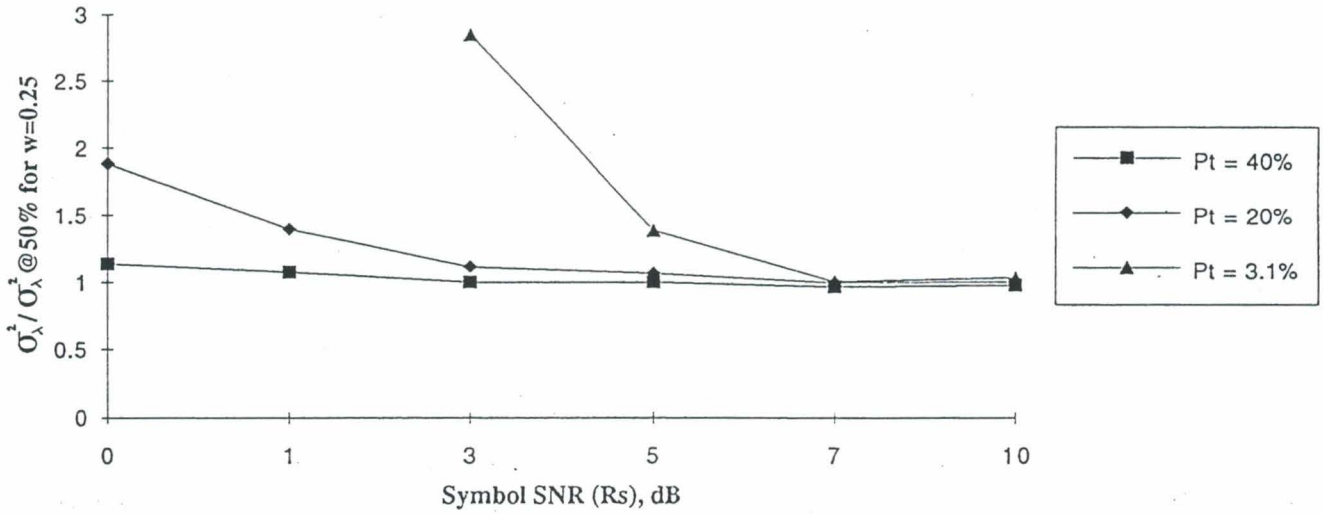

Figure 6b σ_λ^2 vs Symbol SNR for Pt=50% and w=0.25

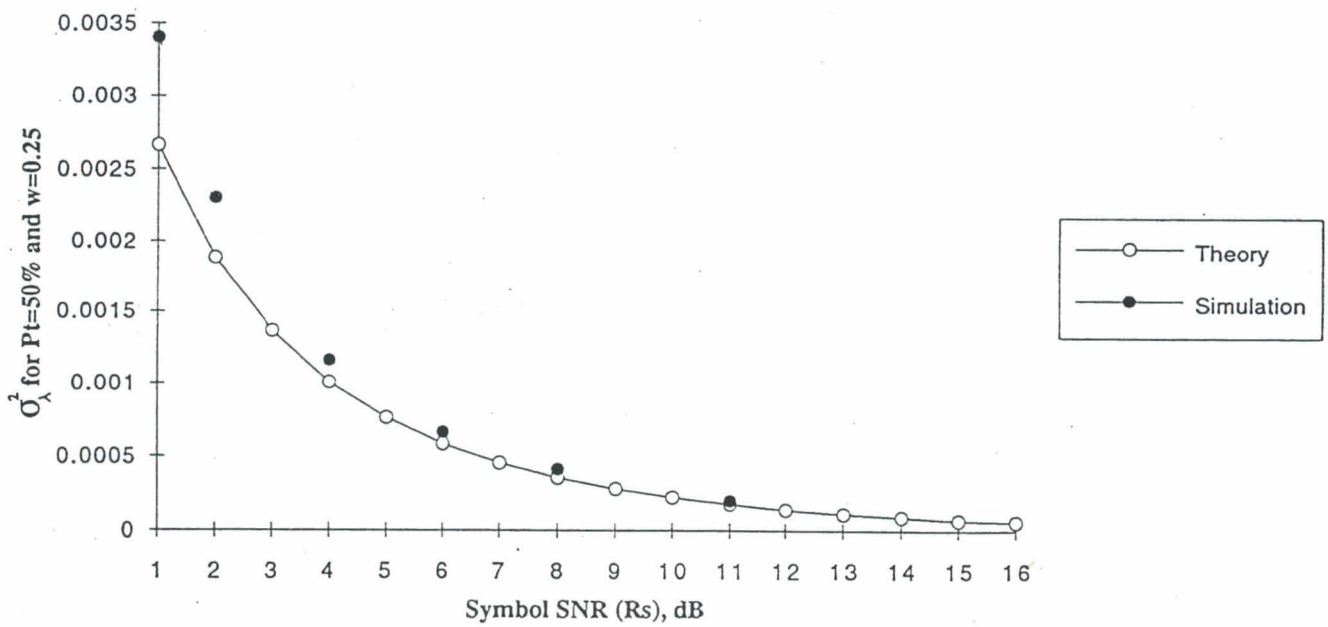

SESSION 3

NAVIGATION

Technical Characteristics and Accuracy Capabilities of Delta Differential One-Way Ranging (ΔDOR) as a Spacecraft Navigation Tool

James S. Border and John A. Koukos
Jet Propulsion Laboratory
California Institute of Technology
Pasadena, California

technical position paper presented at meeting of the
Consultative Committee for Space Data Systems
on
RF & Modulation Standards Approval
DLR, Munich, Germany
September 20, 1993

Abstract

The technique of determining spacecraft angular position by Delta Differential One-Way Ranging (ΔDOR) is described. The dependence of measurement accuracy on parameters which define the spacecraft signal spectrum is shown. To enable a ΔDOR measurement, a spacecraft must emit several tones. A narrow tone spacing is required for integer cycle phase ambiguity resolution, while a wider tone spacing is required for high measurement accuracy. An illustration of ΔDOR measurement accuracy, using the Mars Observer spacecraft, is presented. Guidelines for specifying spacecraft tone spectra are presented based on typical accuracy and ambiguity resolution needs, on frequency allocation for deep space tracking, on the efficient use of spacecraft signal power, and on the efficient use of ground tracking resources.

1. Introduction

Very Long Baseline Interferometry (VLBI) is a technique that allows determination of angular position for distant radio sources by measuring the geometric time delay between received radio signals at two geographically separated stations. The observed time delay is a function of the known baseline vector joining the two radio antennas and the direction to the radio source.

An application of VLBI is spacecraft navigation in deep space missions where the measurements at two stations of the phases of tones emitted from a spacecraft are differenced and compared against similarly differenced phase measurements of angularly nearby quasar radio signals. This application of VLBI is known as Delta Differential One-Way Ranging (ΔDOR).

As such, this technique may necessitate intra-agency cooperation because stations from different agencies can be used as ΔDOR data collectors for deep space navigation purposes. The NASA Deep Space Network (DSN) has used this technique operationally in a number of missions including Voyager, Magellan, and Vega. Currently, JPL navigation teams are employing ΔDOR in the Mars Observer and Galileo missions.

This technical position paper intends to provide implementation and performance details of the ΔDOR technique in order to support forging CCSDS[1] standards for spacecraft VLBI, given the increasing popularity of this method among space agency navigators.

2. ΔDOR and Quasars

An interferometer processes signals recorded at two stations that are geographically separated. The vector $\vec{B}$ from the first to the second station antenna is called the baseline vector. If the direction $\hat{s}$ of an extraterrestrial radio source forms an angle θ with the baseline vector, then a single radio frequency (RF) source signal wavefront arrives at the two ends of the baseline with a time difference given approximately by

$$\tau_g = -\frac{1}{c}\left(\vec{B} \bullet \hat{s}\right) = -\frac{B}{c}\cos\theta \qquad (1)$$

assuming that $B = |\vec{B}|$. This geometric time delay is an observable quantity with a maximum possible value equal to earth radius/c, or 0.021 sec, and a rate of change due to earth rotation up to 3.0 μsec/sec.

The advantage of very long baselines can be shown by differentiating the above equation with respect to geometric delay:

$$\frac{\partial\theta}{\partial\tau_g} = \frac{c}{B\sin\theta} \; . \qquad (2)$$

In the above equation the longer the baseline B, the smaller the angular position error for a given error in observed time delay. DSN baseline lengths are between 8,000 and 10,000 km, which yield angular position errors of about 30 nanoradians provided that measurement error in observed time delay is not larger than 1 nanosecond. Note that 30 nrad corresponds to about 22 km plane-of-sky position accuracy at a distance equal to that of Jupiter from the sun.

A ΔDOR measurement is generated from one-way range measurements made between a spacecraft and each of two ground antennas, and an interferometric time delay measurement of a natural radio source made using the same two antennas.

For a spacecraft, one-way range is determined locally at each station by extracting the phases of two or more tones emitted by the spacecraft. One-way range measurements contain unknown biases due to spacecraft clock offset, receiver clock offset, and ground station instrumental delay. Differential one-way range (DOR) measurements are formed by subtracting the one-way range measurements generated at two stations. The station differencing eliminates the effect of the spacecraft clock offset, but DOR measurements are biased by ground station clock offsets and instrumental delays. The observed quantity in a DOR measurement is analogous to the interferometric delay which may be measured for a broadband radio source as in Eq. (1).

To generate a ΔDOR measurement, an interferometric delay measurement of an extragalactic radio source (quasar) is subtracted from a spacecraft DOR measurement. Each station is configured to acquire data from the quasar in frequency channels centered on the

[1]Consultative Committee for Space Data Systems

spacecraft tone frequencies. This receiver configuration choice ensures that the spacecraft-quasar differencing eliminates the effects of ground station clock offsets and instrumental delays. In fact more is accomplished. By selecting a quasar which is close in an angular sense to the spacecraft, and by observing the quasar at nearly the same time as the spacecraft, the effects of errors in the modeled station locations, earth orientation, and transmission media delays are diminished. A ΔDOR measurement determines the angular position of a spacecraft in the inertial reference frame defined by the quasars.

The spacecraft and quasar observables are derived from processing digital samples of the radio signals received at each station. The spacecraft tone phases may be extracted using either open-loop or closed-loop techniques, but the quasar radio signal must be recorded open-loop. The quasar data samples from two stations must be transmitted to a central processing facility for delay measurement extraction. The DSN stations currently generate open loop recordings of both quasar and spacecraft signals, though an experimental closed-loop tone tracker is now being used during spacecraft observations for realtime validation. The same instrumental receiver chain, to the point of signal digitization, must be used for both spacecraft and quasar data acquisition.

The RF signals are selectively downconverted and filtered to generate several baseband channels. Normally, one baseband channel is centered on each spacecraft tone. The instantaneous channel bandwidth is typically in the range of a few hundred kiloHertz to a few MegaHertz. The DSN operational system, referred to as the Narrow Channel Bandwidth (NCB) VLBI System [Liewer 1988], uses a 250 kHz channel bandwidth. The analog signal in each channel is digitally sampled at the Nyquist rate, and then either recorded or input to the tone tracker. For DSN data acquisition, data samples are transmitted to the Network Operations Control Center at JPL for observable extraction.

For spacecraft data processing, an *a priori* tone phase model is computed, based on the nominal measurement geometry and transmitter frequency. A search in frequency is conducted to locate the actual tone frequency, and then tone phase is extracted using a phase-locked loop. This procedure is repeated for each tone at each station. Denote the station-differenced received phase, for a spacecraft tone with transmitter frequency ω_i, by $\phi_S(\omega_i)$. Then the spacecraft delay observable is given by

$$\tau_g^{S/C} = \frac{\phi_S(\omega_2) - \phi_S(\omega_1)}{\omega_2 - \omega_1}. \tag{3}$$

The frequency separation between the two outermost DOR tones is referred to as the spanned bandwidth of the spacecraft signal.

For quasar data processing, the data samples in each baseband channel from two stations are cross-correlated to produce an estimate of interferometric phase $\phi_Q(\overline{\omega}_i)$ at the channel centroid frequency $\overline{\omega}_i$ [Thomas 1987]. Interferometric phase for a broadband radio source is analogous to station-differenced phase for a sinusoidal radio source. The quasar delay observable is given by

$$\tau_g^{QSR} = \frac{\phi_Q(\overline{\omega}_2) - \phi_Q(\overline{\omega}_1)}{\overline{\omega}_2 - \overline{\omega}_1}. \tag{4}$$

The centroid of the receiver bandpass for channel i takes the role of the discrete frequency of DOR tone i.

3. Spacecraft DOR Tone Structure

A spacecraft transponder must emit several tones (referred to as DOR tones) spanning some bandwidth to enable a DOR measurement. The DOR tones are generated by modulating a pure sine wave or pure square wave onto the downlink carrier at either S-band, X-band, or Ka-band. Requirements on the number of DOR tones, tone frequencies, and tone power are based on the expected *a priori* knowledge of spacecraft angular position and on the required differential range measurement accuracy, as discussed below. Generally, a narrow spanned bandwidth is needed for integer cycle ambiguity resolution based on *a priori* knowledge of spacecraft angular position, while a wide spanned bandwidth is needed for high measurement accuracy.

Tones generated by modulating a carrier signal by a single square wave provide a low performance option. The ratio of maximum spanned bandwidth to minimum spanned bandwidth, for tones above the detection threshold, is usually in the range of 1 to 6. To provide higher performance (i.e. a wider spanned bandwidth with more power in the outer tones), while still providing a spanned bandwidth narrow enough for integer cycle ambiguity resolution, more DOR tones are needed. Sine waves are normally used in multi-tone systems based on efficiency considerations.

For example, ΔDOR measurements were made for the Voyager spacecraft using high order harmonics of the 360 kHz telemetry square wave subcarrier signal. More accurate ΔDOR measurements have been made of the Mars Observer spacecraft using two sine wave signals (3.825 MHz and 19.125 MHz) modulated onto the downlink carrier.

It is preferable for DOR tones to be frequency coherent with the downlink carrier. This facilitates the detection of weak DOR tones by allowing the use of a phase model derived from the received carrier signal. Also, the transmitted spanned bandwidth of the DOR tones, which must be known for the generation of a differential range observable from received phase measurements, will in this case be a defined multiple of the transmitted carrier frequency.

The most usual DOR tone modulation formats are presented next.

3.1 DOR Tones Generated from Modulation by Two Sinewaves

Two sinusoidal tones with circular frequencies ω_1 and ω_2 are phase modulated on the downlink carrier signal with peak modulation indices m_1 and m_2, respectively:

$$s(t) = \sqrt{2P_T}\cos(\omega_c t + m_1\sin(\omega_1 t) + m_2\sin(\omega_2 t)). \quad (5)$$

The above expression may be expanded to separate the carrier and main DOR tone components of the signal from higher order harmonics:

$$s(t) = \sqrt{2P_T}[J_0(m_1)J_0(m_2)\cos(\omega_c t) - 2J_1(m_1)J_0(m_2)\sin(\omega_c t)\sin(\omega_1 t) - 2J_0(m_1)J_1(m_2)\sin(\omega_c t)\sin(\omega_2 t) + \textit{higher harmonics}] \quad (6)$$

where J_0 and J_1 are Bessel functions of the first kind. The modulation produces tones at frequencies of $\omega_c \pm \omega_1$ and $\omega_c \pm \omega_2$. Modulation indices may be chosen to put more power in the outer tones, while putting just enough power in the inner tones to provide for ambiguity resolution.

The powers allocated to the carrier and the tones are easily deduced from the above expression:

$$P_c = P_T J_0^2(m_1) J_0^2(m_2),$$
$$P_1 = P_T J_1^2(m_1) J_0^2(m_2), \text{ and}$$
$$P_2 = P_T J_0^2(m_1) J_1^2(m_2). \tag{7}$$

The corresponding modulation losses are expressed as the fractions below:

$$\frac{P_c}{P_T} = J_0^2(m_1) J_0^2(m_2),$$
$$\frac{P_1}{P_T} = J_1^2(m_1) J_0^2(m_2), \text{ and}$$
$$\frac{P_2}{P_T} = J_0^2(m_1) J_1^2(m_2). \tag{8}$$

The above two-sinewave signaling scheme is used on Mars Observer. For Mars Observer the nominal values of the DOR modulation indices are m_1=0.64 rad and m_2=0.32 rad for the f_1=19.125 MHz and f_2=3.825 MHz DOR tones, respectively. Such values yield modulation losses P_c/P_T=-1.14 dB, P_1/P_T=-10.57 dB, and P_2/P_T=-16.94 dB.

3.2 DOR Tones Generated from Modulation by One Squarewave

In this case, one squarewave signal with unit amplitude and frequency ω_1 is phase modulated on the downlink carrier to generate a downlink signal with multiple tones:

$$s(t) = \sqrt{2P_T}\cos(\omega_c t + m_1 \text{sqwv}(\omega_1 t)). \tag{9}$$

The cosine of the sum may be expanded to give:

$$s(t) = \sqrt{2P_T}\cos(m_1 \text{sqwv}(\omega_1 t))\cos(\omega_c t) - \sqrt{2P_T}\sin(m_1 \text{sqwv}(\omega_1 t))\sin(\omega_c t). \tag{10}$$

The second term on the right hand side is a carrier signal multiplied by a square wave with amplitude $\sin(m_1)$. This square wave has a Fourier expansion

$$\sin(m_1 \text{sqwv}(\omega_1 t)) = \sin(m_1)\frac{4}{\pi}\sum_{k=1}^{\infty}\frac{\cos[(2k-1)\omega_1 t]}{2k-1}, \tag{11}$$

and Eq. (10) may be rewritten as

$$s(t) = \sqrt{2P_T}\cos(m_1 \text{sqwv}(\omega_1 t))\cos(\omega_c t) -$$
$$\sqrt{2P_T}\sin(m_1)\frac{4}{\pi}\sum_{k=1}^{\infty}\frac{\cos[(2k-1)\omega_1 t]}{2k-1}\sin(\omega_c t). \tag{12}$$

The second term on the right hand side produces tones at odd multiples of the subcarrier frequency spaced about the carrier. The modulation loss formula for the squarewave harmonics is easily calculated from the coefficients of the above expression:

$$\frac{P_k}{P_T} = \frac{4}{\pi^2}\frac{1}{(2k-1)^2}\sin^2(m_1) \text{ at } \omega_c \pm (2k-1)\omega_1 \text{ for } k = 1,2,3,\ldots \quad (13)$$

Considering that the cosine is an even function, the first term on the right hand side of Eq. (10) would appear to produce a pure carrier signal with $P_c/P_T = \cos^2(m_1)$. However, since the square wave must be band limited, the function $\cos(m_1 \text{sqwv}(\omega_1 t))$ is actually a spike train with period $2\pi/(2\omega_1)$ and amplitude $(1 - \cos m_1)$. This spike train produces even harmonics of the square wave frequency about the carrier signal [Hildebrand and Yunck 1982]. For high rate subcarriers, say above 360 kHz, these tones may be detectable and usable as DOR tones. The power in the even harmonics is proportional to $(1 - \cos m_1)^2$, but the actual power depends on the shape of the subcarrier signal. The total power in the even harmonics, excluding the carrier signal itself, is usually quite small.

When telemetry modulation is imposed on the subcarrier, the odd harmonics are spread and are not usable for DOR measurements. The even harmonics generated from the spike train, on the other hand, remain as pure tones. High order even harmonics of the high rate telemetry subcarrier, at a level of about -30 dB relative to the total signal power, were used as DOR tones for the Voyager and Magellan spacecraft. While such measurements of opportunity may be useful, it is difficult to plan for this case since the spectrum depends on the precise shape of the subcarrier signal.

Normally, low order odd harmonics of the square wave modulation would serve as DOR tones. This scheme was used on the Vega and Phobos missions.

As an example consider a fully suppressed carrier (m_1=90°). Then the suppression of the first two odd square wave harmonics is given by:

$$\frac{P_1}{P_T} = -3.92 \text{ dB and}$$

$$\frac{P_2}{P_T} = -13.46 \text{ dB}. \quad (14)$$

4. Signal Detection Requirements

Signal detection requirements are stated in terms of the voltage signal-to-noise ratio for an 1-sec average. For a sinusoidal spacecraft signal, the requirement may be expressed in terms of tone power to noise power spectral density. For a broadband quasar signal, the requirement may be expressed in terms of source flux, antenna gain, antenna noise temperature, and recorded bandwidth. The requirements given here are not theoretical limits, but rather practical thresholds based on typical system coherence times* and operational data processing methods.

* The system coherence time may be defined as the time for the actual signal phase to wander by 0.1 cycle from the model signal phase.

The requirements are:

$$SNR_{V1}^{S/C} \geq 5.0 \qquad \text{for a spacecraft tone, and} \qquad (A)$$

$$SNR_{V1}^{QSR} \geq 1.3 \qquad \text{for a broadband quasar source,} \qquad (B)$$

where SNR_{V1} is the voltage signal-to-noise ratio for an 1-sec average. The difference in detection criteria is due to the effective coherence time. Quasar signal detection is based on an averaging time of about 60 sec, since geometric delay models for quasar signals are quite well known *a priori*. But spacecraft signal detection must usually be based on an averaging time of order 1 sec, since tone phase models are not well known *a priori*. If the spacecraft transmits a carrier signal which satisfies criterion (A), and if differential range measurements are to be made using side tones which are coherent multiples of the carrier signal, then the detection requirement for the sidetones may be relaxed to

$$SNR_{V1}^{S/C} \geq 1.3 \qquad \text{for a spacecraft tone which is a coherent multiple of a spacecraft carrier signal which satisfies criterion (A).} \qquad (C)$$

For a spacecraft tone, the 1-sec voltage SNR is related to P_{Tone}/N_0, the tone power to noise power in a 1 Hz bandwidth, by

$$SNR_{V1}^{S/C} = \sqrt{\frac{2}{\pi}\frac{2P_{Tone}}{N_0}} \qquad (15)$$

where the factor $2/\pi$ is due to 1-bit sampling of the signal. The factor $2/\pi$ is replaced by unity for a system which supports multi-level sampling. Using Eq. (15), criteria (A) and (C) may be rewritten as

$$\frac{P_{Tone}}{N_0} \geq 13 \text{ dB} \cdot \text{Hz} \qquad \text{for a spacecraft tone,} \qquad (A')$$

$$\frac{P_{Tone}}{N_0} \geq 1 \text{ dB} \cdot \text{Hz} \qquad \text{for a spacecraft tone which is a coherent multiple of a spacecraft carrier signal which satisfies criterion (A').} \qquad (C')$$

For a broadband quasar signal, the 1-sec voltage SNR is related to system parameters by [Thomas 1981]

$$SNR_{V1}^{QSR} = K_L \frac{2}{\pi}\sqrt{\frac{T_{q1}T_{q2}}{T_{s1}T_{s2}}}\sqrt{N_b} \qquad (16)$$

where K_L is the system loss factor (0.8 to 1.0), the factor $2/\pi$ is due to 1-bit sampling, T_{qi}, T_{si} are the correlated source temperature and system noise temperature at antenna i, and N_b is the number of data samples in 1 second. The correlated source temperature for antenna i is given approximately by

$$T_{qi} = 0.00030\ \varepsilon_i\ \pi\ r_i^2\ S_c \qquad (17)$$

where ε_i, r_i are the efficiency and radius (m) for antenna i and S_c is the correlated source flux (Jansky or Jy). For the DSN NCB VLBI System operating at X-band, K_L = 0.8, ε = 0.60 for a 70-m diameter antenna at 10° elevation, ε = 0.68 for a 34-m diameter antenna at 10° elevation, $T_s \approx$ 30 K, and N_b = 500,000. Using these nominal values in Eqs (16) and (17), the detection criterion (B) is restated in terms of minimum required correlated source flux for DSN antenna pairs in Table 1.

Table 1. Minimum correlated source flux for signal detection at X-band using the NCB VLBI System.

DSN Antenna Pair	Minimum Correlated Flux
70m-70m	0.16 Jy
70m-34m	0.30 Jy
34m-34m	0.60 Jy

5. ΔDOR Measurement Accuracy

The *precision* of a spacecraft DOR measurement, given by Eq. (19) below, depends on the received tone power to noise power ratio and on the spanned bandwidth of the DOR tones. But the *accuracy* of a ΔDOR measurement, given by the sum of Eqs. (19) through (28) below, also depends on the precision of the quasar delay measurement, on knowledge of the quasar position, on clock stability, on instrumental phase response, and on uncertainties in earth platform models and transmission media delays. An error budget for a ΔDOR measurement depends on observation geometry and all of these factors. Specifications for DOR tone power level and spanned bandwidth are based on total ΔDOR measurement accuracy, rather than only on spacecraft DOR measurement precision. Simplified formulae are given here for evaluating ΔDOR measurement accuracy to provide a basis for developing transponder specifications.

Normally, a ΔDOR pass consists of three "scans" of data recording each of a few minutes duration. The observing sequence is spacecraft-quasar-spacecraft. A ΔDOR observable is generated from the linear combination of the three measurements which eliminates linear temporal errors. The observed quantity in a ΔDOR observation is time delay.

5.1 Spacecraft SNR

The precision of measurement of tone phase, for T_L sec of data, is described by the error in the tone phase measurement:

$$\varepsilon_\varphi = \frac{1}{2\pi\sqrt{T_L SNR_{V1}^{S/C}}} \text{ cycles.} \qquad (18)$$

A DOR measurement is formed from tone phase measurements, received at two stations, as in Eq. (3). Assuming that the four tones have the same received power to noise ratio, the delay error ε_τ is given by

$$\varepsilon_\tau = \frac{2}{2\pi f_{BW}\sqrt{\frac{T_{obs}}{N_c} SNR_{V1}^{S/C}}} \text{ sec} \tag{19}$$

where f_{BW} is the spanned bandwidth (Hz), T_{obs} is the observation scan length (sec), and N_c is the number of channels of data recorded by time multiplexing. Set N_c to unity if data channels are recorded in parallel.

5.2 Quasar SNR

The quasar delay measurement error is given by [Thomas 1981]

$$\varepsilon_\tau = \frac{\sqrt{2}}{2\pi f_{BW}\sqrt{\frac{T_{obs}}{N_c} SNR_{V1}^{QSR}}} \text{ sec.} \tag{20}$$

The spanned bandwidth for the quasar measurement must be selected to be the same as for the spacecraft tones to ensure cancellation of the effects of dispersive instrumental phase shifts.

5.3 Quasar Position

Uncertainty in the position coordinates of the reference quasar will cause a ΔDOR delay error through the relation given by Eq. (1). Assuming a spherical position uncertainty of ε_θ rad, the delay error is

$$\varepsilon_\tau = \frac{B_p}{c}\varepsilon_\theta \text{ sec} \tag{21}$$

where B_p is the projected baseline length.

5.4 Clock Instability

Instability in the station frequency standard or temporal instabilities in instrumental components cause a delay error which depends on the time separation between the spacecraft and quasar observations. The delay error is given by

$$\varepsilon_\tau = \sqrt{2} T_{S/C-QSR}\varepsilon_{\Delta f/f} \text{ sec} \tag{22}$$

where $T_{S/C-QSR}$ (sec) is the time separation between the spacecraft and quasar observations and $\varepsilon_{\Delta f/f}$ is the composite Allan standard deviation of the station frequency standard and frequency distribution system.

5.5 Instrumental Phase Ripple

A quasar signal is affected by the station instrumental phase response across the bandpass, whereas a spacecraft tone is affected by the instrumental phase shift at the tone frequency. A deviation of the phase response from a smooth phase versus frequency transfer function is referred to as phase ripple. Instrumental phase ripple of ε_ϕ deg causes a delay error of

$$\varepsilon_\tau = \sqrt{2}\sqrt{2}\frac{1}{f_{BW}}\frac{\varepsilon_\phi}{360} \text{ sec} \tag{23}$$

assuming the phase ripple is independent in each channel and at each station, and assuming that the phase ripple averages to zero for the quasar measurement.

5.6 Station Location

Uncertainty in station coordinates causes a delay error which depends on the spacecraft-quasar angular separation. Assuming a spherical uncertainty ε_{stn} in baseline position components, the delay error is

$$\varepsilon_\tau = \Delta\theta\frac{\varepsilon_{STN}}{c} \text{ sec} \tag{24}$$

where $\Delta\theta$ is the spacecraft-quasar angular separation (rad).

5.7 Earth Orientation

Uncertainty in the orientation of the Earth in inertial space causes a delay error of the same form as station location uncertainty. The delay error is

$$\varepsilon_\tau = \Delta\theta\frac{\varepsilon_{UTPM}}{c} \text{ sec} \tag{25}$$

where ε_{UTPM} is the positional uncertainty in UT1-UTC and polar motion at the Earth's surface.

5.8 Troposphere

Uncertainty in the zenith tropospheric delay, primarily due to variations in the wet component, causes a systematic delay error of

$$\varepsilon_\tau = \frac{\rho_z}{c}\left|\frac{1}{\sin\gamma_{S/C}} - \frac{1}{\sin\gamma_{QSR}}\right| \text{ sec} \tag{26}$$

where ρ_z is the zenith uncertainty, $\gamma_{S/C}$ is the spacecraft elevation angle, and γ_{QSR} is the quasar elevation angle. There is a term of this form for each station.

5.9 Ionosphere

The ionospheric error depends on signal frequency and path delay uncertainty after calibration. A rough empirical formula, based on comparisons of ionospheric calibrations derived from Faraday rotation measurements with dual frequency quasar VLBI measurements [Edwards 1991], is given by

$$\varepsilon_\tau = \frac{(1.46 + 16.9\Delta\theta)}{f_{RF}^2} \times 10^{-9} \text{ sec} \qquad (27)$$

where $\Delta\theta$ is the spacecraft-quasar angular separation (rad) and f_{RF} is the signal radio frequency (GHz).

5.10 Solar Plasma

The solar plasma error depends on signal frequency and proximity of the the signal raypaths to the sun. An estimate for the delay error is given by [Callahan 1978]

$$\varepsilon_\tau = \frac{0.013}{f_{RF}^2}[\sin(SEP)]^{-1.3}\left(\frac{B_p}{v_{SW}}\right)^{0.75} \times 10^{-9} \text{ sec} \qquad (28)$$

where SEP is the sun-radio source angular separation, B_p is the projected baseline length (km) at the point of signal closest approach to the sun, v_{SW} (km/sec) is the solar wind velocity, and f_{RF} is the signal frequency (GHz). There is a term of this form for both the spacecraft and the quasar.

5.11 Root-Sum-Square

The predicted ΔDOR measurement accuracy is computed as the RSS of the above ten terms. Equation (2) may be used to relate delay measurement accuracy to angular position accuracy.

6. Mars Observer ΔDOR Error Budget

The formulae of Section 5 show how ΔDOR measurement accuracy depends on spacecraft transponder parameters, on observation geometry and scan length, on instrumental stability, and on the accuracy of external calibrations. Nominal values for these parameters, applicable for the cruise phase of the Mars Observer mission and for data acquisition using the DSN NCB VLBI System, are given in Table 2. Figure 1 shows the error budget which corresponds to these parameter values.

Table 2. Nominal parameter values for evaluation of Mars Observer ΔDOR error budget.

Term	Description	Nominal Value
P_{Tone}/N_0	DOR tone power to noise power spectral density	25 dB•Hz
K_L	System loss factor (quasar data acquisition)	0.8
N_b	Number of quasar data samples per second	500,000
T_{si}	System noise temperature, antenna i	Antenna 1: 30 K Antenna 2: 30 K
ε_i	Efficiency, antenna i	Antenna 1: 0.60 Antenna 2: 0.68
r_i	Radius, antenna i	Antenna 1: 35 m Antenna 2: 17 m
S_c	Correlated source flux	0.8 Jy
f_{BW}	Spanned bandwidth	38.25 MHz
T_{obs}	Observation scan length	S/C: 10 min QSR: 14 min
N_c	Number of time-multiplexed frequency channels	4
ε_θ	Quasar position uncertainty	5 nrad
B_p	Projected baseline length	8000 km
$T_{S/C\text{-}QSR}$	Time separation between S/C and QSR observation	12.5 min
$\varepsilon_{\Delta f/f}$	Clock Instability	10^{-14}
ε_ϕ	Instrumental phase ripple	0.5 deg
$\Delta\theta$	Spacecraft-quasar angular separation	10 deg
ε_{stn}	Baseline coordinate uncertainty, each component	3 cm
ε_{UTPM}	Baseline orientation uncertainty, each component	5 cm†
ρ_z	Zenith troposphere delay uncertainty, each station	4 cm
$\gamma_{S/C}$	Spacecraft elevation angle	Antenna 1: 20 deg Antenna 2: 25 deg
γ_{QSR}	Quasar elevation angle	Antenna 1: 25 deg Antenna 2: 20 deg
f_{RF}	Signal radio frequency	8.4 GHz
SEP	Sun-Earth-Source angle	50 deg
v_{SW}	Solar wind velocity	400 km/sec

† Realtime prediction uncertainty for UT1-UTC is 30 cm. A processing delay of 1 week is necessary to obtain 5 cm accuracy for earth orientation calibrations.

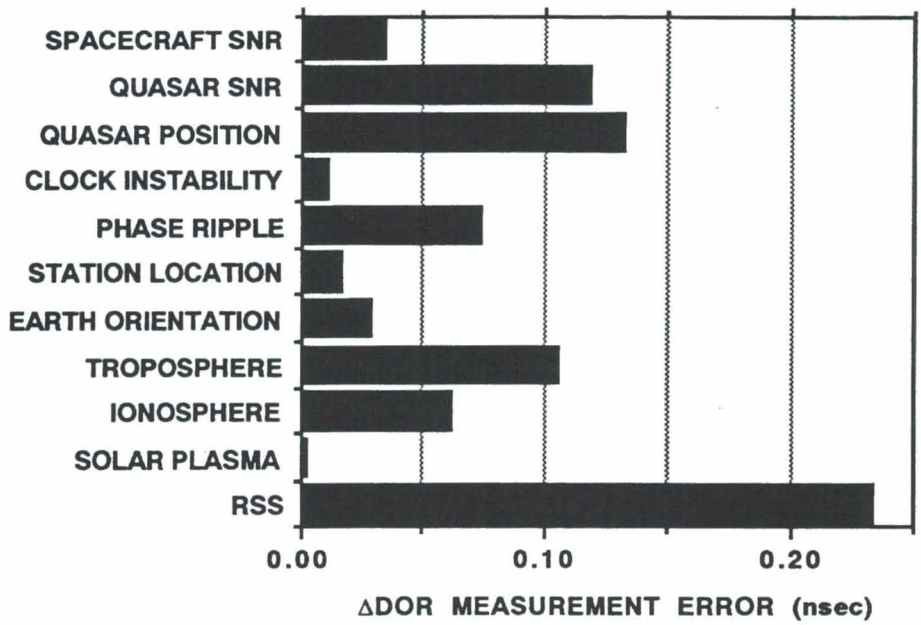

Figure 1. ΔDOR error budget (1-σ) for Mars Observer, based on the nominal parameter values given in Table 2.

The RSS ΔDOR measurement accuracy of 0.23 nsec, shown in Fig. 1, provides an angular position accuracy of 9 nrad for a projected baseline length of 8000 km. The dominant errors due to quasar SNR, quasar position, instrumental phase ripple, troposphere, and ionosphere vary considerably with observing schedule and geometry, so that actual performance for Mars Observer ΔDOR accuracy falls within a range of values from 0.1 nsec to 0.7 nsec. The DOR tones emitted by the Mars Observer transmitter clearly enable ΔDOR measurement accuracy, using the DSN, of better than 1 nsec.

Perhaps the single most important parameter in the error budget is the spanned bandwidth of the spacecraft DOR tones. Doubling this bandwidth, while holding other parameters fixed, will halve the errors due to spacecraft SNR, quasar SNR, and instrumental phase ripple. Once antennas and data acquisition terminals are implemented, little control is available over the other parameters which affect quasar SNR and instrumental phase ripple. For example, the quasar scan length must be increased by a factor of four to halve the error due to quasar SNR if other parameters are held fixed.

7. Integer Cycle Phase Ambiguity Resolution

Only the fractional part of signal phase can be measured; the integer part must be determined from *a priori* knowledge. This phase ambiguity leads to a ΔDOR time delay ambiguity equal to the reciprocal of the minimum spanned bandwidth. For ambiguity resolution at the 99% confidence level, the spacecraft geometric delay must be known *a priori* in the radio reference frame to 1/6 of the reciprocal minimum spanned bandwidth.

Delay ambiguities in observables generated from wider spanned bandwidths are resolved successively by using delay estimates from the narrower spanned bandwidths.

For example, the angular position of the spacecraft must be known *a priori* with a 1-σ accuracy of 1 μrad to confidently resolve the ambiguity in a ΔDOR measurement which was made by using a 5 MHz spanned bandwidth and a 10,000 km projected baseline length. This level of accuracy is normally achieved using a few passes of Doppler and range data.

Once the delay ambiguity has been resolved for a spanned bandwidth of f_{BW1}, then the ambiguity may be resolved for a spanned bandwidth of ηf_{BW1}, provided that

$$\eta \leq 1/(6\sigma_{\phi 1}), \tag{29}$$

where $\sigma_{\phi 1}$ is an upper bound on the 1-σ dispersive error (cycles) in the channel-differenced, station-differenced phase measurement used to generate delay at the spanned bandwidth f_{BW1}. Dispersive errors, caused by system thermal noise, instrumental phase ripple, and interchannel oscillator phase drift, are conservatively bounded by 0.03 cycle, indicating that spanned bandwidth may reliably increase by a factor of 5.5.

In a multi-tone system, a tone frequency ratio of $f_2/f_1 = 12$ is consistent with a jump of at most 5.5 in spanned bandwidth. The ambiguity is first resolved using the carrier tone and one DOR tone at frequency separation f_1 from the carrier. Next, the ambiguity at spanned bandwidth $2f_1$ is resolved. The resulting delay estimate is used to resolve the ambiguity at spanned bandwidth f_2-f_1, which may finally be used to resolve the ambiguity at spanned bandwidth $2f_2$. Note that $f_2/f_1 = 12$ follows from $(f_2-f_1)/(2f_1) = 5.5$.

Dispersive phase measurement errors may be considerably less than 0.03 cycle for a highly linear ground receiver system operating with strong signal levels. For this case use Eq. (29) to determine the greatest allowable jump in spanned bandwidth.

8. Proposed Spacecraft DOR Tone Spectra

The material developed in Sections 1 through 8 may be used to derive specifications for the number of spacecraft DOR tones, tone powers, and tone frequencies, given mission navigation accuracy requirements. Guidelines for DOR tone spectra are presented here based on typical accuracy and ambiguity resolution needs, on frequency allocation for deep space tracking, on the efficient use of spacecraft signal power, and on the efficient use of ground tracking resources. The case of a single spacecraft in interplanetary cruise is considered first. Next, the special case of differential VLBI measurements made between two spacecraft is considered.

8.1 Cruise Navigation Support: Ambiguity Resolution and Measurement Accuracy

A minimum spanned bandwidth of 5 MHz or less is recommended so that integer cycle delay ambiguities may be resolved, for the longest baselines, using only 1 μrad *a priori* knowledge of spacecraft angular position. This spanned bandwidth may be realized using the carrier signal and the first harmonic of a DOR tone whose frequency is 5 MHz or less. The required *a priori* knowledge may be obtained by using Doppler or range data, or by using the unambiguous ΔVLBI delay rate observables which can always be generated from

the phase measurements used to generate a ΔDOR observable, or by making a ΔDOR measurement using the spacecraft telemetry signal. For some cases the *a priori* trajectory knowledge may be much better than 1 μrad, and the minimum spanned bandwidth may be much greater than 5 MHz.

The final ΔDOR measurement is derived using the widest spanned bandwidth provided by the DOR tones. Measurement accuracy, as a function of spanned bandwidth, is plotted in Fig. 2. The separate errors due to spacecraft SNR, quasar SNR, and instrumental phase ripple are shown; the RSS of all other measurement system errors is shown with label "other errors"; the total RSS error is shown. This error computation assumes that data are acquired at X-band using a DSN 70m-34m antenna pair with the NCB VLBI System, the quasar flux is 0.5 Jy, and the received spacecraft DOR tone power to noise spectral density is 15 dB•Hz. All other assumptions are as given in Table 2.

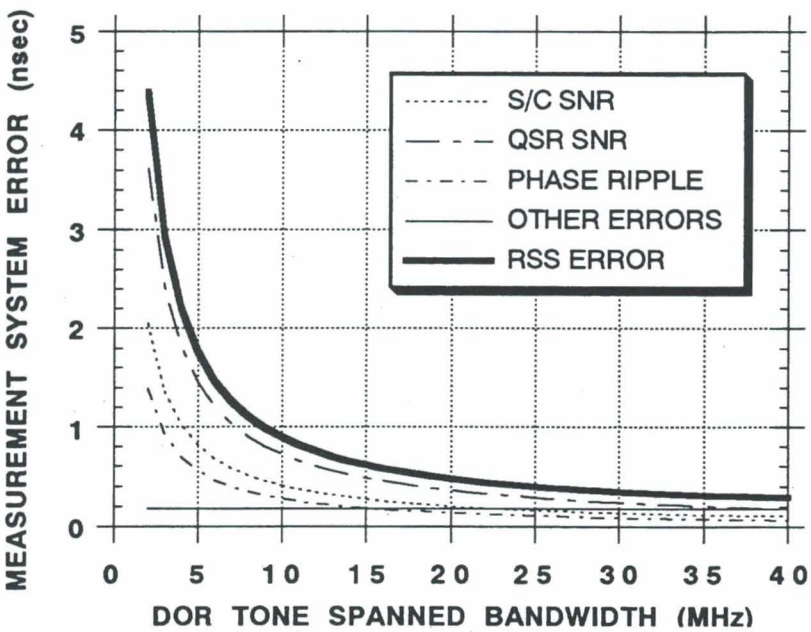

Figure 2. Typical ΔDOR measurement system errors at X-band as a function of spacecraft tone spanned bandwidth.

As seen from Fig. 2, a spanned bandwidth of 35 MHz or greater is needed to reduce the errors which depend on spanned bandwidth to a level comparable with typical values for other measurement system errors. Measurements generated using a more narrow spanned bandwidth do not make efficient use of DSN resources, since more station time is required to obtain the same level of trajectory accuracy. For this same reason, it is recommended that the received power to noise spectral density ratio be at least 15 dB•Hz for the outer most DOR tones. If the signal level is much less than 15 dB•Hz, then the spacecraft scan length must be much longer than the quasar scan length to reduce the error due to spacecraft SNR to a level comparable with the error due to quasar SNR. The inner DOR tones, which are only used for ambiguity resolution, need only be strong enough to detect.

The frequency bandwidth allocation for deep space tracking is 10 MHz at S-band (2.3 GHz), 50 MHz at X-band (8.4 GHz), and 400 MHz at Ka-band (32 GHz). The recommendations, which are consistent with these allocations, are given in Table 3.

Table 3. Proposed spacecraft DOR tone spectra for deep space tracking.

Frequency Band	Proposed DOR Tone Spectra		Accuracy*
	Number of DOR Tones	DOR Tone Frequencies (Approximate)	
S-band	1	4 MHz	41 nrad
X-band	2	4 MHz and 20 MHz	9 nrad
Ka-band	3	4 MHz, 20 MHz, and 120 MHz	7 nrad

* The assumptions used in this accuracy prediction are as given in Table 2 except: signal frequency is 2.3 GHz for S-band, 8.4 GHz for X-band, 32 GHz for Ka-band; DOR tone power to noise power spectral density is 15 dB•Hz; system noise temperature is 30 K for S-band and X-band, and 60 K for Ka-band; quasar flux is 0.5 Jy for S-band and X-band, and 0.25 Jy for Ka-band; charged particle errors are scaled by inverse frequency squared. Error is converted from nsec to nrad assuming 8000 km baseline projection.

The DOR measurements are generated using the $\pm 1^{st}$ harmonics of the DOR tones. At S-band, one tone provides for ambiguity resolution and provides the widest bandwidth that fits within the allocation. At X-band, two tones are generally needed to provide for both ambiguity resolution and for high accuracy. At Ka-band, a wider spanned bandwidth is necessary to reduce the size of the error due to quasar SNR, since, for Ka-band relative to X-band, quasar flux is reduced and system noise temperature is higher. Three tones are needed at Ka-band to provide for successive ambiguity resolution and to produce a sufficiently wide spanned bandwidth.

The proposed tone frequencies listed in Table 3 are meant to be approximate values, not exact values. For example, at X-band, one tone in the range of 2 to 5 MHz, and a second tone in the range of 17.5 to 24 MHz, satisfies all the guidelines.

The ΔDOR measurement accuracy shown in Table 3 is the typical value attained today using the DSN NCB VLBI System for S-band or X-band. The value shown for Ka-band is a projection. It should be noted that a number of sources of error, such as quasar position, quasar SNR, and uncalibrated tropospheric delay, could be significantly reduced in the future. Thus total measurement accuracy could possibly be improved by incorporating a wider spacecraft DOR tone spanned bandwidth or by transmitting more power in the outer DOR tones.

8.2 Special Cases: Spacecraft-Spacecraft ΔVLBI

When one spacecraft is approaching a planet at which another spacecraft is already in orbit or landed on the surface, then ΔVLBI measurements between the two spacecraft can provide target-relative angular position. When two or more spacecraft are operating in orbit or on the surface of the same planet, then earth-based Same-Beam Interferometry (SBI) measurements can increase both the efficiency and the accuracy of positioning. For these applications, to achieve the best performance, there are additional compatibility requirements on the signal spectra of the spacecraft to be jointly observed. The signal requirements depend on the characteristics of the ground receiver system and on the

navigation performance requirements. The relevant issues are introduced here, but detailed design criteria are not given.

8.2A Spacecraft-Target ΔVLBI. Studies have shown that the use of spacecraft-spacecraft ΔVLBI for planetary approach navigation can reduce targeting errors by a factor of two to three relative to solutions based on Doppler, range, and spacecraft-quasar ΔDOR [Edwards *et al.* 1991]. The ΔDOR technique employs observations of two radio sources at the same frequency in order to eliminate the effects of dispersive phase shifts in the station receiver chain. To make ΔVLBI measurements between two spacecraft, either the two spacecraft must emit DOR tones at or near the same frequencies, or external calibrations must be used to reduce the effects of dispersive instrumental phase shifts. Here, "near the same frequency" means that both signals must fall within the same baseband receiver channel, and that each spacecraft must provide the same spanned bandwidth. Instrumental effects are analyzed in [Border *et al.* 1992].

The DSN NCB VLBI System has 250 kHz baseband channels. Each channel is downconverted from RF using an analog mixing signal. An arbitrary phase shift is introduced in each channel by this process. For spacecraft-spacecraft ΔVLBI, where the two spacecraft do not emit compatible signals, the receiver system must be calibrated either by observing a quasar or by injecting a comb of calibration tones locally at each station. These calibration techniques are operationally cumbersome and degrade the data accuracy.

The spacecraft signal compatibility requirements could be relaxed if the station receiver system digitized the entire passband before downconverting selected portions of the spectrum to baseband. In an all-digital system, the two spacecraft need not transmit at the same frequencies, spacecraft tone phases could be extracted locally in realtime, and spacecraft-spacecraft ΔVLBI observables could be generated immediately following acquisition.

8.2B Orbiter-Orbiter SBI. For two planetary orbiters, SBI data are generated from carrier phase measurements acquired simultaneously at two stations from the two spacecraft. The SBI data sense the relative motion of the spacecraft in the plane of the sky. Studies have shown that SBI data, when combined with Doppler data, can improve orbital accuracy by an order of magnitude relative to solutions generated from only Doppler data [Folkner and Border 1992]. No DOR tones are needed to enable this measurement; each spacecraft must transmit a carrier signal. Data arcs of 1 to 2 hr are needed. A carrier phase bias must be estimated for each arc; ambiguity resolution is not required. The spacecraft signals should be in the same RF band, but there are no further compatibility requirements for this application.

8.2C Lander-Rover SBI. The SBI measurement becomes extremely accurate as the angular separation between radio sources decreases. For the case of a rover and lander, accuracy as good as 10 prad is possible. Studies have shown that SBI measurements, combined with line-of-sight range measurements, could enable nearly instantaneous earth-based positioning of a rover relative to a lander at the 1-m level [Kahn *et al.* 1992]. To achieve this level of accuracy, the phase ambiguity must be resolved in the carrier cycle.

It follows from the analysis in Section 7 that carrier cycle ambiguity resolution requires either several DOR tones at intermediate frequencies, or a ground receiver system with high phase-linearity. Also, as for spacecraft-spacecraft ΔVLBI, the signals from the two

spacecraft must be at or near the same frequencies, unless the station receiver system digitizes the entire passband before downconversion to baseband.

As in the case of two orbiters, relative positioning information for a lander and rover may be obtained from an arc of SBI data without resolving the carrier cycle ambiguity. Only a carrier signal from each spacecraft is needed to enable this measurement. The performance for this case depends on the length of the data arc.

9. VLBI Compared to other Navigation Techniques

Earth-based radio metric tracking is the primary source of navigational data during interplanetary cruise. Recent studies [e.g. Thurman and Estefan 1993] predict that angular accuracy as good as 50 nrad can be inferred, in some cases, from long arcs of line-of-sight Doppler data. The advantages of using ΔDOR measurements are:

- ΔDOR provides a direct geometric measure of plane-of-sky position. Orbit solutions based on ΔDOR data show differing sensitivities to system errors, as compared to orbit solutions based on only line-of-sight measurements. Solutions which incorporate ΔDOR do not have singularities at low geocentric declinations or other adverse geometries.

- Comparable trajectory accuracy is obtained using either short arc (few days) or long arc (few months) solutions when ΔDOR data are used. Spacecraft state can be recovered more quickly following a maneuver.

- Navigation requirements can be satisfied by 1 hr of tracking time per week, thus reducing both the duration and number of weekly tracking passes.

- ΔDOR data may be acquired in a listen-only mode; an uplink is not required.

- ΔDOR data can provide improved angular accuracy.

10. Summary

A ΔDOR measurement is generated by comparing, at two ground stations, the phases of two or more tones emitted by a spacecraft, and by measuring the difference in time of arrival, at the same two stations, of a broadband quasar signal.

The DOR tones are generated by modulating a pure sine wave or pure square wave onto the downlink carrier at either S-band or X-band or Ka-band. A single square wave provides a lower DOR measurement accuracy compared to sine waves that are normally used in multi-tone systems for measurements of higher accuracy. The DOR measurements are usually generated using the $\pm 1^{st}$ harmonics of the DOR tones. A narrow spanned bandwidth must be provided for delay ambiguity resolution, whereas a wide spanned bandwidth is needed for high measurement accuracy.

It is preferable for DOR tones to be frequency coherent with the downlink carrier. This facilitates the detection of weak DOR tones by allowing the use of a phase model derived from the received carrier signal.

Signal detection requires a threshold of $\frac{P_{Tone}}{N_0} \geq 13$ dB • Hz for a spacecraft tone alone as compared to a threshold of $\frac{P_{Tone}}{N_0} \geq 1$ dB • Hz for a spacecraft tone which is a coherent submultiple of a spacecraft carrier signal .

The ΔDOR measurement error is typically dominated by uncertainties due to quasar SNR, quasar position, instrumental phase ripple, and troposphere. Doubling the spanned bandwidth of the spacecraft DOR tones, while holding other parameters fixed, will halve the errors due to spacecraft SNR, quasar SNR, and instrumental phase ripple.

At S-band, one tone provides for ambiguity resolution and provides the widest bandwidth that fits within the allocation. At X-band, two tones are generally needed to provide for both ambiguity resolution and for high accuracy. At Ka-band, a wider spanned bandwidth is necessary to control the size of the error due to quasar SNR. Three tones are needed at Ka-band to provide for ambiguity resolution and to produce a sufficiently wide spanned bandwidth.

Acknowledgments

The research described in this paper was performed at the Jet Propulsion Laboratory, California Institute of Technology, under contract with the National Aeronautics and Space Administration.

References

J. S. Border, W. M. Folkner, R. D. Kahn, and K. S. Zukor, "Precise Tracking of the Magellan and Pioneer Venus Orbiters by Same-Beam Interferometry, Part I: Data Accuracy Analysis," The Telecommunications and Data Acquisition Progress Report 42-110, Jet Propulsion Laboratory, California Institute of Technology, Pasadena, California, August, 1992, pp. 1-20.

P. S. Callahan, "An Analysis of Viking S-X Doppler Measurements of Solar Wind Columnar Content Fluctuations," The Deep Space Network Progress Report 42-44, Jet Propulsion Laboratory, California Institute of Technology, Pasadena, California, April, 1978, pp. 75-81.

C. D. Edwards, "Ionospheric Errors for Phobos ΔVLBI," JPL Internal Document IOM 335.1-91-21, Jet Propulsion Laboratory, California Institute of Technology, Pasadena, California, July 8, 1991.

C. D. Edwards, Jr., W. M. Folkner, J. S. Border, and L. J. Wood, "Spacecraft-Spacecraft Very Long Baseline Interferometry for Planetary Approach Navigation," Spaceflight Mechanics 1991, Vol. 75, Advances in the Astronautical Sciences, Univelt, Inc., San Diego.

W. M. Folkner and J. S. Border, "Orbiter-Orbiter and Orbiter-Lander Tracking Using Same-Beam Interferometry," The Telecommunications and Data Acquisition Progress Report 42-109, Jet Propulsion Laboratory, California Institute of Technology, Pasadena, California, May, 1992, pp. 74-86.

C. E. Hildebrand and T. P. Yunck, "Addendum to 'A Surprising Discovery in the Spectrum of the Voyager 2 X-band Signal'," JPL Internal Document IOM 335.4-98, Jet Propulsion Laboratory, California Institute of Technology, Pasadena, California, March 1, 1982.

R. D. Kahn, W. M. Folkner, C. D. Edwards, and A. Vijayaraghavan, "Position Determination of a Lander and Rover at Mars With Earth-Based Differential Tracking," Jet Propulsion Laboratory TDA Progress Report 42-108, February, 1992, pp. 279-293.

K. M. Liewer, "DSN Very Long Baseline Interferometry System Mark IV-88," The Telecommunications and Data Acquisition Progress Report 42-93, Jet Propulsion Laboratory, California Institute of Technology, Pasadena, California, May, 1988, pp. 239-246.

J. B. Thomas, "An Error Analysis for Galileo Angular Position Measurements with the Block I ΔDOR System," JPL Internal Document EM 335-26, Jet Propulsion Laboratory, California Institute of Technology, Pasadena, California, November 11, 1981.

J. B. Thomas, "Interferometry Theory for the Block II Processor," JPL Publication 87-29, Jet Propulsion Laboratory, California Institute of Technology, Pasadena, California, October 15, 1987.

S. W. Thurman and J. A. Estefan, "Radio Doppler Navigation of Interplanetary Spacecraft Using Different Data Processing Modes," paper AAS-93-163, AAS/AIAA Spaceflight Mechanics Meeting, Pasadena, CA, February 22-24, 1993.

SESSION 4

REQUIRED BANDWIDTH,

SPURIOUS EMISSION, AND

INTERFERENCE SUSCEPTIBILITY

REQUIRED BANDWIDTH, UNWANTED EMISSION, AND DATA POWER EFFICIENCY FOR RESIDUAL AND SUPPRESSED CARRIER SYSTEMS--A COMPARATIVE STUDY[1]

Tien M. Nguyen and Warren L. Martin
National Aeronautics and Space Administration
Jet Propulsion Laboratory
California Institute of Technology
4800 Oak Grove Drive
Pasadena, California 91109

ABSTRACT

This paper presents a new concept for required bandwidth along with a method for computing this bandwidth and the associated unwanted emission for the classes of PCM/PSK/PM, PCM/PM and BPSK signals. The PCM/PSK/PM signals considered here employ either a square wave or sine wave subcarrier with NRZ data format. On the other hand, the PCM/PM and BPSK signals use either a Bi-phase or an NRZ data format. Furthermore, the optimum required bandwidth in the presence of noise and the data power efficiency for these modulation schemes will also be investigated. The term "data power efficiency" as considered in this paper consists of two principal components, namely, the amount of power contained in the data channel, and the Symbol Signal-to-Noise Ratio (SSNR) degradation due to the presence of InterSymbol Interference (ISI) for a specified required bandwidth. This paper evaluates both of these components numerically for the modulation schemes considered and the results are then compared.

[1] The work described in this paper was carried out at the Jet Propulsion Laboratory, California Institute of Technology, under contract with the National Aeronautics and Space Administration.

1. INTRODUCTION

The topic of occupied bandwidth for the space telemetry signals has been investigated in great detail in the recent past [1-6]. The the space telemetry signals examined in [1-6] employed both residual and suppressed carrier modulation techniques. This paper presents a method to calculate the required bandwidth for PCM/PSK/PM signals with squarewave and sinewave subcarriers, PCM/PM and BPSK with both NRZ and Bi-phase data formats. The data power efficiency among these modulation techniques will be evaluated and compared. As mentioned earlier, the term "power data efficiency" considered here also includes the effects of ISI on the Symbol Error Rate (SER) performance degradation. In addition, the results for the optimum bandwidth in the presence of noise will also be presented and compared with the others.

For space applications, the typical signal recommended by the international Consultative Committee for Space Data Systems (CCSDS) is the residual carrier signal using the subcarrier to separate the data from the RF residual carrier, namely PCM/PSK/PM signals [7]. Mathematically, the PCM/PSK/PM signal can be expressed by

$$s_1(t) = \sqrt{2}\, A\sin[\omega_c t + md(t)P(t)] \tag{1}$$

where A is the rms voltage, ω_c is the angular carrier center frequency in rads/sec, m is the modulation index in radian, d(t) is the NRZ binary valued data sequence with symbol period T, and P(t) is the subcarrier waveform. Expanding Eqn (1) one obtains

$$s_1(t) = \sqrt{2}\, A[\sin(\omega_c t)\cos(mP(t)) + d(t)\cos(\omega_c t)\sin(mP(t))] \tag{2}$$

The subcarrier waveforms recommended by the CCSDS are the squarewave and sinewave for deep space and near earth missions, respectively [7]. Hence, one has PCM/PSK/PM-Squarewave and PCM/PSK/PM-Sinewave for squarewave and sinewave subcarriers, respectively. Currently, the CCSDS has expressed considerable interest in eliminating the subcarrier to conserve bandwidth [8-9]. The transmitting signal format without the subcarrier becomes PCM/PM. The mathematical expression for PCM/PM signal is given by

$$s_2(t) = \sqrt{2}\, A\sin[\omega_c t + md(t)] \tag{3}$$

Expanding Eqn (3) we get:

$$s_2(t) = \sqrt{2}\, A[\sin(\omega_c t)\cos(m) + d(t)\cos(\omega_c t)\sin(m)] \tag{4}$$

where the data sequence d(t) can be formated either in the form of NRZ or Bi-phase. Therefore, one has PCM/PM/NRZ and PCM/PM/Bi-phase for NRZ and Bi-phase data formats, respectively.

The mathematical expression for suppressed carrier modulation, namely BPSK signal, is defined as follow

$$s_3(t) = \sqrt{2}\, Ad(t)\sin[\omega_c t] \tag{5}$$

again, the data sequence d(t) can be either NRZ or Bi-phase. Thus, one has BPSK/NRZ and BPSK/Bi-phase for NRZ and Bi-phase data formats, respectively. In the following sections, the terms required bandwidth as well as unwanted spurious emissions will be defined and a method for calculating these quantities will be presented. Moreover, the optimum bandwidth in the presence of noise and the data power efficiency will also be investigated in detail.

This paper is organized in the following manner. Section 2 defines the term "required bandwidth" and presents a method to calculate this quantity for various modulation schemes mentioned above. Section 3 explains the term "unwanted spurious emission" and shows how this quantity can be computed. The data power efficiency is considered in Section 4. The term data power efficiency calculated in this section consists of two components, namely, the power contained in the data channel for the required bandwidths of 2/T and 4/T (Where T denotes the symbol period), and the symbol SNR degradation in the data channel for various values of required bandwidths. Section 5 shows how to calculate the optimum required bandwidth in the presence of the white Gaussian noise. The discussions and main conclusions are presented in Sections 6 and 7, respectively.

2. REQUIRED BANDWIDTH: DEFINITION AND ANALYSIS

2.1 DEFINITION

The term "Required Bandwidth" used through this paper is defined as follow:

> "The required bandwidth is the width of a frequency band such that, within the lower and the upper frequency limits, the total power contained in this frequency band is equal to a specified percentage of the total power. This specified percentage is determined in such a way that the transmitted data power and the required bandwidth will meet the required link performance margin and bandwidth assignment."

2.2 REQUIRED BANDWIDTH FOR PCM/PSK/PM WITH SQUAREWAVE

When P(t) is a unit power squarewave subcarrier of frequency f_{sc}. It has been shown in [2] that the required bandwidth for this case is given by

$$\frac{8\sin^2(m)}{\pi^3} \sum_{k\geq 1} \frac{1}{(2k-1)^2} \int_{-\pi(M-n(2K-1))}^{\pi(M-n(2K-1))} [\sin(x)/x]^2\, dx + \cos^2(m) = p\% \tag{6}$$

Where M is the normalized required bandwidth with p% power containment-to-bit rate ratio, i.e.,

$$M = BW_1/R_s \tag{7}$$

and n is the subcarrier frequency-to-bit rate ratio, i.e.,

$$n = f_{sc}/R_s, \text{ where n is integer and } R_s = 1/T \text{ is the data rate} \tag{8}$$

and p% is the percentage of power containment in the data component. The plot of Eqn (6) for various values of n and m is shown in Figure 1. This figure shows the power containment as a function of the one-sided bandwidth-to-symbol rate ratio. As an example, for 99 % power containment, the one-sided bandwidth is about $328R_s$ for m = 1.2 rad and n = 9 [2,3,6]. While, form Figure 1, the one-sided bandwidth for 90 % only requires about $29R_s$. Therefore, if 90 % of the power meets the desired link performance margins then the required bandwidth will be $29R_s$ which is 11 times less than the bandwidth required for 99 % power containment.

2.3 REQUIRED BANDWIDTH FOR PCM/PSK/PM WITH SINEWAVE

When P(t) is a sinewave subcarrier, it has been shown in Reference 2 that the required bandwidth for this case is given by

$$J_0^2(m) + 2 \sum_{k \text{ even}}^{L} J_k^2(m) + \sum_{h \text{ odd}}^{L} J_h^2(m) a_h(L) = p\% \tag{9}$$

where $a_h(L)$ is defined as

$$a_h(L) = \int_{-Lfsc}^{Lfsc} [S_d(f-hf_{sc}) + S_d(f+hf_{sc})]df \tag{10}$$

Here f_{sc} and Lf_{sc} are defined as nR_s and the required bandwidth with p% power containment, respectively. The required bandwidth BW_2-to-bit rate ratio is found to be

$$M_2 = BW_2/R_s = Ln \tag{11}$$

Note that $S_d(t)$ is the power spectral density (PSD) for NRZ data which is defined as

$$S_d(f) = T \frac{\sin^2(\pi fT)}{(\pi fT)^2} \tag{12}$$

where T is the symbol period. Figure 2 illustrates a plot of Eqn (9) for various values of n and m. This figure shows that, for n = 9, m = 1.2 rad, the required one-sided bandwidth for 90 % power containment is about $9R_s$. On the other hand, the required bandwidth for 99 % power containment is about $27R_s$ which is 3 times greater than the bandwidth required for 90 % power containment.

2.4 REQUIRED BANDWIDTH FOR PCM/PM WITH BI-PHASE DATA FORMAT

From Eqn (4), the PSD of the PCM/PM with Bi-phase data format can be shown to be:

$$S_2(f) = \cos^2(m)\,\delta(f - f_c) + T\,\mathrm{Sin}^2(m)\,\frac{\sin^4(\pi(f-f_c)T/2)}{(\pi(f-f_c)T/2)^2} \tag{13}$$

Using Eqn (13), the required bandwidth can be easily evaluated. The relationship between the required bandwidth with p% power containment and the modulation index is found as follow:

$$p\% = \frac{2\sin^2(m)}{\pi}\int_{-M_3\pi/2}^{M_3\pi/2}[\sin^4(x)/x^2]dx + \cos^2(m) \tag{14}$$

where

$$M_3 = \frac{BW_3}{R_s} \tag{15}$$

where BW_3 is the required bandwidth for Bi-phase case. This result is the same as the one found in Reference 3. The plot of Eqn (14) is shown in Figure 3 for various values of m. As an example, for m = 1.2 rad, the required bandwidths for 95 % and 99 % power containment are $5R_s$ and $26R_s$, respectively.

2.5 REQUIRED BANDWIDTH FOR PCM/PM WITH NRZ DATA FORMAT

Again, from Eqn (4), the PSD of the PCM/PM with NRZ data format can be shown to be:

$$S_2(f) = \cos^2(m)\,\delta(f - f_c) + T\,\mathrm{Sin}^2(m)\,\frac{\sin^2(\pi(f-f_c)T)}{(\pi(f-f_c)T)^2} \tag{16}$$

Using Eqn (16), the required bandwidth can be easily evaluated. The relationship between the required bandwidth with p% power containment and the modulation index is found to be:

$$p\% = \frac{\sin^2(m)}{\pi}\int_{-M_4\pi}^{M_4\pi}[\sin^2(x)/x^2]dx + \cos^2(m) \tag{17}$$

where

$$M_4 = \frac{BW_4}{R_s} \tag{18}$$

Here BW_4 denotes the required bandwidth for NRZ case. Illustrated in Figure 4 is the plot of Eqn (17). This figure shows the power containment as a function of the normalized bandwidth with the

modulation index m as a parameter. For instance, the required bandwidths for 95 % and 99 % power containment are $1.6R_s$ and $9R_s$, respectively, for m = 1.2 rad.

2.6 REQUIRED BANDWIDTH FOR BPSK WITH BI-PHASE DATA FORMAT

From Eqn (5), the PSD of the BPSK with Bi-phase data format can be shown to be:

$$S_3(f) = T \frac{\sin^4(\pi(f-f_c)T/2)}{(\pi(f-f_c)T/2)^2} \tag{19}$$

Using Eqn (19), the required bandwidth can be easily evaluated. The relationship between the required bandwidth with p% power containment is found to be:

$$p\% = \frac{2}{\pi} \int_{-M_5\pi/2}^{M_5\pi/2} [\sin^4(x)/x^2]dx \tag{20}$$

where

$$M_5 = \frac{BW_5}{R_s} \tag{21}$$

here BW_5 is the required bandwidth for BPSK/Bi-phase case. The plot of Eqn (20) is shown in Figure 5. As an example, the required one-sided bandwidths for 95 % and 99 % power containment are $6.5R_s$ and $31R_s$, respectively.

2.7 REQUIRED BANDWIDTH FOR BPSK WITH NRZ DATA FORMAT

Again, from Eqn (5), the PSD of the BPSK with NRZ data format can be shown to have the following form:

$$S_2(f) = T \frac{\sin^2(\pi(f-f_c)T)}{(\pi(f-f_c)T)^2} \tag{22}$$

Using Eqn (22), the required bandwidth can be easily evaluated. The relationship between the required bandwidth with p% power containment is given as

$$p\% = \frac{1}{\pi} \int_{-M_6\pi}^{M_6\pi} [\sin^2(x)/x^2]dx \tag{23}$$

where

$$M_6 = \frac{BW_6}{R_s} \tag{24}$$

here BW_6 denotes the required bandwidth for BPSK/NRZ case. Illustrated in Figure 5 is the plot of Eqn (23). This figure shows the power containment as a function of the normalized bandwidth. For example, the required one-sided bandwidths for 95 % and 99 % power containment are $2R_s$ and $11R_s$, respectively.

3. UNWANTED EMISSION: DEFINITION AND ANALYSIS

3.1 DEFINITION

The term "Unwanted Emission" used through this paper is defined as follow:

> "The unwanted emission is the amount of emission such that, below the lower and above the upper frequency limits, the total power contained in the unwanted emission is equal to a percentage of the total power."

3.2 ANALYSIS

By definition, the unwanted emission can have both continuous and discrete components. In the followings, the unwanted emission caused by each component will be calculated separately for each type of modulation scheme considered above. Notice that form the PSD, we observe that only PCM/PSK/PM/sinewave subcarrier have both discrete and continuous components and the rest has only continuous component.

From Eqn (6), the unwanted spurious emission, denote as SE1%, for PCM/PSK/PM with squarewave subcarrier can be evaluated using the following equation

$$SE1\% = 1 - \frac{8\sin^2(m)}{\pi^3} \sum_{k\geq 1} \frac{1}{(2k-1)^2} \int_{-\pi(M-n(2K-1))}^{\pi(M-n(2K-1))} [\sin(x)/x]^2 \, dx - \cos^2(m) \qquad (25)$$

From Eqn (9), for PCM/PSK/PM with sinewave subcarrier, the unwanted spurious emission due to continuous spectrum, denoted by $SE2_c\%$, is given by

$$SE2_c\% = 1 - J_0^2(m) - 2\sum_{k \text{ even}}^{\infty} J_k^2(m) - \sum_{h \text{ odd}}^{L} J_h^2(m) a_h(L) \qquad (26)$$

and the unwanted spurious emission, denoted by $SE2_d\%$, due to the discrete component is given by

$$SE2_d\% = 2 \sum_{k \text{ even}}^{\infty} J_k^2(m) \qquad (27)$$

The unwanted spurious emission for PCM/PM/Bi-phase, denoted by SE3%, can be evaluated by using, from Eqn (14)

$$SE3\% = 1 - \frac{2\sin^2(m)}{\pi} \int_{-M_3\pi/2}^{M_3\pi/2} [\sin^4(x)/x^2]dx - \cos^2(m) \quad (28)$$

From Eqn (17), the unwanted spurious emission for PCM/PM/NRZ, denoted by SE4%, can be evaluated by using, from Eqn (14)

$$SE4\% = 1 - \frac{\sin^2(m)}{\pi} \int_{-M_4\pi}^{M_4\pi} [\sin^2(x)/x^2]dx - \cos^2(m) \quad (29)$$

Similarly, from Eqn (20), the unwanted spurious emission for BPSK/Bi-phase, denoted by SE5%, is given by

$$SE5\% = 1 - \frac{2}{\pi} \int_{-M_5\pi/2}^{M_5\pi/2} [\sin^4(x)/x^2]dx \quad (30)$$

From Eqn (23), the unwanted spurious emission for BPSK/NRZ, denoted by SE6%, is given by

$$SE6\% = 1 - \frac{2}{\pi} \int_{-M_6\pi}^{M_6\pi} [\sin^2(x)/x^2]dx \quad (31)$$

The unwanted spurious emission for each modulation type is calculated and the results are presented in Table 1. This table shows the results for one-sided bandwidth of $2R_s$ and $4R_s$ for both BPSK and PCM/PM signal with m = 1.3 rad for PCM/PM, and one-sided bandwidth of $20R_s$ for PCM/PSK/PM signals with m = 1.3 rad and n = 3,9.

4. DATA POWER EFFICIENCY

4.1 POWER CONTAINED IN THE DATA CHANNEL

The power contained in the data channel for a specified bandwidth can be calculated from the results presented in Section 2. From Eqns (6), (9), (14), (17), (20) and (23), the power contained in the data channel can be calculated. Notice that for BPSK signals, the power contained in the data channel are calculated using the same equations as (20) and (23) for BPSK/Bi-phase and BPSK/NRZ, respectively.

For PCM/PSK/PM/Squarewave subcarrier, the data power containment, denoted as P1%, is given by

$$p1\% = \frac{8\sin^2(m)}{\pi^3} \sum_{k\geq 1} \frac{1}{(2k-1)^2} \int_{-\pi(M-n(2K-1))}^{\pi(M-n(2K-1))} [\sin(x)/x]^2 \, dx \quad (32)$$

For PCM/PSK/PM/Sinewave subcarrier, the data power containment, denoted as P2%, is given by

$$P2\% = \sum_{h \text{ even}}^{L} J_h^2(m)\, a_h(L) \tag{33}$$

For PCM/PM/Bi-phase, the data power containment, denoted as P3%, is given by

$$P3\% = \frac{2\sin^2(m)}{\pi} \int_{-M_3\pi/2}^{M_3\pi/2} [\sin^4(x)/x^2]dx \tag{34}$$

For PCM/PM/NRZ, the data power containment, denoted as P4%, is given by

$$P4\% = \frac{\sin^2(m)}{\pi} \int_{-M_4\pi}^{M_4\pi} [\sin^2(x)/x^2]dx \tag{35}$$

The power containment in the data channel for each modulation type is evaluated and the numerical results are also presented in Table 1, for the sake of comparison. This table shows the calculations of the data power efficiency for one-sided bandwidth of $2R_s$ and $4R_s$ for both BPSK and PCM/PM signal with m = 1.3 rad for PCM/PM, and one-sided bandwidth of $20R_s$ for PCM/PSK/PM signals with m = 1.3 rad and n = 3, 9.

4.2 SYMBOL SNR DEGRADATION DUE TO ISI

When the RF filter bandwidth becomes less than the main spectrum hump of the modulated carrier, the information-bearing pulses are spread out in time. Each pulse is overlaid with the tails of previous pulses and the precursors of the subsequent ones, and this so-called Intersymbol Interference (ISI) behaves like an additional random noise. This additional random noise can cause potential degradation to the receiver. In addition, excessive filtering of the pulse can also cause a loss of symbol energy during the symbol time. The effects of symbol energy's loss for specified bandwidths are already examined in Section 4.1 for the required bandwidth of $2R_s$ and $4R_s$. This section investigates the effects of ISI on the symbol SNR degradation.

The effects of the ISI on the performance degradation of the PCM/PM receivers have been investigated in [8-9]. [8-9] evaluated the SSNR degradation of both PCM/PM/NRZ and PCM/PM/Bi-phase receivers for an ideal low-pass filter. The results presented in [8-9] can be extended for PCM/PSK/PM and BPSK signal formats.

To extend the results in [8-9], it is necessary to give a brief summary on the key results presented in [8-9]. It has been shown in [8] that, for $BT \geq 1$ (where B denotes the required bandwidth), the average probability of error is given by:

$$P_e = \int_{\theta_e} P_e(\theta_e) P(\theta_e) d\theta_e \tag{36}$$

TTable 1: Data Power Efficiency and Unwanted Spurious Emission For Various Modulation Techniques Under Investigation

Modulation Type	Data Power Efficiency Without Filtering	Unwanted Spurious Emission		Remark
		Continuous Component	Discrete Component	
BPSK/NRZ	95 % (BW = $2R_s$)	5 % (BW = $2R_s$)	0 %	
	97.5 % (BW = $4R_s$)	2.5 % (BW = $4R_s$)		
BPSK/Bi-Phase	85.57 % (BW = $2R_s$)	14.43 % (BW = $2R_s$)	0 %	Recommend Filtering
	92.51 % (BW = $4R_s$)	7.49 % (BW = $4R_s$)		
PCM/PM/NRZ (m =1.3 rad)	88.2 % (BW = $2R_s$)	4.64 % (BW = $2R_s$)	0 %	
	90.5 % (BW = $4R_s$)	2.3 % (BW = $4R_s$)		
PCM/PSK/Bi-Phase (m =1.3 rad)	79.45 % (BW = $2R_s$)	13.40 % (BW = $2R_s$)	0 %	Recommend Filtering
	85.89 % (BW = $4R_s$)	6.95 % (BW = $4R_s$)		
PCM/PSK/PM - Squarewave (BW = $20R_s$) (m=1.3 rad)	86.23 % (n = 3)	6.61 % (n = 3)	0 %	Recommend Filtering
	74.84 % (n = 9)	18.01 % (n = 9)		
PCM/PSK/PM - Sinewave (BW = $20R_s$) (m=1.3 rad)	54.56 % (n = 3)	0.28 % (n = 3)	6.71 (n = 3)	
	54.16 % (n = 9)	0.69 % (n = 9)	6.70 % (n = 9)	

where $P_e(\theta_e)$ is the conditional probability of error and $P(\theta_e)$ is the probability density function (pdf) of the carrier tracking phase error θ_e. If the number of pulses, M, before and after the present pulse being detected is bewteen 1 and 2, i.e., $1 \leq M \leq 2$, then direct computation of the conditional error probability $P_e(\theta_e)$ is feasible through the following equation [8]

$$P_e(\theta_e) = (1/2)[(1/2^{2M}) \sum_{\substack{k=2^{2M} \\ \text{combinations}}} \text{erfc}\{\sqrt{E_s/N_o}[1 + \Sigma' d_k \lambda_k]\cos\theta_e\} \quad (37)$$

As an example, for M = 1, Eqn (37) becomes

$$\begin{aligned} P_e(\theta_e) = {} & (1/2)[(1/4)\text{erfc}\{\sqrt{E_s/N_o}(1+\lambda_{-1}+\lambda_{+1})\cos\theta_e\} \\ & + (1/4)\text{erfc}\{\sqrt{E_s/N_o}(1+\lambda_{-1}-\lambda_{+1})\cos\theta_e\} \\ & + (1/4)\text{erfc}\{\sqrt{E_s/N_o}(1-\lambda_{-1}+\lambda_{+1})\cos\theta_e\} \\ & + (1/4)\text{erfc}\{\sqrt{E_s/N_o}(1-\lambda_{-1}-\lambda_{+1})\cos\theta_e\}] \end{aligned} \quad (38)$$

where $d_k = \pm 1$ with $\Pr\{d_k = +1\} = \Pr\{d_k = -1\} = 1/2$, and

$$\lambda_k = \frac{\int_0^T g(t)g(t+kT)\,dt}{\int_0^T |g(t)|^2\,dt} \quad (39)$$

where g(t) is defined as

$$g(t) = P(t) * h(t) \quad (40)$$

where * denotes the convolution.

For both PCM/PM/NRZ and PCM/PM/Bi-phase, the symbol energy is defined as

$$E_s = A^2\sin^2(m_T)\int_0^T |g(t)|^2\,dt \quad (41)$$

Note that P(t) denotes the pulse shape of the data and h(t) denotes the impulse response of the equivalent low-pass filter of the RF bandpass filter with the required bandwidth B.

When the loop signal-to-noise ratio is high the Tikhonov pdf can be approximated by

$$P(\theta_e) \approx \exp(-\theta_e^2/2\sigma^2)/[2\pi\sigma^2]^{-1/2}, \quad -\infty < \theta_e < \infty \quad (42)$$

For perfect NRZ data stream and high-data-rate case ($B_L/R_s << 0.1$, where B_L and R_s denote the one-sided carrier loop bandwidth and the symbol rate, respectively), the variance of the carrier tracking phase error is found to be

$$\sigma^2 = (1/\rho_o) + (B_L/R_s)\tan^2(m_T) \tag{43}$$

and, for perfect Bi-ϕ data format σ^2 becomes

$$\sigma^2 = (1/\rho_o) + (I/C)\tan^2(m_T) \tag{44}$$

where ρ_o is the carrier loop SNR which is found to be

$$\rho_o = \frac{(E_s/N_o)}{(B_L/R_s)\tan^2(m_T)} \tag{45}$$

and I/C is the interference-to-carrier ratio which is given by

$$\begin{aligned} I/C = {} & (1/2) + (9/16)(B_L/R_s)^{-1} \\ & - (3/4)(B_L/R_s)^{-1}\exp\{-(2/3)(B_L/R_s)\}[\cos\{(2/3)(B_L/R_s)\} \\ & + 3\sin\{(2/3)(B_L/R_s)\}] \\ & + (3/16)(B_L/R_s)^{-1}\exp\{-(4/3)(B_L/R_s)\}[\cos\{(4/3)(B_L/R_s)\} \\ & + 3\sin\{(4/3)(B_L/R_s)\}] \end{aligned} \tag{46}$$

[8] has shown that, for ideal low-pass filter and perfect data stream, the output of the filter for NRZ data format, denoted by $g_{NRZ}(t+kT)$, is given by

$$g_{NRZ}(t+kT_s) = \frac{1}{\pi}[si\{2\pi B(t+T(k+1/2))\} - si\{2\pi B(t+T(k-1/2))\}] \tag{47}$$

For Bi-ϕ data format one gets

$$\begin{aligned} g_{Bi\text{-}\phi}(t+kT_s) = {} & \frac{1}{\pi}[si\{2\pi B(t+T(k+1/2))\} + si\{2\pi B(t+T(k-1/2))\} \\ & - 2si(2\pi B(t+kT)] \end{aligned} \tag{48}$$

where B is the one-sided bandwidth of the low-pass filter and it can be set equal to the required bandwidth, and

$$si(x) = \int_0^X [\sin(u)/u]du \tag{49}$$

For PCM/PSK/PM with $n \geq 3$, the variance of the carrier tracking phase error becomes

$$\sigma^2 = (1/\rho_o) \tag{50}$$

For PCM/PSK/PM-squarewave, the carrier loop SNR is identical to PCM/PM (see Eqn (45)). However, for PCM/PSK/PM-sinewave, the carrier loop SNR becomes

$$\rho_o = \frac{J_0^2(m_T)(E_s/N_o)}{2(B_L/R_s)J_1^2(m_T)} \tag{51}$$

where E_s is given by

$$E_s = 2A^2J_1^2(m_T)\int_0^T |g(t)|^2\, dt \tag{52}$$

For BPSK, the loop SNR, ρ, of a Costas is given by [10]

$$\rho = \frac{A^2}{N_0B_L} S_L \tag{53}$$

where S_L is the squaring loss which is given by the simple relation

$$S_L = \frac{K_1^2}{K_1K_2 + K_LK} \tag{54}$$

where

$$K_1 = \int_{-\infty}^{\infty} S_d(f)\,|G(j2\pi f)|^2\, df \tag{55}$$

$$K_2 = \frac{\int_{-\infty}^{\infty} S_d(f)\,|G(j2\pi f)|^4\, df}{\int_{-\infty}^{\infty} S_d(f)\,|G(j2\pi f)|^2\, df} \tag{56}$$

$$K_L = \frac{\int_{-\infty}^{\infty} |G(j2\pi f)|^4\, df}{\int_{-\infty}^{\infty} |G(j2\pi f)|^2\, df} \tag{57}$$

$$K = \frac{BT}{E_s/N_0} \tag{58}$$

where $S_d(f)$ denotes the power spectral density of the data modulation d(t), $G(j2\pi f)$ is the transfer function of the low-pass arm filter. Again, the parameter B in Eqn (47) is the single-sided noise bandwidth of the low-pass arm filter of the Costas loop, i.e.,

$$B = \int_{-\infty}^{\infty} |G(j2\pi f)|^2 \, df \tag{59}$$

Note that B can have the same value as the required bandwidth.

For NRZ and Bi-phase data modulation, the power spectral densities are identical to Eqns (12) and (19), respectively. Furthermore, for n-pole Butterworth filter, the transfer function of the arm filter is

$$|G(j2\pi f)|^2 = [1 + (f/f_c)^{2n}]^{-1} \tag{60}$$

where f_c is the 3-dB bandwidth which is related to the single-sided noise bandwidth B of the arm filter:

$$f_c = (2Bn/\pi)\sin(\pi/2n) \tag{61}$$

For ideal arm filter, i.e. rectangular frequency response, the squaring loss S_L becomes

$$S_L = \frac{K_3^2}{K_3 + [BT/(E_s/N_0)]} \tag{62}$$

where

$$K_3 = \frac{2}{\pi}\left[si(2\pi BT) - \frac{\sin^2(\pi BT)}{\pi BT}\right] \tag{63}$$

and Si(x) is defined in Eqn (49).

In the absence of ISI, the average BER, PE_0, for an uncoded channel is well-known to be given by:

$$PE_0 = \frac{1}{2}\,\mathrm{erfc}\left(\sqrt{(E_s/N_0)_0}\right) \tag{64}$$

where $(E_s/N_0)_0$ is the required symbol SNR to achieve a desired SER, PE_0, for unlimitted bandwidth case.

In the presence of bandlimiting channel, the average SER, PE_1, for an uncoded channel can be calculated from Eqn (36). Let $(E_s/N_0)_1$ be the required symbol SNR to achieve a desired SER, PE_1, for bandlimiting case. Thus, if we fix the SER, i.e.,

$PE_0 = PE_1 = SER_0$ (a desired value)

then the symbol SNR degradation in dB for this specified SER_0 is defined as:

$$\Delta(dB) = (E_s/N_0)_0 - (E_s/N_0)_1 \quad (65)$$

The value of $(E_s/N_0)_0$ can be computed by using Eqn (53). To compute $(E_s/N_0)_1$ for PCM/PM/NRZ, we substitute Eqns (37) and (42) into Eqn (36) with the carrier tracking jitter (σ^2) given by Eqn (43) and performing numerical integration on the digital computer. Having $(E_s/N_0)_0$ and $(E_s/N_0)_1$, one can calculate the Symbol SNR degradation in dB using Eqn (54). The calculated symbol SNR degradation in dB for various modulation types are presented in Table 2. Table 2 shows the results for m = 1.3 rad, $(2B_L/R_s)$ = 0.001 at SER = 10^{-5}. Note that the carrier loop SNR (ρ_0) is fixed in the calculation of the symbol SNR degradation for all cases.

Table 2. Symbol SNR degradation in dB due to ISI for various Modulation Schemes at SER = 10^{-5}

Modulation Type	Symbol SNR Degradation (dB)	
	BT = 1	BT = 2
PCM/PSK/PM-Squarewave ($m = 1.3$ rad, $2B_L/R_s = 0.001$)	0.75	0.15
PCM/PSK/PM-Sinewave ($m = 1.3$ rad, $2B_L/R_s = 0.001$)	0.75	0.18
PCM/PM/NRZ ($m = 1.3$ rad, $2B_L/R_s = 0.001$)	0.85	0.21
PCM/PM/Bi-Phase ($m = 1.3$ rad, $2B_L/R_s = 0.001$)	6.30	0.34
BPSK/NRZ ($2B_L/R_s = 0.001$)	0.74	0.17
BPSK/Bi-Phase ($2B_L/R_s = 0.001$)	6.30	0.29

5. OPTIMUM REQUIRED BANDWIDTH IN THE PRESENCE OF NOISE

This section focuses on the calculation of the optimum required bandwidth in the presence of the white Gaussian noise for BPSK signals only. Extension of the method presented here to other modulation types is straight forward. The term "optimum required bandwidth" considered in this section is defined as the bandwidth that is required to achieve the same amount of power contained in the signal as in the noise. When the required bandwidth exceeds that of the optimum required bandwidth, the noise power will exceed that of the signal power and hence degrades the system performance.

Let P_t be the total transmitted power, and P_s be the signal power. The signal power-to-the total transmitted power can be defined as follow

$$\frac{P_s}{P_t} = \int_{-BW}^{BW} S(f)\, df \qquad (66)$$

where BW is the required bandwidth and S(f) is the PSD of the transmitted signal. As an example, for BPSK/Bi-phase and BPSK/NRZ, the PSD's are given by Eqns (19) and (22), respectively.

Similarly, the noise power-to-the total transmitted power is given by

$$\frac{P_n}{P_t} = \frac{2N_0BW}{P_t} \qquad (67)$$

where N_0 is one-sided spectral density of the noise. Note that Eqn (52) can be rewritten in terms of the normalized bandwidth M, i.e., $M = BW/R_s$, and the Symbol Signal-to-Noise Ratio (SSNR), $SSNR = E_s/N_0 = P_tT/N_0$, as follow

$$\frac{P_n}{P_t} = \frac{2M}{SSNR} \qquad (68)$$

Dividing Eqn (51) by (53) we obtain

$$\frac{P_s}{P_n} = \frac{SSNR}{2M} \int_{-BW}^{BW} S(f)\, df \qquad (69)$$

where the optimum bandwidth is selected in such a way that the ratio in Eqn (54) is unity. The plots of Eqns (51), (53) and (54) are shown in Figures 6-9. Figures 6-7 show the results for BPSK/NRZ, and Figures 8-9 are for BPSK/Bi-phase. These figures plot the percentage of power containment as a function of the normalized bandwidth with SSNR as parameter. These figures show that for SSNR = 10 dB, the optimum bandwidths for both BPSK/NRZ and BPSK/Bi-phase are about $5R_s$. Furthermore, maximum P_s/P_n occurs at $BW = R_s$ for BPSK/NRZ, and at $BW = 2R_s$ for BPSK/Bi-phase.

6. DISCUSSIONS

For the sake of comparison, the numerical results presented in Figures 1-2, and 3-4 are ploted in Figures 10-11 and 12, respectively. Figures 10-11 compare the required bandwidth between PCM/PSK/PM-squarewave and PCM/PSK/PM-sinewave. Figure 12 compares the bandwidth between PCM/PM/NRZ and PCM/PM/Bi-phase. It is clearly shown in Figures 10-11 that as the desired signal power containment increases above 90 %, the required bandwidth for PCM/PSK/PM-squarewave increases much faster than that of

PCM/PSK/PM-sinewave. As mentioned earlier, for 99 % power containment, the one-sided bandwidths for PCM/PSK/PM-squarewave and PCM/PSK/PM-sinewave are about $328R_s$ and $27R_s$, respectively, for m = 1.2 rad and n = 9. Hence, for PCM/PSK/PM-squarewave signal with high data rate, it is suggested that the required bandwidth should be calculated before the frequency assignment.

Figure 12 shows that for signal power containment below 95 %, the required bandwidth for PCM/PM/Bi-phase is approximately twice that of PCM/PM/NRZ. But when the signal power containment exceeds 95 %, the required bandwidth for PCM/PM/Bi-phase grows exponentially as compare to PCM/PM/NRZ. The same is true for BPSK/Bi-phase and BPSK/NRZ. This is demonstrated in Figure 5. Based on the numerical results shown in Figures 5, 10, 11 and 12, BPSK/NRZ and PCM/PM/NRZ signals require the least bandwidth and PCM/PSK/PM-squarewave requires the most bandwidth.

It is also shown in Table 1 that for a fixed one-sided bandwidth of $2R_s$, BPSK/NRZ and PCM/PM/NRZ have the most power in the data channel as compare to the other modulation schemes. Concerning the unwanted spurious emission, the use of squarewave subcarrier and Bi-phase data format produce more out-of-band power than the sinewave subcarrier and NRZ data format.

Table 2 exemplifies the effects of ISI on the symbol SNR degradations when the required bandwidths are at R_s (BT = 1) and $2R_s$ (BT = 2). The results show that PCM/PM/NRZ provides relatively good performance as compared with the others. For instance, for BT =2, the symbol SNR degradations associated with PCM/PSK/PM-Square, PCM/PSK/PM-Sine, PCM/PM/NRZ, PCM/PM/Bi-phase, BPSK/NRZ and BPSK/Bi-phase are about 0.15, 0.18, 0.21, 0.34, 0.17 and 0.29, respectively.

7. CONCLUSION

Based on the detail investigation presented in this paper, the following conclusions can be reached. In order to achieve the same data power containment, the use of residual carrier modulation technique will require more bandwidth than the suppressed carrier modulation technique. In particular, BPSK/NRZ provides the best compromise between data power efficiency and unwanted emission as compared to BPSK/Bi-phase, PCM/PM/NRZ, PCM/PM/Bi-phase, PCM/PSK/PM-squarewave and PCM/PSK/PM-sinewave. However, PCM/PM/NRZ also provides compatible performance, in terms of high power containment and low level of unwanted emission, as compared to BPSK/NRZ. It is clearly shown in this paper that the use of subcarrier requires much larger bandwidth than that of the systems without using subcarrier. Because frequency spectrum is a scarce resource, it is recommended that the use of subcarrier should not be employed at high data rate, and that PCM/PM/NRZ modulation scheme should be used in place of PCM/PSK/PM.

ACKNOWLEDGEMENT

The authors are indebted to F. Bornkamp for his comments and suggestions in the calculation of the optimum bandwidth presented in Section 5. The work described in this paper was carried out at the Jet Propulsion Laboratory, California Institute of Technology, under contract with the National Aeronautics and Space Administration.

REFERENCES

[1] Tien M. Nguyen, "Occupied Bandwidth of Square Waveform/Sine Waveform as Subcarrier in Residual Carrier Systems," JPL-IOM 3396-86-144, internal document, October 11, 1986, Jet Propulsion Laboratory, Pasadena, CA.

[2] Tien M. Nguyen, "Closed Form Expressions for Computing the Occupied Bandwidth of PCM/PSK/PM Signals," 1991 IEEE International Symposium on EMC Proceedings, New Jersey.

[3] Tien M. Nguyen, "Computation of the Occupied Bandwidth for PCM/PSK/PM Signals," A-E-91-13, CCSDS, Subpanel 1E meeting, Salzburg, Austria, May 1992.

[4] Tien M. Nguyen, "Occupied Bandwidth for PCM/PSK/PM and PCM/PM Signals-A Comparative Study," A-E-90-15, CCSDS, Subpanel 1E meeting, Salzburg, Austria, May 1992.

[5] Jean Luc Gerner, "A Position Paper on Occupied Bandwidth of Space Telemetry Signals," CCSDS, Subpanel 1E Meeting, September 1991, Orlando, Florida.

[6] Jacques Fois Pelayo, "PCM/PSK/PM and PCM-SPL/PM Signals-Occupied Bandwidth and BER," European Space Agency, ESTEC, Noordwijk, the Netherlands, October 1992.

[7] Consultative Committee for Space Data Systems, Recommendations for Space Data System Standards, Radio Frequency and Modulation Systems, Part I, Earth Stations and Spacecraft, CCSDS 401.0-B, Blue Book, CCSDS Secretariat, Communications and Data System Division, (Code OS), NASA, Washington D.C.

[8] Tien M. Nguyen, Behavior of PCM/PM Receivers in Non-Ideal Channels, Part I: Separate Effects of Imperfect Data Streams and BandLimiting Channels on Performances," CCSDS, Subpanel 1E Meeting, January 1993, Pasadena, California.

[9] Tien M. Nguyen, Behavior of PCM/PM Receivers in Non-Ideal Channels, Part II: Combined Effects of Imperfect Data Streams and BandLimiting Channels on Performances," CCSDS, Subpanel 1E Meeting, January 1993, Pasadena, California.

[10] Joseph Yuen, "Deep Space Telecommunications Systems Engineering," Chapter 3, Plenum Press, New York, 1983.

Figure 1. Required Bandwidth for PCM/PSK/PM-Square

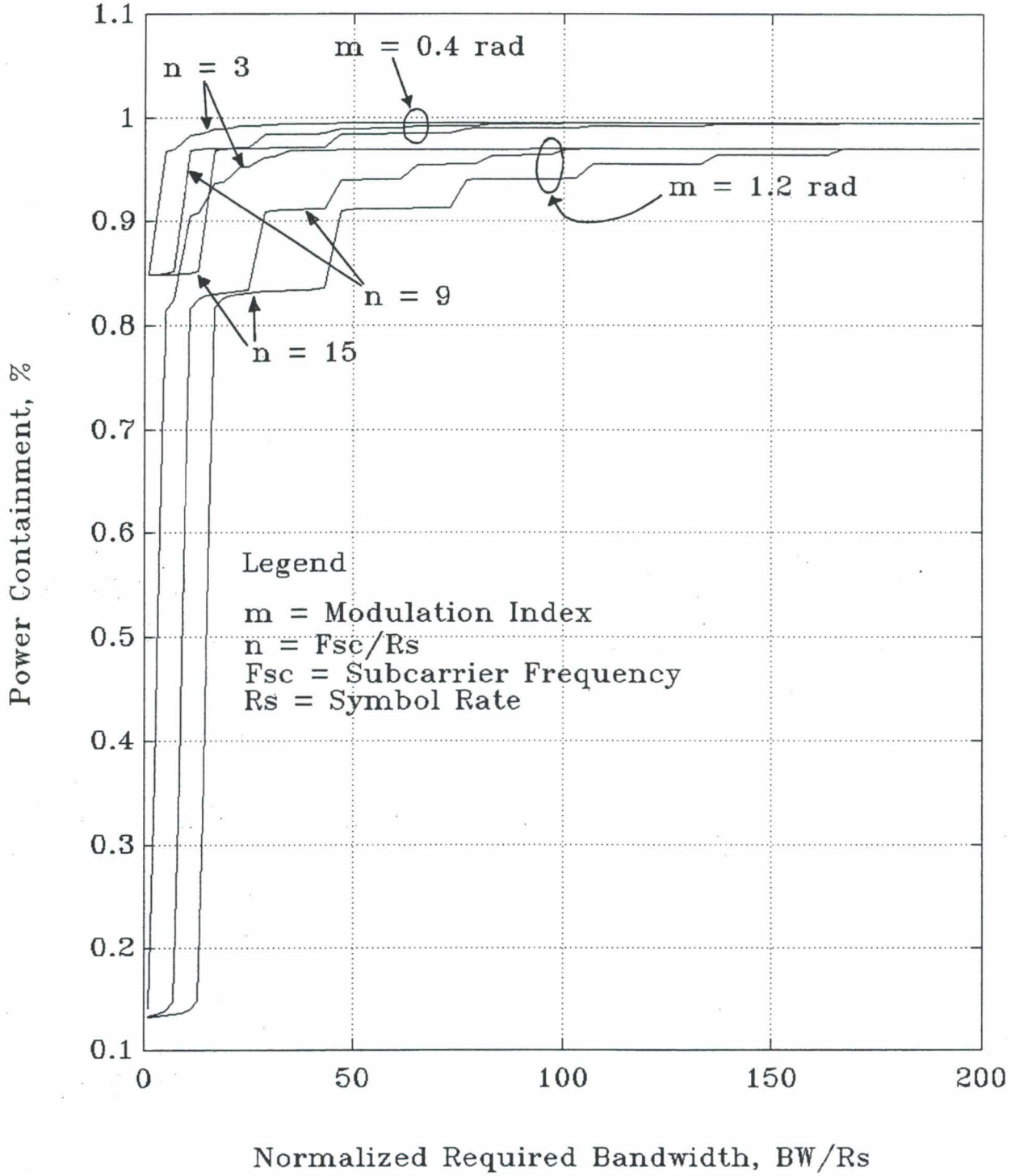

Figure 2. Required Bandwidth for PCM/PSK/PM–Sinewave

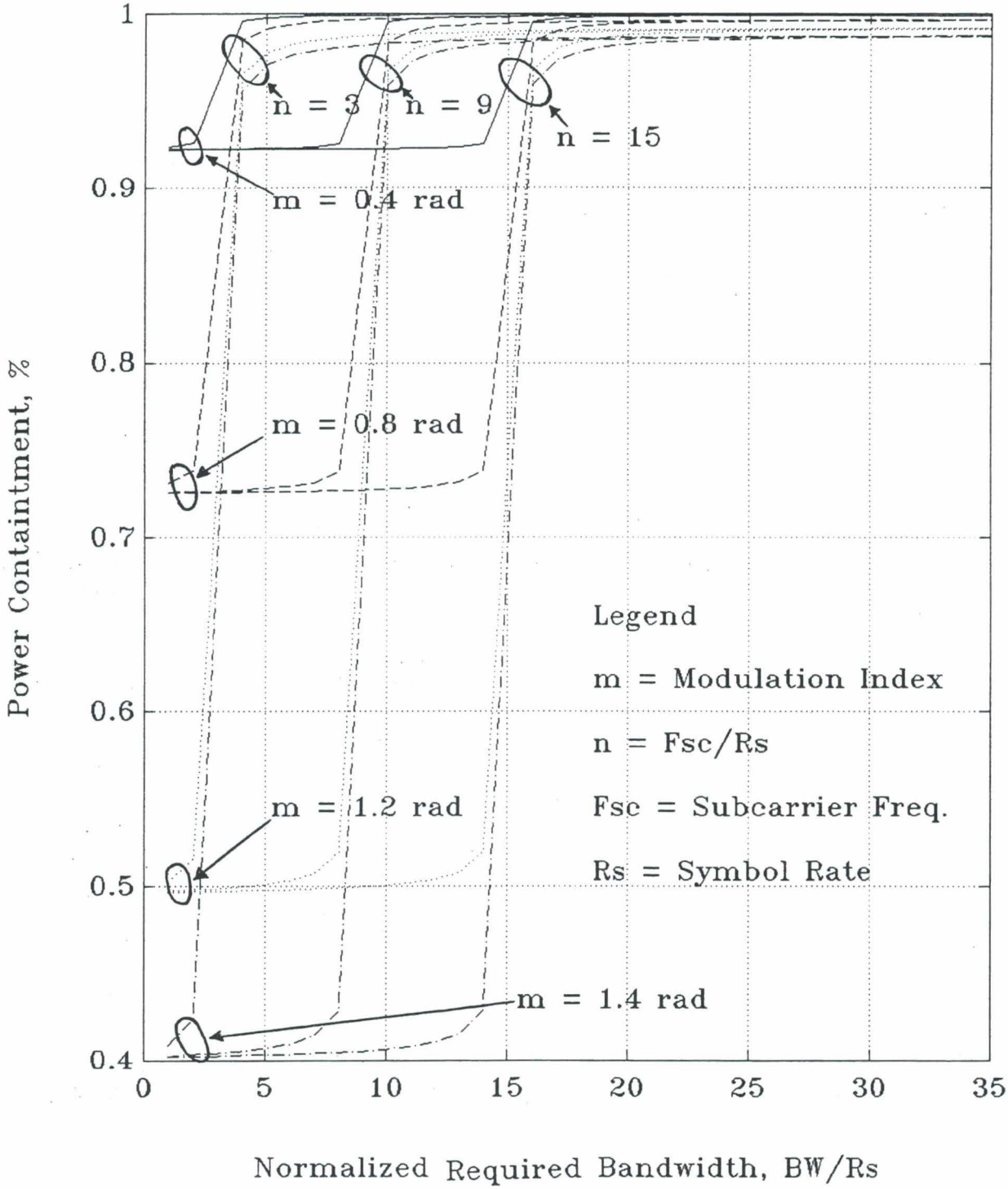

Figure 3 . Required Bandwith for PCM/PM/Bi-Phase

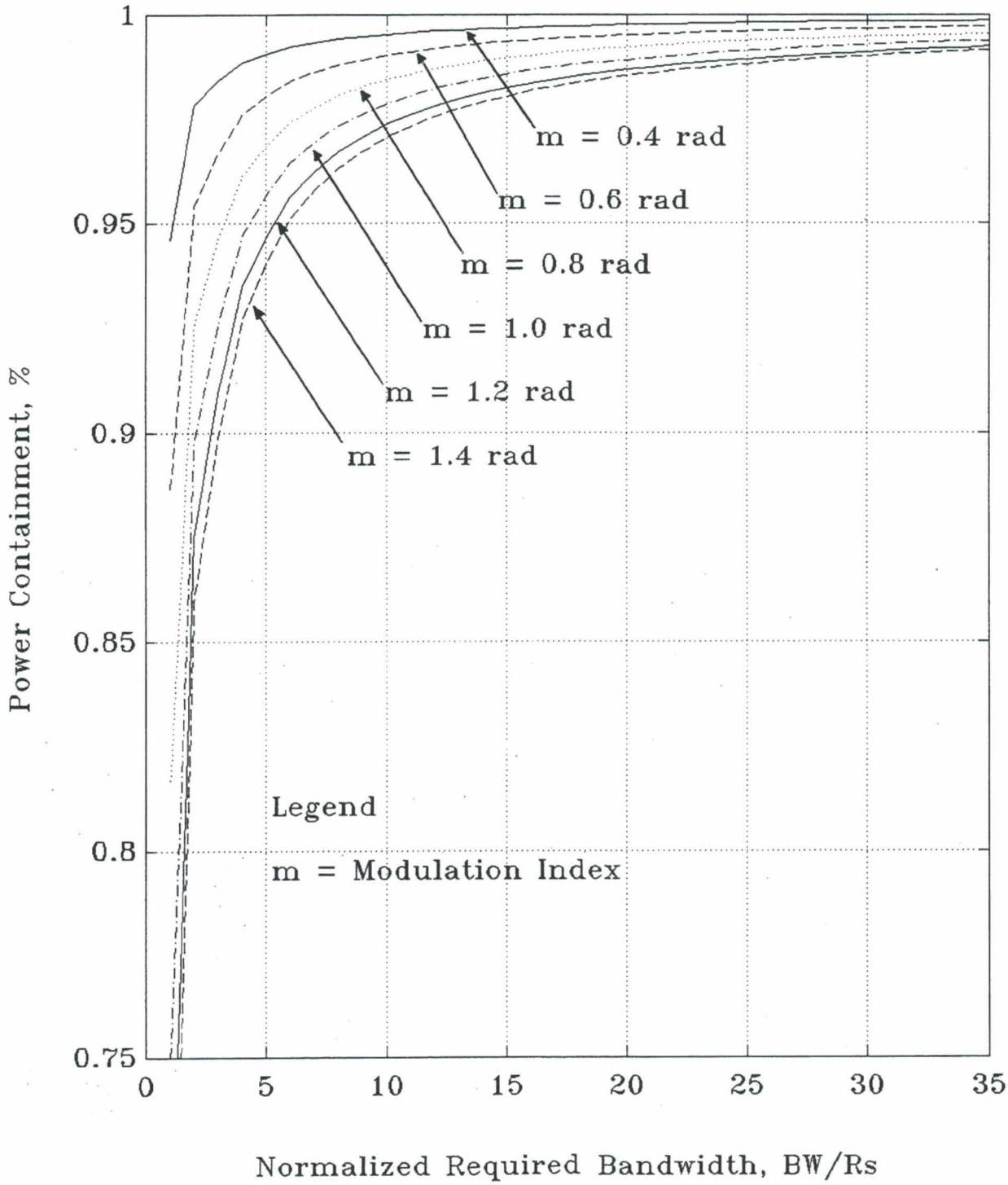

Figure 4. Required Bandwith for PCM/PM/NRZ

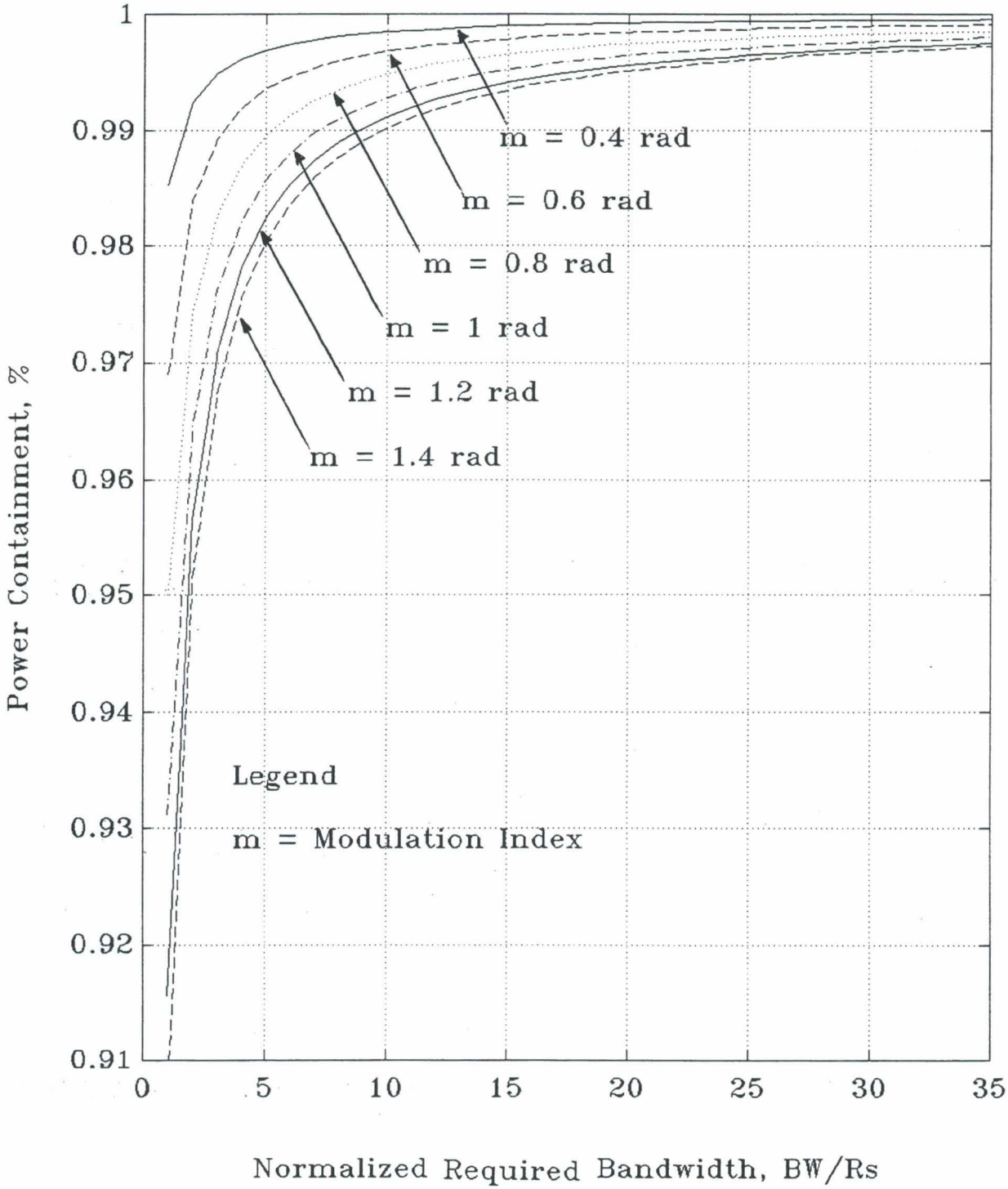

Figure 5. Required Bandwidth for BPSK Signals

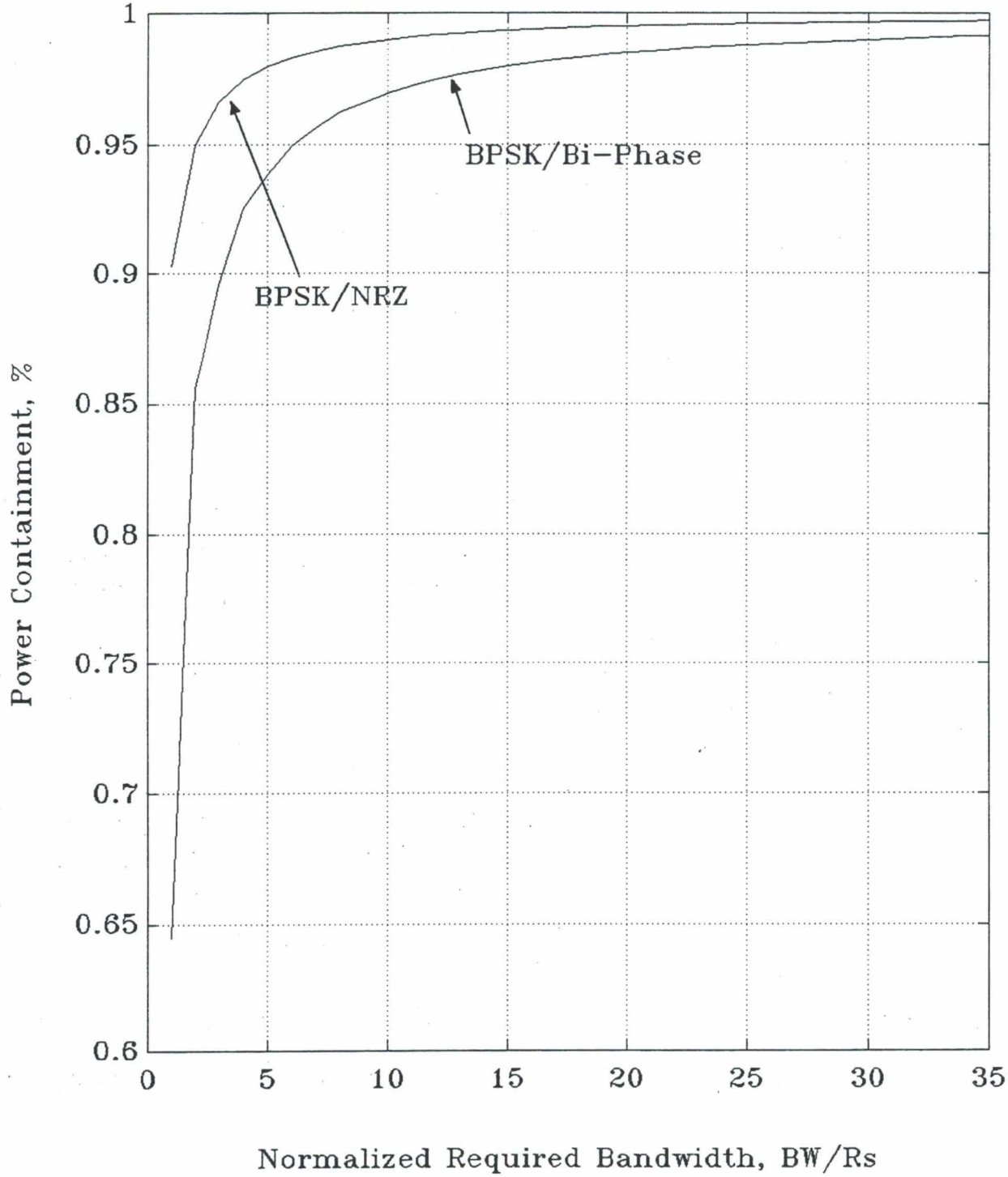

Figure 6. BPSK/NRZ in the Presence of Noise

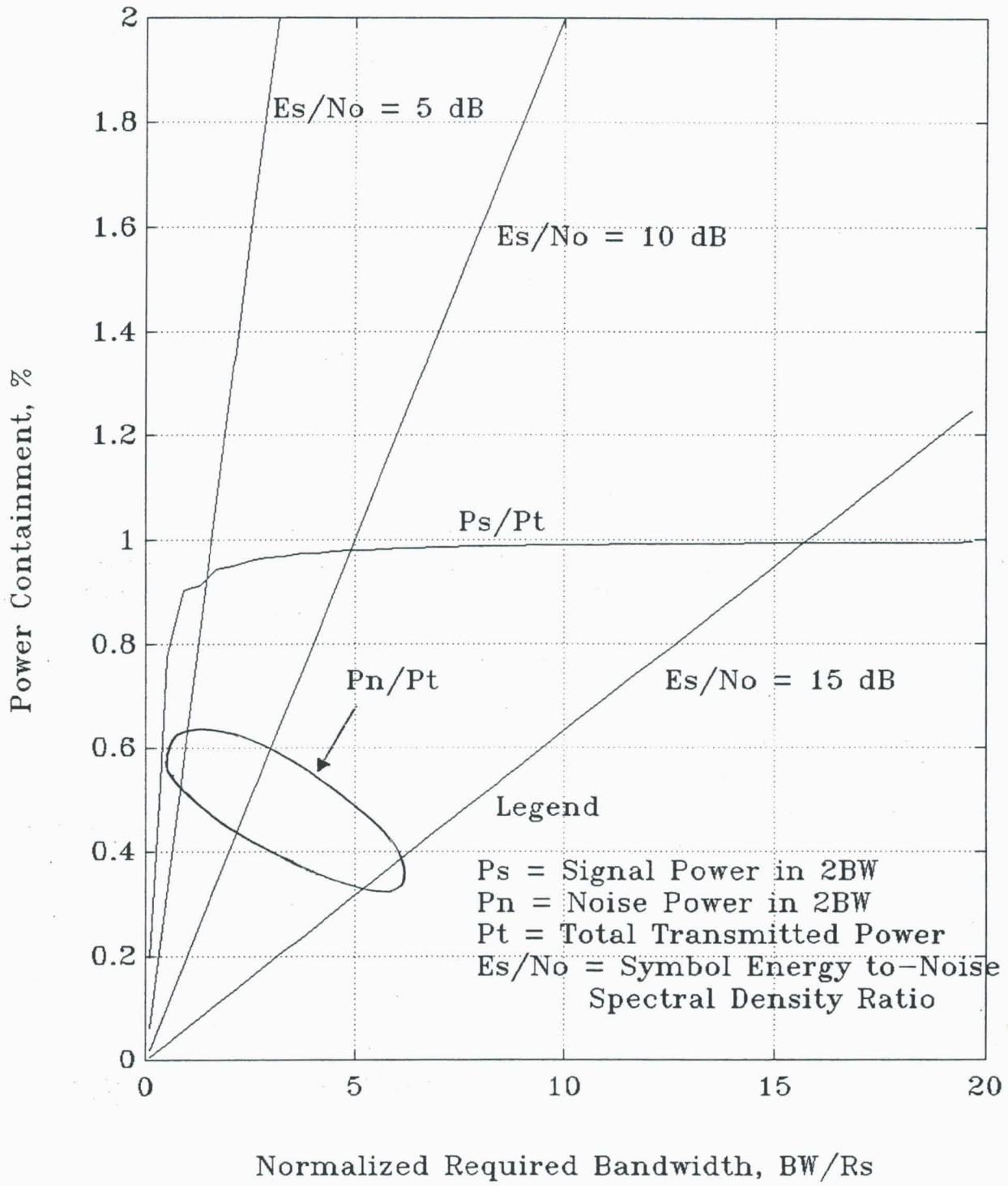

Figure 7. BPSK/NRZ in the Presence of Noise

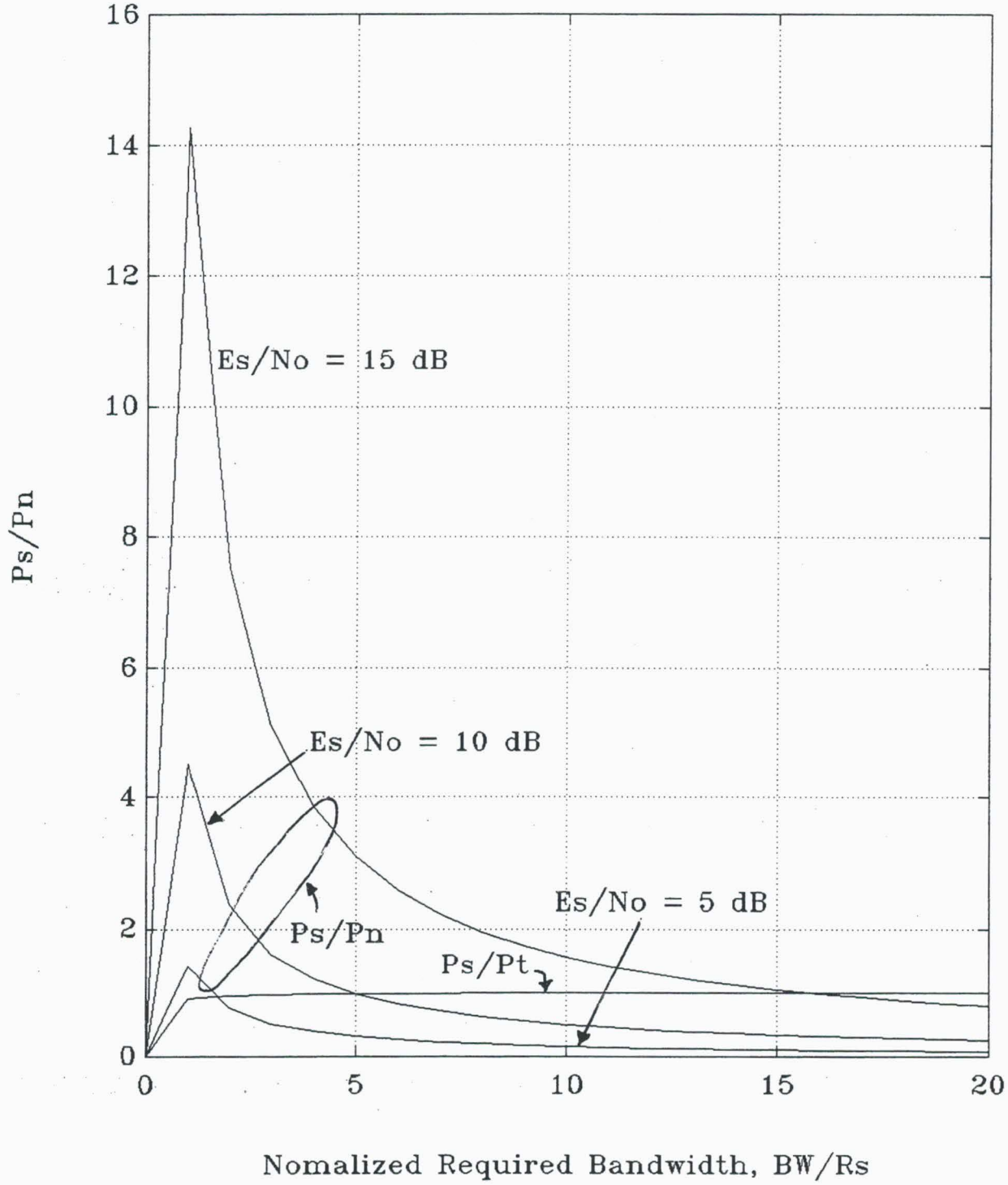

Figure 8. BPSK/Bi-Phase in the Presence of Noise

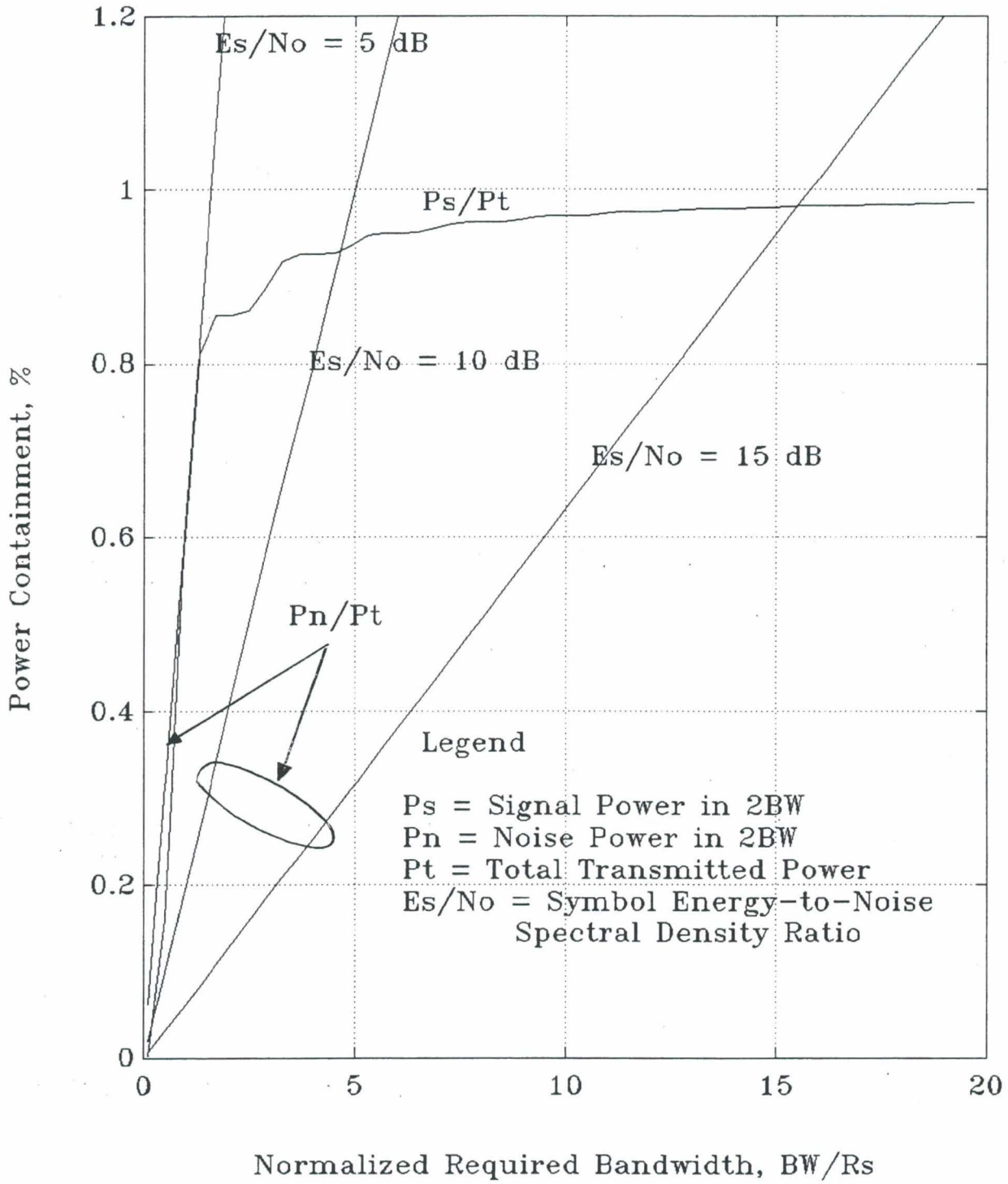

Figure 9. BPSK/Bi-Phase in the Presence of Noise

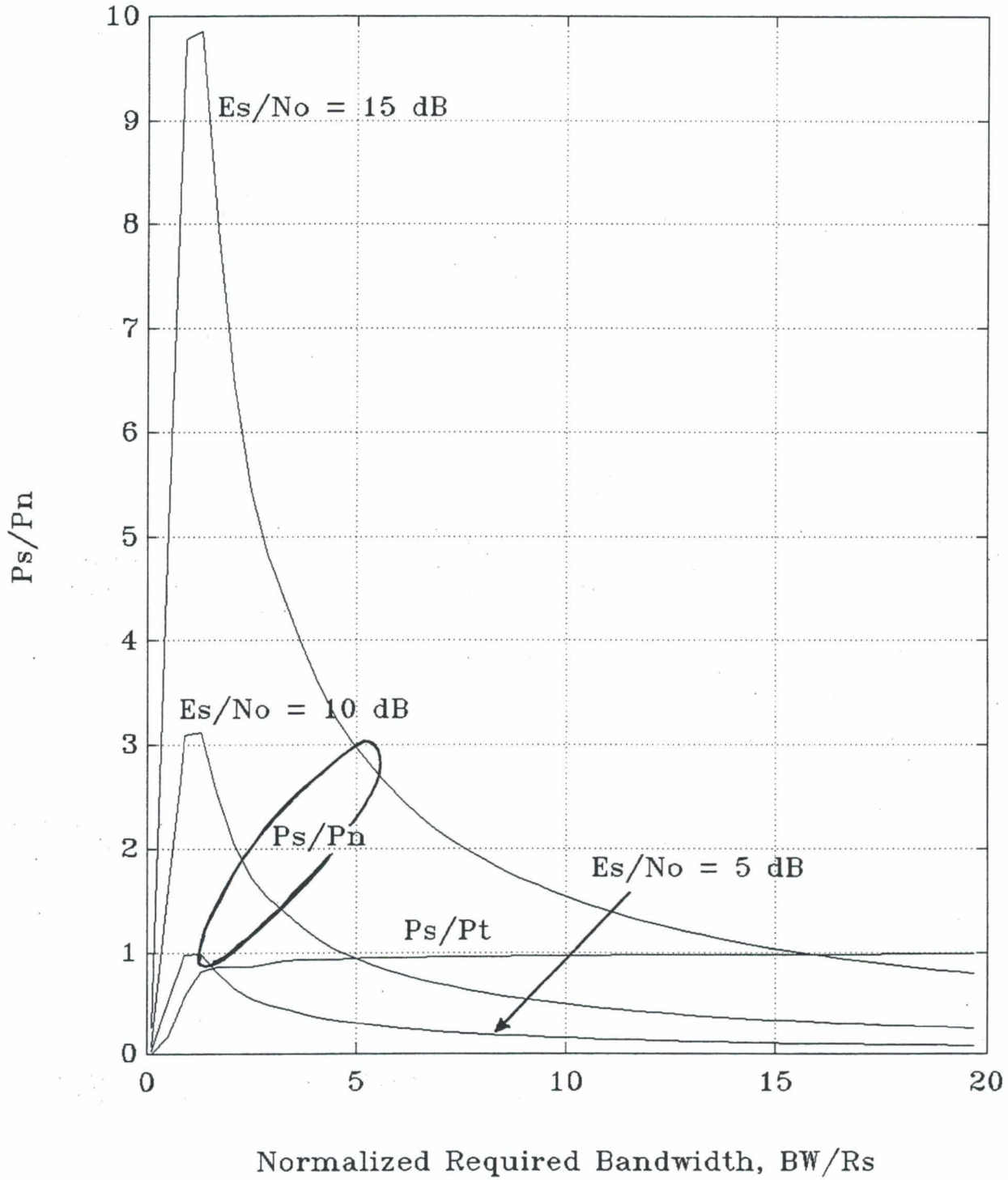

Figure 10 .Comparison of PCM/PSK/PM for m = 1.2 rad

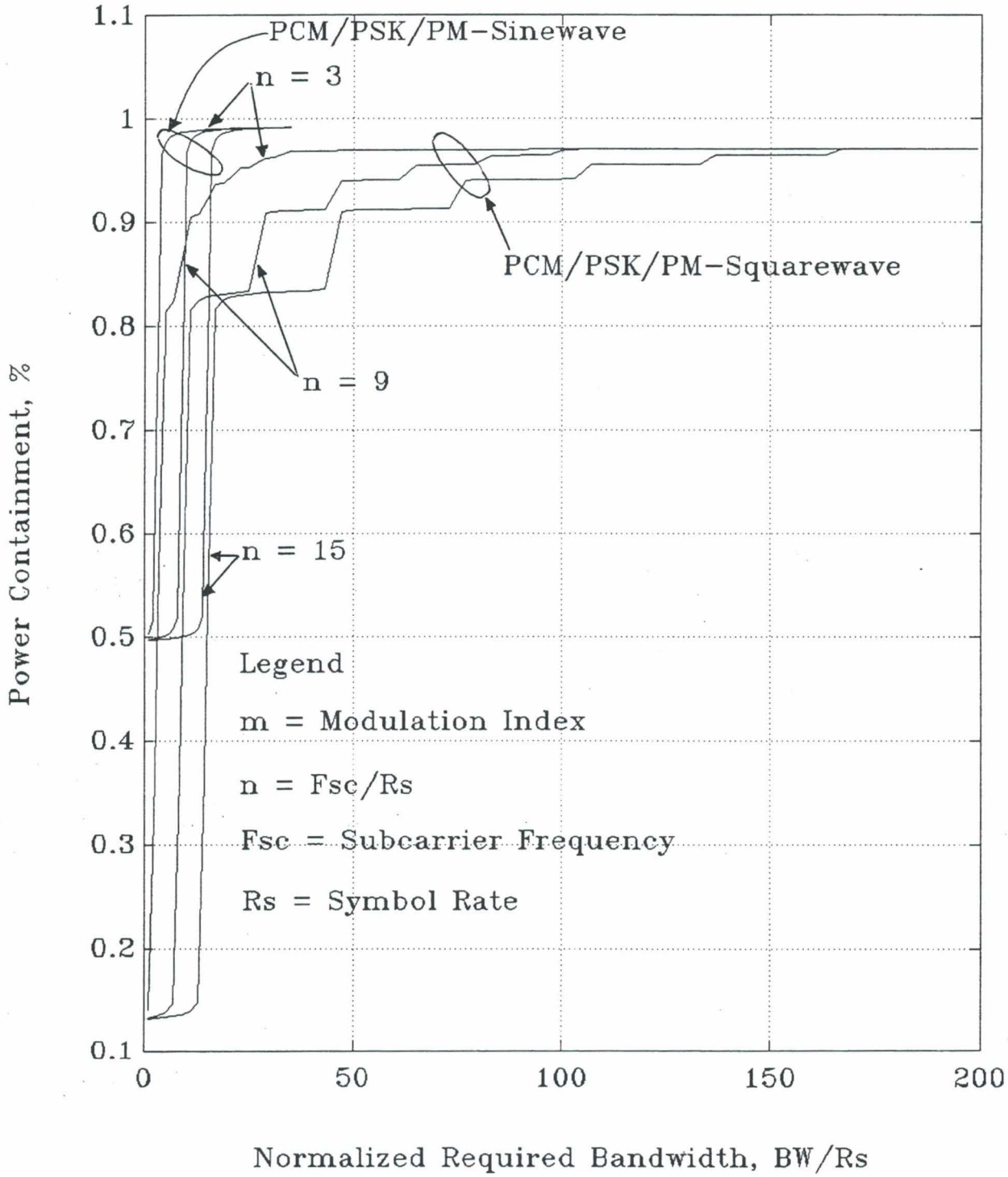

Figure 11 ..Comparison of PCM/PSK/PM for m = 0.4 rad

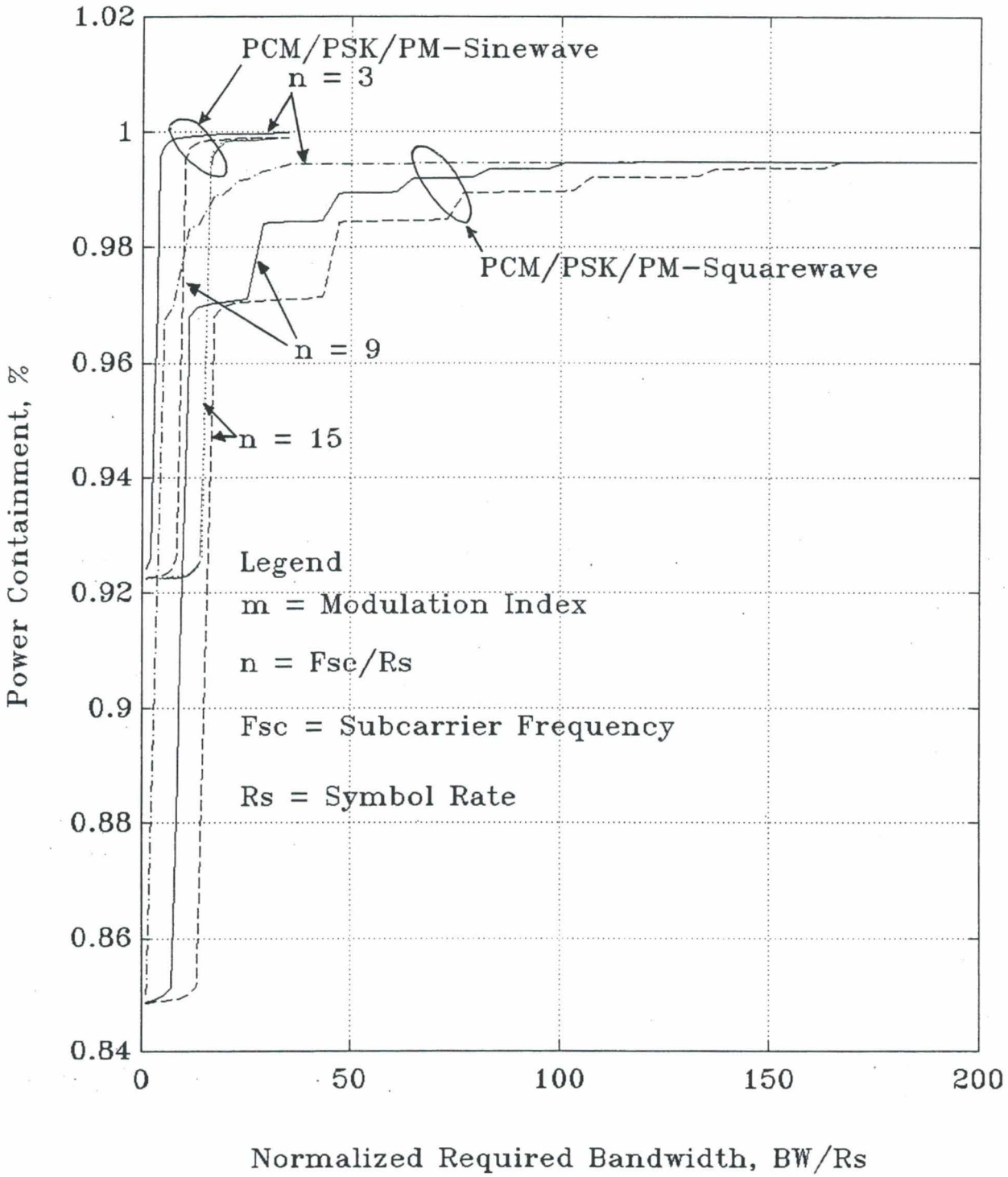

Figure 12. Comparison of PCM/PM Signals

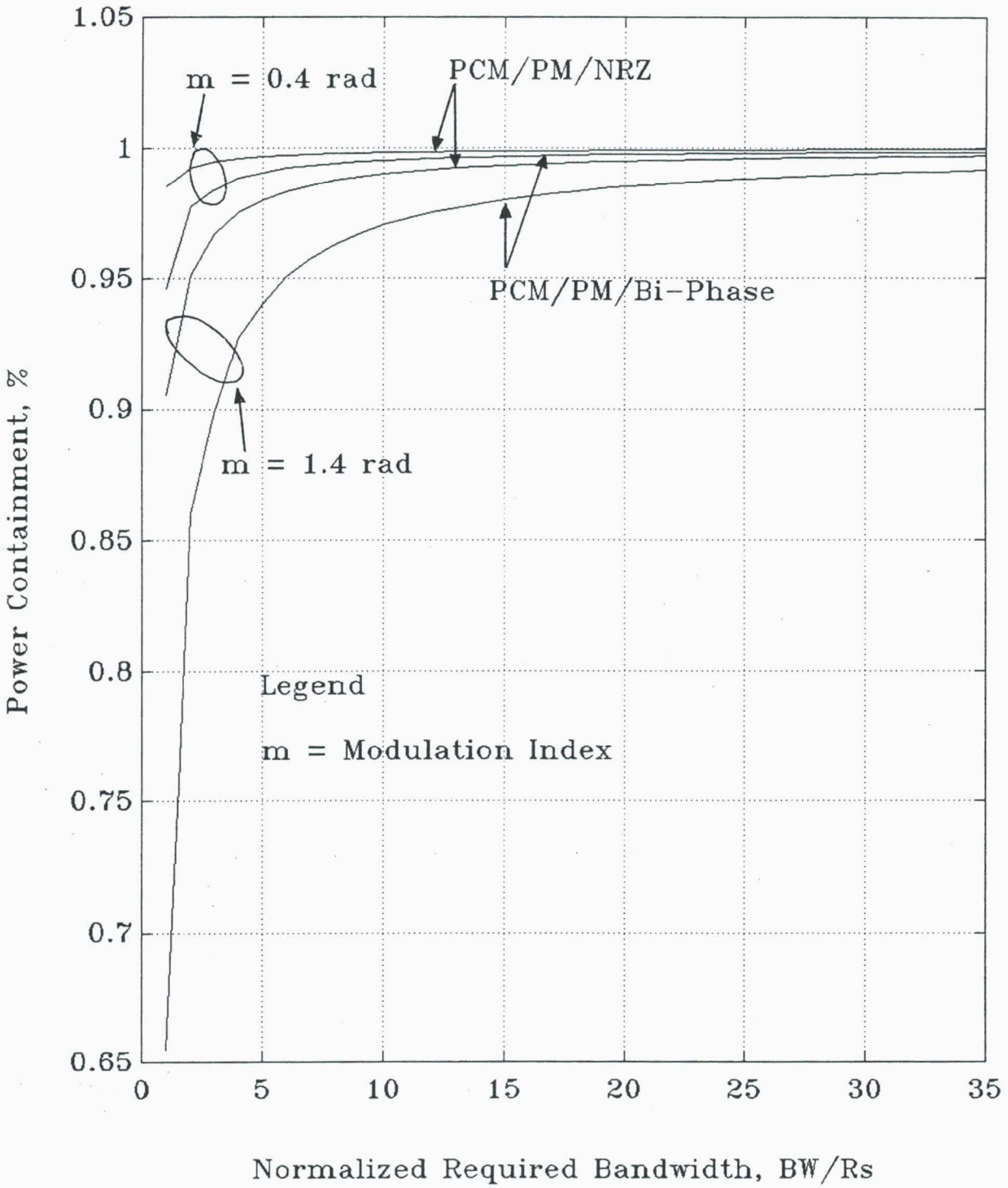

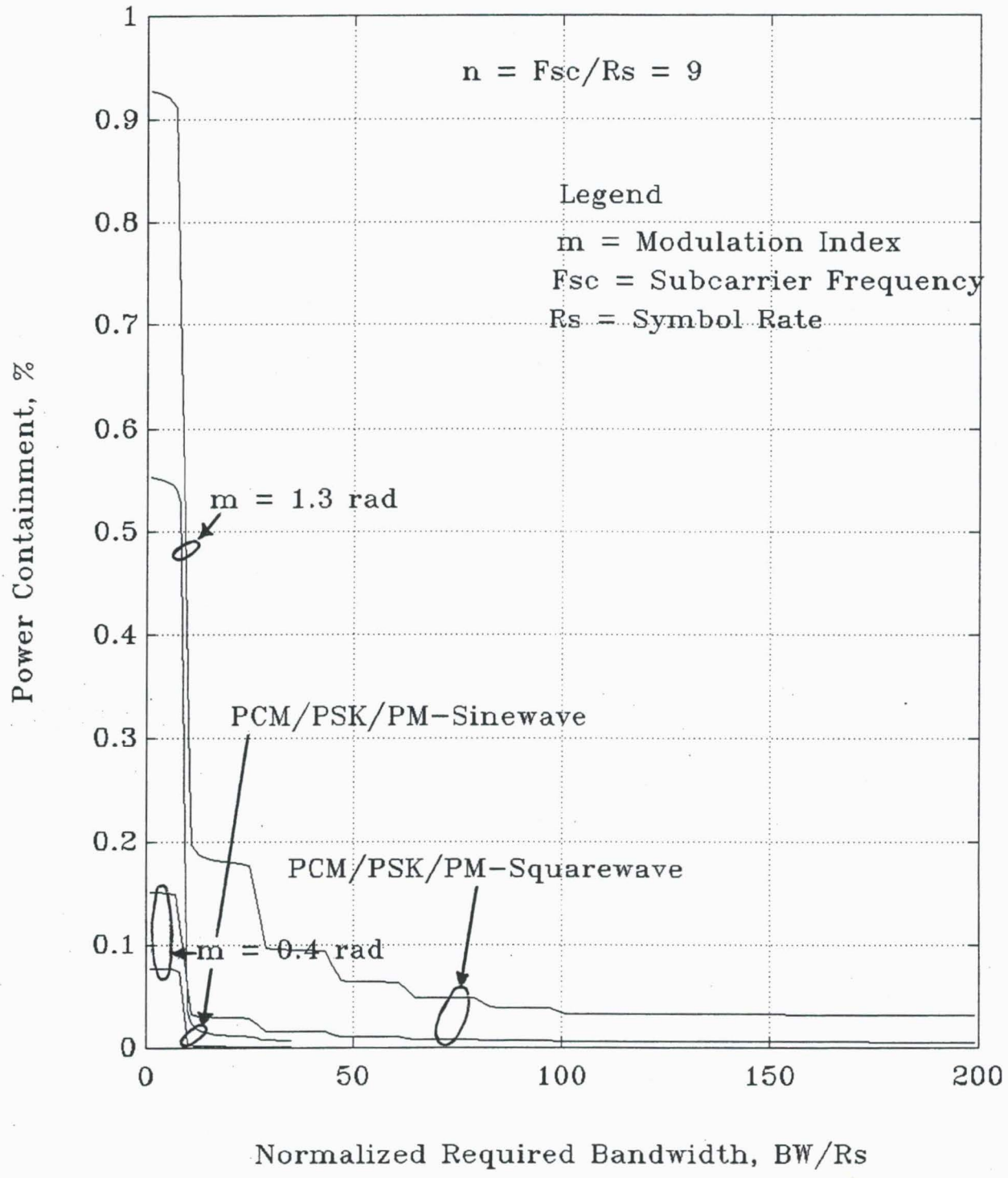

Figure 13. Unwanted Spurious Emission for PCM/PSK/PM Signals

Figure 14. Unwanted Spurious Emission for PCM/PM Signals

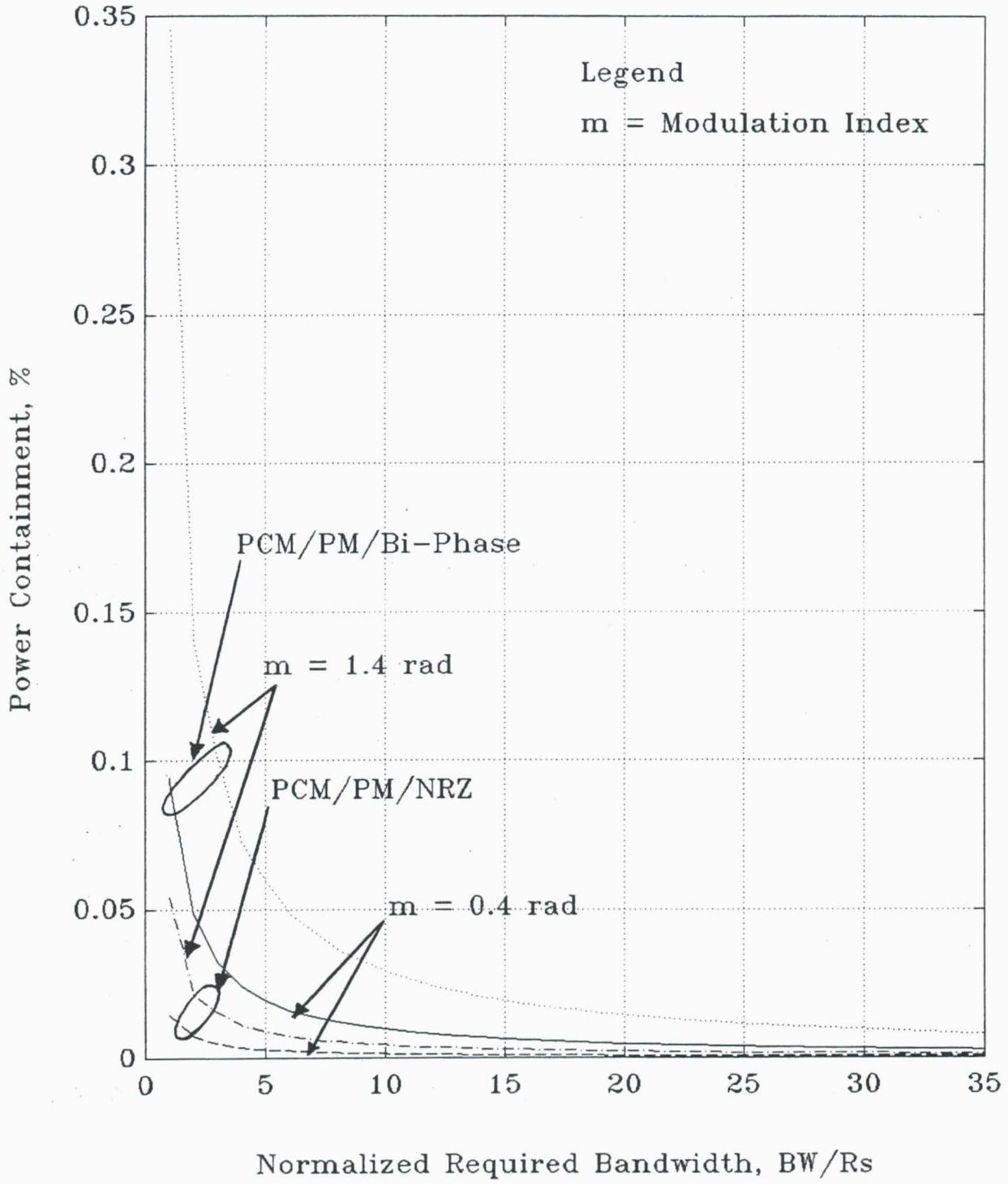

Figure 5. Unwanted Spurious Emission for BPSK Signals

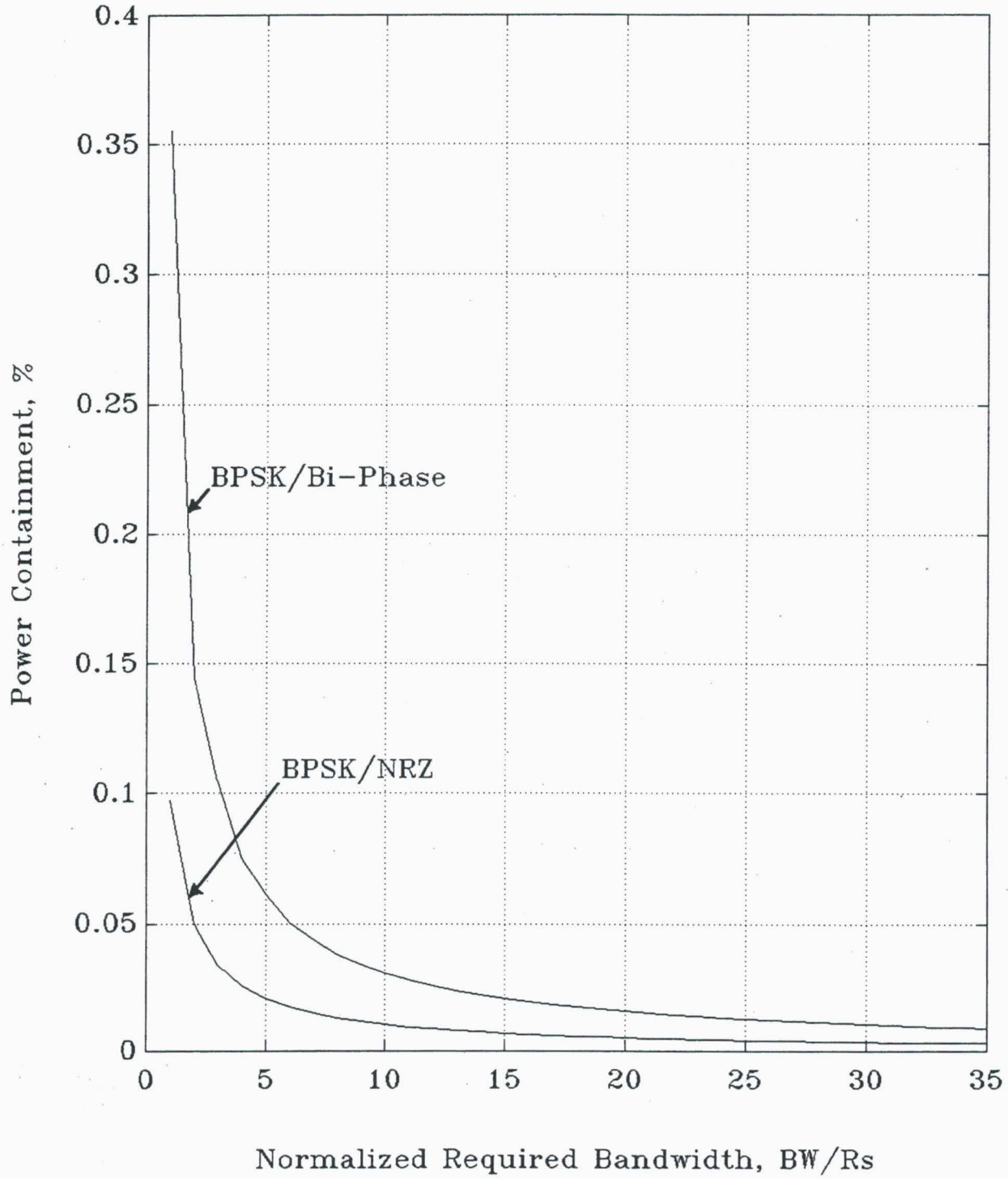

Figure 16. Data Power Containment for PCM/PSK/PM

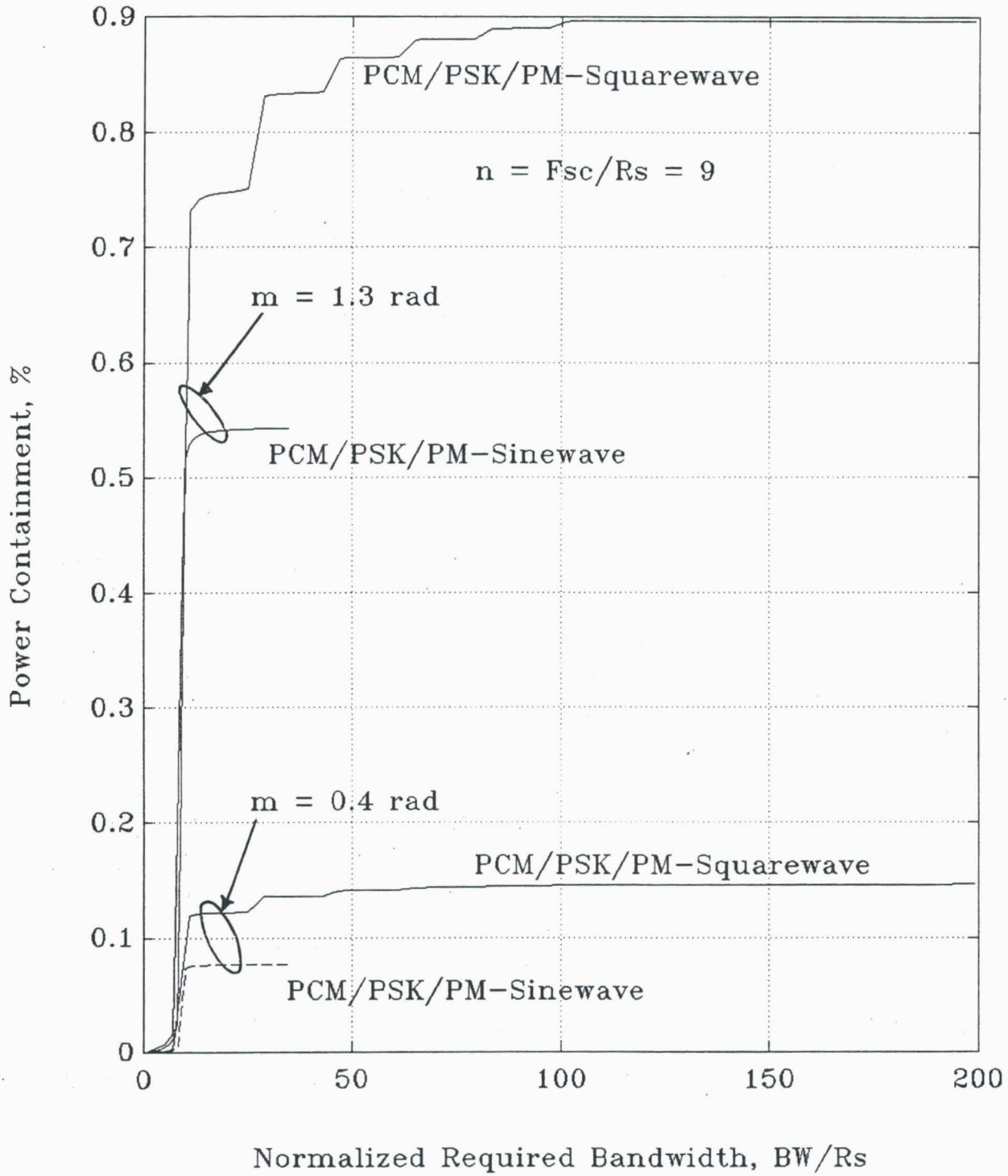

Figure 17. Data Power Containment for BPSK and PCM/PM

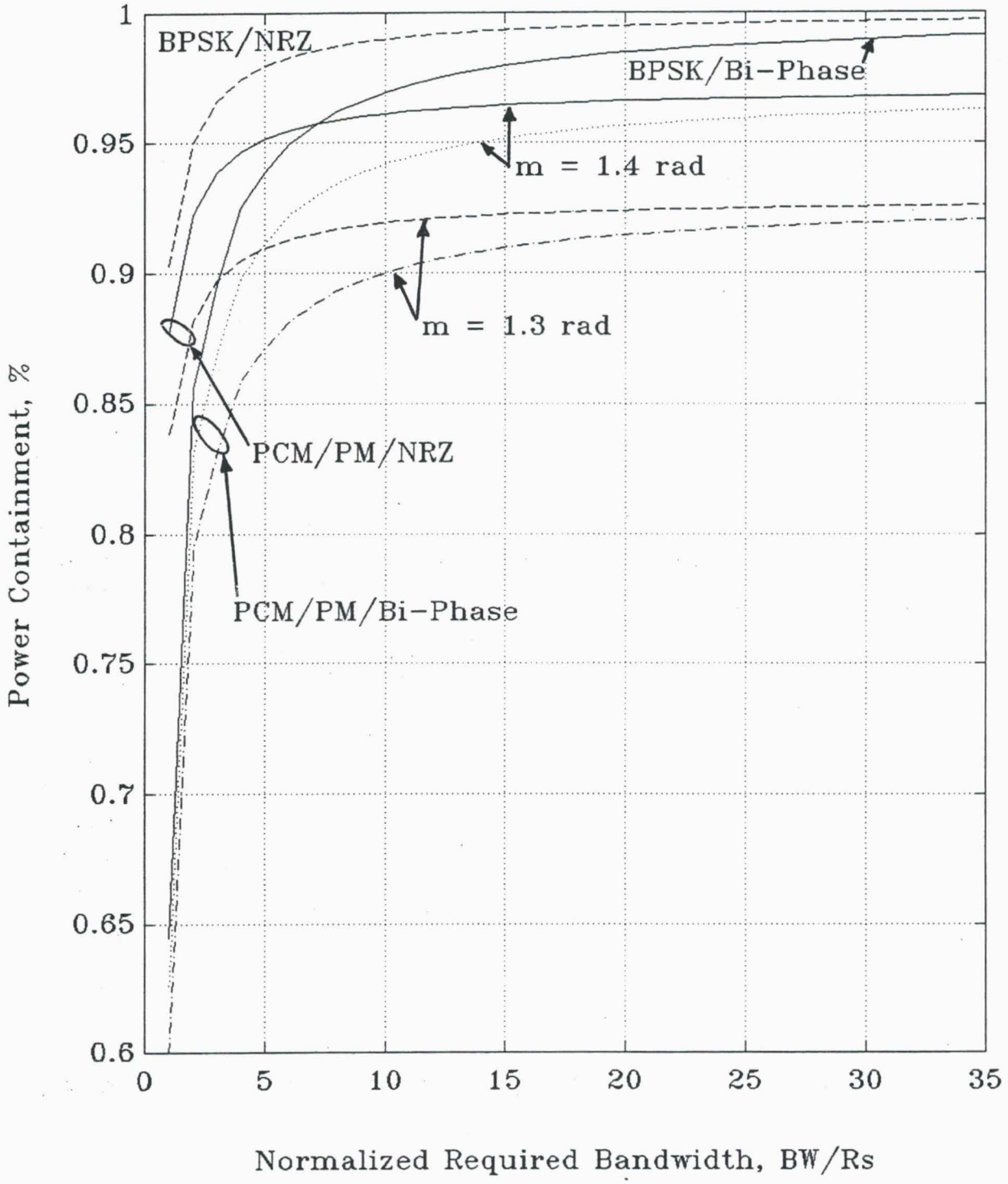

A REVIEW OF THE CURRENT AVAILABLE STUDIES OF THE INTERFERENCE SUSCEPTIBILITY OF VARIOUS MODULATION SCHEMES[1]

Tien Manh Nguyen
National Aeronautics and Space Administration
Jet Propulsion Laboratory
California Institute of Technology
4800 Oak Grove Drive
Pasadena, CA 91109

ABSTRACT

This paper reviews the current available work on interference susceptibility for various modulation schemes. Only known and published work in this area is discussed. This paper classifies the interference signal into three different categories, namely, narrow-band (in-band), wide-band and pulse interference. The purpose of this paper is to provide an overview of the current known work available on the interference susceptibility of various modulation formats for these three types of interference signals. The output of this paper is a recommendation for the Consultative Committee for Space Data Systems (CCSDS) regarding future direction for the interference susceptibility study.

---

[1] The work described in this paper was carried out at the Jet Propulsion Laboratory, California Institute of Technology, under contract with the National Aeronautics and Space Administration.

1. INTRODUCTION

The primary objective of this report is to review in a partly tutorial manner, the current available studies on the interference susceptibility of various signal modulation formats for three types of interference signals, namely, narrow-band (in-band), wide-band and pulse interference. The modulation formats emphasized in this report are:

-PCM/PSK/PM-Squarewave: the NRZ data is phase-shift-keyed onto the squarewave subcarrier and then phase modulated it onto the a sinusoidal carrier;

-PCM/PSK/PM-Sinewave: the NRZ data is phase-shift-keyed onto the sinewave subcarrier and then phase modulated it onto the a sinusoidal carrier;

-PCM/PM/NRZ: the NRZ data is phase modulated directly on the RF residual carrier;

-PCM/PM/Bi-Phase: the Bi-Phase (or Manchester) data is phase modulated directly on the RF residual carrier;

-BPSK/NRZ: the NRZ data is phase-shift-keyed onto the sinusoidal carrier-Note that for this modulation scheme, the RF carrier is fully suppressed;

-BPSK/Bi-Phase: the Bi-Phase data is phase-shift-keyed onto the sinusoidal carrier;

-QPSK: this modulation can be regarded as two BPSK/NRZ systems operating in quadrature

-OQPSK: this is the same as QPSK except that the In-phase (I) channel is offset with respect to the Quadrature (Q) channel by delaying it by an amount equal to half of the symbol rate;

-MSK: is regarded as a form of quadrature amplitude modulation with the modulation frequency (or clock frequency-not the carrier frequency) equal to 1/4 of the bit rate.

-GMSK: this is the same as MSK except that the transmitting pulse is shaped by a Gaussian filter.

The report is subdivided into five remaining sections. Section 2 reviews and discusses the interference susceptibility for narrow-band (in-band) interference. The pulse interference is discussed in Section 3. Section 4 presents the findings on wide-band interference. Section 5 summaries the results found in Sections 2, 3 and 4. Finally, the conclusion and recommendation of the report are presented in Section 6.

2. INTERFERENCE SUSCEPTIBILITY OF VARIOUS MODULATION FORMATS IN THE NARROW-BAND INTERFERENCE ENVIRONMENT

2.1 INTERFERENCE SUSCEPTIBILITY OF PCM/PSK/PM MODULATION FORMAT

Sue and Rosenbaum [1-4] has investigated the effects of the CW interference on the performance degradation of the PCM/PSK/PM receivers. The work done by Sue and Rosenbaum are based on the coherent detection of the residual modulated signals with squarewave [Sue, 1-3] and sinewave [Rosenbaum, 4] as subcarriers.

Sue analyzed the performance degradation of the telemetry system due to the presence of CW interference. His results are based on the assumption that the carrier tracking, subcarrier tracking and symbol synchronization are perfect. Hence, the effects of the phase error due to noise and interference in the carrier tracking loop have been neglected. In the determination of the symbol error rate (SER), P_S, Sue also assumed that the phase of the CW interference is a random variable uniformly distributed over $(0, 2\pi)$. The essential of Sue's work is the use of the squarewave as subcarrier instead of sinewave. If one let S(t) and I(t) be the transmitted and interference signals, respectively, then

$$S(t) = \sqrt{2}A\sin(\omega_C t + mP(t)\,d(t) + \Theta) \tag{1}$$

$$I(t) = \sqrt{2}B\sin(\omega_C t + \omega_{SC} t + \Delta\omega t + \beta) \tag{2}$$

where A and B are the RMS voltages of S(t) and I(t), ω_C is the carrier frequency in radians/seconds, P(t) is the subcarrier, d(t) is the binary data stream, $\Delta\omega$ is the interference offset frequency in radians/seconds relative to the subcarrier frequency (ω_{SC}), ϕ is the phase angle of the desired signal S(t), m is the modulation index and β is the phase angle of the interference signal I(t) which is assumed to be a random variable with uniform distribution in $[0, 2\pi]$.

For sinewave subcarrier, the SER is given by [4]

$$P_S = \frac{1}{2\pi}\int_0^{2\pi} \operatorname{erfc}\left[\sqrt{\frac{E_S}{N_0}}\,(1 + R\cos(\beta))\right] d\beta \tag{3}$$

For squarewave subcarrier, the SER is found to be [1]

$$P_S = \frac{1}{2\pi}\int_0^{2\pi} \text{erfc}\left[\sqrt{\frac{E_S}{N_0}}\left(1+\frac{2}{\pi}R\cos(\beta)\right)\right] d\beta \qquad (4)$$

where E_S/N_0 is the symbol Signal-to-Noise Ratio (SNR), R is the Interference-to-Signal Ratio (ISR). The SERs shown in Eqns (3) and (4) have assumed that the offset frequency of the interference signal is zero.

Based on Eqns (3) and (4), it is clear that, for a fixed Symbol SNR, the squarewave subcarrier makes the receiver less susceptible to in-band interference by about 4 dB. But on the other hand, the squarewave subcarrier makes the receiver susceptible to out-of-band interference due to the translation mechanism of the squarewave subcarrier.

2.2 INTERFERENCE SUSCEPTIBILITY OF PCM/PM MODULATION FORMAT

Currently, to the best knowledge of the author, the interference susceptibility for PCM/PM modulation format has not been investigated yet. Therefore, there are no results available for the effects of CW interference on the performance degradation of the PCM/PM receivers.

2.3 INTERFERENCE SUSCEPTIBILITY OF BPSK MODULATION FORMAT

A single constant amplitude, CW in-band additive interference to a coherent BPSK receiver has been analyzed by Rosenbaum [4]. The SER for this case is found to be the same as Eqn (1) for perfect carrier tracking, subcarrier tracking and symbol synchronization. However the results presented in [4] appears to apply only for the NRZ data format under perfect carrier tracking assumption. For Bi-phase data format, it is anticipated that the results will be slightly different.

The numerical results presented in [4] show that when the value of R (the interference-to-carrier signal ratio) is about - 30 dB or less, the SER performance degradation due to the CW in-band interference becomes negligible. The SER performance becomes unacceptable (more than 0.5 dB) when $R \geq -15$ dB.

2.4 INTERFERENCE SUSCEPTIBILITY OF QPSK/OQPSK MODULATION FORMATS

The effects of CW cochannel (in-band) interference on the performance of QPSK receiver have been investigated in [5-8]. [5-7] examined the effects of CW interference in the linear channel, and [8] considered the nonlinear channel.

The numerical results presented in [5-8] show that the SER performance experiences more degradation in the nonlinear channel than in the linear channel. Furthermore, the results also show that, for nonlinear channel caused by TWTA, the SER performance degradation due to the presence of cochannel interference is more than that of the channel employed hardlimiter. The different in term of symbol SNR degradation between the TWTA and hardlimiter is about 0.2 dB for the interference-to-carrier signal ratio, R, of -15 dB. In addition, for R = -15 dB, the symbol SNR degradation due to the presence of CW cochannel interference for a harlimiter channel is about 1.2 dB. For linear channel, the QPSK signal is more susceptible to the CW in-band interference than BPSK signal. It was found that QPSK signal makes the receiver more susceptible to in-band interference by about 2 dB in terms of interference-to-carrier signal ratio as compared to BPSK.

2.5 INTERFERENCE SUSCEPTIBILITY OF MSK/GMSK MODULATION FORMAT

The effects of CW interference on MSK signal reception have been investigated by Shabsigh [9]. [9] also derived the SER for fading MSK signal and fading interference. It was found in [9] that MSK is more immune to CW in-band interference than BPSK. MSK has about 1.8 dB power advantage over BPSK in CW in-band interference environment.

For GMSK, currently, to the best knowledge of the author, there are no work done available in this area. Therefore, there are no results available for the effects of CW in-band interference on the performance degradation of the GMSK receiver.

3. INTERFERENCE SUSCEPTIBILITY OF VARIOUS MODULATION FORMATS IN THE PULSE INTERFERENCE ENVIRONMENT

3.1 INTERFERENCE SUSCEPTIBILITY OF PCM/PSK/PM MODULATION FORMAT

Currently, to the best knowledge of the author, the interference susceptibility for PCM/PSK/PM modulation format in the presence of pulse interference environment has not been investigated yet. Therefore, there are no results available for the effects of pulse interference on the performance degradation of the PCM/PM receivers.

3.2 INTERFERENCE SUSCEPTIBILITY OF PCM/PM MODULATION FORMAT

Currently, to the best knowledge of the author, the interference susceptibility for PCM/PM modulation format in the presence of pulse interference environment has not been investigated yet. Therefore, there are no results available for the effects of pulse interference on the performance degradation of the PCM/PM receivers.

3.3 INTERFERENCE SUSCEPTIBILITY OF BPSK MODULATION FORMAT

The deleterious effects of the pulse Radio Frequency Interference (RFI) on the (1) tracking performance of a BPSK receiver, and (2) coded Bit Error Rate (BER) performance of the nonlinear satellite communication channel have been investigated in [10-11].

[10] has examined the tracking performance of a Costas loop in the presence of single and multiple in-band pulsed RFI signals and receiver additive white Gaussian noise. [10] pointed out that when the effective RFI power is not sufficiently large to capture the loop, there exists static phase error biases which cause the loop to lock at a phase between that of the desired signal and the composite RFI. In addition, [10] also indicated that there is an increase in the rms phase jitter over the nominal design. These two effects will degrade the BER performance of the receiver. However, [10] did not evaluate the BER performance degradation due to the presence of the pulsed RFI.

[11] evaluated the coded BER degradation of a BPSK receiver due to the presence of the pulsed CW or pulsed noise RFI. This paper predicted the BER at the output of a Viterbi decoder, based on the assumption that convolutional coding is employed. The numerical results show that as the coding rate increases the coded BER degradation decreases. The bit SNR degradations due to infinite noise RFI with 10 % duty cycle and BT = 10 (B = filter bandwidth, T = bit rate) with transponder hardlimiter, Δ(dB), for $10^{-4} \leq$ BER $\leq 10^{-2}$ are approximately 6.3 dB $\leq \Delta$(dB) $\leq$ 4.2 dB and 3.4 dB $\leq \Delta$(dB) $\leq$ 2.7 dB, for coding rate of 1/2 and 1/3, respectively.

3.4 INTERFERENCE SUSCEPTIBILITY OF QPSK/OQPSK MODULATION FORMATS

Currently, to the best knowledge of the author, the interference susceptibility for QPSK/OQPSK modulation formats in the presence of pulse interference environment has not been investigated yet. Therefore, there are no results available for the effects of pulse interference on the performance degradation of the QPSK/OQPSK receivers.

3.5 INTERFERENCE SUSCEPTIBILITY OF MSK/GMSK MODULATION FORMATS

Currently, to the best knowledge of the author, the interference susceptibility for MSK and GMSK modulation formats in the presence of pulse interference environment has not been investigated yet. Therefore, there are no results available for the effects of pulse interference on the performance degradation of the MSK and GMSK receivers.

4. INTERFERENCE SUSCEPTIBILITY OF VARIOUS MODULATION FORMATS IN THE WIDEBAND INTERFERENCE ENVIRONMENT

Currently, to the best knowledge of the author, the interference susceptibility for PCM/PSK/PM, PCM/PM, BPSK, QPSK, OQPSK and MSK modulation formats in the presence of wideband interference environment has not been investigated yet. Therefore, there are no results available for the effects of wideband interference on the performance degradation of these modulation schemes.

4. SUMMARY

The current work on the interference susceptibility of various modulation schemes under three different interference environments presented in the above sections can be summarized in Table 1.

5. CONCLUSIONS AND RECOMMENDATIONS

Based on the investigation presented above, it has been found that the interference susceptibility for CW in-band interference has been investigated for PCM/PSK/PM, BPSK, QPSK and MSK. Apparently, the effects of CW in-band interference to the performances of OQPSK, PCM/PM and GMSK receivers have not been investigated. For interference susceptibility in pulsed RFI environments, only coded BPSK is available. Furthermore, there are no work done available on the interference susceptibility in wideband interference environment.

Based on this finding, it is recommended that the CCSDS should invest its effort in completing the investigation on the interference susceptibility for CW in-band interference. To complete the investigation in this area, the following studies are recommended:

- Investigate the effects of CW interference on the performance degradations of PCM/PM and GMSK receivers;

-Extend the current results for BPSK and QPSK to OQPSK.

For interference susceptibility in pulsed RFI environment, the following studies are recommended:

-Extend the current results for coded BPSK to uncoded BPSK, QPSK and OQPSK;

-Assess the impact of pulsed RFIs on the performance degradations of the PCM/PM. PCM/PSK/PM, MSK and GMSK receivers.

Since there are no work available for wideband interference, it is recommended that the CCSDS should also conduct a thorough investigation on the effects of wideband interferences on the performance of various modulation formats described in Section 1.

Acknowledgement

The work described in this paper was carried out at the Jet Propulsion Laboratory, California Institute of Technology, under contract with the National Aeronautics and Space Administration.

Table 1: Research on the Work Done for Interference Susceptibility of Various Modulation Schemes

Modulation Type	CW In-band Interference	Pulsed RFI Interference	Wideband Interference
PCM/PSK/PM (Squarewave)	-Less sensitive, by about 4 dB, as compared to PCM/PSK/PM-Sine -Susceptible to out-of-band interference	Not available	Not available
PCM/PSK/PM (Sinewave)	More sensitive than PCM/PSK/PM-square	Not available	Not available
PCM/PM/NRZ	Not available	Not available	Not available
PCM/PM/Bi-Phase	Not available	Not available	Not available
BPSK	Less sensitive, by about 2 dB, as compared to QPSK	-Only available for convolutional coded BPSK -More susceptible at rate 1/2 than at rate 1/3	Not available
QPSK	More sensitive as compared to BPSK	Not available	Not available
OQPSK	Not available	Not available	Not available
MSK	Less sensitive as compared to BPSK (has 1.8 dB, in term of CNR, advantage over BPSK)	Not available	Not available
GMSK	Not available	Not available	Not available

REFERENCES

[1] M. K. Sue, "Performance Degradation of the Block IV Telemetry System Due to the Presence of a CW Interference," The TDA Progress Report, 32-69, March and April 1982, JPL, Pasadena.

[2] M. K. Sue, "Telemetry Degradation Due to a CW RFI Induced Carrier Tracking Error for the Block IV Receiving System With Maximum Likelihood Convolutional Decoding," The TDA Progress Report, 42-61, November-December 1980, JPL, Pasadena.

[3] M. K. Sue, "Block IV Receiver Tracking Loop Performance in the Presence of a CW RFI" The TDA Progress Report, 42-60, September and October 1980, JPL, Pasadena.

[4] A. S. Rosenbaum, "PSK Error Performance with Gaussian Noise and Interference," The Bell System Technical Journal, February 1960.

[5] V. K. Bhargava, D. Haccoun, R. Maytyas, P. P. Nuspl, Digital Communications by Satellite, John Wiley & Son, New York, 1981.

[6] V. K. Prabhu, "Error Rate Considerations for Coherent Phase-Shift Keyed Systems with Cochannel Interference," The Bell Systems Technical Journal, Volume 48, March 1969.

[7] O. Shimbo, R. Fang, "Effects of Cochannel Interference and Gaussian Noise in m-ary PSK Systems," COMSAT Technical Review, Volume 3, No. 1, Spring 1973.

[8] David J. Kennedy, Osamu Shimbo, "Cochannel Interference in Nonlinear QPSK Satellite Systems," IEEE Transactions on Communications, Vol. Com-29, No. 5 May 1981.

[9] Omar A. H. Shabsigh, "On the Effects of CW Interference on MSK Signal Reception," IEEE Transactions on Communications, Vol. Com-30, No. 8, August 1982.

[10] Marvin K. Simon, "The Performance of Suppressed Carrier Receivers in a Pulse RFI Environment," IEEE Transactions on Communications, Vol. Com-28, No. 5, May 1980.

[11] Aaron Weinberg, "The Impact of Pulsed RFI on the Coded BER Performance of the Nonlinear Satellite Communication Channel," IEEE Transactions on Communications, Vol. Com-29, No. 5, May 1981.

THE JOINT CCSDS-SFCG MODULATION STUDY--

A COMPARISON OF MODULATION SCHEMES[1]

Warren L. Martin and Tien M. Nguyen
National Aeronautics and Space Administration
Jet Propulsion Laboratory
California Institute of Technology
4800 Oak Grove Drive
Pasadena, California 91109

ABSTRACT

This paper compares the various modulation schemes, namely, PCM/PSK/PM, PCM/PM and BPSK. The subcarrier wave form for PCM/PSK/PM can be either square wave or sine wave, and the data format for PCM/PM and BPSK can be either NRZ or Bi-phase. The benchmarks used for this comparative study are the required bandwidth, power efficiency, spurious emission and interference susceptibility.

[1] The work described in this paper was carried out at the Jet Propulsion Laboratory, California Institute of Technology, under contract with the National Aeronautics and Space Administration.

1.0 INTRODUCTION

During the CCSDS Subpanel 1E (RF and Modulation) meeting at JPL from 8-12 February 1993 the SFCG's representative requested that Subpanel 1E study several modulation schemes and provide a comparison of their performance. Several attributes such as bandwidth needed, power efficiency, spurious emissions, and interference susceptibility were the benchmarks suggested for comparison.

As the presently allocated frequency bands become more congested, it is imperative that the most bandwidth-efficient communication methods be utilized. Additionally, space agencies are under constant pressure to reduce costs. Budget constraints result in simpler spacecraft carrying less communications capability as well as reduced staffing at the earth stations used to capture the data. Therefore, the power-efficiency of each modulation scheme becomes an important discriminator in the evaluation process.

The following paper explores both those modulation schemes which have been traditionally employed by space agencies and newer techniques promising significantly improved communications channel efficiencies. Supporting analysis for this work was done by Tien M. Nguyen and can be found in References 1, 2, and 3.

2.0 BANDWIDTH MEASUREMENT

2.1 Traditional Modulation Methods

Traditionally, space agencies have employed subcarriers for both telecommand and telemetry data transmissions. Subcarriers provided a simple method for separating different types of data as well as ensuring no overlap between the modulated data's frequency spectra and the RF carrier. It was not uncommon for early spacecraft to have two or more subcarriers.

Subcarrier modulation suffered the disadvantages of greater spacecraft complexity, additional losses in the modulation/demodulation process, and a large occupied bandwidth. An effort was made to mitigate the latter effect by specifying that Category A missions utilize sinewave subcarriers while Category B missions should use squarewave subcarriers (CCSDS Recommendation 401 (2.4.5) B-1). Although requiring more bandwidth, square wave subcarriers were found to be acceptable for deep space missions because the weaker signals from such spacecraft, together with the separately allocated frequency bands, ensured that spacecraft transmissions would not interfere with one another. They offered the advantage of being less susceptible to in-band interference.

In the 1960s and 1970s, when data rates were low and only 2 or 3 channels required, the added complexity and spectrum utilization required when using subcarriers could be tolerated. Since then, missions have become more complex, technology has matured, and the radio frequency spectrum has become more congested. Greater data rates require higher frequency subcarriers which expand the occupied bandwidth increasing the likelihood of overlapping downlinks from different spacecraft which could interfere with one another.

Fortunately, new modulation techniques and improved data formatting can significantly reduce the amount of bandwidth needed to transmit information. Reference 4 describes a Packet Telemetry data format recommended by the Consultative Committee for Space Data Systems (CCSDS). These formats include a Transfer Frame into which Data Packets are placed. Three bits in the header of each Transfer Frame can be set by the user to indicate the type of data in that frame. Thus, the CCSDS *Packet Telemetry* system can provide up to eight separate and independent virtual channels.

The eight virtual channels are equivalent to eight separate, but simultaneous, data streams from the spacecraft. But, rather than employing eight subcarriers, these Transfer Frames (channels) are transmitted consecutively in a single data stream. By combining the CCSDS *Packet Telemetry* format with one of the direct modulation schemes discussed in this paper, and applying some judicious filtering, it is now possible to transmit messages at a high rate while using a comparatively small bandwidth. Before describing these alternative modulation systems, a reference for bandwidth measurement must be established.

2.2 Occupied Bandwidth

Several years ago the International Telecommunications Union (ITU) established criteria for quantifying the bandwidth used by a telecommunications system. Termed *Occupied Bandwidth*, Section RR1-18, Paragraph 6.17, of the ITU's *Radio Regulations* defined the term as:

> *Occupied Bandwidth: The width of a frequency band such that, below the lower and above the upper frequency limits, the mean power emitted are each equal to a specified percentage $\beta/2$ of the total mean power of a given emission.*
>
> *Unless otherwise specified by the CCIR for the appropriate class of emission, the value of $\beta/2$ should be taken as 0.5%.*

Under the ITU definition, the *Occupied Bandwidth* is that span of frequencies which contains 99% of the emitted power. Where digital communications are concerned, *Occupied Bandwidths* of unfiltered signals tend to be very large. Some people believe that *Occupied Bandwidth* is not a useful concept for digital communications systems absent some degree of filtering.

The ITU partially recognized this difficulty with *Occupied bandwidth* and created an alternative measure called *Necessary Bandwidth*. It is defined as:

> *Necessary Bandwidth: For a given class of emission, the width of the frequency band which is just sufficient to ensure the transmission of information at the rate and with the quality required under the specified conditions.*

Here, the problem is one of uncertainty. To a large extent "quality" is a subjective concept. While a specific standard could be adopted, the ITU has not done so. Moreover, no attention is paid to power efficiency which can be very important in space communications systems. Generally, *Necessary Bandwidth* is not deemed to be a useful measure for space communications systems.

2.3 Required Bandwidth

Given the problems with both the *Occupied Bandwidth* and the *Necessary Bandwidth* notions, this paper proposes a new measure called *Required Bandwidth.* For the most part, the definition of *Required Bandwidth* is the same as that for *Occupied Bandwidth.* The principal difference is that a more realistic value for the percentage of power is selected. The proposed definition is:

> *Required Bandwidth: is the width of the frequency band such that, within the lower and upper frequency limits, the total power contained in this frequency band is equal to a specified percentage of the total power [percentage to be specified].*

Note that the definition is not referenced to 99% of the power in the transmitted spectrum as is *Occupied Bandwidth.* This is because filtering is inherent in the concept of *Required Bandwidth.* In simple terms, *Required Bandwidth* is that bandwidth needed to complete a communication *with an acceptable amount of power loss.* For example, a 5% loss in power corresponds to -0.2 dB and a 10% loss is equivalent to -0.45 dB. One of these values should be acceptable to most space missions. Both will significantly reduce the bandwidth needed to transmit a message. As will be demonstrated in the remainder of this paper, accepting a small loss in the system's performance, dramatically reduces the amount of bandwidth needed to complete the communication.

It is assumed that a filter will be employed at an appropriate location in the information transmission system so that *only the Required Bandwidth is transmitted from the spacecraft.* Figure 2-1 is a simplified block diagram of a spacecraft Radio Frequency Subsystem (RFS). Note that filters are located in the ranging channel, at the input to the modulator, and at the output of the power amplifier. All may not be required. The actual number and their locations will depend upon the specific RFS design and the linearity of the multiplier and the power amplifier. Obviously, it is desirable to avoid placing a filter at the output of the power amplifier if at all possible in order to eliminate the RF power loss and prevent a weight increase.

If a filter is required at the power amplifier's output, the *acceptable amount of RF power loss* will need to be established. For the purposes of this paper values of 95% (-0.2 dB) and 90% (-0.45 dB) were selected. A standard called: *Required Bandwidth* will be proposed which utilizes one of these power efficiencies as its reference. It is suggested that the SFCG and CCSDS adopt a Recommendation establishing *Required Bandwidth* as a term of measurement with the associated "acceptable loss".

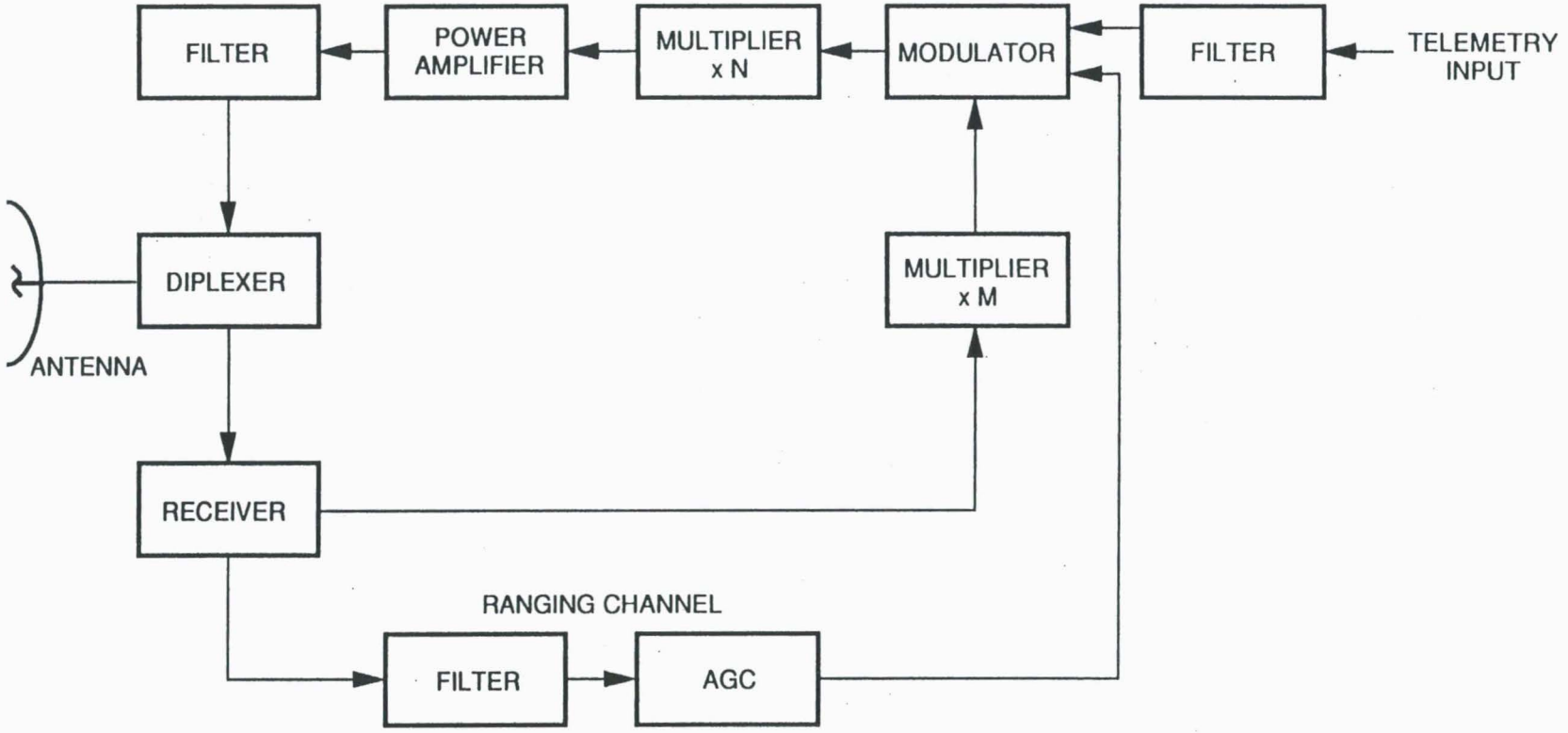

Figure 2-1. Simplified Block Diagram of Spacecraft Radio Frequency Subsystem

3.0 COMPARISON OF MODULATION SCHEMES

Modulation schemes shown in Table 1 were investigated in Reference 1 and are compared in this paper. Modulation methods are listed in the order of increasing bandwidth efficiency (diminishing *Required Bandwidth*).

TABLE 3-1: INVESTIGATED MODULATION SCHEMES

Modulation Type	Description
PCM/PSK/PM squarewave	NRZ data is PSK modulated on a squarewave subcarrier which is then phase modulated on a residual RF carrier.
PCM/PSK/PM sinewave	NRZ data is PSK modulated on a sinewave subcarrier which is then phase modulated on a residual RF carrier.
PCM/PM/Bi-ϕ	Data is Bi-Phase (Manchester) modulated directly on a residual RF carrier.
PCM/PM/NRZ	NRZ data is phase modulated directly on a residual RF carrier.
BPSK/Bi-ϕ	Data is Bi-Phase (Manchester) modulated on an RF carrier fully suppressing it.
BPSK/NRZ	NRZ data is phase modulated directly on an RF carrier fully suppressing it.

To compare the *Required Bandwidths* for the several modulation schemes, power transfer efficiencies of 90% and 95% are used. As noted above, these correspond to power losses of 0.45 dB and 0.2 dB respectively. For each modulation type the bandwidth needed to convey 90% and 95% of the modulated signal will be computed. Bandwidths will be normalized to the data Symbol Rate, R_s, so that the various types can be compared. Additionally, an RF carrier modulation index of 1.2 radians, a value typical for primary telemetry channels having reasonable data rates, was used for evaluating all modulation schemes.

Figure 3-1 shows the frequency spectrum of each of the several modulation schemes shown in Table 3-1. One need look no further than this figure to see that there is a very large disparity in the bandwidths used by the several schemes.

3.1 Subcarrier Modulation Schemes

Subcarriers were routinely used for telemetry channels. Not only did they facilitate separation of different data types, but also they served to separate the data's transmitted spectrum from the RF carrier. Spectral separation was particularly important in the early days of the space program when data rates were low and the data sidebands were frequently indistinguishable from the carrier.

In this analysis, both sinewave and squarewave subcarriers will be examined to determine their effect upon the *Required Bandwidth.*

3.1.1 Squarewave Subcarriers

CCSDS Recommendation 401 (2.4.5) B-1 states that Category B missions should employ squarewave subcarriers. Although requiring a larger bandwidth than sinewave subcarrier modulation schemes, use of squarewave subcarriers does provide slightly better performance at high modulation indices than do sinewave subcarrier systems. This is so because, if the receiver's bandwidth is sufficient, high order harmonics are recoverable whereas the high order Bessel functions, present with sinewave subcarriers at high modulation indices, are not. Figure 3-1 (a) shows the frequency spectrum of a system employing a single squarewave subcarrier. Limited space restricted the ability to show the full spectrum. Odd harmonics of the subcarrier's frequency, each with data sidebands, will be present with diminishing amplitude as the order increases.

Figure 3-2 shows the *Required Bandwidth* for data systems employing squarewave subcarriers. All plots in this paper normalize the *Required Bandwidth* to the data Symbol Rate[1], R_s (e.g., BW/R_s). *Required Bandwidth* is also dependent upon the ratio between the subcarrier's frequency and the Symbol Rate, as well as the RF carrier's modulation index. The reason for the former should be obvious while the latter is because, at lower modulation indices, a greater percentage of the transmitted power will be found in the carrier's comparatively narrow frequency band.

Three values for Subcarrier Frequency/Symbol Rate (n) corresponding to 3, 9, and 15 were evaluated. While these represent the minimum and maximum ratios generally used, some missions have been known to fly ratios as high as 1,000. A brief glance at Figure 3-2 will clearly show the effect of these high ratios on *Required Bandwidth.*

For comparative purposes, the same reference points are used for evaluating both squarewave and sinewave subcarrier modulation methods (e.g., modulation index (m) = 1.2 radians and subcarrier frequency-to-symbol rate ratio (n) = 9). From Figure 3-2, it is clear that the *Required Bandwidth* is quite large for 90% and 95% power efficiencies. Approximately 30 R_s and 75 R_s required for the respective efficiencies. A summary of the results will be found in columns 2 and 3 of Table 3-2 at the end of this section.

As will be shown in 3.1.2, squarewave subcarriers consume substantially more bandwidth than do sinewave subcarriers. Although the modulation/demodulation losses are likely to be greater than for direct modulation schemes, most of the transmitted power is recoverable when using squarewave subcarriers, provided that the earth station receiver's bandwidth is sufficiently wide.

Squarewave subcarriers may still find application in some Category B missions where the data's symbol rate is low and significant data sideband power will fall into the RF carrier phase locked loop's bandwidth if a direct modulation scheme is used.

---

[1] Symbol Rate is equal to the data rate for unencoded transmissions and the encoded bit rate for coded transmissions.

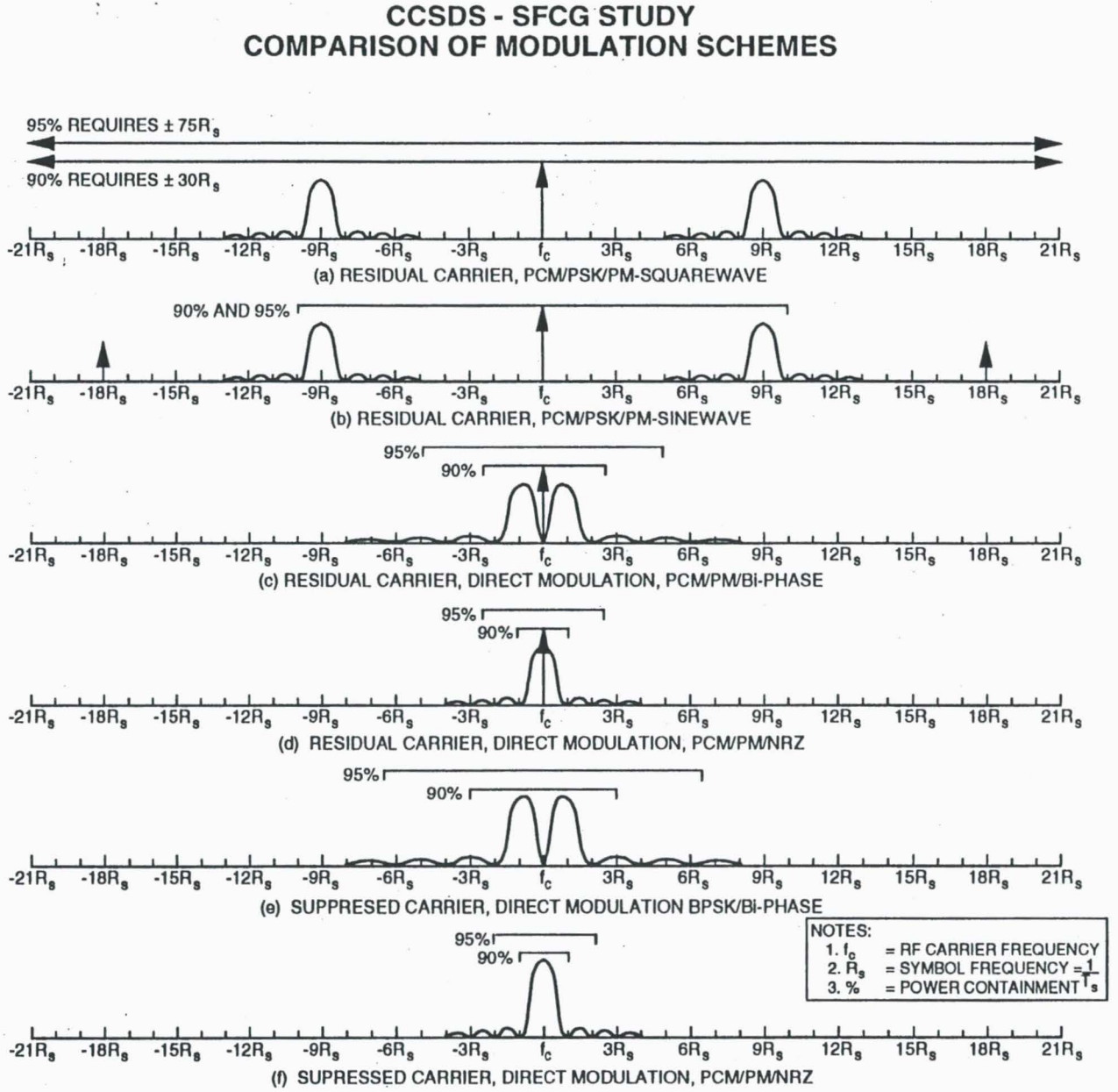

Figure 3-1. Spectra of Various Modulation Methods

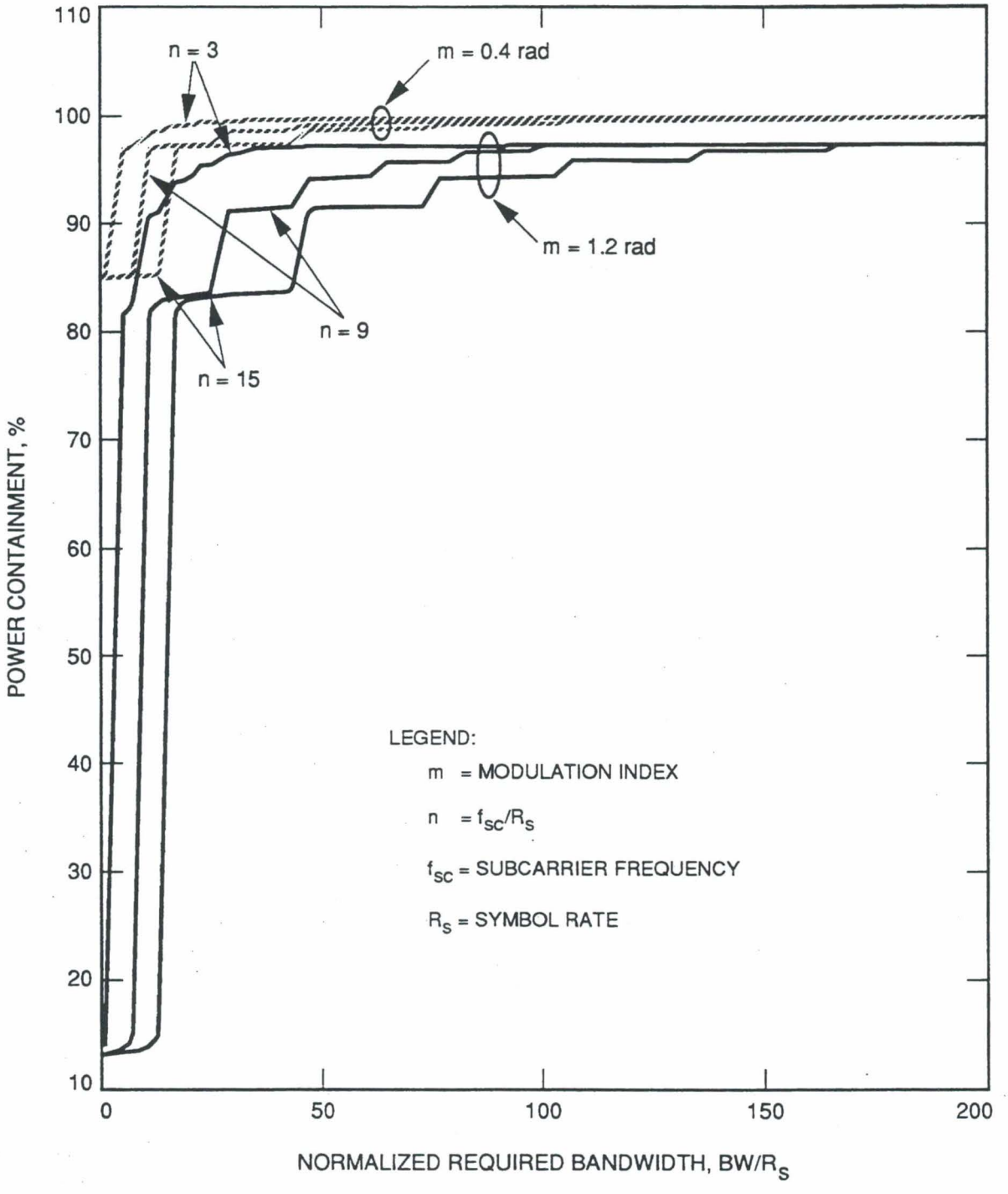

Figure 3-2. Required Bandwidth for PCM/PSK/PM-Squarewave

3.1.2 Sinewave Subcarriers

CCSDS Recommendation 401 (2.4.5) B-1 states that Category A missions should employ sinewave subcarriers. Congestion in the 2 GHz band, combined with the comparatively strong signals from Category A spacecraft, constrain each user to the minimum amount of spectrum necessary for his communication. Sinewave subcarriers require less spectrum bandwidth than do squarewave subcarriers. Although sinewave subcarriers have greater losses, and therefore are less efficient than squarewave subcarriers at high RF modulation indices, the stronger signals from Category A missions largely offset this disadvantage.

Figure 3-1 (b) depicts the frequency spectrum of a system utilizing a single sinewave subcarrier. Unlike the squarewave subcarrier's frequency spectrum, a sinewave subcarrier will have energy at the even harmonics in the form of a Delta function. The Delta function's amplitude will depend upon the RF carrier's modulation index. It is this energy that is lost during the demodulation process and which accounts for the lower efficiency of sinewave subcarrier systems.

Figure 3-3 shows the *Required Bandwidth* for data systems using sinewave subcarriers. As with the squarewave subcarrier plot, the figure normalizes *Required Bandwidth* to the data Symbol Rate, R_S (e.g., BW/R_S) and utilizes a subcarrier frequency-to-symbol rate ratio of 9. Some missions have flown ratios as high as 1,000. A brief glance at Figure 3-3 will clearly show the effect of these high ratios on *Required Bandwidth.*

For a mid-range value of n = 9 and a typical modulation index of 1.2 radians, the *Required Bandwidth* is about 10 times the Symbol Rate, R_S, for both the 90% and 95% Power Containments[2]. Note that a bandwidth approximately 30 times the Symbol Rate is required if the ITU's *Occupied Bandwidth* computation is used. Results of these computations will be found in columns 2 and 3 of Table 3-2.

Although using less bandwidth than squarewave subcarriers, the use of sinewave subcarriers does introduce greater losses than other modulation methods because of the high order Bessel functions which become prominent at high modulation indices. Nevertheless, sinewave subcarriers may still find application in some Category A mission designs where the data's symbol rate is low and significant data sideband power will fall into the RF carrier phase locked loop's bandwidth.

---

[2] Power Containment is that percentage of the total modulated data's power contained in the indicated *Required Bandwidth* for each specific modulation index and subcarrier frequency-to-symbol rate ratio.

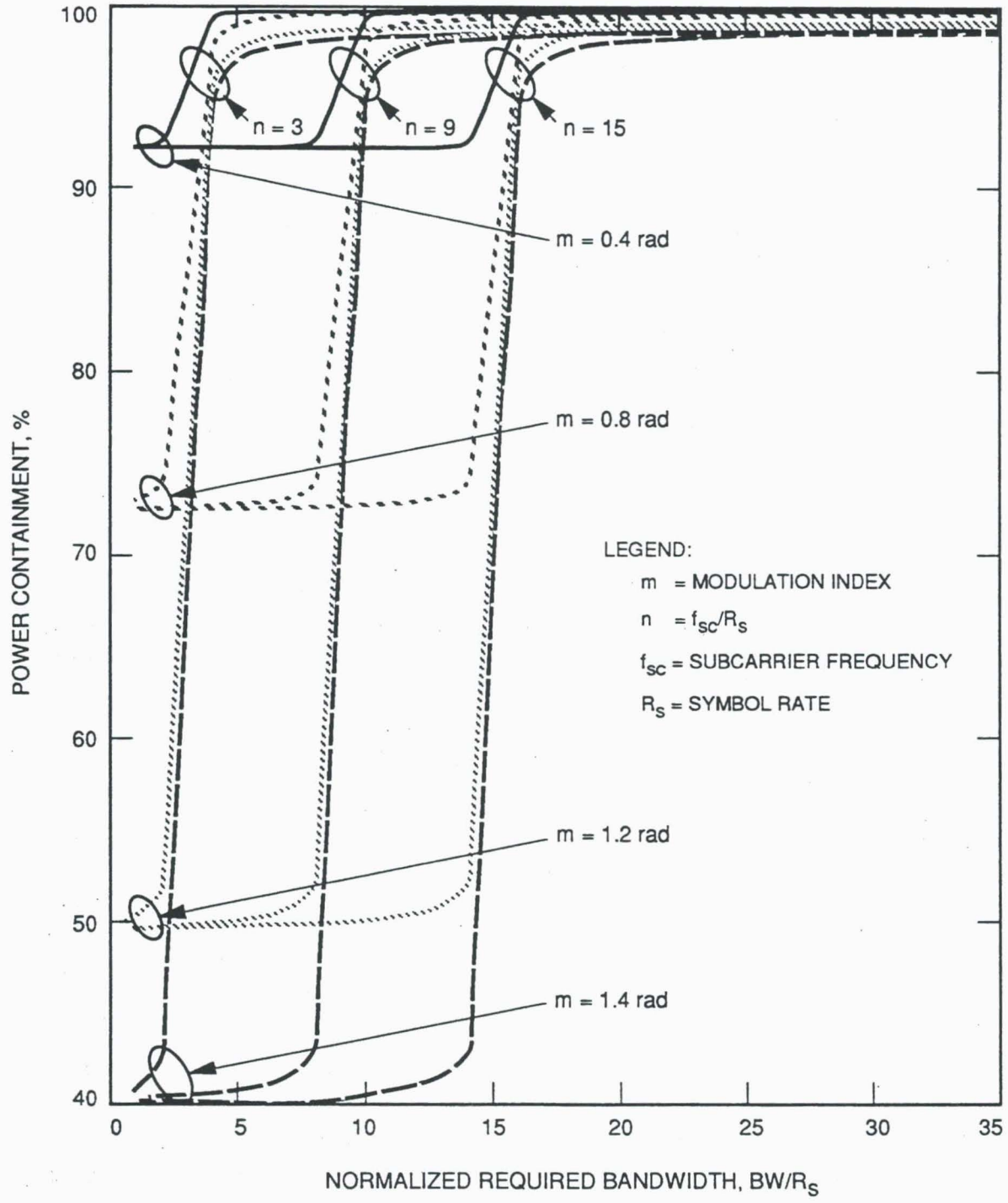

Figure 3-3. Required Bandwidth for PCM/PSK/PM-Sinewave

3.2 Direct Modulation Schemes

As indicated in Table 3-1, several direct modulation schemes were considered. Historically, space agencies used residual carrier systems[3]. This provided a stable reference frequency at the earth station which was used to demodulate the data from the carrier. Alternative, suppressed carrier systems, will be considered following a discussion of traditional residual carrier systems. None of the modulation schemes considered in this section employ subcarriers.

Direct modulation schemes are inherently more bandwidth efficient than those employing subcarriers. This is due, in part, to the way that the ITU defined *Occupied Bandwidth* to be that span of frequencies, covered by the modulated signal, which excludes only the lower 0.5% and the upper 0.5% of the transmitted power. Thus, large frequency gaps between the RF carrier and the subcarrier are included in the *Occupied Bandwidth* calculation despite the fact that there is no significant modulation sideband energy in large portions of these frequency gaps.

3.2.1 Direct Modulation, Residual Carrier, Bi-ϕ

From the view of *Required Bandwidth*, direct modulation with a Bi-ϕ format is a compromise between direct modulation with an NRZ format and a conventional subcarrier telemetry system. It places the modulated data sidebands close to the RF carrier while providing a null in the data's frequency spectrum at the RF carrier's frequency. Figure 3-1 (c) shows the PCM/PM/ Bi-ϕ spectrum which ensures that the carrier will be easily distinguishable from the surrounding data sidebands. The bandwidth advantage of direct modulation schemes is readily apparent in this figure.

Sometimes called Manchester modulation, a Bi-ϕ format is formed by the modulo-2 addition of each data symbol with a squarewave clock whose period is equal to that of a data symbol. In addition to moving the data's spectrum away from the RF carrier's frequency, Bi-ϕ modulation also ensures RF carrier phase transitions during each data symbol.

With random data, this modulation scheme produces a spectrum with a clearly discernable RF carrier component and a $[(\sin^4 x)/(x)^2]$ distribution with peaks at about $\pm$ 0.75 R_s (R_s = symbol frequency, f_s) due to the modulation. A null in the data's spectrum will lie at the RF carrier's frequency, f_c. Additional nulls, on either side of f_c will lie at $\pm$ 2 f_s, $\pm$ 4 f_s, $\pm$ 6 f_s, etc. Figure 3-4 shows the *Required Bandwidth* for various levels of Power Containment. For a modulation index, m, of 1.2 radians, *Required Bandwidths* of 2.5 R_s and 5 R_s are needed for 90% and 95% power containment respectively. A summary of the findings will be found in Table 3-2, columns 2 and 3.

Direct Bi-ϕ modulation is useful when bandwidth conservation is important and the modulated symbol rate is sufficient to ensure that the level of data sideband power, falling in the phase locked loop's bandwidth, is sufficiently low. This modulation scheme should find broad application in future missions having low or moderate data rates or where a stable carrier reference frequency is required.

---

[3] Residual Carrier System is one in which the modulation index is less than $\pm$ 90 degrees so that a small percentage of the total transmitted power remains at the RF carrier frequency.

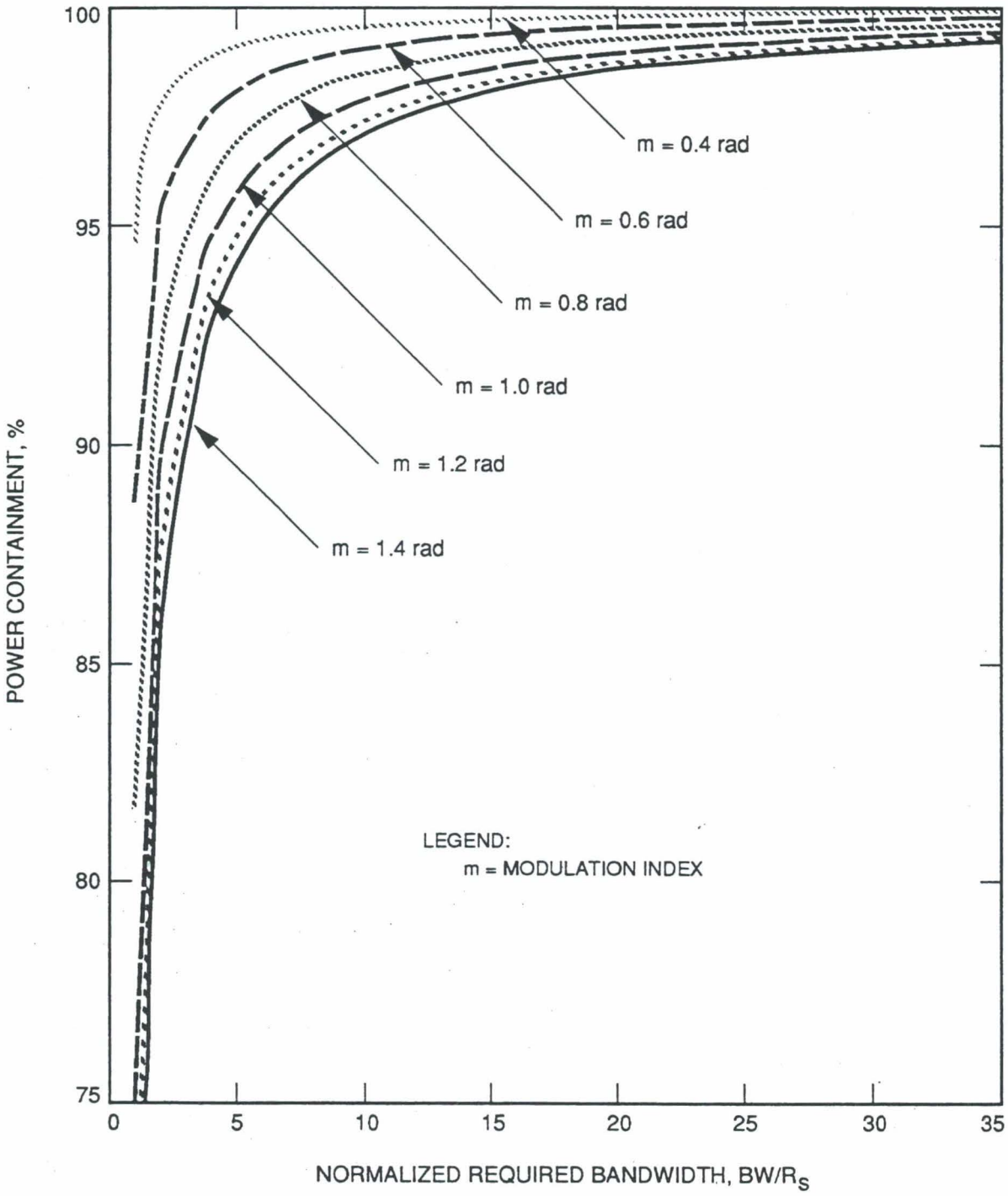

Figure 3-4. Required Bandwidth for PCM/PM/Bi-Phase

3.2.2 Direct Modulation, Residual Carrier, NRZ

Direct Bi-ϕ differs from Direct NRZ modulation in that the double frequency clock component is absent in the latter modulation type. Here, the modulated telemetry data's frequency spectrum is discernably narrower than the one for Bi-ϕ modulation. The RF frequency spectrum for this modulation type will be found in Figure 3-2 (d). For random telemetry data, the power spectrum is described by $[(\sin x/x)^2]$. Here, the peak of the spectrum occurs at the RF carrier's frequency, f_C, and the nulls are at $f_C \pm 1\ f_s, \pm 2\ f_s, \pm 3\ f_s$, etc.

Clearly, the advantage of direct NRZ modulation is the substantially reduced bandwidth needed for communications as compared to the modulation types discussed above. Figure 3-5 shows the *Required Bandwidth* for several levels of power containment. This is the most bandwidth efficient modulation method considered so far. Table 3-2, columns 2 and 3 list the *Required Bandwidth* for 90% and 95% power containment respectively.

PCM/PM/NRZ modulation suffers the disadvantage of placing the peak of the data's frequency spectrum at the RF residual carrier's frequency. Unless the data symbol rate is comparatively high, so as to spread the data sideband's power over a relatively broad frequency range, the RF carrier may be difficult to detect. Additionally, the presence of data power within the earth station's phase locked loop's bandwidth can introduce RF carrier interference with the result that the loop's phase jitter is increased.

Direct NRZ modulation should find application to residual carrier systems when minimum bandwidth utilization is important and when the data rates are moderate to high. When using this modulation type, care must be exercised to ensure that the carrier is sufficiently distinguishable for RF carrier acquisition at the earth station's receiver. Some earth stations may prefer that the telemetry modulation be turned off during the acquisition process. Other earth stations, using a spectrum analyzer in their receiver acquisition system, may experience no difficulty in acquiring the RF carrier with telemetry modulation turned on.

One of NASA's International Solar Terrestrial Physics (ISTP) program's spacecraft named Polar uses this modulation scheme. Polar is an earth orbiter, has a residual carrier, and a data rate of 500 kb/s. A rate ½, constraint length 7 convolutional code concatenated with a Reed-Solomon code increases the symbol rate to slightly above 1 Ms/s. This spacecraft will be launched in mid 1994.

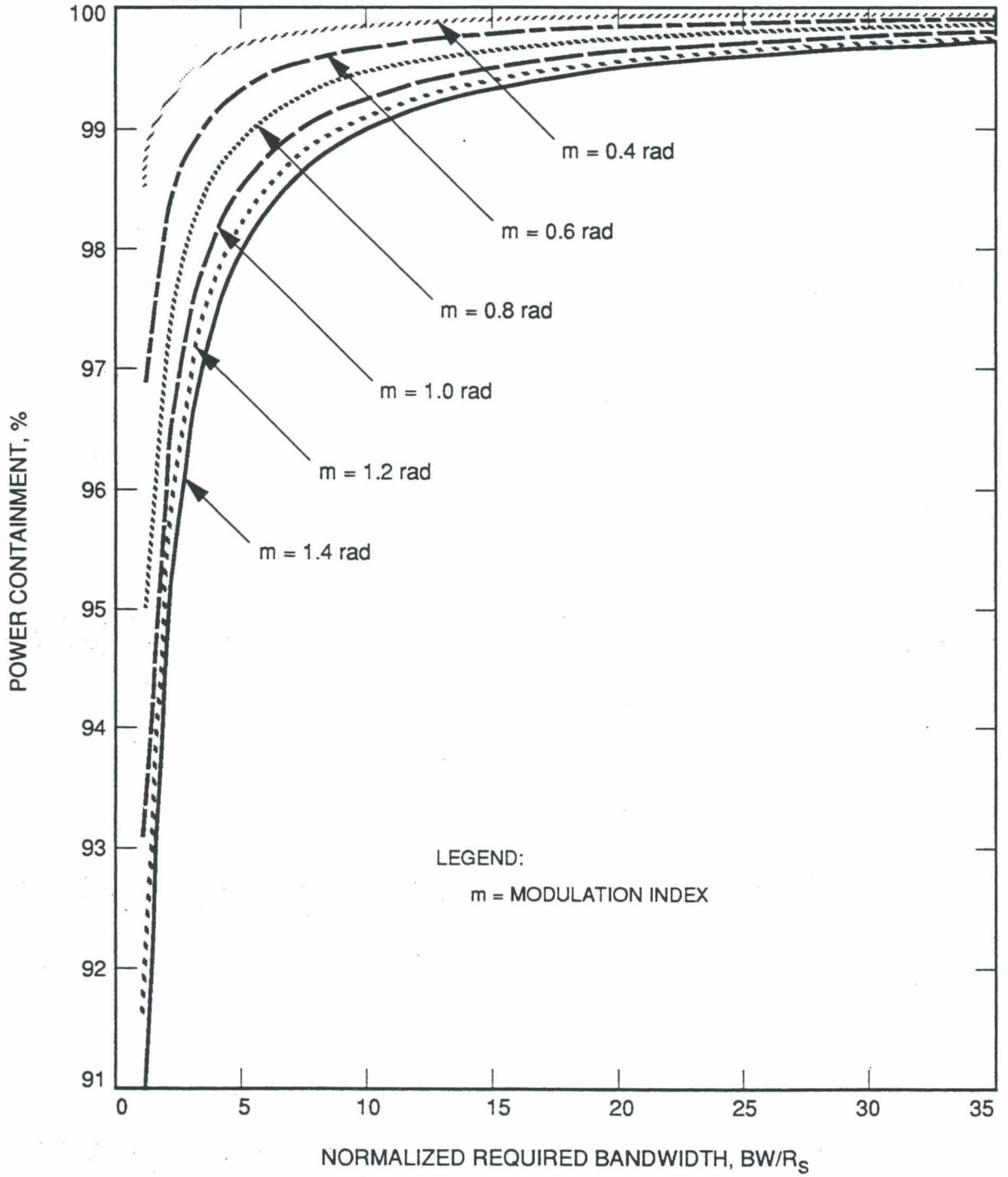

Figure 3-5. Occupied Bandwidth for PCM/PM/NRZ

3.2.3 Suppressed Carrier, Bi-Phase Shift Keyed (BPSK/Bi-ϕ)

BPSK/Bi-ϕ modulation fully suppresses the RF carrier but modulo-2 adds the telemetry data to a squarewave clock at twice the frequency of the telemetry symbol frequency. In this regard, the system is identical to the one described in section 3.2.1 above. Like that modulation scheme described earlier, the data's spectrum will follow a $[(\sin^2 x)/(x)^2]$ distribution with peaks at $\pm$ 2 f_s, $\pm$ 4 f_s, $\pm$ 6 f_s, etc. and a null at the carrier's frequency. However, unlike direct residual carrier Bi-ϕ modulation, there will be no carrier component. The spectrum generated by BPSK/Bi-ϕ is shown in Figure 3-2 (e).

A carrier component is reestablished within the earth station receiver's Costas or Squaring Loop. The result is that all of the transmitted power is placed in the data's sidebands. Since the RF carrier is reconstructed from the data sidebands, virtually all of the transmitted power is available for this purpose as well.

Squaring Loops regenerate the RF carrier by combining signals generated by a reference and a quadrature channel. Noise, as well as signal is present in both channels and both are combined. As a consequence, it is important to have a sufficient signal-to-noise (SNR) ratio in the loop. A minimum SNR of 12 - 15 dB is recommended for such loops to function efficiently.

Figure 3-6 shows the *Required Bandwidth* as a function of power containment. Note that the *Required Bandwidth* is slightly greater for this modulation type than for the residual carrier PCM/PM/Bi-ϕ owing to the lack of RF carrier. This slightly larger *Required Bandwidth* is clearly evident in Table 3-2.

BPSK/Bi-ϕ modulation will find application in high data rate systems where conservation of bandwidth is important and where maximum system performance is required. Some comparatively low rate missions (Galileo-S-Band, Pluto Flyby, and MESUR) are considering the use of BPSK modulation.

3.2.4 Direct Modulation, Suppressed Carrier, NRZ (BPSK/NRZ)

Like direct residual carrier modulation, BPSK/NRZ differs from direct modulation BPSK/Bi-ϕ in that the double frequency clock component is absent in the latter modulation type. In all other respects, the modulation type is the same as BPSK/Bi-ϕ discussed above. The modulated signal's frequency spectrum is shown in Figure 3-2 (f). It reflects the bandwidth conserving nature of this modulation scheme which provides the least *Required Bandwidth* of any of the types considered. Figure 3-6 demonstrates the bandwidth efficiency of BPSK/NRZ modulation as compared with BPSK/Bi-ϕ modulation.

BPSK/NRZ modulation will find application in high data rate systems where bandwidth conservation is of utmost importance and where the complexities of QPSK and N-PSK modulation methods are to be avoided.

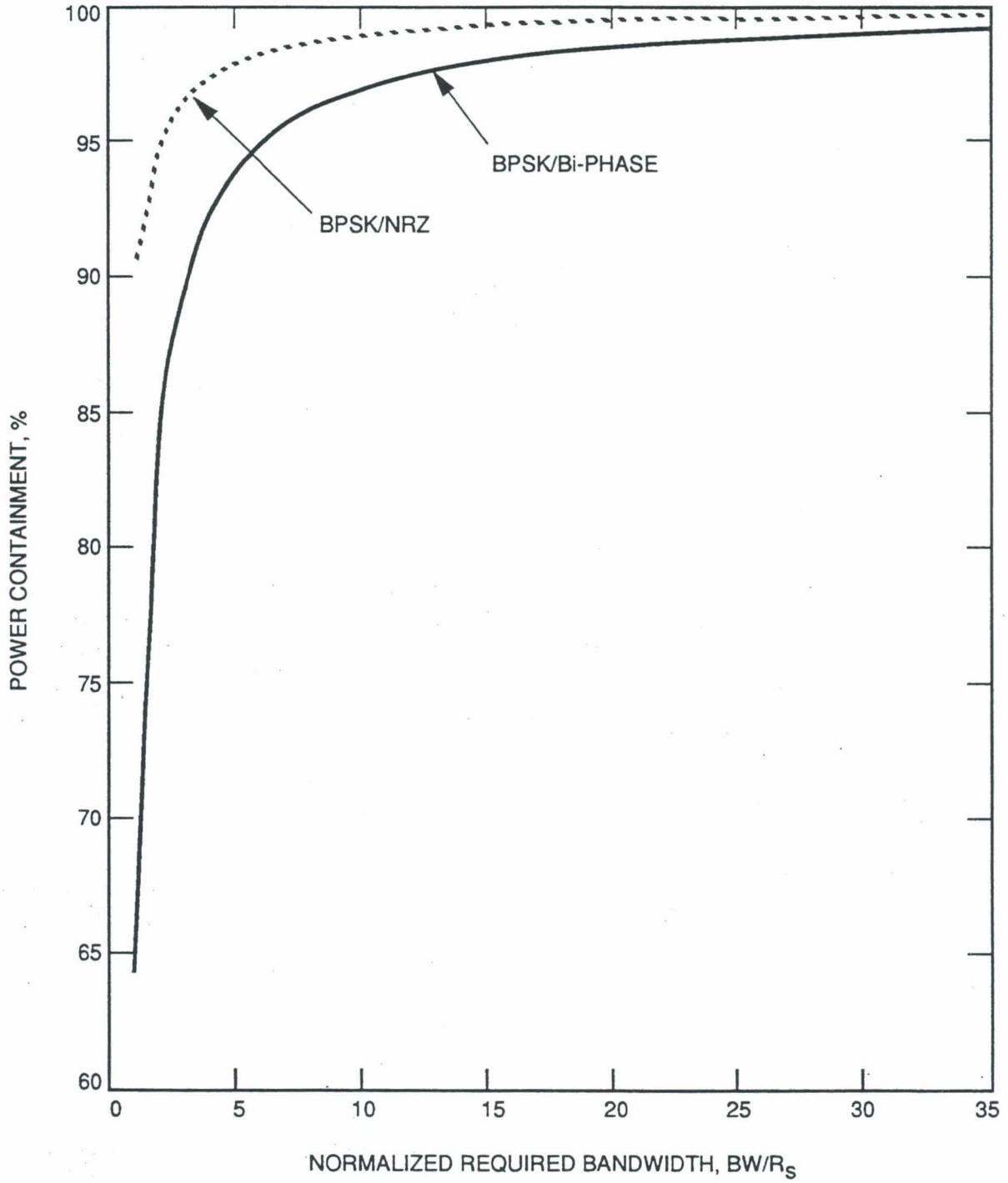

Figure 3-6. Required Bandwidth for BPSK Signals

CCSDS - SFCG STUDY
COMPARISON OF MODULATION SCHEMES

TABLE 3-2: PERFORMANCE SUMMARIES OF MODULATION SCHEMES

Modulation Type	90% Power Containment	95% Power Containment	ISI SNR Reduction dB	ISI SNR Reduction dB	ISI SNR Reduction dB	In-Band Interference Susceptibility
PCM/PSK/PM (Sq) n = 9, m = 1.2 rad.	± 30 R_s	± 75 R_s	0.75 @ ± 10 R_s	0.15 @ ± 20 R_s	0.01 dB @ ± 50 R_s	Less susceptible than PCM/PSK/PM sine by about 4 dB. Susceptible to Out-of-Band interference.
PCM/PSK/PM (Sine) n = 9, m = 1.2 rad.	± 10 R_s	± 10 R_s	0.75 @ ± 10 R_s	0.18 @ ± 20 R_s	0.04 dB @ ± 50 R_s	More susceptible than PCM/PSK/PM square.
PCM/PM/Bi-ϕ m = 1.2 rad.	± 2.5 R_s	± 5 R_s	6.3 @ ± 1 R_s	0.34 @ ± 2R_s	0.20 dB @ ± 5 R_s	No information available.
PCM/PM/NRZ m = 1.2 rad.	± 1.2 R_s	± 2.5 R_s	0.85 @ ± 1 R_s	0.21 @ ± 2 R_s	0.01 dB @ ± 5 R_s	No information available.
BPSK/Bi-ϕ m = ± 90 deg.	± 3 R_s	± 6.5 R_s	6.3 @ ± 1 R_s	0.29 @ ± 2 R_s	0.15 dB @ ± 5 R_s	Less susceptible than QPSK. No information available comparing to modulation types listed above.
BPSK/NRZ m = ± 90 deg.	± 1 R_s	± 2 R_s	0.74 @ ± 1 R_s	0.17 @ ± 2 R_s	0.04 dB @ ± 5 R_s	Likely to be more sensitive than BPSK/Bi-ϕ. No information available as to other modulation types.

4.0 EFFECT OF FILTERING

Filtering of the signal is implicit in the notion of *Required Bandwidth.* This is because the suggested concept involves accepting a small loss in transmitted power in order to obtain a significant saving in bandwidth. Filters should be placed to effectively shape the transmitted signal while minimizing the weight and size of the filter. Options for filter locations were shown in Figure 2-1.

If filtering becomes excessive, whether at the transmitter or receiver, additional losses can be introduced. When the filter's bandwidth is restricted to less than the main lobe of the transmitted data's frequency spectrum, then the shape of the transmitted pulse is changed. Symbols are elongated with the result that one symbol will begin to overlay the following symbol (Reference 1). Termed Intersymbol Interference (ISI), the effect is a loss in symbol energy resulting in a reduced telemetry SNR.

ISI was evaluated for three bandwidths equivalent to $\pm$ 1 R_s, $\pm$ 2 R_s, and $\pm$ 5 R_s (Reference 1). The results will be found in columns 4, 5, and 6 of Table 3-2. Since all filtering was assumed to be at the spacecraft, actual bandwidth, sufficient to handle one, two, or five times the main spectral lobe(s) were used. Transmitter bandwidths are listed below the losses in the ISI columns of Table 3-2. These filter bandwidths also provide an easy method for comparing the *Required Bandwidths* of the several modulation methods.

5.0 SUSCEPTIBILITY TO INTERFERENCE

Reference 3 reviewed the literature to determine whether any comparative studies of susceptibility to interference could be found. Very little information was discovered. The data that was found tended to compare the susceptibility of similar systems rather than different modulation schemes. For example, data was found comparing squarewave and sinewave subcarrier systems. Another study measured the relative performance of BPSK and QPSK systems. None were located which contrasted subcarrier and direct modulation methods.

Despite this lack of information. some simple observations can be made. Generally, the larger the frequency spectrum's width, the less the susceptibility to in-band interference. This results from the logical assumption that individual interference bursts tend to be concentrated in narrow frequency ranges. Therefore, the larger the width of the transmitted data's frequency spectrum, the less susceptible it is to interference in a portion of that band.

This "rule" is one reason why squarewave subcarriers have a distinct advantage over some of the other modulation techniques. Of course, other methods such as high rate convolutional coding and spread spectrum modulation can be used to achieve the same result with any of the direct modulation methods. However, the important point is that restricting the frequency spectrum's width increases the susceptibility to in-band interference.

6.0 CONCLUSIONS AND RECOMMENDATIONS

Because of the difficulties with the ITU definitions for *Occupied Bandwidth* and *Necessary Bandwidth*, it is recommended that both the CCSDS and SFCG adopt a new definition for *Required Bandwidth*. Because filtering is intrinsic in the concept of *Required Bandwidth*, the definition should specify the percentage of power containment (acceptable loss). Suggested levels of 95% (-0.2 dB) and 90% (-0.45 dB) should be considered by both organizations. The definition should be reviewed and agreed upon by both the SFCG and CCSDS.

With regard to modulation schemes, it is recommended that subcarriers should be eliminated from flight systems except in those unusual cases where they are required for some valid technical reason. The excessive amount of bandwidth required by subcarrier modulation systems is graphically summarized in Figure 6-1. Instead, one of the direct modulation schemes described above, together with CCSDS recommended Virtual Channels (Reference 4) should be used to separate the data streams.

Where bandwidth conservation is important, and particularly in high data rate systems, special consideration should be given to PCM/PM/NRZ and BPSK/NRZ formats. *Required Bandwidths* for the several direct, residual carrier, modulation schemes are shown in Figure 6-2. If spectral spreading is needed to meet PFD limitations, then consideration should be given to reducing the transmitter's power and using convolutional encoding to compensate for the diminished power and to spread the spectrum.

Both the CCSDS and SFCG should coordinate and consider adopting Recommendations limiting the use of subcarrier modulation schemes, except in specified circumstances, while favoring specific direct modulation methods. It is likely that the recommended types of modulation will be a function of mission design and data rate.

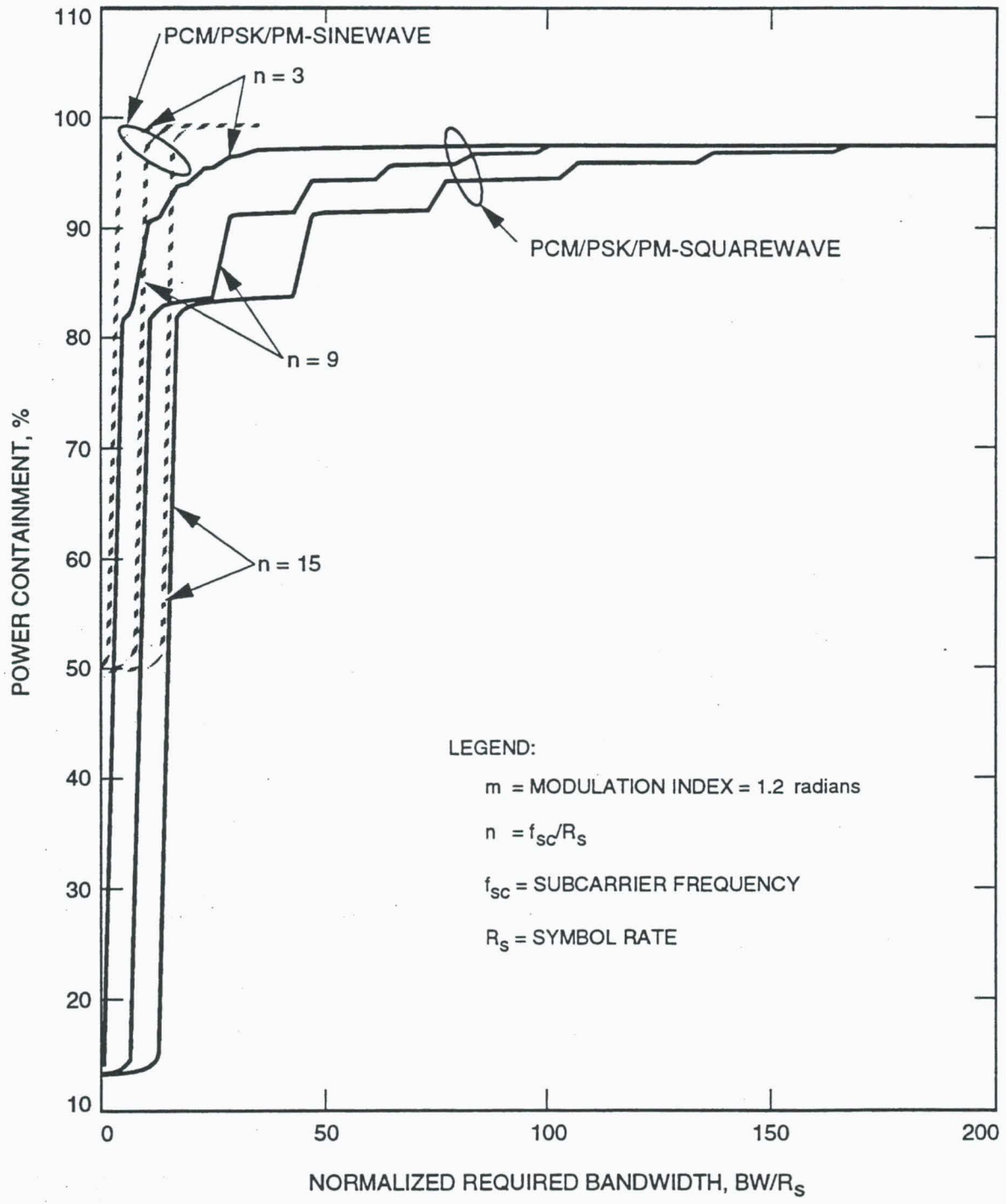

Figure 6-1. Comparison of PCM/PSK/PM

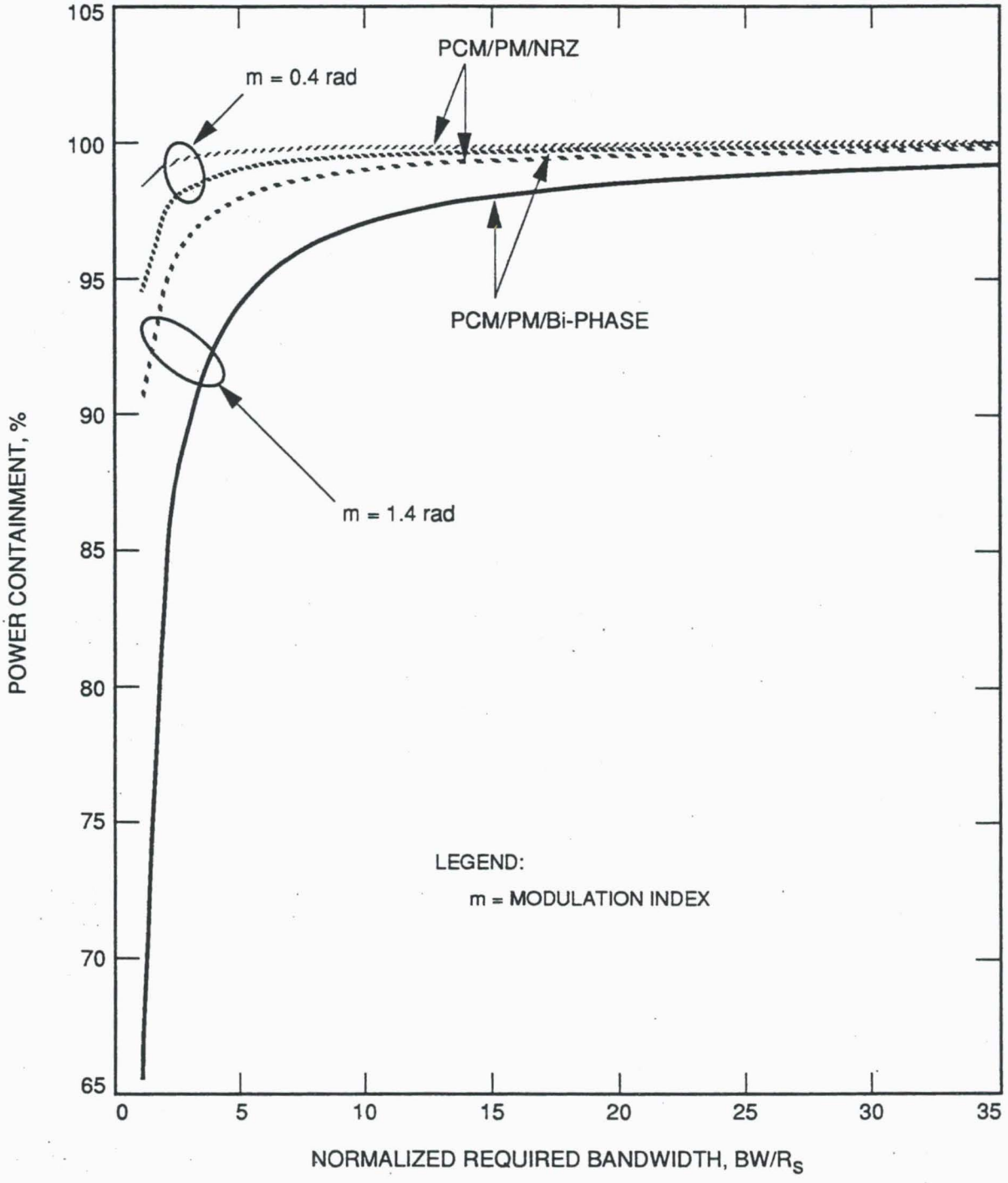

Figure 6-2. Comparison of PCM/PM Signals

REFERENCES

[1] Tien Manh Nguyen and Warren L. Martin, "Required Bandwidth, Unwanted Emission, and Data Power Efficiency for Residual and Suppressed Carrier Systems--A Comparative Study," Consultative Committee for Space Data Systems, Report of the Proceedings of the RF and Modulation Subpanel 1E meeting at the German Space Operations Centre, September 20-24, 1993, CCSDS B20.0-Y-1, February 1994.

[2] Tien Manh Nguyen and Yvette Owens, "Cross-talk in QPSK Communication Systems," Consultative Committee for Space Data Systems, Report of the Proceedings of the RF and Modulation Subpanel 1E meeting at the German Space Operations Centre, September 20-24, 1993, CCSDS B20.0-Y-1, February 1994.

[3] Tien Manh Nguyen, "A Review of the Current Available Studies of the Interference Susceptibility of Various Modulation Schemes," Consultative Committee for Space Data Systems, Report of the Proceedings of the RF and Modulation Subpanel 1E meeting at the German Space Operations Centre, September 20-24, 1993, CCSDS B20.0-Y-1, February 1994.

[4] Consultative Committee for Space Data Systems, Recommendations for Space Data System Standards, Packet Telemetry, CCSDS 102.0-B-2, January 1987.

THE OCCUPIED BANDWIDTH AND SPECTRAL CHARACTERISTICS OF FILTERED/UNFILTERED PSK, MSK AND GMSK

Philippe Michel
European Space Agency
European Space Research and Technology Centre
2200 AG Noordwijk, The Netherlands

ABSTRACT

This paper investigates the 99% occupied bandwidth of unfiltered and filtered telemetry signals employing different types of modulation schemes. The modulation schemes considered in this paper are: BPSK, QPSK, OQPSK, MSK and GMSK.

1. Introduction

The purpose of this paper is to present the 99% occupied bandwidth of a telemetry signal with different types of modulation schemes, namely unfiltered and filtered BPSK QPSK and OQPSK, MSK and GMSK.

2. Power Spectral Density and Occupied Bandwidth

2.0 Definition

In the Radio Regulations, the occupied bandwidth is defined as the bandwidth in which 99% of the transmitted signal power is concentrated.

In this note, we call B_occ the occupied bandwidth. B_occ is equal to 2 times Bp where Bp is the baseband (99%) bandwidth. The transmitted signal 99% power is contained inside [-Bp, Bp].
Rb is the data rate.

2.1 Unfiltered BPSK, QPSK, OQPSK

These modulation schemes have already been extensively addressed, in particular in previous CCSDS position papers. (In particular ref. [1,2] and ref.[3]).

The Power Spectral Density (PSD) of an unfiltered PSK with random data patterns is given by the following equation:

$$PSD = T\left(\frac{\sin\pi fT}{\pi fT}\right)^2$$

were T is the symbol duration. (equal to the bit duration for BPSK and to two times the bit duration for QPSK and OQPSK).

The symbol duration for a QPSK or a OQPSK modulated signal is twice that of a BPSK modulated signal therefore the QPSK or OQPSK transmitted bandwidth is twice less than a BPSK.

Figure 1 shows the spectrum of a unfiltered QPSK signal and the Out-of-Band Power (OBP) versus the normalized frequency. The OBP is defined as the fraction of power outside the normalized bandwidth:

$$OBP(f) = \frac{\int_f^{\infty} PSD(\nu)d\nu}{\int_0^{\infty} PSD(\nu)d\nu}$$

When plotted with a dB scale, Bp corresponds to the value for which the OBP is equal to -20 dB. The occupied bandwidth (B_occ) is therefore equal to twice the value for which the OBP is equal to -20 dB.

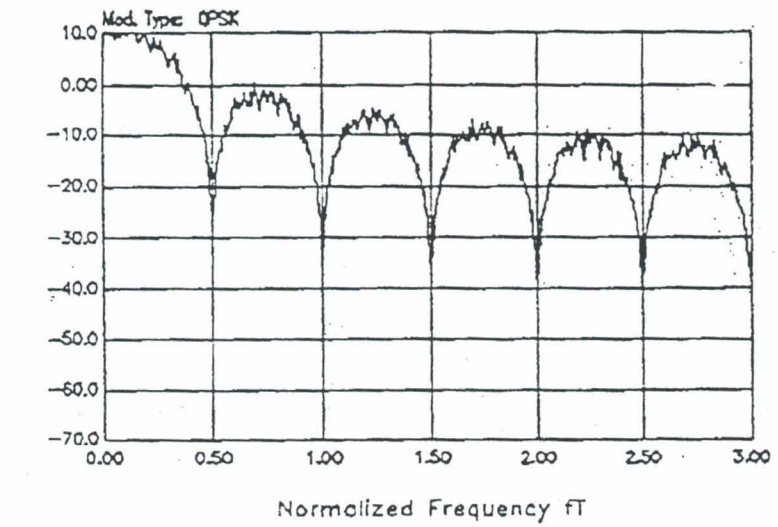

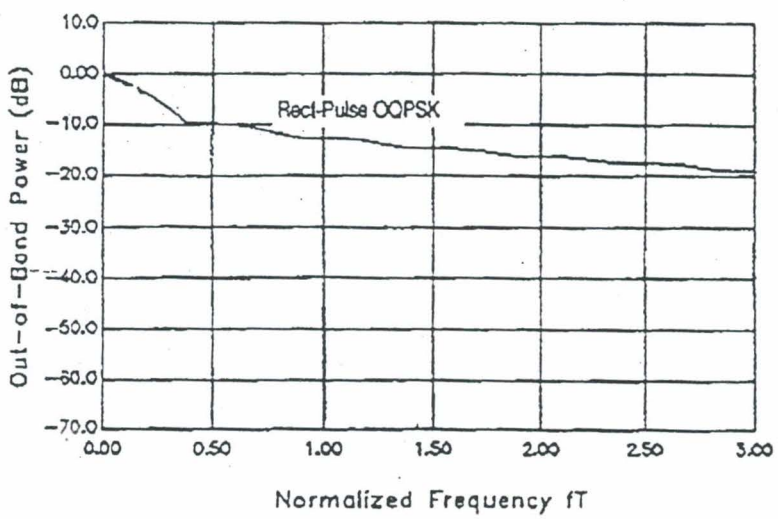

Figure 1

Finally, the occupied bandwidths are:

Unfiltered PSK	Bp	Occupied Bandwidth (B_occ)
Unfiltered BPSK	10.2xRb	20.4xRb
Unfiltered QPSK	5.1xRb	10.2xRb
Unfiltered OQPSK	5.1xRb	10.2xRb

where Rb is the data rate.

2.2 Filtered BPSK, QPSK, OQPSK.

As shown in the previous paragraph, unfiltered PSK modulated signal exhibit a fairly large required bandwidth. Filtering these signals can reduce dramatically the occupied bandwidth.

Ref. [1] shows the occupied bandwidth with a simple one-pole Low Pass Filter applied at the input of the modulator. (This simple filter was selected for demonstration purposes only) With a ratio of the cutoff frequency to the data rate of 2, the occupied bandwidth is roughly reduced by a factor 3, compared to the unfiltered case.

Ref. [2] reports on the occupied bandwidth of a PSK modulated signal filtered with a Butterworth filter with orders ranging from 2 to 4. The response of a Butterworth low pass filter is given by:

$$|H(f)|^2 = \frac{1}{1+(f/f_{3dB})^{2n}}$$

where:

- f3dB: 3 dB bandwidth of the filter
- n : order of the filter.

The results show that with a Butterworth filter of an order 3 and a 3 dB bandwidth roughly equal to the main lobe of the modulation, , 99% of the transmitted energy is concentrated in the main lobe. In other words, for a QPSK signal, the occupied bandwidth is now equal to 1*Rb which represents a reduction of a factor 10 compared to the unfiltered case.

Further bandwidth reduction can be achieved with still fairly simple filters. In particular, if we introduce the classical raised cosine Nyquist function:

$$P_N(f) = \begin{cases} 1, & 0 < |2fT| \le \frac{1-\alpha}{2} \\ \cos^2\left[\frac{\pi}{2\alpha}\left(2fT - \frac{1-\alpha}{2}\right)\right], & \frac{1-\alpha}{2} < |2fT| \le \frac{1+\alpha}{2} \\ 0, & \text{elsewhere} \end{cases}$$

Assuming an equally-splitted filtering between transmitter and receiver and a roll-off factor equal to 0.5, figure 2 shows the PSD and the OBP of the OQPSK filtered with raised cosine filters.

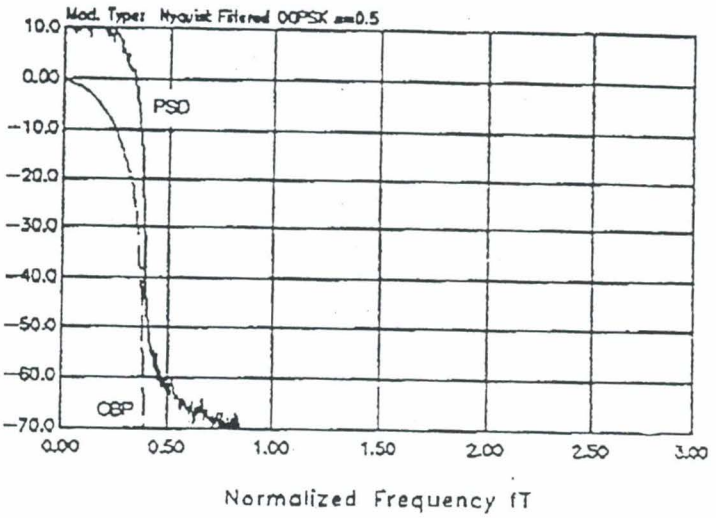

Figure 2

As can be seen from figure 2, the occupied bandwidth is now roughly equal to 0.7xRb.

Finally, the spectral occupancy of filtered PSK can be summarized as follows:

Filtered PSK	Bp	Occupied Bandwidth (B_occ)
One pole filtered BPSK	3.4xRb	6.8xRb
One pole filtered QPSK or OQPSK	1.7xRb	3.4xRb
3-poles Butterworth BPSK	1xRb	2xRb
3-poles Butterworth QPSK or OQPSK	0.5xRb	1xRb
Raised-cosine (roll-off=0.5) BPSK	0.7xRb	1.4xRb
Raised-cosine (roll-off=0.5) QPSK or OQPSK	0.35xRb	0.7xRb

2.3 Minimum Shift Keying (MSK) Modulation Scheme

An MSK signal can be viewed as a Continuous Phase Frequency Shift Keying signal or as an Offset QPSK signal with sinusoidal phase weighting

The PSD of a MSK modulated signal is given by:

$$PSD(f) = \frac{16T}{\pi^2}\left(\frac{\cos 2\pi fT}{1-16(fT)^2}\right)^2$$

Figure 3 (ref.[3]) shows the PSD and the OBP of an MSK signal.

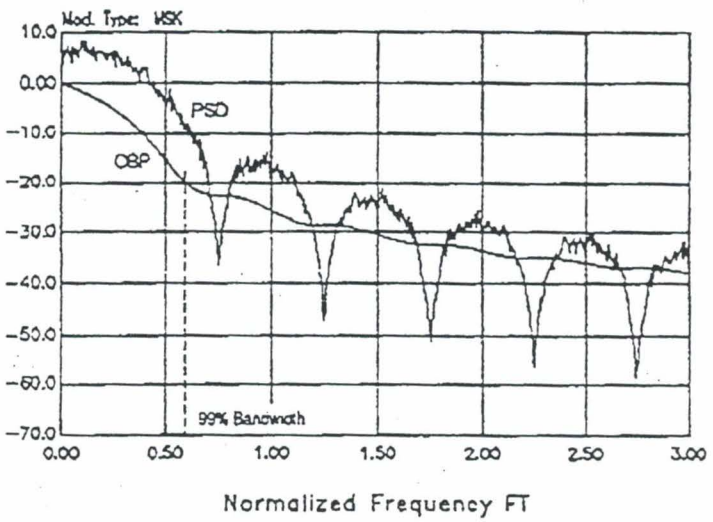

Figure 3

The first null in the PSD of an MSK modulated signal takes place at fT=0.75 and the 99% of the total baseband signal power is concentrated in the interval $|ft| < 0.6$.

The occupied bandwidth is therefore as follows:

MSK	Bp	Occupied Bandwidth (B_occ)
MSK signal	0.6xRb	1.2xRb

2.4 Gaussian Minimum Shift Keying (GMSK)

GMSK modulation is a MSK modulation to which is applied a Gaussian filter. This modulation scheme is attractive due to its constant-envelope and compact-spectrum features. In par-

ticular, the spectral occupancy of the modulated signal can be adjusted by varying the bandwidth of the Gaussian filter (Bg).
Letting Bg to infinite, GMSK turns into an MSK signal. Common values for the product BgT are in the interval 0.25 to 0.5.

Figure 4 shows the PSD of GMSK signals for various values of the parameter BgT.

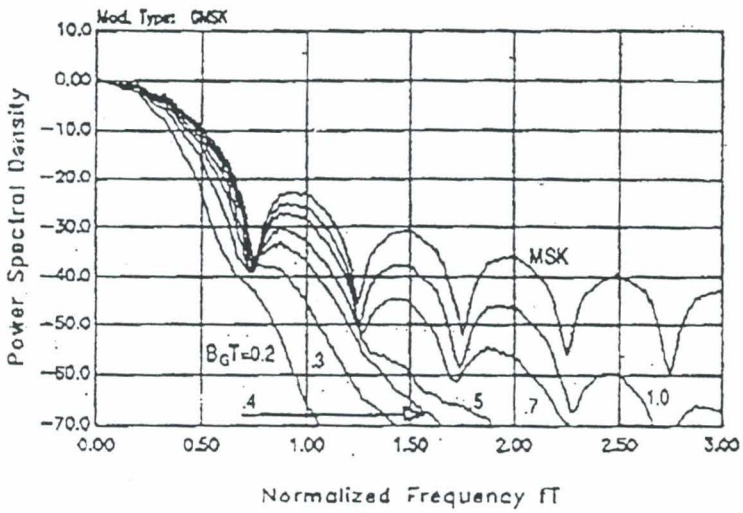

Figure 4

In the case BgT=0.5, the PSD and the OBP are reported in figure 5 (ref.[3]).

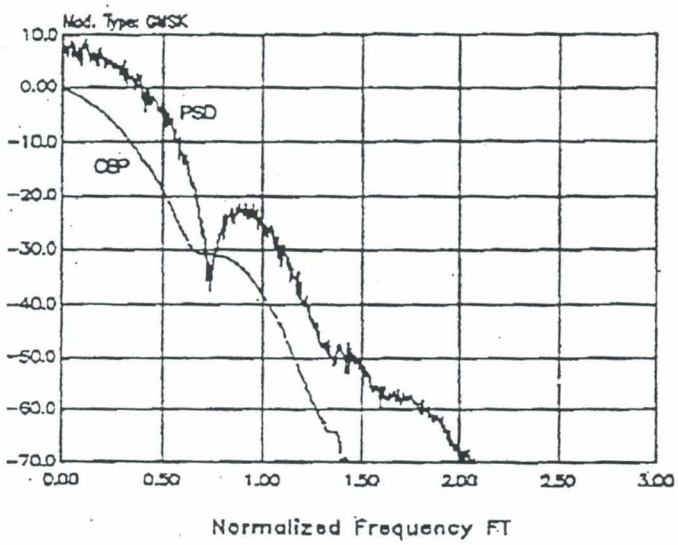

Figure 5

As can be seen from this figure, the occupied bandwidth for a GMSK modulated signal with a filter bandwidth Bg such that BgT=0.5 is as follows:

GMSK	Bp	Occupied Bandwidth (B_occ)
GMSK Signal	0.5xRb	1.0xRb

3 Conclusions

We have reviewed in this paper the bandwidth occupancy of various modulation schemes.

Clearly, unfiltered PSK are not the most attractive from the bandwidth occupancy point of view. A large range of filtering possibilities can be envisaged to reduce the bandwidth occupancy of PSK signals. Alternatively, other modulation techniques such as MSK or GMSK exhibit performances similar to filtered PSK.

Bandwidth occupancy in the range 1 to 2 times the bit rate can easily be achieved which represents a gain of a factor 5 to 10 with respect to unfiltered PSK.

In this paper, the impact of filtering and non linear amplification in terms of sidelobes regrowth and BER degradation has not been assessed.

Regarding the sidelobes regrowth problem after amplification, the actual bandwidth occupancy may slightly be increased (compared to the results given in this paper), but not significantly. For what concerns the out-of-band spurious generation, it is expected, even after non linear amplification, that filtered PSK, MSK and GMSK exhibit better performances than unfiltered PSK and also that they are less sensitive to possible out-of-band interferences.

Regarding BER degradations, GMSK is a constant envelope modulation, therefore insensitive to non linearities. Clearly, filtered PSK is more sensitive than unfiltered PSK to non-linearities. However, the possibility of selecting smooth filtering should allow to keep signal distortions to a low level. As a side effect, the use of error correction coding schemes, by keeping the Eb/No working point low, also helps to minimize the BER degradation due to non-linearities of non constant envelope signals. Practically, depending on the type of non-linearity and on the choice of the filtering scheme, a goal of 0.1 to 0.3 dB of degradation should be achievable.

For category A missions, filtered PSK or MSK or GMSK are very good modulation schemes candidates, compared to traditional residual carrier or unfiltered PSK, to minimize the spectral occupancy and possibly the generation of out of band spurious emissions.

References

[1] J. A Koukos "Occupied Bandwidth of QPSK and MSK Telemetry Systems", Position paper presented in the CCSDS panel 1E, Spring 1993, Pasadena.

[2] M. Outer "Optimal Filtering of PSK to retain 99% power in the Spectral Main Lobe" Position Paper presented in the CCSDS panel 1E, Spring 1990.

[3] University of Pisa, "Advanced Modulation Schemes for Future ESA Standards", ESTEC/Contract #8565/89/NL/JG, Spring 1991.

PCM/PSK/PM AND PCM-SPL/PM SIGNALS-

OCCUPIED BANDWIDTH AND BIT ERROR RATE

Jacques Fois Pelayo, Jean-Luc Gerner

European Space Agency

European Space Research and Technology Centre

2200 AG Noordwijk, The Netherlands

ABSTRACT

This report presents results from a computational technique to determine the occupied bandwidth for a class of PCM/PSK/PM and PCM-SPL/PM signals, and to derive the BER as well, for implementing a study focused to telecommand, telemetry and tracking (TT&C) signals.
Either a squarewave or sinewave subcarrier are considered in this paper for PCM/PSK/PM signals, as well as the cases of filtered or unfiltered signals for both kinds of signals.

The computational technique has been performed by using the TOPSIM simulation package for evaluating the spectra, the occupied bandwidth and the BER.
Furthermore, some data obtained with TOPSIM are processed for getting some interesting plots and for computing approximate formulas of the occupied bandwidth with the aid of MATLAB.

0. INTRODUCTION.

For space applications, the typical signal recommended by the Consultative Committee for Space Data Systems (CCSDS) is the residual carrier signal using the subcarrier for the data.The subcarrier is used to separate the data from the residual carrier and its waveforms recommended by the CCSDS for telemetry transmissions are the squarewave for deep space, and the sinewave for near earth missions.

Concerning the bandwidth, in the International Telecommunications Union (ITU) the occupied bandwidth is defined as :

> ' The width of a frequency band such that, below the lower and above the upper frequency limits, the mean power emitted are each equal to a specified percentage $\beta/2$ of the total mean power of a given emission.Unless otherwise specified by the CCIR for the appropriate class of emissions, the value of $\beta/2$ should be taken as 0.5%. '

For all transmissions, the occupied bandwidth shall be specified.Moreover, a radio frequency spectral mask shall be specified, below which the emitted spectral power density shall lie.

As far as this paper is concerned, two parameters are taken into consideration to perform the computations : the modulation index of the phase modulation and the subcarrier frequency-to-bit-rate ratio.The use of these parameters has to be in agreement with International or European Standards.This paper will consider the parameters more generally for getting an overall study of PCM/PSK/PM and PCM-SPL/PM signals.

1. OCCUPIED BANDWIDTH FOR PCM/PSK/PM SIGNALS

1.1 Sinewave subcarrier.

The occupied bandwidth for a 99% power containment will be computed for PCM/PSK/PM signals when we modulate with a sinewave subcarrier.

The block diagram of the transmitter for these kind of signals is as follows:

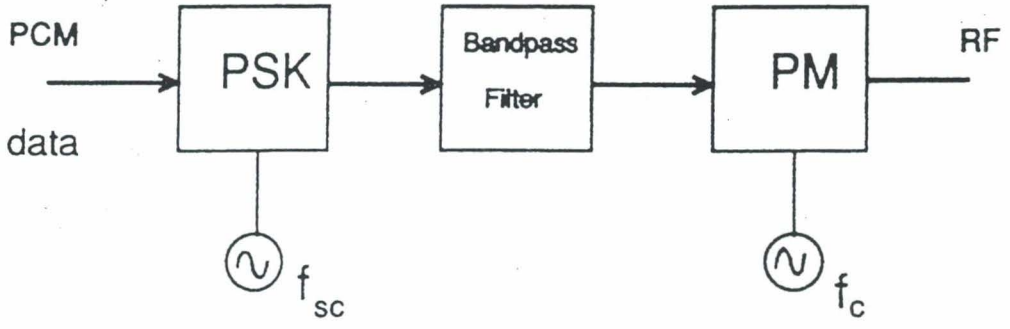

where the filter is optional.

In RF we obtain a signal given in time domain by:

$$s(t) = A\sqrt{2}\sin[w_c t + m\phi(t)]$$

where A is the rms voltage, w_c the angular carrier center frequency in rd/s, m the modulation index in rd and $\phi(t)$ is the PSK modulated signal filtered or not.

The power spectral density of s(t) is:

$$S(f) = A^2[J_0^2(m)\delta(f-f_c) + \sum_{k\ even} J_k^2(m)\{\delta(f-f_c-kf_{sc})+\delta(f-f_c+kf_{sc})\} +$$

$$+ \sum_{h\ odd} J_h^2(m)\{S_d(f-f_c-hf_{sc})+S_d(f-f_c+hf_{sc})\}]$$

where S_d is the power spectral density for PCM data.This expression has been extracted from the A-E-91-13 work paper published by the NASA.

If we sketch the spectrum for these kind of signals we can obtain a plot like the one given in next page. This case is for $f_{sc}=9R_s$, m=0.6 and no filtering, with R_s being the symbol rate of binary data.

POWER SPECTRUM OF Y

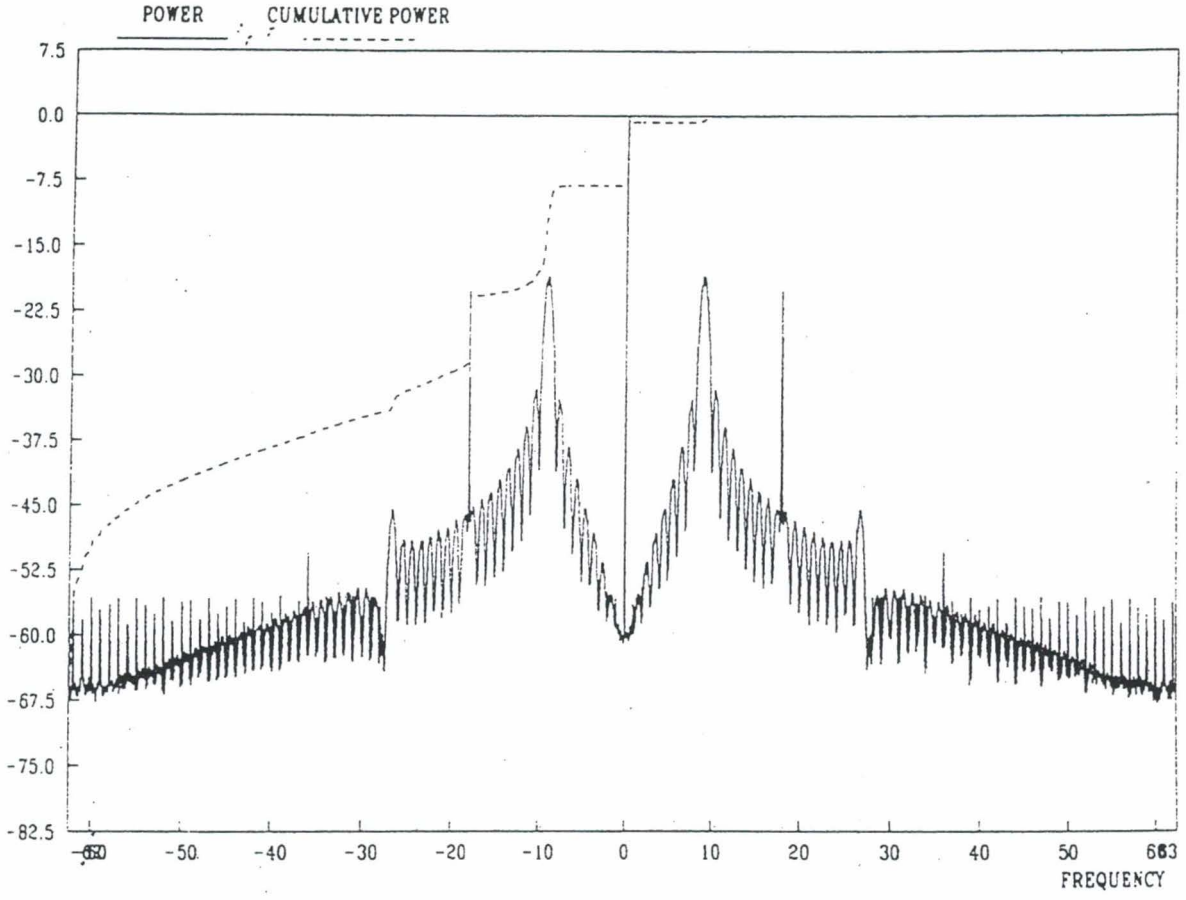

The frequency axis is normalized to the symbol rate R_s and shifted to the carrier frequency, so we can define a parameter $n=f_{so}/R_s$. In fact this parameter n is not a new concept, but only a new way for defining the subcarrier frequency because of the frequency normalization.

In the graphic it is possible to see all the components that form the spectrum, that is, the carrier frequency on the center, replicas of the modulating signal on the odd multiples of n, and spectral lines on the even multiples due to the nature of phase modulation.

The occupied bandwidth is computed for two cases:

a. With no filtering.

The normalized one-sided occupied bandwidth to R_s for a 99% power containment is the following for different values of n and the modulation index m:

n	m= 0.2rd	m= 0.4rd	m= 0.6rd	m= 0.8rd	m= 1.rd	m= 1.1rd	m= 1.2rd	m= 1.35r	m= 1.5rd
3	3.335	4.562	6.017	8.500	9.116	9.372	12.00	12.06	12.90
5	5.305	6.401	10.02	10.62	14.39	14.87	15.16	16.03	20.03
7	7.296	8.36	14.01	14.06	18.58	20.74	21.04	21.42	27.81
9	9.31	10.30	18.02	18.06	22.45	26.66	27.00	27.35	28.58
11	11.30	12.30	22.02	22.04	24.79	32.61	32.98	33.33	33.77
13	13.29	14.27	26.01	26.07	27.79	38.52	38.97	39.32	39.71
15	15.30	16.32	30.01	30.06	30.59	44.46	44.97	45.32	45.65
17	17.29	18.30	34.00	34.05	34.25	50.42	50.96	51.32	51.65
19	19.30	20.29	38.01	38.08	38.27	56.29	56.96	57.32	57.63
21	21.30	22.31	42.01	42.04	42.41	61.93	62.95	63.30	63.61

Using the linear curve fitting technique we can obtain expressions for the occupied bandwidth:

m=0.2rd , BW = (0.999*n + 0.3171)R_s

m=0.4rd , BW = (0.9901*n + 1.461)R_s

m=0.6rd , BW = (1.999*n + 2.1733E-02)R_s

m=0.8rd , BW = (1.922*n + 1.3)R_s

m=1.0rd , BW = (1.732*n + 5.464)R_s

m=1.1rd , BW = (2.942*n + 0.2891)R_s

m=1.2rd , BW = (2.911*n + 1.368)R_s

m=1.35rd, BW = (2.908*n + 1.785)R_s

m=1.5rd , BW = (2.715*n + 5.551)R_s

These results are somewhat deviating from those obtained in the A-E-91-13 NASA work paper.We can now write down a few lines about this suggestion.

We know that the spectrum for PCM/PSK/PM signals contains 2 spectral lines at each side of the carrier and separated both from the carrier by 2*n (with the frequency axis normalized to R_s).The total power contained in these lines is given by $2*J_2^2(m)$ for a 1W normalized signal (for sake of simplicity) and for each modulation index we can obtain the percentage of power contained in these lines which is given by $100*(2*J_2^2(m))\%$:

m(rd)	% power containment	m(rd)	% power cont.
0.2	4.966E-3	1.35	7.614
0.4	7.789E-2	1.5	10.77
0.6	0.3813		
0.8	1.149		
1.0	2.64		
1.1	3.73		
1.2	5.07		

Relating to these results we can remark that for m=0.8rd the 1.149% of total power is contained in the spectral lines, and this means that if we want to compute the bandwidth for the 99% power containment when we use a modulation index of 0.8rd we have, at least, to reach the value of 2*n because it is where the spectral lines are lying.

Our numbers given in the previous table agree with this comment, but not the ones given in the A-E-91-13 NASA work paper.

b. With filtering.

The filter used for filtering the PSK modulated signal is a 1st-order Butterworth filter with a 3dB bandwidth of $2*R_s$ and centered on the subcarrier frequency, i.e.,only the major lobe is being unfiltered.The choice of this filter is a trade-off between the necessity to avoid an unnecessary extension of the occupied bandwidth and the objective to not significantly degrade the performances of the transmission (Bit Error Rate).

The results are given in next page and the expressions for the occupied bandwidth are right below:

m=0.2rd , BW = $(1.002*n + 0.1762)R_s$

m=0.4rd , BW = $(1.002*n + 0.5358)R_s$

m=0.6rd , BW = $(2*n - 4.5264E\text{-}03)R_s$

m=0.8rd , BW = $(2*n + 5.9943E\text{-}02)R_s$

m=1.0rd , BW = $(1.983*n + 0.438)R_s$

m=1.1rd , BW = $(1.995*n + 1.082)R_s$

m=1.2rd , BW = $(2.996*n - 0.1986)R_s$

m=1.35rd, BW = $(3*n + 0.1292)R_s$

m=1.5rd , BW = $(3*n + 0.324)R_s$

n	m= 0.2rd	m= 0.4rd	m= 0.6rd	m= 0.8rd	m= 1.rd	m= 1.1rd	m= 1.2rd	m= 1.35r	m= 1.5rd
3	3.18	3.546	6.014	6.064	6.078	7.066	8.857	9.154	9.358
5	5.184	5.541	10.01	10.09	10.25	11.06	14.79	15.13	15.33
7	7.191	7.540	13.97	14.05	14.09	15.03	20.72	21.11	21.30
9	9.197	9.566	17.98	18.07	18.13	19.02	26.72	27.11	27.30
11	11.19	11.56	21.98	22.06	22.20	23.06	32.72	33.11	33.30
13	13.19	13.56	26.00	26.01	26.17	27.01	38.74	39.16	39.33
15	15.21	15.59	29.96	30.06	30.15	31.06	44.74	45.13	45.33
17	17.21	17.58	33.99	34.06	34.12	34.99	50.74	51.13	51.33
19	19.21	19.57	37.99	38.08	38.14	38.97	56.73	57.13	57.32
21	21.21	21.58	42.00	42.08	42.11	42.97	62.73	63.12	63.32

Conclusions.

1) The spectrum for PCM/PSK/PM signals using sinewave subcarrier is built as follows : First we create a PSK modulating signal which spectrum is well known as the following

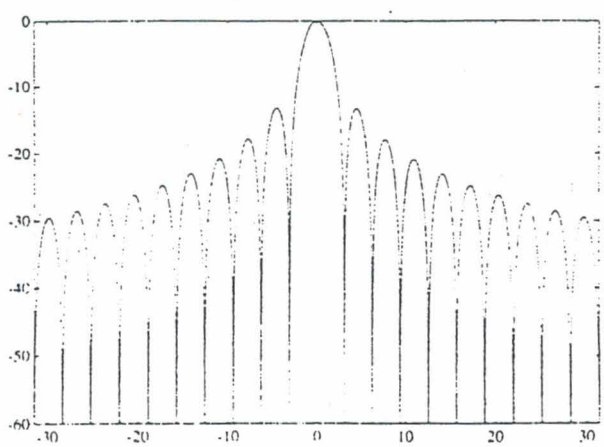

Afterwards, the spectrum obtained by modulating in PM has replicas of the PSK spectrum located at $f_c \pm kf_{sc}$ with k being an odd integer and also there are spectral lines that appear at the frequencies $f_c \pm lf_{sc}$ with l being an even integer, besides the carrier centered at f_c.So, if we shift the spectrum to the carrier frequency and we normalize the frequency axis by the symbol rate R_s, the PCM/PSK/PM spectrum can be plotted as follows:

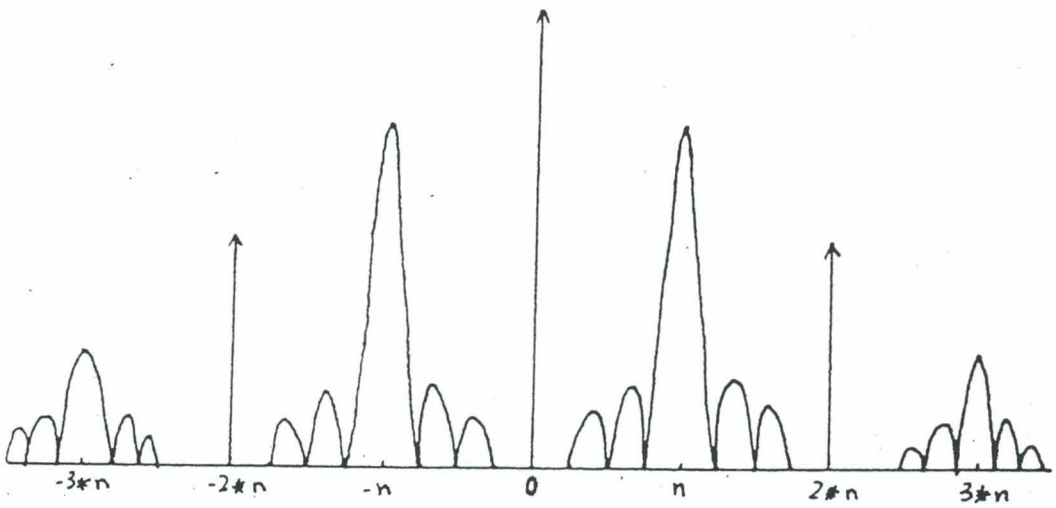

Let's look at some cases.In next pages the spectrum for n=3 and n=21 are sketched with and without filtering.Because of the lower value of n=3, the spectrum obtained is more concentrated around the carrier than the case of n=21.
A consequence of this is that the increase of the occupied bandwidth referring to the value of n is bigger for n=3 than for n=21 when the modulating index is increasing.
This can be seen with the values given in the table for the case of no filtering as follows: for m=0.2, the normalized occupied bandwidth is 3.335 for n=3 and 21.30 for n=21, i.e., almost n in both cases, but in the case of m=1.35 the new values are 12.06 for n=3 (that is, 4*n) and 63.30 for n=21 (that is, 3*n).

Another point is remarkable in these plots.This is that it is easy to find out by inspection that the effect of filtering is more important for the case of n=3 than the case for n=21.

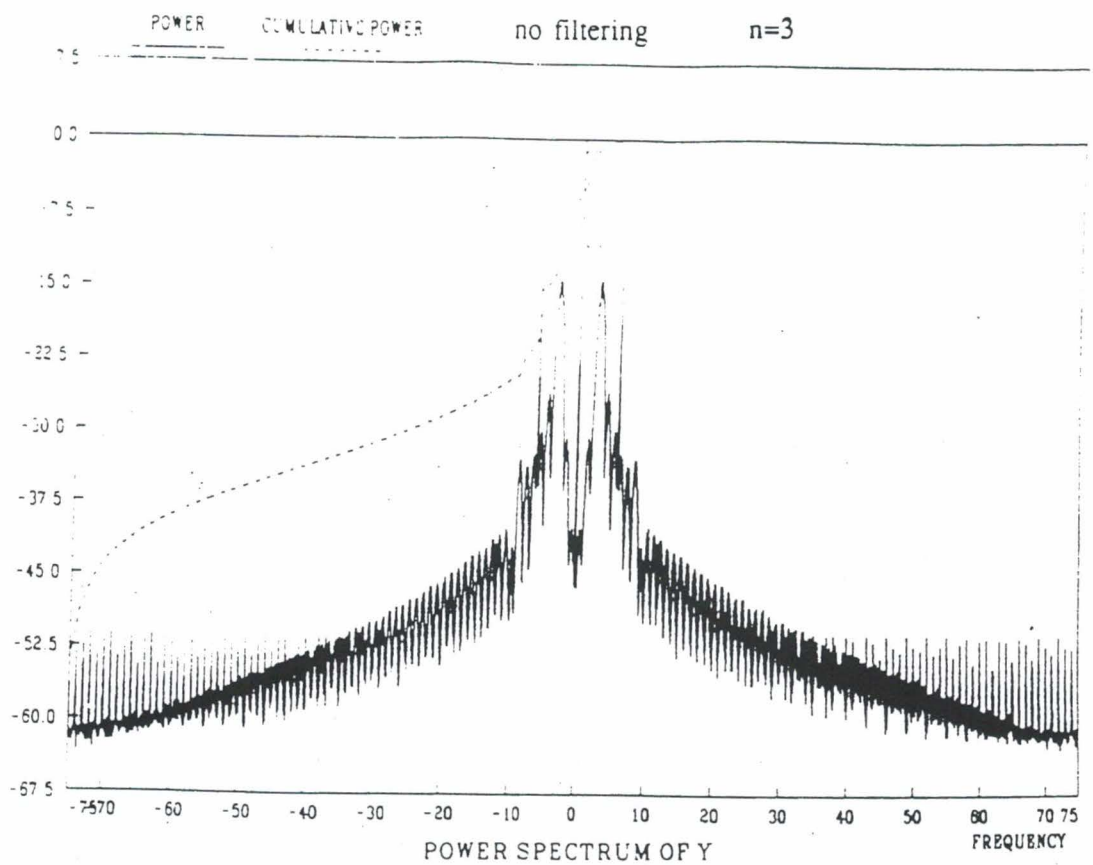
POWER
CUMULATIVE POWER
no filtering
n=3
0.0
-7.5
-15.0
-22.5
-30.0
-37.5
-45.0
-52.5
-60.0
-67.5
-75 -70 -60 -50 -40 -30 -20 -10 0 10 20 30 40 50 60 70 75
FREQUENCY
POWER SPECTRUM OF Y

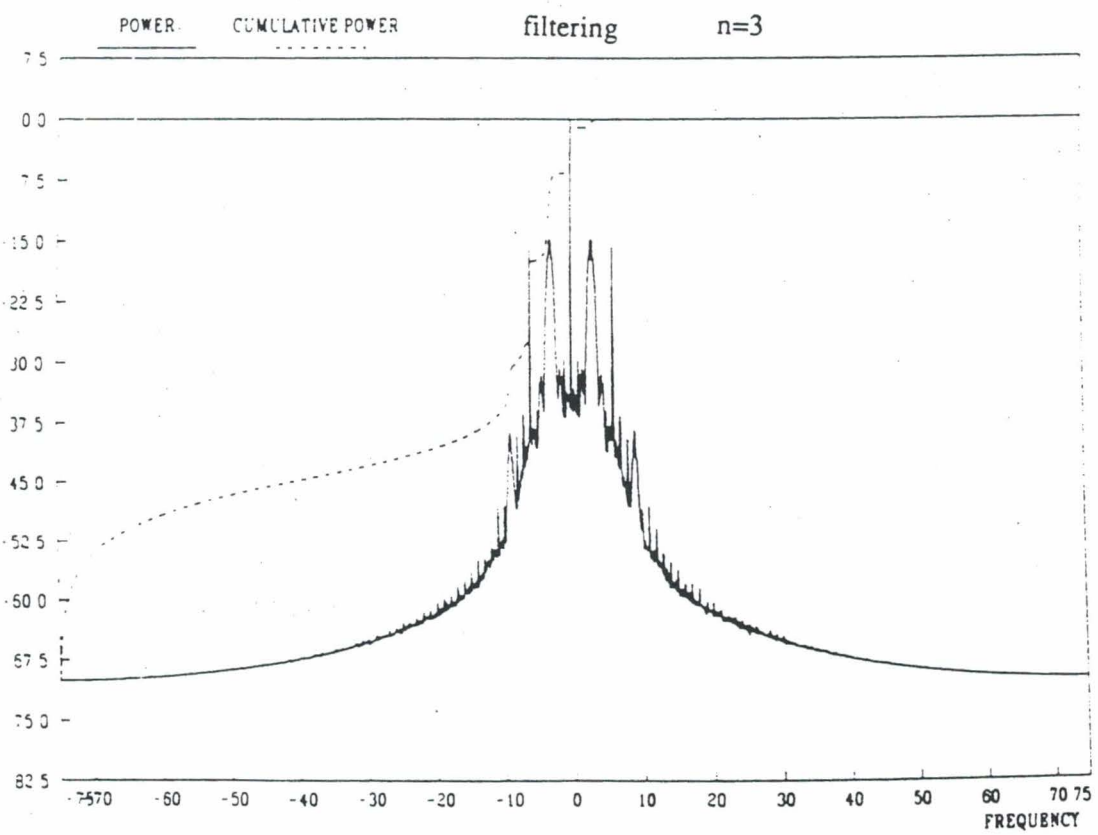
POWER
CUMULATIVE POWER
filtering
n=3
7.5
0.0
-7.5
-15.0
-22.5
-30.0
-37.5
-45.0
-52.5
-60.0
-67.5
-75.0
-82.5
-75 -70 -60 -50 -40 -30 -20 -10 0 10 20 30 40 50 60 70 75
FREQUENCY

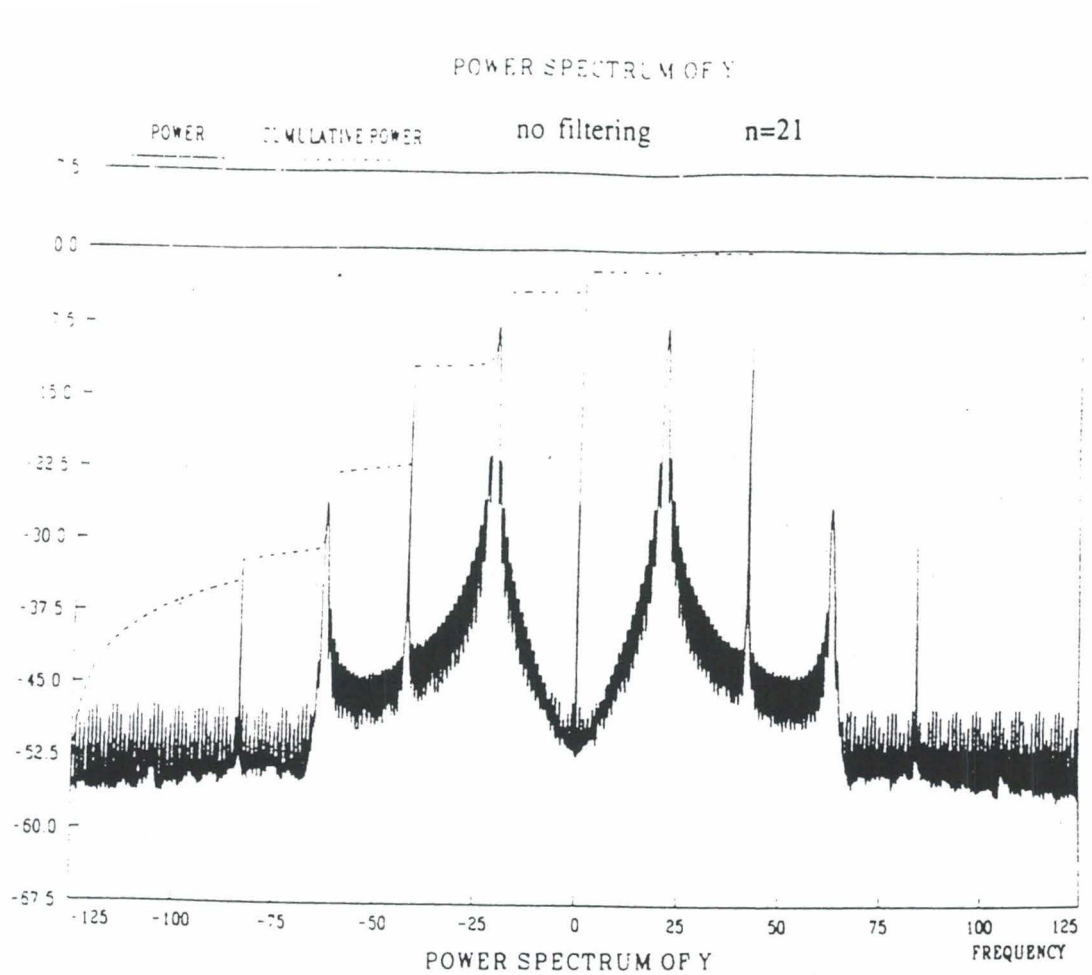
POWER SPECTRUM OF Y
POWER
CUMULATIVE POWER
no filtering
n=21
7.5
0.0
-7.5
-15.0
-22.5
-30.0
-37.5
-45.0
-52.5
-60.0
-67.5
-125
-100
-75
-50
-25
0
25
50
75
100
125
FREQUENCY
POWER SPECTRUM OF Y

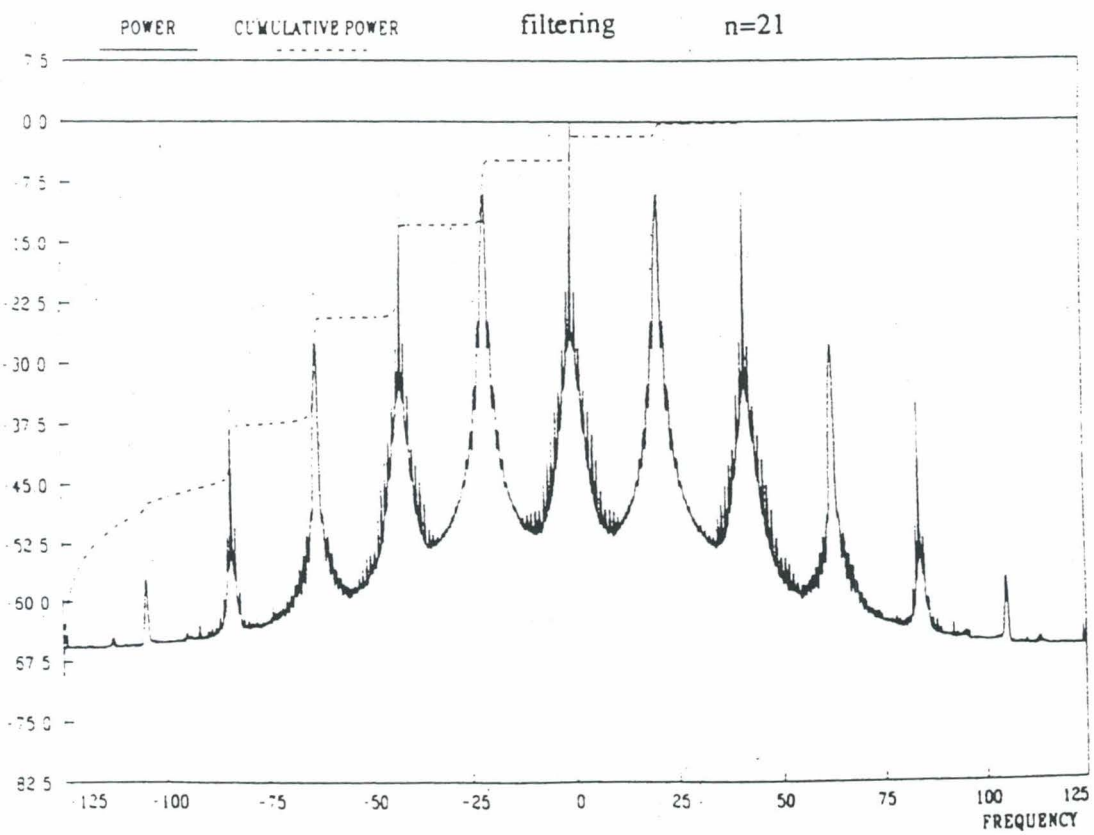
POWER
CUMULATIVE POWER
filtering
n=21
7.5
0.0
-7.5
-15.0
-22.5
-30.0
-37.5
-45.0
-52.5
-60.0
-67.5
-75.0
-82.5
-125
-100
-75
-50
-25
0
25
50
75
100
125
FREQUENCY

2) In next pages, graphics relating to the normalized occupied bandwidth vs. the modulation index are plotted for fixed values of n.The continuous lines are referring to the case of no filtering and the dashed ones to the case of filtering.

In general, we can remark that:

* The effect of filtering for low values of the modulation index is moderate.

* There is almost no difference between filtering and no filtering when we use a modulation index m from 0.6 to 1.0.This happens because of the nature of the phase modulation.For this range of values of m, the occupied bandwidth remains approximately constant around 2*n, and if we look at the spectrum we can observe a spectral line at 2*n surrounded by spectrum components with very low power as compared with the power contained in the spectral line.This makes the spectral line create a high jump when we compute the occupied bandwidth for a 99% power containment for these values of m.

* An analogue situation is evidenced with a modulation index of 1.2.The occupied bandwidth is almost the same for both cases of filtering or not around 3*n.

This happens because in this part of the spectrum there is a second replica of the modulating signal that happens to have an important power containment.

It's likely to remark that this not occurs exactly for lower values of n because the spectrum is more concentrated, i.e., the spectral lines and replicas of modulating signal are surrounded by spectral components with no so low power.And that is the reason also for what the effect of filtering is more important in these cases.

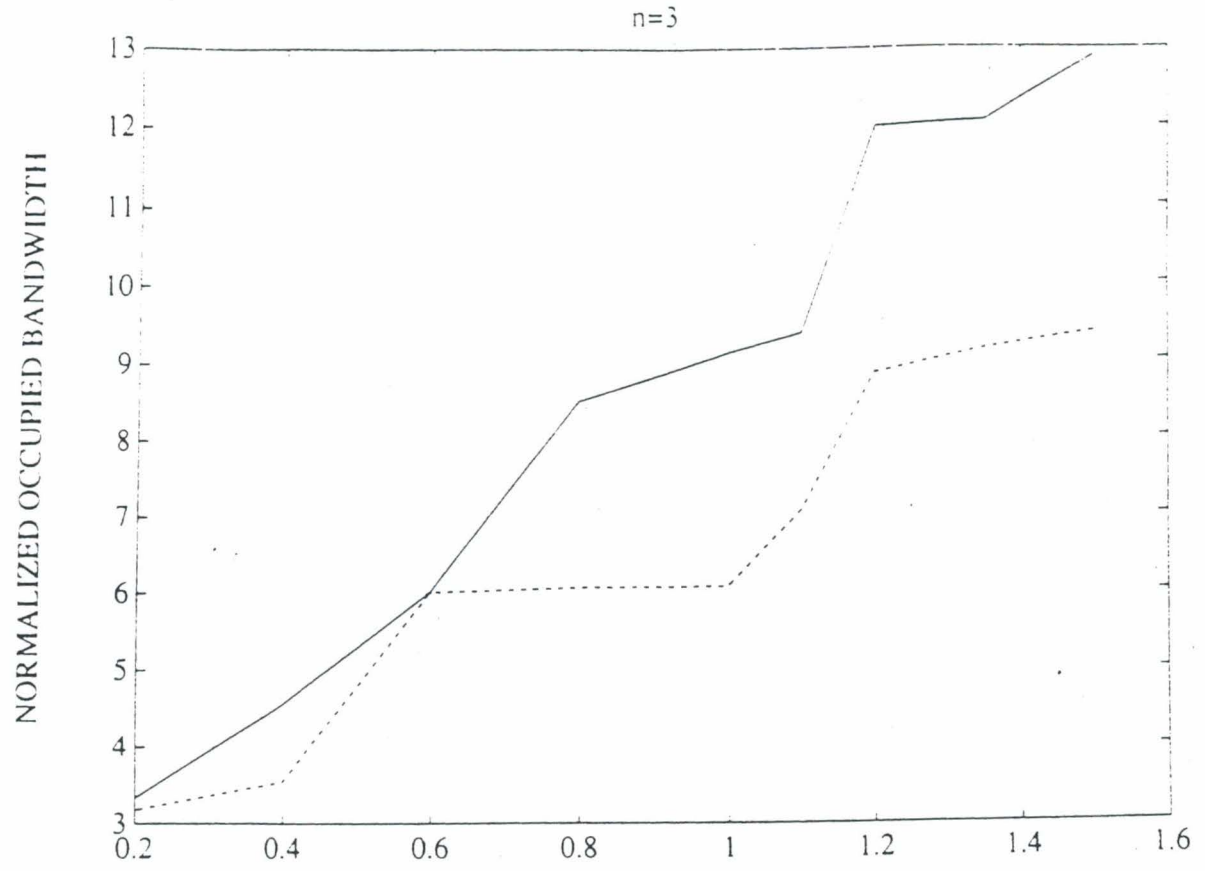
n=3
NORMALIZED OCCUPIED BANDWIDTH
13
12
11
10
9
8
7
6
5
4
3
0.2
0.4
0.6
0.8
1
1.2
1.4
1.6
m

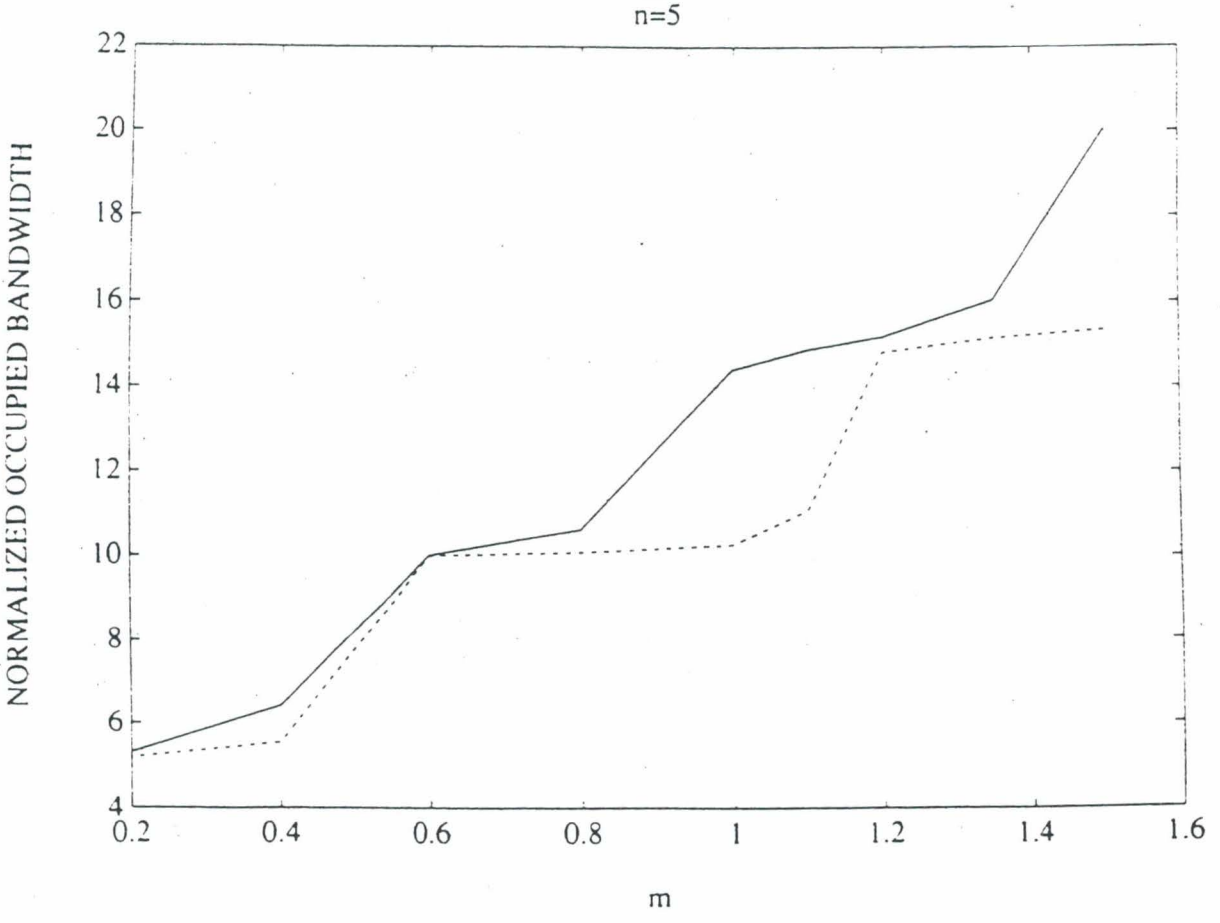
n=5
NORMALIZED OCCUPIED BANDWIDTH
22
20
18
16
14
12
10
8
6
4
0.2
0.4
0.6
0.8
1
1.2
1.4
1.6
m

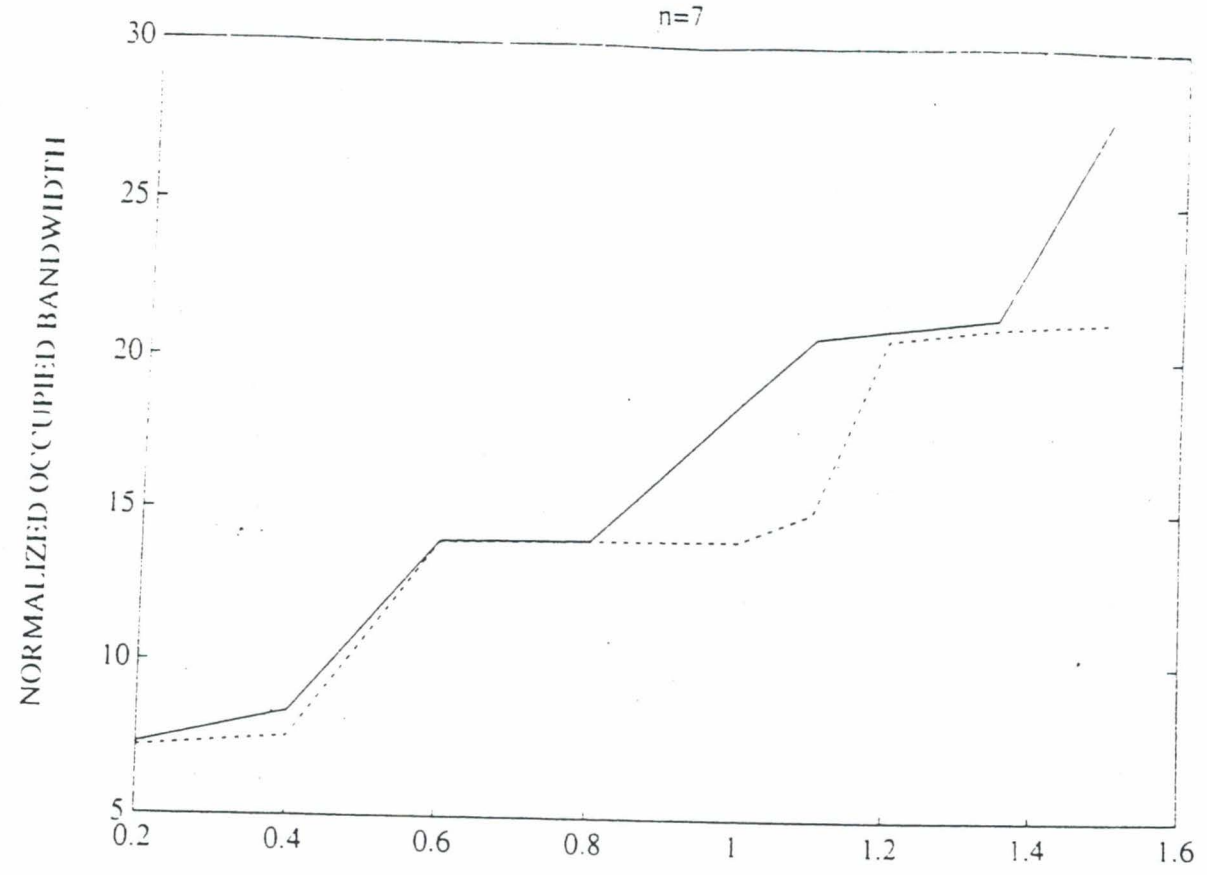
n=7
NORMALIZED OCCUPIED BANDWIDTH
30
25
20
15
10
5
0.2
0.4
0.6
0.8
1
1.2
1.4
1.6
m

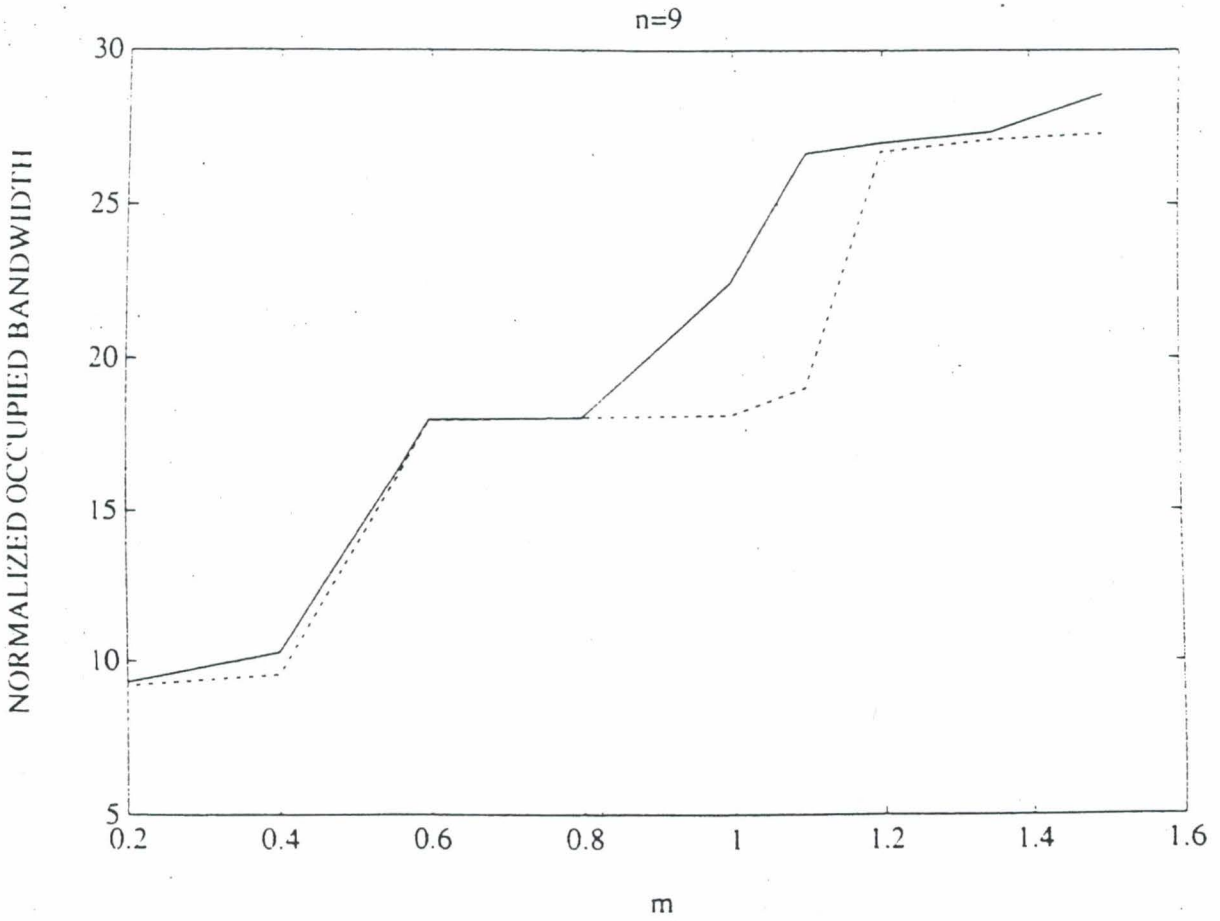
n=9
NORMALIZED OCCUPIED BANDWIDTH
30
25
20
15
10
5
0.2
0.4
0.6
0.8
1
1.2
1.4
1.6
m

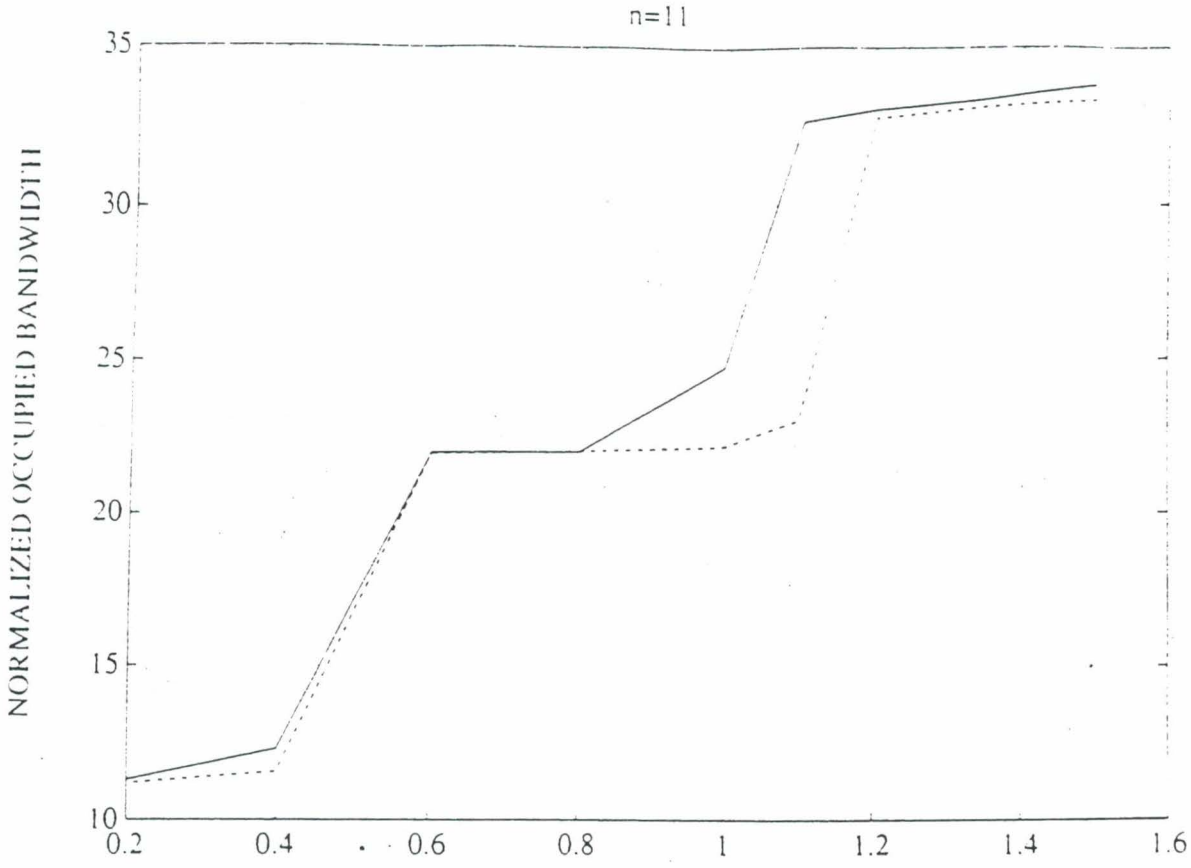
n=11
NORMALIZED OCCUPIED BANDWIDTH
35
30
25
20
15
10
0.2
0.4
0.6
0.8
1
1.2
1.4
1.6
m

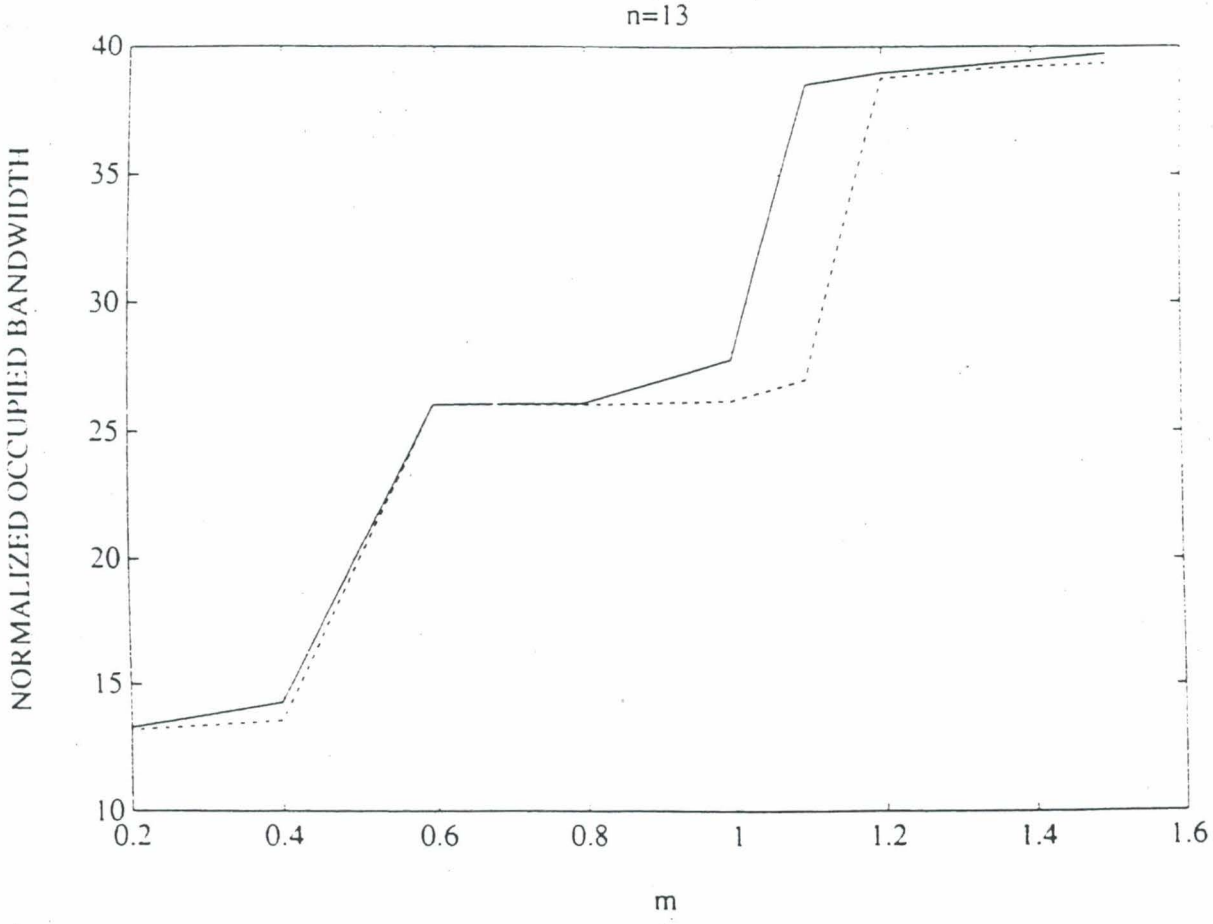
n=13
NORMALIZED OCCUPIED BANDWIDTH
40
35
30
25
20
15
10
0.2
0.4
0.6
0.8
1
1.2
1.4
1.6
m

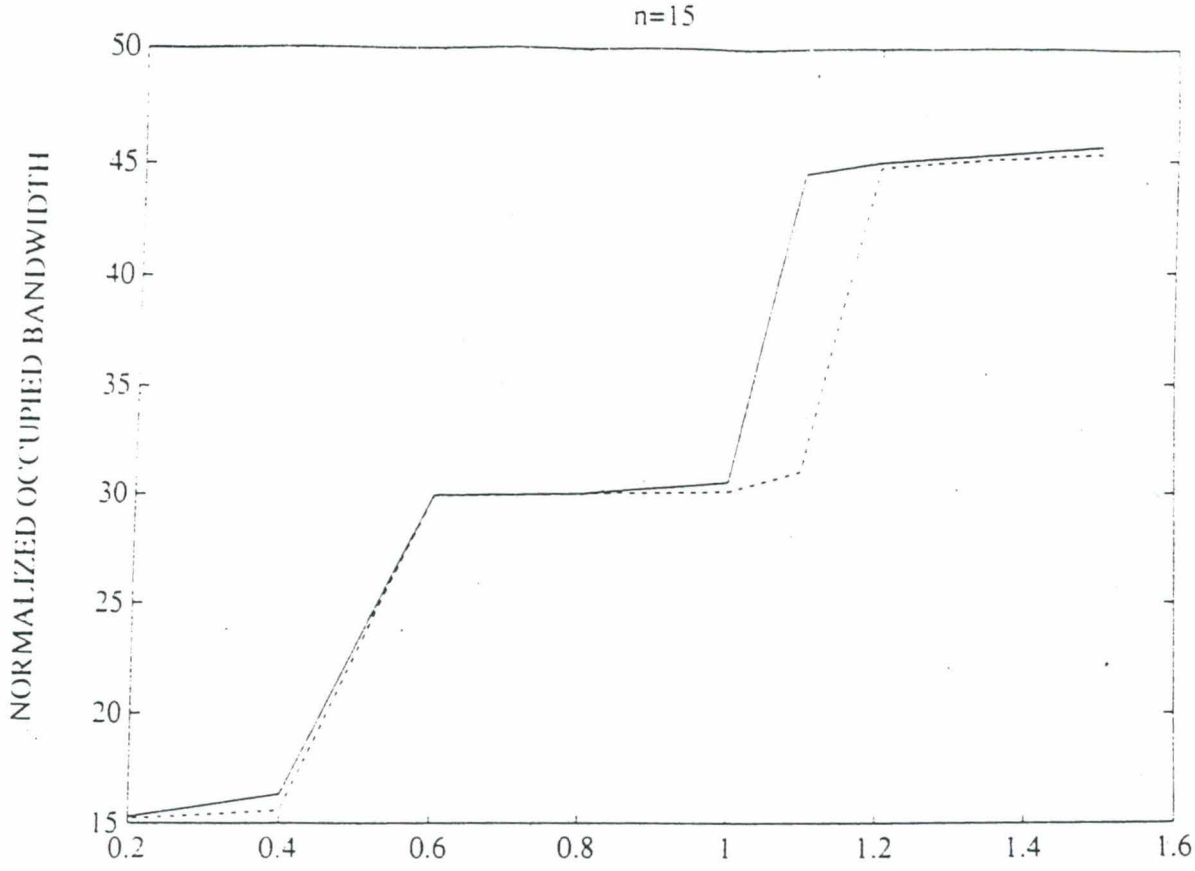
n=15
NORMALIZED OCCUPIED BANDWIDTH
50
45
40
35
30
25
20
15
0.2
0.4
0.6
0.8
1
1.2
1.4
1.6
m

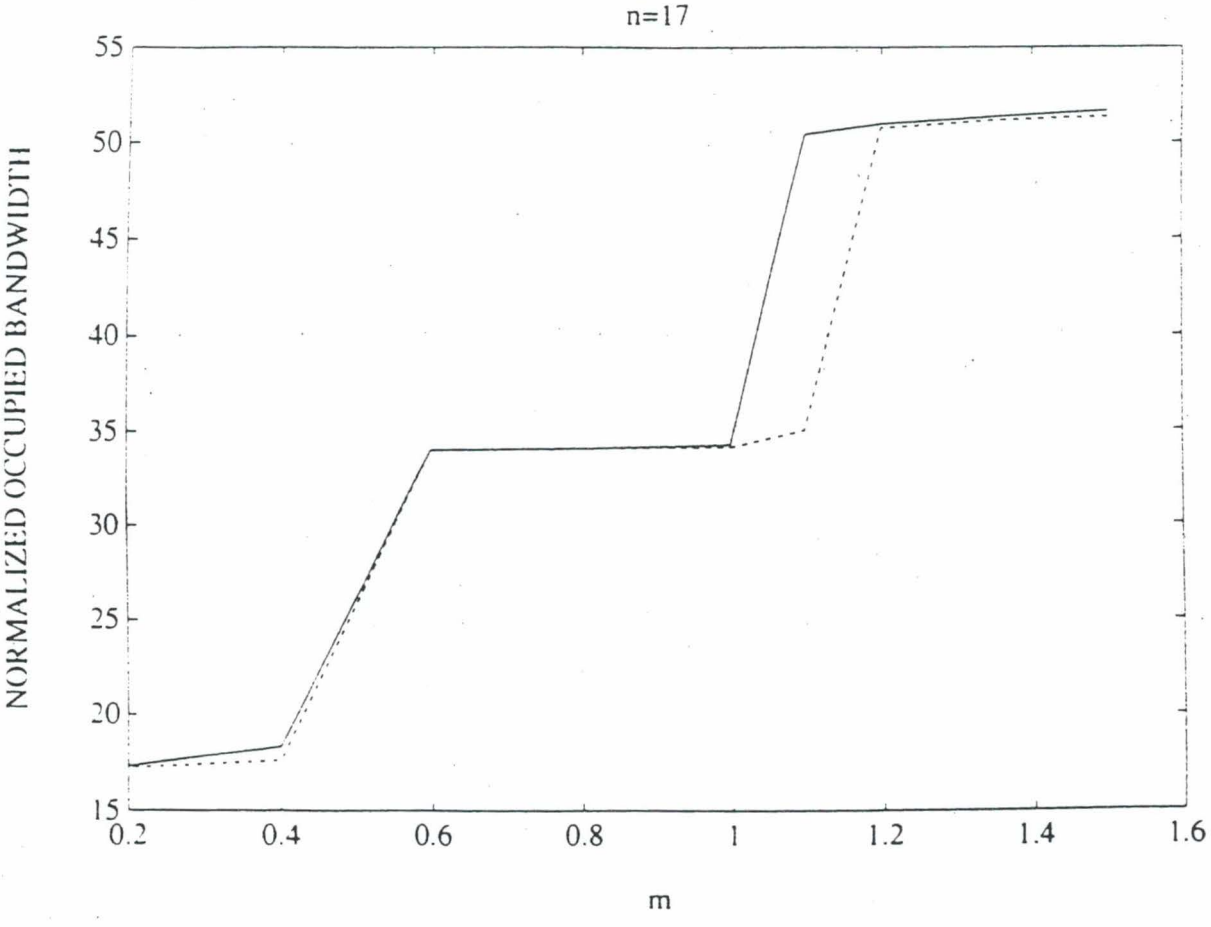
n=17
NORMALIZED OCCUPIED BANDWIDTH
55
50
45
40
35
30
25
20
15
0.2
0.4
0.6
0.8
1
1.2
1.4
1.6
m

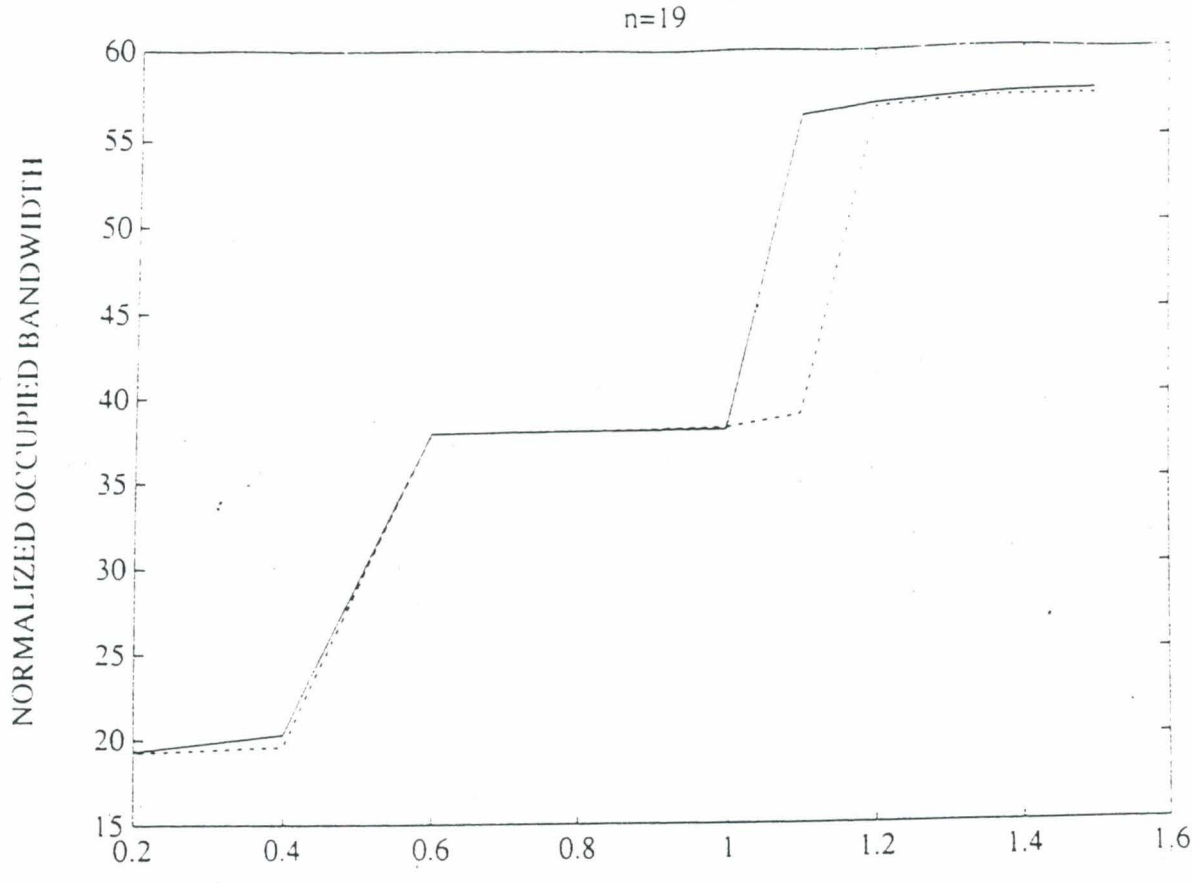
n=19
NORMALIZED OCCUPIED BANDWIDTH
60
55
50
45
40
35
30
25
20
15
0.2
0.4
0.6
0.8
1
1.2
1.4
1.6
m

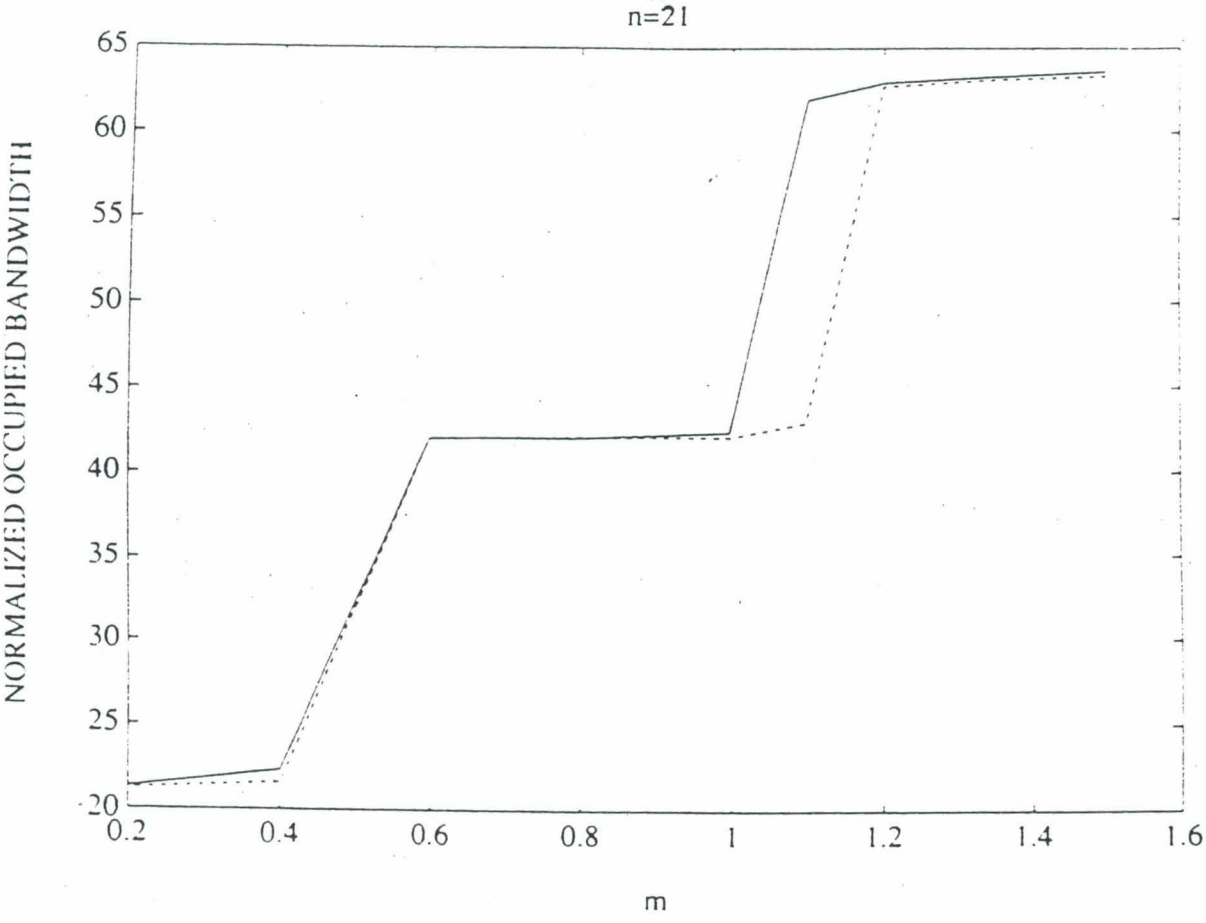
n=21
NORMALIZED OCCUPIED BANDWIDTH
65
60
55
50
45
40
35
30
25
20
0.2
0.4
0.6
0.8
1
1.2
1.4
1.6
m

3) The error induced by using the formulas for the occupied bandwidth obtained with the linear curve fitting technique instead of the values computed by simulation can be calculated as:

$$\varepsilon(\%) = |(T-P)/P| * 100$$

where P is the bandwidth computed by simulation and T the value using the formulas.

For each case, the error is given in % in next tables for the cases of filtering and no filtering.

With no filtering:

n	m= 0.2rd	m= 0.4rd	m= 0.6rd	m= 0.8rd	m= 1.rd	m= 1.1rd	m= 1.2rd	m= 1.35r	m= 1.5rd
3	0.62	2.86	0.03	16.87	16.9	2.74	15.82	12.86	6.17
5	0.13	0.16	0.03	2.73	1.84	0.86	5.03	1.84	4.51
7	0.19	0.38	0.03	4.93	5.34	0.69	3.35	3.36	11.70
9	0.02	0.70	0.04	2.98	6.22	0.40	2.10	2.22	4.92
11	0.05	0.42	0.04	1.82	1.10	0.13	1.24	1.33	4.87
13	0.10	0.43	0.005	0.82	0.68	0.04	0.61	0.68	2.86
15	0.01	0.05	0.01	0.23	2.79	0.09	0.14	0.19	1.37
17	0.03	0.04	0.01	0.22	1.92	0.23	0.21	0.19	0.11
19	0.01	0.08	0.02	0.69	0.26	0.18	0.49	0.49	0.86
21	0.02	0.25	0.02	0.90	1.35	0.23	0.71	0.70	1.64

With filtering:

n	m= 0.2rd	m= 0.4rd	m= 0.6rd	m= 0.8rd	m= 1.rd	m= 1.1rd	m= 1.2rd	m= 1.35rd	m= 1.5rd
3	0.07	0.12	0.31	0.07	5.08	0.01	0.76	0.27	0.36
5	0.04	0.08	0.14	0.30	1	0.03	0.06	0.005	0.04
7	0.01	0.13	0.18	0.07	1.62	0.11	0.26	0.09	0.11
9	0.03	0.12	0.09	0.06	0.85	0.09	0.17	0.07	0.08
11	0.07	0.02	0.07	2.E-4	0.23	0.14	0.11	0.06	0.07
13	0.09	0.01	0.02	0.19	0.18	0.02	0.02	0.09	0.01
15	0.02	0.15	0.12	2.E-4	0.11	0.17	0.003	0.002	0.01
17	0.001	0.06	0.02	1.E-4	0.08	0.02	0.01	0.002	0.01
19	0.02	0.02	0.01	0.05	0.06	0.04	0.01	0.001	0.007
21	0.04	0.01	0.01	0.05	0.07	0.02	0.02	0.01	0.006

Recommendations.

The improvement in spectral efficiency introduced by the effect of filtering is not very important.For this reason, the filters used don't have to be so critical concerning their characteristics.

As a final suggestion, the filters are likely to be implemented in the cases of lower values of the parameter n in particular, and for a modulation index between 1.1rd and 1.2rd in general.

1.2 Squarewave subcarrier.

The block diagram implemented here for computing the bandwidth of 99% power containment is the same as the one used for the case of sinewave subcarrier, but modulating with a squarewave subcarrier :

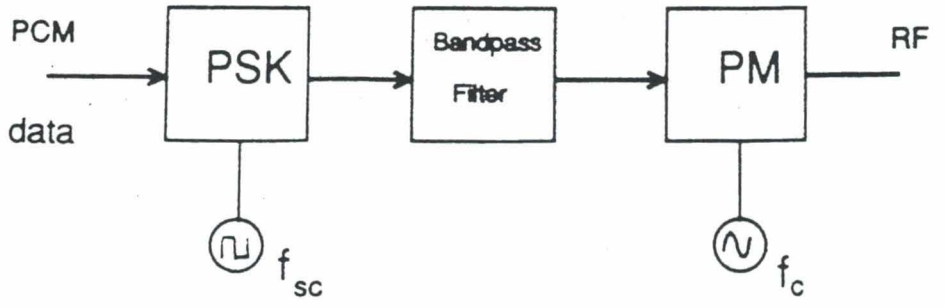

More precisely, the PSK block performed in the simulation is, in fact, an XOR gate.

Now, the power spectral density in RF is given by :

$$S(f) = A^2[\cos^2(m)\delta(f-f_c) + \frac{4}{\pi^2}\sin^2(m)\sum_{K\geq 1}\frac{S_d(f-f_c-(2K-1)f_{sc})+S_d(f-f_c+(2K-1)f_{sc})}{(2K-1)^2}]$$

This expression has also been extracted from the A-E-91-13 NASA work paper.The first term is the residual spectral component and the second is the data component. The data component consists of replicas of the power spectral density for an equiprobable NRZ binary data.

The plot given for the power spectral density is shown in next page for the case of $f_{sc}=9*R_s$, m=0.2rd and unfiltered signal.As in the case of sinewave subcarrier, the frequency axis is shifted to the carrier frequency and normalized to the symbol rate R_s.

It's easy to see that, if we use the parameter $n=f_{sc}/R_s$, i.e., the subcarrier frequency-to-bit-rate ratio, the replicas of the data component are situated exactly in the odd multiples of n.

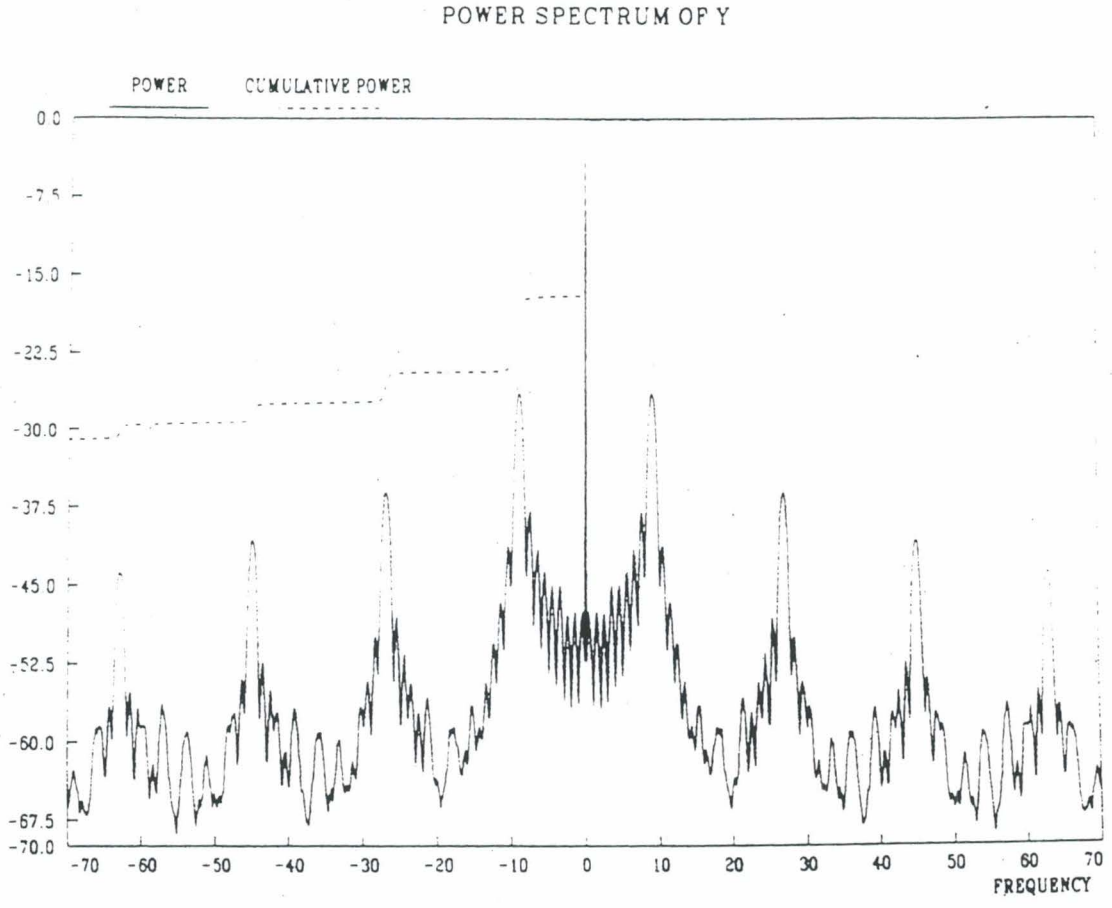
POWER SPECTRUM OF Y
POWER
CUMULATIVE POWER
0.0
-7.5
-15.0
-22.5
-30.0
-37.5
-45.0
-52.5
-60.0
-67.5
-70.0
-70 -60 -50 -40 -30 -20 -10 0 10 20 30 40 50 60 70
FREQUENCY

We are now going to evaluate the occupied bandwidth for the two cases taken into account : filtered and unfiltered signal.

a. With no filtering.

For different values of n and the modulation index m, the one-sided occupied bandwidth normalized to R_s for a 99% of power containment is given in the next table right below:

n	m= 0.2rd	m= 0.4rd	m= 0.6rd	m= 0.8rd	m= 1.0rd	m= 1.1rd	m= 1.2rd	m= 1.35r	m= 1.5rd
3	3.456	15.89	38.96	63.24	87.2	112.5	118.6	121.8	124.0
5	5.553	25.95	64.95	105.1	143.9	175.1	187.5	196.4	226.6
7	7.598	37.27	90.87	147.1	204.7	240.9	260.6	285.6	316.8
9	9.597	45.83	116.8	188.6	262.3	298.1	327.9	356.8	369.6
11	11.67	55.74	142.7	230.4	306.7	363.0	385.9	444.1	453.2
13	13.69	65.67	168.6	272.4	367.3	425.6	455.9	508.5	554.6
15	15.72	75.65	194.4	314.3	433.6	466.4	516.9	584.5	615.5
17	17.68	85.34	220.4	356.2	472.7	528.0	562.2	629.9	665.0
19	19.70	95.31	246.3	398.2	525.1	588.4	627.7	703.8	766.7
21	21.72	105.3	272.2	441.3	583.3	624.3	692.6	776.7	818.3

These results are quite similar to those given in the A-E-91-13 NASA work paper.And the approximate formulas for the occupied bandwidth using the linear curve fitting technique are found to be :

m=0.2rd , $BW = (1.013*n + 0.4862)R_s$

m=0.4rd , $BW = (4.938*n + 1.54)R_s$

m=0.6rd , BW = (12.95*n + 0.1829)R_s

m=0.8rd , BW = (20.97*n + 9.5249E-02)R_s

m=1.0rd , BW = (27.42*n + 9.691)R_s

m=1.1rd , BW = (28.8*n + 36.7)R_s

m=1.2rd , BW = (31.49*n + 35.69)R_s

m=1.35rd , BW = (36.1*n + 27.59)R_s

m=1.5rd , BW = (38.21*n + 32.52)R_s

b. With filtering.

The filter implemented for filtering the signal is a 1st order Butterworth filter with a 3 dB bandwidth of 2*R_s and centered on the subcarrier frequency.The resulting spectrum is plotted immediately below for the case of n=9 and m=0.2rd :

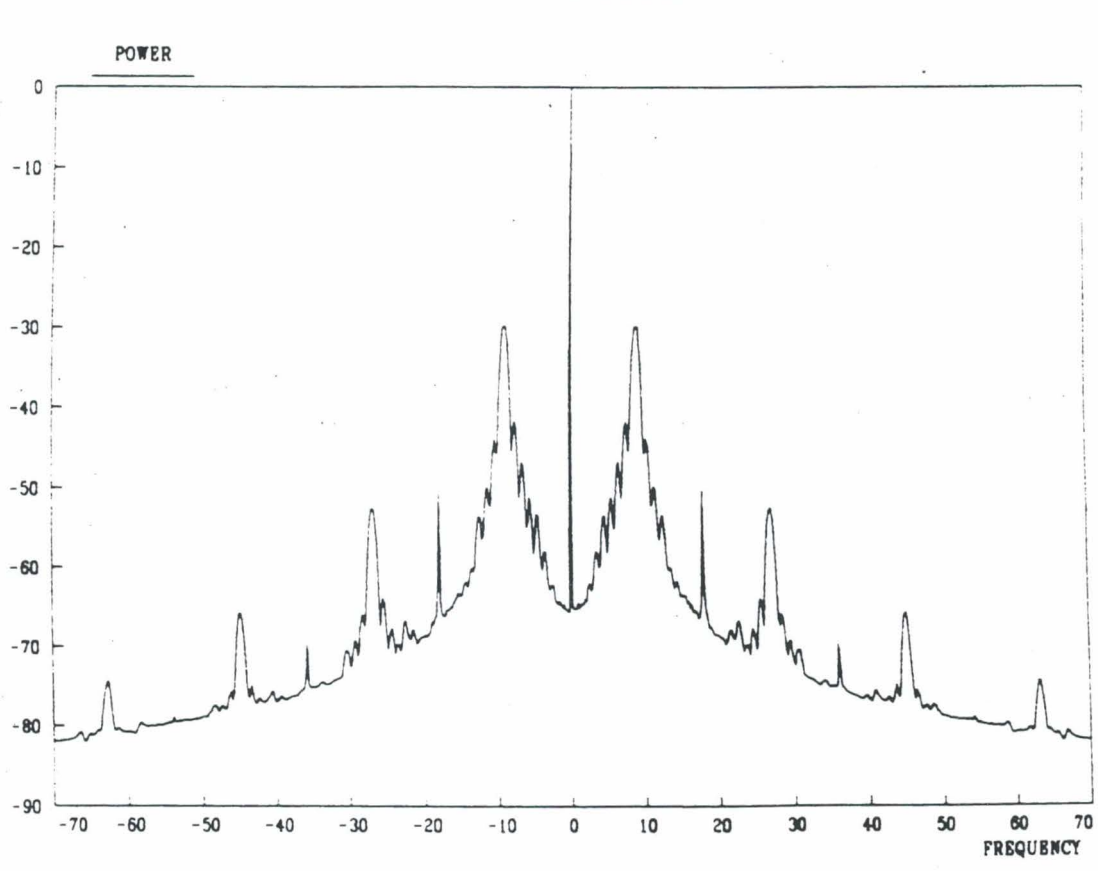

There is something new remarkable and it's that because of the effect of filtering, there are spikes that appear in the even multiples of n.For instance, in the previous plot we are in the case of n=9, and we can observe that the location of the spikes are situated on the normalized frequency axis in values of ±18, ±36, ..., i. e., ±2*n, ±4*n, and so on.As long as the modulation index is increasing, the spikes are increasing in power so that the one located in 2*n becomes the boundary of the occupied bandwidth for a 99% power containment when a large modulation index is required.

This suggestion can be easily found in the next table given of the occupied bandwidth for the 99% power containment :

n	m= 0.2rd	m= 0.4rd	m= 0.6rd	m= 0.8rd	m= 1.0rd	m= 1.1rd	m= 1.2rd	m= 1.35r	m= 1.5rd
3	2.911	3.351	3.599	6.018	6.042	6.047	6.051	6.054	7.423
5	4.778	5.336	5.576	6.681	10.03	10.04	10.05	10.06	10.06
7	6.688	7.343	7.575	8.372	14.02	14.03	14.04	14.05	14.06
9	8.549	9.33	9.56	10.16	18.02	18.05	18.07	18.09	18.1
11	10.70	11.38	11.62	12.56	21.99	22.02	22.05	22.07	22.12
13	12.25	13.33	13.57	14.04	25.60	26.01	26.03	26.05	26.06
15	14.46	15.33	15.59	16.29	29.92	30.01	30.03	30.05	30.06
17	16.32	17.33	17.59	18.17	32.25	33.98	34.06	34.12	34.15
19	18.47	19.36	19.65	20.42	37.74	37.97	38.03	38.08	38.12
21	20.39	21.33	21.59	22.05	41.36	41.99	42.03	42.07	42.09

And the approximate formulas are found to be :

m=0.2rd , BW = (0.9716*n - 0.1056)R_s

m=0.4rd , BW = (0.9997*n + 0.3461)R_s

m=0.6rd , BW = (1.001*n + 0.5744)R_s

m=0.8rd , BW = (0.9374*n + 2.229)R_s

m=1.0rd , BW = (1.946*n + 0.3476)R_s

m=1.1rd , BW = (1.996*n + 6.7869E-02)R_s

m=1.2rd , BW = (1.999*n + 5.8455E-02)R_s

m=1.35rd, BW = (2.001*n + 5.1921E-02)R_s

m=1.5rd , BW = (1.955*n + 0.8191)R_s

Conclusions.

1) For the different values of n, plots comparing the occupied bandwidth for either filtering and no filtering cases are shown in the next 5 pages.We can observe a spectacular decrease of the bandwidth when we filter the signal.

So far, The improvement in spectral efficiency due to the effect of filtering seems to be a good performance for a class of PCM/PSK/PM signal with square-wave subcarrier, but we don't know yet how can be affected the receiving signal. This will be discussed later on this document when the BER is going to be evaluated.

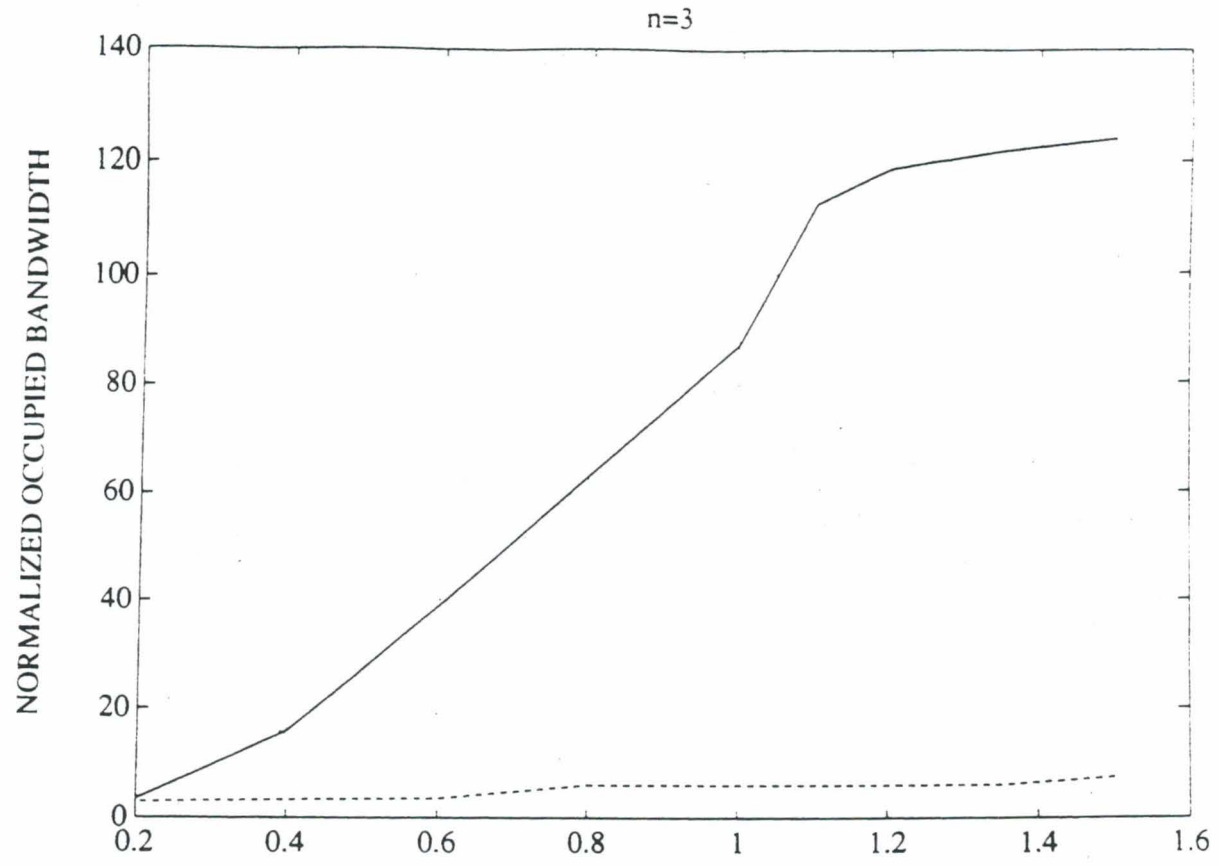
n=3
NORMALIZED OCCUPIED BANDWIDTH
140
120
100
80
60
40
20
0
0.2
0.4
0.6
0.8
1
1.2
1.4
1.6
m

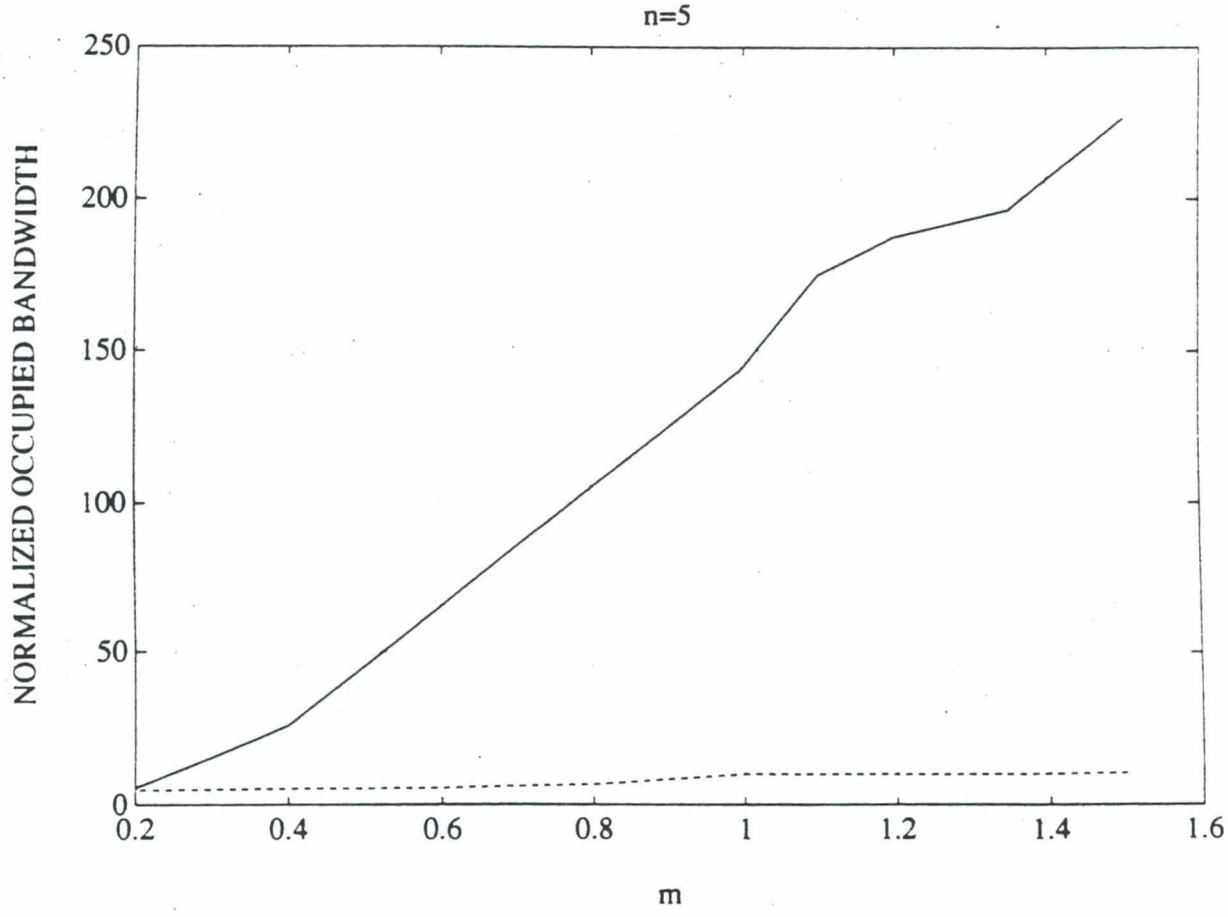
n=5
NORMALIZED OCCUPIED BANDWIDTH
250
200
150
100
50
0
0.2
0.4
0.6
0.8
1
1.2
1.4
1.6
m

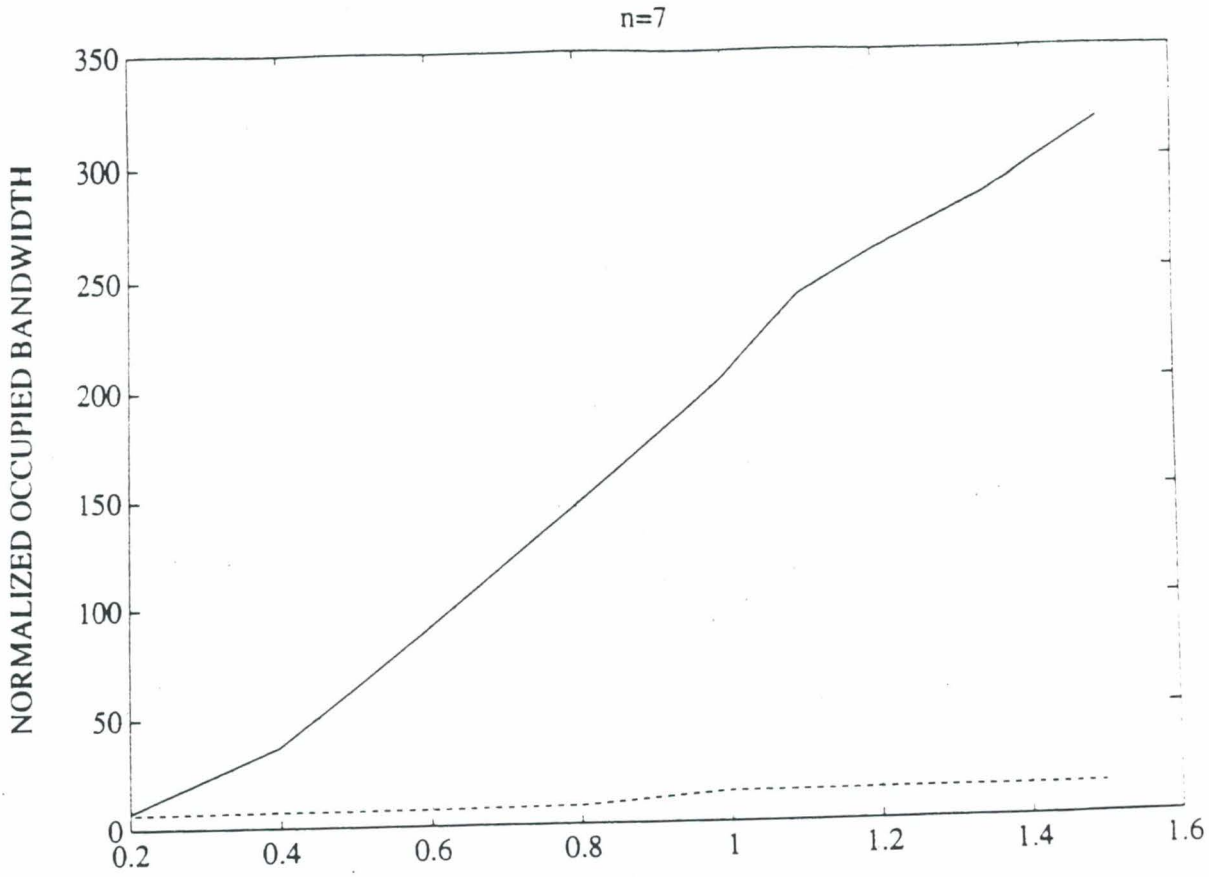
n=7
NORMALIZED OCCUPIED BANDWIDTH
350
300
250
200
150
100
50
0
0.2
0.4
0.6
0.8
1
1.2
1.4
1.6
m

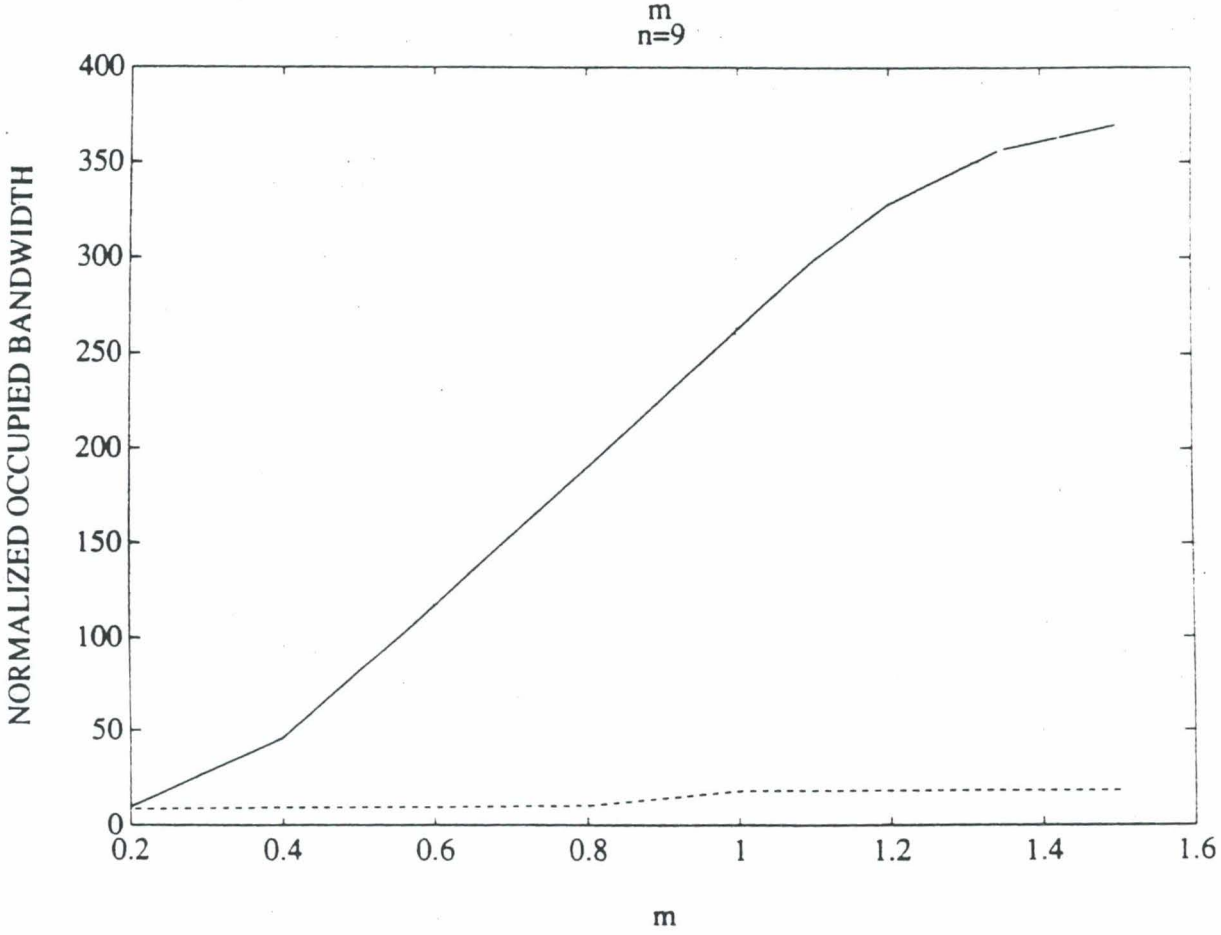
n=9
NORMALIZED OCCUPIED BANDWIDTH
400
350
300
250
200
150
100
50
0
0.2
0.4
0.6
0.8
1
1.2
1.4
1.6
m

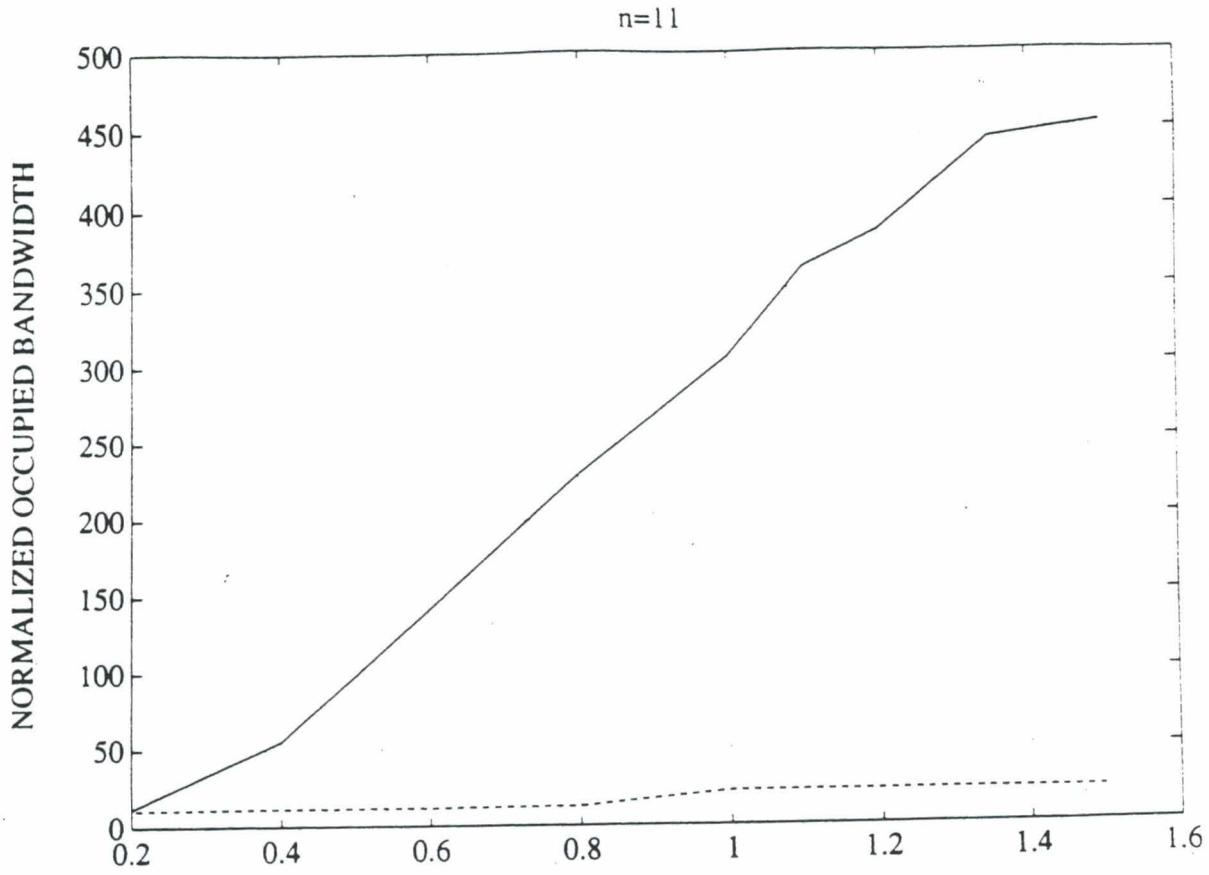
n=11
NORMALIZED OCCUPIED BANDWIDTH
500
450
400
350
300
250
200
150
100
50
0
0.2
0.4
0.6
0.8
1
1.2
1.4
1.6
m

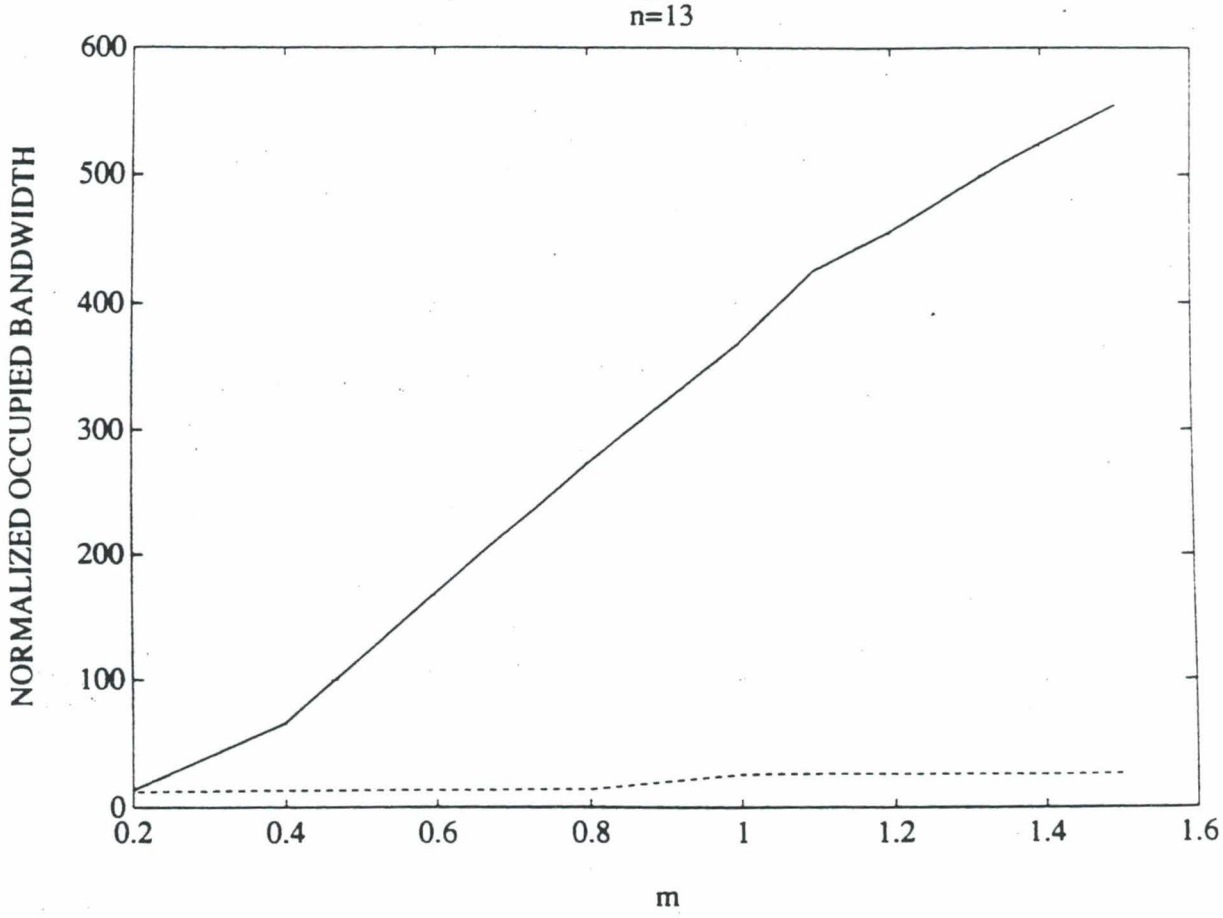
n=13
NORMALIZED OCCUPIED BANDWIDTH
600
500
400
300
200
100
0
0.2
0.4
0.6
0.8
1
1.2
1.4
1.6
m

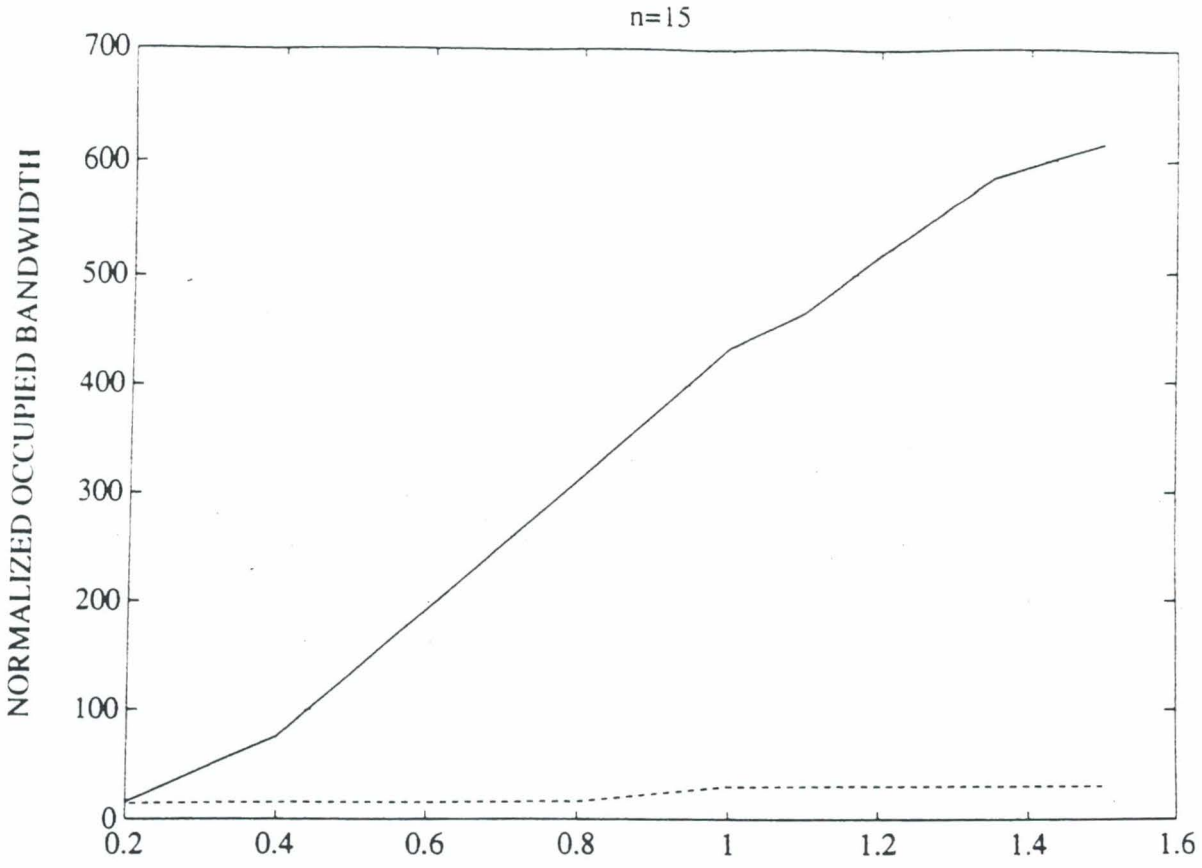
n=15
NORMALIZED OCCUPIED BANDWIDTH
700
600
500
400
300
200
100
0
0.2
0.4
0.6
0.8
1
1.2
1.4
1.6
m

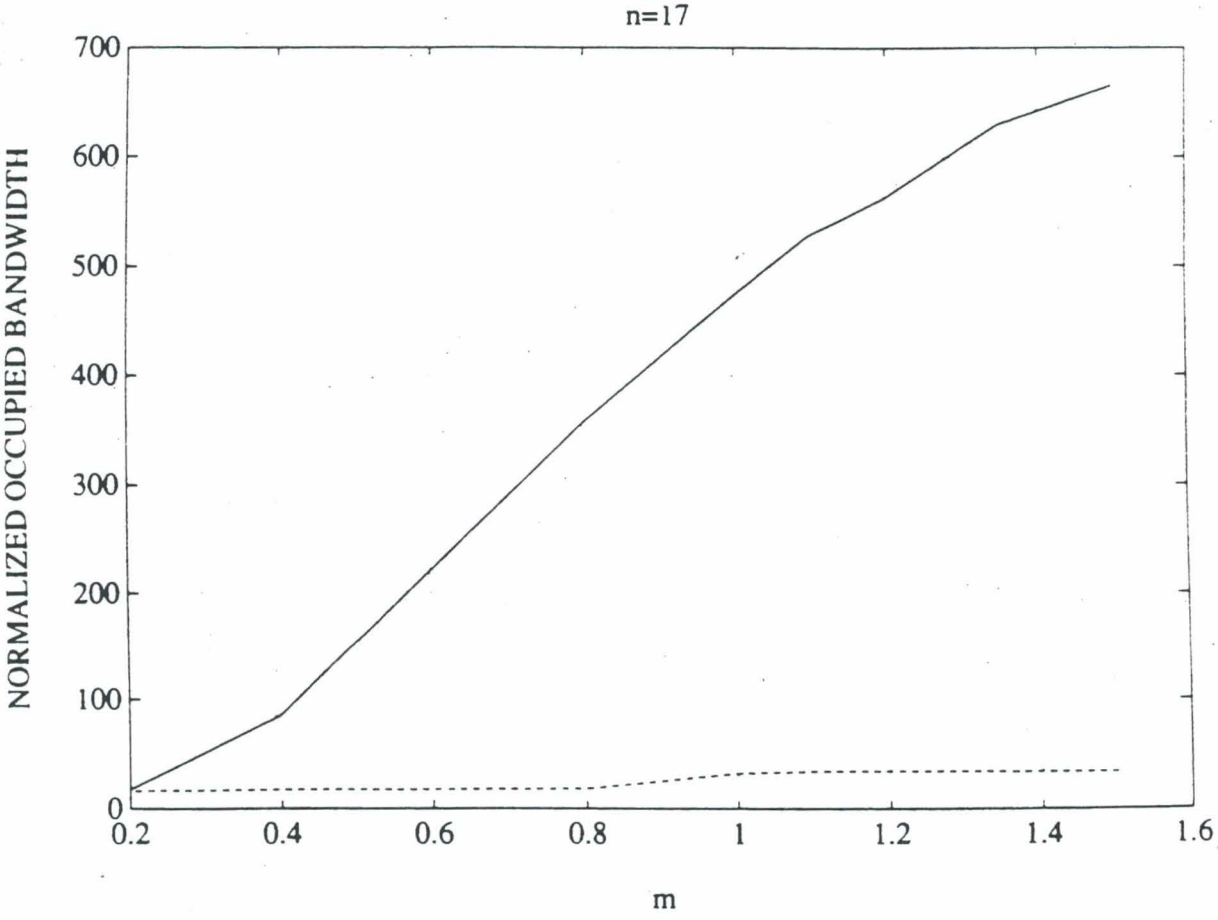
n=17
NORMALIZED OCCUPIED BANDWIDTH
700
600
500
400
300
200
100
0
0.2
0.4
0.6
0.8
1
1.2
1.4
1.6
m

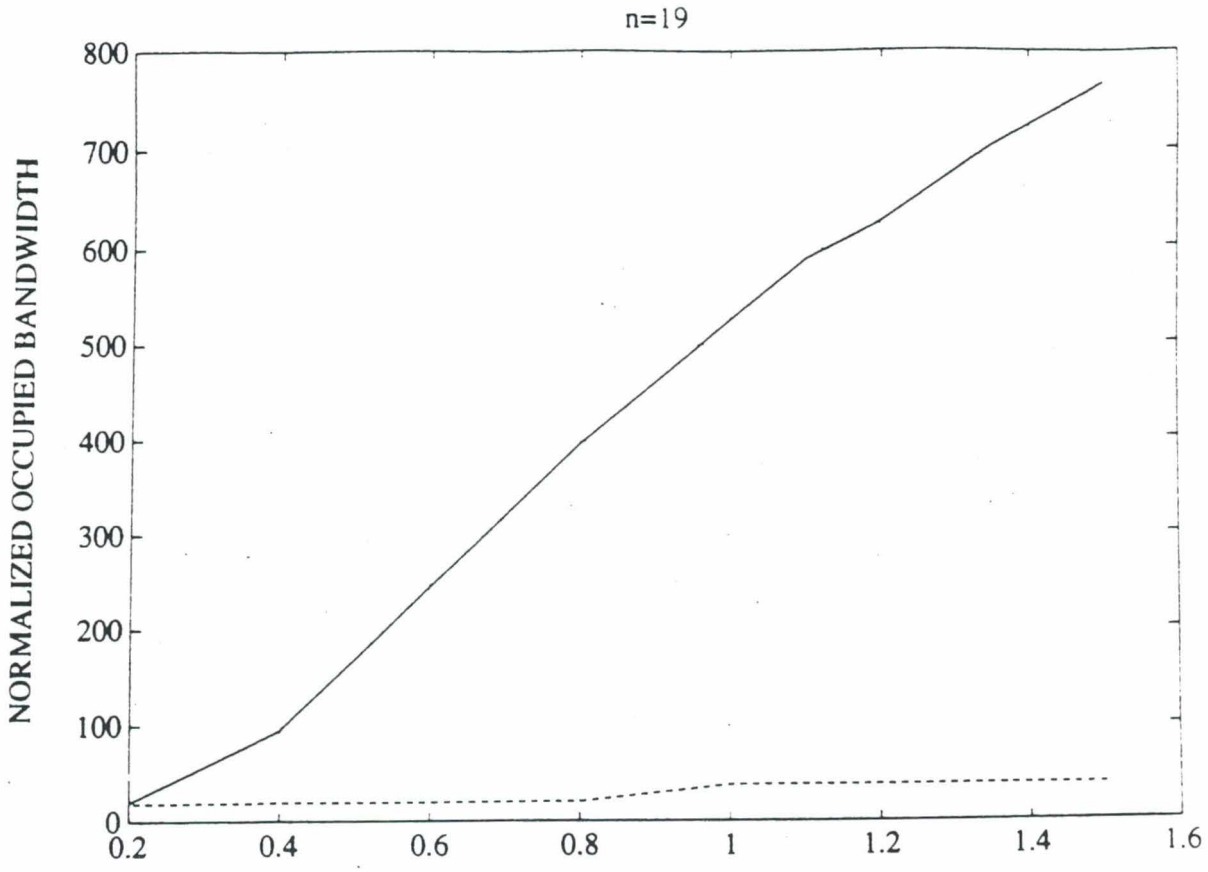
n=19
NORMALIZED OCCUPIED BANDWIDTH
800
700
600
500
400
300
200
100
0
0.2
0.4
0.6
0.8
1
1.2
1.4
1.6
m

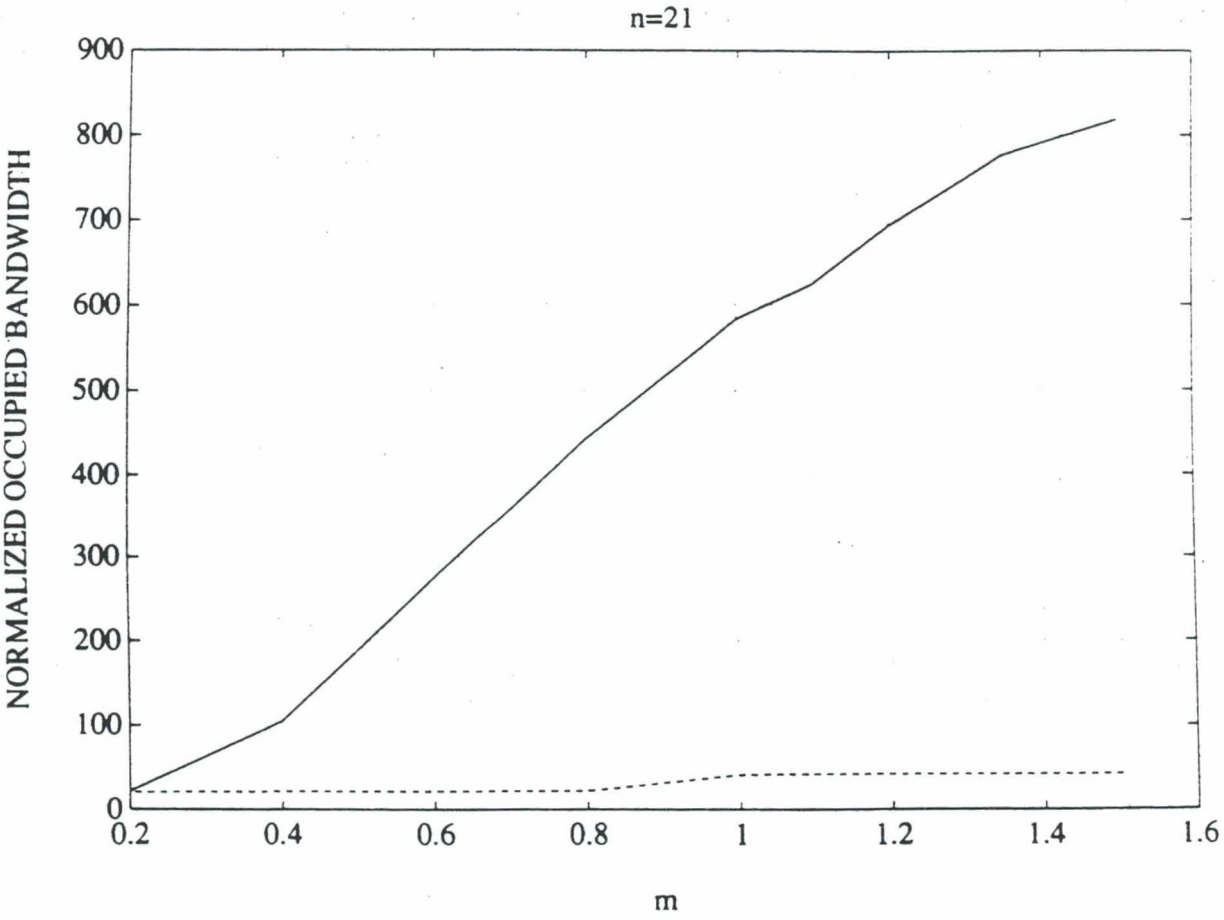
n=21
NORMALIZED OCCUPIED BANDWIDTH
900
800
700
600
500
400
300
200
100
0
0.2
0.4
0.6
0.8
1
1.2
1.4
1.6
m

2) In the same way as in the case of sinewave subcarrier we can evaluate the same error induced when we use the approximate formulas for computing the occupied bandwidth instead of the values computed by simulation.

Proceeding by this way, the error given in % is calculated in the next two tables for unfiltered and filtered signal respectively.

No filtering :

n	m= 0.2rd	m= 0.4rd	m= 0.6rd	m= 0.8rd	m= 1.rd	m= 1.1rd	m= 1.2rd	m= 1.35rd	m= 1.5rd
3	2	2.88	0.17	0.38	5.44	9.37	9.72	11.54	18.66
5	0.04	1.06	0.03	0.17	1.96	3.2	3.01	5.95	1.35
7	0.27	3.13	0.04	0.142	1.5	1.09	1.72	1.88	5.32
9	0.06	0.32	0.08	0.12	2.22	0.72	2.67	1.22	1.85
11	0.4	0.21	0.04	0.14	1.51	2.62	1.01	4.37	0.07
13	0.26	0.08	0.02	0.11	0.31	3.41	2.38	2.31	4.57
15	0.27	0.05	0.01	0.09	2.9	0.49	1.72	2.63	1.59
17	0.1	0.17	0.02	0.1	0.66	0.32	1.56	1.81	2.57
19	0.15	0.05	0.01	0.08	1.05	0.76	0.99	1.37	1.07
21	0.2	0.02	0.02	0.19	0.38	2.75	0.63	1.16	2.03

Filtering :

n	m= 0.2rd	m= 0.4rd	m= 0.6rd	m= 0.8rd	m= 1.rd	m= 1.1rd	m= 1.2rd	m= 1.35rd	m= 1.5rd
3	3.51	0.17	0.6	16.23	2.37	0.14	0.08	0.01	9.95
5	0.54	0.16	0.07	3.52	0.44	0.05	0.05	0.03	0.16
7	0.11	0.01	0.09	4.99	0.38	0.03	0.05	0.05	3.18
9	1.04	0.14	0.24	4.92	0.92	0.12	0.12	0.14	1.76
11	1.1	0.33	0.33	0.16	1.11	0.02	0.01	0.04	0.92
13	2.23	0.11	0.09	2.66	0.16	0.03	0.05	0.04	0.64
15	0.03	0.07	0.04	0.05	1.29	0.01	0.04	0.05	0.26
17	0.53	0.04	0.03	0.03	3.67	0.04	0.06	0.14	0.28
19	0.63	0.09	0.27	1.88	1.1	0.04	0.03	0.01	0.4
21	0.44	0.03	0.04	0.6	0.34	0.01	0.02	0.02	0.5

2.OCCUPIED BANDWIDTH FOR PCM-SPL/PM SIGNALS

The modulating process is now carried away by the following block diagram :

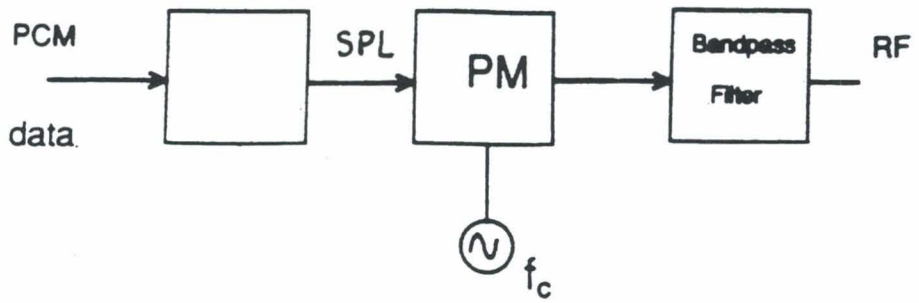

The expression of the space telemetry signal for direct phase modulation of the carrier by the data is well known, but now, when the modulating signal is an baseband biphase encoded data sequence, the power spectral density of this signal is found to be :

$$S(f) = A^2\{\cos^2(m)\delta(f-f_c) + \frac{1}{R_s}\sin^2(m)\frac{\sin^4[\pi(f-f_c)/2R_s]}{[\pi(f-f_c)/2R_s]^2}\}$$

The first term corresponds to the residual carrier and the second to the data component, with m being the modulation index of phase modulation and R_s the bit rate of PCM data, i. e., half bit rate of biphase encoded sequence.

A plot of the spectrum of this kind of signal is given in next page for the case of m=1.0rd and no filtering.The frequency axis is shifted to the carrier frequency f_c and normalized to R_s.

Due to the nature of biphase encoded data sequence, the mean value of the modulating signal is zero so that in radio-frequency the residual carrier and the data component do not overlap in the power spectrum.

POWER SPECTRUM OF YRF

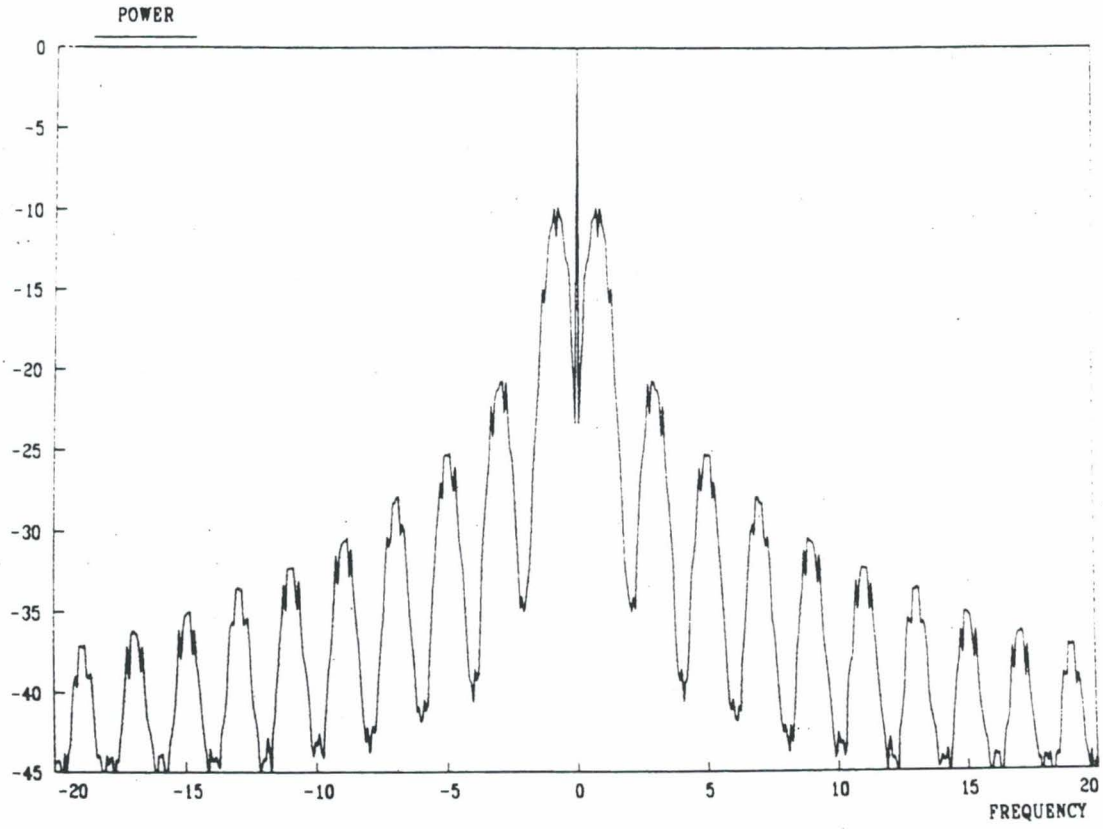

CCSDS recommendations for direct phase modulation do not differ with category A and category B missions.Therefore, the following computations of the occupied bandwidth is applicable to all categories of spacecraft transmitters.

In the other hand, an CCSDS recommendation states that the carrier suppression should not exceed 15 dB.Consequently and by this way, since

$$0.0316227 \leq \cos^2(m) < 1$$

we obtain that

$$0 < m \leq 1.392\text{rd}$$

In practice, m is supposed to be as close as possible to 1.392 in order to concentrate as much power as possible to data component.

The baseband filter implemented is a Butterworth 1st order filter and we will consider three values of the 3 dB cutoff frequency f_{cut} to compute the occupied bandwidth of 99% power containment : $\pm 4R_s$, $\pm 8R_s$ and $\pm 12R_s$.

Thus, for different values of the modulation index m we can fill the table in next page giving the occupied bandwidth normalized to R_s.

It is easy to find out that the effect of filtering is a good performance in reducing the occupied bandwidth defined in terms of the ITU regulations, but a problem could appear, and it is that the bandpass filter is surely difficult to implement because the band is very narrow as compared with the carrier frequency.

That is why it could be a better way to filter in baseband the biphase encoded data sequence in order to perform in radio-frequency afterwards the phase modulation.

In this case, i. e., proceeding to filter before the phase modulation, it is possible to expect the appearance of new spikes in the radio-frequency spectrum due to the effect of filtering.

m	No Filtering	f_{cut} = ± $4R_s$	f_{cut} = ± $8R_s$	f_{cut} = ±$12R_s$
0.2rd	1.3007	1.1308	1.1588	1.1907
0.4rd	5.0550	2.5483	3.0497	3.2238
0.6rd	10.5946	3.2826	4.8441	5.2609
0.8rd	16.5970	4.6038	5.5440	7.1119
1.0rd	21.6450	5.1150	7.0240	8.7993
1.1rd	24.604	5.2500	7.2153	9.0627
1.2rd	26.5313	5.3776	7.3863	9.2510
1.25rd	27.1490	5.4297	7.4733	9.3362
1.35rd	28.7492	5.5455	7.7711	9.5245
1.5rd	29.4053	5.6647	8.4992	10.0558

And the approximate formulas are found to be:

No filtering , $BW = (-6.51*m^2 + 34.7841*m - 6.7081)R_s$

$f_{cut} = \pm 4R_s$, $BW = (-2.864*m^2 + 8.3055*m - 0.4095)R_s$

$f_{cut} = \pm 8R_s$, $BW = (-3.0675*m^2 + 10.5486*m - 0.7028)R_s$

$f_{cut} = \pm 12R_s$, $BW = (-4.7256*m^2 + 14.9178*m - 1.7863)R_s$

With R_s being the symbol rate of the binary data.

The error committed by using these formulas rather than the values obtained by simulation is given in % for each parameter considered in the next table.

m	No Filtering	f_{cut} = ± $4R_s$	f_{cut} = ± $8R_s$	f_{cut} = ±$12R_s$
0.2rd	100.913	0.5518	10.8233	15.3241
0.4rd	21.9338	3.6825	0.7824	6.2325
0.6rd	11.553	7.9254	6.6481	3.8447
0.8rd	2.1428	4.3846	4.1284	0.1639
1.0rd	0.3654	1.6227	3.498	4.4708
1.1rd	3.7667	0.2116	0.3647	1.7367
1.2rd	3.2902	1.0291	2.0581	0.6399
1.25rd	2.0218	1.2464	2.8994	1.5103
1.35rd	1.2635	0.6814	2.2673	2.266
1.5rd	4.813	1.0583	3.3059	0.9746

Curves Power vs. Bandwidth.

Finally, a families of curves giving the power containment versus the considered occupied bandwidth are shown in the next four pages for each case of filtering by taking the modulation index m as a parameter.

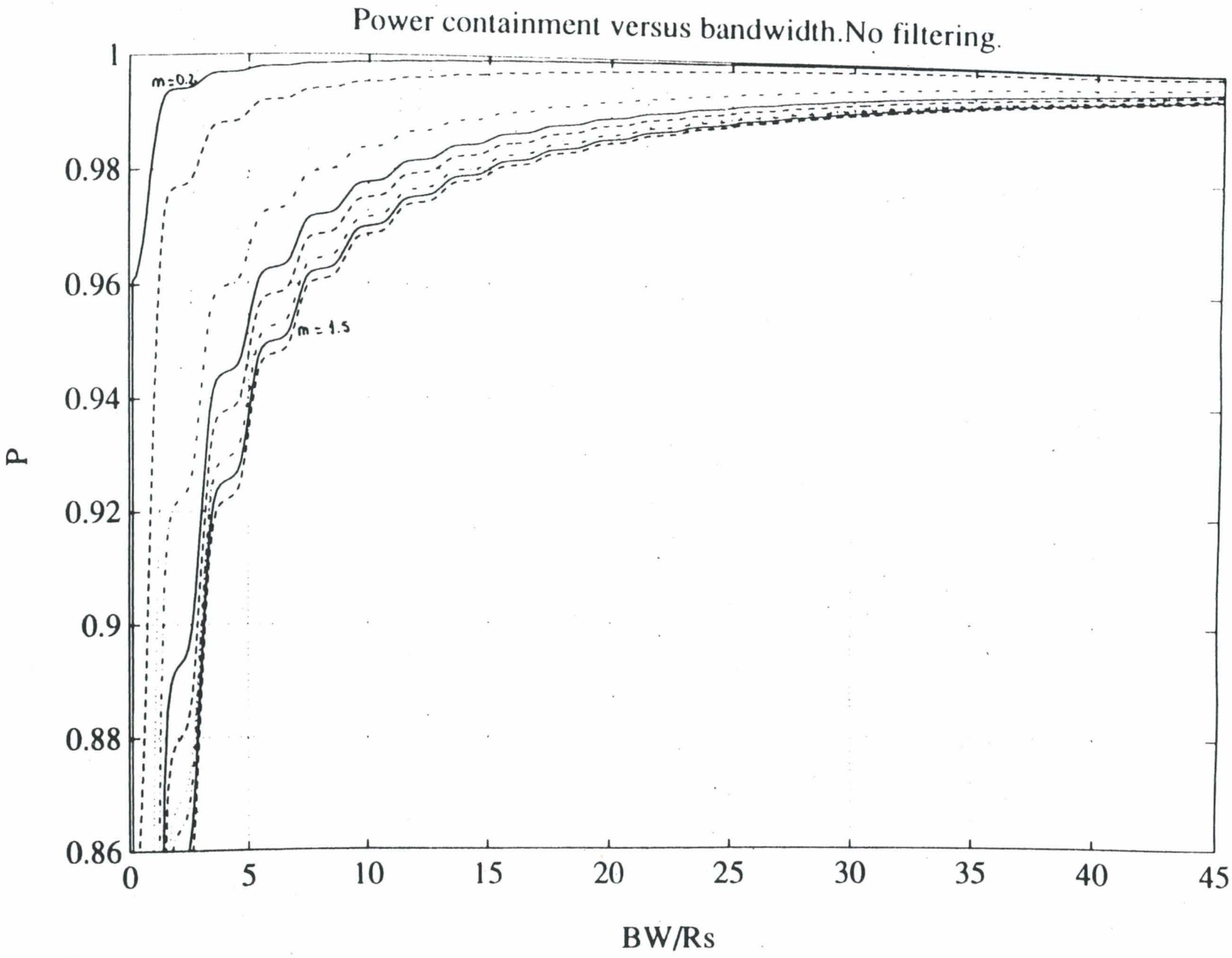
Power containment versus bandwidth.No filtering.
m=0.2
m=1.5
P
BW/Rs
1
0.98
0.96
0.94
0.92
0.9
0.88
0.86
0
5
10
15
20
25
30
35
40
45

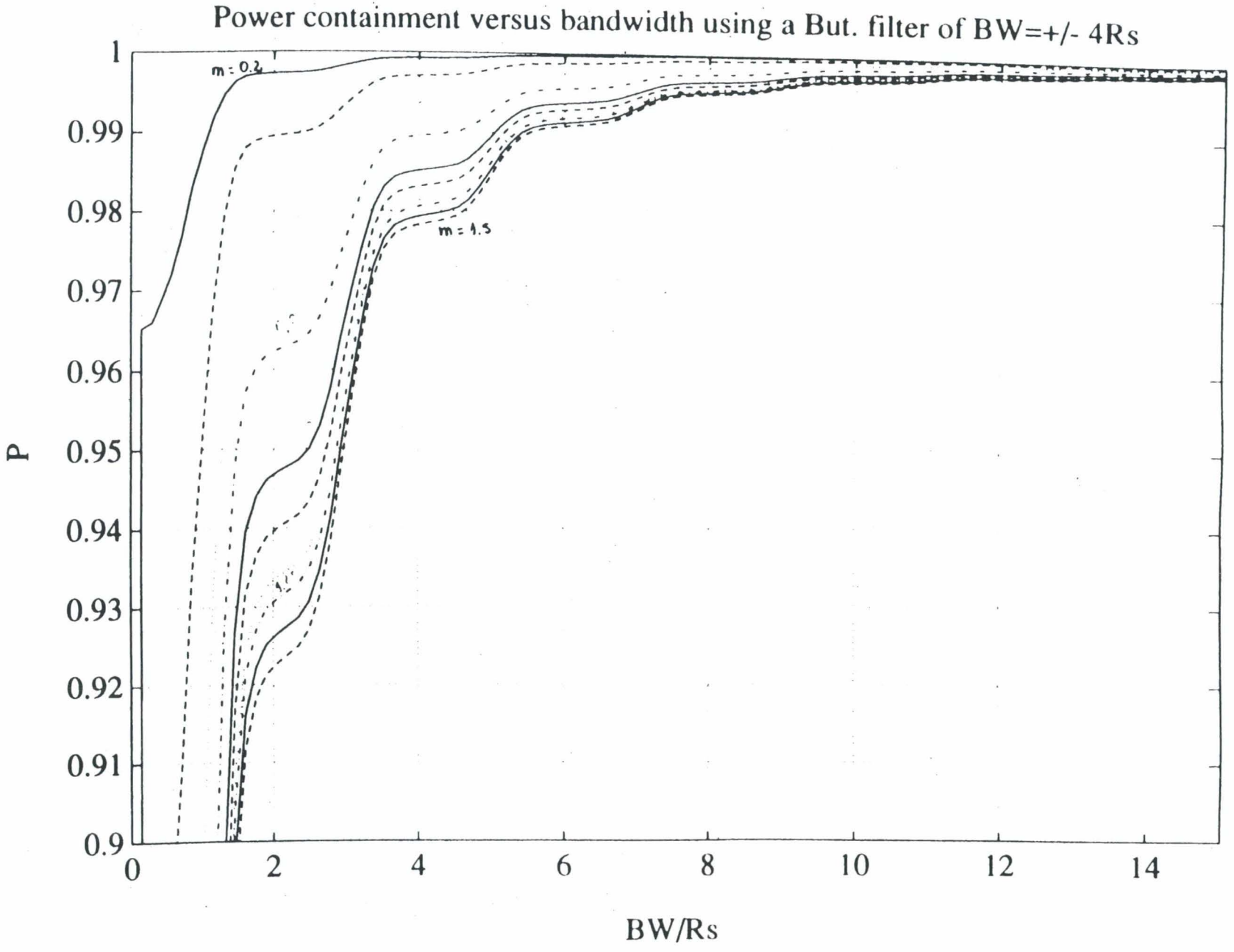
Power containment versus bandwidth using a But. filter of BW=+/- 4Rs
m = 0.2
m = 1.5
P
BW/Rs
1
0.99
0.98
0.97
0.96
0.95
0.94
0.93
0.92
0.91
0.9
0
2
4
6
8
10
12
14

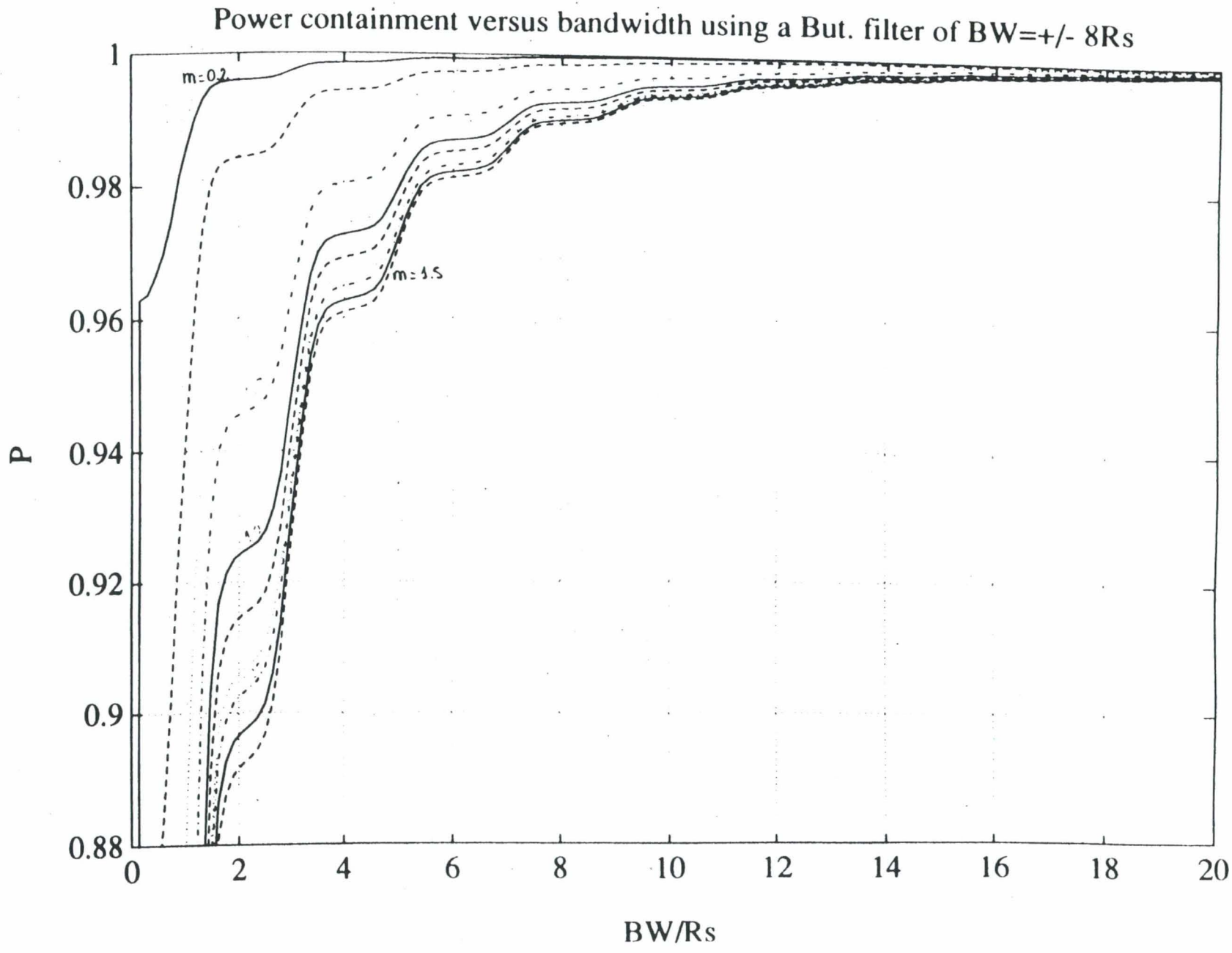
Power containment versus bandwidth using a But. filter of BW=+/- 8Rs
m=0.2
m=1.5
P
BW/Rs
1
0.98
0.96
0.94
0.92
0.9
0.88
0
2
4
6
8
10
12
14
16
18
20

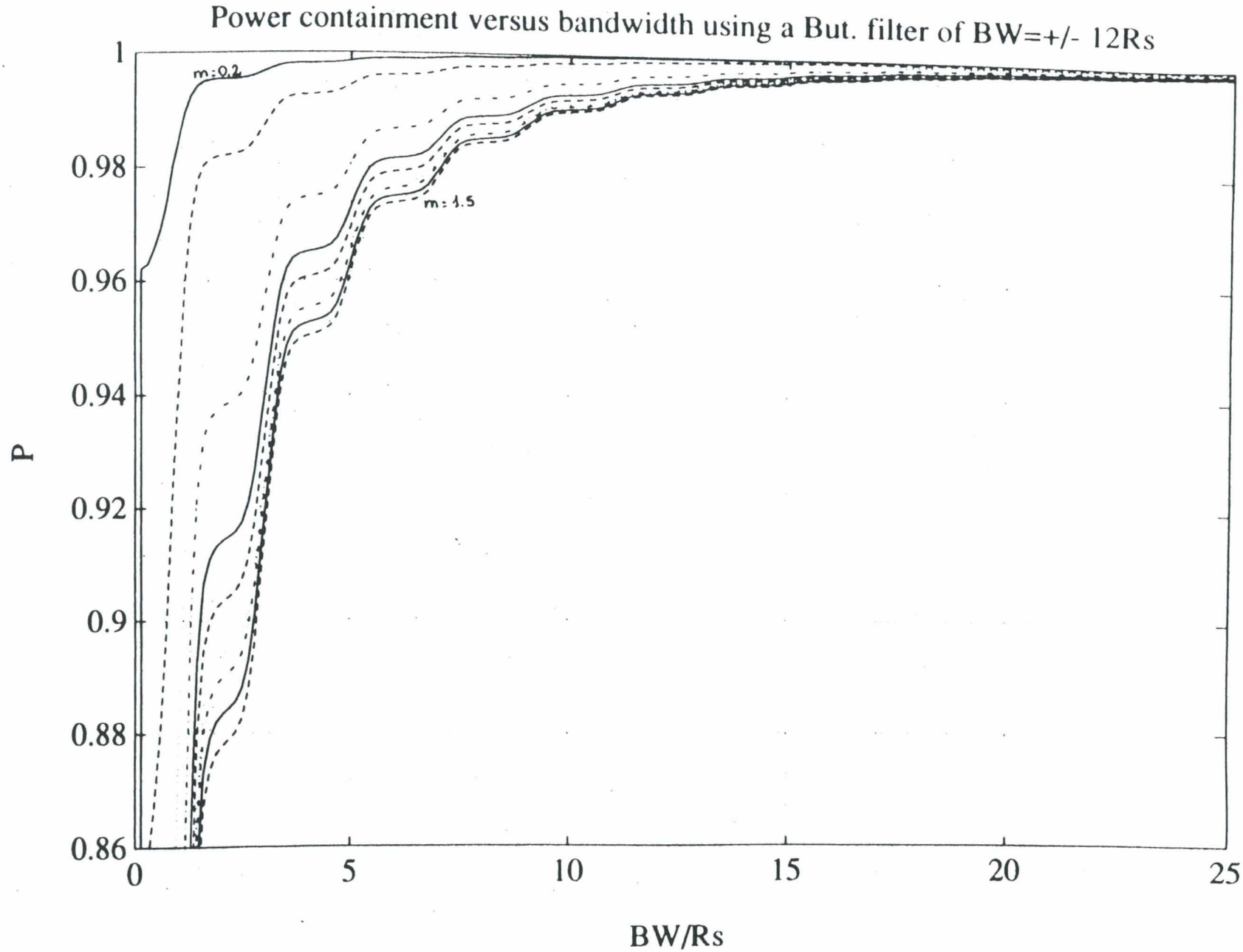
Power containment versus bandwidth using a But. filter of BW=+/- 12Rs
m:0.2
m:1.5
P
BW/Rs
1
0.98
0.96
0.94
0.92
0.9
0.88
0.86
0
5
10
15
20
25

3. BIT ERROR RATE FOR PCM/PSK/PM SIGNALS.

The process to evaluate the Bit Error Rate (BER) has been carried out by demodulating the receiving signal added with noise and comparing the demodulated sequence with the original sequence.

The demodulation has been simulated as shown in the next block diagram :

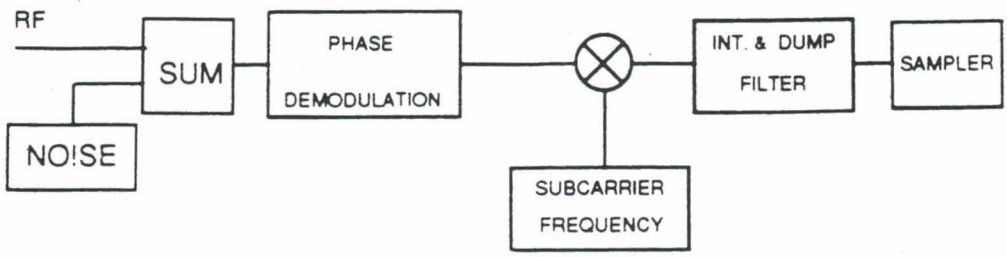

It was not possible to evaluate the BER by using a semianalytic technique because the noise at the output of the phase demodulator is not gaussian.

For each case taken into account, the BER has been calculated for 5 values of the energy-per-bit to noise power spectral density ratio (ETA, also called E_b/N_0), which are in dB : -2, 0, 2, 4, and 6.

Besides, the BER is independent on the value of the phase modulation used so that we can focus the study in a particular case.

3.1 Sinewave subcarrier.

The values selected here are n=9 and m=1.1rd. We choose this value of the modulation index because if we look backward on this document to section 1.1, we concluded that the effect of filtering is particularly efficient in terms of bandwidth occupancy for m =1.1rd.

The values obtained are written in next table for both cases of filtering and no filtering.

E_b/N_0 (dB)	BER (No Filtering)	BER (Filtering)
-2.0	$1.31*10^{-1}$	$1.51*10^{-1}$
0.0	$8.06*10^{-2}$	$9.83*10^{-2}$
2.0	$3.9*10^{-2}$	$5.28*10^{-2}$
4.0	$1.34*10^{-2}$	$2.03*10^{-2}$
6.0	$2.8*10^{-3}$	$5.4*10^{-3}$

and the plot is given in next page. The solid line is referred to the case of no filtering and the dashed one to the case of filtering.

The values for the case of unfiltered signal are more or less equal to the ones expected from the theoretical values.

The curve obtained with the signal filtered shows a degradation of about 0.7 dB due to filtering. For this reason it could be a better way to filter the transmitting signal with a wider filter to limit losses due to filtering for a few tenths of a dB. It could be enough a value of $4R_s$ rather than the value of $2R_s$ used in this document.Besides, proceeding by this way, the impact in bandwidth occupancy will surely not be very important.

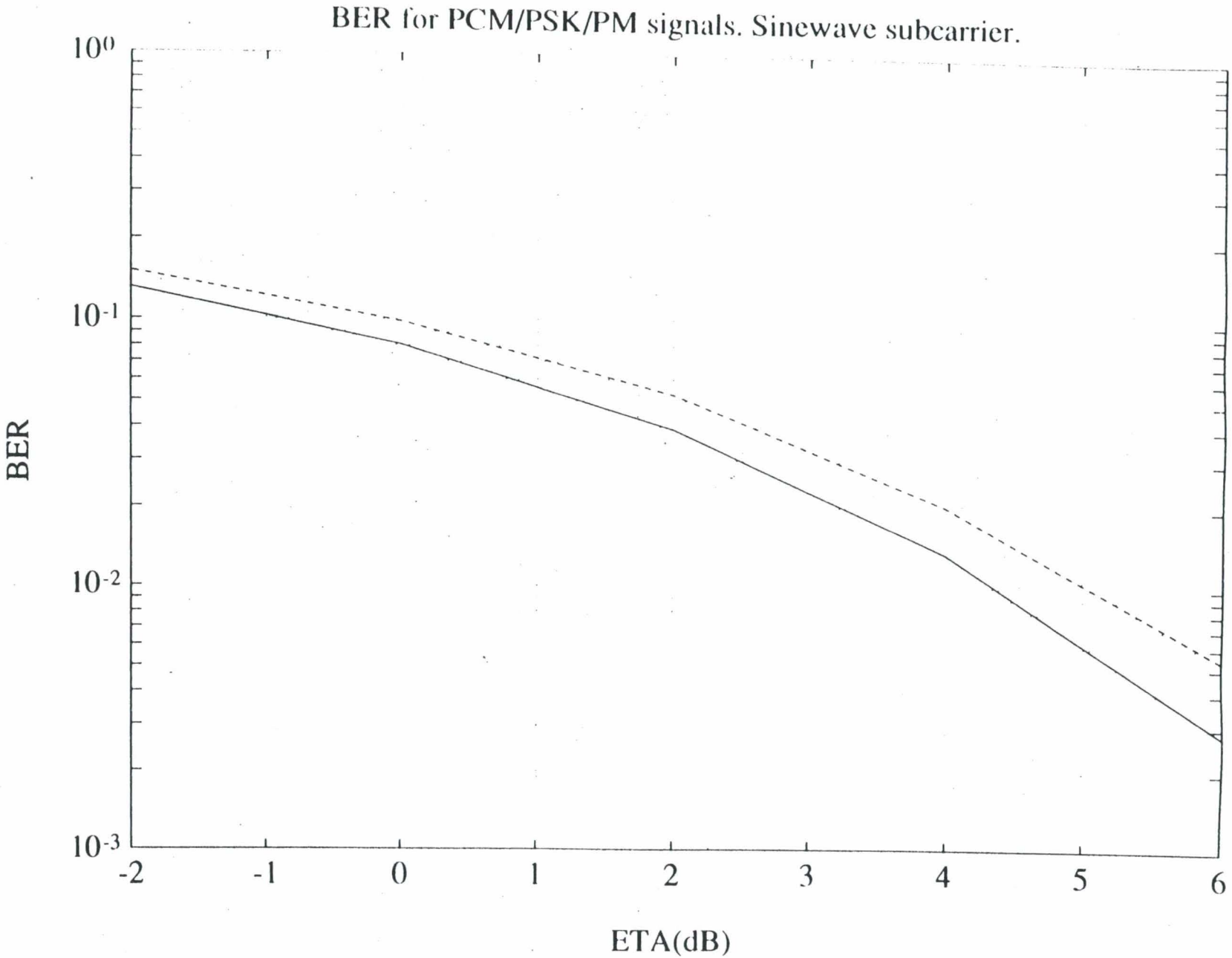
BER for PCM/PSK/PM signals. Sinewave subcarrier.
BER
10^{0}
10^{-1}
10^{-2}
10^{-3}
-2
-1
0
1
2
3
4
5
6
ETA(dB)

3.2 Squarewave subcarrier.

The BER has been calculated for n=3 and m=1.0rd, and the values are found to be :

E_b/N_0 (dB)	BER (No Filtering)	BER (Filtering)
-2.0	$1.40*10^{-1}$	$2.73*10^{-1}$
0.0	$8.80*10^{-2}$	$2.27*10^{-1}$
2.0	$4.30*10^{-2}$	$1.70*10^{-1}$
4.0	$1.60*10^{-2}$	$1.15*10^{-1}$
6.0	$3.51*10^{-3}$	$6.62*10^{-2}$

The values of BER for the case of no filtering are deviated by 0.3dB from the theoretical values of BER for PSK signals.This can be due to the large spectrum of these kind of signals and also because the value of n used is 3, which can be too much close to the carrier.

The plot is given in next page, with the solid line corresponding to the case of no filtering and the dashed one to the case of filtering.

We can remark that the curve of the BER for the case of filtering does not have the same shape as the curve for unfiltered signal.The values obtained lead us to confirm that the filter used is too narrow and severely degrades the link performances.

As we saw in section 1.2, the decrease in bandwidth occupancy by using the filter was very significant, but this has made the system useless because of the poor values of BER.

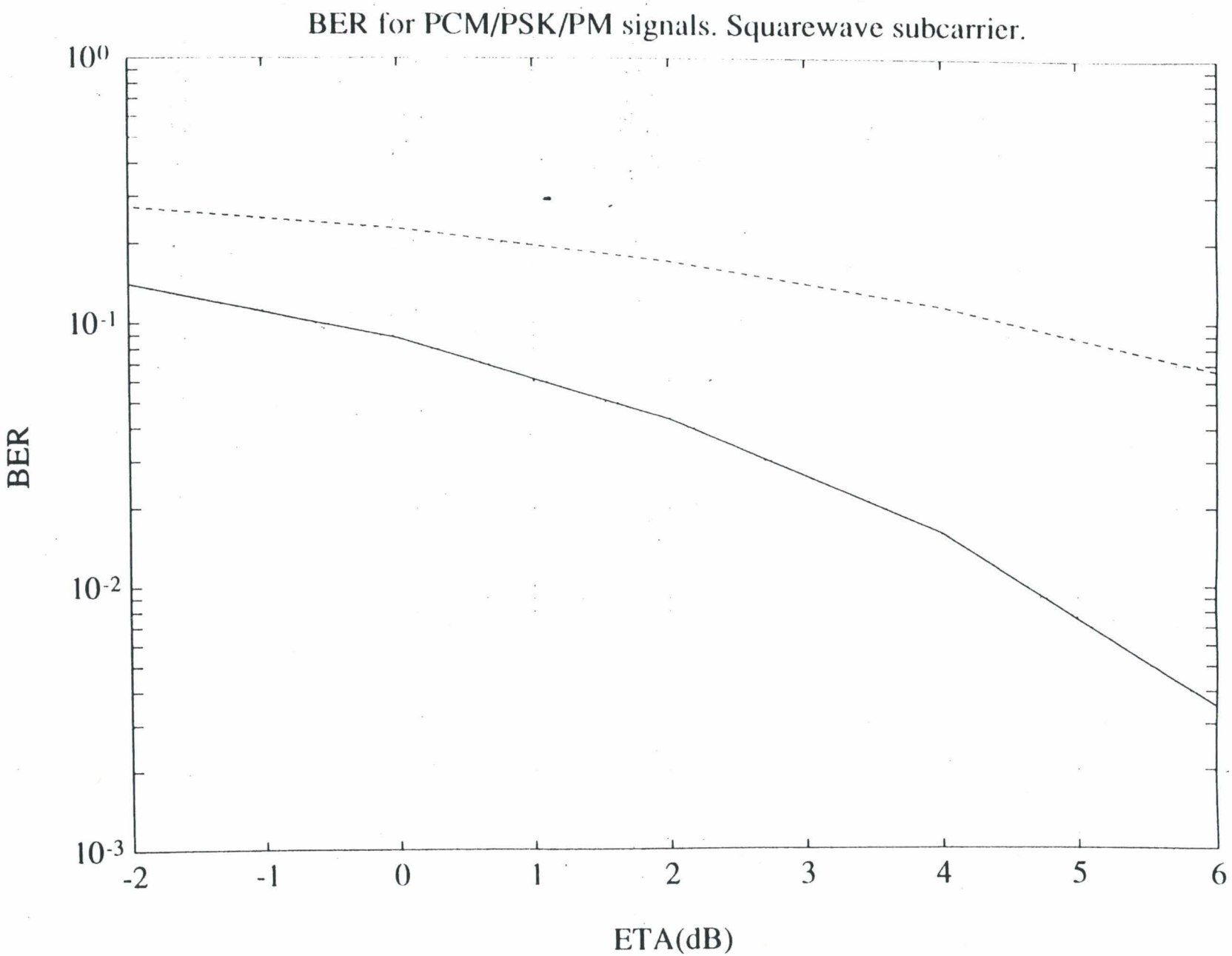
BER for PCM/PSK/PM signals. Squarewave subcarrier.
10^0
10^{-1}
10^{-2}
10^{-3}
BER
-2
-1
0
1
2
3
4
5
6
ETA(dB)

4. BIT ERROR RATE FOR PCM-SPL/PM SIGNALS.

The value of the modulation index used here is m=1.0rd and the values obtained for the BER are given right below in next table for every case of filtering :

E_b/N_0 (dB)	No Filtering	f_{cut} = $\pm 4R_s$	f_{cut} = $\pm 8R_s$	f_{cut} = $\pm 12R_s$
-2.0	$1.48*10^{-1}$	$1.68*10^{-1}$	$1.58*10^{-1}$	$1.51*10^{-1}$
0.0	$9.42*10^{-2}$	$1.13*10^{-1}$	$9.73*10^{-2}$	$9.67*10^{-2}$
2.0	$5.02*10^{-2}$	$6.29*10^{-2}$	$5.35*10^{-2}$	$5.10*10^{-2}$
4.0	$1.94*10^{-2}$	$2.68*10^{-2}$	$2.11*10^{-2}$	$2.03*10^{-2}$
6.0	$4.60*10^{-3}$	$7.10*10^{-3}$	$5.00*10^{-3}$	$4.80*10^{-3}$

The values for the case of no filtering are 0.7 dB deviated from the ones expected theoretically, and the reasons for that deviation could not be clearly identified.However, it appears that this offset is quite similar for all filtering conditions considered, thus rendering valid the results on relative effects on BER of the different filtering schemes simulated as compared to the "no filtering" case.

For the different cases the plot of BER vs. ETA is given in next page.

The solid line corresponds to the case of no filtering, the dotted one to the case of $f_{cut}=\pm 4R_s$, the dashed and dotted one to the case of $f_{cut}=\pm 8R_s$, and the dashed one to the case of $f_{cut}=\pm 12R_s$.

By inspection of the curves we can conclude that the case of filtering with a 3dB double-sided cutoff frequency of $\pm 8R_s$ has only a loss of 0.2 dB from the curve without filtering so that, by this way, we can reach an acceptable trade-off between the bandwidth occupancy and the BER.

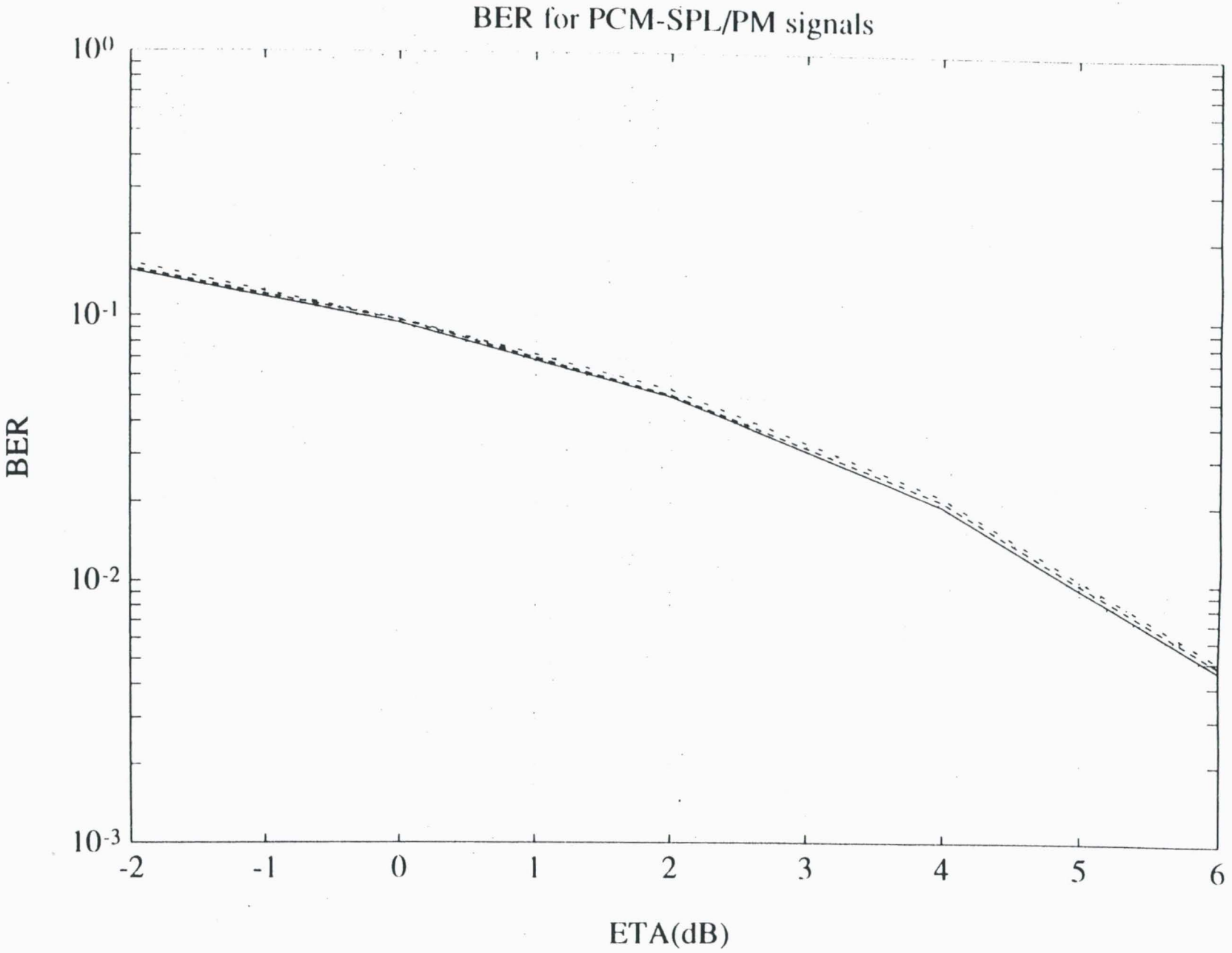
BER for PCM-SPL/PM signals
BER
10^{0}
10^{-1}
10^{-2}
10^{-3}
-2
-1
0
1
2
3
4
5
6
ETA(dB)

5. REFERENCES.

[1] **JEAN-LUC GERNER**, " A position paper on occupied bandwidth of space telemetry signals ", CCSDS report, March 1991.

[2] **TIEN M. NGUYEN**, " Computation of the occupied bandwidth for PCM/PSK/PM signals ", A-E-91-13 CCSDS report, May 1992.

[3] **CCSDS RECOMMENDATIONS FOR RADIO FREQUENCY AND MODULATIONS SYSTEMS**, " Computational method for determining the occupied bandwidth of unfiltered PCM/PSK/PM with sinewave subcarrier signals ", A-E-91-14 CCSDS report, May 1992.

[4] **RICCARDO DE GAUDENZI**, " PCM/PM and PCM/PSK/PM signals. Power Spectral Density calculation ", ESA/ESOC report, 1986.

[5] **ESA**, " Radio Frequency and Modulation Standards ", PSS-04-105 Issue 1, December 1989.

[6] **TOPSIM IV**, Design and implementation of software for simulation and analysis of communications systems, ESA/ESTEC contract No. 6981/86/ML/JG, 1986.

ACKNOWLEDGEMENT.

This document has been written in the European Space Research and Technology Centre of the European Space Agency, ESA/ESTEC, P.O. Box 299, 2200 AG Noordwijk, THE NETHERLANDS from the result of a stage period of four months, July-October 1992.

I would like to thank all the people who oriented me to carry out my training period in ESTEC, Werner Kriedte, the head of the XRT section, Riccardo de Gaudenzi, the secretary of XRT & XRF sections Pauline Martin who helped me to carry a pleasant stage, and everybody else from XRT section, but I would like to thank specially my supervisor Jean-Luc Gerner who helped me to interpret all the results that I have been obtaining and without his attention this work paper should not have ever been published.

Also thanks to all the staff members, stagiaires, young graduate and spanish trainees that I have met in ESTEC who helped me in having a very pleasant stage.

6. APPENDIX. LIST OF PROGRAMS.

The list of programs are given for the cases taken into account : PCM/PSK/PM with sinewave subcarrier, PCM/PSK/PM with squarewave subcarrier and PCM-SPL/PM signals, respectively.

Some subroutines very easy to implement with the aid of the TOPSIM mask have been created for several purposes :

1. **CHAPH2(F0)**. Because of the constraints of the block of TOPSIM called PHAMOD (that only allows baseband inputs), the PSK signal must be shifted into TOPSIM baseband.F0 is the frequency contained into TOPSIM baseband.
2. **CHAPH3(F0)**. It generates a sinusoidal signal into TOPSIM baseband which frequency is given by F0.
3. **PCMSSI** & **PCMSQW**. They make the conversion of analog signals to registers.
4. **BIN(AMP)**. It converts a register into an analog signal.The output analog signal has an amplitude given by the parameter AMP.
5. **REGSQW(P)**. It creates a periodic register.The value of the period is given by P.
6. **SPLCHA(AMP)**. It makes a conversion of code creating an analog biphase encoded data from a register.The resulting output is an analog signal which amplitude is given by the parameter AMP.
7. **REGSPL(P)**. Same as REGSQW(P) but applied to the particular case of SPL data.

```
* Generated by TOPSIM Graphic Editor
* File name: APPO.TOP
PROGRAM  = APPO
GRAPHICS = DISPLAY
*
INITIAL
*
TS      = 1.
NS      = 100
T0      = 20*TS
DELT    = TS/NS
FINTIM  = T0+10013*TS
NDEG    = 0
NGEN    = 1
NSYNC   = 0.
F0      = 400./TS
F01     = 9./TS
AMP     = 1.
NTYP    = 2
NTY     = 2
NP      = 2
BW      = 2./TS
F02     = 2050000./TS
PHA     = 0.
SENS    = 1.1
SPOW    = (1.-0.0746-(COS(SENS)**2))/2.
M       = 1
PARAMETER ETA  = -2.,0.,2.,4.,6.
G       = (NS*DELT*SPOW/M)/(10.**(ETA/10))
N0      = 0.051*NS
MAXEYE  = 0.95*NS
*
DYNAMIC
*
L1X < PNSEQ (NDEG, NGEN, NSYNC, NS)
YMOD < PSKMOD (F0, AMP) < L1X
YFIL < FILBUT (NTYP, NP, F0, BW, AMP) < YMOD
YSUB < CHAPH2 (F01) < YFIL
YRF < PHAMOD (F02, AMP, PHA, SENS) < YSUB
YNOI < NBWN (G, F02)
Y < BPSUM (F02) < YRF, YNOI
YDEM < PHADEM < Y
YSIG < CHAPH3 (F01)
YDE < DELAY (N0) < YSIG
YMUL < MULTBB < YDE, YDEM
YID < INTDUM (NS, N0) < YMUL
XCLK < CLOCK (NS, MAXEYE)
YSH < SHOLD < XCLK, YID
L1OUT < PCMSSI < YSH
*
END
```

```
* Generated by TOPSIM Graphic Editor
* File name: SQMOD.TOP
PROGRAM  = SQMOD
GRAPHICS = DISPLAY
*
INITIAL
*
TS      = 1.
NS      = 240
DELT    = TS/NS
T0      = 20*TS
FINTIM  = T0+10014*TS
NDEG    = 0
NGEN    = 1
NSYNC   = 0.
P       = TS/5.
AMP     = 1.
F02     = 2.05E6/TS
PHA     = 0.
SENS    = 1.0
NTYP    = 1
NP      = 2
BW      = 11./TS
SPOW    = (1.-(COS(SENS)**2))/2.
M       = 1
ETA     = 4.
*PARAMETER ETA = -2.,0.,2.,4.,6.
G       = (NS*DELT*SPOW/M)/(10.**(ETA/10))
*N0      = 0.01*NS
N0      = 0.
MAXEYE  = 0.9*NS
*
DYNAMIC
*
L1X < PNSEQ (NDEG, NGEN, NSYNC, NS)
L1Y < REGSQW (P)
YNR < BIN (AMP) < L1Y
YDE < DELAY (N0) < YNR
L1Z < RXOR < L1X,L1Y
Y1 < BIN (AMP) < L1Z
*YFIL < FILBUT (NTYP, NP, 0., BW, AMP) < Y1
YRF < PHAMOD (F02, AMP, PHA, SENS) < Y1
YNOI < NBWN (G, F02)
Y < BPSUM (F02) < YRF,YNOI
YREC < PHADEM < Y
YMUL < MULTBB < YDE, YREC
YID < INTDUM (NS, N0) < YMUL
XCLK < CLOCK (NS, MAXEYE)
YSH < SHOLD < XCLK, YID
L1OUT < PCMSQW < YSH
*
END
```

```
* Generated by TOPSIM Graphic Editor
* File name: SPLCOD.TOP
PROGRAM  = SPLCOD
GRAPHICS = DISPLAY
*
INITIAL
*
TS      = 1.
NS      = 80
T0      = 20*TS
DELT    = TS/NS
FINTIM  = T0+10013*TS
NDEG    = 0
NGEN    = 1
NSYNC   = 0.
AMP     = 1.
F0      = 2.05E6/TS
PHA     = 0.
SENS    = 1.0
SPOW    = (1.-(COS(SENS)**2))/2.
M       = 1
PARAMETER ETA = -2.,0.,2.,4.,6.
G       = (NS*DELT*SPOW/M)/(10.**(ETA/10))
BW      = 8./TS
N0      = 0.025*NS
*N0      = 0.
MAXEYE  = 0.95*NS
P       = TS/1.
*
DYNAMIC
*
L1X < PNSEQ (NDEG, NGEN, NSYNC, NS)
YSAL < SPLCHA (AMP) < L1X
*YSAL1 < FILBUT (1, 2, 0., 12./TS, AMP) < YSAL
YRF < PHAMOD (F0, AMP, PHA, SENS) < YSAL
YTFIL < FILBUT (2, 2, F0, BW, AMP) < YRF
YNOI < NBWN (G, F0)
Y < BPSUM (F0) < YTFIL, YNOI
YREC < PHADEM < Y
YSQ < REGSPL (P)
YDE < DELAY (N0) < YSQ
YMUL < MULTBB < YDE, YREC
YID < INTDUM (NS, N0) < YMUL
XCLK < CLOCK (NS, MAXEYE)
YSH < SHOLD < XCLK, YID
L1OUT < PCMSQW < YSH
*
END
```

SESSION 5

SPACECRAFT TRANSPONDER

DEEP SPACE TRANSPONDER DEVELOPMENT

L. Popken
European Space Research and Technology Centre
RF System Division (XRT)
European Space Agency, Keplerlaan 1
P.O. Box, 2200 AG Noordwijk, The Netherlands

ABSTRACT

This paper presents the activities of ESA/ESTEC on the development of the deep space transponder (DST). The paper discusses the revision of the development objectives along with the main design approach and DST frequency plans. Additionally, the paper presents the tasks planned for the coming year.

1 Activity Programmatics

The first status report [1] had provided the rationale for the new development, together with a summary of the first design activities and some critical design issues driving the transponder architectural definition. The functional partitioning of the digital receiver and impacts of the coherent frequency turnaround from X- to Ka-Band on the upconverted transmit phase jitter were discussed.
The first design phase was concluded by June '92 and provided the transponder overall design going along with a definition down to component levels in the analog and digital unit domains. The technical handouts from the final presentation [2] for this first activity were presented to the CCSDS at their last meeting.

In the sequence of planned contracts the second phase for the development of the transponder started in May '93. The industrial team is formed by DASA, former MBB, (D) as prime contractor who are responsible for the overall design and breadboarding, and with Satellites International Ltd. (GB) as subcontractor in charge of the digital demodulator, and with InformationsKontroll (N) responsible for the breadboard check-out equipment.

In addition, two other supporting but secondary activities (one at Univ. Edinburgh, the other at ESTEC) are performed which investigate the possibilities of onboard carrier post-filtering for jitter reduction in the coherent turnaround (see also [1]), and the prospects and implementation issues of onboard ranging signal regeneration for the ESA/MPTS and NASA/JPL/DSN ranging signals and codes.

1.1 Revision of Development Objectives

For the development of the new transponder it is most important for ESA to acquire at an early stage the programmatic and also financial support from potential future deep space missions who potentially would embark on the new TT&C equipment. From trade-offs and discussions with mission study teams at system and subsystem levels, such as for the Rosetta mission, over the last year some important conclusions had to be incorporated into the transponder development; this shall ensure the continuation of the activity also beyond the

present Phase 2. The system and mission needs and the corresponding implications on the transponder design are as follows:

- The new transponder shall be used as fully operational (i.e. not just experimental) and shall be compliant with the usual requirements and constraints applicable to TT&C onboard subsystems. This immediately implies that at system level there is presently no need identified by ESA to consider any Ka-Band for telecommand uplink; among other reasons, the TC omni-coverage requirement and its implementation dictate the choice for an uplink frequency-band (if single) not higher than X-Band which already imposes receive antenna coverage complications relative to the advantages of S-Band in this respect.
- For a (deep) space mission supported by European ground stations any necessary upgrading of the groundstation network is usually at the cost of the first mission requiring the upgrading. Therefore, projects prefer to use already existing ground equipments, probably at the expense of shifting complexity towards the space segment, e.g. to use X-Band telemetry instead of Ka-Band telemetry although the required onboard resource envelope (DC power, antenna size etc.) might exceed those needs implied by a Ka-Band telemetry for the same telemetry capacity.
  Telecommanding a spacecraft within X-Band from an ESA groundstation would also require upgradings of the existing RF frontends which, however, would be much less expensive than any groundstation upgrading towards Ka-Band telemetry.
- In conclusion and for important programmatic reasons, the new transponder in its baseline is an X-to-X-Band (749/880) transponder with the manufacturing option for Ka-Band telemetry (3344) at minimum hardware modifications or additions. No other alternatives are considered during the design. The Ka-Band instead of X-Band telemetry does not necessitate any exciter external to the basic transponder but can be accommodated within the same physical dimensions of the unit which will be of a fixed number of modules.

The industrial team was requested to review the transponder design achieved earlier during Phase 1 [2] by taking the above aspects into full consideration for the detailed design and for the definition of the breadboard.

2 Main Design Approach

During the development of the dual-mode S-Band transponders for data-relay some rather general but important design approach-experiences were gained which are closely followed also for the DST.

There is no attempt made for re-using or re-starting from the frequency plan of the traditional S-Band TT&C transponders from which conventional X-Band transponders (with probably slaved Ka-Band exciters) are derived by basically adding complexity i.e. additional front-end converters but maintaining the unit's basic functional and also hardware partitionings. Instead, the frequency plan was designed from scratch, taking into account the benefits (but also the limitations) of new devices such as DDS's (direct digital synthesizers) for the receive and transmit chains. (DDS's were sucessfully implemented in a new dual-mode S-Band transponder.)

For an overall optimization much effort was spent first on the transponder architectural and interface definition plus design, before starting on any details e.g. of the digital demodulator which is considered at a lower design level; (this approach is reflected also by the contractual hierarchy and work-sharing in the industrial consortium).

Careful appreciation of phase noise effects and corresponding analysis trade-offs led to the choice of deriving all LO mixing frequencies from the TCXO master oscillator, and to implement a short-loop closure for the receiver demodulator instead of the different long-loop approaches in existing transponders. No frequency upconversion is applied to the two NCO output signals in the transponder, in order to account properly for the inherent and peculiar NCO spurious characteristics, apart of selecting the most adequate ratios of clocking rates and output frequencies from these devices.

Other design objectives were the maximum commonality of the LO section shared between receiver and transmitter, and to find a design for the X-to-X-Band frequency plan which at a minimum number of modifications can be used for the option of Ka-Band telemetry. In total, some 65 (!) different frequency plans very identified and analyzed by the contractor in terms of the various design aspects before having achieved the agreed baseline.

As the frequency plan design was evolving, parallel measurement tests were conducted to verify the phase noise performances in particular of the NCO's and DAC's (Digital-to-Analog Converters) forming the DDS's.

The achieved confidence in the feasibility of the revised frequency plan allows us to precede now with the further detailed design also of the digital section for which no significant change is anticipated relative to the baseline established during Phase 1.

3 DST Frequency Plans

For the design the following general guide-lines applied:

- minimum number of frequency-multiplier stages, i.e. choosing frequency-conversion factors such that maximum commonality w.r.t. their factorisation was achieved,
- limitation of single-stage frequency multiplication to a factor of e.g. 11 in order to facilitate signal filtering, (DRO clean-up loops are not excluded and are slaved to TCXO, i.e. not to any VCO, because short-loop closure implies LO frequencies to be derived from TCXO),
- receiver and transmitter passbands are determined by maximum of 3MHz ranging signals, (ΔDOR signal modulation is separately covered by dedicated wideband modulator),
- receiver and transmitter noise bandwidths not exceeding 4 MHz,
- consequently, the final receiver IF, and the receiver and transmitter NCO frequencies are in the order of 20 MHz,
- to facilitate signal filtering the relative frequency-spacing of all LO frequencies should be at least two times the relative RF passband corner frequencies,
- for spurious noise-control from the NCO's the clocking frequency should be at least three times the output frequency (optimally, a factor of about 4 is desired),

- the clock frequency of applicable CMOS NCO devices is less than 80 MHz, or 70 MHz considering some margin, (GaAs DDS devices are considered as backup alternative at the expense of higher power consumptions),
- according to results from Phase 1 the input clock frequency to the digital section is 4/3 times the final IF of the receiver.

The found optimum conversion from an X/X- to X/Ka-transponder requires

- the addition of one frequency-multiplier in the final LO-path,
- the addition of one frequency-multiplier providing the third LO frequency, and
- the replacement of the X/X-transponder output mixer by a two-mixer stage.

Up to the 2-nd IF in the transmit chain there are no changes required for the X/Ka-option relative to the X/X-baseline.

Figs. 1 and 2 from [3] show the two principle frequency plans (not functional or hardware blockdiagrams) for the X/X- and X/Ka-transponders. Although indicated, the 32 MHz frequency will not be output from a TCXO in an actual implementation but will be derived from a frequency generation slaved to a TCXO with a more convenient output frequency. For the final implementations of the frequency plans there exist various alternatives.

Currently, the intermodulation analyses and the associated filter definitions for the frequency plans are finalized.

4 Tasks Planned for the Coming Year

By the end of 1994 the DST X-Band receiver breadboard will be developed; this includes the complete LO synthesizer but not the transmitter frequency upconversion chain.

As the next step during the coming weeks the receiver breadboard will be defined further in terms of electrical signal interfaces between the different modules. The test plan will be established with emphasis primarily on functional and phase noise and detection performance verifications; but some relaxations will be granted e.g. in terms of final X-Bandd LNA noise figure performance and input filtering which would be cost-drivers deemed unnecessary at this breadboarding stage.

Specific tasks cover the integrations of

- the X-Band receiver and the LO synthesizer,
- the signal generator including the receiver and transmitter DDS's,
- TCXO and slaved PLL,
- Digital Unit, with
  - Architectural and algorithmic design and verification of the DST specific IC as defined during Phase 1, applying VHDL as design entry,
  - Field-Programmable-Gate-Array (FPGA) IC-implementation for the breadboard,
  - Implementation of the digital unit comprising the FPGA's and the microprocessor (1750 instruction set).

Further progress reports will be provided to the CCSDS as the development will precede.

It is intended to continue the development beyond 1994 within a not yet approved Phase 3 in 1995, which shall breadboard the transmitter upconversion chain for either the X-Band baseline or the Ka-Band option, pending the preferences as implied by a potential future mission application.

References

[1] Deep Space Transponder Development, 'Activity Rationale, Current Status and Further Planning, Design Issues,' L. Popken (ESA/ESTEC, XRT), Report to the CCSDS, 17 March 1992.

[2] Deep Space Transponder, Final Presentation Handouts by DASA (D) and SIL (GB), ESA-Contract No. 8742/90/NL/PB(SC), July 3rd, 1992. Presented to the CCSDS Meeting, Febr. 8-12, 1993.

[3] Deep Space Transponder, Design Notes by DASA (D), Working Meeting, July 26, 1993.

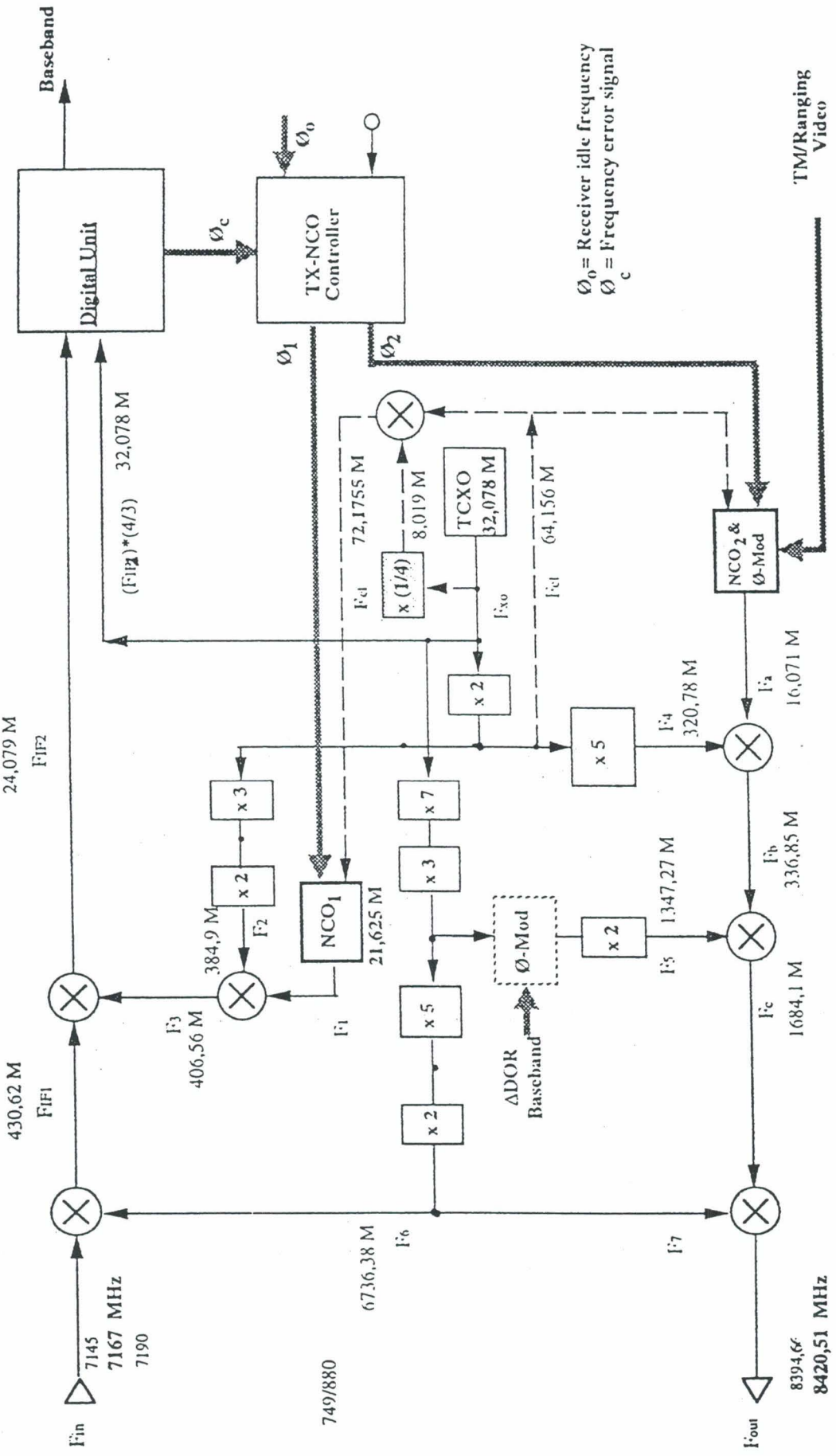

Fig. 1: X/X DST Frequency Plan Schematic [3]

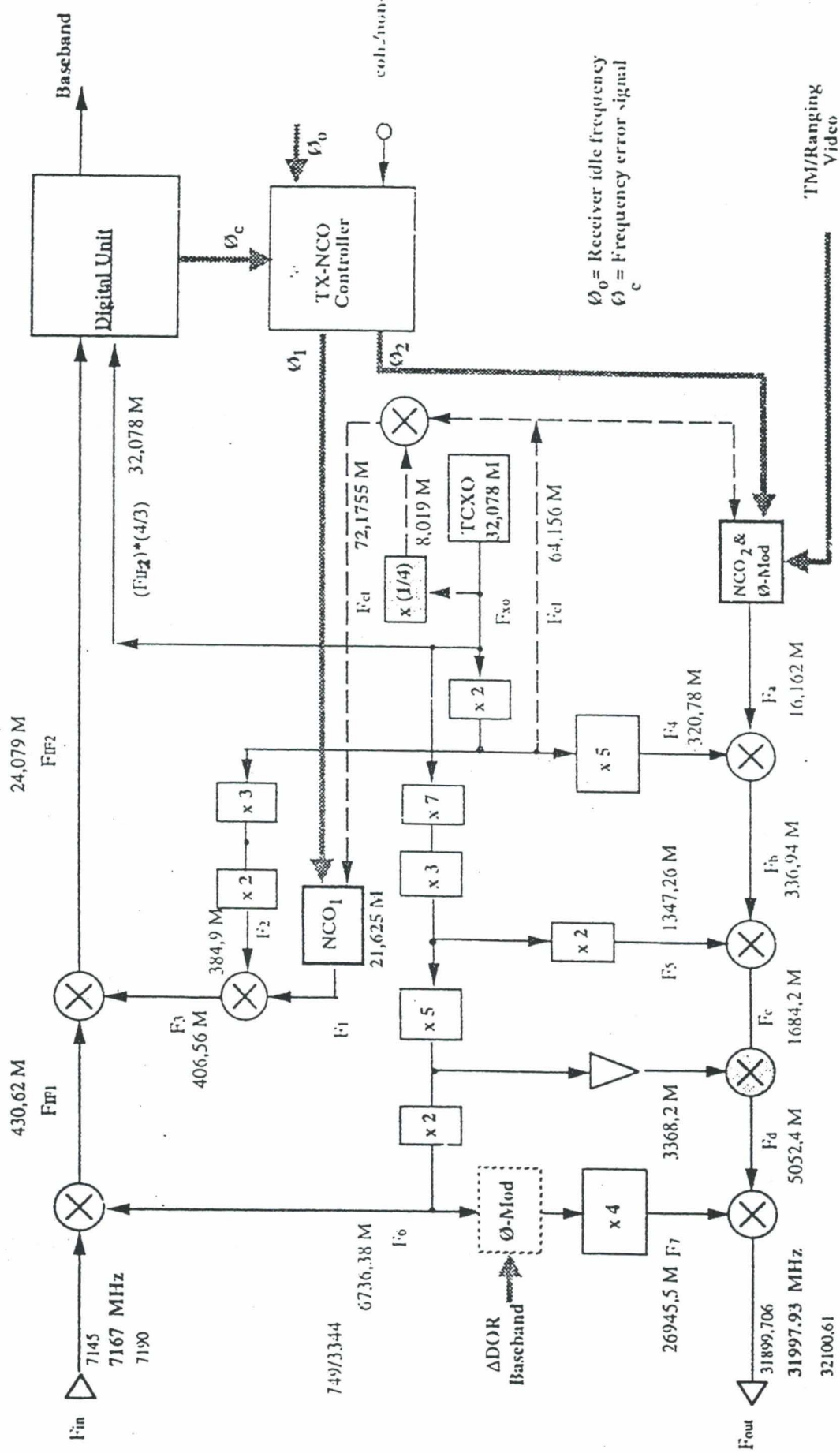

Fig. 2: X/Ka DST Frequency Plan Schematic [3]

Preliminary Design and Implementation of the Baseline Digital Baseband Architecture for Advanced Deep Space Transponders[1]

T. M. Nguyen
Communications Systems Research Section

H.-G. Yeh
Spacecraft Telecommunications Equipment Section

National Aeronautics and Space Administration

Jet Propulsion Laboratory

California Institute of Technology

Pasadena, California

Abstract

This article investigates and identifies the baseline design and implementation of the digital baseband architecture for advanced deep space transponders. Trade studies on the selection of the number of bits for the analog-to-digital converter (ADC) and optimum sampling schemes are presented. In addition, the proposed optimum sampling scheme is analyzed in detail. Descriptions of possible implementations for the digital baseband (or digital front end) and digital phase-locked loop (DPLL) for carrier tracking are also described.

I. Introduction

Future NASA missions will require cheaper, smaller, and more energy-efficient spacecraft telecommunication equipment. These requirements motivated this study on advanced transponders for deep space applications. Recently, a study [1] has investigated various digital baseband architectures for future deep space transponders. Three different architectures were proposed for near-term, intermediate, and long-term solutions. The purpose of this article is to investigate and identify the baseline design and the conceptual implementation of the digital baseband architecture for a short-term solution.

The baseline architecture will use advanced digital technologies and signal-processing techniques for improved performance along with attractive functionality and adaptability to mission requirements. The identified architecture should also meet the interface constraint to minimize the cost of the design. The baseline architecture was developed based on the current configuration of the Cassini Deep Space Transponder (DST) [2]. The proposed architecture will maintain the analog IF section and the automatic gain control (AGC) loop at the first IF mixer identical to the current Cassini DST. However, the second IF will be redesigned to ease the digitization of baseband functions. In addition, the command detector unit (CDU) function, along with its modifications, will be included as a whole in the advanced DST. A description of the CDU and its modifications can be found in [1].

The simplified block diagram of the baseline architecture for the receiver of the DST is shown in Fig. 1. For this baseline architecture, the analog phase-locked loop

1. The work described in this paper was carried out at the Jet Propulsion Laboratory, California Institute of Technology, under contract with the National Aeronautics and Space Administration.

(APLL) for carrier tracking is replaced by a hybrid digital phase-locked loop (DPLL) and the ranging signal is extracted by filtering and turning the signal around without further signal processing (analog turnaround ranging). To simplify the hardware, the sampling frequency will be selected so that it is compatible with the sampling rate requirement of the CDU. A detailed description of the baseline architecture shown in Fig. 1 can also be found in [1].

This article begins with the trade studies for the selection of the number of bits for the ADC and the optimum sampling technique. Based on the selected optimum sampling scheme, the implementation of the baseband digital front end for simplified hardware was analyzed and proposed. Next, preliminary results related to the design and conceptual implementation of the DPLL for carrier tracking are presented and discussed. Finally, the article concludes with a summary of the salient features associated with this baseline design and direction of future work.

II. Selection of Number of Bits for the ADC

The number of bits required for the ADC at the second IF will determine the setting of the power for the AGC, the carrier signal-to-noise (SNR) degradation due to quantization, and the saturation noise. This section summarizes the results presented by Nguyen.[1] The carrier SNR degradation due to digitization, Δ, in the presence of Gaussian noise, is given by Nguyen[2] as

$$\Delta = \left(1 + \frac{P_N}{\sigma^2}\left(1 + \frac{P_S}{P_n}\right)\right)^{-1} \tag{1}$$

where

$$\frac{P_N}{\sigma^2} = 2\left(K^2+1\right)F(K) - \frac{2K}{\sqrt{2\pi}}e^{\left(-\frac{K^2}{2}\right)}$$

$$+ \frac{K^2}{12(M-1)^2}\left(1 - 2F(K)\right) \tag{2}$$

$$\frac{P_S}{P_n} = \left(\frac{P_S}{N_0}\right)\left(\frac{2}{F_S}\right) \tag{3}$$

$$K = \frac{1}{LF} \tag{4}$$

$$F(K) = \frac{1}{\sqrt{2\pi}}\int_K^\infty e^{\left(-\frac{u^2}{2}\right)}du \tag{5}$$

Note that (P_N/σ^2) denotes the quantization noise plus saturation noise-to-carrier signal power ratio; (P_S/P_n) denotes input carrier power-to-noise power ratio; N_0 is the one-sided input noise power density; F_S is the sampling frequency; $M = 2^{N-1}$, where N is the number of bits (including sign); and LF is the loading factor defined as follows:

$$LF = \frac{\text{rms amplitude of the total input signal}}{\text{ADC saturation voltage}} \tag{6}$$

The optimum values for K for various values of N have been calculated in [3], and the corresponding optimum LF as a function of N is depicted in Fig. 2. From the optimum values of N and LF found in Fig. 2, one can calculate the corresponding values of (P_N/σ^2) using Eq. (2). Using the calculated (P_N/σ^2) together with Eq. (1), one can calculate the carrier SNR degradation due to digitization. The results are plotted in Fig. 3 for 0 dB-Hz $< P_S/N_0 <$ 50 dB-Hz and 1 MHz $< F_S <$ 36 MHz. Note that for 0 dB-Hz $< P_S/N_0 <$ 50 dB-Hz and 1 MHz $< F_S <$ 36 MHz, one has: $1 + P_S/P_n \approx 1$. Using this approximation, the results are shown in Fig. 3.

Therefore, to achieve the digitization with a degradation in carrier SNR of less than 0.1 dB and to meet the required dynamic range of $6N$ dB for the input carrier signal, the required number of bits is $N \geq 4$ bits. In addition, the higher the number of bits that one selects, the less susceptible to interference the signal will be.[3] Consequently, the required number of bits for the ADC should be selected such that 4 bits $\leq N \leq$ 8 bits.

III. Optimum Sampling Scheme

A. Review of Current Sampling Techniques

Currently, there are several techniques for sampling the band-pass signals [4]: in-phase and quadrature (I&Q) baseband sampling with analog quadrature, I&Q sampling with analog Hilbert transform, band-pass sampling with

[1] T. M. Nguyen, "Selection of the A/D Sampling Frequency and Number of Bits for the Advanced Transponder," JPL Interoffice Memorandum 3313-92-024 (internal document), Jet Propulsion Laboratory, Pasadena, California, April 20, 1992, revised May 18, 1992.

[2] Ibid.

[3] J. Berner, "Number of Bits Required in Block-V ADC," JPL Interoffice Memorandum 3338-90-048 (internal document), Jet Propulsion Laboratory, Pasadena, California, March 26, 1990.

digital quadrature mixers, and band-pass sampling with digital Hilbert transform. Based upon the investigation in [4], the band-pass sampling technique with digital quadrature mixers is recommended (see Fig. 5) for the baseline design of the advanced transponder because of the following reasons:

(1) No phase and amplitude imbalances because the mixing is done in digital domain.

(2) The digital low-pass filter (LPF) using finite-impulse response (FIR) filter provides constant group delay that is very important for ranging and Doppler information.

(3) Only one ADC is required.

(4) If the sampling period is exactly $1/4F_{IF}$, then the reference of I&Q components reduces to an alternating sequence.

It will be shown later that the hardware implementation can be simplified by using the last property with some modification. Before describing how to implement the "digital front end" for the advanced transponder, the digital front end needs to be defined.

The digital front end of the transponder (see Figs. 1 and 4) is designed to accept an IF analog signal and output digital baseband I&Q components for further processing by the remainder of transponder. The purpose of the digital front end is to provide the transponder with a demodulation capability from an IF-to-baseband digital signal.

B. Conceptual Implementation of the Digital Front End

To implement the digital front end (see Fig. 4), one must set up the criteria for selecting both the optimum sampling frequency and the analog IF. First, there are several criteria for selecting the optimum sampling frequency, namely,

(1) The hardware implementation should be simple.

(2) The sampling frequency should be sufficiently high to meet the required number of samples per symbol for the CDU and the carrier tracking loop.

(3) The sampling frequency should be sufficiently high to prevent aliasing of the baseband signal with the images that occur at the sampling rate.

(4) The sampling frequency selected should meet the current specification of the analog-to-digital (A/D) technology with reasonable cost.

Based on these criteria, the sampling frequency, F_S, must be selected to satisfy the following conditions [5–7]:

$$F_S \geq 2BW \tag{7}$$

$$\frac{2}{(l+1)}\left(F_{IF} - \frac{BW}{2}\right) \leq F_S \leq \frac{2}{(l+1)}\left(F_{IF} + \frac{BW}{2}\right) \tag{8}$$

where BW is the bandwidth of the band-pass signal in hertz, F_{IF} is the center of the IF band, and l is a positive integer. In order to simplify the hardware implementation, one chooses equality in Eq. (7) and an odd integer for l in Eq. (8):

$$F_S = 2pBW \tag{9}$$

$$nF_S = F_{IF} - \frac{BW}{2} \tag{10}$$

where $p \geq 1$ and $n = (l+1)/2$.

Solving for the sampling frequency in terms of F_{IF}, one gets

$$F_S = \frac{4pF_{IF}}{(1+4np)} \tag{11}$$

for $p = 1$, Eq. (11) reduces to

$$F_S = \frac{4F_{IF}}{(1+4n)} \tag{12}$$

where n satisfies the following inequality

$$n \leq \left[\frac{F_{IF}}{2BW} - \frac{1}{4}\right] \tag{13}$$

where $[x]$ is the smallest integer that is less than or equal to x. It should be mentioned that the sampling scheme proposed is known as the under-sampling scheme. Note that, in practice, to simplify the I&Q sampling technique using digital quadrature mixers (see Fig. 5) to the configuration shown in Fig. 7(a), the sampling frequency must

be chosen as $4F_{IF}$ [8–10].[3] However, using Eq. (12) one can avoid selecting a high sampling frequency (and hence achieve a more energy efficient spacecraft). As an example for the proposed under-sampling scheme, let the IF be 5 MHz and the bandwidth of the signal be 36 kHz; then using Eq. (13), one obtains $n \leq 69$. If one selects $n = 6$, then the sampling frequency required for this case is, from Eq. (12), $F_S = 0.8$ MHz. Figures 7(b) and (c) illustrate and compare the two sampling schemes discussed above.

Secondly, one must select the IF so that the analog circuitry in the transponder can be designed and built easily. There are several criteria for selecting the IF, namely,

(1) The quadrature sampling error caused by spectral bands overlapping [7] must be avoided by selecting the upper cutoff frequency of the band-pass filter (BPF) equal to an integer multiple of the bandwidth, i.e.,

$$F_{IF} + \frac{BW}{2} = cBW \tag{14}$$

where c is a positive integer.

(2) For minimum hardware implementation, F_{IF} and F_S should satisfy Eq. (12).

(3) F_{IF} must be chosen such that the associated band-pass filter in the analog-mixing and filtering circuitry is realizable. The passband of this filter must pass the required number of sidelobes of the command signal and possibly the highest ranging clock frequency.

(4) F_{IF} must be chosen by taking into consideration the throughput limitation of the digital filters of the digital front end.

(5) F_{IF} must be chosen to provide minimum carrier delay variation.

To show that Eq. (12) can be used to select the sampling frequency for hardware simplification, look at the mathematical model for the uplink signal, $S(t)$:

$$S(t) = \sqrt{2P}\sin\left((\omega + \omega_d)t + \Theta(t) + \varphi\right) \tag{15}$$

where

P = total received power

ω = angular carrier frequency

ω_d = Doppler angular frequency offset

$\Theta(t)$ = phase modulation $= md(t)\sin(\omega_{SC}t) + m_R R(t)$

φ = phase offset

m = command modulation index

$d(t)$ = command non-return-to-zero (NRZ) data

ω_{SC} = command subcarrier frequency

m_R = ranging modulation index

$R(t)$ = ranging signal

Without loss of generality, one can set $\omega = \omega_{IF} = 2\pi F_{IF}, \omega_d = 0, \varphi = 0$, and can expand Eq. (15) to get

$$S(t) = \sqrt{2P}\left[\cos(\Theta(t))\sin(2\pi F_{IF}t) + \sin(\Theta(t))\cos(2\pi F_{IF}t)\right] \tag{16}$$

The first term in Eq. (16) represents the carrier component, and the second is the command signal component.

Assume that the I&Q components of Eq. (15) are extracted by using analog quadrature mixers as shown in Fig. 6. If the cutoff frequency of the LPF is such that it rejects higher-order harmonics components and passes only the first harmonic component without distortion, then the output I&Q components are

$$I(t) = \frac{1}{2}\sin(\Theta(t)) \tag{17}$$

$$Q(t) = \frac{1}{2}\cos(\Theta(t)) \tag{18}$$

Note that Eqs. (17) and (18) have been normalized by $\sqrt{2P}$. If one assumes that the ranging signal is off, then the $I(t)$ and $Q(t)$ shown in Eqs. (17) and (18) become

$$I(t) = \frac{1}{2}d(t)\sin(m\sin(\omega_{SC}t)) \approx d(t)J_1(m)\sin(\omega_{SC}t) \tag{19}$$

$$Q(t) = \frac{1}{2}\cos(m\sin(\omega_{SC}t)) \approx \frac{1}{2}J_0(m) \tag{20}$$

[3] M. J. Agan and C. R. Pasqualino, "AMT Modem Digital Front End," JPL Interoffice Memorandum AMT:331-5-90-0 (internal document), Jet Propulsion Laboratory, Pasadena, California, October 1990.

Note that the I-component contains the command information and the Q-component contains the amplitude of the carrier component.

A sample of the signal expressed in Eq. (16) is obtained by using the sampling frequency derived in Eq. (12). At this sampling frequency, one has

$$t = kT_S = \frac{k(4n+1)}{4\mathrm{F}_{IF}},\ k = 0, 1, 2, 3, 4,\ \ldots \tag{21}$$

where T_S denotes the sampling period. Substituting Eq. (21) into Eq. (16) and evaluating it for $k = 0, 1, 2, 3, 4, \ldots$, one sees that Eq. (16) generates the following sequence:

$$\sqrt{2P}\sin(\Theta(0)), \sqrt{2P}\cos(\Theta(T_S)), -\sqrt{2P}\sin(\Theta(2T_S)),$$

$$-\sqrt{2P}\cos(\Theta(3T_S)), \sqrt{2P}\sin(\Theta(4T_S)),$$

$$\sqrt{2P}\cos(\Theta(5T_S)), -\sqrt{2P}\sin(\Theta(6T_S)),$$

$$-\sqrt{2P}\cos(\Theta(7T_S)), \sqrt{2P}\sin(\Theta(8T_S)),$$

$$\sqrt{2P}\cos(\Theta(9T_S)), \ \ldots$$

Taking the above sequence and multiplying by the $\{1, 1, -1, -1, 1, 1, -1, -1, 1, 1, \ldots\}$ sequence, one gets

$$\sqrt{2P}\sin(\Theta(0)), \sqrt{2P}\cos(\Theta(T_S)), \sqrt{2P}\sin(\Theta(2T_S)),$$

$$\sqrt{2P}\cos(\Theta(3T_S)), \sqrt{2P}\sin(\Theta(4T_S)),$$

$$\sqrt{2P}\cos(\Theta(5T_S)), \sqrt{2P}\sin(\Theta(6T_S)),$$

$$\sqrt{2P}\cos(\Theta(7T_S)), \sqrt{2P}\sin(\Theta(8T_S)),$$

$$\sqrt{2P}\cos(\Theta(9T_S)), \ \ldots$$

Note that this sequence alternates between samples of $I(t)$ and $Q(t)$ shown in Eqs. (18) and (19) with only a scaling factor difference. The above sequence can be simply expressed as

$$I(0), Q(T_S), I(2T_S), Q(3T_S), I(4T_S), Q(5T_S),$$

$$I(6T_S), Q(7T_S), I(8T_S), Q(9T_S), \ \ldots$$

Based on these results, the optimum implementation of the digital front end for the baseline design of the advanced transponder is shown in Fig. 7. As shown in this section, using the sampling frequency derived in Eq. (12), one can simplify the hardware. The hardware simplification is exactly the same as for the case when the sampling frequency is $4F_{IF}$ [9][4] except when using lower F_S, and hence lower power consumption.

IV. Design and Implementation of the Carrier Tracking Loop

A. Description of the Carrier APLL and Transformation Techniques

The block diagram of the analog carrier tracking loop for the Cassini DST is depicted in Fig. 8. Based on the current design, an architecture of the DPLL for computer simulation is developed. Presently, the analog carrier tracking loop is Type I, second order PLL with the following characteristics:

$$AK = \text{loop gain} = 2.4 \times 10^7 \tag{22}$$

$$B(S) = \frac{1}{(1+\tau_{RC}S)}, \tau_{RC} = 1.6 \times 10^{-5} \tag{23}$$

$$F(S) = \frac{1+\tau_2 S}{1+\tau_1 S}, \tau_1 = 4707, \tau_2 = 0.0442 \tag{24}$$

$$V(S) = \frac{1}{(1+\tau_V S)}, \tau_V = 1.0 \times 10^{-6} \tag{25}$$

$$K(S) = \frac{1}{S} \tag{26}$$

Note that $B(S)$ is the typical LPF, $F(S)$ is the loop filter, $V(S)$ is the rolloff filter of the voltage control oscillator (VCO), and $K(S)$ is the VCO integrator.

Let $G(S)$ be the transfer function of the analog loop defined as follows:

[4] Ibid.

$$G(S) = B(S)F(S)V(S) \tag{27}$$

From the analog characteristics of the loop, there are four different techniques (cases 1–4) to design the equivalent digital loop

(1) Bilinear Transformation Method. This method preserves the phase characteristics in the narrow passband when mapping the APLL into the digital domain with high sampling frequency. The mapping from analog (S-domain) to digital domain (Z-domain) can be achieved by direct substitution of the following equation into the analog transfer function [11–13]:

$$S = \frac{2}{T_S}\frac{(Z - 1)}{(Z + 1)} \tag{28}$$

(2) Impulse-Invariant Transformation Method. This mapping technique preserves the impulse response at the sampling points. The relationship between the S-variable and Z-variable is given by [12–13]

$$S = \frac{(Z-1)}{T_S Z} \tag{29}$$

However, the corresponding digital transfer function cannot be obtained by substituting Eq. (28) directly into the analog transfer function as in case (1) above. Let $g(t)$ be the impulse response of $G(S)$, i.e., $g(t) = L^{-1}\{G(S)\}$, where L^{-1} $\{.\}$ denotes the inverse Laplace transform of $\{.\}$. Thus, the digital approximation of the analog transfer function $G(S)$ is given by

$$G_D(Z) = T_S\left(z\{g(t)|_{t=nT_s}\}\right) \tag{30}$$

where $z\{.\}$ is the z-transform of $\{.\}$. Note that the analog transfer function $G(S)$ considered in this article is defined in Eq. (27).

(3) Step-Invariant Transformation Method. This method preserves the step response at the sampling points when mapping S-domain to Z-domain. The relationship between S- and Z-variables is given in [12]:

$$S = \frac{(Z-1)}{T_S} \tag{31}$$

Similar to case (2), the equivalent digital transfer function of the open loop cannot be found by substituting Eq. (31) directly into the analog transfer function. The relationship between the analog and digital transfer function is [12, 13]

$$G_D(Z) = \frac{Z-1}{Z}\left(z\left\{\left\lfloor L^{-1}\left[\frac{G(S)}{S}\right]\right\rfloor_{t=nT_S}\right\}\right) \tag{32}$$

where $z\{.\}$ and $G(S)$ are defined the same as above.

(4) Rational Transformation Method. This mapping technique is identical to the impulse-invariant transformation technique [11, 12].

B. Recursive Implementation of the Carrier DPLL

To obtain the digital approximation of the carrier APLL described in Section IV.A, each functional block in the analog loop, i.e., $B(S)$, $F(S)$, $V(S)$, and $K(S)$, can be mapped directly into the Z-domain using bilinear transformation or the composite function $B(S)F(S)V(S)$ using impulse-invariant (or step-invariant) transformation. These mappings are accomplished by applying Eqs. (28), (30), and (32), depending on the type of transformation used. Following are the recursive implementations of the digital transfer functions.

1. Recursive Implementation of $B(S)$, $F(S)$, $V(S)$, and $K(S)$ Using Bilinear Transformation. To obtain the digital approximation of the analog loop using bilinear transformation, one substitutes Eq. (28) into Eqs. (23)–(26) to get the Z-domain representations for the LPF $B(S)$, loop filter $F(S)$, VCO rolloff filter $V(S)$, and the integrator $K(S)$. The results are

$$B(Z) = \frac{(1 + Z^{-1})}{(A_{00}Z^{-1} + A_{11})} \tag{33}$$

$$F(Z) = \frac{(A_0 Z - B_0)}{(A_1 Z - B_1)} \tag{34}$$

$$K(Z) = \frac{T_S(Z+1)}{2(Z-1)} \tag{35}$$

where

$$A_{00} = 1 - C_0,\ A_{11} = 1 + C_0 \tag{36}$$

$$A_0 = 1 + a_o,\ A_1 = 1 + b_0,\ B_0 = a_0 - 1,\ B_1 = b_0 - 1 \tag{37}$$

and

$$C_0 = \frac{2\tau_{RC}}{T_S},\ a_0 = \frac{2\tau_2}{T_S},\ b_0 = \frac{2\tau_1}{T_S} \tag{38}$$

Note that the Z-domain representation for $V(S)$ is exactly the same as Eq. (33), except that C_0 is replaced by

$$C_0 = \frac{2\tau_V}{T_S} \tag{39}$$

The digital closed-loop transfer function, $H(Z)$, for this case is given by

$$H(Z) = \frac{AK\big(B(Z)F(Z)V(Z)K(Z)\big)}{\big[1 + AK\big(B(Z)F(Z)V(Z)K(Z)\big)\big]} \tag{40}$$

Plots of the analog and digital closed-loop phase and magnitude responses are shown in Figs. 9(a) and 9(b). These figures show that for sampling frequencies below 100 kHz, distortions in phase and magnitude can occur for the digital approximation loop. In addition, the figures show that for sampling frequencies greater than or equal to 100 kHz the response of the digital loop approaches that of the analog counterpart. Hence, the minimum sampling frequency for this case is 100 kHz. Figures 10(a), (b), and (c) show the recursive implementation of the LPF $B(Z)$, integrator $K(Z)$, and loop filter $F(Z)$.

The implementation of the rolloff filter $V(Z)$ is similar to that of the LPF $B(Z)$.

2. Recursive Implementation of the Analog Transfer Function *G(S)* and *K(S)* Using Impulse-Invariant Transformation. To obtain the equivalent digital approximation for the integrator $K(S)$, one substitutes Eq. (29) into Eq. (26) to get

$$K(Z) = \frac{ZT_S}{(Z-1)} \tag{41}$$

The digital approximation for the analog transfer function $G(S)$ (see Eq. (27)) is obtained by finding the inverse Laplace transform of $G(S)$ and then substituting the result into Eq. (30). Evaluating Eq. (30), one has

$$G_D(Z) = T_S \left[\frac{\alpha_0}{1 - Z^{-1}e^{-aT_S}} + \frac{\alpha_1}{1 - Z^{-1}e^{-bT_S}} + \frac{\alpha_2}{1 - Z^{-1}e^{-cT_S}} \right] \tag{42}$$

where

$$\alpha_0 = \frac{\tau_1 - \tau_2}{(\tau_1 - \tau_{RC})(\tau_1 - \tau_V)} \tag{43}$$

$$\alpha_1 = \frac{\tau_{RC} - \tau_2}{(\tau_{RC} - \tau_1)(\tau_{RC} - \tau_V)} \tag{44}$$

$$\alpha_2 = \frac{\tau_V - \tau_2}{(\tau_2 - \tau_1)(\tau_V - \tau_{RC})} \tag{45}$$

and

$$a = \frac{1}{\tau_1},\ b = \frac{1}{\tau_{RC}},\ c = \frac{1}{\tau_V} \tag{46}$$

The digital closed-loop transfer function for this case is given by

$$H(Z) = \frac{AK\big(G_D(Z)K(Z)\big)}{\big[1 + AK\big(G_D(Z)K(Z)\big)\big]} \tag{47}$$

From Eq. (47), the plots of the phase and magnitude responses can be obtained for the digital approximation loop. Figures 11(a) and 11(b) illustrate the closed-loop phase and magnitude responses for both analog and digital loops. The figures show that the response of the digital loop approximated by using impulse-invariant transformation is the same as the analog loop when the sampling frequency is higher than or equal to 100 kHz. When the sampling frequency is less than 100 kHz, the digital loop can encounter serious distortion in both phase and amplitude. The recursive implementations $G_D(Z)$ and $K(Z)$ using impulse-invariant transformation are shown in Figs. 12(a) and 12(b).

3. Recursive Implementation of the Analog Transfer Function $G(S)$ and $K(S)$ Using Step-Invariant Transformation. Digital approximations $K(Z)$ and $G_D(Z)$ for $K(S)$ and $G(S)$ using step invariant transformation can be obtained by using Eqs. (31) and (32). The results are

$$K(Z) = \frac{T_S}{(Z-1)} \tag{48}$$

$$G_D(Z) = \beta_0 + \beta_1 \left[\frac{1 - Z^{-1}}{1 - Z^{-1}e^{-aT_S}}\right] + \beta_2 \left[\frac{1 - Z^{-1}}{1 - Z^{-1}e^{-bT_S}}\right] + \beta_3 \left[\frac{1 - Z^{-1}}{1 - Z^{-1}e^{-cT_S}}\right] \tag{49}$$

where

$$\beta_0 = \frac{\alpha_0}{a} + \frac{\alpha_1}{b} + \frac{\alpha_2}{c} \tag{50}$$

$$\beta_1 = -\frac{\alpha_0}{a},\ \beta_2 = -\frac{\alpha_1}{b},\ \beta_3 = -\frac{\alpha_2}{c} \tag{51}$$

The parameters α_0, α_1, a, b, and c are defined in Eqs. (43)–(46), respectively. Again, Eq. (47) can be used to evaluate the closed-loop transfer function for this case. The plots of the closed-loop transfer functions for both analog and digital loops are shown in Figs. 13(a) and 13(b). The figures show that the magnitude response approaches the analog response when the sampling frequency is higher than or equal to 100 kHz. However, the phase response suffers serious distortion when the sampling frequency is less than 1 MHz. Thus, in order to achieve the same response as the analog loop, the digital approximation loop using step-invariant transformation must be sampled at least at 1 MHz, i.e., this method requires a 10 times higher sampling frequency than the previous methods. The recursive implementations of $G_D(Z)$ and $K(Z)$ using step-invariant transformation are shown in Figs. 14(a) and 14(b).

V. Conclusions and Future Work

This article presented preliminary results on the design and implementation of the baseline digital baseband architecture for future deep space transponders, and also presented trade studies on: (1) the number of bits required by the ADC, (2) the sampling and IF for hardware simplification, and (3) the optimum sampling technique. A conceptual implementation of the proposed optimum sampling technique was presented and discussed. In addition, the phase and amplitude responses of digital approximations of the analog loop were briefly investigated. It was found that in order to achieve the same closed-loop responses as the analog counterpart, the step-invariant transformation method requires a higher sampling frequency than the other methods.

Furthermore, this article identified various architectures for possible implementation of the digital carrier tracking loop. The architecture that was found to provide the smallest phase jitter and fastest response is appropriate for the advanced transponder.

Acknowledgments

The authors thank S. Kayalar for his useful comments and suggestions, C. Kyriacou and A. Kermode for their constant support, and S. Hinedi for many useful discussions on the implementation and design of the digital phase-locked loop.

References

[1] T. M. Nguyen, S. Kayalar, H.-G. Yeh, and C. Kyriacou, "Advanced Transponders for Deep Space Applications," *Proceedings of IEEE Conference on Aerospace Applications*, Steamboat Springs, Colorado, January 30–February 3, 1993.

[2] N. Mysoor, J. Perret, and A. Kermode, "An X-Band Spacecraft Transponder for Deep Space Applications-Design Concepts and Breadboard Performance," *IEEE Transactions on Microwave Theory and Techniques*, vol. 40, no. 6, pp. 1192–1198, June 1992.

[3] G. A. Gray and G. W. Zeoli, "Quantization and Saturation Noise Due to Analog-to-Digital Conversion," *IEEE Transactions on Aerospace and Electronics Systems*, vol. 7, no. 1, pp. 222–223, January 1971.

[4] R. Sadr and M. Shahshahani, "On Sampling Band-Pass Signal," *TDA Progress Report 42-96*, vol. October–December 1988, Jet Propulsion Laboratory, Pasadena, California, pp. 14–20, February 15, 1989.

[5] A. Kohlenberg, "Exact Interpolation of Bandlimited Functions," *J. Appl. Phys.*, vol. 24, no. 12, p. 1432, December 1953.

[6] J. L. Brown, Jr., "On Quadrature Sampling of Bandpass Signals," *IEEE Trans, Aer. Elec. Sys.*, vol. AES-15, no. 3, pp. 366–371, May 1979.

[7] C. E. Persons, "Quadrature Sampling Error Formula," *J. Acoust. Soc. Am.*, vol. 57, no. 2, p. 511, February 1975.

[8] T. Hack, "I/Q Sampling Yields Flexible Demodulators," *RF Design*, vol. 14, no. 4, pp. 40–43, April 1991.

[9] R. Cali and G. Ferrari, "Algorithms for Computing Phase and AGC in Digital PLL Receivers," *RF Design*, vol. 15, no. 11, pp. 33–40, October 1992.

[10] R. Sfeir, S. Aguirre, and W. J. Hurd, "Coherent Digital Demodulation of a Residual Carrier Signal Using IF Sampling," *TDA Progress Report 42-78*, vol. April–June 1984, Jet Propulsion Laboratory, Pasadena, California, pp. 135–142, August 15, 1984.

[11] L. R. Rabiner and B. Gold, *Theory and Applications of Digital Signal Processing*, Englewood Cliffs, New Jersey: Prentice-Hall, 1975.

[12] W. D. Stanley, *Digital Signal Processing*, Reston, Virginia: Reston Publishing Co., 1975.

[13] K. Ogata, *Discrete Time Control Systems*, Englewood Cliffs, New Jersey: Prentice-Hall, 1987.

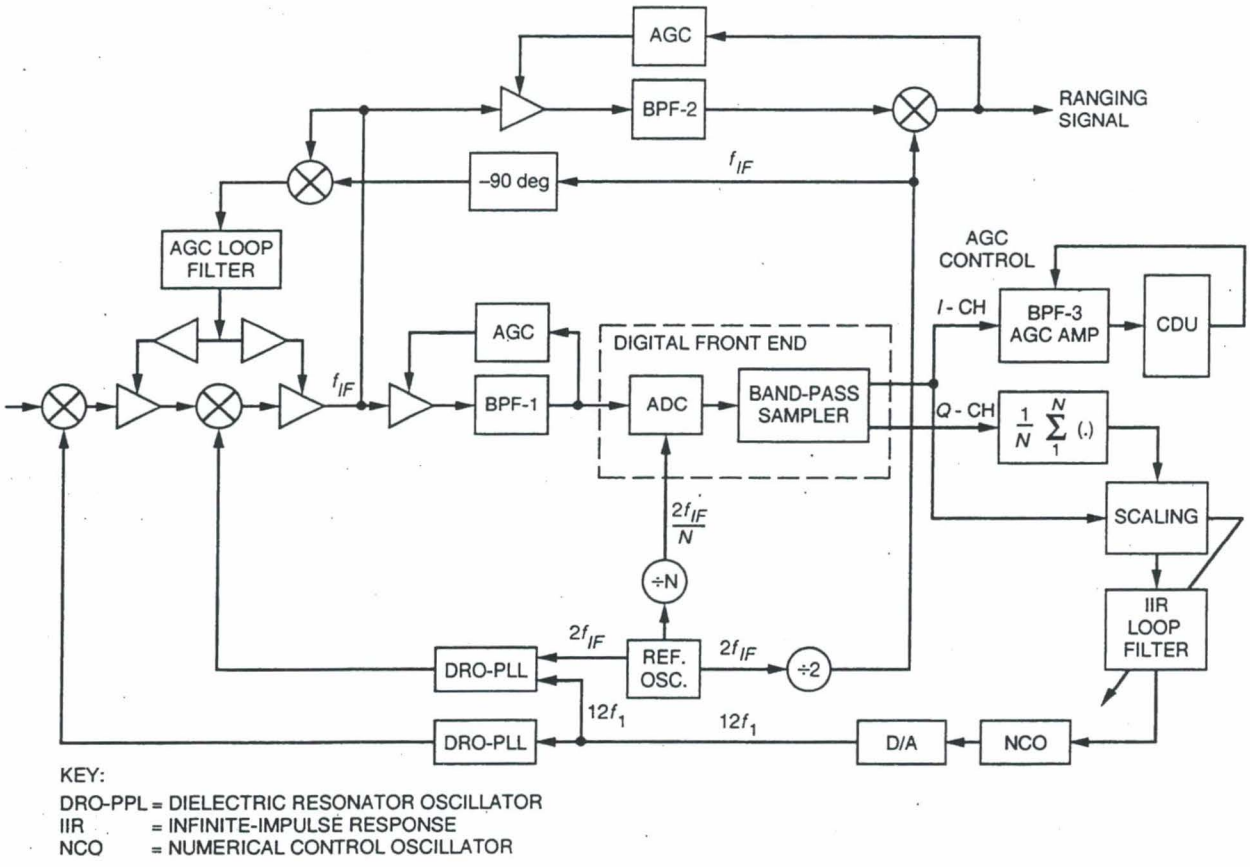

Fig. 1. Proposed baseline architecture for the advanced deep space transponder—a basic digital structure with analog turnaround ranging.

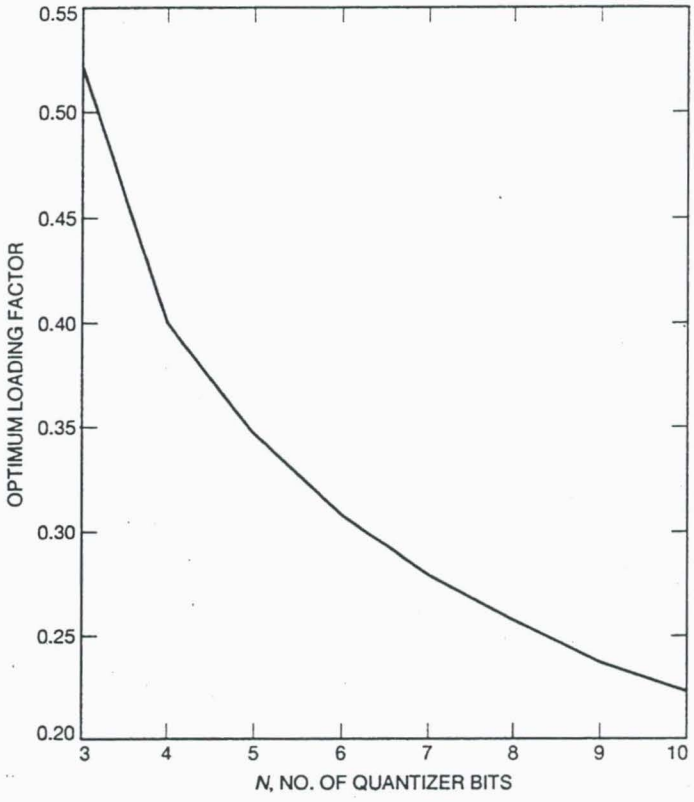

Fig. 2. Optimum loading factor as a function of *N*.

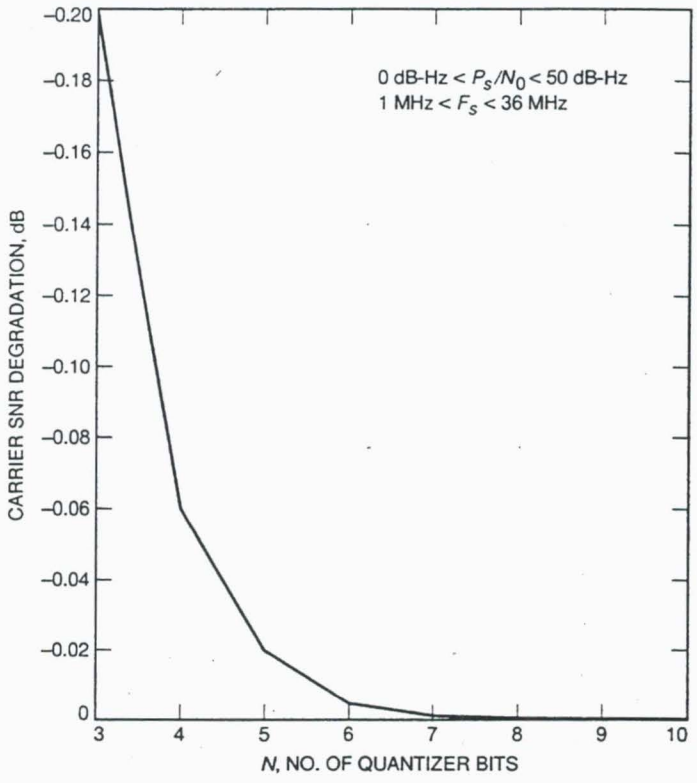

Fig. 3. Carrier SNR degradation as a function of *N*.

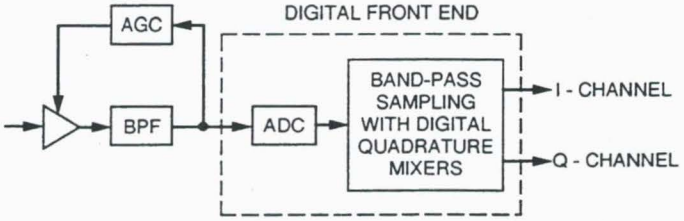

Fig. 4. A simplified block diagram of the proposed configuration for the digital front end of the transponder.

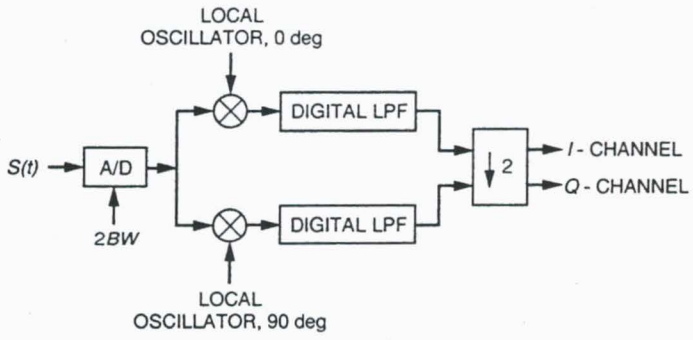

Fig. 5. I&Q sampling technique with digital quadrature mixers.

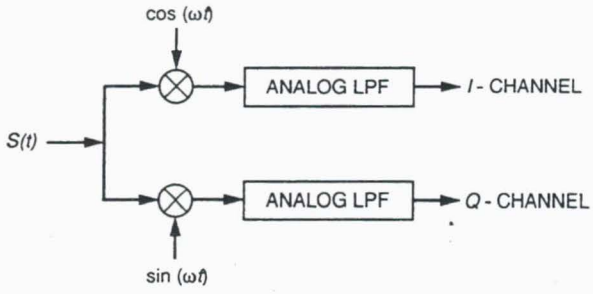

Fig. 6. I&Q extraction using the analog mixer approach.

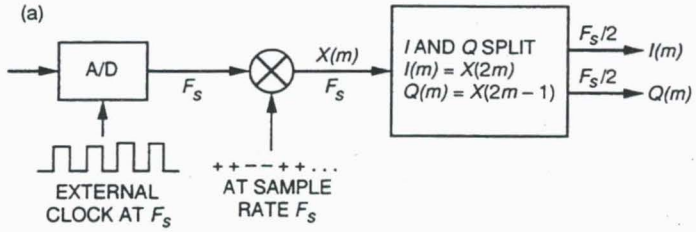

$$F_S = \frac{4F_{IF}}{(4n+1)}, \; n = 0,1,2,3, \ldots$$

$$n \leq \left[\frac{F_{IF}}{2BW} - \frac{1}{4} \right]$$

$[X]$ = SMALLEST INTEGER $\leq X$

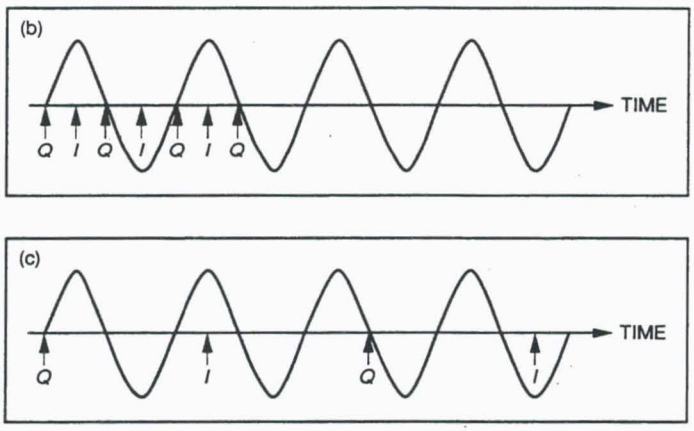

Fig. 7. Implementation and illustrations of the I&Q sampling technique: (a) proposed implementation using digital quadrature mixers; (b) illustration of over-sampling scheme, $F_C = 4F_{IF}$; and (c) illustration of under-sampling scheme, $F_S = \frac{4F_{IF}}{(4n+1)}$, $n = 6$.

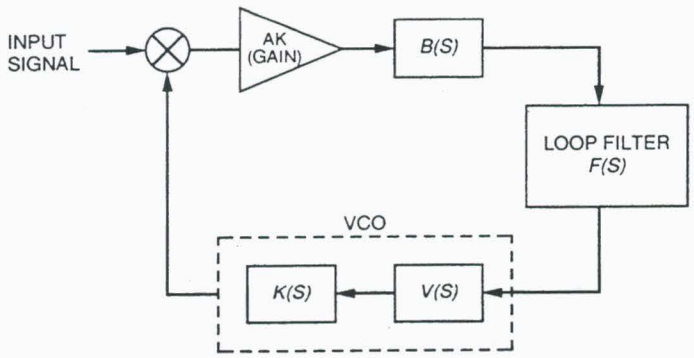

Fig. 8. Analog model of the Cassini carrier-tracking phase-locked loop—a short-loop version.

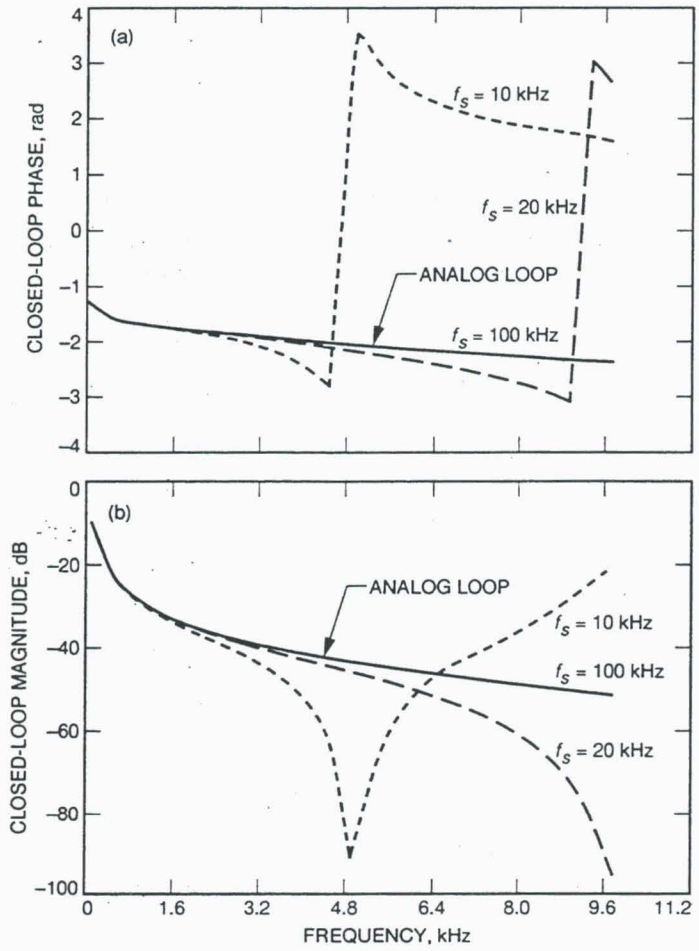

Fig. 9. Plots of two closed-loop responses for the digital loop using the bilinear transformation method: (a) phase response and (b) magnitude response.

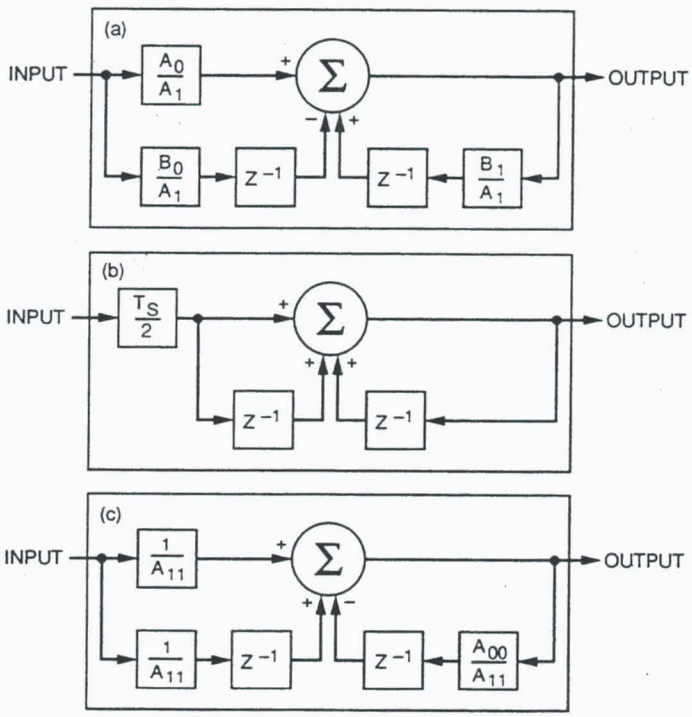

Fig. 10. Recursive implementation of the digital loop using the bilinear transformation method: (a) low-pass filter $B(Z)$, (b) integrator $K(Z)$, and (c) loop filter $F(Z)$.

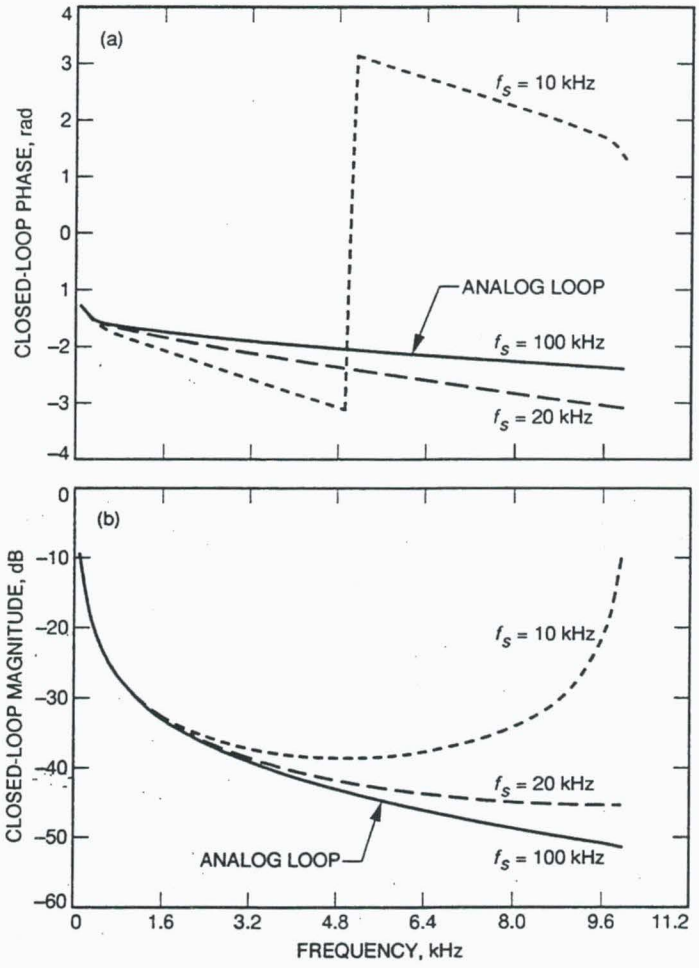

Fig. 11. Plots of two closed-loop responses for the digital loop using the impulse-invariant transformation method: (a) phase response and (b) magnitude response.

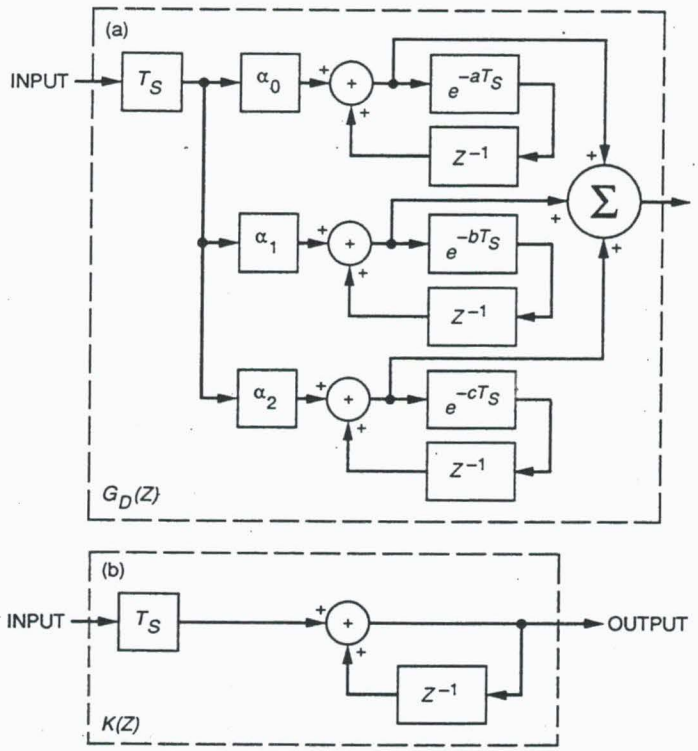

Fig. 12. Recursive implementation of the digital loop using the impulse-invariant transformation method: (a) open-loop transfer function $G_D(Z)$ and (b) integrator $K(Z)$.

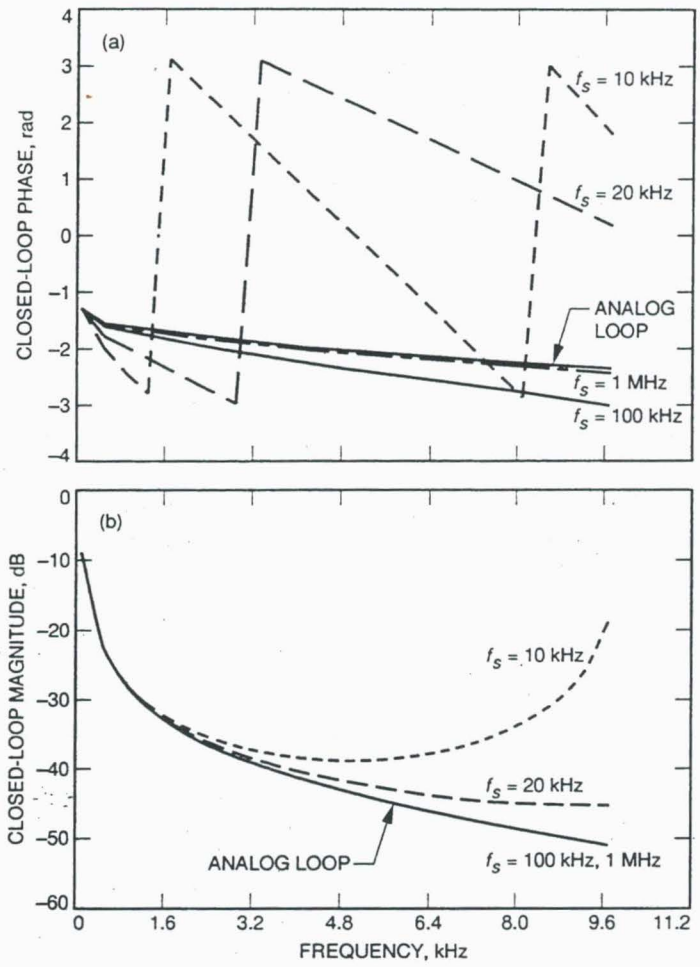

Fig. 13. Plots of two closed-loop responses for the digital loop using the step-invariant transformation method: (a) phase response and (b) magnitude response.

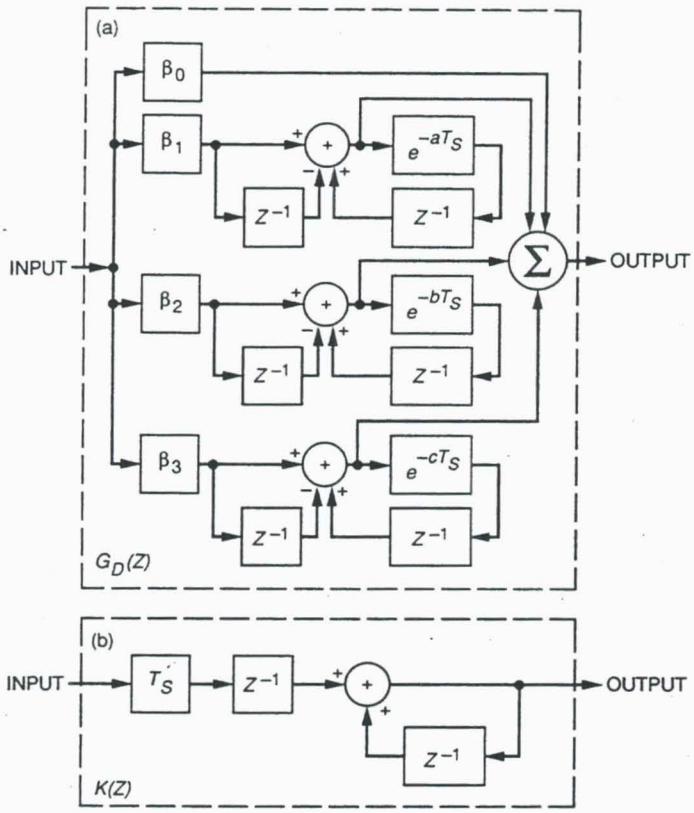

Fig. 14. Recursive implementation of the digital loop using the step-invariant transformation method: (a) open-loop transfer function $G_D(Z)$ and (b) integrator $K(Z)$.

Selection of Ka-Band Transponder Turnaround Frequency Ratios

John Alexander Koukos
National Aeronautics and Space Administration
Jet Propulsion Laboratory
California Institute of Technology
Pasadena, California

I. Introduction

The Consultative Committee for Space Data Systems (CCSDS) has issued recommendations specifying Transponder Turn-around Frequency Ratios (TTFR) for S-band and X-band coherent earth-to-space and space-to-earth links. The new transponders designed for missions such as NASA/JPL Cassini include downlink and/or uplink Ka-band links in the 31.8-32.3 GHz and 34.2-34.7 GHz bands respectively.

This paper summarizes the reasoning behind the selection of the 749/3344 TTFR for the X_{up}/Ka_{down} two-way links and the 3597/3344 or the 3599/3344 TTFR for the X_{up}/Ka_{down} two-way links by the Advanced Transponder Development Group at JPL. The transponder multiplier (TM) 749 has already been adopted by blue recommendations 2.6.2 and 2.6.6B as part of the X and X/S-band TTFRs 749/880 and 749/240 respectively. Thus only the selection of TMs 3344 and 3597 or 3599 will be discussed here and the optimum TTFR will be selected.

II. Coherent Frequency Channels

The deep space bands, for tracking support purposes, are subdivided into 42 channels associated with a given transponder ratio. The basis for the determination of these channels is the S-band downlink center frequency (2295 MHz) designated to channel 14 (total of 27 channels inside the S-band downlink allocation). Adjacent channels in the S-band downlink frequency range are spaced $\frac{10}{27}$ MHz apart, therefore a channel frequency is computed by subtracting $\frac{10}{27}$ MHz from the higher channel or adding $\frac{10}{27}$ MHz to the lower channel frequency :

$$F_{ch}(n\pm1) = F_{ch}(n) \pm \frac{10}{27}\ MHz, \quad n=2, \ldots,41 \tag{1}$$

where $F_{ch}(n)$ is the frequency in MHz of channel n with 6 decimal digits accuracy (to Hz level).

Channel frequencies f_{ch} for another band are generated by multiplying the corresponding S-band downlink channel frequency F_{ch} by the ratio TM/240 :

$$f_{ch}(n) = F_{ch} \times \frac{TM}{240} \qquad (2)$$

where TM is the transponder multiplier factor of that frequency band as shown in Table 1a.

Table 1a. Transponder Multipliers Factors

Frequency Band and Link	S Up	X Up	X Down	Ka Down *	Ka Up *	Ka Up *
TM	221	749	880	3344	3597	3599

* TM factor has not been adopted by the CCSDS yet.

Using equations (1) and (2) and the values of TMs in Table 1a above, a list of channel frequencies for deep space research bands S, X and Ka is generated in Table 1b.

III. Criteria for Selection of TTFR in the Ka Band

Criterion 1 : TMs that generate frequencies near the center of the Ka-band allocation should be selected. For this purpose, distances of mid-channel 21 from the center of the uplink (34450 MHz) and downlink (32050 MHz) bands are listed in Table 2 for all uplink (3563-3635) and downlink (3314-3386) TMs. As seen in Table 2, uplink TM 3599 and downlink TM 3348 generate the shortest distances (4.31 and 1.41 MHz respectively) for channel 21 from the centers of the Ka-bands.

Criterion 2 : The selection of a TTFR should provide the maximum number of channels for simultaneous coherent operation within the boundaries allocated for deep space research for the following combination of bands :

A. X band in the uplink and X and Ka bands in the downlink ;

B. X in the uplink and Ka band in the downlink.

C. Ka band in the uplink and X and Ka bands in the downlink ;

Tables 3a, 3b and 3c list all combinations of uplink versus downlink TMs that generate frequencies according to the criteria 1A, 1B and 1C above respectively. Each table entry contains 3 numbers, the first number is the total number of coherent channels per TTFR, the second and the third numbers are the first and the last coherent channel numbers respectively (in the sense of Table 2 channel enumeration) for the same TTFR. As shown in :

a. Table 3a, uplink TMs 3563-3635 and downlink TMs 3332-3364 form 17×37=629 TTFRs with a (maximum) number of 35 coherent channels according to criterion 1A above;

b. Table 3b, uplink TMs 3563-3635 and downlink TMs 3334-3364 form 16×37=592 TTFRs with a (maximum) number of 37 coherent channels according to criterion 1B above ;

c. Table 3c, uplink TMs 3583-3611 and downlink TMs 3332-3364 form 17×15=255 TTFRs with a (maximum) number of 37 coherent channels according to criterion 1C above.

Criterion 3 : The uplink factor should be an odd multiple of the base frequency and the downlink factor should be an even multiple of the base frequency to avoid feeding downlink RF spurious signals to the uplink RF channels inside the transponder or via the S/C microwave path including the S/C antennas. Similarly, the first IF should be an odd multiple of the base frequency, while the Local Oscillator (LO) should be an even multiple of the base frequency.

Criterion 4 : The downlink multiplication factor is generated by cascaded "×N" multipliers in a high-to-low order multiplication chain. Each multiplier is followed by a passive bandpass filters able to reject all other than the N-th harmonic. In such case the multiplication factor N cannot be higher than 19, because the BPF cannot be made arbitrarily narrow in order to reject all adjacent harmonics. Tables 4a,b list the prime multiplication factors for uplink and downlink TMs. The downlink TMs with prime multiplication factors ≤ 19 are the following :

3328, 3332, 3344, 3360, 3366, and 3380.

Of the above candidate downlink TMs only 3344 and 3360 satisfy maximum channel coherence criterion 2. However lately, usage of a Dielectric Resonator Oscillator (DRO) controlled by phase lock loop (PLL), in either single or double IF stage Advanced Transponder designs, made possible multiplication factors much higher than 19 (e.g. 73 in the Cassini Transponder), because the PLL acts as a very narrowband filter rejecting all other spurious harmonics.
The multiplier chain implementations of the chosen factors use the same downlink and first local oscillator prime factor in order to minimize the delay in the spacecraft receiver's closed loop path. If multiplication factors ≤ 19 are not found, only then different downlink and first LO factors are implemented (see Figures 1-6).

Criterion 5 : The chosen downlink TM should allow a maximum VCO multiplier implementation flexibility. Of the above downlink TMs, TM 3332 can be implemented with VCO frequencies 2F1 and 4F1, TM 3344 with 2F1, 4F1 and 8F1 and 3360 with 2F1, 4F1, 6F1, 8F1, 10F1 and 12F1, where F1 is the base frequency (e.g. F1=9542438 Hz).

Criterion 6 : An Automatic Gain Control (AGC) performance limitation requires an upper boundary of 2.5 GHz for the first IF frequency. However, an AGC implementation in a more recent Advanced Transponder design allows up to 10 GHz. Also a lower boundary of 250 MHz is necessary due to wide turnaround ranging limitations. Table 5 lists the uplink factors for a given downlink factor and specified VCO frequency.

Criterion 7 : The turnaround ratio separation should be greater than 7% to assure a realizable diplexer and to minimize diplexer implementation losses and cost. Table 6 lists the satisfactory ratios for a specified Voltage Controlled Oscillator (VCO) frequency.

Criterion 8 : The selected downlink TMs should generate channels that avoid potential interference with the intersatellite service allocation in the 32-33 GHz band. Table 8 lists all downlink TMs versus the number of channels generated in the [31.8, 32] GHz band, non-overlapping with the intersatellite service allocation. As shown in Table 7, downlink TM 3332 generates a maximum number of 39 channels in the Ka-band downlink allocation below 32 GHz, TM 3328 generates 33 and TM 3344 generates 18 such channels. All the other candidate downlink TM (3360, 3366 and 3380) channels do interfere with the intersatellite band, [Ref. 3].

Criterion 9 : If Differential One-Way Ranging (DOR) tones are part of the spacecraft downlink signaling scheme, then a downlink TM is selected so that the downlink carrier together with the DOR tones fall within the Ka-band deep space allocation. For example, if a maximum DOR tone generation capability of ±100 MHz from the carrier is required, then the available downlink frequency range is reduced to 31.9-32.2 GHz. In this case downlink TM 3332 can only be implemented for channels 22-37, TM 3344 for channels 5-37 and 3360 for channels 5-28, [Ref. 2].

IV. Proposed Frequency Schemes

Next a series of Transponder Frequency Schematics illustrates the merits of the investigated TTFRs 3597/3344, 3599/3344 and 749/3344, [Ref. 4].

Figures 1-6 show Ka-Up/Ka-Down frequency schemes, implemented with **Cascaded Multipliers** ≤19, for the 3597/3344 and 3599/3344 TTFRs, using criteria 2 and 3. The TMs used for uplink, downlink, first Local Oscillator (LO), and first IF are listed in Tables 8 a,b. VCO frequencies used are 2F1, 4F1 and 8F1.

Figures 7-12 show Ka-band transponder implementations using **DROs**.

Specifically, Figure 7 implementation has a TTFR=3599/3344, with double conversion, Ka- and S-band DROs and Ka-band Phase Modulator (PM). Both receiver DROs are phase-locked from the 12F1 Voltage Controlled Crystall Oscillator (VCXO). The receiver fixed frequency oscillator is 2F2, in the coherent mode and 12F0 in the non-coherent mode.

In Figure 8, TTFR=3599/3344, with single conversion, a Ka-band DRO and Ka-band PM. The DRO is phased locked from the 12F1 and the receiver fixed frequency oscillator is 2F2. The non-coherent mode uses a 12F0 oscillator. This design can also be implemented for the 3597/3344 TTFR.

In Figure 9, TTFR=3597/3344, with double conversion, a Ka-band and S-band DROs, and a Ka-band PM. Both DROs are phase-locked from the 11F1 , and the receiver fixed frequency reference oscillator is 2F2. The non-coherent DRO is locked to a 11F0 oscillator. The 11F1 and 11F0 oscillators are used to reduce the complexity of LO and non-coherent carrier generation circuitry.

In Figure 10, TTFR=3597/3344, with single conversion, a Ka-band DRO and a Ka-band PM. The DRO is phase-locked from the 11F1 , and the receiver fixed frequency reference oscillator

is 2F2 for the coherent mode. The non-coherent mode uses a 11F0 oscillator.

Notice that the dual conversion designs (Fig 7, 9) require two LO loops in the receiver and are more complex than the single conversion designs. The two single conversion designs (Fig 8,10) require tighter filtering but only one LO loop.

Figure 11 depicts a DRO implementation of X/Ka band Reduced Function Transponder, TTFR=749/3344, featuring double conversion with a UHF Coaxial Resonator Oscillator (CRO), and an X-band PM. The CRO is phase-locked from a 12F1, and the reference oscillator is 2F2. Since the downlink TM 3344 is also an integer multiple of 11, the use of 11F0 oscillator reduces the complexity of the non-coherent carrier generation circuitry. The design eliminates a Ka-band DRO and other loop components to reduce complexity, size, mass, power and cost.

Finally, Figure 12 illustrates the usage of DROs in the design of an X-band Transponder upgrade with two Ka-band front end modules heterodyning the uplink from 3599F1 to 749F1 and the downlink from 880F1 to 3344F1. The X-band module features a double conversion, with an X-band DRO and an L-band Surface acoustic wave Resonator Oscillator (SRO).

V. Conclusions

TTFR 3599/3344 is the desired choice because :

1. For uplink TM 3599 the distance of mid-channel 21 from the center of the uplink band (34.45 GHz) is the shortest = 4.31 MHz. For downlink TM 3344 the distance of mid-channel 21 from the center of the downlink band (32.05 GHz) is the fourth shortest = 36.87 MHz (Criterion 1).

2. Provides a maximum number of coherent channels (Criterion 2).

3. TM 3599 is an odd number and TM 3344 is an even number (Criterion 3).

4. TM 3344 allows implementations with cascaded multipliers because it contains factors ≤ 19 : $3344 = 2 \times 2 \times 2 \times 2 \times 11 \times 19$ and $3599\text{-}3344 = 255 = 3 \times 5 \times 17$. Also DRO implementations are possible at a greater cost (Criterion 4).

5. TM 3344 allows VCO implementation with frequencies 2F1, 4F1 and 8F1 (Criterion 5).

6. Allows AGC implementations with VCO frequencies 2F1, 4F1 and 8F1 (Criterion 6).

7. Turnaround Ratio Separation $= \frac{3599-3344}{3599} = 14.11\% > 7\%$ (Criterion 7).

8. TM 3344 creates 18 channels non-interfering with the intersatellite band (Criterion 8).

9. TM 3344 creates 33 channels that contain 100 MHz DOR tones inside the downlink Ka-band allocation (Criterion 9).

VI. Acknowledgment

I wish to acknowledge the contributions of F. Davarian, D. Bishop (JPL Telecommunications Systems Section 339) and A. Kermode, N. Mysoor, E. Watson, C. Kyriakou, J. Lane (Spacecraft Telecommunications Equipment Section 336), in putting together this paper.

The research described in this paper was carried out by the Jet Propulsion Laboratory, California Institute of Technology, under contract with the National Aeronautics and Space Administration.

VII. References

1. N. R. Mysoor, J. D. Perret, and A. W. Kermode, "An X-Band Spacecraft Transponder for Deep Space Applications - Design Concepts and Breadboard Performance," IEEE Trans. Microwave Theory Tech., vol MTT-40, no. 6, pp. 1192-1198, June 1992.

2. R. Y. Watson and A. W. Kermode, "Transponder Implementation of Channel Plan Frequency Turnaround Ratio", IOM 336-90-210, internal document, December 19, 1992.

3. D. F. Bishop, "Turnaround Ratios for Deep Space Network Systems at Ka-Band," JPL IOM 3396-90-89, internal document, November 19, 1990.

4. Advanced Transponder Development/FY 92 End Year Report, JPL D-10515, internal document.

24-Aug-93 J. A. KOUKOS

TABLE 1b : DSN CHANNEL FREQUENCIES IN THE S, X AND Ka BANDS

TM => CHANNEL #	S-Band Up 221	S-Band Down, MHz 240	X-Band Up, MHz 749	X-Band Down, MHz 880	Ka-Band Down, MHz 3344	Ka-Band Up, MHz 3597	Ka-Band Up, MHz 3599	Ka-Band Up, MHz 3583	Ka-Band Down, MHz 3332
1		2290.185185	7147.286265	8397.345679	31909.913580	34324.150463	34343.235340	34190.556327	31795.404321
2		2290.555556	7148.442130	8398.703704	31915.074074	34329.701389	34348.789352	34196.085648	31800.546296
3		2290.925926	7149.597994	8400.061728	31920.234568	34335.252315	34354.343364	34201.614969	31805.688272
4		2291.296296	7150.753858	8401.419753	31925.395062	34340.803241	34359.897377	34207.144290	31810.830247
5	2110.243056	2291.666667	7151.909722	8402.777778	31930.555556	34346.354167	34365.451389	34212.673611	31815.972222
6	2110.584105	2292.037037	7153.065586	8404.135802	31935.716049	34351.905093	34371.005401	34218.202932	31821.114198
7	2110.925154	2292.407407	7154.221451	8405.493827	31940.876543	34357.456019	34376.559414	34223.732253	31826.256173
8	2111.266204	2292.777778	7155.377315	8406.851852	31946.037037	34363.006944	34382.113426	34229.261574	31831.398148
9	2111.607253	2293.148148	7156.533179	8408.209877	31951.197531	34368.557870	34387.667438	34234.790895	31836.540123
10	2111.948302	2293.518519	7157.689043	8409.567901	31956.358025	34374.108796	34393.221451	34240.320216	31841.682099
11	2112.289352	2293.888889	7158.844907	8410.925926	31961.518519	34379.659722	34398.775463	34245.849537	31846.824074
12	2112.630401	2294.259259	7160.000772	8412.283951	31966.679012	34385.210648	34404.329475	34251.378858	31851.966049
13	2112.971451	2294.629630	7161.156636	8413.641975	31971.839506	34390.761574	34409.883488	34256.908179	31857.108025
14	2113.312500	2295.000000	7162.312500	8415.000000	31977.000000	34396.312500	34415.437500	34262.437500	31862.250000
15	2113.653549	2295.370370	7163.468364	8416.358025	31982.160494	34401.863426	34420.991512	34267.966821	31867.391975
16	2113.994599	2295.740741	7164.624228	8417.716049	31987.320988	34407.414352	34426.545525	34273.496142	31872.533951
17	2114.335648	2296.111111	7165.780093	8419.074074	31992.481481	34412.965278	34432.099537	34279.025463	31877.675926
18	2114.676698	2296.481481	7166.935957	8420.432099	31997.641975	34418.516204	34437.653549	34284.554784	31882.817901
19	2115.017747	2296.851852	7168.091821	8421.790123	32002.802469	34424.067130	34443.207562	34290.084105	31887.959877
20	2115.358796	2297.222222	7169.247685	8423.148148	32007.962963	34429.618056	34448.761574	34295.613426	31893.101852
21	2115.699846	2297.592593	7170.403549	8424.506173	32013.123457	34435.168981	34454.315586	34301.142747	31898.243827
22	2116.040895	2297.962963	7171.559414	8425.864198	32018.283951	34440.719907	34459.869599	34306.672068	31903.385802
23	2116.381944	2298.333333	7172.715278	8427.222222	32023.444444	34446.270833	34465.423611	34312.201389	31908.527778
24	2116.722994	2298.703704	7173.871142	8428.580247	32028.604938	34451.821759	34470.977623	34317.730710	31913.669753
25	2117.064043	2299.074074	7175.027006	8429.938272	32033.765432	34457.372685	34476.531636	34323.260031	31918.811728
26	2117.405093	2299.444444	7176.182870	8431.296296	32038.925926	34462.923611	34482.085648	34328.789352	31923.953704
27	2117.746142	2299.814815	7177.338735	8432.654321	32044.086420	34468.474537	34487.639660	34334.318673	31929.095679
28	2118.087191	2300.185185	7178.494599	8434.012346	32049.246914	34474.025463	34493.193673	34339.847994	31934.237654
29	2118.428241	2300.555556	7179.650463	8435.370370	32054.407407	34479.576389	34498.747685	34345.377315	31939.379630
30	2118.769290	2300.925926	7180.806327	8436.728395	32059.567901	34485.127315	34504.301698	34350.906636	31944.521605
31	2119.110340	2301.296296	7181.962191	8438.086420	32064.728395	34490.678241	34509.855710	34356.435957	31949.663580
32	2119.451389	2301.666667	7183.118056	8439.444444	32069.888889	34496.229167	34515.409722	34361.965278	31954.805556
33	2119.792438	2302.037037	7184.273920	8440.802469	32075.049383	34501.780093	34520.963735	34367.494599	31959.947531
34		2302.407407	7185.429784	8442.160494	32080.209877	34507.331019	34526.517747	34373.023920	31965.089506
35		2302.777778	7186.585648	8443.518519	32085.370370	34512.881944	34532.071759	34378.553241	31970.231481
36		2303.148148	7187.741512	8444.876543	32090.530864	34518.432870	34537.625772	34384.082562	31975.373457
37		2303.518519	7188.897377	8446.234568	32095.691358	34523.983796	34543.179784	34389.611883	31980.515432
38		2303.888889	7190.053241	8447.592593	32100.851852	34529.534722	34548.733796	34395.141204	31985.657407
39		2304.259259	7191.209105	8448.950617	32106.012346	34535.085648	34554.287809	34400.670525	31990.799383
40		2304.629630	7192.364969	8450.308642	32111.172840	34540.636574	34559.841821	34406.199846	31995.941358
41		2305.000000	7193.520833	8451.666667	32116.333333	34546.187500	34565.395833	34411.729167	32001.083333
42		2305.370370	7194.676698	8453.024691	32121.493827	34551.738426	34570.949846	34417.258488	32006.225309
Deep-	2110	2290	7145	8400	31800	34200	34200	34200	31800
Alloc	2120	2300	7190	8450	32300	34700	34700	34700	32300
Near	2025	2200	7190	8450	32000	<== intersatellite	======>		32000
Alloc	2110	2290	7235	8500	33000	service			33000

Table 2 : Mid Channel 21 Distance in MHz from the Center of Ka-Band versus Transponder Multiplier (TM).

U/L TM	Distance, MHz	U/L TM	Distance, MHz	D/L TM	Distance, MHz	D/L TM	Distance, MHz
3563	-340.324	3601	23.4609	3314	-324.076	3352	39.709
3565	-321.176	3603	42.6094	3316	-304.93	3354	58.8555
3567	-302.031	3605	61.7539	3318	-285.783	3356	78.002
3569	-282.887	3607	80.9023	3320	-266.637	3358	97.1484
3571	-263.738	3609	100.0469	3322	-247.49	3360	116.295
3573	-244.59	3611	119.195	3324	-228.344	3362	135.441
3575	-225.445	3613	138.34	3326	-209.195	3364	154.59
3577	-206.297	3615	157.488	3328	-190.051	3366	173.736
3579	-187.152	3617	176.633	3330	-170.904	3368	192.881
3581	-168.004	3619	195.781	3332	-151.756	3370	212.029
3583	-148.859	3621	214.926	3334	-132.611	3372	231.176
3585	-129.711	3623	234.074	3336	-113.465	3374	250.32
3587	-110.566	3625	253.223	3338	-94.3164	3376	269.469
3589	-91.418	3627	272.367	3340	-75.1699	3378	288.615
3591	-72.2695	3629	291.516	3342	-56.0254	3380	307.76
3593	-53.125	3631	310.66	3344	-36.877	3382	326.908
3595	-33.9805	3633	329.805	3346	-17.7305	3384	346.055
3597	-14.832	3635	348.953	3348	1.41602	3386	365.201
3599	4.31641			3350	20.5625		

30-Jul-93 J. A. Koukos

Table 3a : X-up/X, Ka down

downlink\uplink	3563			3565			3567			3569			3571			3573			3575			3577			3579		
3314	2	36	37	2	36	37	2	36	37	2	36	37	2	36	37	2	36	37	2	36	37	2	36	37	2	36	37
3316	6	32	37	6	32	37	6	32	37	6	32	37	6	32	37	6	32	37	6	32	37	6	32	37	6	32	37
3318	10	28	37	10	28	37	10	28	37	10	28	37	10	28	37	10	28	37	10	28	37	10	28	37	10	28	37
3320	13	25	37	13	25	37	13	25	37	13	25	37	13	25	37	13	25	37	13	25	37	13	25	37	13	25	37
3322	17	21	37	17	21	37	17	21	37	17	21	37	17	21	37	17	21	37	17	21	37	17	21	37	17	21	37
3324	21	17	37	21	17	37	21	17	37	21	17	37	21	17	37	21	17	37	21	17	37	21	17	37	21	17	37
3326	24	14	37	24	14	37	24	14	37	24	14	37	24	14	37	24	14	37	24	14	37	24	14	37	24	14	37
3328	28	10	37	28	10	37	28	10	37	28	10	37	28	10	37	28	10	37	28	10	37	28	10	37	28	10	37
3330	32	6	37	32	6	37	32	6	37	32	6	37	32	6	37	32	6	37	32	6	37	32	6	37	32	6	37
3332	35	3	37	35	3	37	35	3	37	35	3	37	35	3	37	35	3	37	35	3	37	35	3	37	35	3	37
3334	35	3	37	35	3	37	35	3	37	35	3	37	35	3	37	35	3	37	35	3	37	35	3	37	35	3	37
3336	35	3	37	35	3	37	35	3	37	35	3	37	35	3	37	35	3	37	35	3	37	35	3	37	35	3	37
3338	35	3	37	35	3	37	35	3	37	35	3	37	35	3	37	35	3	37	35	3	37	35	3	37	35	3	37
3340	35	3	37	35	3	37	35	3	37	35	3	37	35	3	37	35	3	37	35	3	37	35	3	37	35	3	37
3342	35	3	37	35	3	37	35	3	37	35	3	37	35	3	37	35	3	37	35	3	37	35	3	37	35	3	37
3344	35	3	37	35	3	37	35	3	37	35	3	37	35	3	37	35	3	37	35	3	37	35	3	37	35	3	37
3346	35	3	37	35	3	37	35	3	37	35	3	37	35	3	37	35	3	37	35	3	37	35	3	37	35	3	37
3348	35	3	37	35	3	37	35	3	37	35	3	37	35	3	37	35	3	37	35	3	37	35	3	37	35	3	37
3350	35	3	37	35	3	37	35	3	37	35	3	37	35	3	37	35	3	37	35	3	37	35	3	37	35	3	37
3352	35	3	37	35	3	37	35	3	37	35	3	37	35	3	37	35	3	37	35	3	37	35	3	37	35	3	37
3354	35	3	37	35	3	37	35	3	37	35	3	37	35	3	37	35	3	37	35	3	37	35	3	37	35	3	37
3356	35	3	37	35	3	37	35	3	37	35	3	37	35	3	37	35	3	37	35	3	37	35	3	37	35	3	37
3358	35	3	37	35	3	37	35	3	37	35	3	37	35	3	37	35	3	37	35	3	37	35	3	37	35	3	37
3360	35	3	37	35	3	37	35	3	37	35	3	37	35	3	37	35	3	37	35	3	37	35	3	37	35	3	37
3362	35	3	37	35	3	37	35	3	37	35	3	37	35	3	37	35	3	37	35	3	37	35	3	37	35	3	37
3364	35	3	37	35	3	37	35	3	37	35	3	37	35	3	37	35	3	37	35	3	37	35	3	37	35	3	37
3366	33	3	35	33	3	35	33	3	35	33	3	35	33	3	35	33	3	35	33	3	35	33	3	35	33	3	35
3368	29	3	31	29	3	31	29	3	31	29	3	31	29	3	31	29	3	31	29	3	31	29	3	31	29	3	31
3370	26	3	28	26	3	28	26	3	28	26	3	28	26	3	28	26	3	28	26	3	28	26	3	28	26	3	28
3372	22	3	24	22	3	24	22	3	24	22	3	24	22	3	24	22	3	24	22	3	24	22	3	24	22	3	24
3374	18	3	20	18	3	20	18	3	20	18	3	20	18	3	20	18	3	20	18	3	20	18	3	20	18	3	20
3376	15	3	17	15	3	17	15	3	17	15	3	17	15	3	17	15	3	17	15	3	17	15	3	17	15	3	17
3378	11	3	13	11	3	13	11	3	13	11	3	13	11	3	13	11	3	13	11	3	13	11	3	13	11	3	13
3380	7	3	9	7	3	9	7	3	9	7	3	9	7	3	9	7	3	9	7	3	9	7	3	9	7	3	9
3382	4	3	6	4	3	6	4	3	6	4	3	6	4	3	6	4	3	6	4	3	6	4	3	6	4	3	6
3384	0	0	0	0	0	0	0	0	0	0	0	0	0	0	0	0	0	0	0	0	0	0	0	0	0	0	0
3386	0	0	0	0	0	0	0	0	0	0	0	0	0	0	0	0	0	0	0	0	0	0	0	0	0	0	0

Table 3a : X-up/X, Ka down (cont)

downlink\uplink	3581			3583			3585			3587			3589			3591			3593			3595			3597		
3314	2	36	37	2	36	37	2	36	37	2	36	37	2	36	37	2	36	37	2	36	37	2	36	37	2	36	37
3316	6	32	37	6	32	37	6	32	37	6	32	37	6	32	37	6	32	37	6	32	37	6	32	37	6	32	37
3318	10	28	37	10	28	37	10	28	37	10	28	37	10	28	37	10	28	37	10	28	37	10	28	37	10	28	37
3320	13	25	37	13	25	37	13	25	37	13	25	37	13	25	37	13	25	37	13	25	37	13	25	37	13	25	37
3322	17	21	37	17	21	37	17	21	37	17	21	37	17	21	37	17	21	37	17	21	37	17	21	37	17	21	37
3324	21	17	37	21	17	37	21	17	37	21	17	37	21	17	37	21	17	37	21	17	37	21	17	37	21	17	37
3326	24	14	37	24	14	37	24	14	37	24	14	37	24	14	37	24	14	37	24	14	37	24	14	37	24	14	37
3328	28	10	37	28	10	37	28	10	37	28	10	37	28	10	37	28	10	37	28	10	37	28	10	37	28	10	37
3330	32	6	37	32	6	37	32	6	37	32	6	37	32	6	37	32	6	37	32	6	37	32	6	37	32	6	37
3332	35	3	37	35	3	37	35	3	37	35	3	37	35	3	37	35	3	37	35	3	37	35	3	37	35	3	37
3334	35	3	37	35	3	37	35	3	37	35	3	37	35	3	37	35	3	37	35	3	37	35	3	37	35	3	37
3336	35	3	37	35	3	37	35	3	37	35	3	37	35	3	37	35	3	37	35	3	37	35	3	37	35	3	37
3338	35	3	37	35	3	37	35	3	37	35	3	37	35	3	37	35	3	37	35	3	37	35	3	37	35	3	37
3340	35	3	37	35	3	37	35	3	37	35	3	37	35	3	37	35	3	37	35	3	37	35	3	37	35	3	37
3342	35	3	37	35	3	37	35	3	37	35	3	37	35	3	37	35	3	37	35	3	37	35	3	37	35	3	37
3344	35	3	37	35	3	37	35	3	37	35	3	37	35	3	37	35	3	37	35	3	37	35	3	37	35	3	37
3346	35	3	37	35	3	37	35	3	37	35	3	37	35	3	37	35	3	37	35	3	37	35	3	37	35	3	37
3348	35	3	37	35	3	37	35	3	37	35	3	37	35	3	37	35	3	37	35	3	37	35	3	37	35	3	37
3350	35	3	37	35	3	37	35	3	37	35	3	37	35	3	37	35	3	37	35	3	37	35	3	37	35	3	37
3352	35	3	37	35	3	37	35	3	37	35	3	37	35	3	37	35	3	37	35	3	37	35	3	37	35	3	37
3354	35	3	37	35	3	37	35	3	37	35	3	37	35	3	37	35	3	37	35	3	37	35	3	37	35	3	37
3356	35	3	37	35	3	37	35	3	37	35	3	37	35	3	37	35	3	37	35	3	37	35	3	37	35	3	37
3358	35	3	37	35	3	37	35	3	37	35	3	37	35	3	37	35	3	37	35	3	37	35	3	37	35	3	37
3360	35	3	37	35	3	37	35	3	37	35	3	37	35	3	37	35	3	37	35	3	37	35	3	37	35	3	37
3362	35	3	37	35	3	37	35	3	37	35	3	37	35	3	37	35	3	37	35	3	37	35	3	37	35	3	37
3364	35	3	37	35	3	37	35	3	37	35	3	37	35	3	37	35	3	37	35	3	37	35	3	37	35	3	37
3366	33	3	35	33	3	35	33	3	35	33	3	35	33	3	35	33	3	35	33	3	35	33	3	35	33	3	35
3368	29	3	31	29	3	31	29	3	31	29	3	31	29	3	31	29	3	31	29	3	31	29	3	31	29	3	31
3370	26	3	28	26	3	28	26	3	28	26	3	28	26	3	28	26	3	28	26	3	28	26	3	28	26	3	28
3372	22	3	24	22	3	24	22	3	24	22	3	24	22	3	24	22	3	24	22	3	24	22	3	24	22	3	24
3374	18	3	20	18	3	20	18	3	20	18	3	20	18	3	20	18	3	20	18	3	20	18	3	20	18	3	20
3376	15	3	17	15	3	17	15	3	17	15	3	17	15	3	17	15	3	17	15	3	17	15	3	17	15	3	17
3378	11	3	13	11	3	13	11	3	13	11	3	13	11	3	13	11	3	13	11	3	13	11	3	13	11	3	13
3380	7	3	9	7	3	9	7	3	9	7	3	9	7	3	9	7	3	9	7	3	9	7	3	9	7	3	9
3382	4	3	6	4	3	6	4	3	6	4	3	6	4	3	6	4	3	6	4	3	6	4	3	6	4	3	6
3384	0	0	0	0	0	0	0	0	0	0	0	0	0	0	0	0	0	0	0	0	0	0	0	0	0	0	0
3386	0	0	0	0	0	0	0	0	0	0	0	0	0	0	0	0	0	0	0	0	0	0	0	0	0	0	0

Table 3a : X-up/X, Ka down (cont)

downlink\uplink	3599			3601			3603			3605			3607			3609			3611			3613			3615		
3314	2	36	37	2	36	37	2	36	37	2	36	37	2	36	37	2	36	37	2	36	37	2	36	37	2	36	37
3316	6	32	37	6	32	37	6	32	37	6	32	37	6	32	37	6	32	37	6	32	37	6	32	37	6	32	37
3318	10	28	37	10	28	37	10	28	37	10	28	37	10	28	37	10	28	37	10	28	37	10	28	37	10	28	37
3320	13	25	37	13	25	37	13	25	37	13	25	37	13	25	37	13	25	37	13	25	37	13	25	37	13	25	37
3322	17	21	37	17	21	37	17	21	37	17	21	37	17	21	37	17	21	37	17	21	37	17	21	37	17	21	37
3324	21	17	37	21	17	37	21	17	37	21	17	37	21	17	37	21	17	37	21	17	37	21	17	37	21	17	37
3326	24	14	37	24	14	37	24	14	37	24	14	37	24	14	37	24	14	37	24	14	37	24	14	37	24	14	37
3328	28	10	37	28	10	37	28	10	37	28	10	37	28	10	37	28	10	37	28	10	37	28	10	37	28	10	37
3330	32	6	37	32	6	37	32	6	37	32	6	37	32	6	37	32	6	37	32	6	37	32	6	37	32	6	37
3332	35	3	37	35	3	37	35	3	37	35	3	37	35	3	37	35	3	37	35	3	37	35	3	37	35	3	37
3334	35	3	37	35	3	37	35	3	37	35	3	37	35	3	37	35	3	37	35	3	37	35	3	37	35	3	37
3336	35	3	37	35	3	37	35	3	37	35	3	37	35	3	37	35	3	37	35	3	37	35	3	37	35	3	37
3338	35	3	37	35	3	37	35	3	37	35	3	37	35	3	37	35	3	37	35	3	37	35	3	37	35	3	37
3340	35	3	37	35	3	37	35	3	37	35	3	37	35	3	37	35	3	37	35	3	37	35	3	37	35	3	37
3342	35	3	37	35	3	37	35	3	37	35	3	37	35	3	37	35	3	37	35	3	37	35	3	37	35	3	37
3344	35	3	37	35	3	37	35	3	37	35	3	37	35	3	37	35	3	37	35	3	37	35	3	37	35	3	37
3346	35	3	37	35	3	37	35	3	37	35	3	37	35	3	37	35	3	37	35	3	37	35	3	37	35	3	37
3348	35	3	37	35	3	37	35	3	37	35	3	37	35	3	37	35	3	37	35	3	37	35	3	37	35	3	37
3350	35	3	37	35	3	37	35	3	37	35	3	37	35	3	37	35	3	37	35	3	37	35	3	37	35	3	37
3352	35	3	37	35	3	37	35	3	37	35	3	37	35	3	37	35	3	37	35	3	37	35	3	37	35	3	37
3354	35	3	37	35	3	37	35	3	37	35	3	37	35	3	37	35	3	37	35	3	37	35	3	37	35	3	37
3356	35	3	37	35	3	37	35	3	37	35	3	37	35	3	37	35	3	37	35	3	37	35	3	37	35	3	37
3358	35	3	37	35	3	37	35	3	37	35	3	37	35	3	37	35	3	37	35	3	37	35	3	37	35	3	37
3360	35	3	37	35	3	37	35	3	37	35	3	37	35	3	37	35	3	37	35	3	37	35	3	37	35	3	37
3362	35	3	37	35	3	37	35	3	37	35	3	37	35	3	37	35	3	37	35	3	37	35	3	37	35	3	37
3364	35	3	37	35	3	37	35	3	37	35	3	37	35	3	37	35	3	37	35	3	37	35	3	37	35	3	37
3366	33	3	35	33	3	35	33	3	35	33	3	35	33	3	35	33	3	35	33	3	35	33	3	35	33	3	35
3368	29	3	31	29	3	31	29	3	31	29	3	31	29	3	31	29	3	31	29	3	31	29	3	31	29	3	31
3370	26	3	28	26	3	28	26	3	28	26	3	28	26	3	28	26	3	28	26	3	28	26	3	28	26	3	28
3372	22	3	24	22	3	24	22	3	24	22	3	24	22	3	24	22	3	24	22	3	24	22	3	24	22	3	24
3374	18	3	20	18	3	20	18	3	20	18	3	20	18	3	20	18	3	20	18	3	20	18	3	20	18	3	20
3376	15	3	17	15	3	17	15	3	17	15	3	17	15	3	17	15	3	17	15	3	17	15	3	17	15	3	17
3378	11	3	13	11	3	13	11	3	13	11	3	13	11	3	13	11	3	13	11	3	13	11	3	13	11	3	13
3380	7	3	9	7	3	9	7	3	9	7	3	9	7	3	9	7	3	9	7	3	9	7	3	9	7	3	9
3382	4	3	6	4	3	6	4	3	6	4	3	6	4	3	6	4	3	6	4	3	6	4	3	6	4	3	6
3384	0	0	0	0	0	0	0	0	0	0	0	0	0	0	0	0	0	0	0	0	0	0	0	0	0	0	0
3386	0	0	0	0	0	0	0	0	0	0	0	0	0	0	0	0	0	0	0	0	0	0	0	0	0	0	0

Table 3a : X-up/X, Ka down (cont)

dnlink\uplink	3617			3619			3621			3623			3625			3627			3629			3631			3633			3635		
3314	2	36	37	2	36	37	2	36	37	2	36	37	2	36	37	2	36	37	2	36	37	2	36	37	2	36	37	2	36	37
3316	6	32	37	6	32	37	6	32	37	6	32	37	6	32	37	6	32	37	6	32	37	6	32	37	6	32	37	6	32	37
3318	10	28	37	10	28	37	10	28	37	10	28	37	10	28	37	10	28	37	10	28	37	10	28	37	10	28	37	10	28	37
3320	13	25	37	13	25	37	13	25	37	13	25	37	13	25	37	13	25	37	13	25	37	13	25	37	13	25	37	13	25	37
3322	17	21	37	17	21	37	17	21	37	17	21	37	17	21	37	17	21	37	17	21	37	17	21	37	17	21	37	17	21	37
3324	21	17	37	21	17	37	21	17	37	21	17	37	21	17	37	21	17	37	21	17	37	21	17	37	21	17	37	21	17	37
3326	24	14	37	24	14	37	24	14	37	24	14	37	24	14	37	24	14	37	24	14	37	24	14	37	24	14	37	24	14	37
3328	28	10	37	28	10	37	28	10	37	28	10	37	28	10	37	28	10	37	28	10	37	28	10	37	28	10	37	28	10	37
3330	32	6	37	32	6	37	32	6	37	32	6	37	32	6	37	32	6	37	32	6	37	32	6	37	32	6	37	32	6	37
3332	35	3	37	35	3	37	35	3	37	35	3	37	35	3	37	35	3	37	35	3	37	35	3	37	35	3	37	35	3	37
3334	35	3	37	35	3	37	35	3	37	35	3	37	35	3	37	35	3	37	35	3	37	35	3	37	35	3	37	35	3	37
3336	35	3	37	35	3	37	35	3	37	35	3	37	35	3	37	35	3	37	35	3	37	35	3	37	35	3	37	35	3	37
3338	35	3	37	35	3	37	35	3	37	35	3	37	35	3	37	35	3	37	35	3	37	35	3	37	35	3	37	35	3	37
3340	35	3	37	35	3	37	35	3	37	35	3	37	35	3	37	35	3	37	35	3	37	35	3	37	35	3	37	35	3	37
3342	35	3	37	35	3	37	35	3	37	35	3	37	35	3	37	35	3	37	35	3	37	35	3	37	35	3	37	35	3	37
3344	35	3	37	35	3	37	35	3	37	35	3	37	35	3	37	35	3	37	35	3	37	35	3	37	35	3	37	35	3	37
3346	35	3	37	35	3	37	35	3	37	35	3	37	35	3	37	35	3	37	35	3	37	35	3	37	35	3	37	35	3	37
3348	35	3	37	35	3	37	35	3	37	35	3	37	35	3	37	35	3	37	35	3	37	35	3	37	35	3	37	35	3	37
3350	35	3	37	35	3	37	35	3	37	35	3	37	35	3	37	35	3	37	35	3	37	35	3	37	35	3	37	35	3	37
3352	35	3	37	35	3	37	35	3	37	35	3	37	35	3	37	35	3	37	35	3	37	35	3	37	35	3	37	35	3	37
3354	35	3	37	35	3	37	35	3	37	35	3	37	35	3	37	35	3	37	35	3	37	35	3	37	35	3	37	35	3	37
3356	35	3	37	35	3	37	35	3	37	35	3	37	35	3	37	35	3	37	35	3	37	35	3	37	35	3	37	35	3	37
3358	35	3	37	35	3	37	35	3	37	35	3	37	35	3	37	35	3	37	35	3	37	35	3	37	35	3	37	35	3	37
3360	35	3	37	35	3	37	35	3	37	35	3	37	35	3	37	35	3	37	35	3	37	35	3	37	35	3	37	35	3	37
3362	35	3	37	35	3	37	35	3	37	35	3	37	35	3	37	35	3	37	35	3	37	35	3	37	35	3	37	35	3	37
3364	35	3	37	35	3	37	35	3	37	35	3	37	35	3	37	35	3	37	35	3	37	35	3	37	35	3	37	35	3	37
3366	33	3	35	33	3	35	33	3	35	33	3	35	33	3	35	33	3	35	33	3	35	33	3	35	33	3	35	33	3	35
3368	29	3	31	29	3	31	29	3	31	29	3	31	29	3	31	29	3	31	29	3	31	29	3	31	29	3	31	29	3	31
3370	26	3	28	26	3	28	26	3	28	26	3	28	26	3	28	26	3	28	26	3	28	26	3	28	26	3	28	26	3	28
3372	22	3	24	22	3	24	22	3	24	22	3	24	22	3	24	22	3	24	22	3	24	22	3	24	22	3	24	22	3	24
3374	18	3	20	18	3	20	18	3	20	18	3	20	18	3	20	18	3	20	18	3	20	18	3	20	18	3	20	18	3	20
3376	15	3	17	15	3	17	15	3	17	15	3	17	15	3	17	15	3	17	15	3	17	15	3	17	15	3	17	15	3	17
3378	11	3	13	11	3	13	11	3	13	11	3	13	11	3	13	11	3	13	11	3	13	11	3	13	11	3	13	11	3	13
3380	7	3	9	7	3	9	7	3	9	7	3	9	7	3	9	7	3	9	7	3	9	7	3	9	7	3	9	7	3	9
3382	4	3	6	4	3	6	4	3	6	4	3	6	4	3	6	4	3	6	4	3	6	4	3	6	4	3	6	4	3	6
3384	0	0	0	0	0	0	0	0	0	0	0	0	0	0	0	0	0	0	0	0	0	0	0	0	0	0	0	0	0	0
3386	0	0	0	0	0	0	0	0	0	0	0	0	0	0	0	0	0	0	0	0	0	0	0	0	0	0	0	0	0	0

30-Jul-93 J. A. Koukos

Table 3b : Ka-up / Ka-down Coherency Test :

downlink\uplink	3563			3565			3567			3569			3571			3573			3575			3577			3579		
3314	2	36	37	2	36	37	2	36	37	2	36	37	2	36	37	2	36	37	2	36	37	2	36	37	2	36	37
3316	6	32	37	6	32	37	6	32	37	6	32	37	6	32	37	6	32	37	6	32	37	6	32	37	6	32	37
3318	10	28	37	10	28	37	10	28	37	10	28	37	10	28	37	10	28	37	10	28	37	10	28	37	10	28	37
3320	13	25	37	13	25	37	13	25	37	13	25	37	13	25	37	13	25	37	13	25	37	13	25	37	13	25	37
3322	17	21	37	17	21	37	17	21	37	17	21	37	17	21	37	17	21	37	17	21	37	17	21	37	17	21	37
3324	21	17	37	21	17	37	21	17	37	21	17	37	21	17	37	21	17	37	21	17	37	21	17	37	21	17	37
3326	24	14	37	24	14	37	24	14	37	24	14	37	24	14	37	24	14	37	24	14	37	24	14	37	24	14	37
3328	28	10	37	28	10	37	28	10	37	28	10	37	28	10	37	28	10	37	28	10	37	28	10	37	28	10	37
3330	32	6	37	32	6	37	32	6	37	32	6	37	32	6	37	32	6	37	32	6	37	32	6	37	32	6	37
3332	36	2	37	36	2	37	36	2	37	36	2	37	36	2	37	36	2	37	36	2	37	36	2	37	36	2	37
3334	37	1	37	37	1	37	37	1	37	37	1	37	37	1	37	37	1	37	37	1	37	37	1	37	37	1	37
3336	37	1	37	37	1	37	37	1	37	37	1	37	37	1	37	37	1	37	37	1	37	37	1	37	37	1	37
3338	37	1	37	37	1	37	37	1	37	37	1	37	37	1	37	37	1	37	37	1	37	37	1	37	37	1	37
3340	37	1	37	37	1	37	37	1	37	37	1	37	37	1	37	37	1	37	37	1	37	37	1	37	37	1	37
3342	37	1	37	37	1	37	37	1	37	37	1	37	37	1	37	37	1	37	37	1	37	37	1	37	37	1	37
3344	37	1	37	37	1	37	37	1	37	37	1	37	37	1	37	37	1	37	37	1	37	37	1	37	37	1	37
3346	37	1	37	37	1	37	37	1	37	37	1	37	37	1	37	37	1	37	37	1	37	37	1	37	37	1	37
3348	37	1	37	37	1	37	37	1	37	37	1	37	37	1	37	37	1	37	37	1	37	37	1	37	37	1	37
3350	37	1	37	37	1	37	37	1	37	37	1	37	37	1	37	37	1	37	37	1	37	37	1	37	37	1	37
3352	37	1	37	37	1	37	37	1	37	37	1	37	37	1	37	37	1	37	37	1	37	37	1	37	37	1	37
3354	37	1	37	37	1	37	37	1	37	37	1	37	37	1	37	37	1	37	37	1	37	37	1	37	37	1	37
3356	37	1	37	37	1	37	37	1	37	37	1	37	37	1	37	37	1	37	37	1	37	37	1	37	37	1	37
3358	37	1	37	37	1	37	37	1	37	37	1	37	37	1	37	37	1	37	37	1	37	37	1	37	37	1	37
3360	37	1	37	37	1	37	37	1	37	37	1	37	37	1	37	37	1	37	37	1	37	37	1	37	37	1	37
3362	37	1	37	37	1	37	37	1	37	37	1	37	37	1	37	37	1	37	37	1	37	37	1	37	37	1	37
3364	37	1	37	37	1	37	37	1	37	37	1	37	37	1	37	37	1	37	37	1	37	37	1	37	37	1	37
3366	35	1	35	35	1	35	35	1	35	35	1	35	35	1	35	35	1	35	35	1	35	35	1	35	35	1	35
3368	31	1	31	31	1	31	31	1	31	31	1	31	31	1	31	31	1	31	31	1	31	31	1	31	31	1	31
3370	28	1	28	28	1	28	28	1	28	28	1	28	28	1	28	28	1	28	28	1	28	28	1	28	28	1	28
3372	24	1	24	24	1	24	24	1	24	24	1	24	24	1	24	24	1	24	24	1	24	24	1	24	24	1	24
3374	20	1	20	20	1	20	20	1	20	20	1	20	20	1	20	20	1	20	20	1	20	20	1	20	20	1	20
3376	17	1	17	17	1	17	17	1	17	17	1	17	17	1	17	17	1	17	17	1	17	17	1	17	17	1	17
3378	13	1	13	13	1	13	13	1	13	13	1	13	13	1	13	13	1	13	13	1	13	13	1	13	13	1	13
3380	9	1	9	9	1	9	9	1	9	9	1	9	9	1	9	9	1	9	9	1	9	9	1	9	9	1	9
3382	6	1	6	6	1	6	6	1	6	6	1	6	6	1	6	6	1	6	6	1	6	6	1	6	6	1	6
3384	2	1	2	2	1	2	2	1	2	2	1	2	2	1	2	2	1	2	2	1	2	2	1	2	2	1	2
3386	0	0	0	0	0	0	0	0	0	0	0	0	0	0	0	0	0	0	0	0	0	0	0	0	0	0	0

30-Jul-93 J. A. Koukos

Table 3b : Ka-up / Ka-down Coherency Test (Cont)

downlink\uplink	3581			3583			3585			3587			3589			3591			3593			3595			3597		
3314	2	36	37	2	36	37	2	36	37	2	36	37	2	36	37	2	36	37	2	36	37	2	36	37	2	36	37
3316	6	32	37	6	32	37	6	32	37	6	32	37	6	32	37	6	32	37	6	32	37	6	32	37	6	32	37
3318	10	28	37	10	28	37	10	28	37	10	28	37	10	28	37	10	28	37	10	28	37	10	28	37	10	28	37
3320	13	25	37	13	25	37	13	25	37	13	25	37	13	25	37	13	25	37	13	25	37	13	25	37	13	25	37
3322	17	21	37	17	21	37	17	21	37	17	21	37	17	21	37	17	21	37	17	21	37	17	21	37	17	21	37
3324	21	17	37	21	17	37	21	17	37	21	17	37	21	17	37	21	17	37	21	17	37	21	17	37	21	17	37
3326	24	14	37	24	14	37	24	14	37	24	14	37	24	14	37	24	14	37	24	14	37	24	14	37	24	14	37
3328	28	10	37	28	10	37	28	10	37	28	10	37	28	10	37	28	10	37	28	10	37	28	10	37	28	10	37
3330	32	6	37	32	6	37	32	6	37	32	6	37	32	6	37	32	6	37	32	6	37	32	6	37	32	6	37
3332	36	2	37	36	2	37	36	2	37	36	2	37	36	2	37	36	2	37	36	2	37	36	2	37	36	2	37
3334	37	1	37	37	1	37	37	1	37	37	1	37	37	1	37	37	1	37	37	1	37	37	1	37	37	1	37
3336	37	1	37	37	1	37	37	1	37	37	1	37	37	1	37	37	1	37	37	1	37	37	1	37	37	1	37
3338	37	1	37	37	1	37	37	1	37	37	1	37	37	1	37	37	1	37	37	1	37	37	1	37	37	1	37
3340	37	1	37	37	1	37	37	1	37	37	1	37	37	1	37	37	1	37	37	1	37	37	1	37	37	1	37
3342	37	1	37	37	1	37	37	1	37	37	1	37	37	1	37	37	1	37	37	1	37	37	1	37	37	1	37
3344	37	1	37	37	1	37	37	1	37	37	1	37	37	1	37	37	1	37	37	1	37	37	1	37	37	1	37
3346	37	1	37	37	1	37	37	1	37	37	1	37	37	1	37	37	1	37	37	1	37	37	1	37	37	1	37
3348	37	1	37	37	1	37	37	1	37	37	1	37	37	1	37	37	1	37	37	1	37	37	1	37	37	1	37
3350	37	1	37	37	1	37	37	1	37	37	1	37	37	1	37	37	1	37	37	1	37	37	1	37	37	1	37
3352	37	1	37	37	1	37	37	1	37	37	1	37	37	1	37	37	1	37	37	1	37	37	1	37	37	1	37
3354	37	1	37	37	1	37	37	1	37	37	1	37	37	1	37	37	1	37	37	1	37	37	1	37	37	1	37
3356	37	1	37	37	1	37	37	1	37	37	1	37	37	1	37	37	1	37	37	1	37	37	1	37	37	1	37
3358	37	1	37	37	1	37	37	1	37	37	1	37	37	1	37	37	1	37	37	1	37	37	1	37	37	1	37
3360	37	1	37	37	1	37	37	1	37	37	1	37	37	1	37	37	1	37	37	1	37	37	1	37	37	1	37
3362	37	1	37	37	1	37	37	1	37	37	1	37	37	1	37	37	1	37	37	1	37	37	1	37	37	1	37
3364	37	1	37	37	1	37	37	1	37	37	1	37	37	1	37	37	1	37	37	1	37	37	1	37	37	1	37
3366	35	1	35	35	1	35	35	1	35	35	1	35	35	1	35	35	1	35	35	1	35	35	1	35	35	1	35
3368	31	1	31	31	1	31	31	1	31	31	1	31	31	1	31	31	1	31	31	1	31	31	1	31	31	1	31
3370	28	1	28	28	1	28	28	1	28	28	1	28	28	1	28	28	1	28	28	1	28	28	1	28	28	1	28
3372	24	1	24	24	1	24	24	1	24	24	1	24	24	1	24	24	1	24	24	1	24	24	1	24	24	1	24
3374	20	1	20	20	1	20	20	1	20	20	1	20	20	1	20	20	1	20	20	1	20	20	1	20	20	1	20
3376	17	1	17	17	1	17	17	1	17	17	1	17	17	1	17	17	1	17	17	1	17	17	1	17	17	1	17
3378	13	1	13	13	1	13	13	1	13	13	1	13	13	1	13	13	1	13	13	1	13	13	1	13	13	1	13
3380	9	1	9	9	1	9	9	1	9	9	1	9	9	1	9	9	1	9	9	1	9	9	1	9	9	1	9
3382	6	1	6	6	1	6	6	1	6	6	1	6	6	1	6	6	1	6	6	1	6	6	1	6	6	1	6
3384	2	1	2	2	1	2	2	1	2	2	1	2	2	1	2	2	1	2	2	1	2	2	1	2	2	1	2
3386	0	0	0	0	0	0	0	0	0	0	0	0	0	0	0	0	0	0	0	0	0	0	0	0	0	0	0

Table 3b : Ka-up / Ka-down Coherency Test (Cont)

downlink\uplink	3599			3601			3603			3605			3607			3609			3611			3613			3615		
3314	2	36	37	2	36	37	2	36	37	2	36	37	2	36	37	2	36	37	2	36	37	2	36	37	2	36	37
3316	6	32	37	6	32	37	6	32	37	6	32	37	6	32	37	6	32	37	6	32	37	6	32	37	6	32	37
3318	10	28	37	10	28	37	10	28	37	10	28	37	10	28	37	10	28	37	10	28	37	10	28	37	10	28	37
3320	13	25	37	13	25	37	13	25	37	13	25	37	13	25	37	13	25	37	13	25	37	13	25	37	13	25	37
3322	17	21	37	17	21	37	17	21	37	17	21	37	17	21	37	17	21	37	17	21	37	17	21	37	17	21	37
3324	21	17	37	21	17	37	21	17	37	21	17	37	21	17	37	21	17	37	21	17	37	21	17	37	21	17	37
3326	24	14	37	24	14	37	24	14	37	24	14	37	24	14	37	24	14	37	24	14	37	24	14	37	24	14	37
3328	28	10	37	28	10	37	28	10	37	28	10	37	28	10	37	28	10	37	28	10	37	28	10	37	28	10	37
3330	32	6	37	32	6	37	32	6	37	32	6	37	32	6	37	32	6	37	32	6	37	32	6	37	32	6	37
3332	36	2	37	36	2	37	36	2	37	36	2	37	36	2	37	36	2	37	36	2	37	36	2	37	36	2	37
3334	37	1	37	37	1	37	37	1	37	37	1	37	37	1	37	37	1	37	37	1	37	37	1	37	37	1	37
3336	37	1	37	37	1	37	37	1	37	37	1	37	37	1	37	37	1	37	37	1	37	37	1	37	37	1	37
3338	37	1	37	37	1	37	37	1	37	37	1	37	37	1	37	37	1	37	37	1	37	37	1	37	37	1	37
3340	37	1	37	37	1	37	37	1	37	37	1	37	37	1	37	37	1	37	37	1	37	37	1	37	37	1	37
3342	37	1	37	37	1	37	37	1	37	37	1	37	37	1	37	37	1	37	37	1	37	37	1	37	37	1	37
3344	37	1	37	37	1	37	37	1	37	37	1	37	37	1	37	37	1	37	37	1	37	37	1	37	37	1	37
3346	37	1	37	37	1	37	37	1	37	37	1	37	37	1	37	37	1	37	37	1	37	37	1	37	37	1	37
3348	37	1	37	37	1	37	37	1	37	37	1	37	37	1	37	37	1	37	37	1	37	37	1	37	37	1	37
3350	37	1	37	37	1	37	37	1	37	37	1	37	37	1	37	37	1	37	37	1	37	37	1	37	37	1	37
3352	37	1	37	37	1	37	37	1	37	37	1	37	37	1	37	37	1	37	37	1	37	37	1	37	37	1	37
3354	37	1	37	37	1	37	37	1	37	37	1	37	37	1	37	37	1	37	37	1	37	37	1	37	37	1	37
3356	37	1	37	37	1	37	37	1	37	37	1	37	37	1	37	37	1	37	37	1	37	37	1	37	37	1	37
3358	37	1	37	37	1	37	37	1	37	37	1	37	37	1	37	37	1	37	37	1	37	37	1	37	37	1	37
3360	37	1	37	37	1	37	37	1	37	37	1	37	37	1	37	37	1	37	37	1	37	37	1	37	37	1	37
3362	37	1	37	37	1	37	37	1	37	37	1	37	37	1	37	37	1	37	37	1	37	37	1	37	37	1	37
3364	37	1	37	37	1	37	37	1	37	37	1	37	37	1	37	37	1	37	37	1	37	37	1	37	37	1	37
3366	35	1	35	35	1	35	35	1	35	35	1	35	35	1	35	35	1	35	35	1	35	35	1	35	35	1	35
3368	31	1	31	31	1	31	31	1	31	31	1	31	31	1	31	31	1	31	31	1	31	31	1	31	31	1	31
3370	28	1	28	28	1	28	28	1	28	28	1	28	28	1	28	28	1	28	28	1	28	28	1	28	28	1	28
3372	24	1	24	24	1	24	24	1	24	24	1	24	24	1	24	24	1	24	24	1	24	24	1	24	24	1	24
3374	20	1	20	20	1	20	20	1	20	20	1	20	20	1	20	20	1	20	20	1	20	20	1	20	20	1	20
3376	17	1	17	17	1	17	17	1	17	17	1	17	17	1	17	17	1	17	17	1	17	17	1	17	17	1	17
3378	13	1	13	13	1	13	13	1	13	13	1	13	13	1	13	13	1	13	13	1	13	13	1	13	13	1	13
3380	9	1	9	9	1	9	9	1	9	9	1	9	9	1	9	9	1	9	9	1	9	9	1	9	9	1	9
3382	6	1	6	6	1	6	6	1	6	6	1	6	6	1	6	6	1	6	6	1	6	6	1	6	6	1	6
3384	2	1	2	2	1	2	2	1	2	2	1	2	2	1	2	2	1	2	2	1	2	2	1	2	2	1	2
3386	0	0	0	0	0	0	0	0	0	0	0	0	0	0	0	0	0	0	0	0	0	0	0	0	0	0	0

Table 3b : Ka-up / Ka-down Coherency Test (Cont)

dnlink\uplink	3617			3619			3621			3623			3625			3627			3629			3631			3633			3635		
3314	2	36	37	2	36	37	2	36	37	2	36	37	2	36	37	2	36	37	2	36	37	2	36	37	2	36	37	2	36	37
3316	6	32	37	6	32	37	6	32	37	6	32	37	6	32	37	6	32	37	6	32	37	6	32	37	6	32	37	6	32	37
3318	10	28	37	10	28	37	10	28	37	10	28	37	10	28	37	10	28	37	10	28	37	10	28	37	10	28	37	10	28	37
3320	13	25	37	13	25	37	13	25	37	13	25	37	13	25	37	13	25	37	13	25	37	13	25	37	13	25	37	13	25	37
3322	17	21	37	17	21	37	17	21	37	17	21	37	17	21	37	17	21	37	17	21	37	17	21	37	17	21	37	17	21	37
3324	21	17	37	21	17	37	21	17	37	21	17	37	21	17	37	21	17	37	21	17	37	21	17	37	21	17	37	21	17	37
3326	24	14	37	24	14	37	24	14	37	24	14	37	24	14	37	24	14	37	24	14	37	24	14	37	24	14	37	24	14	37
3328	28	10	37	28	10	37	28	10	37	28	10	37	28	10	37	28	10	37	28	10	37	28	10	37	28	10	37	28	10	37
3330	32	6	37	32	6	37	32	6	37	32	6	37	32	6	37	32	6	37	32	6	37	32	6	37	32	6	37	32	6	37
3332	36	2	37	36	2	37	36	2	37	36	2	37	36	2	37	36	2	37	36	2	37	36	2	37	36	2	37	36	2	37
3334	37	1	37	37	1	37	37	1	37	37	1	37	37	1	37	37	1	37	37	1	37	37	1	37	37	1	37	37	1	37
3336	37	1	37	37	1	37	37	1	37	37	1	37	37	1	37	37	1	37	37	1	37	37	1	37	37	1	37	37	1	37
3338	37	1	37	37	1	37	37	1	37	37	1	37	37	1	37	37	1	37	37	1	37	37	1	37	37	1	37	37	1	37
3340	37	1	37	37	1	37	37	1	37	37	1	37	37	1	37	37	1	37	37	1	37	37	1	37	37	1	37	37	1	37
3342	37	1	37	37	1	37	37	1	37	37	1	37	37	1	37	37	1	37	37	1	37	37	1	37	37	1	37	37	1	37
3344	37	1	37	37	1	37	37	1	37	37	1	37	37	1	37	37	1	37	37	1	37	37	1	37	37	1	37	37	1	37
3346	37	1	37	37	1	37	37	1	37	37	1	37	37	1	37	37	1	37	37	1	37	37	1	37	37	1	37	37	1	37
3348	37	1	37	37	1	37	37	1	37	37	1	37	37	1	37	37	1	37	37	1	37	37	1	37	37	1	37	37	1	37
3350	37	1	37	37	1	37	37	1	37	37	1	37	37	1	37	37	1	37	37	1	37	37	1	37	37	1	37	37	1	37
3352	37	1	37	37	1	37	37	1	37	37	1	37	37	1	37	37	1	37	37	1	37	37	1	37	37	1	37	37	1	37
3354	37	1	37	37	1	37	37	1	37	37	1	37	37	1	37	37	1	37	37	1	37	37	1	37	37	1	37	37	1	37
3356	37	1	37	37	1	37	37	1	37	37	1	37	37	1	37	37	1	37	37	1	37	37	1	37	37	1	37	37	1	37
3358	37	1	37	37	1	37	37	1	37	37	1	37	37	1	37	37	1	37	37	1	37	37	1	37	37	1	37	37	1	37
3360	37	1	37	37	1	37	37	1	37	37	1	37	37	1	37	37	1	37	37	1	37	37	1	37	37	1	37	37	1	37
3362	37	1	37	37	1	37	37	1	37	37	1	37	37	1	37	37	1	37	37	1	37	37	1	37	37	1	37	37	1	37
3364	37	1	37	37	1	37	37	1	37	37	1	37	37	1	37	37	1	37	37	1	37	37	1	37	37	1	37	37	1	37
3366	35	1	35	35	1	35	35	1	35	35	1	35	35	1	35	35	1	35	35	1	35	35	1	35	35	1	35	35	1	35
3368	31	1	31	31	1	31	31	1	31	31	1	31	31	1	31	31	1	31	31	1	31	31	1	31	31	1	31	31	1	31
3370	28	1	28	28	1	28	28	1	28	28	1	28	28	1	28	28	1	28	28	1	28	28	1	28	28	1	28	28	1	28
3372	24	1	24	24	1	24	24	1	24	24	1	24	24	1	24	24	1	24	24	1	24	24	1	24	24	1	24	24	1	24
3374	20	1	20	20	1	20	20	1	20	20	1	20	20	1	20	20	1	20	20	1	20	20	1	20	20	1	20	20	1	20
3376	17	1	17	17	1	17	17	1	17	17	1	17	17	1	17	17	1	17	17	1	17	17	1	17	17	1	17	17	1	17
3378	13	1	13	13	1	13	13	1	13	13	1	13	13	1	13	13	1	13	13	1	13	13	1	13	13	1	13	13	1	13
3380	9	1	9	9	1	9	9	1	9	9	1	9	9	1	9	9	1	9	9	1	9	9	1	9	9	1	9	9	1	9
3382	6	1	6	6	1	6	6	1	6	6	1	6	6	1	6	6	1	6	6	1	6	6	1	6	6	1	6	6	1	6
3384	2	1	2	2	1	2	2	1	2	2	1	2	2	1	2	2	1	2	2	1	2	2	1	2	2	1	2	2	1	2
3386	0	0	0	0	0	0	0	0	0	0	0	0	0	0	0	0	0	0	0	0	0	0	0	0	0	0	0	0	0	0

30-Jul-93 J. A. Koukos

Table 3c : Ka-up/X-down,Ka-down Coherency Test :

downlink\uplink	3563			3565			3567			3569			3571			3573			3575			3577			3579		
3314	2	38	39	4	36	39	4	36	39	4	36	39	4	36	39	4	36	39	4	36	39	4	36	39	4	36	39
3316	2	38	39	6	34	39	8	32	39	8	32	39	8	32	39	8	32	39	8	32	39	8	32	39	8	32	39
3318	2	38	39	6	34	39	9	31	39	12	28	39	12	28	39	12	28	39	12	28	39	12	28	39	12	28	39
3320	2	38	39	6	34	39	9	31	39	13	27	39	15	25	39	15	25	39	15	25	39	15	25	39	15	25	39
3322	2	38	39	6	34	39	9	31	39	13	27	39	16	24	39	19	21	39	19	21	39	19	21	39	19	21	39
3324	2	38	39	6	34	39	9	31	39	13	27	39	16	24	39	19	21	39	23	17	39	23	17	39	23	17	39
3326	2	38	39	6	34	39	9	31	39	13	27	39	16	24	39	19	21	39	23	17	39	26	14	39	26	14	39
3328	2	38	39	6	34	39	9	31	39	13	27	39	16	24	39	19	21	39	23	17	39	26	14	39	30	10	39
3330	2	38	39	6	34	39	9	31	39	13	27	39	16	24	39	19	21	39	23	17	39	26	14	39	30	10	39
3332	2	38	39	6	34	39	9	31	39	13	27	39	16	24	39	19	21	39	23	17	39	26	14	39	30	10	39
3334	2	38	39	6	34	39	9	31	39	13	27	39	16	24	39	19	21	39	23	17	39	26	14	39	30	10	39
3336	2	38	39	6	34	39	9	31	39	13	27	39	16	24	39	19	21	39	23	17	39	26	14	39	30	10	39
3338	2	38	39	6	34	39	9	31	39	13	27	39	16	24	39	19	21	39	23	17	39	26	14	39	30	10	39
3340	2	38	39	6	34	39	9	31	39	13	27	39	16	24	39	19	21	39	23	17	39	26	14	39	30	10	39
3342	2	38	39	6	34	39	9	31	39	13	27	39	16	24	39	19	21	39	23	17	39	26	14	39	30	10	39
3344	2	38	39	6	34	39	9	31	39	13	27	39	16	24	39	19	21	39	23	17	39	26	14	39	30	10	39
3346	2	38	39	6	34	39	9	31	39	13	27	39	16	24	39	19	21	39	23	17	39	26	14	39	30	10	39
3348	2	38	39	6	34	39	9	31	39	13	27	39	16	24	39	19	21	39	23	17	39	26	14	39	30	10	39
3350	2	38	39	6	34	39	9	31	39	13	27	39	16	24	39	19	21	39	23	17	39	26	14	39	30	10	39
3352	2	38	39	6	34	39	9	31	39	13	27	39	16	24	39	19	21	39	23	17	39	26	14	39	30	10	39
3354	2	38	39	6	34	39	9	31	39	13	27	39	16	24	39	19	21	39	23	17	39	26	14	39	30	10	39
3356	2	38	39	6	34	39	9	31	39	13	27	39	16	24	39	19	21	39	23	17	39	26	14	39	30	10	39
3358	2	38	39	6	34	39	9	31	39	13	27	39	16	24	39	19	21	39	23	17	39	26	14	39	30	10	39
3360	2	38	39	6	34	39	9	31	39	13	27	39	16	24	39	19	21	39	23	17	39	26	14	39	30	10	39
3362	2	38	39	6	34	39	9	31	39	13	27	39	16	24	39	19	21	39	23	17	39	26	14	39	30	10	39
3364	2	38	39	6	34	39	9	31	39	13	27	39	16	24	39	19	21	39	23	17	39	26	14	39	30	10	39
3366	0	0	0	2	34	35	5	31	35	9	27	35	12	24	35	15	21	35	19	17	35	22	14	35	26	10	35
3368	0	0	0	0	0	0	1	31	31	5	27	31	8	24	31	11	21	31	15	17	31	18	14	31	22	10	31
3370	0	0	0	0	0	0	0	0	0	2	27	28	5	24	28	8	21	28	12	17	28	15	14	28	19	10	28
3372	0	0	0	0	0	0	0	0	0	0	0	0	1	24	24	4	21	24	8	17	24	11	14	24	15	10	24
3374	0	0	0	0	0	0	0	0	0	0	0	0	0	0	0	0	0	0	4	17	20	7	14	20	11	10	20
3376	0	0	0	0	0	0	0	0	0	0	0	0	0	0	0	0	0	0	1	17	17	4	14	17	8	10	17
3378	0	0	0	0	0	0	0	0	0	0	0	0	0	0	0	0	0	0	0	0	0	0	0	0	4	10	13
3380	0	0	0	0	0	0	0	0	0	0	0	0	0	0	0	0	0	0	0	0	0	0	0	0	0	0	0
3382	0	0	0	0	0	0	0	0	0	0	0	0	0	0	0	0	0	0	0	0	0	0	0	0	0	0	0
3384	0	0	0	0	0	0	0	0	0	0	0	0	0	0	0	0	0	0	0	0	0	0	0	0	0	0	0
3386	0	0	0	0	0	0	0	0	0	0	0	0	0	0	0	0	0	0	0	0	0	0	0	0	0	0	0

Table 3c : Ka-up/X-down,Ka-down Coherency Test (Cont) :

downlink\uplink	3581			3583			3585			3587			3589			3591			3593			3595			3597		
3314	4	36	39	4	36	39	4	36	39	4	36	39	4	36	39	4	36	39	4	36	39	4	36	39	4	36	39
3316	8	32	39	8	32	39	8	32	39	8	32	39	8	32	39	8	32	39	8	32	39	8	32	39	8	32	39
3318	12	28	39	12	28	39	12	28	39	12	28	39	12	28	39	12	28	39	12	28	39	12	28	39	12	28	39
3320	15	25	39	15	25	39	15	25	39	15	25	39	15	25	39	15	25	39	15	25	39	15	25	39	15	25	39
3322	19	21	39	19	21	39	19	21	39	19	21	39	19	21	39	19	21	39	19	21	39	19	21	39	19	21	39
3324	23	17	39	23	17	39	23	17	39	23	17	39	23	17	39	23	17	39	23	17	39	23	17	39	23	17	39
3326	26	14	39	26	14	39	26	14	39	26	14	39	26	14	39	26	14	39	26	14	39	26	14	39	26	14	39
3328	30	10	39	30	10	39	30	10	39	30	10	39	30	10	39	30	10	39	30	10	39	30	10	39	30	10	39
3330	33	7	39	34	6	39	34	6	39	34	6	39	34	6	39	34	6	39	34	6	39	34	6	39	34	6	39
3332	33	7	39	37	3	39	37	3	39	37	3	39	37	3	39	37	3	39	37	3	39	37	3	39	37	3	39
3334	33	7	39	37	3	39	37	3	39	37	3	39	37	3	39	37	3	39	37	3	39	37	3	39	37	3	39
3336	33	7	39	37	3	39	37	3	39	37	3	39	37	3	39	37	3	39	37	3	39	37	3	39	37	3	39
3338	33	7	39	37	3	39	37	3	39	37	3	39	37	3	39	37	3	39	37	3	39	37	3	39	37	3	39
3340	33	7	39	37	3	39	37	3	39	37	3	39	37	3	39	37	3	39	37	3	39	37	3	39	37	3	39
3342	33	7	39	37	3	39	37	3	39	37	3	39	37	3	39	37	3	39	37	3	39	37	3	39	37	3	39
3344	33	7	39	37	3	39	37	3	39	37	3	39	37	3	39	37	3	39	37	3	39	37	3	39	37	3	39
3346	33	7	39	37	3	39	37	3	39	37	3	39	37	3	39	37	3	39	37	3	39	37	3	39	37	3	39
3348	33	7	39	37	3	39	37	3	39	37	3	39	37	3	39	37	3	39	37	3	39	37	3	39	37	3	39
3350	33	7	39	37	3	39	37	3	39	37	3	39	37	3	39	37	3	39	37	3	39	37	3	39	37	3	39
3352	33	7	39	37	3	39	37	3	39	37	3	39	37	3	39	37	3	39	37	3	39	37	3	39	37	3	39
3354	33	7	39	37	3	39	37	3	39	37	3	39	37	3	39	37	3	39	37	3	39	37	3	39	37	3	39
3356	33	7	39	37	3	39	37	3	39	37	3	39	37	3	39	37	3	39	37	3	39	37	3	39	37	3	39
3358	33	7	39	37	3	39	37	3	39	37	3	39	37	3	39	37	3	39	37	3	39	37	3	39	37	3	39
3360	33	7	39	37	3	39	37	3	39	37	3	39	37	3	39	37	3	39	37	3	39	37	3	39	37	3	39
3362	33	7	39	37	3	39	37	3	39	37	3	39	37	3	39	37	3	39	37	3	39	37	3	39	37	3	39
3364	33	7	39	37	3	39	37	3	39	37	3	39	37	3	39	37	3	39	37	3	39	37	3	39	37	3	39
3366	29	7	35	33	3	35	33	3	35	33	3	35	33	3	35	33	3	35	33	3	35	33	3	35	33	3	35
3368	25	7	31	29	3	31	29	3	31	29	3	31	29	3	31	29	3	31	29	3	31	29	3	31	29	3	31
3370	22	7	28	26	3	28	26	3	28	26	3	28	26	3	28	26	3	28	26	3	28	26	3	28	26	3	28
3372	18	7	24	22	3	24	22	3	24	22	3	24	22	3	24	22	3	24	22	3	24	22	3	24	22	3	24
3374	14	7	20	18	3	20	18	3	20	18	3	20	18	3	20	18	3	20	18	3	20	18	3	20	18	3	20
3376	11	7	17	15	3	17	15	3	17	15	3	17	15	3	17	15	3	17	15	3	17	15	3	17	15	3	17
3378	7	7	13	11	3	13	11	3	13	11	3	13	11	3	13	11	3	13	11	3	13	11	3	13	11	3	13
3380	3	7	9	7	3	9	7	3	9	7	3	9	7	3	9	7	3	9	7	3	9	7	3	9	7	3	9
3382	0	0	0	4	3	6	4	3	6	4	3	6	4	3	6	4	3	6	4	3	6	4	3	6	4	3	6
3384	0	0	0	0	0	0	0	0	0	0	0	0	0	0	0	0	0	0	0	0	0	0	0	0	0	0	0
3386	0	0	0	0	0	0	0	0	0	0	0	0	0	0	0	0	0	0	0	0	0	0	0	0	0	0	0

Table 3c : Ka-up/X-down,Ka-down Coherency Test (Cont) :

downlink\uplink	3599			3601			3603			3605			3607			3609			3611			3613			3615		
3314	4	36	39	4	36	39	4	36	39	4	36	39	4	36	39	4	36	39	4	36	39	2	36	37	2	36	37
3316	8	32	39	8	32	39	8	32	39	8	32	39	8	32	39	8	32	39	8	32	39	6	32	37	6	32	37
3318	12	28	39	12	28	39	12	28	39	12	28	39	12	28	39	12	28	39	12	28	39	10	28	37	10	28	37
3320	15	25	39	15	25	39	15	25	39	15	25	39	15	25	39	15	25	39	15	25	39	13	25	37	13	25	37
3322	19	21	39	19	21	39	19	21	39	19	21	39	19	21	39	19	21	39	19	21	39	17	21	37	17	21	37
3324	23	17	39	23	17	39	23	17	39	23	17	39	23	17	39	23	17	39	23	17	39	21	17	37	21	17	37
3326	26	14	39	26	14	39	26	14	39	26	14	39	26	14	39	26	14	39	26	14	39	24	14	37	24	14	37
3328	30	10	39	30	10	39	30	10	39	30	10	39	30	10	39	30	10	39	30	10	39	28	10	37	28	10	37
3330	34	6	39	34	6	39	34	6	39	34	6	39	34	6	39	34	6	39	34	6	39	32	6	37	32	6	37
3332	37	3	39	37	3	39	37	3	39	37	3	39	37	3	39	37	3	39	37	3	39	35	3	37	35	3	37
3334	37	3	39	37	3	39	37	3	39	37	3	39	37	3	39	37	3	39	37	3	39	35	3	37	35	3	37
3336	37	3	39	37	3	39	37	3	39	37	3	39	37	3	39	37	3	39	37	3	39	35	3	37	35	3	37
3338	37	3	39	37	3	39	37	3	39	37	3	39	37	3	39	37	3	39	37	3	39	35	3	37	35	3	37
3340	37	3	39	37	3	39	37	3	39	37	3	39	37	3	39	37	3	39	37	3	39	35	3	37	35	3	37
3342	37	3	39	37	3	39	37	3	39	37	3	39	37	3	39	37	3	39	37	3	39	35	3	37	35	3	37
3344	37	3	39	37	3	39	37	3	39	37	3	39	37	3	39	37	3	39	37	3	39	35	3	37	35	3	37
3346	37	3	39	37	3	39	37	3	39	37	3	39	37	3	39	37	3	39	37	3	39	35	3	37	35	3	37
3348	37	3	39	37	3	39	37	3	39	37	3	39	37	3	39	37	3	39	37	3	39	35	3	37	35	3	37
3350	37	3	39	37	3	39	37	3	39	37	3	39	37	3	39	37	3	39	37	3	39	35	3	37	35	3	37
3352	37	3	39	37	3	39	37	3	39	37	3	39	37	3	39	37	3	39	37	3	39	35	3	37	35	3	37
3354	37	3	39	37	3	39	37	3	39	37	3	39	37	3	39	37	3	39	37	3	39	35	3	37	35	3	37
3356	37	3	39	37	3	39	37	3	39	37	3	39	37	3	39	37	3	39	37	3	39	35	3	37	35	3	37
3358	37	3	39	37	3	39	37	3	39	37	3	39	37	3	39	37	3	39	37	3	39	35	3	37	35	3	37
3360	37	3	39	37	3	39	37	3	39	37	3	39	37	3	39	37	3	39	37	3	39	35	3	37	35	3	37
3362	37	3	39	37	3	39	37	3	39	37	3	39	37	3	39	37	3	39	37	3	39	35	3	37	35	3	37
3364	37	3	39	37	3	39	37	3	39	37	3	39	37	3	39	37	3	39	37	3	39	35	3	37	35	3	37
3366	33	3	35	33	3	35	33	3	35	33	3	35	33	3	35	33	3	35	33	3	35	33	3	35	33	3	35
3368	29	3	31	29	3	31	29	3	31	29	3	31	29	3	31	29	3	31	29	3	31	29	3	31	29	3	31
3370	26	3	28	26	3	28	26	3	28	26	3	28	26	3	28	26	3	28	26	3	28	26	3	28	26	3	28
3372	22	3	24	22	3	24	22	3	24	22	3	24	22	3	24	22	3	24	22	3	24	22	3	24	22	3	24
3374	18	3	20	18	3	20	18	3	20	18	3	20	18	3	20	18	3	20	18	3	20	18	3	20	18	3	20
3376	15	3	17	15	3	17	15	3	17	15	3	17	15	3	17	15	3	17	15	3	17	15	3	17	15	3	17
3378	11	3	13	11	3	13	11	3	13	11	3	13	11	3	13	11	3	13	11	3	13	11	3	13	11	3	13
3380	7	3	9	7	3	9	7	3	9	7	3	9	7	3	9	7	3	9	7	3	9	7	3	9	7	3	9
3382	4	3	6	4	3	6	4	3	6	4	3	6	4	3	6	4	3	6	4	3	6	4	3	6	4	3	6
3384	0	0	0	0	0	0	0	0	0	0	0	0	0	0	0	0	0	0	0	0	0	0	0	0	0	0	0
3386	0	0	0	0	0	0	0	0	0	0	0	0	0	0	0	0	0	0	0	0	0	0	0	0	0	0	0

Table 3c : Ka-up/X-down,Ka-down Coherency Test (Cont) :

dnlink\uplink	3617			3619			3621			3623			3625			3627			3629			3631			3633			3635		
3314	0	0	0	0	0	0	0	0	0	0	0	0	0	0	0	0	0	0	0	0	0	0	0	0	0	0	0	0	0	0
3316	3	32	34	0	0	0	0	0	0	0	0	0	0	0	0	0	0	0	0	0	0	0	0	0	0	0	0	0	0	0
3318	7	28	34	3	28	30	0	0	0	0	0	0	0	0	0	0	0	0	0	0	0	0	0	0	0	0	0	0	0	0
3320	10	25	34	6	25	30	3	25	27	0	0	0	0	0	0	0	0	0	0	0	0	0	0	0	0	0	0	0	0	0
3322	14	21	34	10	21	30	7	21	27	3	21	23	0	0	0	0	0	0	0	0	0	0	0	0	0	0	0	0	0	0
3324	18	17	34	14	17	30	11	17	27	7	17	23	4	17	20	1	17	17	0	0	0	0	0	0	0	0	0	0	0	0
3326	21	14	34	17	14	30	14	14	27	10	14	23	7	14	20	4	14	17	0	0	0	0	0	0	0	0	0	0	0	0
3328	25	10	34	21	10	30	18	10	27	14	10	23	11	10	20	8	10	17	4	10	13	1	10	10	0	0	0	0	0	0
3330	29	6	34	25	6	30	22	6	27	18	6	23	15	6	20	12	6	17	8	6	13	5	6	10	1	6	6	0	0	0
3332	32	3	34	28	3	30	25	3	27	21	3	23	18	3	20	15	3	17	11	3	13	8	3	10	4	3	6	1	3	3
3334	32	3	34	28	3	30	25	3	27	21	3	23	18	3	20	15	3	17	11	3	13	8	3	10	4	3	6	1	3	3
3336	32	3	34	28	3	30	25	3	27	21	3	23	18	3	20	15	3	17	11	3	13	8	3	10	4	3	6	1	3	3
3338	32	3	34	28	3	30	25	3	27	21	3	23	18	3	20	15	3	17	11	3	13	8	3	10	4	3	6	1	3	3
3340	32	3	34	28	3	30	25	3	27	21	3	23	18	3	20	15	3	17	11	3	13	8	3	10	4	3	6	1	3	3
3342	32	3	34	28	3	30	25	3	27	21	3	23	18	3	20	15	3	17	11	3	13	8	3	10	4	3	6	1	3	3
3344	32	3	34	28	3	30	25	3	27	21	3	23	18	3	20	15	3	17	11	3	13	8	3	10	4	3	6	1	3	3
3346	32	3	34	28	3	30	25	3	27	21	3	23	18	3	20	15	3	17	11	3	13	8	3	10	4	3	6	1	3	3
3348	32	3	34	28	3	30	25	3	27	21	3	23	18	3	20	15	3	17	11	3	13	8	3	10	4	3	6	1	3	3
3350	32	3	34	28	3	30	25	3	27	21	3	23	18	3	20	15	3	17	11	3	13	8	3	10	4	3	6	1	3	3
3352	32	3	34	28	3	30	25	3	27	21	3	23	18	3	20	15	3	17	11	3	13	8	3	10	4	3	6	1	3	3
3354	32	3	34	28	3	30	25	3	27	21	3	23	18	3	20	15	3	17	11	3	13	8	3	10	4	3	6	1	3	3
3356	32	3	34	28	3	30	25	3	27	21	3	23	18	3	20	15	3	17	11	3	13	8	3	10	4	3	6	1	3	3
3358	32	3	34	28	3	30	25	3	27	21	3	23	18	3	20	15	3	17	11	3	13	8	3	10	4	3	6	1	3	3
3360	32	3	34	28	3	30	25	3	27	21	3	23	18	3	20	15	3	17	11	3	13	8	3	10	4	3	6	1	3	3
3362	32	3	34	28	3	30	25	3	27	21	3	23	18	3	20	15	3	17	11	3	13	8	3	10	4	3	6	1	3	3
3364	32	3	34	28	3	30	25	3	27	21	3	23	18	3	20	15	3	17	11	3	13	8	3	10	4	3	6	1	3	3
3366	32	3	34	28	3	30	25	3	27	21	3	23	18	3	20	15	3	17	11	3	13	8	3	10	4	3	6	1	3	3
3368	29	3	31	28	3	30	25	3	27	21	3	23	18	3	20	15	3	17	11	3	13	8	3	10	4	3	6	1	3	3
3370	26	3	28	26	3	28	25	3	27	21	3	23	18	3	20	15	3	17	11	3	13	8	3	10	4	3	6	1	3	3
3372	22	3	24	22	3	24	22	3	24	21	3	23	18	3	20	15	3	17	11	3	13	8	3	10	4	3	6	1	3	3
3374	18	3	20	18	3	20	18	3	20	18	3	20	18	3	20	15	3	17	11	3	13	8	3	10	4	3	6	1	3	3
3376	15	3	17	15	3	17	15	3	17	15	3	17	15	3	17	15	3	17	11	3	13	8	3	10	4	3	6	1	3	3
3378	11	3	13	11	3	13	11	3	13	11	3	13	11	3	13	11	3	13	11	3	13	8	3	10	4	3	6	1	3	3
3380	7	3	9	7	3	9	7	3	9	7	3	9	7	3	9	7	3	9	7	3	9	7	3	9	4	3	6	1	3	3
3382	4	3	6	4	3	6	4	3	6	4	3	6	4	3	6	4	3	6	4	3	6	4	3	6	4	3	6	1	3	3
3384	0	0	0	0	0	0	0	0	0	0	0	0	0	0	0	0	0	0	0	0	0	0	0	0	0	0	0	0	0	0
3386	0	0	0	0	0	0	0	0	0	0	0	0	0	0	0	0	0	0	0	0	0	0	0	0	0	0	0	0	0	0

Table 4a : Coherent Uplink Prime Multiplication Factors

UPLINK FACTOR	PRIME MULTIPLICATION FACTORS
3563	7 x 509
3565	5 x 23 x 31
3567	3 x 29 x 41
3569	43 x 83
3571	3571
3573	3 x 3 x 397
3575	5 x 5 x 11 x 13
3577	7 x 7 x 73
3579	3 x 1193
3581	3581
3583	3583
3585	3 x 5 x 239
3587	17 x 211
3589	37 x 97
3591	3 x 3 x 3 x 7 x 19
3593	3593
3595	5 x 719
3597	3 x 11 x 109
3599	59 x 61
3601	13 x 277
3603	3 x 1201
3605	5 x 7 x 103
3607	3607
3609	3 x 3 x 401
3611	23 x 157
3613	3613
3615	3 x 5 x 241
3617	3617
3619	7 x 11 x 47
3621	3 x 17 x 71
3623	3623
3625	5 x 5 x 5 x 29
3627	3 x 3 x 13 x 31
3629	19 x 191
3631	3631
3633	3 x 7 x 173
3635	5 x 727

Table 4b : Coherent Downlink Prime Multiplication Factors

DOWNLINK FACTOR	PRIME MULTIPLICATION FACTORS
3314	2 x 1657
3316	2 x 2 x 829
3318	2 x 3 x 7 x 79
3320	2 x 2 x 2 x 5 x 83
3322	2 x 11 x 151
3324	2 x 2 x 3 x 277
3326	2 x 1663
3328	2 x2 x2 x2 x2 x2 x 2 x 2 x 13
3330	2 x 3 x3 x5 x 37
3332	2 x 2 x 7 x7 x 17
3334	2 x 1667
3336	2 x 2 x 2 x 3 x 139
3338	2 x 1669
3340	2 x 2 x 5 x 167
3342	2 x 3 x 557
3344	2 x 2 x 2 x 2 x 11 x 19
3346	2 x 7 x 239
3348	2 x 2 x 3 x3 x3 x 31
3350	2 x 5 x5 x 67
3352	2 x 2 x 2 x 419
3354	2 x 3 x13 x 43
3356	2 x 2 x 839
3358	2 x 23 x 73
3360	2 x 2 x 2 x 2 x 3 x 5 x 7
3362	2 x 41 x 41
3364	2 x 2 x 29 x 29
3366	2 x 3 x3 x11 x 17
3368	2 x 2 x 2 x 421
3370	2 x 5 x 337
3372	2 x 2 x 3 x 281
3374	2 x 7 x 241
3376	2 x 2 x 2 x 2 x 211
3378	2 x 3 x 563
3380	2 x 2 x 5 x13 x 13
3382	2 x 19 x 89
3384	2 x 2 x 2 x 3 x3 x 47

Table 5 : Uplink TMs satisfying AGC Limitations (100 MHz < IF Frequency < 10 GHz) versus VCO Frequency.

DOWN FACTOR	2f1	4f1	8f1	12f1
3332	3583 - 3591	3583 - 3595	N/A	N/A
3334	3583 - 3603	3583 - 3607	3583 - 3599	N/A
3360	3583 - 3615	3583 - 3615	3583 - 3615	3583 - 3615

Table 6 : Uplink TMs satisfying Diplexer Limitations (TTFR Separation ≥ 7%) versus VCO Frequency.

DOWLINK FACTOR	2f1	4f1	8f1	12f1
3332	3583 - 3591	3583 - 3595	N/A	N/A
3334	3583 - 3603	3583 - 3607	3583 - 3599	N/A
3360	3595 - 3615	3595 - 3615	3595 - 3615	3595 - 3615

Table 7 : Downlink Ka-Band TM's versus number of Channels in the [31.8, 32] GHz Band

D/L TM	# Channels	D/L TM	# Channels	D/L TM	# Channels
3314	7	3340	25	3364	0
3316	11	3342	22	3366	0
3318	15	3344	18	3368	0
3320	18	3346	14	3370	0
3322	22	3348	11	3372	0
3324	26	3350	7	3374	0
3326	29	3352	3	3376	0
3328	33	3354	0	3378	0
3330	37	3356	0	3380	0
3332	39	3358	0	3382	0
3334	37	3360	0	3384	0
3336	33	3362	0	3386	0
3338	29				

Table 8a - 3597/3344 Turnaround Ratio Multiplier Implementation Uplink, Downlink, 1st LO and 1st IF Factors

	FACTORS	PRIME MULTIPLICATION FACTOR
UPLINK	3597	3 x 11 x 109
DOWNLINK	3344	2 x 2 x 2 x 2 x 11 x 19
FIRST LO	3432	2 x 2 x 2 x 3 x 11 x 13
FIRST IF	165	3 x 5 x 11

Table 8b - 3599/3344 Turnaround Ratio Multiplier Implementation Uplink, Downlink, 1st LO and 1st IF Factors

	FACTORS	PRIME MULTIPLICATION FACTOR
UPLINK	3599	59 x 61
DOWNLINK	3344	2 x 2 x 2 x 2 x 11 x 19
FIRST LO	3344	2 x 2 x 2 x 2 x 11 x 19
FIRST IF	255	3 x 5 x 17

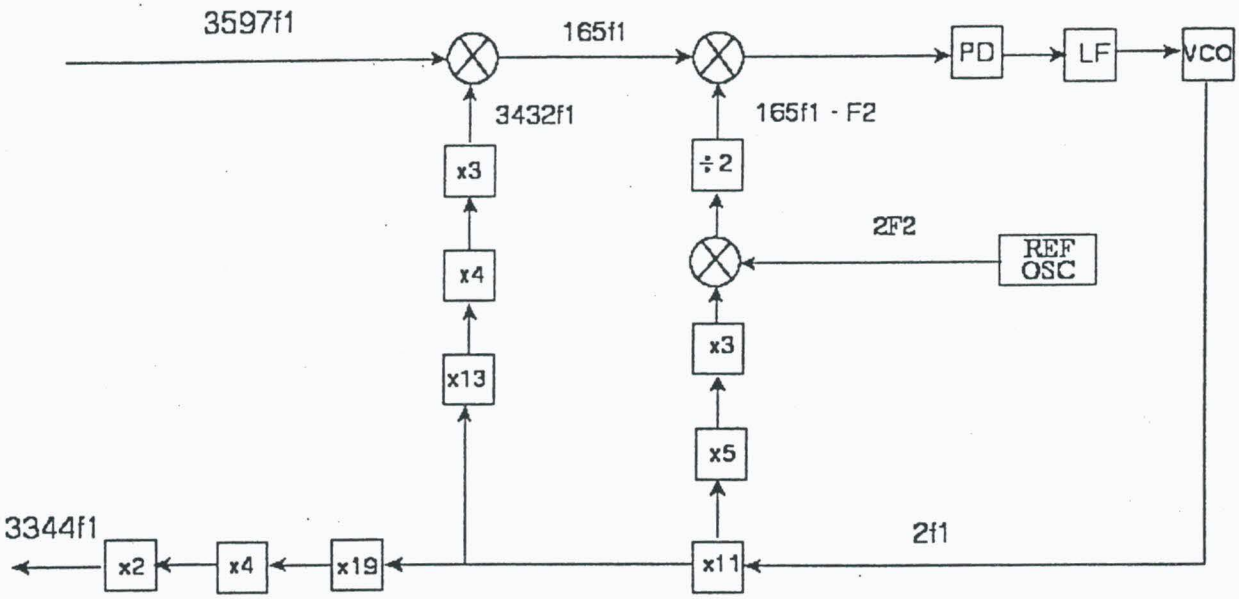

FIGURE 1 - 3597/3344 RATIO KA-BAND RECEIVER BLOCK DIAGRAM WITH A VCO FREQUENCY OF 2f1

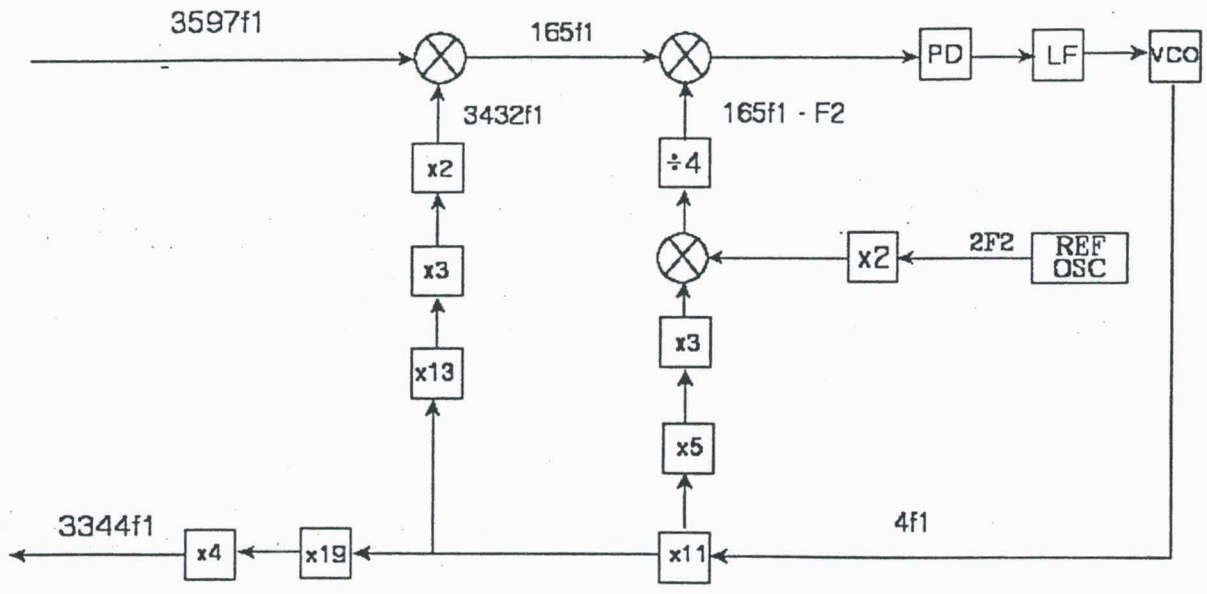

FIGURE 2 - 3597/3344 RATIO KA-BAND RECEIVER BLOCK DIAGRAM WITH A VCO FREQUENCY OF 4f1

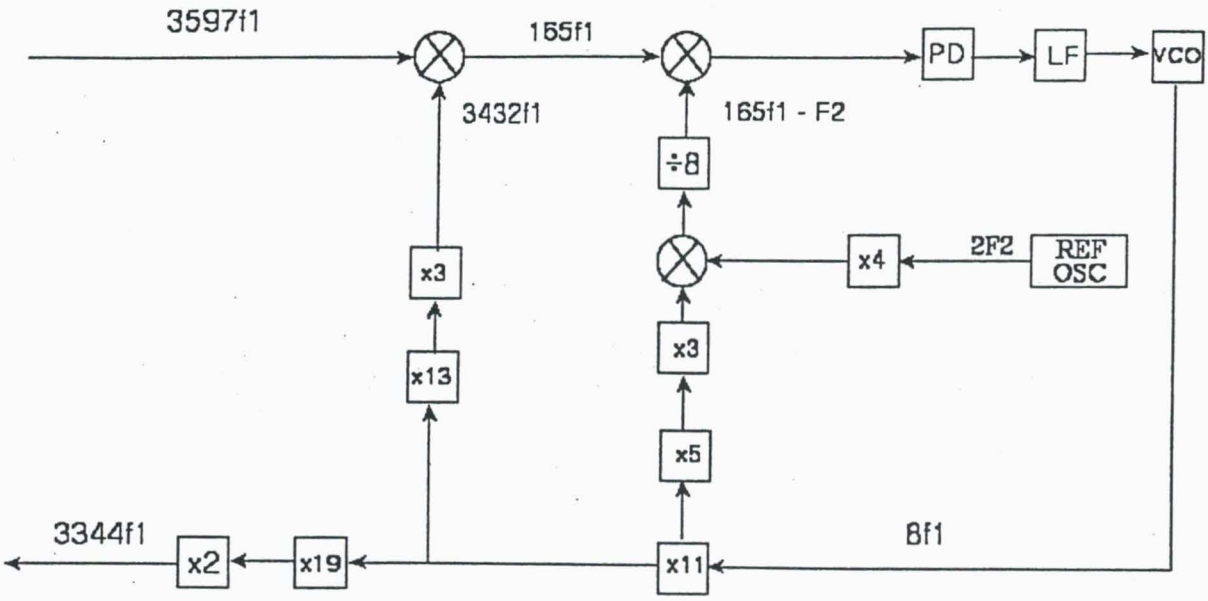

FIGURE 3 - 3597/3344 RATIO KA-BAND RECEIVER BLOCK DIAGRAM WITH A VCO FREQUENCY OF 8f1

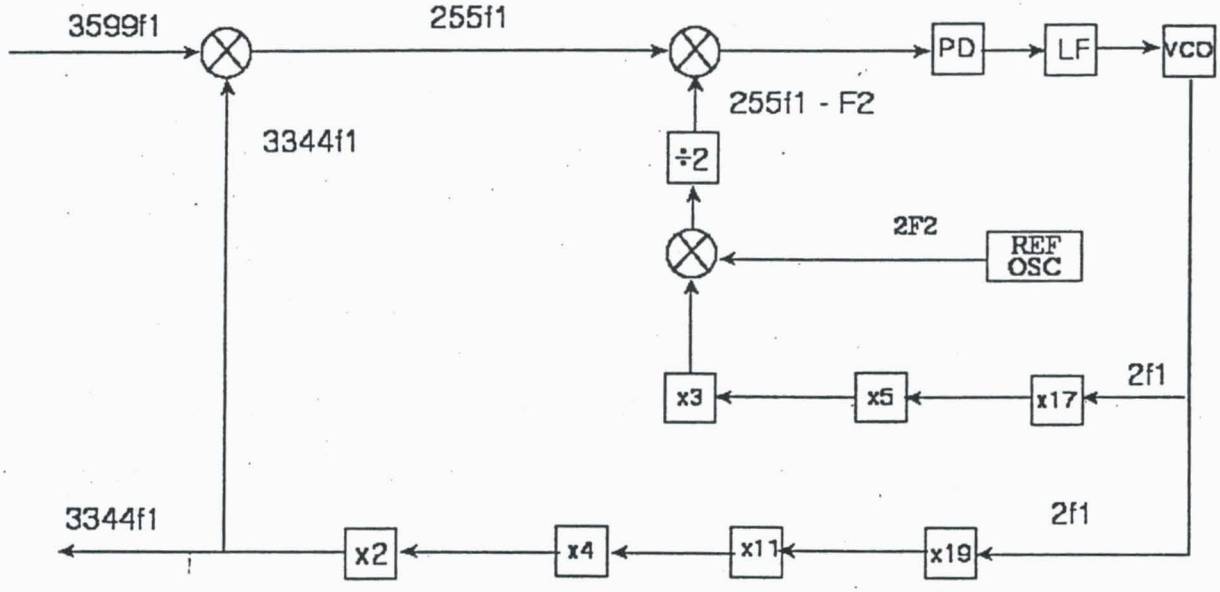

FIGURE 4 - 3599/3344 RATIO KA-BAND RECEIVER BLOCK DIAGRAM WITH A VCO FREQUENCY OF 2f1

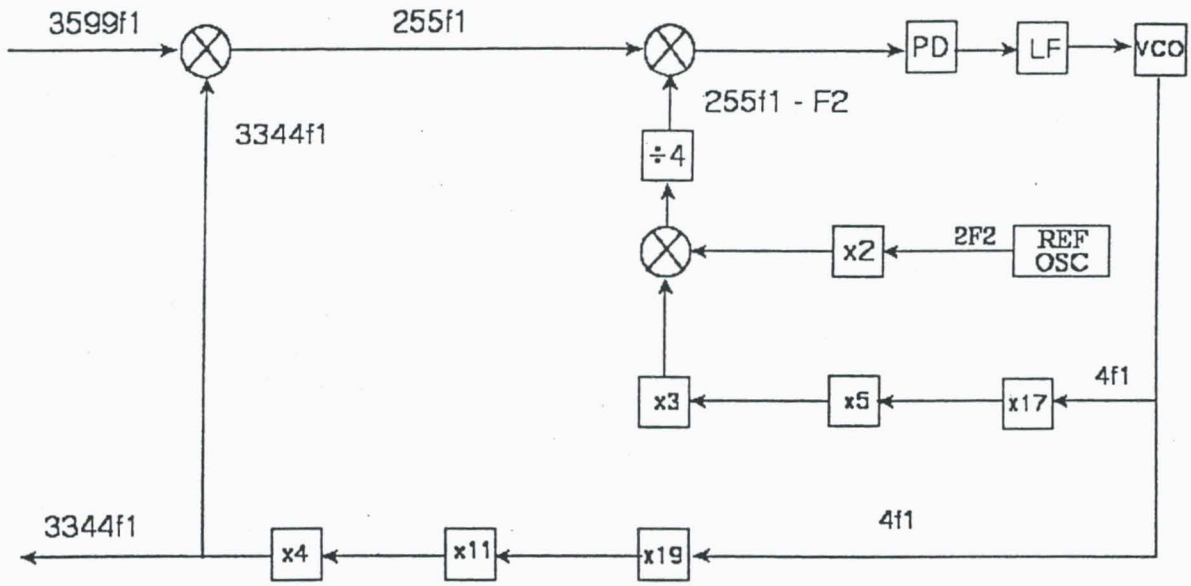

FIGURE 5 - 3599/3344 RATIO KA-BAND RECEIVER BLOCK DIAGRAM WITH A VCO FREQUENCY OF 4f1

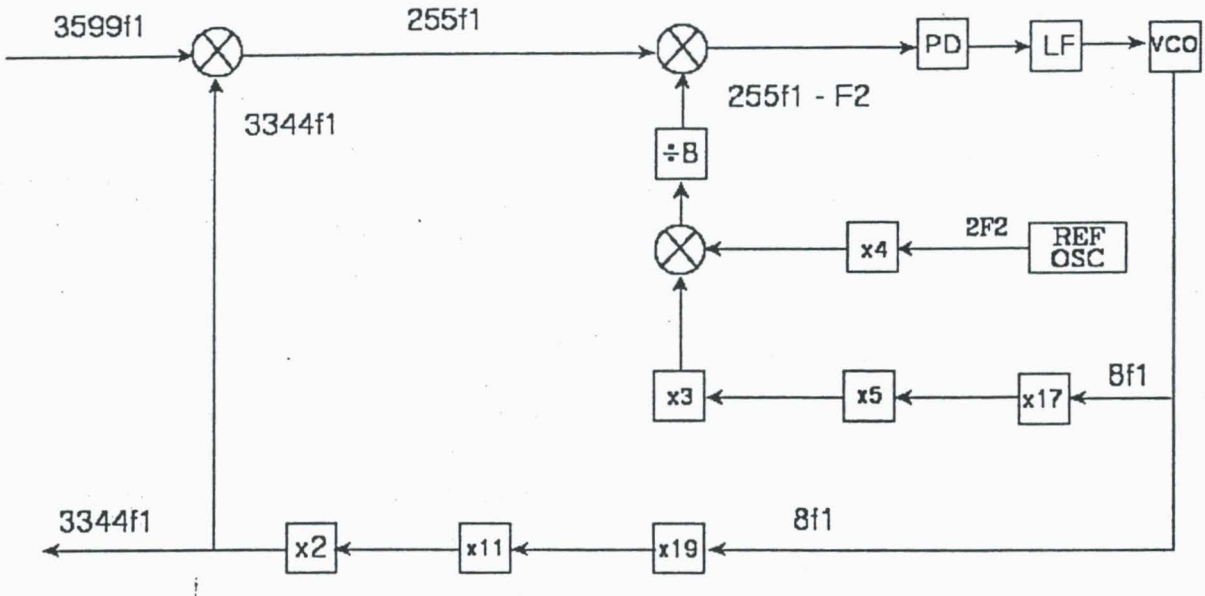

FIGURE 6 - 3599/3344 RATIO KA-BAND RECEIVER BLOCK DIAGRAM WITH A VCO FREQUENCY OF 8f1

Figure 7: 3599/3344 F1 Double Conversion Frequency Scheme: Design 1

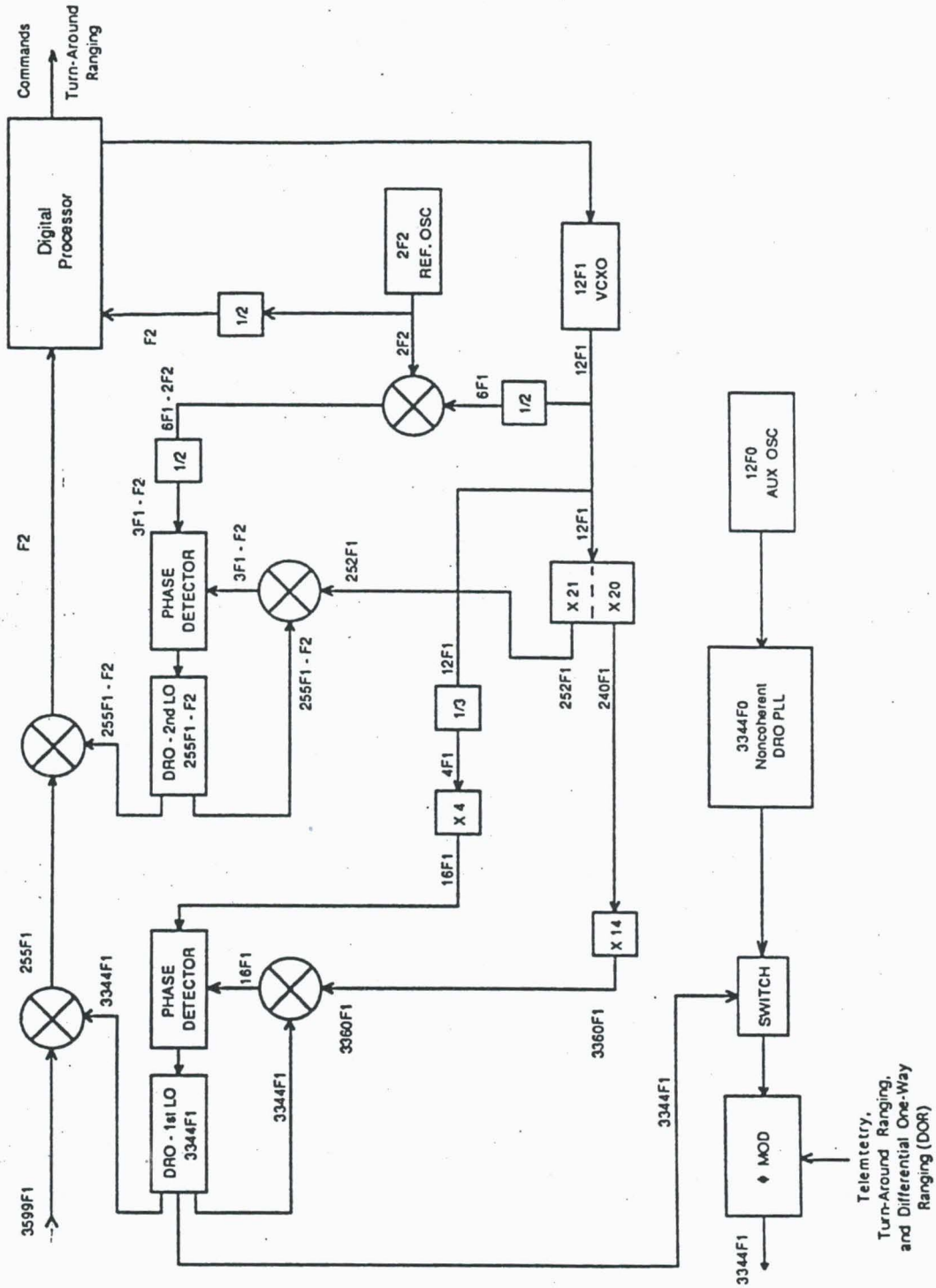

Figure 8: 3599/3344 F1 Single Conversion Frequency Scheme: Design 2

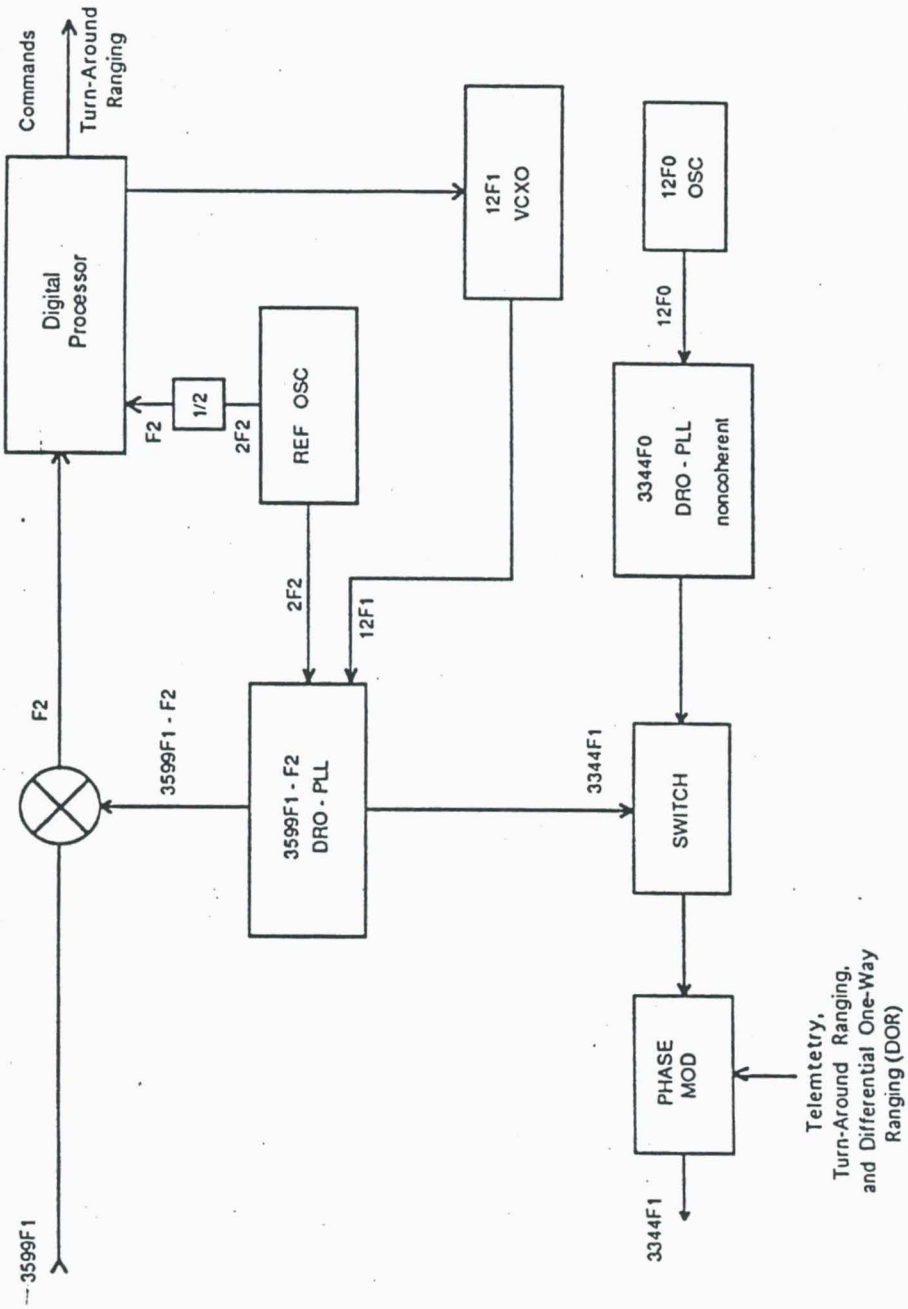

Figure 9: 3597/3344 F1 Double Conversion Frequency Scheme: Design 3

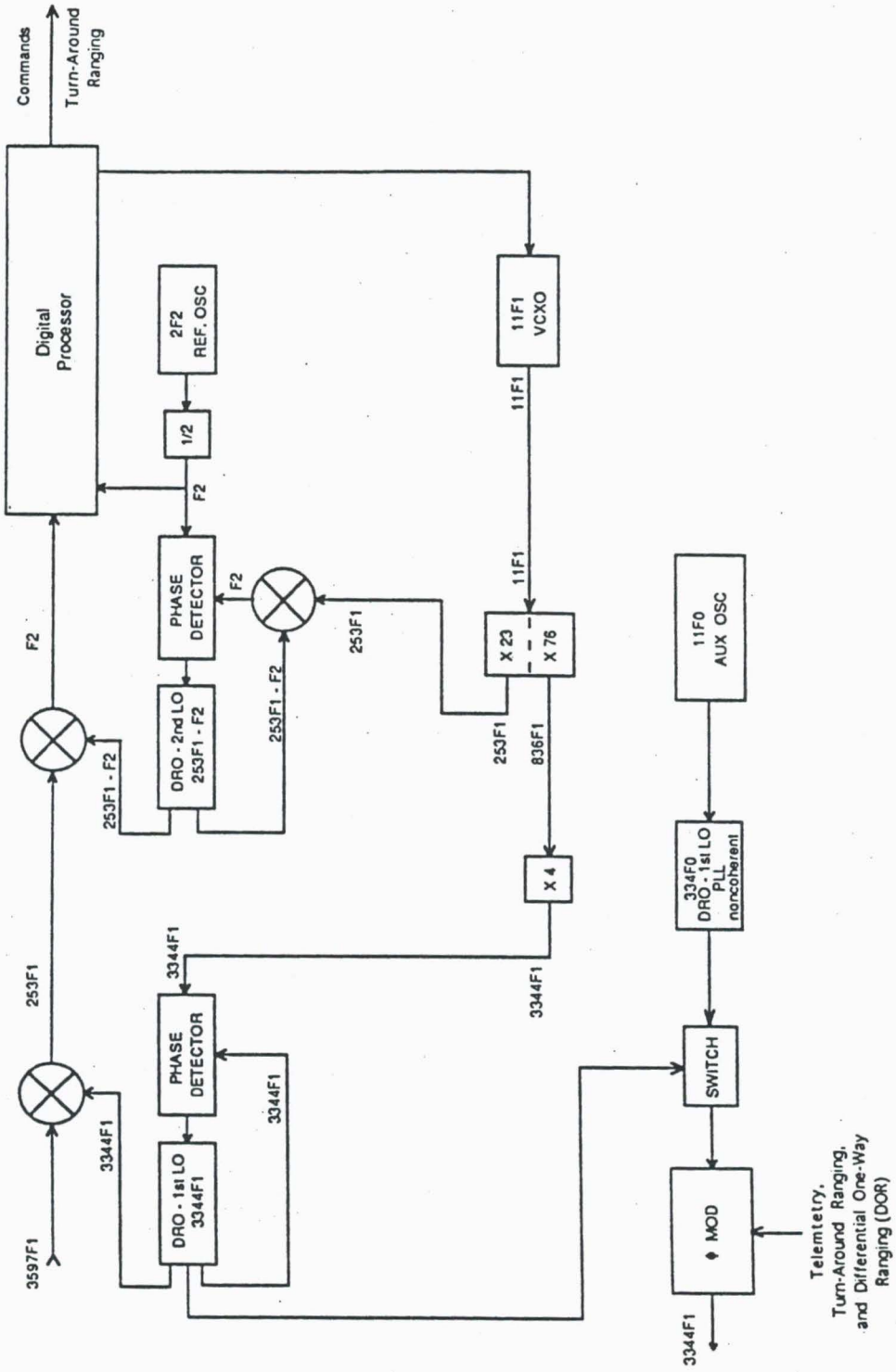

Figure 10: 3597/3344 F1 Single Conversion Frequency Scheme: Design 4

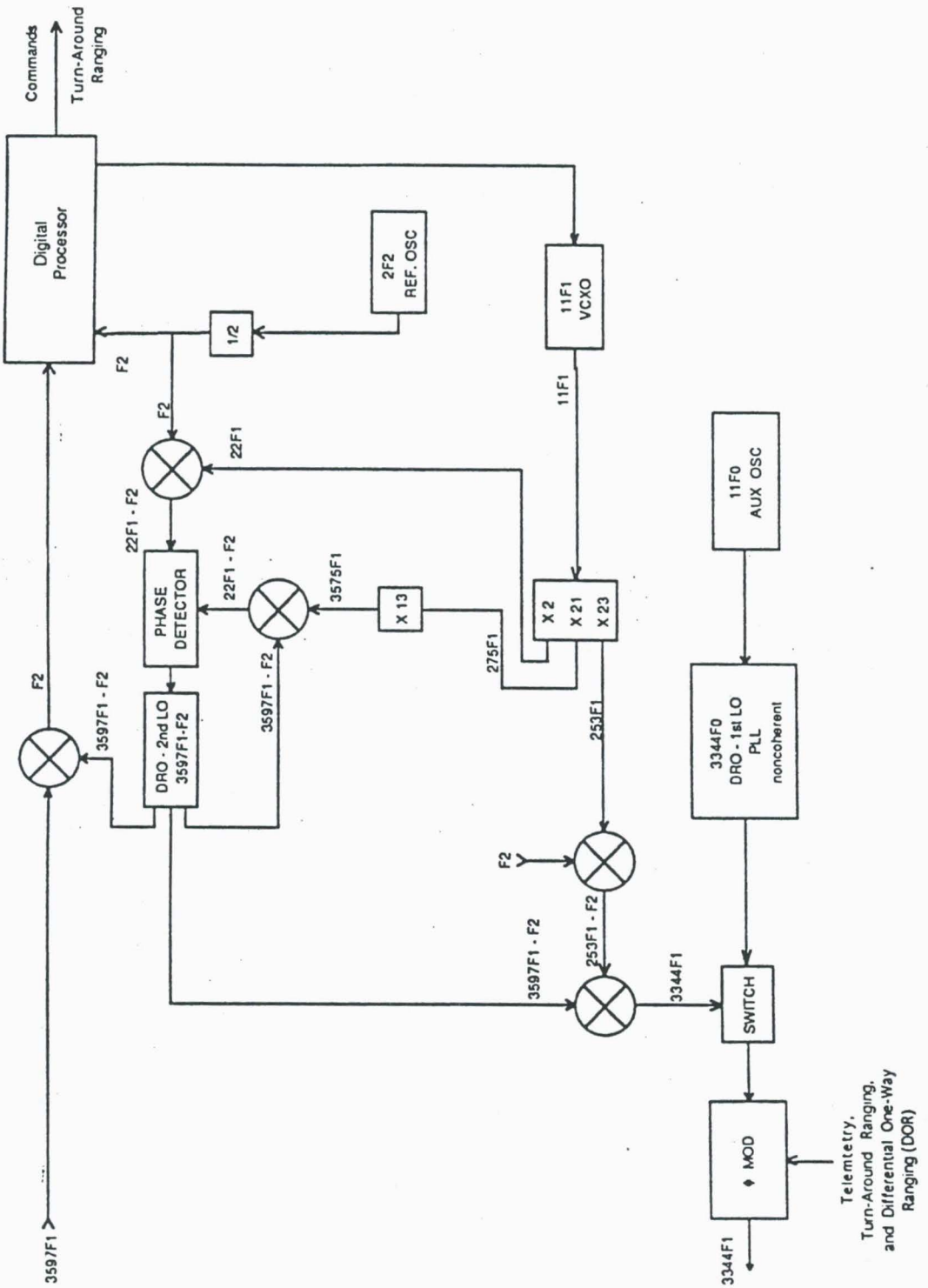

Figure 11 749/3344 F1 Reduced Function Transponder Design 2

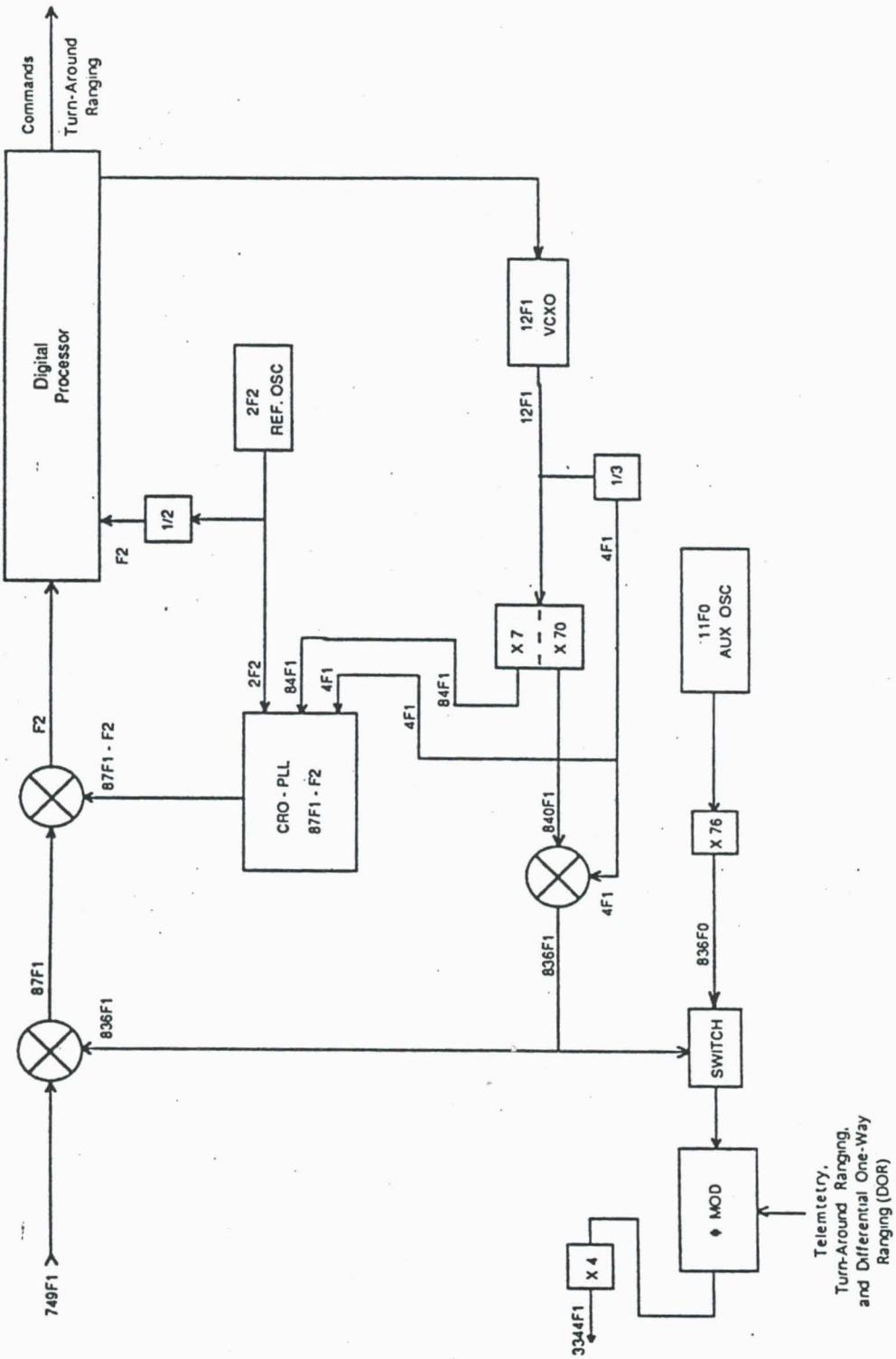

Fig. 12 Ka-Band DST Breadboard Upgrade

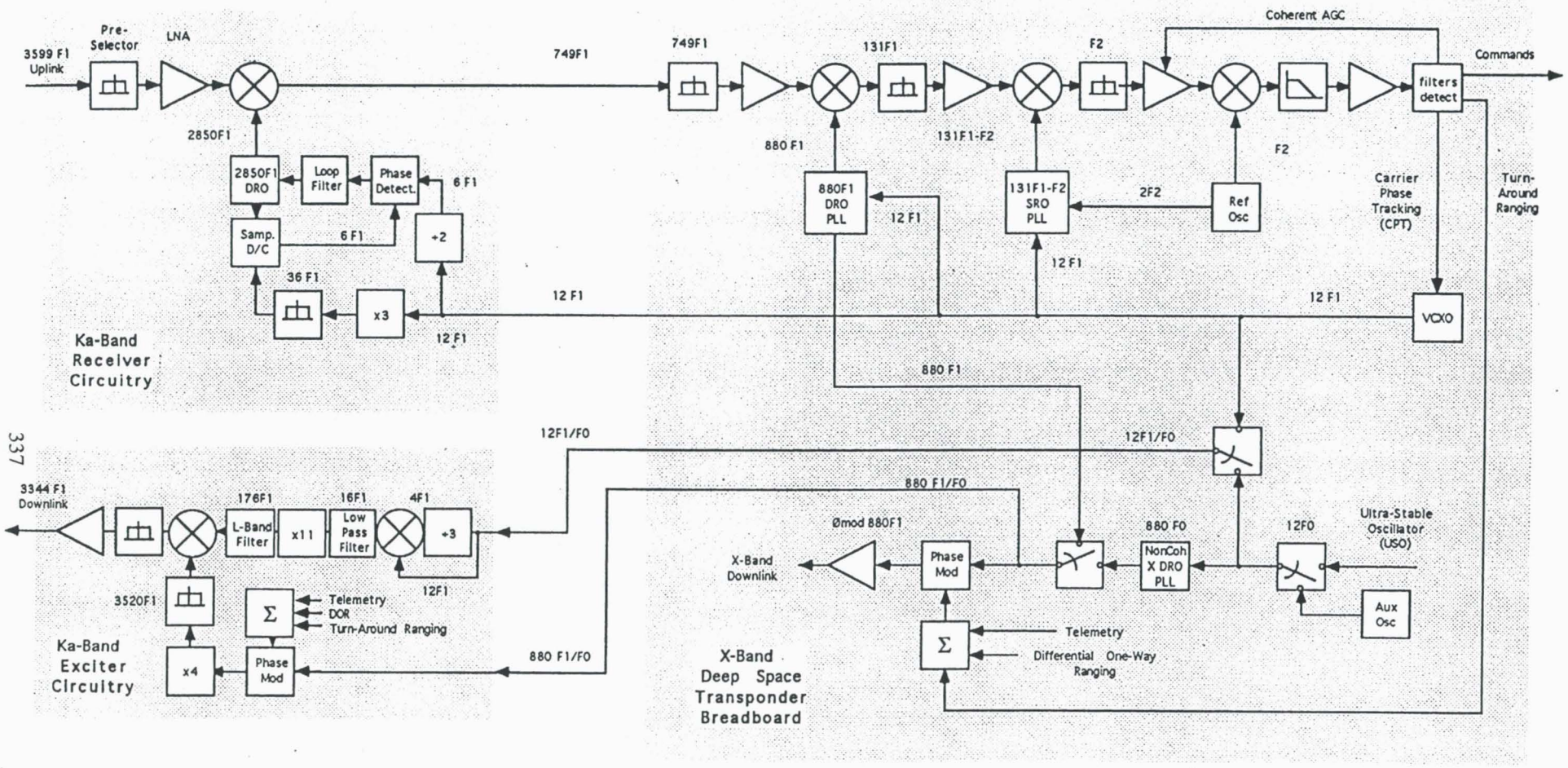

John P. Lane
2/25/93

SESSION 6

MODULATION AND CODING

CURRENT RESEARCH ON THE TCM

COMMUNICATIONS SYSTEMS

Warner Miller
National Aeronautics and Space Administration
Goddard Space Flight Center
Greenbelt, Maryland 20771

ABSTRACT

This report provides information regarding NASA's interest in TCM communications systems along with the recent TCM testing at White Sands Ground Station (WSGT) in New Mexico. The measurement results are presented for two codes, namely, pragmatic code and four dimensional rotationally invariant code.

TCM Overview

- TCM Invented by G. Ungerbeck in 1976
- Intended for applications that are both power and bandwidth limited channels.
- Applied to wireline modems under CCITT recommendation V.32 starting in 1984.
- Testing of the concepts by NASA and COMSAT/Intelsat but no operational SATCOM hardware to date.

NASA's Interest

- Both the KSA and SSA modes of TDRSS are becoming saturated.
- With 8PSK TCM as opposed to the existing 4PSK R=1/2 convolutional codes the information rate of the KSA or the SSA transponders can be doubled.
- This higher rate can be used to increase the amount of user data and/or reduce the users contact time.

8PSK TCM Versus NASA STD RS 1/2, K=7 Convolutional Code With QPSK

Quantity	8PSK-TCM	QPSK-R=1/2
Bandwidth	Equal	Equal
Information Rate	2X-3X	X
Modem Eb/No Req'd	Y+2-3dB	Y
Symbol Sync. Technique	Early/Late Gate w/Soft Decisions	Early/Late Gate w/Hard Decisions
Symbol Sync. BW	W	W
Carrier Sync.	Costas Crossover Loop w/8 Level Decisions	Costas Crossover Loop 4 Level Decisions
Carrier Loop BW	Z/8	Z
Threshold Effects	Code & Carrier	Code

Recent TCM Testing at WSGT

- NMSU under a grant from NASA has just completed a series of TCM Tests
- 8PSK TCM was used with two codecs
- The NMSU codec employed the pragmatic code with bandwidth improvement of 2 and theorical coding gain of 3dB over uncoded PSK
- The Norte Dame codec employed a 4 dimensional rotationally invariant code with bandwidth improvement of 2.5 and theorical coding gain of 1.8dB

Test System Diagram

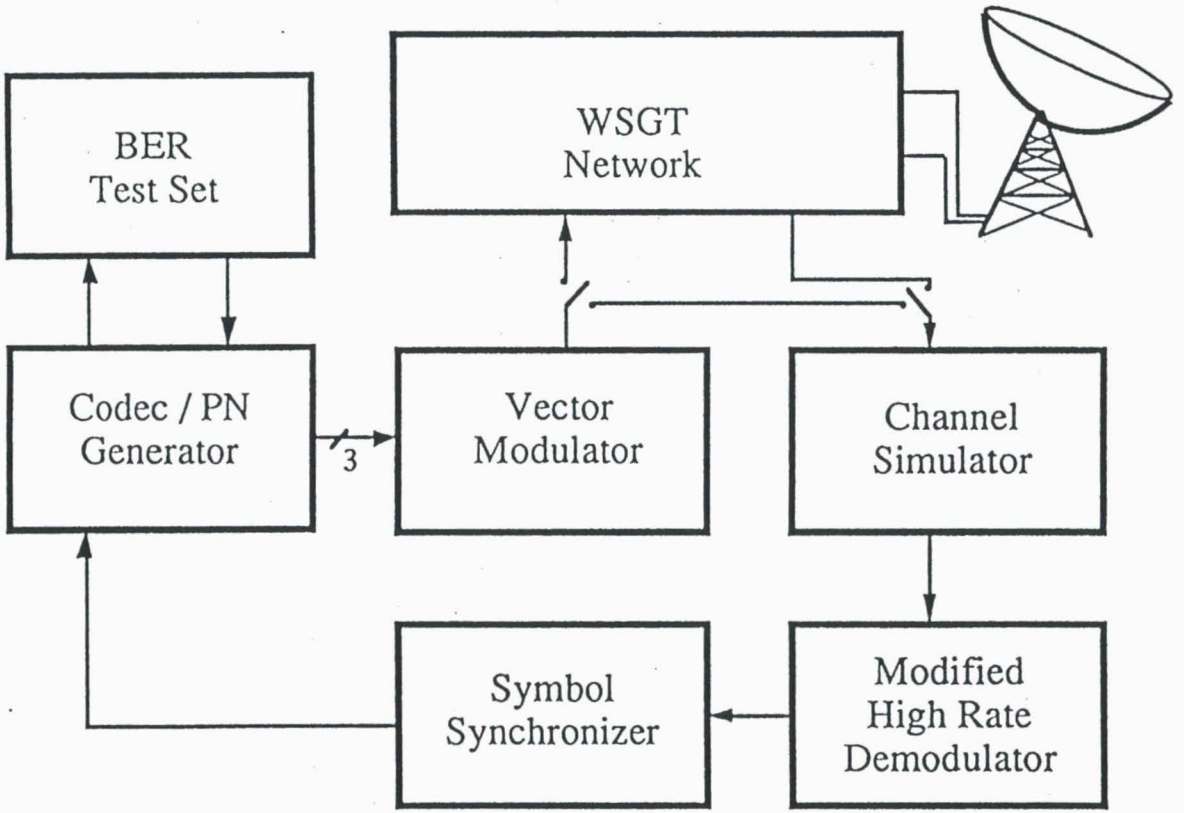

Translation Verification

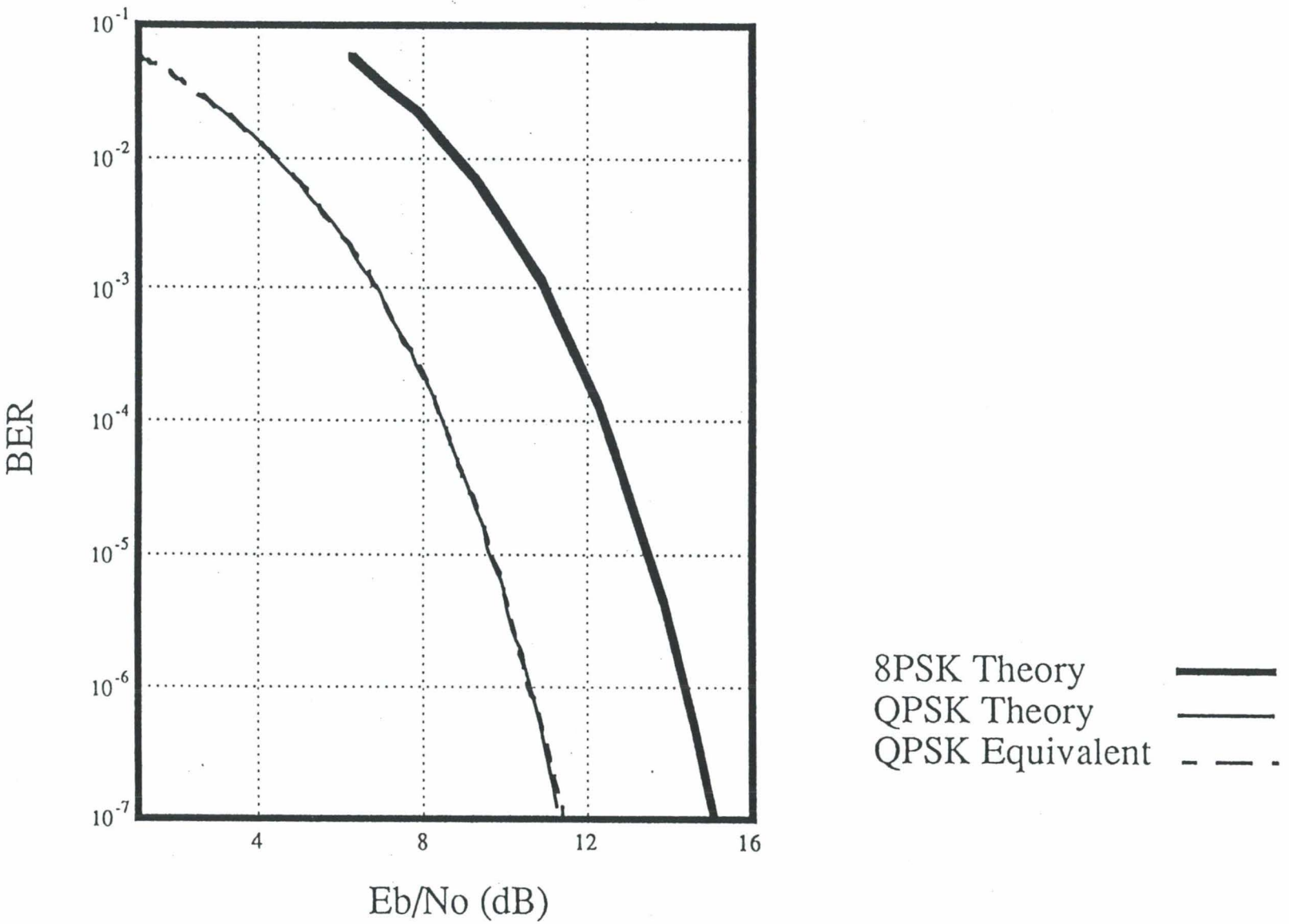

Baseline Comparison

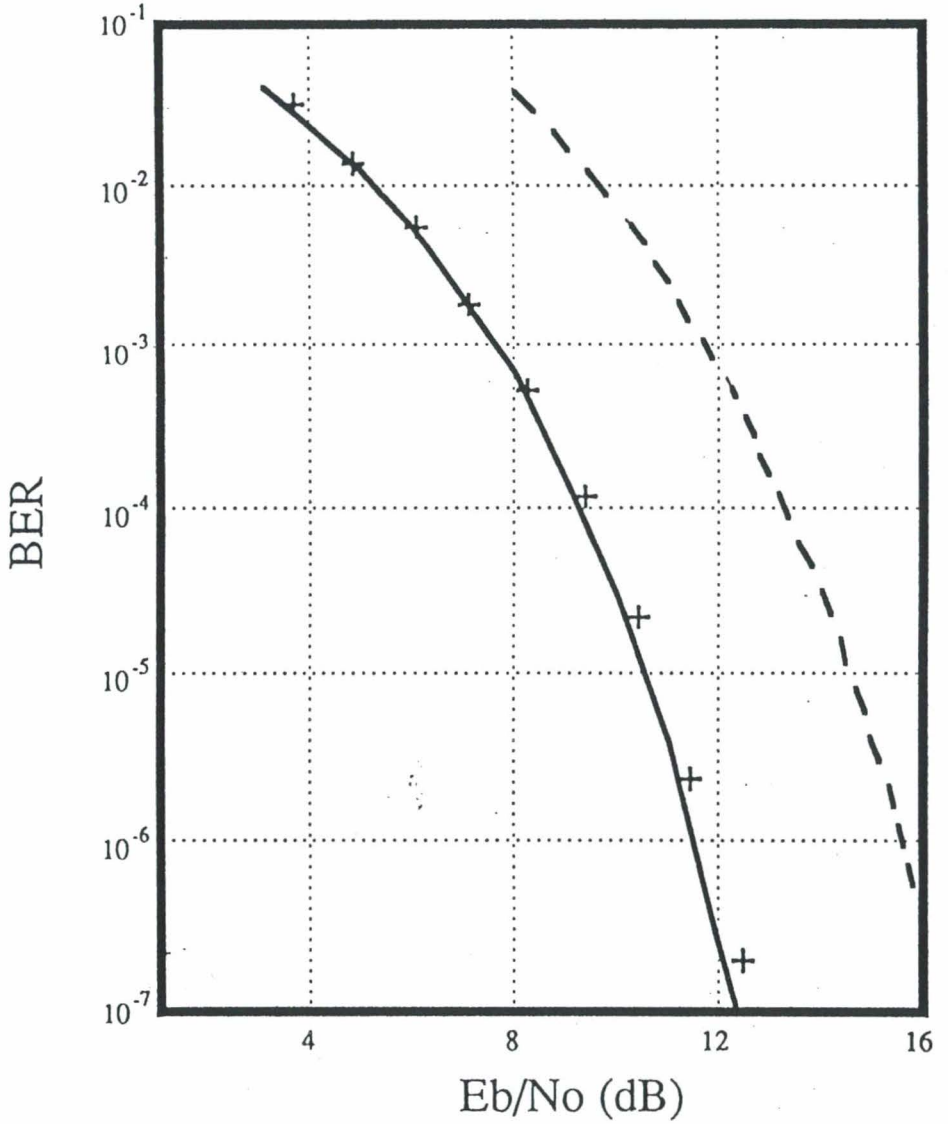

8PSK Measured ----

QPSK Measured ——

QPSK Equivalent + + +

Uncoded S-band Performance

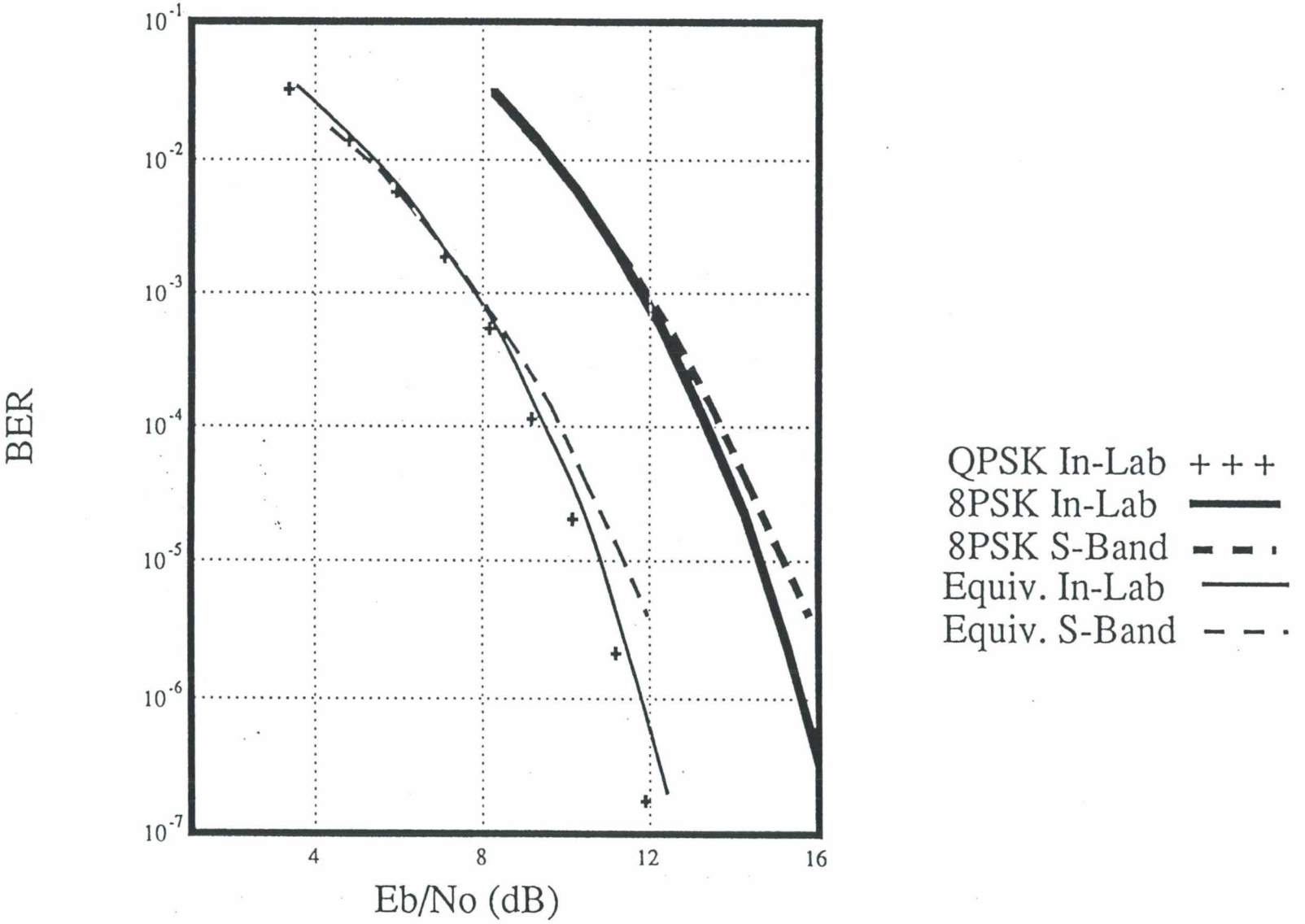

S-Band Performance of NMSU TCM Codec

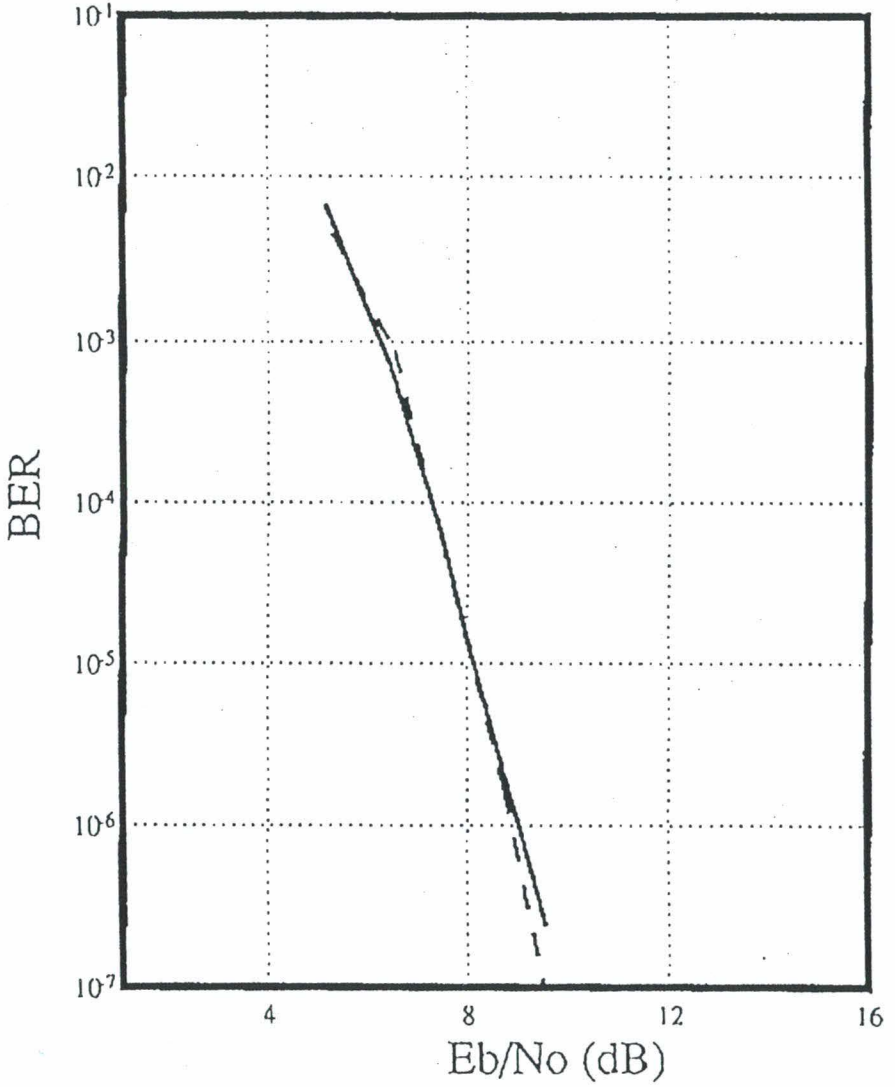

In-Lab Performance - - - -
S-Band Performance ____

NMSU S-Band Performance

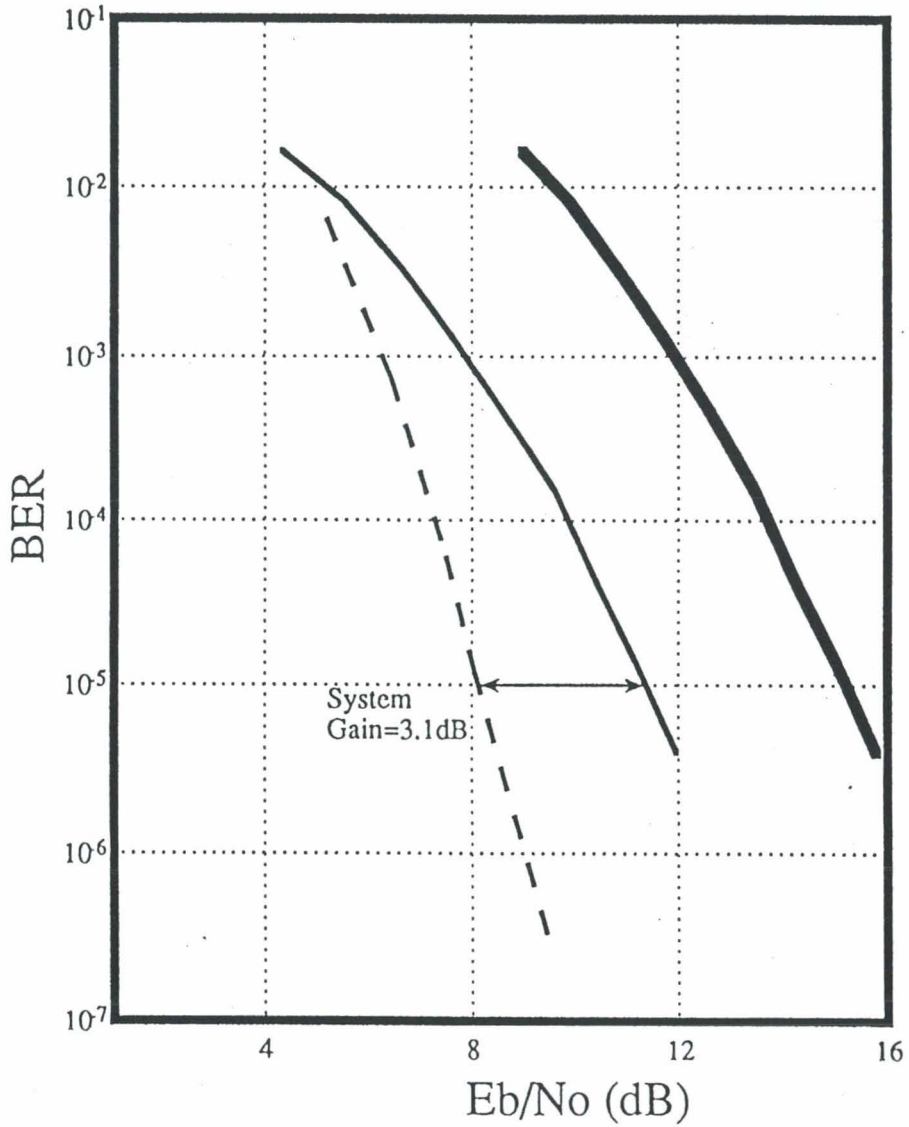

Coded Performance ----

8PSK Measured ━━━

QPSK Equivalent ——

UND S-Band Performance

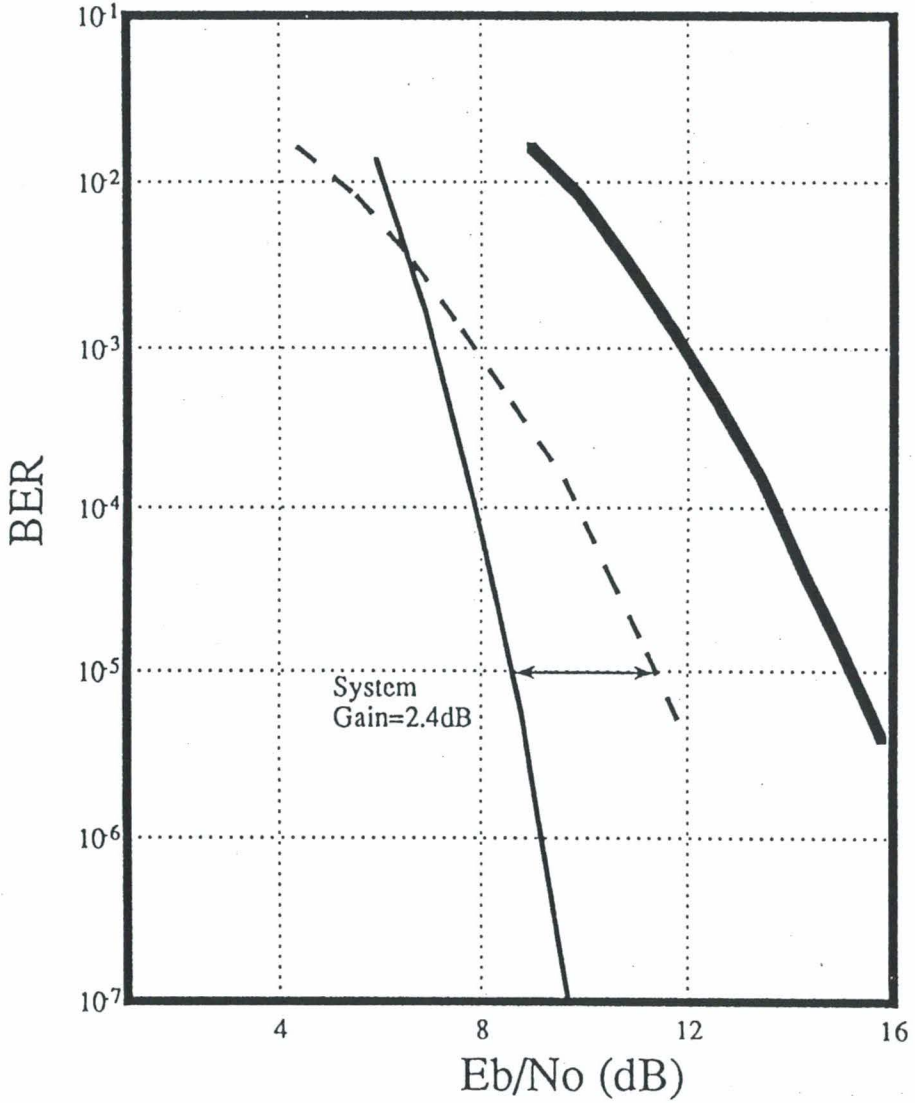

Coded Performance ----

8PSK Measured ——

QPSK Equivalent ——

Additional MPSK and TCM Testing

- Test performance of TDRSS KSA Transponder with 450MBPS 8PSK data (October '93).
- Test performance of TDRSS SSA Transponder with TCM 8PSK at Symbol Rates up to 12 MSPS (March '94).
- Use NASA Lewis advanced programmable digital modem to test various pulse shaping and equalization schemes with the SSA Transponder (March '94).

BANDWIDTH EFFICIENT CODING:

THEORETICAL LIMITS AND REAL ACHIEVEMENTS[1]

Daniel J. Costello, Jr., Servanne Couturier, Yannick Levy,
Diane G. Mills, Lance C. Perez, and Fu-Quan Wang
University of Notre Dame
Department of Electrical Engineering
Notre Dame, IN 46556

ABSTRACT

This paper presents an interim report on the error control techniques for satellite and space communications under NASA Grant NAG5-557. The paper reports a restatement of the channel capacity bound along with other practical bounds for various modulation schemes. Furthermore, this paper also provides a specific bound for a specified signaling method and spectral efficiency.

[1] The work described in this paper was carried out at the University of Notre Dame, under contract with the National Aeronautics and Space Administration.

Introduction

- In his seminal 1948 paper "*The Mathematical Theory of Communication*", Claude E. Shannon derived the "channel coding theorem" which gave an explicit upper bound, called the channel capacity, on the rate at which "information" could be transmitted reliably on a given communication channel.
- Shannon's result was an existence theorem and did not give specific codes to achieve the bound. Some skeptics have claimed that the dramatic performance improvements predicted by Shannon are not achievable in practice.
- The advances made in the area of coded modulation in the past decade have made communications engineers optimistic about the possibility of achieving or at least coming close to channel capacity. Here we consider this possibility in the light of current research results.

Channel Capacity

With respect to coding and coded modulation, the most relevant of Shannon's results is the "noisy channel coding theorem for continuous channels with average power limitations."

This theorem states that for any transmission rate R less than or equal to the channel capacity, C, there exists a coding scheme that achieves an arbitrarily small probability of error!

Conversely, if R is greater than C, no coding scheme can achieve reliable communication, *regardless of complexity.*

Shannon then shows that the capacity, C, of a continuous additive white Gaussian noise (AWGN) channel with bandwidth B and assuming Nyquist signaling is given by

$$C = B \log_2 \left(1 + \frac{E_s}{N_0}\right) bits/sec, \tag{1}$$

where E_s is the average signal energy in each signaling interval T and $N_0/2$ is the two sided noise power spectral density.

This bound represents the absolute best performance possible for a communication system on the AWGN channel.

Restatement of the Capacity Bound

- Shannon's capacity bound can be put in a form more useful for the present discussion by introducing the parameter η, called spectral efficiency, to represent the average number of information bits transmitted per signaling interval.
- From Shannon's bound, it follows that

$$0 \leq R \leq C \ \ bits/sec,$$

and hence

$$0 \leq \eta \leq C/B \ \ bits/signal.$$

- Substituting the relation

$$E_s/N_0 = \eta E_b/N_0,$$

where E_b is the average energy per information bit, into equation (1) and performing some minor manipulations yields

$$E_b/N_0 \geq \frac{2^\eta - 1}{\eta}, \tag{2}$$

which relates the spectral efficiency, η, to the signal-to-noise ratio (SNR), E_b/N_0.

- The bound of equation (2) manifests the fundamental tradeoff between spectral efficiency and SNR. That is, increased spectral efficiency can be reliably achieved only with a corresponding increase in SNR.

Interpretation of the Capacity Curve

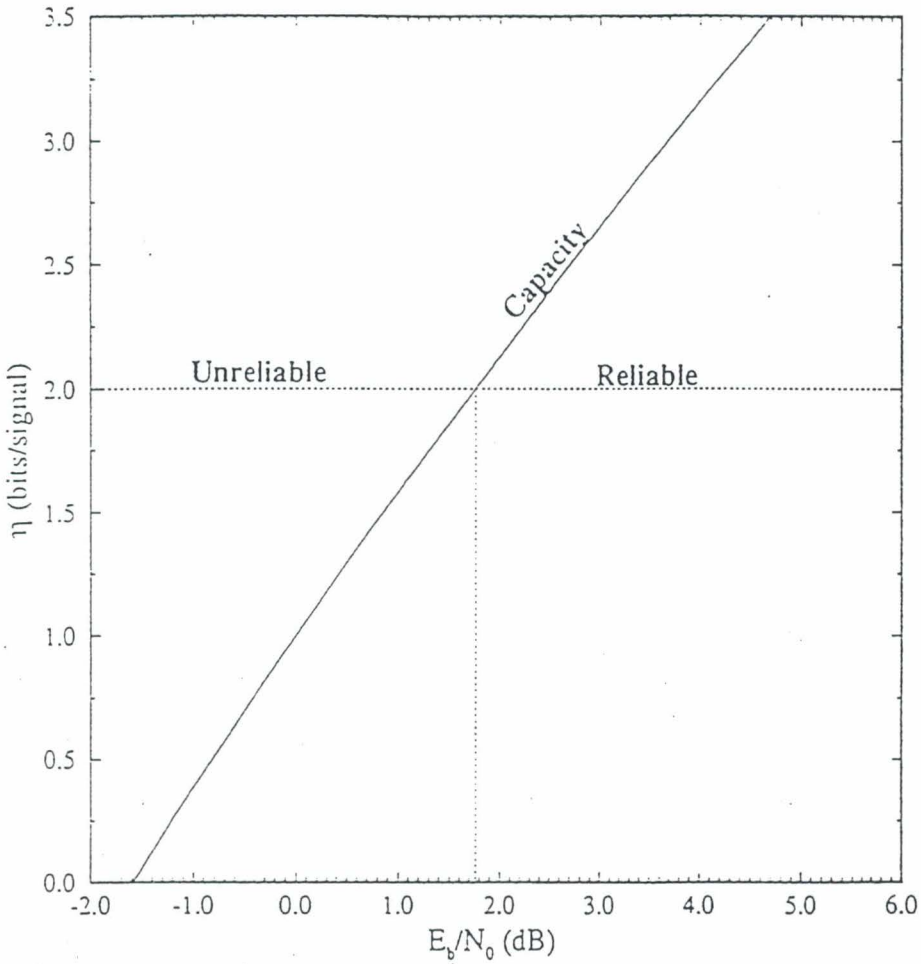

- Shannon's bound gives the minimum signal-to-noise ratio (SNR) required to achieve a specific bandwidth efficiency with an arbitrarily small probability of error.
- *Example*: With $\eta = 2$ information bits per channel signal, there exists a coding scheme that operates reliably with an SNR of 1.76dB.
- Conversely, any coding scheme sending $\eta = 2$ information bits per signal with an SNR *less than* 1.76dB will be unreliable, *regardless of complexity*.

Interpretation of the Capacity Curve

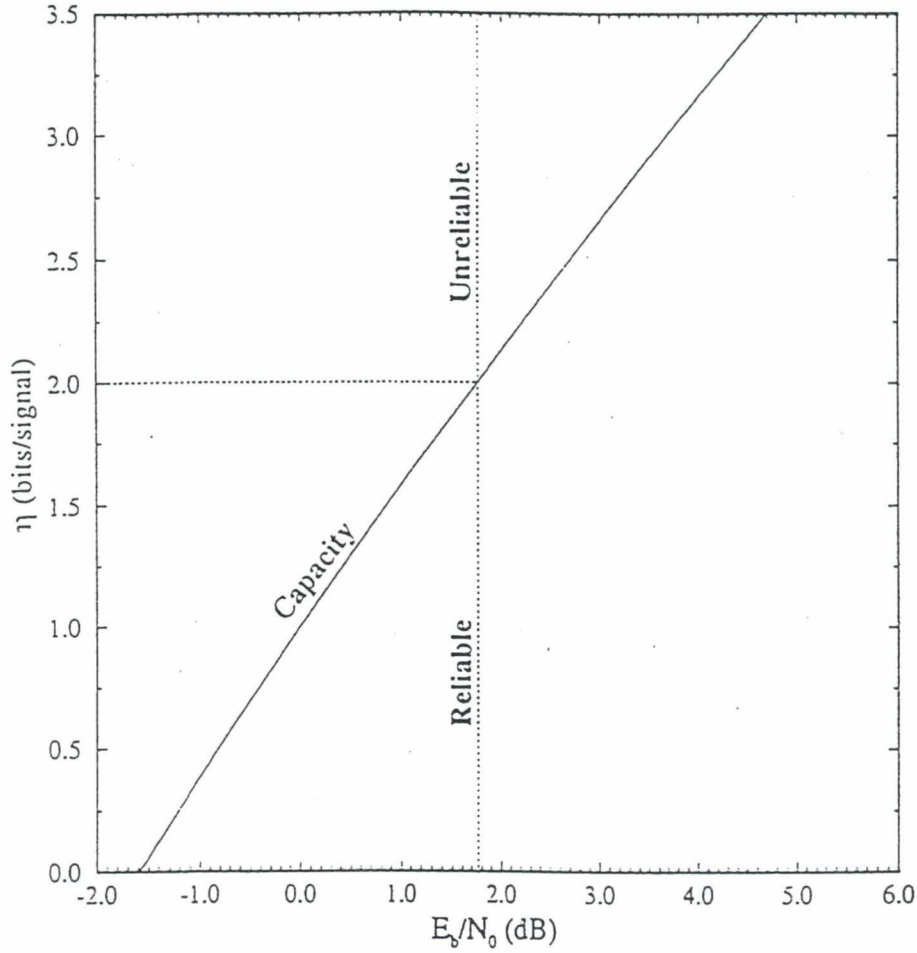

- Alternatively, Shannon's bound gives the maximum achievable spectral efficiency for a specific signal-to-noise ratio (SNR).
- *Example*: With an SNR of $E_b/N_0 = 1.76$db, there exists a coding scheme cabable of transmitting reliably with a spectral efficiency of $\eta = 2$ bits per signal.
- Conversely, any coding scheme operating with an SNR of $E_b/N_0 = 1.76$dB and attempting to transmit *more than* $\eta = 2$ bits per sign will be unrealiable *regardless of complexity.*

NASA (2,1,6) Convolutional Code

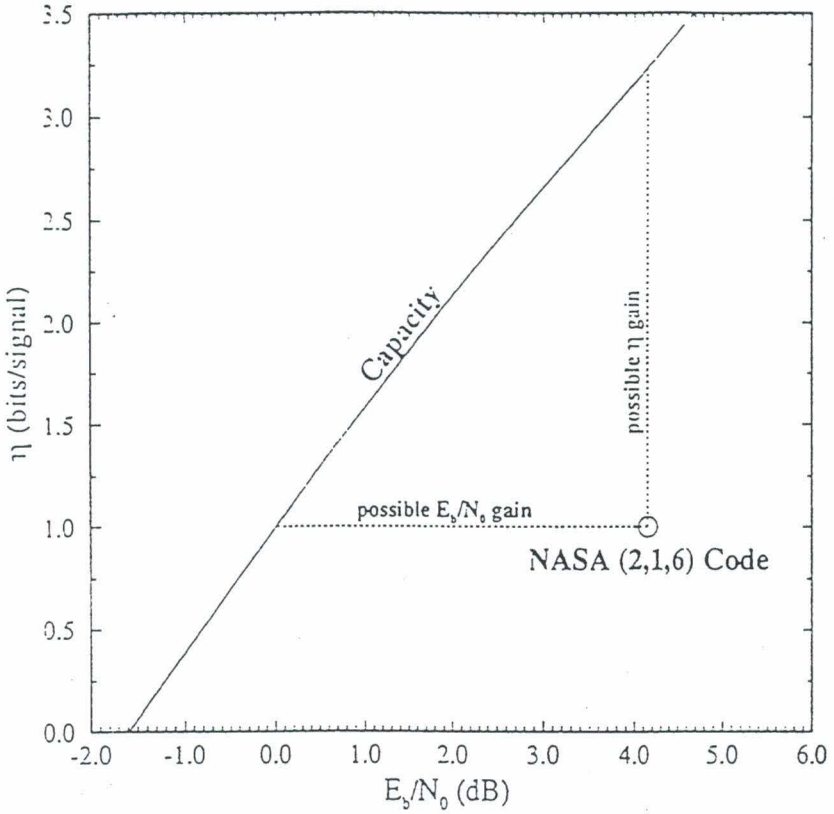

- Historically, most real communications systems operated well below capacity.
- *Example*: The NASA standard rate (2,1,6) convolutional code with QPSK modulation achieves a spectral efficiency of $\eta = 1$ bit/signal and requires a signal-to-noise ratio (SNR) of $E_b/N_0 =$ 4.15 dB to achieve error free (10^{-5} bit error rate) communication.
- An ideal system operating with the same $E_b/N_0 = 4.15$dB can achieve error free communication with a spectral efficiency as high as $\eta = C = 3.235$ bits per signal.

OR

An ideal system operating with the same spectral efficiency of $\eta = 1$ bit per signal would require an SNR of only $E_b/N_0 = 0.0$ dB

A New Optimal (2,1,14) Convolutional Code

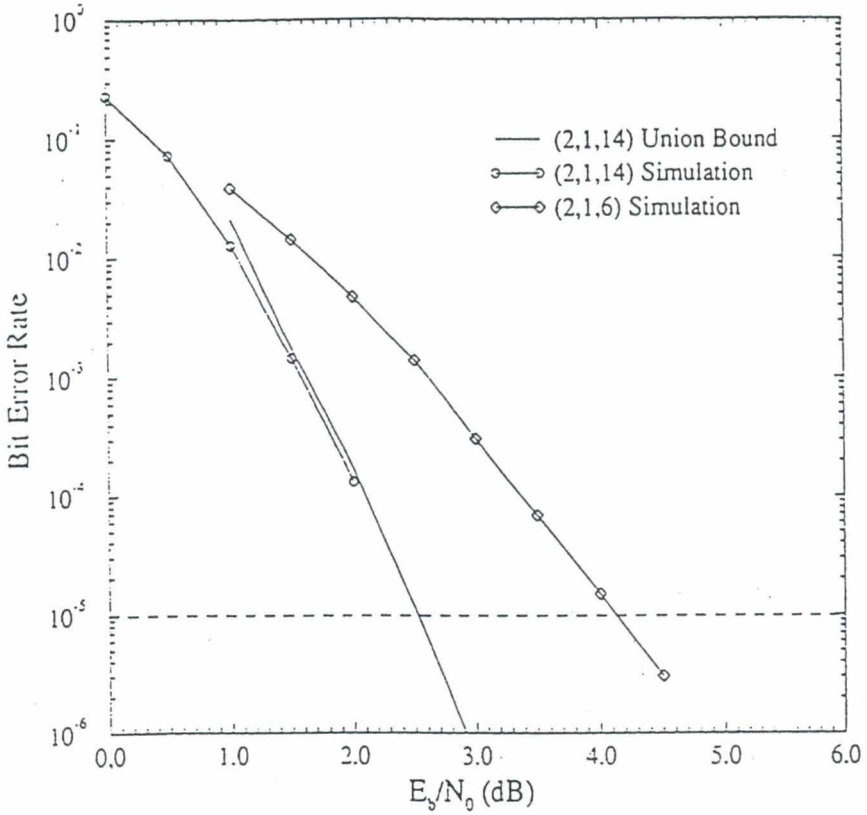

- A computer search has found the optimum distance spectrum (ODS) (2,1,14) convolutional code.
- This code has optimum minimum free Hamming distance, $d_{free} = 18$, and the smallest number of nearest neighbors, $N_{free} = 26$, of any constraint length 15 code.
- The performance of this code is 1.65 dB better than the (2,1,6) code, but is still 2.5dB away from capacity.

Optimal (2,1,14) Convolutional Code

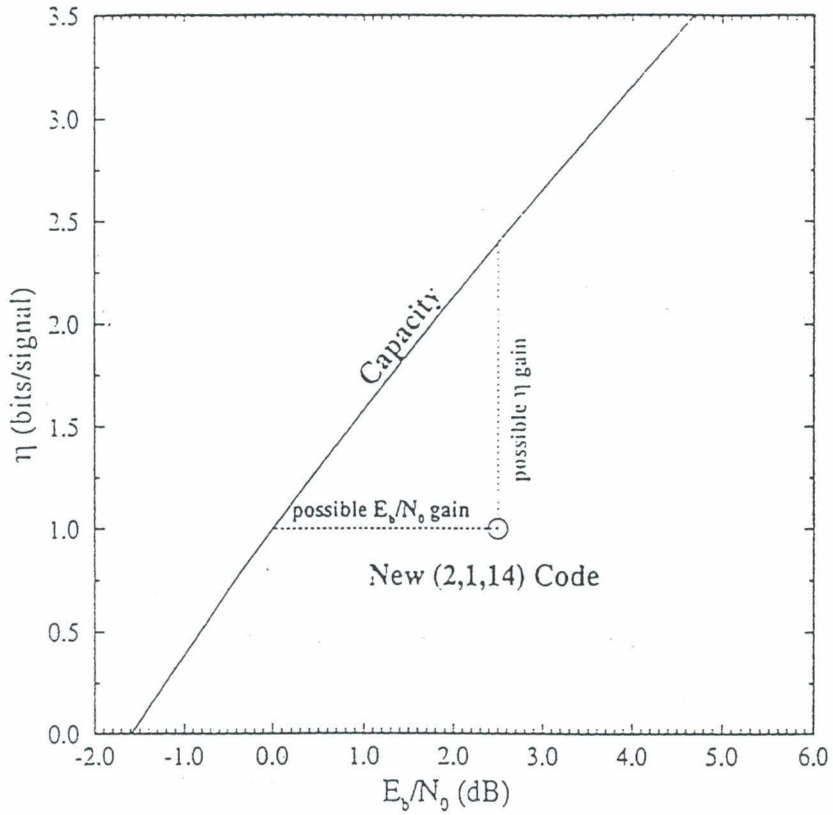

- The new optimal (2,1,14) convolutional code requires a signal-to-noise ratio (SNR) of $E_b/N_0 = 2.5$ dB to achieve error free (10^{-5} bit error rate) communication.
- An ideal system operating with the same $E_b/N_0 = 2.5$dB can achieve error free communication with a spectral efficiency as high as $\eta = C = 2.4$ bits per signal.

OR

An ideal system operating with the same spectral efficiency of $\eta = 1$ bit per signal would require an SNR of only $E_b/N_0 = 0.0$ dB.

Practical Bounds

- In real communication systems, there are many practical considerations that take precedence over Shannon's bound in design decisions.
- For example, satellite communication systems that use nonlinear travelling wave tube amplifiers (TWTA's) require constant envelope signaling such as M-ary phase shift keying (MPSK).
- Thus, even *if* Shannon's results firmly stated that capacity at a spectral efficiency of $\eta = 3$ bits per signal can be achieved with a (4,3,8) convolutional code using 16 QAM, it would not be feasible to do so on the TWTA satellite link.
- It therefore seems reasonable to ask what is the minimum SNR required to achieve reliable communication, *given* a particular modulation scheme and a spectral efficiency, η.

A Signal Specific Bound

- For the discrete input, continuous output, memoryless AWGN channel with M-ary one dimensional amplitude modulation (AM) or two dimensional (PSK, QAM) modulation and equiprobable signaling, the capacity bound becomes

$$\eta^* = \log_2(M) - \frac{1}{M}\sum_{i=0}^{M-1} E\left\{\log_2 \sum_{j=0}^{M-1} \exp\left[\frac{|a^i + n - a^j|^2 - |n|^2}{N_0}\right]\right\}, \quad (3)$$

- Here

$$\left\{a^j, j = 0, 1, \ldots M-1\right\} \quad (4)$$

is an M-ary modulations set, a^j is a channel signal, n is a Gaussian distributed noise random variable with mean 0 and variance $N_0/2$, and E is the expectation operator.

- For a specified signaling method and spectral efficiency, this bound can be used to compute the minimum SNR required to achieve reliable communication.

Interpretation of the Signal Specific Bound

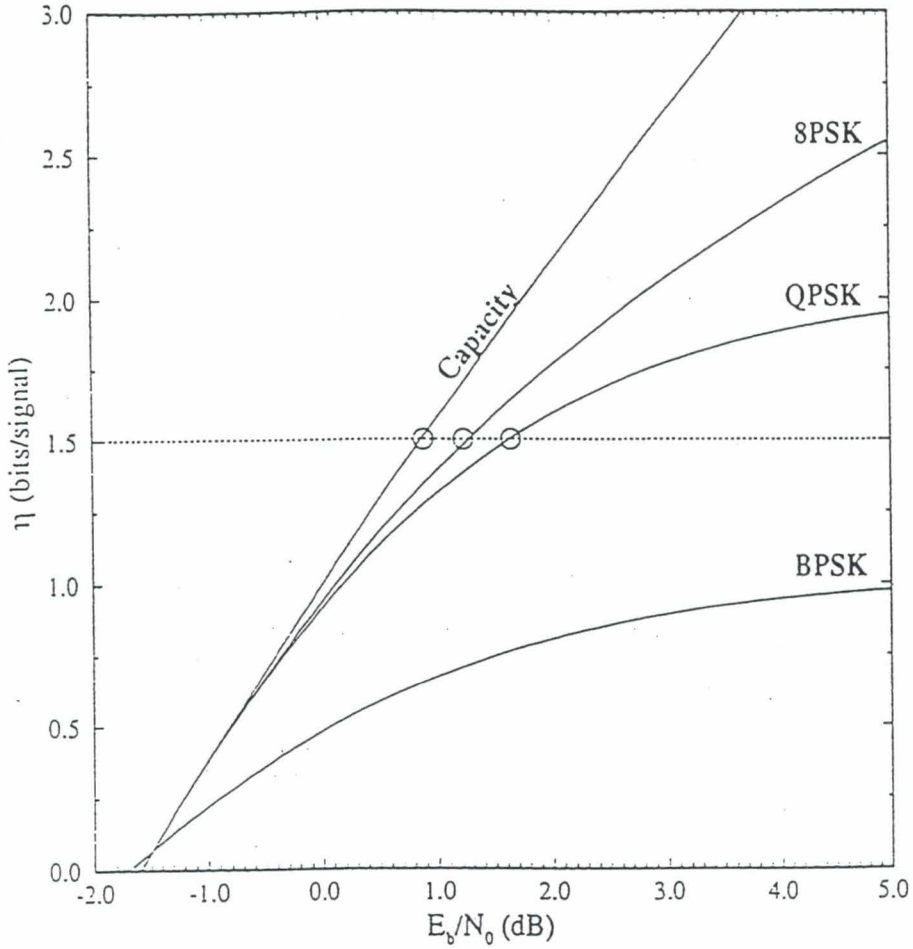

- To send $\eta = 1.5$ information bits per signaling interval, an ideal system *using QPSK modulation* requires a minimum SNR of $E_b/N_0 =$ 1.64dB. This is 0.76 dB more than an ideal system without any modulation constraints.
- To send $\eta = 1.5$ information bits per signaling interval, an ideal system *using 8PSK modulation* requires a minimum SNR of $E_b/N_0 =$ 1.22dB. This is 0.34 dB more than an ideal system without any modulation constraints.

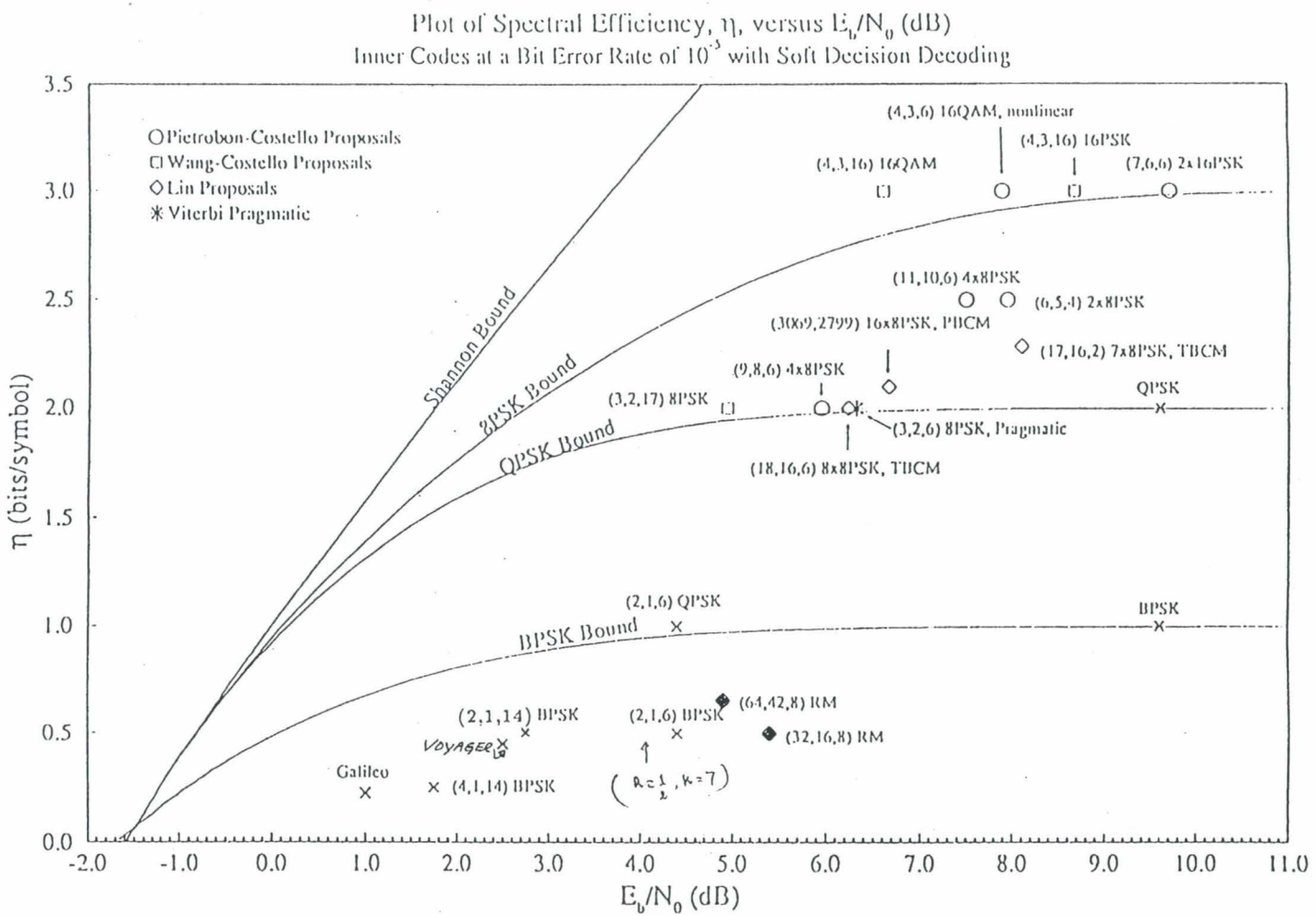
Plot of Spectral Efficiency, η, versus E_b/N_0 (dB)
Inner Codes at a Bit Error Rate of 10^{-5} with Soft Decision Decoding
○ Pietrobon-Costello Proposals
□ Wang-Costello Proposals
◇ Lin Proposals
✳ Viterbi Pragmatic
Shannon Bound
8PSK Bound
QPSK Bound
BPSK Bound
(4,3,6) 16QAM, nonlinear
(4,3,16) 16QAM
(4,3,16) 16PSK
(7,6,6) 2x16PSK
(11,10,6) 4x8PSK
(6,5,4) 2x8PSK
(3069,2799) 16x8PSK, PBCM
(17,16,2) 7x8PSK, TBCM
(9,8,6) 4x8PSK
(3,2,17) 8PSK
QPSK
(3,2,6) 8PSK, Pragmatic
(18,16,6) 8x8PSK, TBCM
(2,1,6) QPSK
BPSK
(2,1,14) BPSK
VOYAGER
(2,1,6) BPSK
(64,42,8) RM
(32,16,8) RM
Galileo
(4,1,14) BPSK
(R=1/2, K=7)
η (bits/symbol)
E_b/N_0 (dB)
3.5
3.0
2.5
2.0
1.5
1.0
0.5
0.0
-2.0
-1.0
0.0
1.0
2.0
3.0
4.0
5.0
6.0
7.0
8.0
9.0
10.0
11.0

All results are with soft decision decoders.

1 NASA Codes: denoted by $\times$

Galileo: This is the concatenated code used on the Galileo probe.

(4,1,14) BPSK The is the (4.1.14) convolutional code developed by JPL.

Voyager: This is the concatenated code used on the Voyager probe.

(2,1,6) BPSK: This is the NASA standard (2.1.6) convolutional code with BPSK modulation.

(2,1,6) QPSK: This is the NASA standard (2.1.6) convolutional code with QPSK modulation.

2 Pietrobon-Costello Codes: denoted by $\bigcirc$

(6,5,4) 2x8PSK: This is a rate 5/6, 16 state, trellis code using 2x8PSK modulation with Viterbi decoding. It has a spectral efficiency of $\eta = 2.5$ bits/signal and is 45° rotationally invariant. A Viterbi decoder for this code has been built by Steven Pietrobon and tested at New Mexico State.

(9,8,6) 4x8PSK: This is a rate 8/9, 64 state, trellis code using 4x8PSK modulation with Viterbi decoding. It has a spectral efficiency of $\eta = 2.0$ bits/signal and is 45° rotationally invariant.

(11,10,6) 4x8PSK: This is a rate 10/11, 64 state, trellis code using 4x8PSK modulation with Viterbi decoding. It has a spectral efficiency of $\eta = 2.5$ bits/signal and is 45° rotationally invariant.

(7,6,6) 2x16PSK: This is a rate 6/7, 64 state, trellis code using 2x16PSK modulation with Viterbi decoding. It has a spectral efficiency of $\eta = 3.0$ bits/signal and is 45° rotationally invariant.

(4,3,6) 16QAM, nonlinear: This is a nonlinear rate 3/4, 16 state, trellis code using 16QAM modulation with Viterbi decoding. It has a spectral efficiency of $\eta = 3.0$ bits/signal and is 90° rotationally invariant.

3 Wang-Costello Codes: denoted by $\square$

(3,2,17)8PSK: This is a rate 2/3, memory 17, trellis code using 8PSK modulation and sequential decoding with a modified Fano algorithm. It has a spectral efficiency of $\eta = 2.0$ bits/signal and is 180° rotationally invariant.

(4,3,16) 16PSK: This a rate 3/4, memory 16, trellis code using 16PSK modulation and sequential decoding with a modified Fano algorithm. It has a spectral efficiency of $\eta = 3.0$ bits/signal and is 180° rotationally invariant.

(4,3,16) 16QAM: This is a rate 3/4, memory 16, trellis code using 16QAM modulation and sequential decoding with a modified Fano algorithm. It has a spectral efficiency of $\eta = 3.0$ bits/signal and is 180° rotationally invariant.

4 Lin Codes: denoted by ◇

(32,16,8) RM: This is a rate 16/32=0.5, 64 state Reed-Muller code using BPSK modulation and Viterbi decoding.

(64,42,8) RM: This is a rate 42/64=0.656, 1024 state Reed-Muller code using BPSK modulation and Viterbi decoding.

(17,16,2) 7x8PSK, TBCM: This is rate 16/17, 4 state, block coded modulation scheme using 7x8PSK modulation with Viterbi decoding. It has a spectral efficiency of $\eta = 2.286$ bits/signal and is 180° rotationally invariant.

(18,16,6) 8x8PSK, TBCM: This is a 2-level trellis code using 8x8PSK modulation. The first level has 64 states and is decoded with a Viterbi decoder. The second level has 8 states and is deocded with a Viterbi decoder. It has a spectral efficiency of $\eta = 2.0$ bits/symbol and is 180° rotationally invariant.

(3069,2799) 16x8PSK, PBCM: This is a 3x3 product block coded modulation scheme. The horizontal codes are BCH codes and the vertical code is a 3-level block code. It is decoded using suboptimal multi-stage decoding. It has a spectral efficiency of $\eta = 2.1$ bits/signal and is 45° rotationally invariant.

5 Viterbi Pragmatic Code: denoted by *

(3,2,6) 8PSK, Pragmatic: This is a rate 2/3, 64 state, trellis code using 8PSK modulation and Viterbi decoding. It uses the NASA standard (2,1,6) convolutional code as its basis and is suboptimal. It can be decoded using essentially the same Viterbi decoding chip that is used to decode the NASA standard convolutional code.

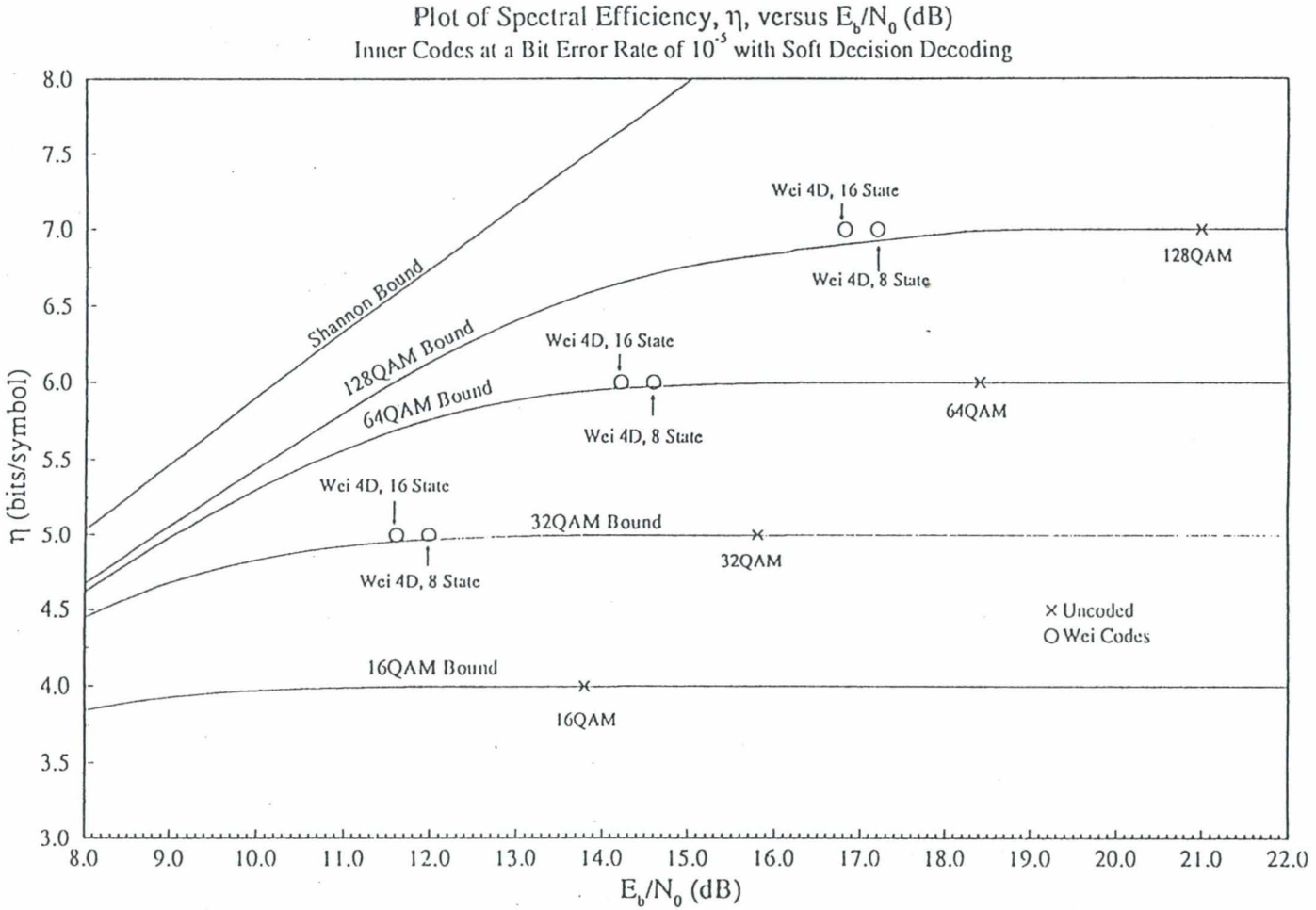
Plot of Spectral Efficiency, η, versus E_b/N_0 (dB)
Inner Codes at a Bit Error Rate of 10^{-5} with Soft Decision Decoding
η (bits/symbol)
E_b/N_0 (dB)
Shannon Bound
128QAM Bound
64QAM Bound
32QAM Bound
16QAM Bound
Wei 4D, 16 State
Wei 4D, 8 State
128QAM
64QAM
32QAM
16QAM
× Uncoded
O Wei Codes

Notes About the Graph

All results are with soft decision decoders.

1 Uncoded Systems: denoted by $\times$

16QAM: Performance of uncoded 16QAM with a spectral efficiency of $\eta = 4$ bits/symbol from simulation results.

32QAM: Performance of uncoded 32QAM with a spectral efficiency of $\eta = 5$ bits/symbol from simulation results.

64QAM: Performance of uncoded 64QAM with a spectral efficiency of $\eta = 6$ bits/symbol from simulation results.

128QAM: Performance of uncoded 128QAM with a spectral efficiency of $\eta = 7$ bits/symbol from simulation results.

2 Wei Codes: denoted by $\bigcirc$

Wei 4D, 8 state: This is Wei's 8 state code using a 4-dimensional constellation (of any size). Performance taken from "Coset Codes - Part 1: Introduction and Geometrical Classification." by G. David Forney. The performance was estimated taking into account the minimum squared Euclidean distance and the number of nearest neighbors. Thus, this point shows effective coding gain at a bit-error-rate (BER) of 10^{-5}.

Wei 4D, 16 state: This is Wei's 16 state code using a 4-dimensional constellation (of any size). Performance taken from "Coset Codes - Part 1: Introduction and Geometrical Classification." by G. David Forney. The performance was estimated taking into account the minimum squared Euclidean distance and the number of nearest neighbors. Thus, this point shows effective coding gain at a bit-error-rate (BER) of 10^{-5}.
This code with a 2x192QAM constellation is being considered by CCITT for the V.FAST ultimate modem standard.

Performance of Trellis Coded Modulation with 8PSK Through TDRSS

By
William Osborne
Ted Wolcott
New Mexico State University
Las Cruces, New Mexico

Abstract

The need to increase data-rate capabilities of the Tracking and Data Relay Satellite System (TDRSS) has prompted NASA to investigate bandwidth-efficient modulation schemes. Based upon current technology the most promising scheme is Trellis-Coded Modulation (TCM) operating with Octal Phase Shift Keying (8PSK). In conjunction with NASA, New Mexico State University's Manuel Lujan Jr. Center for Space Telemetering and Telecommunications Systems has constructed a system to test this new candidate TDRSS modulation scheme, TCM 8PSK. This system was tested through the TDRSS channel to demonstrate that this coding scheme operates as well over the actual channel as it has in lab experiments and simulations. Two interchangeable codecs, implementing separate TCM techniques, were tested. The results of this experiment and subsequent data analysis are presented in this paper.

Background

As the National Aeronautics and Space Administration moves into the 21st century with programs like Space Station Freedom and the new Landsat mission, transmission demands on the Tracking and Data Relay Satellite System (TDRSS) will very likely exceed the available bandwidth. Under NASA grant NAG 5-1491, the Manuel Lujan Jr. Center for Space Telemetering and Telecommunications Systems at New Mexico State University is studying techniques for increasing the data-rate capabilities of TDRSS. These techniques include the use of advanced bandwidth-efficient modulation formats to increase the data rate that can be sustained in a TDRSS transponder and the use of lossless bandwidth compression of the data to be transmitted to lower the data rate required from the user spacecraft.

Currently, TDRSS operates with coded QPSK. Use of uncoded 8PSK would decrease the bandwidth requirement by a factor of 3, while allowing more information to be transmitted with each symbol. The problem with implementing uncoded 8PSK is a significant decrease in performance. The error rates experienced by an uncoded 8PSK system are much higher due to constellation points in closer proximity to one another. In order to make up for the lost performance, error-correction coding must be used. But coding decreases the amount of information carried by individual symbols and therefore decreases the data throughput.

The best solution to this problem is a code that performs well with a minimum of bandwidth expansion. A coding scheme that meets these tough requirements is Trellis-Coded Modulation (TCM). In fact, laboratory tests have shown that 8PSK operating with TCM can perform at error rates lower than uncoded QPSK while transmitting at least as much information in each symbol. This scheme had never been tested through the actual TDRSS channel. It was not known if the channel would affect the coding scheme in a way that was unaccounted for in previous laboratory tests and simulations.

Tests were performed through the TDRSS channel with the help of the White Sands Ground Terminal (WSGT) and NASA. For the test, two TCM codecs (coders/decoders) were developed. One, built by NMSU, is a rate 2/3 Pragmatic Codec [3], while the other is a rate 5/6 TCM codec built by the University of Notre Dame and the University of South Australia [2]. Whereas the NMSU codec focuses on minimizing the system's error rate while maintaining two data bits per symbol, as in uncoded QPSK, the UND/USA codec transmits two and one-half data bits per symbol while still exhibiting a gain in system performance.

All tests were performed at 1 million symbols per second (1Msps). The rate was limited by the operational range of the support hardware and not by the codecs themselves.

Test System Configuration & Operation

A block diagram of the test system constructed by NMSU along with its interface with the WSGT network is shown in Figure 1. This network uses a small dish antenna from which the test signal is transmitted to simulate a user satellite. The signal is then received through TDRSS and routed back to the transmitter for analysis. The test system was designed to interface directly with this equipment. This required only two connections between the test system and the WSGT network. A 370MHz 8PSK data signal was supplied by the test system to the transmission side of the network. That data signal was then converted to

the S or K band frequency and routed through the TDRSS channel. The signal was recovered at 370MHz from the network at the return point.

As shown in Figure 1, the system starts and ends with the Bit Error Rate (BER) Test Set, where the pseudo-random bit sequence to be transmitted is created. This data sequence is supplied to the codec in operation and the PN Generator, which is used to create parallel channels of pseudo-random data for uncoded tests. Three parallel bits of coded or uncoded data are then supplied to the Vector Modulator for 8PSK modulation. The data is modulated on a 370MHz carrier for transmission over the channel and supplied to the WSGT network or routed directly to the test system's receive side or laboratory tests.

The receive side of the test system starts with a channel simulator that adds white noise to the data signal, rotates the data's phase for elimination of phase ambiguity, and conditions the signal for interface with the demodulator. The signal is then demodulated by a Harris High Rate Demodulator modified for 8PSK operation [1]. After demodulation, the bit clock is recovered from the demodulated signal by the Symbol Synchronizer, which also converts the received analog data signal into 5 bits of digital phase information. This data is then decoded and returned to the BER Test Set for measurement.

The two codecs used in the test operate similarly. The NMSU Pragmatic Codec uses the pragmatic TCM standard invented by Viterbi [4] to implement TCM using a currently available binary Viterbi decoder. The codec was implemented using two separate channels. The inboard channel processes a pseudo-random bit sequence using a standard rate 1/2, constraint length 7 convolutional encoder, creating two of the three symbol bits. The outboard channel simply passes a parallel pseudo-random bit sequence to the output as the third symbol bit. When the TCM sequence is decoded, the Viterbi decoder returns the convolutionally encoded bit while the outboard bit is returned by independent decision logic. Since the performance of the inboard bit alone is of most interest, these channels were kept separate in order to measure their performances individually.

The UND/USA codec uses a 4-dimensional signal set, each symbol consisting of a pair of 2-dimensional 8PSK signals [2]. Five data bits are encoded onto the 4-dimensional symbol, thereby achieving a code rate of 5/6 — 6 codebits per 5 data bits. This gives the code a slightly higher spectral efficiency. Differential encoding is used to achieve phase invariance.

System Gain Measurement

System gain is a performance measure defined as the gain in error rate performance seen at the output of the decoders, compared to an equivalent uncoded QPSK modem's performance. More precisely, system gain is the gain in bit energy to noise ratio (Eb/No) at an error rate of 1×10^{-5} demonstrated by the coded 8PSK system over an equivalent uncoded QPSK system.

In order to measure system gain as defined, an equivalent QPSK performance curve must be developed from the uncoded 8PSK performance curve. This is done by mapping from the 8PSK curve to the equivalent QPSK curve through a function of the BER. Each point on the measured curve is translated by ΔdB, where Δ is a function of BER defined by the graph in Figure 2.

Verification of this technique was performed by mapping the theoretical 8PSK BER curve to an equivalent QPSK curve. This curve was then compared to QPSK theory. As shown in Figure 3, the equivalent QPSK curve and the theoretical QPSK curve are identical to within a tenth of a decibel.

Uncoded System Performance

The first test performed was the measurement of the unmodified system performance. The performance of the unmodified HRD was measured and compared to similar data supplied with the equipment. Figure 4 shows the BER curve measured in the laboratory. These curves correspond to well within acceptable measurement error.

Once modifications were made to the HRD to allow it to demodulate 8PSK data, a baseline uncoded performance curve was measured. This curve is shown in Figure 5. Included in this figure is the uncoded QPSK curve measured before modification and the translated equivalent QPSK curve. An important feature of this graph is the slight flare present in the equivalent curve as Eb/No increases, as compared to the measured QPSK curve. This is to be expected, since the 8PSK modem also flares. This flare is due to increased sensitivity of an 8PSK system to phase noise. With smaller values of Eb/No, this phase noise is swamped by the white noise and is not a factor in the maximum likelihood decision process. The 8PSK uncoded baseline curve and its equivalent QPSK curve will be used to measure system gain for all in-lab codec tests.

The baseline measurement was repeated through both the S-band and K-band channels to allow proper system gain measurement under these conditions. Figure 6 and Figure 7 show the S-band and K-band uncoded 8PSK baseline performance curves. The in-lab baseline curve is

included in both to demonstrate the additional flare present in each channel. This is due to the significant levels of phase jitter on the channels that were not present during the in-lab test. The K-band channel shows less flare, indicating that the equipment in this link contributed less phase noise to the channel than the corresponding equipment in the S-band link.

NMSU Pragmatic Codec Performance

While in the laboratory, the performance of the NMSU Pragmatic Codec was measured. The resulting curve is shown in Figure 8. Included in this graph are the measured performance of the codec, the uncoded baseline measured in the lab and the equivalent uncoded QPSK curve. The system gain is 2.5dB at a BER of 1×10^{-5}, as shown. This measurement is slightly below theoretical predictions.

The performance was measured again through the TDRSS S-band and K-band channels. As shown in Figures 9 and 10, neither channel adversely affected the codec's performance.

Compared to the in-lab results, the system gain was measured to be higher through each of the TDRSS channels. These results, shown in graphs similar to the in-lab measurement, are shown in Figures 11 and 12. The S-band and K-band results demonstrate a system gain of 3.1dB and 2.9dB compared to the in-lab measurement of 2.5dB.

The increase in system gain is due to the ability of the codec to operate at lower levels of Eb/No where it is unaffected by the phase jitter that produces the flare associated with the uncoded system. In effect, the coded system is credited with fixing one of the major problems with the uncoded 8PSK system — flare caused by phase jitter at high signal-to-noise ratios.

The variation in system gain from one channel to the other is a result of to the difference in phase jitter in the different systems. Recall that the K-band network produced less phase noise than the S-band network. Although the codec operates almost identically through the two channels, it corrects for more performance loss in the S-band channel. Therefore, the coded system receives more credit, in the form of a higher system gain, through the S-band channel.

UND/USA Rate 5/6 TCM Codec

The in-lab tests showed that the UND/USA codec performs with a system gain of 1.8dB. The measurements made are shown in Figure 13. This system gain is less than that measured for the NMSU codec, but the UND/USA codec operates with a higher spectral bandwidth efficiency.

Due to time and scheduling constraints, this codec was only tested through the S-band TDRSS channel. As shown in Figure 14, this codec was also unaffected by the TDRSS channel, operating with performance almost identical to that measured in the laboratory.

Again, the system gain through the actual channel was measured to be slightly higher than that measured in the laboratory tests. The UND/USA codec performed with 2.4dB of system gain through the S-band channel, as shown in Figure 15. This increase in system gain of .6dB corresponds to the same increase for the NMSU codec when measured through the S-band channel.

Conclusion

Through its research in conjunction with NASA, New Mexico State University's Center for Space Telemetering and Telecommunications believes it has found a strong candidate for a modulation scheme to be used for high data-rate applications through the TDRSS channel in the near future. The test of 8PSK TCM through the satellite system proved to be successful.

The test performed at WSGT by NMSU demonstrated that 8PSK with trellis coding is a modulation scheme that will increase the data-rate capabilities through the TDRSS spacecraft while still achieving better BER versus signal-to-noise ratio performance than uncoded QPSK. This will help with the high demands expected to be placed on the TDRSS network by programs such as Space Station Freedom and the new Landsat mission.

Two TCM codecs, implementing different levels of bandwidth efficiency, were tested and proved to be unaffected by the TDRSS channel. The codec designed and built by NMSU achieved a system gain of approximately 3dB over the S-band and K-band channels while increasing the data rate per unit of occupied bandwidth by a factor of 2. The second codec, built by the University of Notre Dame with the University of South Australia, demonstrated a coding gain of 2.4dB over the S-band channel with a 2.5-to-1 increase in data rate per unit bandwidth.

The modulation technique was not fully tested. Further tests performed at rates higher than 1Msps are required to stress the channel. S-band service should be tested at 6 or 12Msps, while K-band service should be tested with data rated in the 300 to 600Msps range. Tests must also be performed to investigate the effects of RFI and burst errors on the performance of TCM.

Overall, the proof-of-concept test was deemed a success. It was shown that the TDRSS channel did not degrade the TCM format in any unusual way. The researchers at NMSU are

confidant that this modulation scheme will pass all future tests and can safely be selected as one of the modulation schemes for future high-rate TDRSS applications.

References

[1] Osborne, William P. and Jerry Stolarczyk, "Modification of the TDRSS High Rate Demodulator for 8-PSK Operation," Technical Report NMSU-ECE-92-010, New Mexico State University, New Mexico, May 1992.

[2] Pietrobon, Steven S., "Trellis Coding With Multidimensional Signal Sets and Rotationally Invariant Trellis Codes," Doctoral Dissertation, University of Notre Dame, Illinois, December 1990.

[3] Ross, Michael D., "High Speed Architecture for the Decoding of Trellis-Coded Modulation," Doctoral Dissertation,New Mexico State University, New Mexico, December 1992.

[4] Viterbi, Andrew J., Jack K. Wolf, Ephraim Zehavi and Roberto Padovani, "A Pragmatic Approach to Trellis-Coded Modulation," IEEE Communications Magazine, Vol. 27, No. 7, pp. 11-19, July 1989.

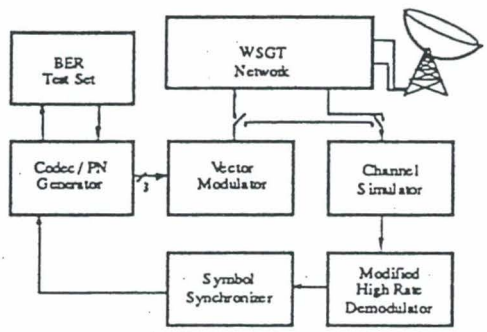

Figure 1/Test System Diagram

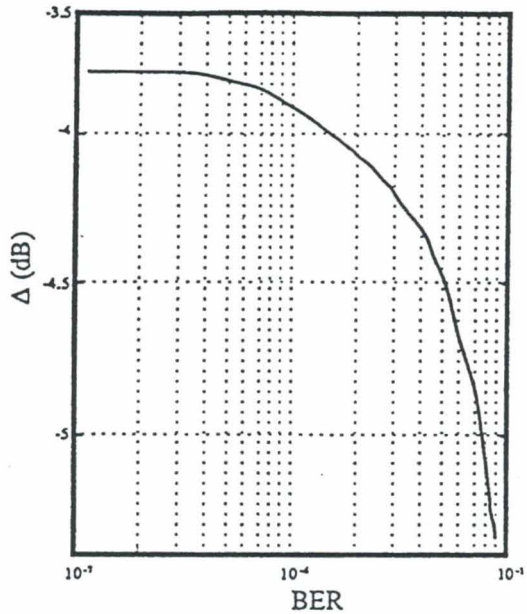

Figure 2/Translation Map

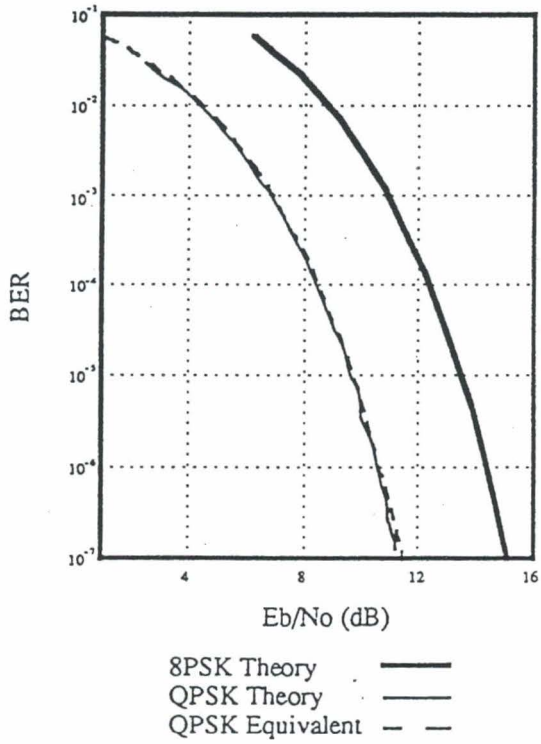

Figure 3/Translation Verification Curve

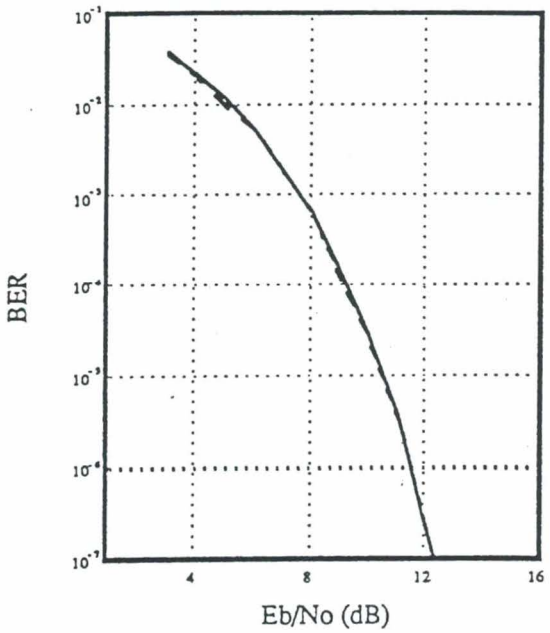

Figure 4/QPSK Baseline

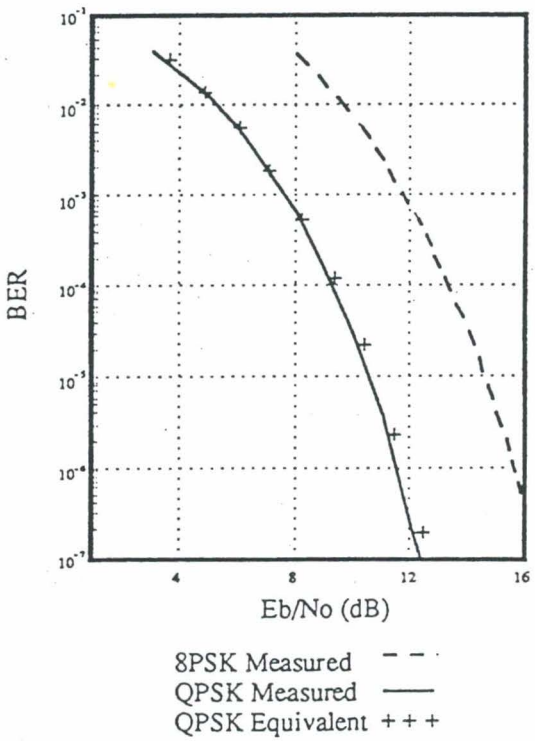

Figure 5/Baseline Comparison

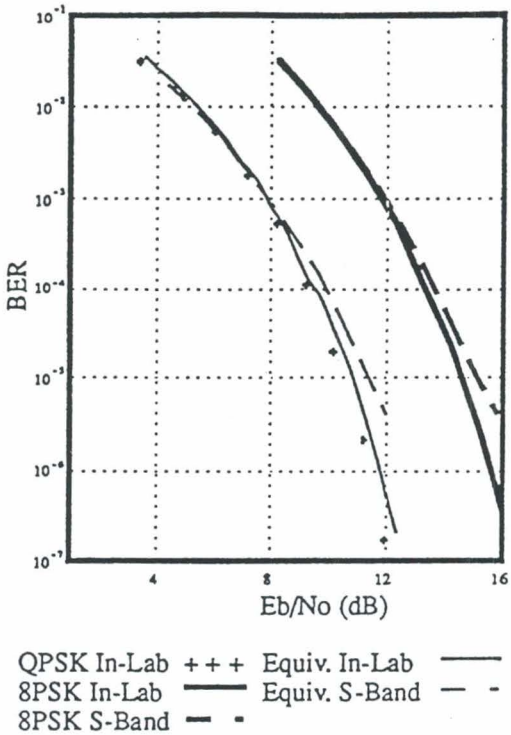

Figure 6/Uncoded S-Band Performance

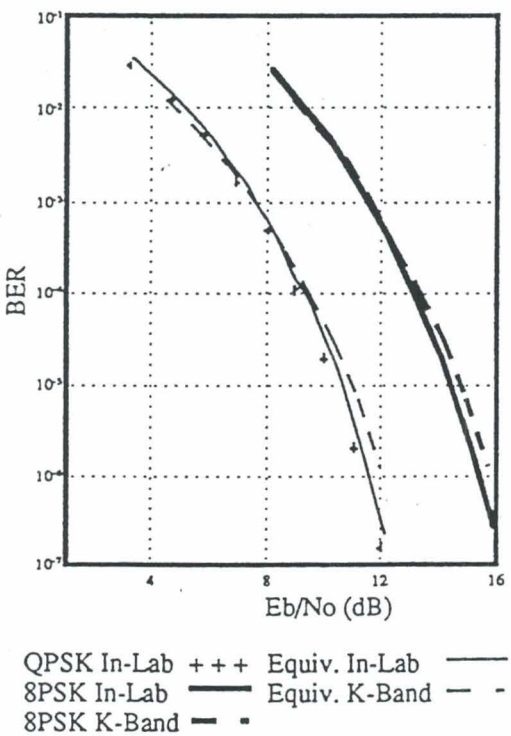

Figure 7/Uncoded K-Band Performance

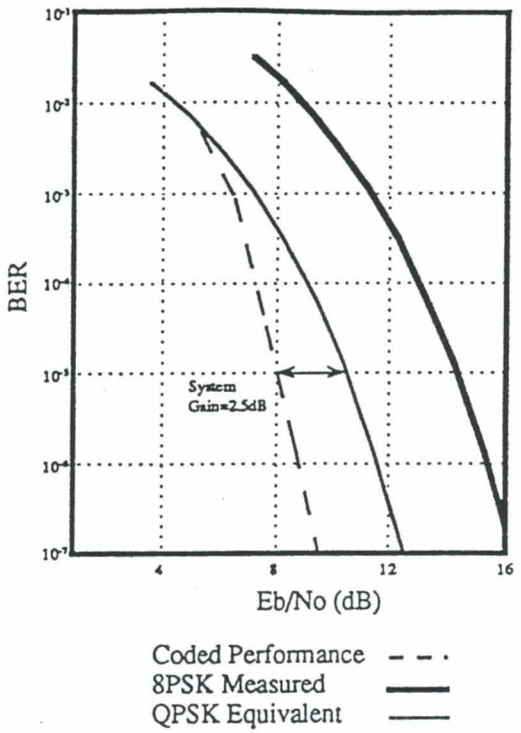

Figure 8/NMSU In-Lab Performance

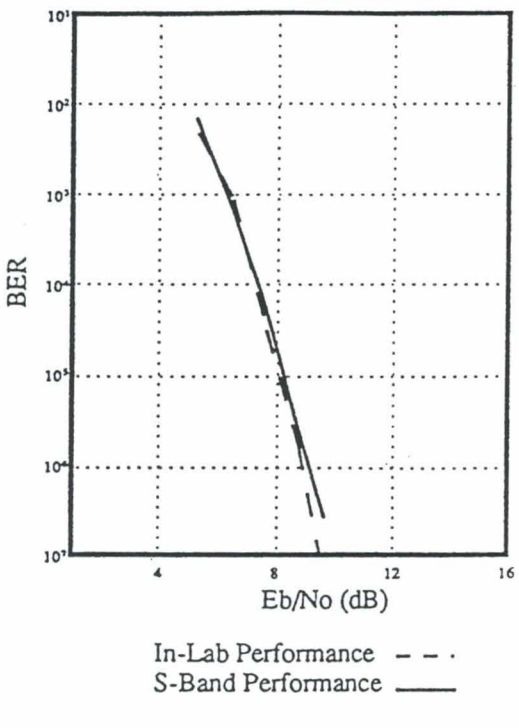

Figure 10/K-Band Performance Comparison

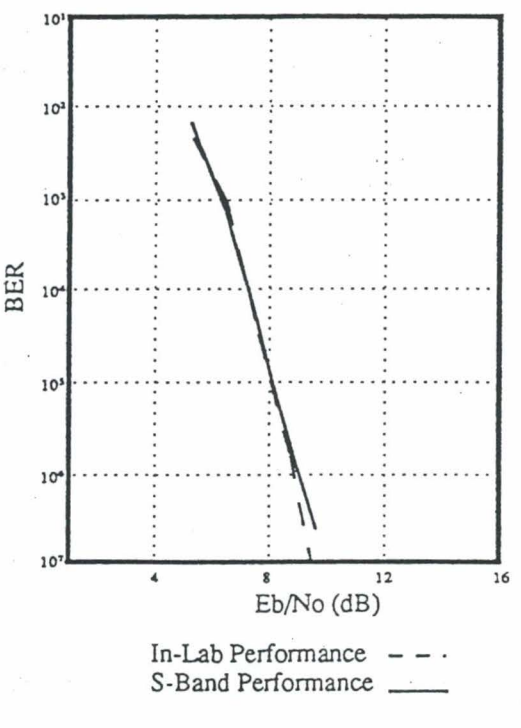

Figure 9/S-Band Performance Comparison

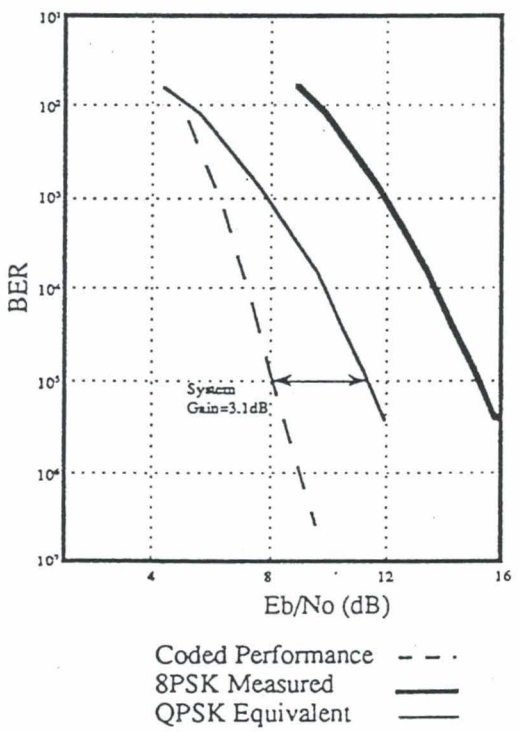

Figure 11/NMSU S-Band Performance

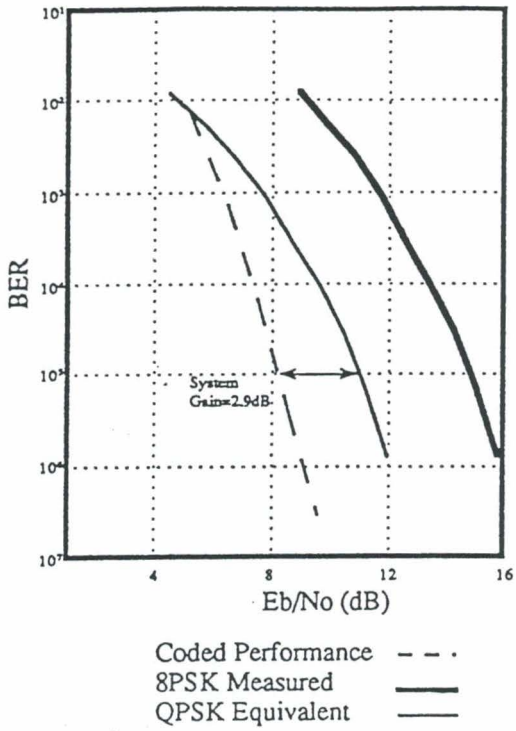

Figure 12/NMSU K-Band Performance

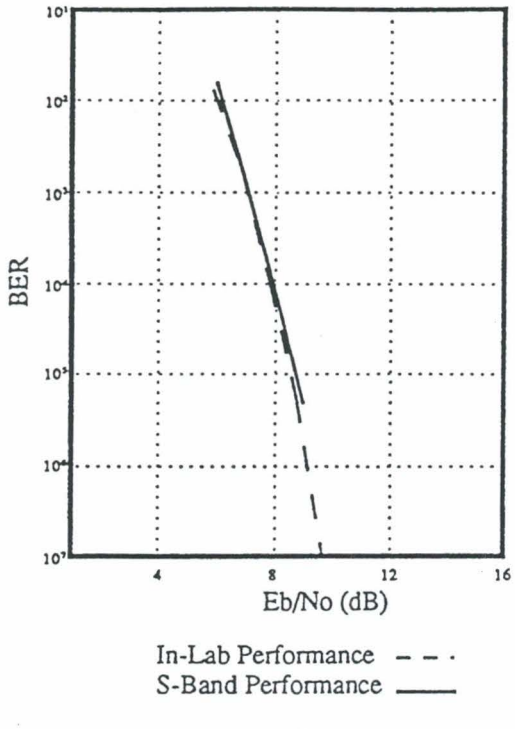

Figure 14/S-Band Performance Comparison

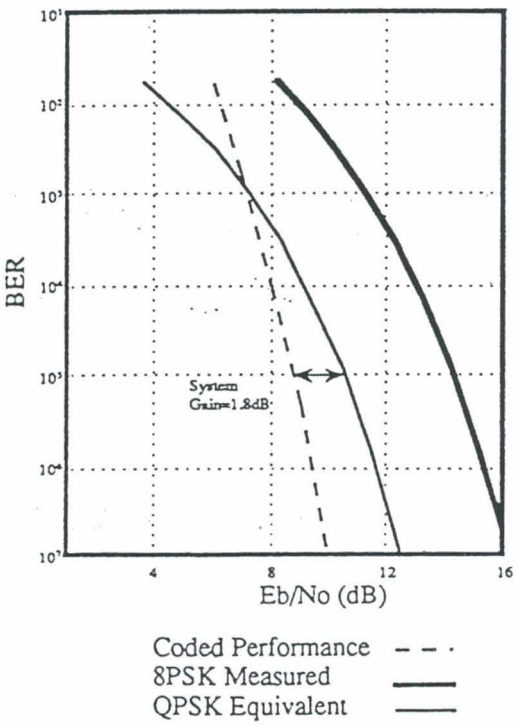

Figure 13/UND In-Lab Performance

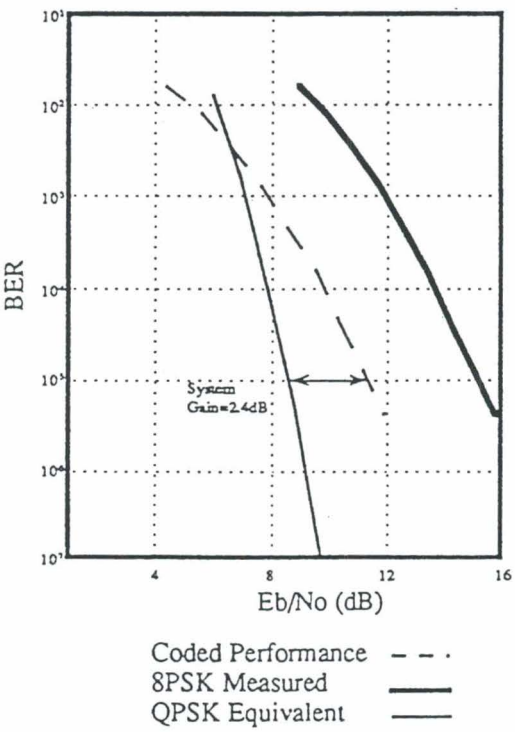

Figure 15/S-Band Performance

THE IMPACT OF LOW SNR WITH ADVANCED CHANNEL CODING ON THE CARRIER ACQUISITION, TRACKING AND SYMBOL SYNCHRONIZATION

Manfred Otter
European Space Agency
European Space Operations Centre
6100 Darmstadt, Germany

ABSTRACT

This paper presents a first-order analysis on the impact of low Signal-to-Noise Ratio (SNR) with advanced channel coding on the performance of the carrier acquisition, tracking and symbol synchronization. The analysis has assumed the squaring loss is constant for the range of symbol SNRs considered in this paper. Furthermore, it also is assumed that the tracking jitter of the symbol synchronizer is derived based on the linear model.

Impact of low Signal to Noise Ratio with advanced Channel Coding on Carrier Acquisition, Tracking and Symbol Synchronisation as a function of Data Rates

Channel coding can substantially improve the quality of a transmission link. This is in particular useful for power limited communication systems, or systems with very low residual error rate requirements. Complex but powerful channel coding techniques have become very attractive with the enormously increased computing power of modern processor generations. The CCSDS is currently considering to adopt one or more new channel codes as a standard. The performance of likely candidates is illustrated in the figures on pages 4 and 5, which have been extracted from TDA Progress Report 42-97, "Performance of Concatenated Codes Using 8-Bit and 10-Bit Reed Solomon Codes", January-March 1989. Key characteristics are given in the table below:

	Rate and Length	Code Rate	Coding Gain	PFD Reduct.	E_b/N_o for BER=10^{-6}	E_s/N_o for BER=10^{-6}
Uncoded	R = 1, K = 1	1	0	0	10.4 dB	10.4 dB
Code 1	R=1/2, K=7, (255,223)	0.437	8.0 dB	-11.6 dB	2.4 dB	- 1.2 dB
Code 2	R=1/2, K=15, (255,223)	0.437	8.8 dB	-12.4 dB	1.6 dB	- 2.0 dB
Code 3	R=1/4, K=15, (255,223)	0.218	9.5 dB	-16.1 dB	0.9 dB	- 5.7 dB
Code 4	R=1/6, K=15, (1023,959)	0.156	9.8 dB	-17.8 dB	0.6 dB	- 7.5 dB

These codes are very powerful with respect to coding gain but the demodulator must be designed to handle the extremely low signal to noise ratios in the carrier tracking loop (in case of a suppressed carrier system), the subcarrier tracking loop (in case of a residual carrier system) and the bit synchronizer.

The tables below give an idea what typical performance characteristics could be expected for a second order tracking loop (either for carrier or subcarrier recovery) and for a bit synchroniser loop. Regarding bit synchronisers, several implementations are possible and the calculated data must be considered as a rough estimation of achievable performance.

In order to acquire and track a low power signal, the loop bandwidth B_l has to be small. The required loop bandwidth is determined by the signal to noise density ratio C/N_o, the squaring loss and the required signal to noise ratio in the loop, typically 15 dB. The natural frequency ω_n is determined by the following relation for a second order loop [1]:

$$\omega_n = \frac{2B_l}{\xi + \frac{1}{4\xi}} \quad [rad/s]$$

For the damping factor $\xi = 0.7$, $\omega_n = 1.89\ B_l$

The maximum permissable rate of input frequency change is given by [1]:

$$\Delta\dot{\omega} = \omega_n^2 \quad [rad/s^2]$$

$$\Delta\dot{f} = 0.57\ B_l^2 \quad [Hz/s]$$

The pull-in or acquisition time is given by [1]:

$$t_p \cong 4.2\frac{\Delta f^2}{B_l^3} \quad [s]$$

For determining Δf , it has been assumed that the Doppler uncertainty can be predicted with an error of better than 1%.

The pull-in range is given by [2]:

$$\Delta\omega_m \cong 2\omega_n\ (\xi+0.6) \quad [rad/s]$$

$$\Delta f_m \cong 0.785\ B_l \quad [Hz]$$

Relative timing errors σ_ε/T for in-phase/mid-phase and early-late-gate bit synchronisers are given in [2] and the equation below lists one example. B_L is the loop bandwidth of the synchroniser loop, and T is the bit time:

$$\frac{\sigma_\varepsilon}{T} \cong \sqrt{\frac{B_L T}{8\ (E_s/N_o)}}$$

It should be noted that the characteristics given below are based on specific implementations and assumptions. They are only intended to give an idea on the order of magnitude to be expected and to point out where the difficulties will be encountered. Frequency uncertainties, for example, can vary over a wide range depending on the type of orbit and the accuracy with which predictions can be made. In general, it can be stated that near earth missions involve typically high data rate transmissions and high frequency uncertainties. Deep space missions have often very low data rates but also very good frequency predictions. From that point of view the conditions are favourable for application of the new channel coding schemes to a variety of missions but the complexity of the channel decoders is likely to put a limit on the highest data rates that can be transmitted.

PERFORMANCE CHARACTERISTICS FOR CODE 1				
Data rate	10	100	1000	b/s
Es/No	-1.2	-1.2	-1.2	dB
C/No	8.8	18.8	28.8	dBHz
Squaring loss	6	6	6	dB
Requ. S/N In The Loop	15	15	15	dB
Carrier recovery loop bandwidth Bl	0.0602	0.602	6.025	Hz
Maximum relative velocity	8	8	8	km/s
Subcarrier frequency	120	120	120	kHz
Max. subcarrier frequency offset [1% error on Doppler]	0.032	0.032	0.032	Hz
Max. frequeny change rate for S/C	0.0020	0.206	20.695	Hz/s
Pull-in (acquisition) time	19.7	0.019	0.0002	s
Pull-in range	0.0473	0.473	4.73	Hz
Bit Synchroniser loop bandwidth for 5% error	0.1517	1.517	15.1715	Hz

PERFORMANCE CHARACTERISTICS FOR CODE 4				
Data rate	10	100	1000	b/s
Es/No	-7.6	-7.6	-7.6	dB
C/No	2.4	12.4	22.4	dBHz
Squaring loss	6	6	6	dB
Requ. S/N In The Loop	15	15	15	dB
Carrier Recovery loop bandwidth Bl	0.014	0.14	1.4	Hz
Maximum relative velocity	8	8	8	km/s
Subcarrier frequency	120	120	120	kHz
Max. Subcarrier Frequency Offset [1% error on Doppler]	0.032	0.032	0.032	Hz
Max. frequeny change rate for S/C	0.0001	0.011	1.08	Hz/s
Pull-in (acquisition) time	1635	1.64	0.0016	s
Pull-in range	0.0108	0.108	1.084	Hz
Bit Synchroniser loop bandwidth for 5% error	0.035	0.35	3.47	Hz

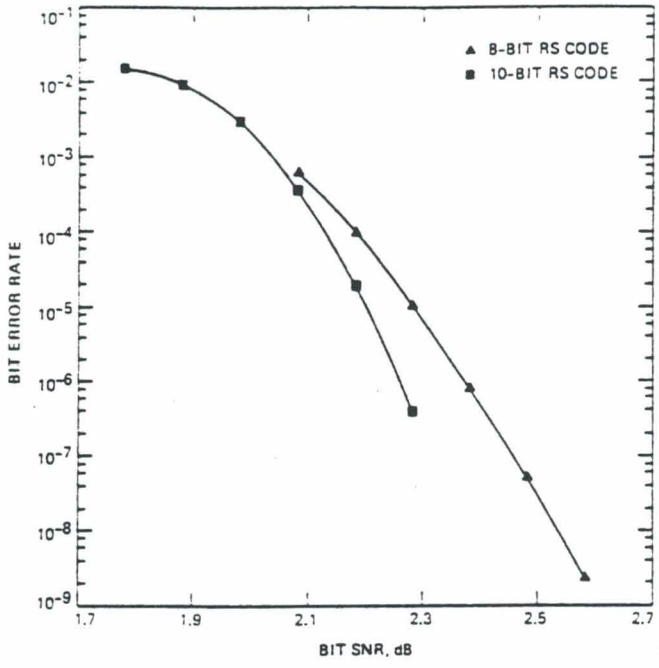

Concatenated code performance comparison: 8-bit (255,223) and 10-bit (1023,959) RS concatenated with (7,1/2) convolutional.

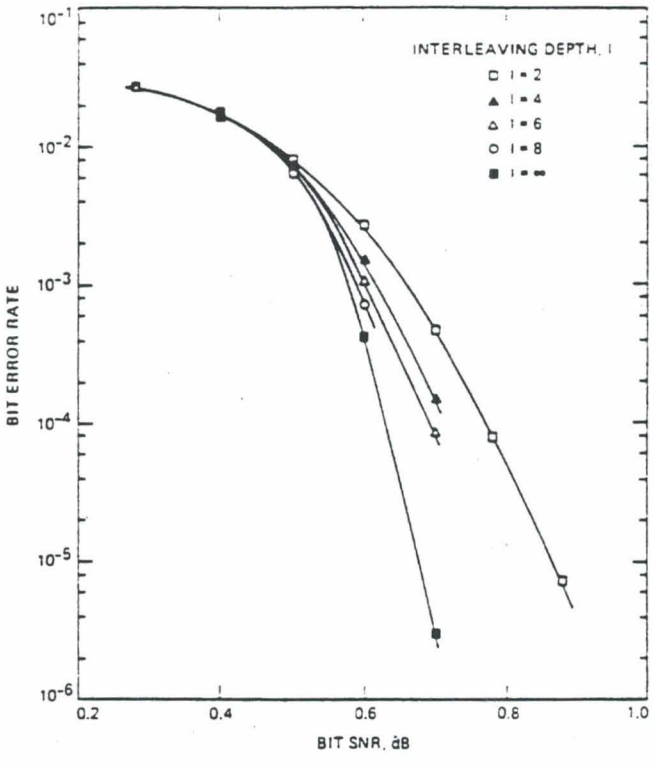

Concatenated code performance: (15,1/4) convolutional and 10-bit (1023,959) RS.

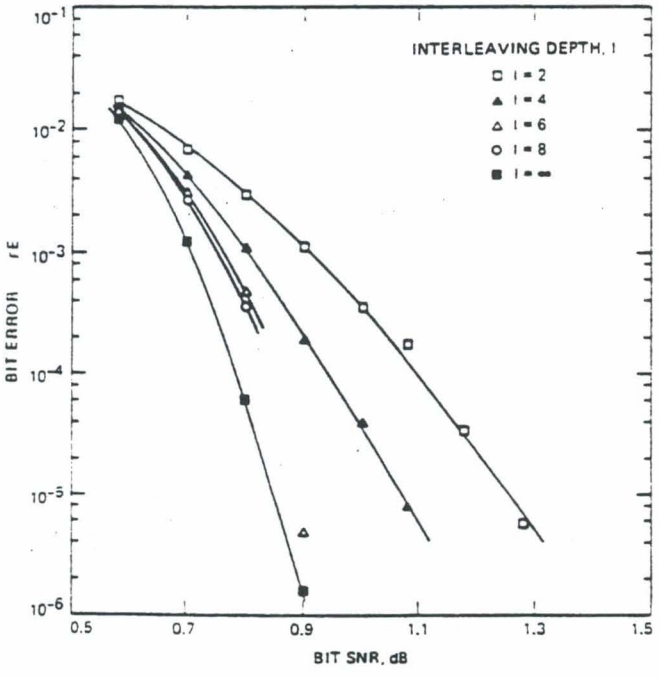

Concatenated code performance: (15,1/4) convolutional and 8-bit (255,223) RS.

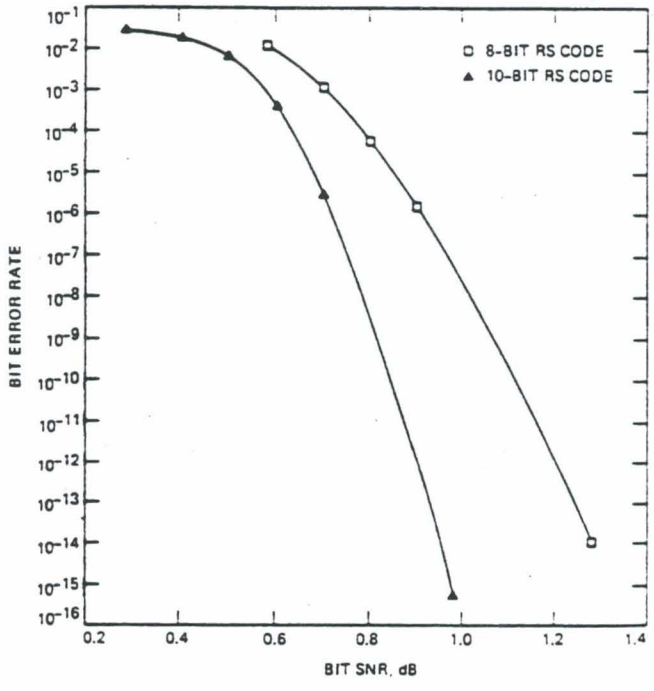

Concatenated code performance comparison: 8-bit (255,223) and 10-bit (1023,959) RS concatenated with (15,1/4) convolutional.

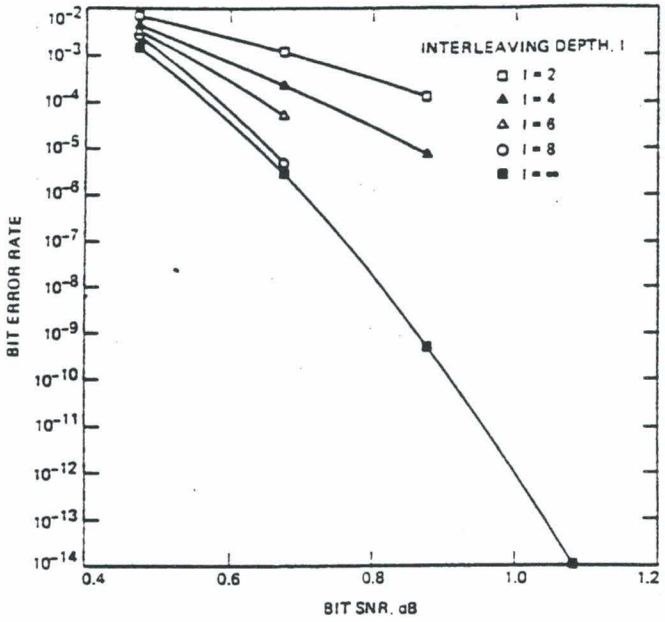

Concatenated code performance: (15,1/6) convolutional and 8-bit (255,223) RS.

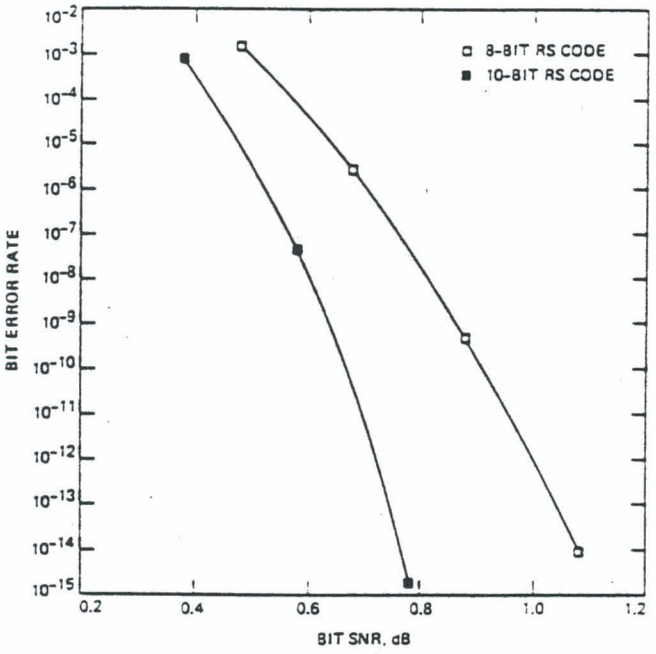

Concatenated code performance comparison: 8-bit (255,223) and 10-bit (1023,959) RS concatenated with (15,1/6) convolutional.

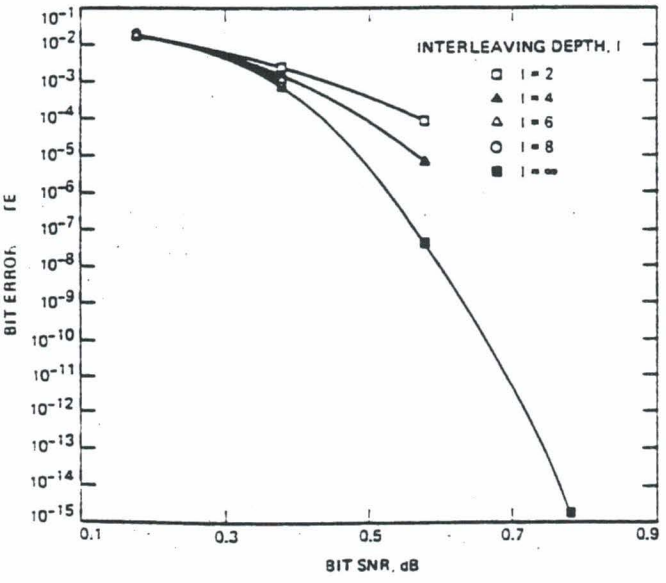

Concatenated code performance: (15,1/6) convolutional and 10-bit (1023,959) RS.

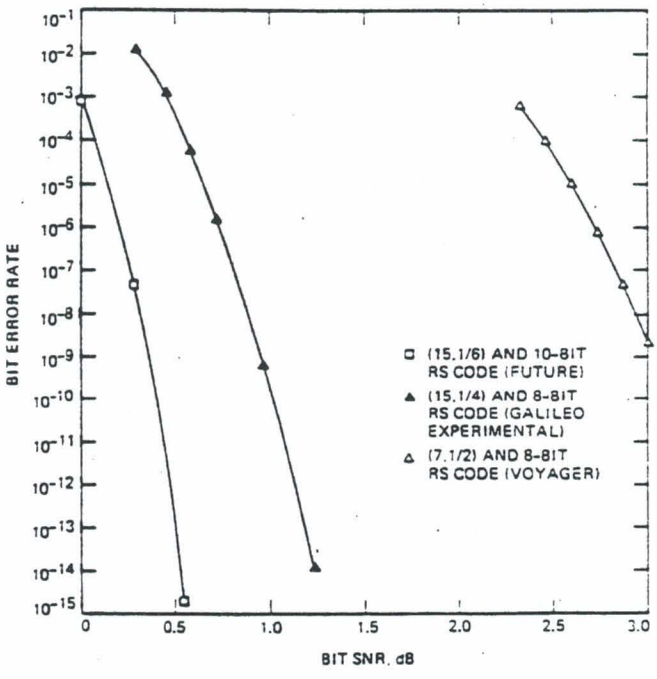

Comparison of three concatenated codes.

CONCLUSIONS

The critical part of the demodulator is the carrier or subcarrier acquisition and tracking. Carrier recovery circuits would not be feasible if the data rates were low and frequency deviations due to e.g. Doppler were above medium.

For data rates of more than a few hundred bits/s on a subcarrier and small frequency offsets, operation at the low signal to noise ratios under consideration is possible. However, a major portion of the total signal power has to be allocated to the carrier in order to cope with orbital dynamic effects on the signal. For data rates below approximately 100 b/s, very powerful coding does consequently not offer advantages anymore. In practice it makes only sense to use very powerful coding for data rates above a few kb/s.

The bit synchroniser is expected to have in principle no problems when operating at the above conditions.

REFERENCES

[1] Gardner, F.M. *Phase Lock Techniques*, John Wiley & Sons, New York, 1966

[2] Spilker, J.J. *Digital Communications by Satellite*, PRENTICE HALL, INC., New Jersey, 1977

ADVANTAGES OF RATE 1/4 AND 1/6 CONVOLUTIONAL CODING FOR DATA RELAY SATELLITES

Jean-Luc Gerner
European Space Agency
European Space Research and Technology Centre
2200 AG Noordwijk, The Netherlands

ABSTRACT

This paper investigates the usefulness of convolutional codes with rates 1/4 and 1/6 for Low Earth Orbiter (LEO) missions supported by the Data Relay Satellites (DRSs). The communications link budgets for these codes are calculated for the telemetry links via European Space Agency (ESA)/DRS. Based on these calculations, the impact of low/high rate constraint length convolutional codes on deep space missions and on the DRS users can be assessed.

1. INTRODUCTION

The 2 GHz band (S-Band) is widely used for Telemetry, Tracking and Command (TT&C) links between spacecraft and the ground. When it comes to radiocommunications, Radio Regulations differentiate two families of spacecraft: Category A and Category B.

- *Category A* spacecraft are those which altitude above the Earth is less than 2.0×10^6km. This category embraces a wide variety of spacecraft which communication features depend heavily on their orbit type:

  a. Spacecraft in geostationary earth orbit (GEO) are relatively high above the Earth (36,000 km) in a fixed position. Most of them are telecommunication satellites which transmit TT&C signals in their payload band. They do not make use of the 2 GHz band during normal operations;

  b. Spacecraft in low earth orbit (LEO), typically a few hundreds to a few thousands kilometers are heavy S-Band users for TT&C. The Category A part of the S-Band is densely occupied and these users are invited to restrict as much as possible their occupied bandwidth. Link budgets are generally comfortable but signal dynamics (Doppler rate) are rather high especially at the lowest altitudes;

  c. Spacecraft in non-circular orbits.

- *Category B* spacecraft are operating at distances from the Earth of more than 2.0×10^6 km. They operate in a less crowed part of the S-Band and are thus submitted to less restrictive bandwidth constraints. Link budgets are in general very critical, owing to the enormous distances between spacecraft and Earth but signal dynamics (Doppler rate) are low.

To be completed, this list should mention the LEO spacecraft which communicate with the ground via a Data Relay Satellite located in GEO orbit. The advantage offered by such a system is the quasi-permanent communication coverage. On the other hand, Radio Regulations limit the allowed power flux density that a satellite may radiate on the Earth surface. These constraints impose limits on the radiated power in both directions of the LEO - GEO link, thus rendering link budgets in general rather critical.

As a result of this quick survey, it appears that two categories of missions experience the same criticality in link budgets: Deep Space missions and LEO missions when they communicate via a DRS. The Jet Propulsion Laboratory (JPL) studied recently for the Deep Space Network (DSN) a new set of forward error correction codes designed to allow link budget improvements on downlinks with a very limited added complexity onboard the spacecraft.

The purpose of this paper is to investigate the usefullness of these codes for LEO missions supported by a DRS System.

2. SOME OUTCOMES OF NASA CODES SEARCH

In general, the most critical part of a Deep Space radio communication link is the telemetry downlink, because of the required telemetry data rate and because onboard transmit power resources are limited. Therefore, a lot of efforts is put in implementing forward error correction coding schemes which offer significant reduction in data error rates while allowing for a simple encoder design. On the other hand, the complexity of the decoder, to be installed into the ground stations, is considered less critical.

The coding schemes which are presently recommended by CCSDS for telemetry links are (ref [5]):

- Convolutional Code with rate r = 1/2 and constraint length k = 7;
- Reed-Solomon Code 8-bit (255,223). Interleaving may be used with depths of I = 1,2,3,4,5.

For best performances, these two codes may be concatenated, the Convolutional Code being . then the inner code and the Reed - Solomon Code being the outer code.

Many articles were published into the Telecommunication and Data Acquisition (TDA) Progress Reports (ref [1] to [4]), dealing with the search of more performing coding schemes. They are based on the same concept of concatenation of an inner Convolutional Code with an outer Reed-Solomon code, but with codes parameters which differ from the CCSDS recommended ones. Some of the basic results are provided below for Convolutional Code only (table 1) and for various types of concatenated codes (table 2).

Convolutional Coding BER = 10^{-4}	Eb/No (dB) (information data)	Es/No (dB) (channel symbols)
CV (7,1/2)	3.6	0.6
CV (15,1/4)	2.2	- 3.8
CV (15,1/6)	2.0	- 5.8

Table 1: Required Eb/No for a BER of 10^{-4} with 3 different types of Convolutional Codes

Concatenated Coding BER = 10^{-6} *10^{-8}*	Eb/No (dB) (information data)	Es/No (dB) (channel symbols)
CV (7,1/2) RS 8 b, I > 4	2.4 *2.5*	- 1.2 *- 1.1*
CV (15,1/4) RS 10 b, I infinite	0.7 *0.8*	- 5.6 *- 5.5*
CV (15,1/6) RS 10 b, I > 8	0.4 *0.7*	- 7.5 *- 7.4*

Table 2: Required Eb/No for BER of 10^{-6} and 10^{-8} with 3 different types of Concatenated Coding schemes

3. LOW RATES CONVOLUTIONAL CODES FOR DRS USERS

Spacecraft in low earth orbit which require continuous communication with the ground have their communications relayed via a Data Relay System. We can identify two categories of DRS users:

- those who need to transmit to ground data at moderate to high rates. They operate either in S-Band (2 GHz) up to 3 Mb/s or in Ku/Ka-Band (13-15/25-27 GHz) for data rates up to a few hundred Mb/s. They operate through a steerable directive antenna and the power flux density limitations on the earth surface do not directly affect the communication system.

- those whose communication needs are limited to a few kb/s, in general for TT&C purposes. These users operate in S-Band via a fixed omni-coverage antenna to meet reliability requirements on the TT&C system, and therefore radiate basically over the 4 π steradians. Their telemetry transmissions capabilities are thus restricted to the maximum power flux density (PFD) of -154dBW/m^2/4kHz that they may radiate on the Earth surface in the 1525-2300 GHz band, together with the protection requirements in the other bands.

For this category of S-Band low data rate users , link budget margins are very often marginal, due to above mentioned PFD restrictions, and this inspite of the spectrum spreading techniques that they employ (table 3). Table 4 provides a comparison of Deep Space and Low Data Rate DRS users with regard to the use of low rate / high constraint length codes for telemetry links.

Parameter	Characteristic
Carrier frequency F_T	$2200 < F_T < 2290$ MHz In coherent mode, related to the receive frequency: $F_T = 240/221 \times F_R$
Modulation	USQPN Both I and Q channels are spread with a PN code XORed with the data prior to entering the modulator
Code type	Gold code (2^{11}-1) in non-coherent mode Truncated maximal length (2^{18}-1) code synchronized with receive code in coherent mode
Code rate	Coherently related with F_T and equal to (31/240x96) x F_T (about 3 Mc/s)
Data rate restriction	Maximum symbol rate of 300 ks/s per channel

Table 3: Return link Spread Spectrum communications via a Data Relay System

As can be seen from table 4, DRS low data rate users may take great advantage in the implementation of Convolutional Codes with higher gain. Unlike Deep Space missions, the limitations on these spacecraft is not technical but rather regulatory (PFD limitations).

The link budget (LBT) of table 5 is typical of a return link for a 2 GHz user of the ESA Data Relay System. Link budget has been computed with 3 different assumptions on convolutional coding, basically rates 1/2, 1/4 and 1/6. Coding gains are estimates for a BER of 10^{-5}.
On top of the LBT are provided the basic geographical data necessary to the computation. The station is assumed to be in Toulouse (south of France).
The first section of the LBT addresses the LEO->GEO link, i.e. from the user to the DRS satellite. The PFD on the Earth surface is computed with the assumption that the antenna is radiating equally in all directions (worst case).
The second part of the LBT addresses the GEO->Ground link, i.e. from the DRS satellite to the ground station. The feeder link operates at 20.2 GHz. Atmospheric attenuation was computed for a 99.9% availability at 20.2 GHz in Toulouse.
The link budgets were established with a 3dB system margin.

ITEM	DEEP SPACE	DRS
Impact on occupied bandwidth of the increase of channel symbol rate (x2 or x3) as compared with R=1/2	Owing to the low telemetry data rates as compared with the ranging signal bandwidth and the carrier frequency, symbol rate increase has *no significant impact.*	*No impact* on occupied bandwidth, determined by the PN spreading code but reduction of operational data rate range from 150kb/s for R=1/2 to: 75kb/s for R=1/4 50 kb/s for R=1/6
Reduction of channel Es/No in the receiver bit synchronizer	Existing NASA ground receiver can operate down to Es/No = -8 dB	*Not compatible with existing ESA/NASA ground receivers.* ESA receiver threshold is Es/No=-1dB for a symbol rate of 1kb/s. Upgrade necessary.
Link budget improvement by 1 or 2 dB	Of high interest to save onboard power or alternatively operate with smaller antenna size	Of high interest to reduce transmit power presently rather high for small users operating with omnidirectional antennas
Slight increase of onboard encoder complexity	Very limited impact	Very limited impact
Latency	Not critical	Not critical

Table 4: Impact of low rate/high constraint length convolutional codes on Deep Space missions and on DRS users

The following comments can be drawn out of the computations of this LBT:

- the replacement of a rate 1/2 code by a rate 1/4 or 1/6 can allow a typical low rate DRS user to save 3 to 3.5 Watts RF power, which leads to a reduction of 13 to 15 Watts DC power, a non negligeable saving for a small satellite.
- alternatively, a high rate code allows to increase the telemetry data rate by roughly 50% while remaining within the PFD limits on the Earth surface.
- higher rate codes implies that the demodulator/bit synchroniser will have to operate under lower signal-to-noise conditions. Existing Data Relay Systems receivers are not specified for it.

4. CONCLUSION

A new set of better performing convolutional codes has been studied by NASA/JPL for the purpose of improving performance capabilities of Deep Space missions. It has been demonstrated that these codes used as stand-alone can improve the link by almost 2 dB in certain conditions and by probably more than 2 dB when concatenated with a properly selected Reed-Solomon code.

Data Relay Systems users operating at low data rates in S-Band (2GHz) could also take advantage of these codes for their telemetry communication links. The only drawback which was found in the use of these codes is the need for the receiver bit synchroniser to operate under low signal-to-noise conditions, for which the present equipments are not designed.

The gain brought by the rate 1/6 code as compared with the rate 1/4 looks rather marginal and the trade-off against decoder complexity should allow to make the decision.

Table 5/a: Link Budget Table for a telemetry link via ESA DRS

31-AUG-1993 PERF. OF A RETURN LINK VIA DRS, LOW RATE, FOR CONV. CODES R=1/2, 1/4, 1/6
09:55:45 AM
CCSDS_CONVCO BW..MHz 12 BER=10^-5 GS=Toulouse

G/S TOULOUSE					
G/S LONGITUDE.....deg	1	east	(long. west : neg. value)		
DRS LONG. worst case.deg	59	east			
G/S LATTITUDE...l....deg	45				
G/S LONGITUDE/DRS..L.deg	58				
EARTH RADIUS....R.....km	6,378				
DRS ORBIT ALTITUDE.Do.km	35,786				
SPACECR ORBIT ALTIT.H.km	700				
GRAZING ANGLE (min)..deg	5.0195				
		USER->DRS			
		R=1/2	R=1/4	R=1/6	
TX EIRP .....dBW		2.86	1.16	1.06	
TX PATH LOSSES.....dB		1.00	1.00	1.00	
TX A GAIN.....dB		-6.00	-6.00	-6.00	
TX POWER.....dBW		9.86	8.16	8.06	
TX Power.....W		9.68	6.55	6.40	
TX MODUL. LOSS.....dB		0.00	0.00	0.00	
TX OTHER DEGRAD.....dB		0.00	0.00	0.00	
FREQUENCY.....MHz		2250.00	2250.00	2250.00	
Chip Rate.....Mb/s		3.29	3.29	3.29	
SLANT RANGE.....km		44140.00	44140.00	44140.00	
PATH LOSS.....dB		192.38	192.38	192.38	
POINT.LOSS.....dB		0.00	0.00	0.00	Null because included into of Antenna gain
POL.LOSS.....dB		0.30	0.30	0.30	
ATMOSPH. LOSS.....dB		0.00	0.00	0.00	Est. for a beam not entering the near atmosphere (< 30 km)
.....					
PFD-Earth....dBw/m2/4kHz		-154.18	-155.88	-155.98	Assumes antenna radiating as much towards the Earth as towar
.....					
RX ANT GAIN.....dB		34.70	34.70	34.70	Only indicative, not used in calculation
ANT NOISE TEMP.....K					
LOSS TEMP.....K					
POINT & CABL LOSSES...dB					
DIPLEXER L.....dB					
RX NF.....dB					
RX AMBIENT TEMP.....K					
RX EFF. NOISE TEMP...dBK					
RX G/T.....dB/K		6.80	6.80	6.80	(2) ESA DRS data
RX RECEIVED POWER....dBw		-155.12	-156.82	-156.92	
RX C/NO.....dBHz		45.58	43.88	43.78	
		DRS->GRD			
TX sign. EIRP twd RX.dBW		25.34	23.65	23.55	
Rel.Sat.Deg.(mod.loss)dB		0.50	0.50	0.50	
OHMIC LOSSES.....dB		1.50	1.50	1.50	
TX A GAIN.....dB		37.80	37.80	37.80	
TX POWER.....dBw		14.77	14.77	14.77	
C/(C+N) (TWTA).....dB		-25.23	-26.92	-27.02	C/(C+N)=1/(1+N/C) and C/N=C/No+10LogBW
FREQUENCY.....MHz		20200.00	20200.00	20200.00	Max freq.

Table 5/b: Link Budget Table for a telemetry link via ESA DRS

SLANT RANGE	km	40211.27	40211.27	40211.27
PATH LOSS	dB	210.64	210.64	210.64
POINT.LOSS	dB	0.00	0.00	0.00
POL.LOSS	dB	0.10	0.10	0.10
ATMOSPH. LOSS	dB	15.30	15.30	15.30
RX ANT GAIN	dB	64.80	64.80	64.80
ANT NOISE TEMP	K	262.20	262.20	262.20
LOSS TEMP	K	290.00	290.00	290.00
POINT & CABLE LOSS	dB	1.00	1.00	1.00
DIPLEXER LOSS	dB	0.00	0.00	0.00
RX NF	dB	3.50	3.50	3.50
RX AMBIENT TEMP	K	290.00	290.00	290.00
RX EFF. NOISE TEMP	dBK	28.60	28.60	28.60
RX G/T	dB/k	36.20	36.20	36.20
RX RECEIVED POWER	dB	-136.89	-138.59	-138.69
RX C/NO	dBHz	64.11	62.41	62.31
Net. C/No	dBHz	45.52	43.82	43.72
Modul. loss	dB	0.00	0.00	0.00
Relay Sat.Deg	dB	0.50	0.50	0.50
RFI Loss	dB	0.00	0.00	0.00
CCI/ACI Loss	dB	0.00	0.00	0.00
DEM & SS LOSSES	dB	1.50	1.50	1.50
DATA RATE	kbps	4.00	4.00	4.00
Eb/No	dB	7.50	5.80	5.70
Required Eb/No	dB	4.50	2.80	2.70
Es/No at demod.input	dB	1.50	-3.20	-5.10
SYSTEM MARGIN	dB	3.00	3.00	3.00

REFERENCE DOCUMENTS

(1) Breadboarding of DRS SS Receiver and Modem
OPS/SCED/16655/TB/AOC July 89

(2) DRS Satellite Performance Specifications
SP 7-1-1 October 89

(3) DRS G/S System Performance Specification
SP 7-2-1 October 89

(4) Propagation margins for DRS antenna
J.P. Baptista XEP/119/PB (12/6/89)

(5) Convolutional codes
R=1/2 CCSDS Standard
R=1/4 K=15 developed by JPL
R=1/6 K=15 developed by JPL

Range = SQRT(Do^2 + 2R(Do+R)(1-coslcosL))

(4) For 99.9 percent availability 1G/S (TLSE)

Not used in computation
Id.
Id.
Id.
Id.
Id.
Id.
Id.

(3)

Relay Degrad due to AM/PM, Phase Noise, etc. estimated

Adjacent or Cochannel interference (cochannel when SMA)
(1)

(5)

REFERENCE DOCUMENT

[1] Frame Error Rate of the NASA Cocatenated Coding System, L. Swanson and K. -M. Cheung, TDA Progress Report 42-106, August 15, 1991

[2] Performance of Concatenated Codes using 8-bit and 10-bit Reed Solomon Codes, F. Pollara and K. -M. Cheung, TDA Progress Report 42-97, January - March 89

[3] A new code for Galileo, S. Dolinar, TDA Progress Report 42-93, January - March 1988

[4] In search of a 2-dB coding gain, J. H. Yuen and Q. D. Vo, TDA Progress Report 42-83, July - September 85

[5] Telemetry Channel Coding, CCSDS 101.0-B-3, Blue Book, may 92

PERFORMANCE OF RF DOWNLINK WITH PERIODIC DATA FRAME[1]

John Alexander Koukos
National Aeronautics and Space Administration
Jet Propulsion Laboratory
California Institute of Technology
4800 Oak Grove Drive
Pasadena, CA 91109

ABSTRACT

Telemetry of discrete spectrum components induced by the periodicity of an Attached Sync Marker may coincide with the RF carrier frequency, causing unwanted interference while tracking the RF carrier. However, with the CCSDS recommended frame length of 10200, the power of all harmonics created by this periodicity is always 50 dB below the overall data power, hence there is no significant interference imposed on the carrier tracking. Additionally, it is found that insertion of the pseudo randomizer reduces the intensity of all harmonics caused by bursts of 1's and 0's, and therefore decreases any potential interference to the carrier tracking.

[1] The work described in this paper was carried out at the Jet Propulsion Laboratory, California Institute of Technology, under contract with the National Aeronautics and Space Administration.

I. Introduction

Telemetry discrete spectral components, due to the periodicity of the Attached Sync Marker (ASM) and burst of 1's or 0's, may coincide with the RF carrier, and thus cause unwanted interference. This paper investigates whether such an interference can arise in the telemetry downlink. Also spectral plots of the CCSDS pseudorandomizer [Ref 1., 2.] are presented.

II. Spectral Components due to Periodic Sync Word

According to the CCSDS telemetry format, each data frame is separated form the previous one by a 32 bit synchronization (sync) word written in hexadecimal form as 1ACFFC1D. The periodicity of the sync word creates discrete harmonics in the telemetry data spectrum. In this section, the possibility of such spectral components, causing interference to the RF carrier, is investigated.

We assume, for the sake of analysis, an all-zero frame with length N_f and a sync word with length N_s. Let $A_m=\pm 1$ be the amplitude of the mth bit of the sync word, T_b the duration of data bit. The duration of a frame plus the sync word becomes $T_0=(N_f+N_s)T_b$. The baseband telemetry periodic data waveform y(t)=sync(t)+frame(t) can be expanded into Fourier series as :

$$y(t) = \sum_{n=-\infty}^{\infty} Y_n e^{j\omega_0 t}, \qquad \omega_0 \equiv \frac{2\pi}{(N_s+N_f)T_b} \tag{1}$$

where the spectral components Y_n can be computed from the Fourier transform as

$$Y_n = \frac{1}{T_0}\int_0^{T_0} y(t)e^{-jn\omega_0 t}dt = \frac{1}{T_0}\left[\sum_{m=0}^{N_s-1}\int_{mT_b}^{(m+1)T_b} A_m e^{jn\omega_0 t}dt - \int_{N_sT_b}^{(N_s+N_f)T_b} e^{-jn\omega_0 t}dt\right] \tag{2}$$

Carrying out the integration yields the following expression for the spectral component Y_n

$$Y_n = \frac{1}{N_s+N_f}\,Sinc\left(\pi\frac{n}{N_s+N_f}\right)\sum_{m=0}^{N_s-1} A_m e^{-j\pi n\frac{2m+1}{N_s+N_f}} - \frac{N_f}{N_s+N_f}\,Sinc\left(\pi n\frac{N_f}{N_s+N_f}\right) e^{-j\pi n\frac{2N_s+N_f}{N_s+N_f}} \tag{3}$$

Spectral component Y_0 for $N_s=32$ becomes :

$$Y_0 = \frac{1}{N_s+N_f}\sum_{m=0}^{N_s-1} A_m + \frac{N_f}{N_s+N_f} = \frac{1}{32+n_f}(19-13) + \frac{N_f}{32+N_f} = \frac{6+N_f}{32+N_f} \tag{4}$$

The power spectral density of the baseband waveform y(t) contains discrete components at $\pm n\omega_0$

$$S_y(f) = \sum_{n=-\infty}^{\infty} |Y_n|^2\,\delta(f-nf_0) \tag{5}$$

In Fig. 1, plots of (5) up to n=100, for N_f=10200, 1020, 102 demonstrate the dramatic increase in the power of the sync word harmonics, as the frame length becomes shorter. However, for the CCSDS recommended frame length of 10200, the power of all harmonics other than the fundamental is always 50 dB below the overall data power.

If y(t) modulates a square wave subcarrier / carrier, then the power spectral density of the resulting PCM/PSK/PM signal centered around the carrier is the following :

$$S_M(f) = S_M^{+}(f-f_c) + S_M^{-}(f+f_c); \qquad where:$$

$$S_M^{+}(f-f_c) \equiv \frac{2}{\pi^2}\left[\sum_{k=1}^{\infty}\frac{S_y(f-f_c-(2k-1)f_{sc}) + S_y(f-f_c+(2k-1)f_{sc})}{(2k-1)^2}\right], \tag{6}$$

$$S_M^{-}(f+f_c) \equiv \frac{2}{\pi^2}\left[\sum_{k=1}^{\infty}\frac{S_y(f+f_c+(2k-1)f_{sc}) + S_y(f+f_c-(2k-1)f_{sc})}{(2k-1)^2}\right]$$

For computational simplicity we choose to perform our analysis around the positive carrier frequency where the modulation spectrum is $S_M^{+}(\nu)$, $\nu \equiv f-f_c$:
Substituting expression (5) for $S_y(f)$ in (7), yields an expression for the discrete power spectrum of the PCM/PSK/PM signal :

Fig. 1 : Power Spectral Density of Baseband Telemetry

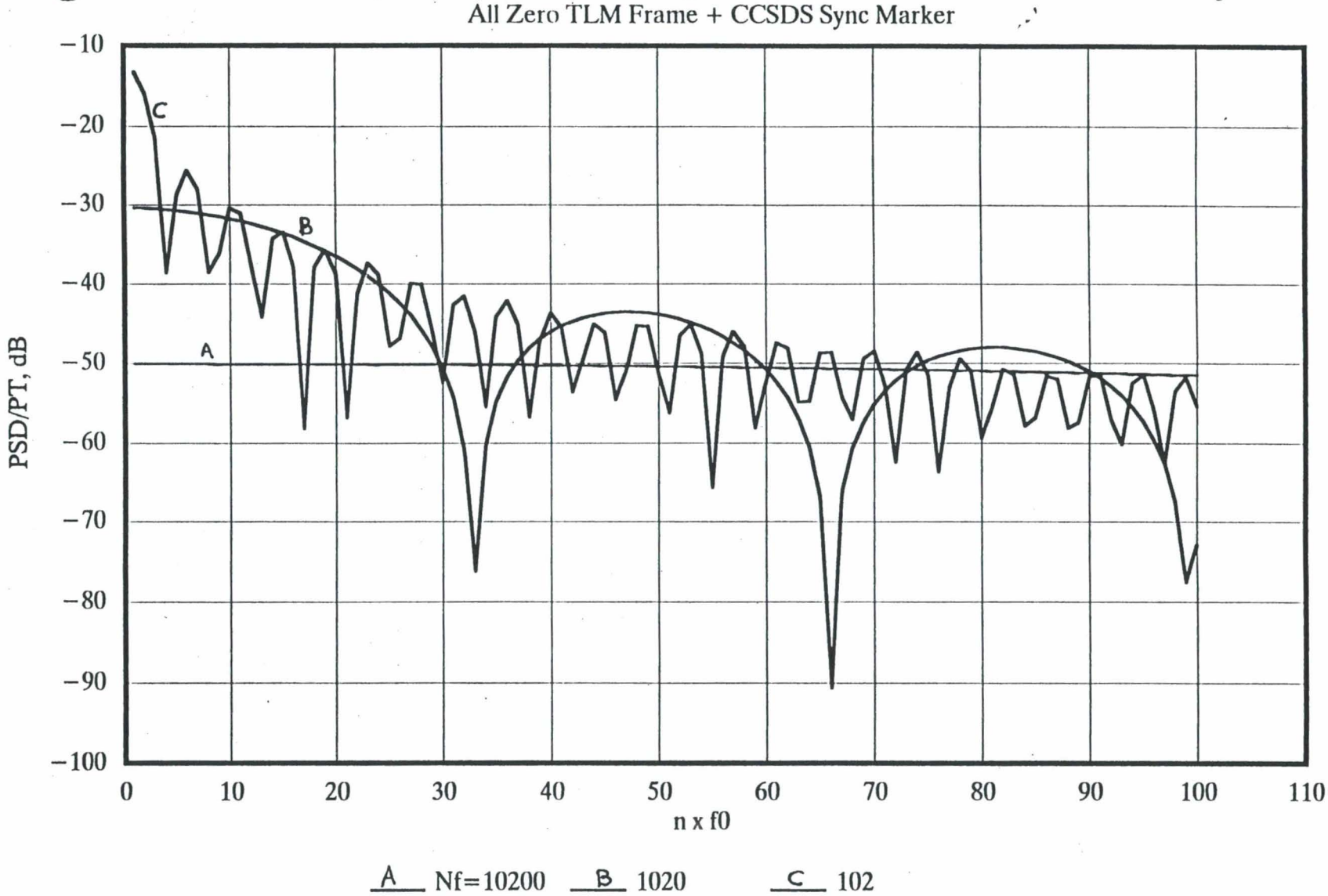

Ns=32 bit at Sync Marker
f0=1/T0=1/(Ns+Nf)Tb

$$S_M^{+}(\nu) \equiv \frac{2}{\pi^2}\left[\sum_{k=1}^{\infty} \frac{S_y(\nu-(2k-1)f_{sc}) + S_y(\nu+(2k-1)f_{sc})}{(2k-1)^2}\right] \quad (7)$$

$$S_M^{+}(\nu) \equiv \frac{2}{\pi^2}\sum_{k=1}^{\infty}\frac{1}{(2k-1)^2}\sum_{n=-\infty}^{\infty} |Y_n|^2 \left[\delta(\nu-nf_0-(2k-1)f_{sc}) + \delta(\nu-nf_0+(2k-1)f_{sc})\right] \quad (8)$$

Discrete harmonics of eg. (8) coincide (and therefore interfere) with the carrier if the following Diophantine equation has at least one solution :

$$nf_0-(2k-1)f_{sc} = 0, \qquad k=1,2,3,\ldots, \text{ and } n=1,2,3,\ldots \quad (9)$$

Using the definition for f_0 from (1) and setting $x_b \equiv f_{sc}/R_b$, $(R_b=1/T_b)$, the above equation becomes :

$$n-(2k-1)(N_s+N_f)x_b = 0, \qquad n,k=1,2,3,\ldots \quad (10)$$

Equation (10) has an infinite number of discrete solutions if the subcarrier-frequency-to-bit-rate ratio x_b is an integer. As shown in the solutions presented in Table 1, below the interfering harmonic power on the carrier is negligible compared to the overall data power in the link.

Table 1 : Solutions of (10) with k=1

x_b	2			1.875
N_f	10200	1020	102	10200
n	20464	2104	268	19185
$\lvert Y_n\rvert^2$, dB	-149.91	-155.74	-144.99	-152.36

III. CCSDS Pseudo-Randomizer

In order to avoid inadvertent creation of telemetry harmonics falling on the carrier frequency, CCSDS recommends "XORing" a pseudorandom sequence of length=255 bits with the transfer frame. The pseudorandom sequence is generated using the following polynomial :

$$h(x) = x^8+x^7+x^5+x^3+1$$

Since there is such a repetitive pattern inside a transfer frame, there exist a possibility of undesirable harmonics generation. However, simulation of a random number generator with

probability of zero = 0.1 in the Comdisco SPW™ (See Fig. 2) demonstrated that inserting the pseudorandomizer keeps all harmonics 40 dB below total signal power.

In Fig. 3 the histogram and the spectrum of the random number generator is plotted with prob-of-zero = 0.1. A DC component is 5 db (or less) below the total signal power as expected.

In Fig. 4 we see that by inserting the randomizer the DC component has been dispersed and all harmonics lie 40 db below the total signal power.

III. Conclusions

Repetitive patterns such as Sync Markers do not generate significant interference to the carrier. However bursts of 1's or 0's generate strong components that may fall on the carrier frequency, therefore insertion of pseudorandomization in the tranfer frame has been appropriately recommended by CCSDS.

IV. References

1. CCSDS Blue Book : "TELEMETRY CHANNEL CODING", CCSDS 101.0-B-3, May 1982.

2. CCSDS Green Book : "TELEMETRY - Summary of Concept and Rational", CCSDS 100.0-G-1, December 1987.

Fig. 2 : CCSDS Pseudo-Randomizer

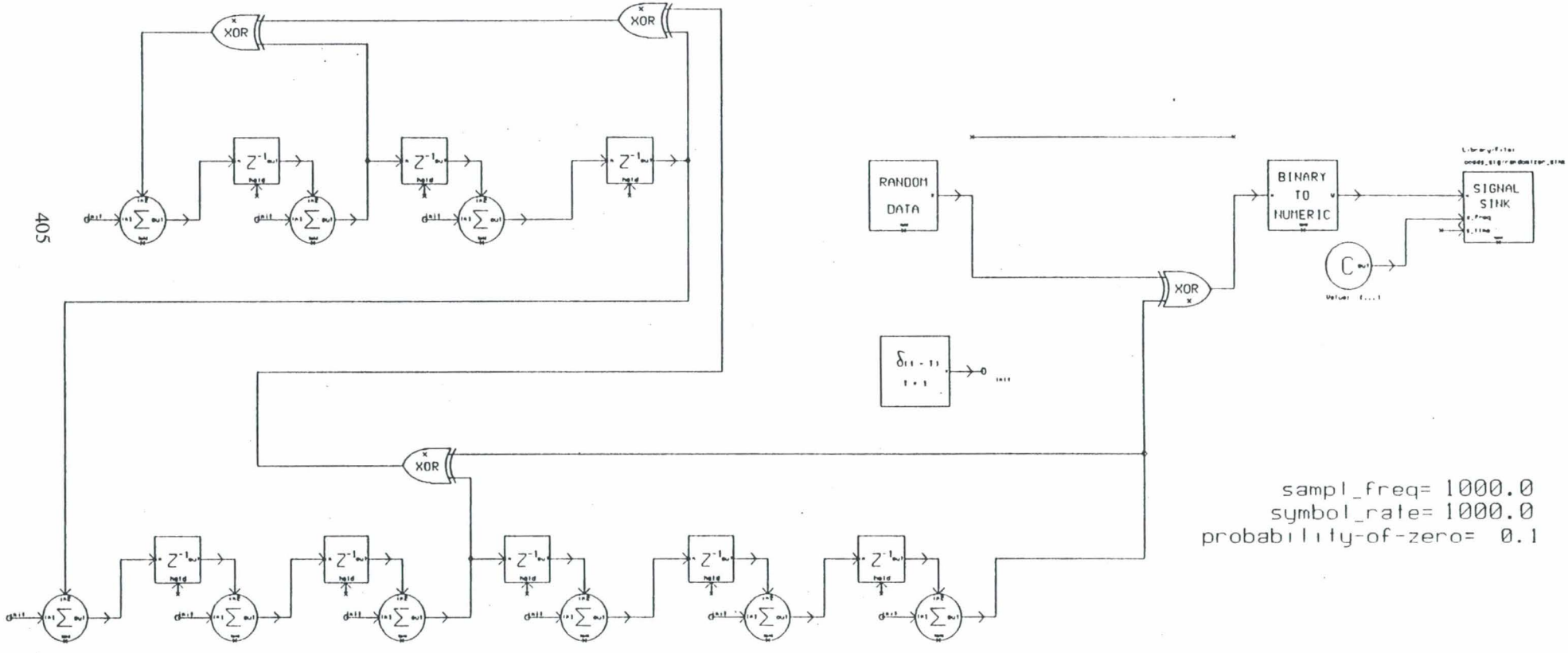

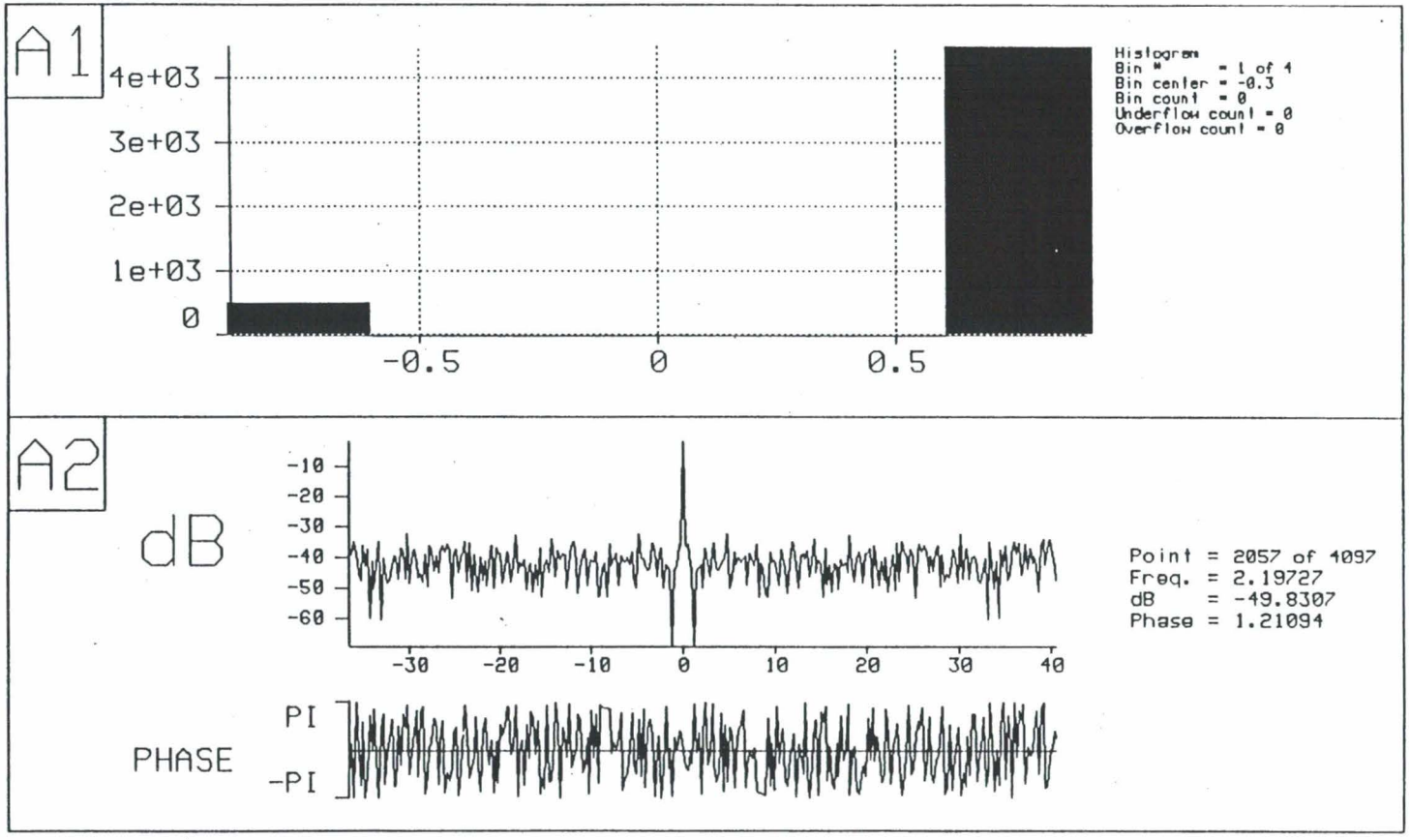

FIG. 3 A1: Histogram of 1's versus 0's for a random number generator with prob-of-zero = 0.1.

A2 : FFT of a 4092 bit stream, showing a strong DC component.

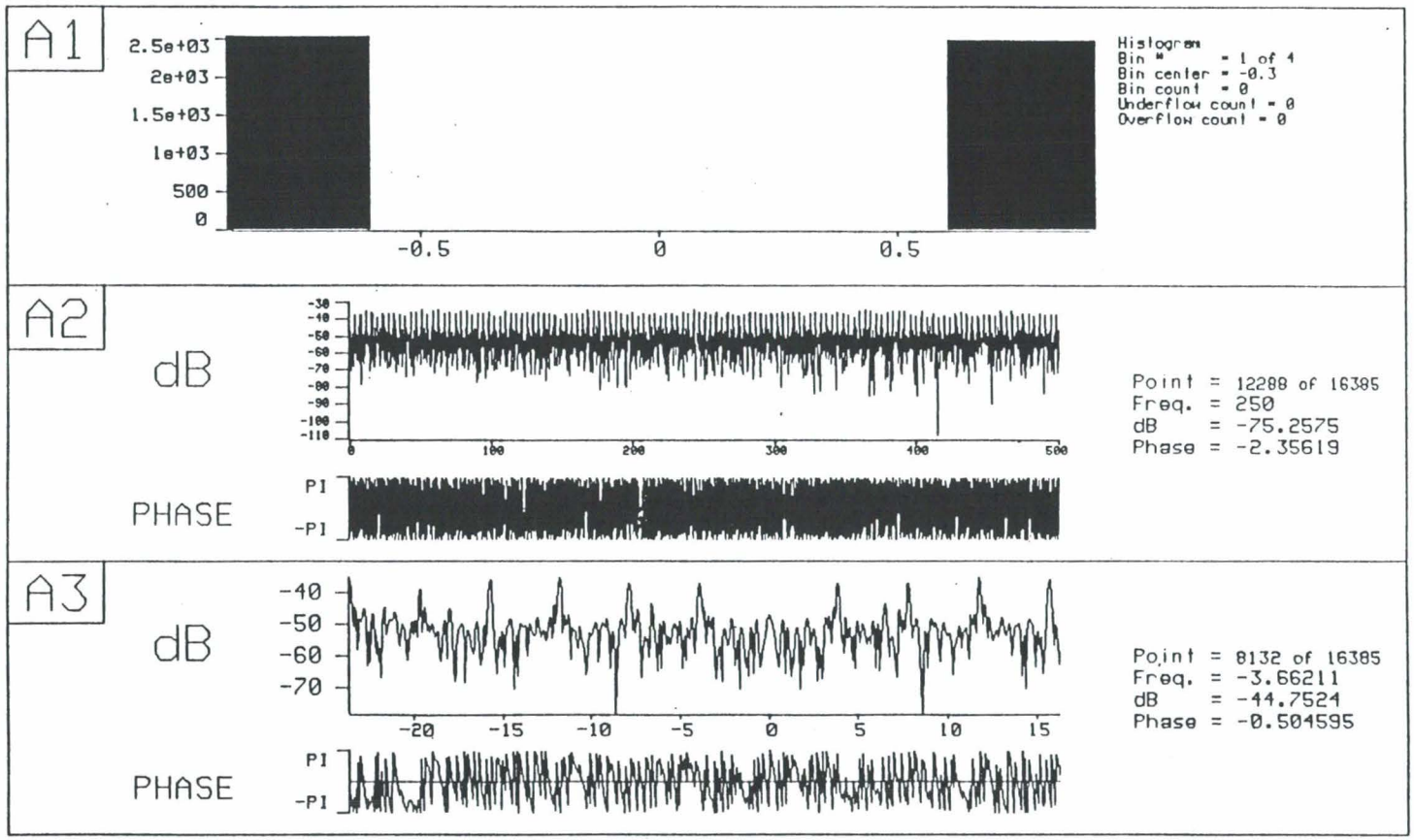

FIG. 4 A1: Histogram of 1's and 0's after the insertion of the pseudorandomizer. An almost 50% zero - 50% one situation.

A2: FFT of 16384 bits. All harmonics are approximately 40 dB or below the total signal power.

A3: FFT detail around the DC component. No significant DC component exists.

SESSION 7

K_A- BAND EXPERIMENT

AND WEATHER MODELS

Ka-Band Link Experiment (KaBLE) Description and Preliminary Results

S. Hinedi
National Aeronautics and Space Administration
Jet Propulsion Laboratory
California Institute Of Technology
4800 Oak Grove Dr.
Pasadena, CA 91109

Abstract

This paper describes the Ka-Band Link Experiment (KaBLE) with the Mars Observer (MO) spacecraft. The objectives of KaBLE are discussed and a comparison using flight tests between X-Band and Ka-Band reception is presented.

1 Introduction

The Ka-band Link Experiment (KaBLE) with the Mars Observer (MO) spacecraft is part of an on-going effort to establish viability of the 34/32 GHz frequency bands for communication with deep space spacecraft. The overall objective of the experiment is to evaluate for the first time, the performance of a spacecraft to ground communication link (downlink) at 33.7 GHz (Ka-Band) relative to a 8.4 GHz (X-Band) downlink, currently the highest Deep Space Network (DSN) operating frequency. This information will used to design future deep space missions which will operate at Ka-Band.

Figure 1 depicts DSS-13 (R&D station) and DSS-24 (operational station) "ideal Ka-band" with an absolute maximum performance advantage of about 12 dB (based solely on the frequency ratio) which is unattainable in any real situation. The current expectation is

for a 6 dB advantage of Ka-band over X-band assuming spacecraft (s/c) systems are of equal performance. However, with current s/c flight qualified technology, and equal s/c antennas, the real expected advantage would be only 2.4 dB into DSS-24 with an operational Ka-band capability devised with our current technology, and about 2 dB for the actual DSS-13. Within the next three years, it is expected that the performance of either of these antennas will improve by about 2 dB. We expect parallel improvements in s/c efficiencies.

2 KaBLE Description

This section presents a technical description of the experiment in the context of the MO mission, as depicted in Fig. 2. The primary engineering objective is to measure and document the performance of Ka-band and X-band downlinks using the same path simultaneously, so that an accurate comparison can be made. The second objective is to receive coded telemetry at a data rate of 250 bits/sec. A third objective is to measure the s/c to earth distance using Ka-band downlink in conjunction with X-band ranging.

The Ka-band downlink on MO is generated directly from the X-band downlink at the High Gain Antenna (HGA) as shown in Fig. 3. A 14 dB coupler diverts 28 dBm (about 3%) to a $\times 4$ frequency multiplier producing a 14.3 dBm Ka-band signal. This is conducted via waveguide to a feed at the focal point of the 28 cm diameter subreflector that serves as the Ka-band antenna. The experiment design makes use of the fact that the Ka-band phase modulation index is 4 times the X-band modulation index. The telemetry experiment was planned at a rate of 250 bps in January 5-18, 1993 when Ka-band is first enabled as this is the only time the Ka-band link margin will be sufficient. A link analysis is shown in Fig. 4.

As part of the experiment, all measurements and events will be time-tagged relative to the station Frequency and Timing Subsystem (FTS) so that they can be retrieved and cross-referenced chronologically. The following parameters have been measured and recorded at intervals of 1 minute ($\pm$ 1 msec), except as noted:

Atmospheric temperature, pressure and humidity

Wind speed and direction

Rain and rain rate

Water Vapor and droplets in antenna beam

Antenna physical temperature

Antenna pointing angles and pointing errors

Subreflector position

System noise temperature at X and Ka-band

Carrier SNR at X and Ka

Symbol SNR at X and Ka (only for 250 bps)

Ranging delay difference X vs. Ka-band

Start and end of pass (per occurrence)

Start of acquisition/reacquisition (per occurrence)

Times of carrier, subcarrier and symbol lock (per occurrence)

Times of loss of lock (per occurrence)

Ka and X-band spectra (as required)

The following parameters were computed:

Received carrier at X and Ka-band

Total signal power at X and Ka-band

Ratio of Ka-band to X-band carrier SNR and total power ratio

X-band vs. Ka-band carrier phase differentials

Doppler residuals (Ka-band at DSS-13 vs X-band at DSS-15)

Bit error rate at Ka-band vs. X-band

Antenna gain vs. elevation vs. weather parameters

Antenna pointing errors vs. elevation vs. weather

A Data Handling Terminal (DHT) has been provided as the KaBLE user interface to the station. The DHT provides interfaces with two Advanced Receivers (ARX's) and the station

monitor and control (M & C) subsystem. The software in the DHT accomplishes data acquisition, processing, plotting, recording, retrieval, manipulation, and display requirements.

3 KaBLE Experiment Results

The KaBLE system diagram is shown in Fig. 5 where the microwave subsystem contains the Ka-band and X-band low noise amplifiers (LNA's) followed by downconversion to the 200-300 MHz range. The Ka and X-band intermediate frequency (IF) signals are then distributed through the IF distribution assembly to various subsystems that include a multi-tone receiver, a Doppler tuner, two advanced receivers and two total power radiometers. The Doppler tuner operates only on the Ka-band signal as the latter experiences more Doppler shifts. The Doppler tuner uses frequency predicts to remove most Ka-band Doppler rate so that the demodulation process is easier. The multi-tone receiver operates on the carrier components and uses information provided by the X-band signal to lock and demodulate the Ka-band signal even for extremely weak scenarios. The ARX's output soft symbols which are then decoded to obtain the bits. The two bit streams (from X and Ka) are then compared in the DHT to provide a Bit Error Rate (BER) measurement on the Ka-band signal assuming that the X-band signal is ideal (which is reasonable due to the high symbol SNR). Figure 6(a) depicts the received P_T/N_0 in dB-Hz from the time the HGA is deployed (which is 100 days after launch). A minimum of 29 dB-Hz is required to receive a 250 bps telemetry, which is possible for the first 15 days only. Figure 6(b) shows the telemetry margin (in dB) as a function of days from launch. With an EIRP of 49.5 dB and elevation angle of 30 deg, a positive telemetry margin is available for about 15 days only.

The first few days of the experiment experienced an extremely unfavorable whether during which the X-band signal was observed but not the Ka-band signal. With better weather and after last minute debugging in the system configuration, both the X and Ka band signals were received and tracked simultaneously. Telemetry was received only for one day at Ka-band

and decoded successfully. Figure 7(a) and (b) depict the X and Ka-band carrier in dB-Hz as a function of time on January 8th, 1993. Note the X-band signal was fading during that time period due to pointing problems from the spacecraft. During that same period, the Ka-band signal was lost as expected. The X-band signal was about 55 dB-Hz while the Ka-band signals was in the range of 10-15 dB-Hz. During that same period, the difference between X-band received frequency and one fourth of Ka-band received frequency is shown in Fig. 8 which clearly indicates a small difference when both signals are tracked. Figure 9 (a) and (b) depicts the received P_c/N_0 in dB-Hz for both X and Ka-band signals on January 16th, 1993 and the relative frequencies as observed by the ARX's. The measurements agree well with the predicts and the Ka-band signals looked stationary to the ARX as most Doppler was removed by the Doppler tuner. Figure 10 (a) and (b) depict P_c/N_0 in dB-Hz for both X and Ka-band for the first 9 days of the experiment. Note the irregularity in the Ka-band signal P_c/N_0 due to the weather.

As for the telemetry reception, that was performed on January 17th, 1993 with total received Ka-band power as depicted in Fig. 11. Only few hours of telemetry was received when the P_T/N_0 was about 28 dB-Hz. The effective E_b/N_0 is depicted in Fig. 12 as a function of time. From 6 to 9 hours (UTC), E_b/N_0 was between 0 and 1 dB. In addition, Fig. 12 shows the elevation angle and system temperature of both X and Ka-band signals. Finally, the BER measurements are depicted in Fig. 13 as a function of E_b/N_0. the measurements agree well with the simulations for E_b/N_0 between 0 and 1 dB.

4 Conclusion

For the first time in the history of the DSN, a Ka-band signal has been received and demodulated from a deep space spacecraft. The carrier tracking measurements agree well with predictions. As for telemetry detection, not enough data was collected to confirm, with high confidence, the models. But the little data collected agrees well with predictions.

REFERENCES

1. J. W. Layland, *Draft Ka-band Thrust Paper*, Interoffice Memorandum (3300-92-342), December 10, 1992

2. S. A. Butman, J. G. Meeker, *Ka-Band Link Experiment Plan*, JPL D-8799, August 1991.

ACKNOWLEDGEMENT

The work described in this paper was carried out at the Jet Propulsion Laborartory, California Institute of Technology, under contract with the National Aeronautics and Space Administration. The KaBLE experiment was initially led by Stan Butman and later by Gordon Wood. A lot of the figures presented in this document were taken from "OSC Advanced Systems Review", June 1993. I would also like to thank Tom Rebold for his help.

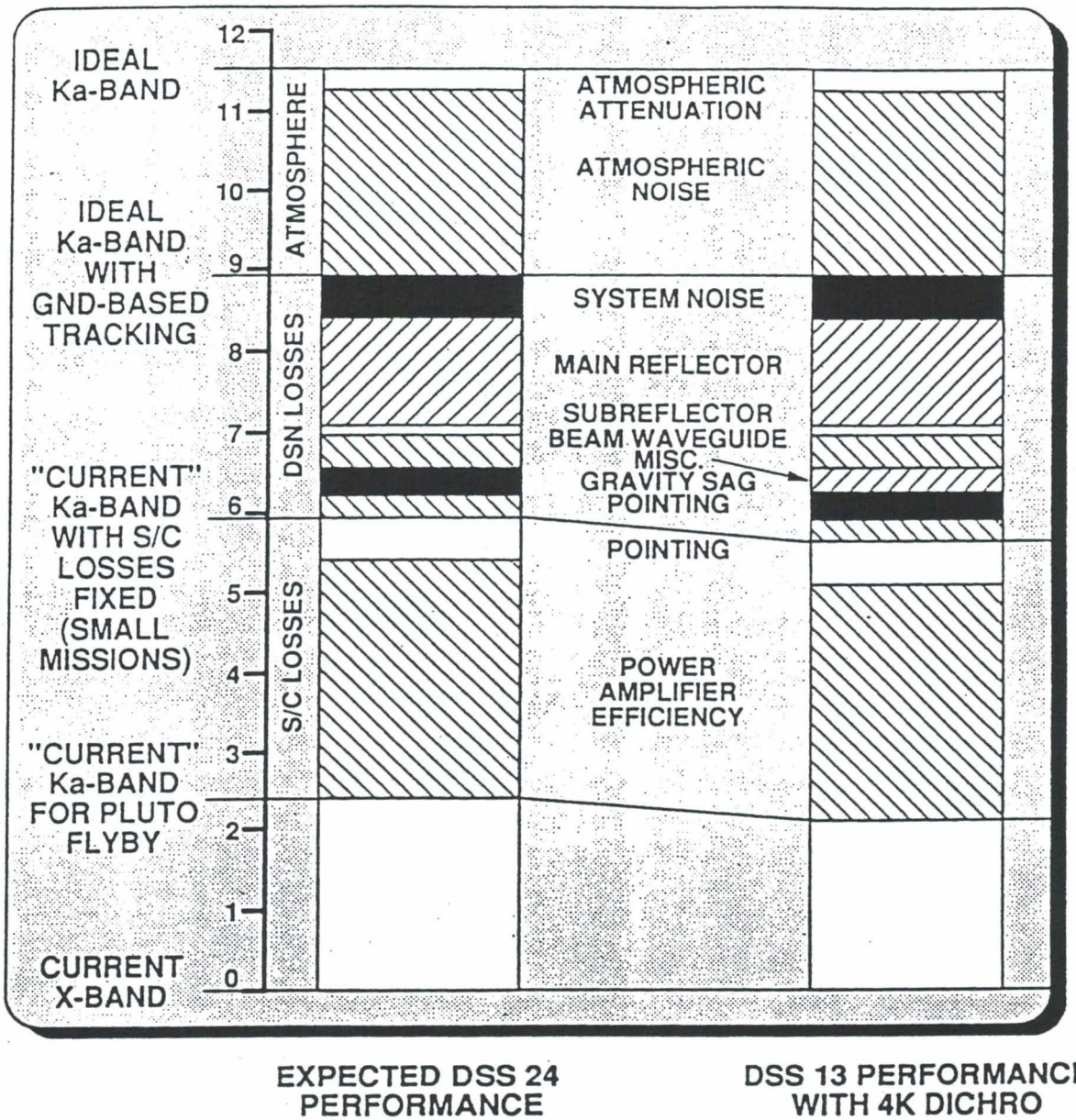

Figure 1. Ka-band Advantage over X-band.

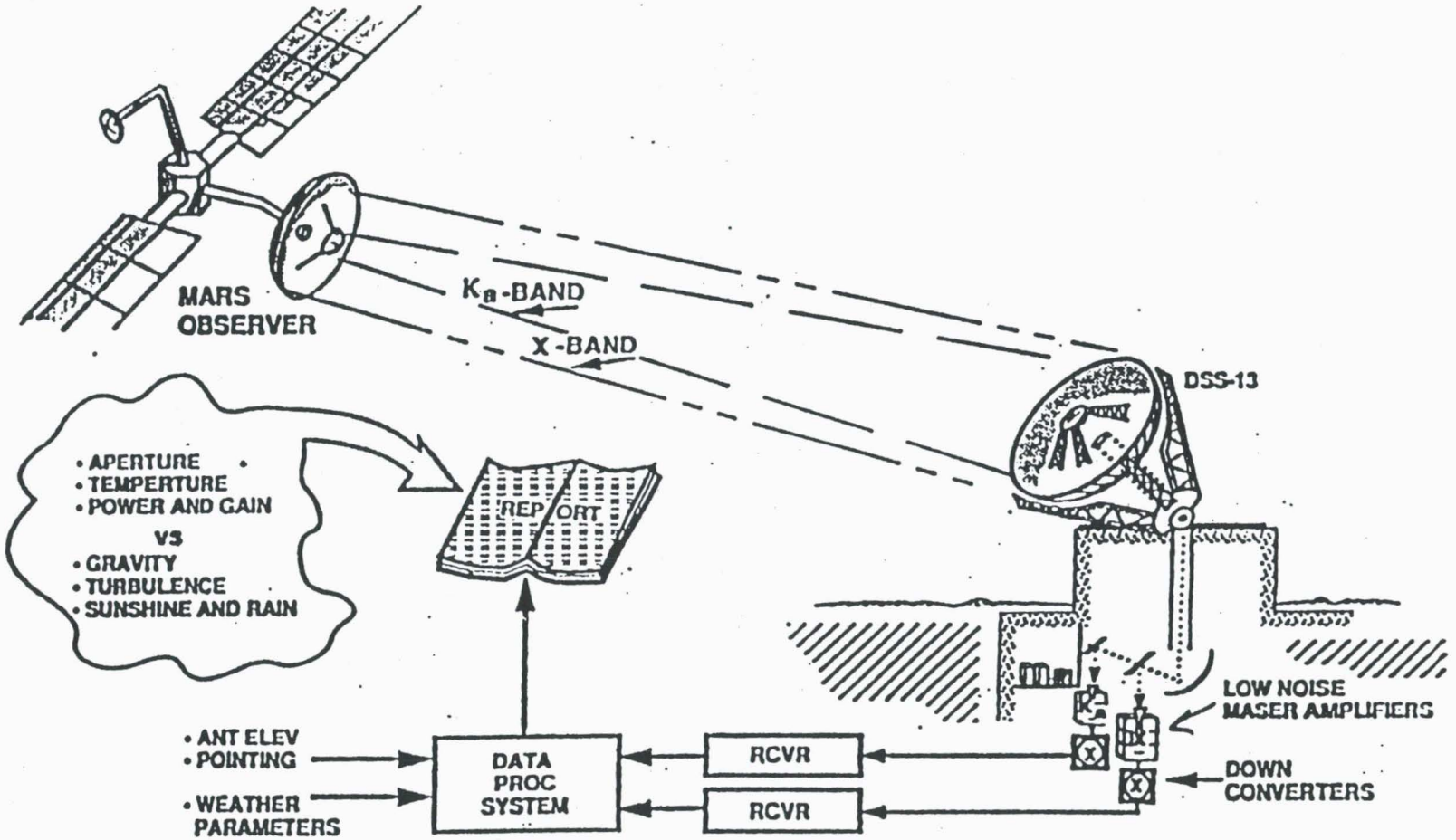

Figure 2 KaBLE Concept.

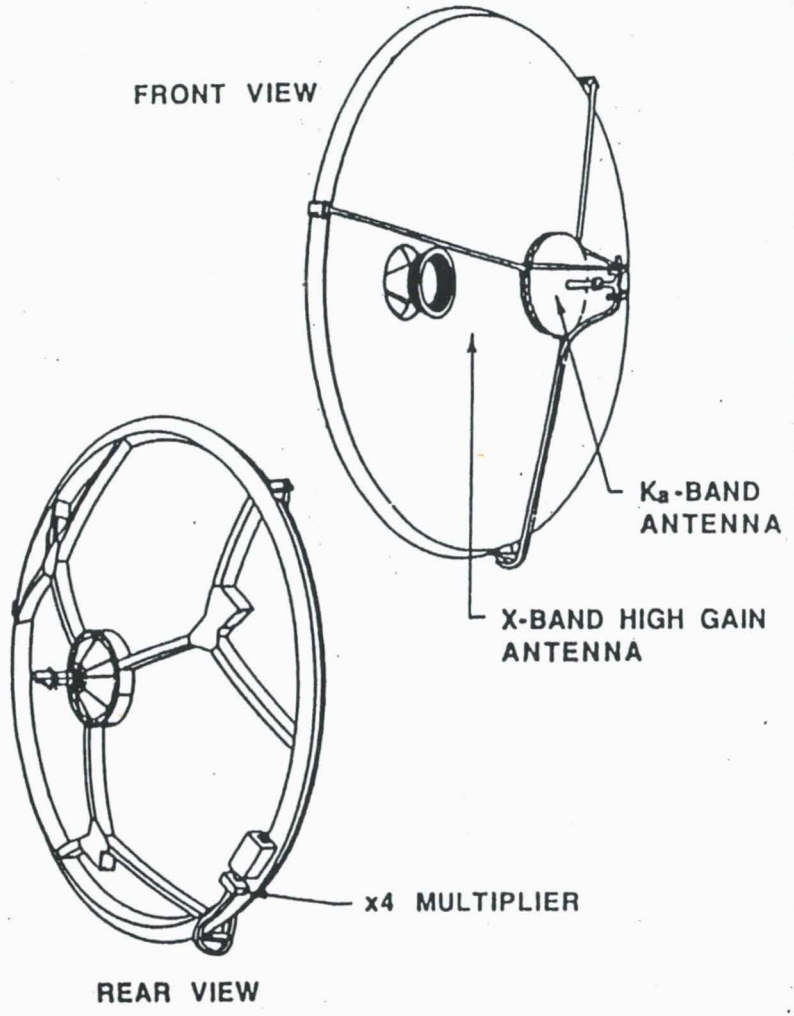

HIGH-GAIN ANTENNA

	X-BAND	K_a-BAND
• DIAMETER, m	1.5	0.28
• 1dB BEAM, deg	0.9	1.3
• GAIN, dBi	40.2	37.0
• POWER, dBm	46.5	14.3
• CIRCUIT LOSS, dB	-3.6	-1.5
• POINTING LOSS, dB	-0.9	-0.5
• EIRP, dBmi	82.2	49.3

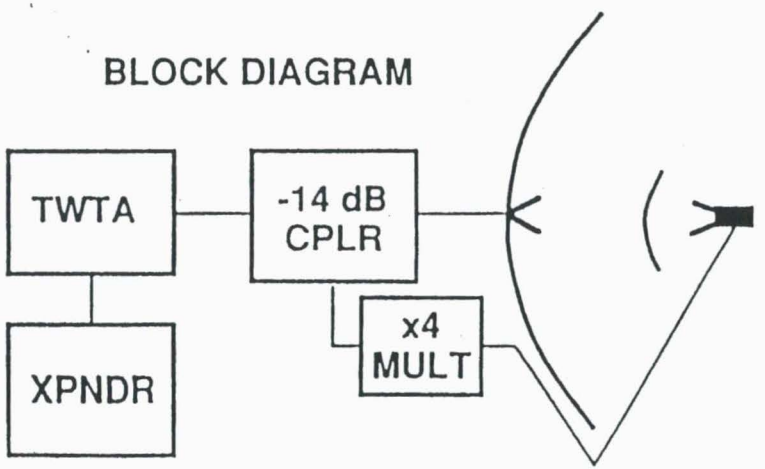

Figure 3. Mars Observer KaBLE Spacecraft Equipment.

	X-BAND		Ka-BAND	
DOWNLINK FREQUENCY (GHz)	8.417716050		33.67086420	
SPACECRAFT PARAMETERS	MEAN	VAR	MEAN	VAR
RF POWER OUTPUT (dBm)	46.53	.0171	14.3	.1013
CIRCUIT LOSS (dB)	-3.66	.0202	-1.5	.0224
HGA GAIN (dBi)	40.20	.0267	37.0	.0067
POINTING LOSS (dB)	-0.85	.0075	-0.5	.0038
EIRP (dBmi)	**82.22**	**.0715**	**49.3**	**.1342**
SPACE LOSS (@ 1AU) (dB)	**-274.45**	**.0000**	**-286.5**	**.0000**
GROUND SYSTEM PARAMETERS (DSS 13 AT 50 DEG EL, 90% WEATHER)				
ATMO. ATTENUATION (dB)	-0.00	.0000	-0.3	.0004
ANTENNA GAIN (dBi)	68.11	.0056	77.9	.1204
SYSTEM NOISE TEMP(-dBK)	-14.00	.0099	-15.9	.0267
GND, STA & COSMIC 22K			22K	
ATMOSPHERIC 3K			17K	
G/T (dBi/K)	**54.11**	**.0155**	**61.7**	**.1475**
POINTING LOSS (dB)	-0.10	.0000	-0.5	.0017
PLRZN & CKT LOSS (dB)	-0.01	.0003	-0.2	.0004
BOLTZMANN CNST (-dBm/K/Hz)	198.60	.0000	198.6	.0000
PT/No (dB-Hz) @ 1AU	**60.37**	**.0873**	**22.4**	**.2838**
At the end of the Telemetry Experiment Jan 18 1993 at 0.37 AU				
PT/No =	69.00	.0873	31.0	.2838
At Solar Conjunction Dec 27 1993, at 2.45 AU				
PT/No =	52.59	.0873	14.6	.2838
The above must be corrected for lower DSS 13 elevation and Sun effects which increase system temperature to an estimated 100K at X-band and 110k at Ka-band (TBD VARIANCE), so that				
PT/No =	46.59	TBD	10.1	TBD

Figure 4. Link Design Control Table.

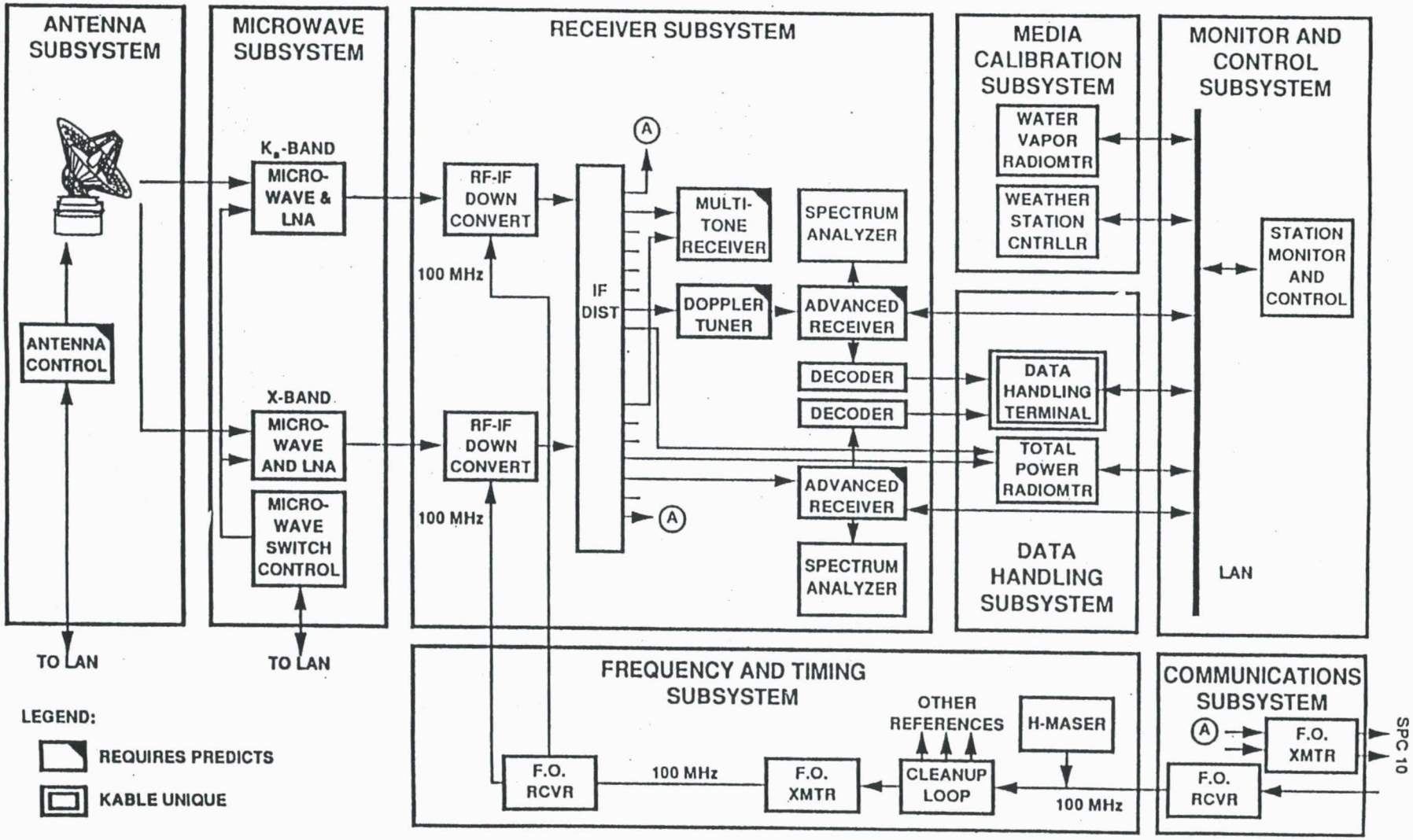

Figure 5. DSS-13 KaBLE System Diagram.

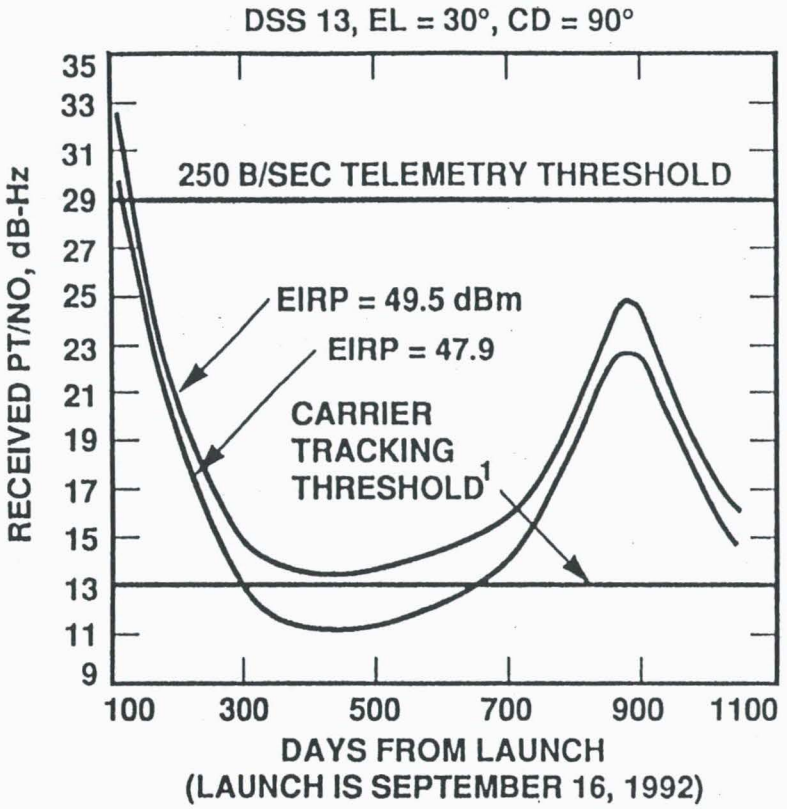

(a) Received P_T/N_0, dB-Hz.

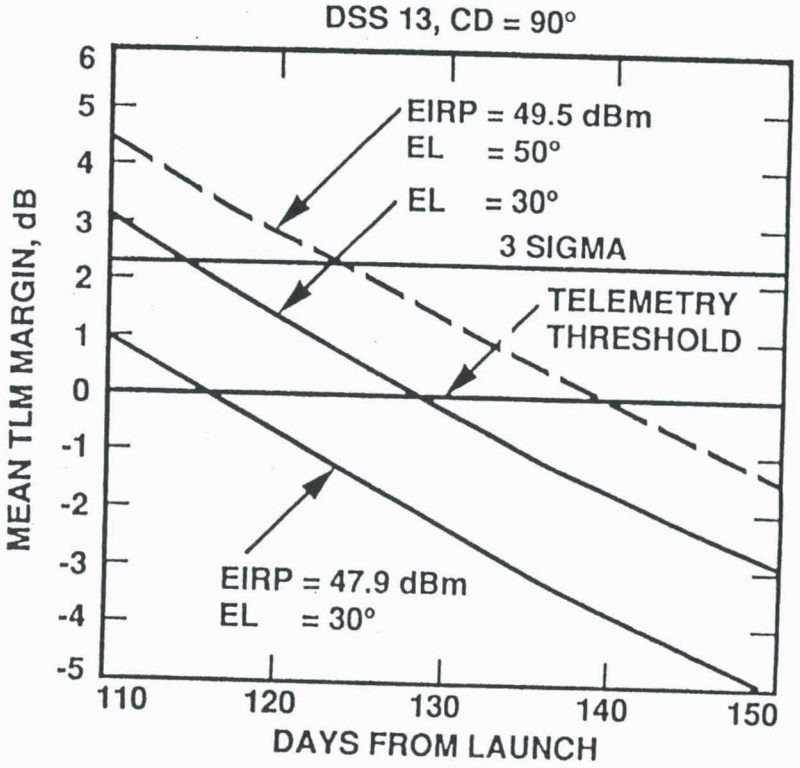

(b) Mean Telemetry Margin, dB.

Figure 6. KaBLE Kink Profile.

(a) X-band P_c/N_0, dB-Hz.

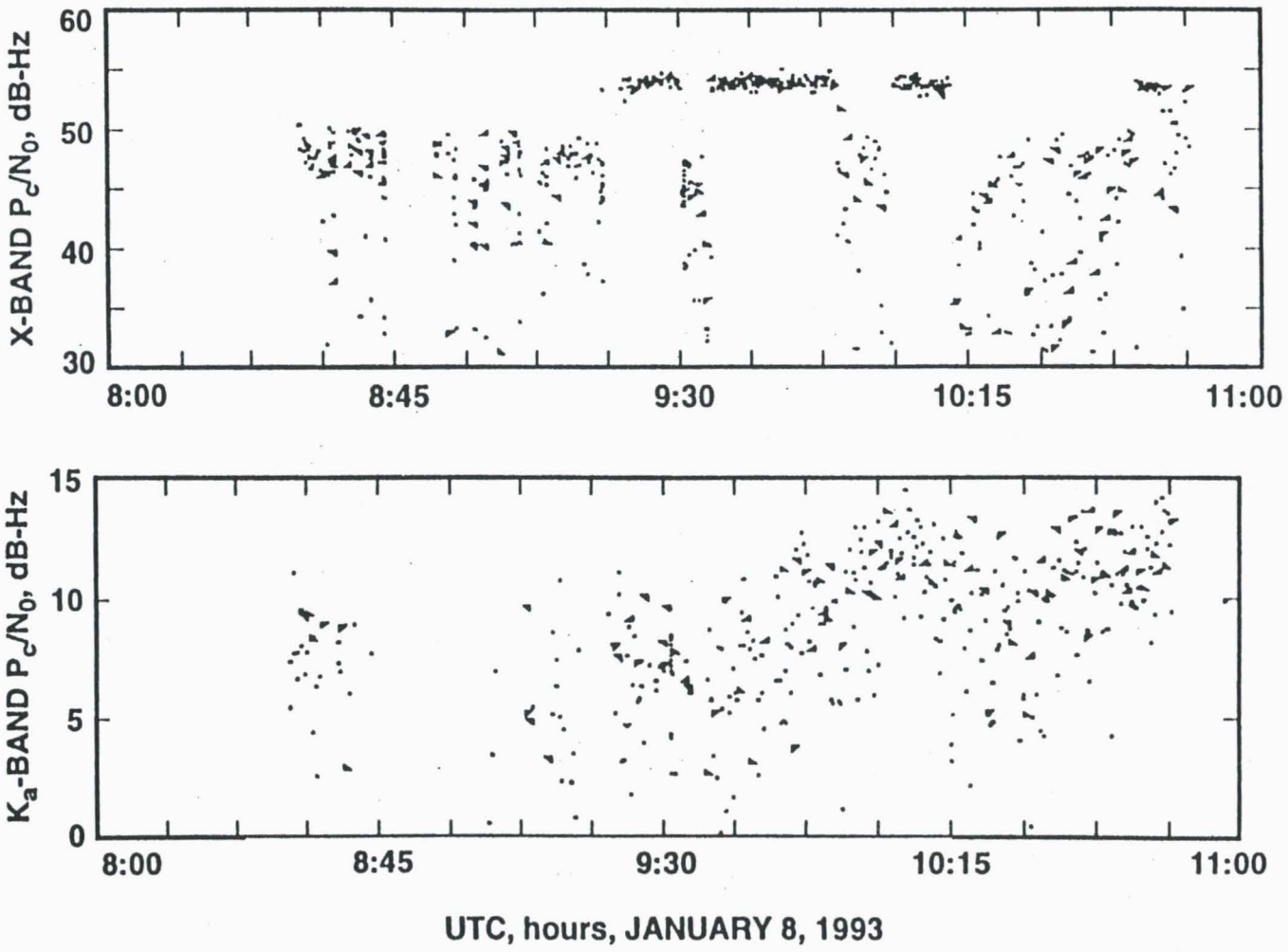

(b) Ka-band P_c/N_0, dB-Hz.

Figure 7. Received SNR of X-band and Ka-band Carrier Signal from Mars Observer.

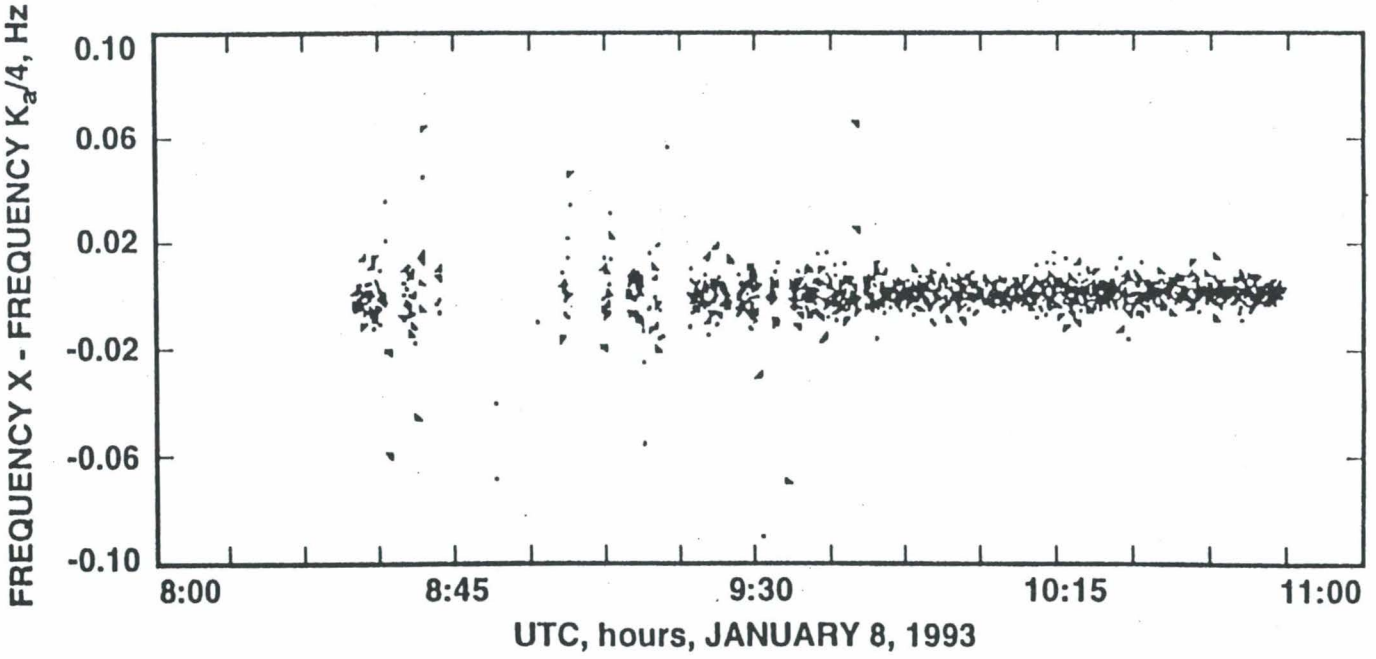

Figure 8. Difference between X-band and 1/4 Ka-band received frequencies.

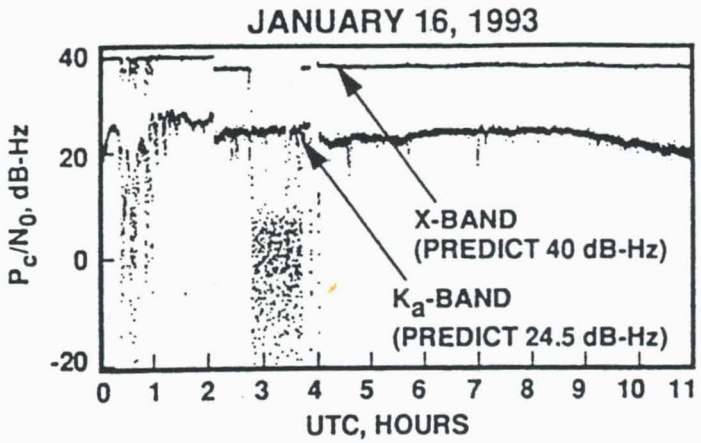

(a) Carrier P_c/N_0, dB-Hz.

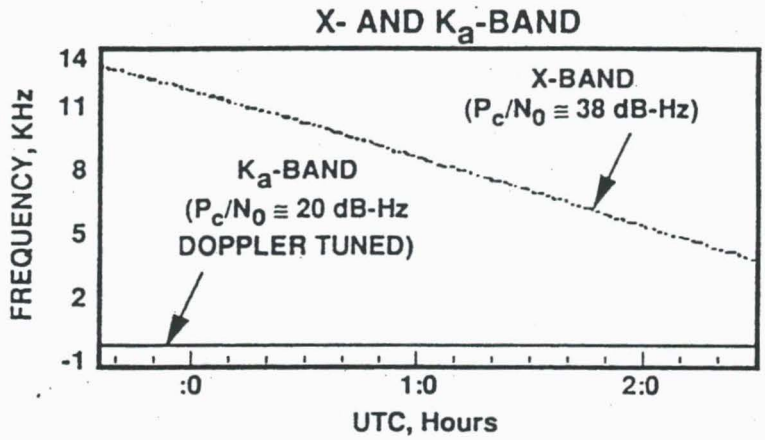

(b) Doppler tuned frequency.

Figure 9. Received signal on January 16th, 1993.

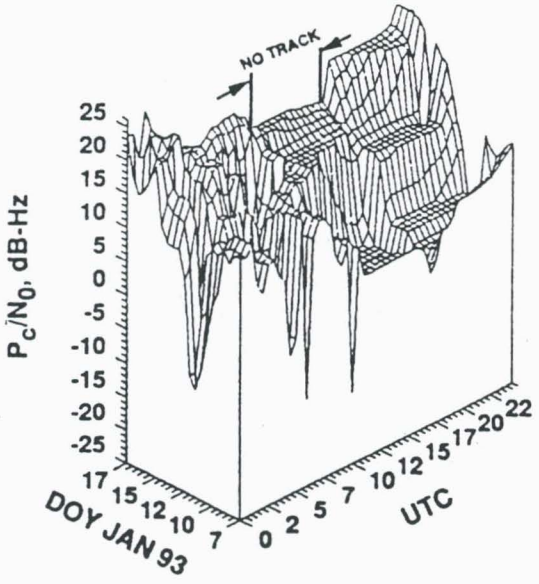

(a) Ka-band.

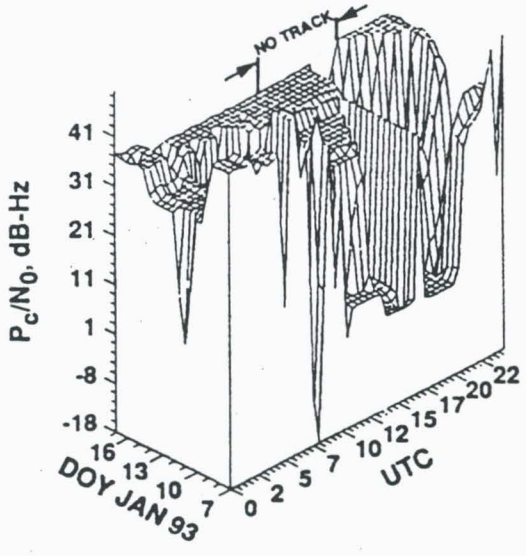

(b) X-band.

Figure 10. Three-dimensional plot of Carrier SNR's.

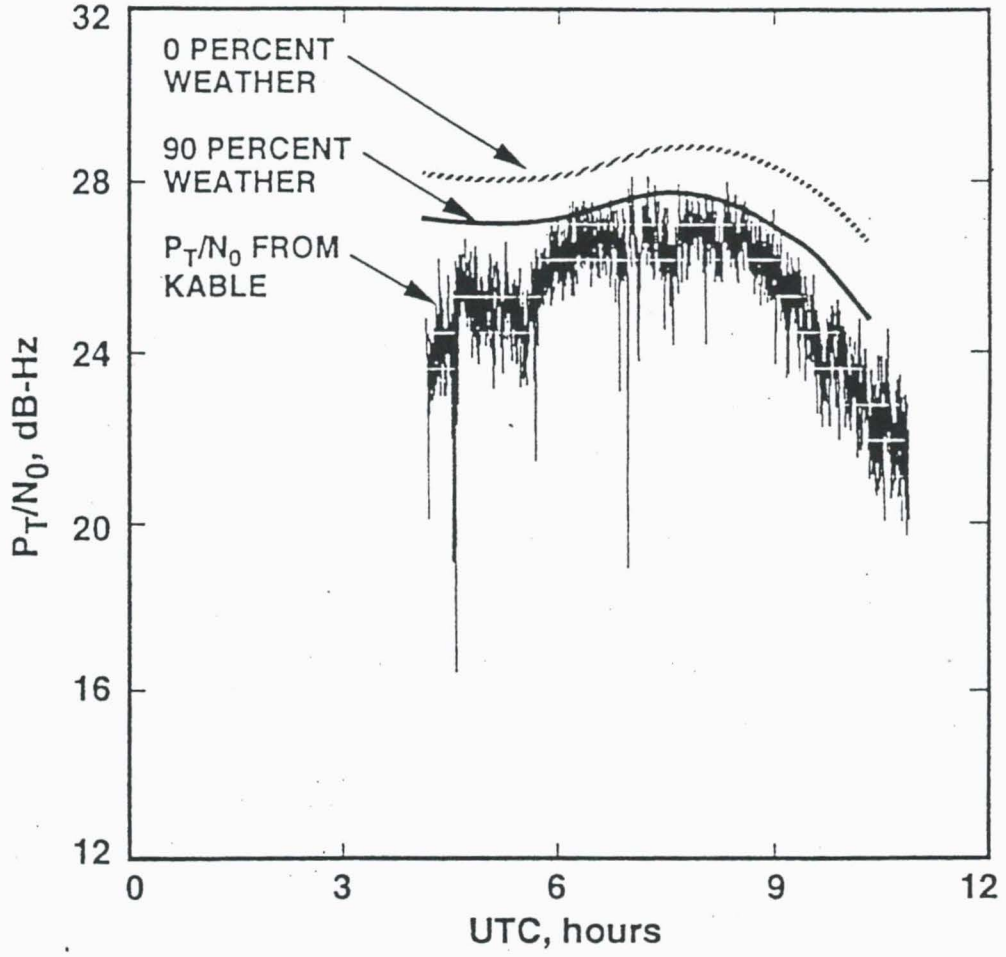

Figure 11. Ka-band received power during telemetry demonstration.

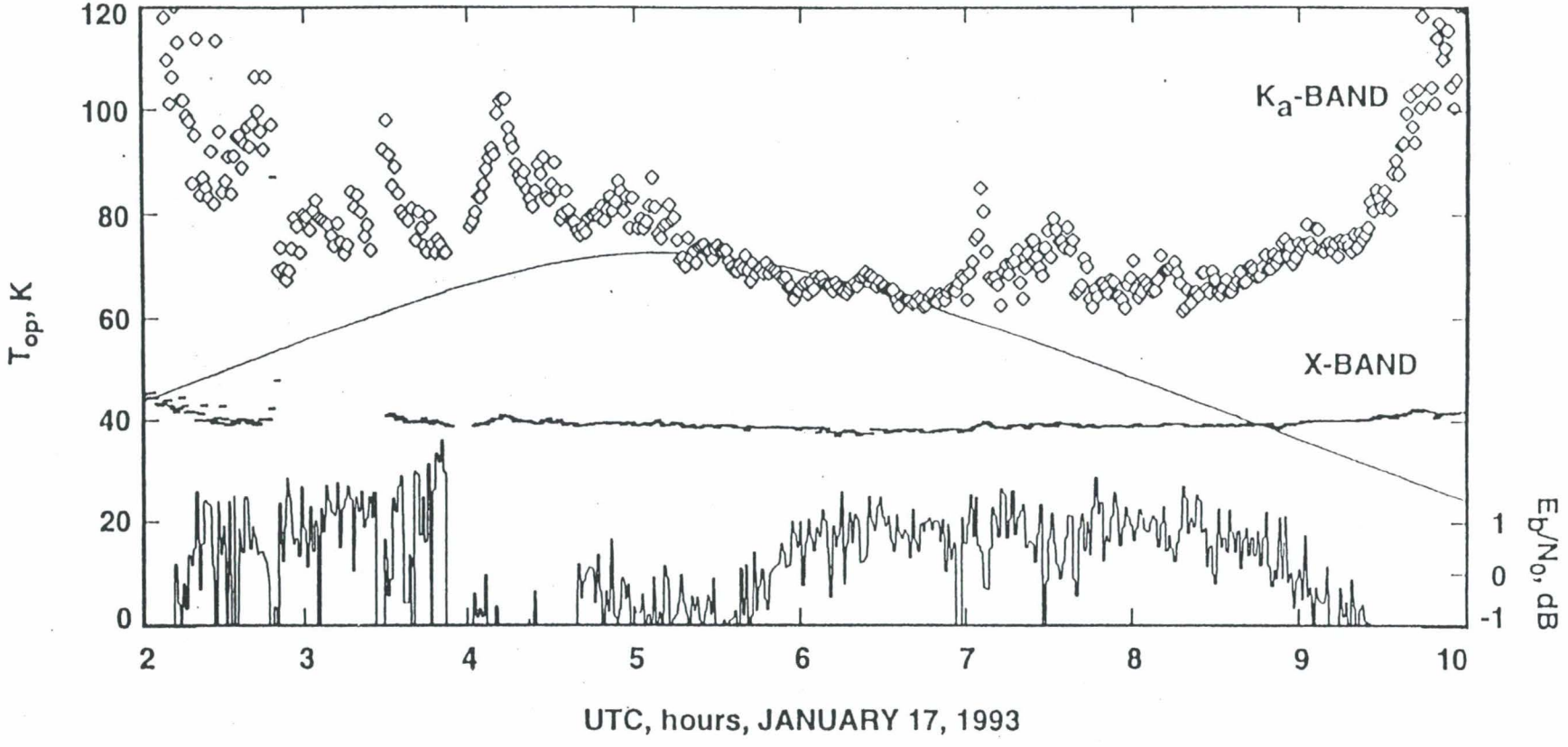

Figure 12. Ka-band E_b/N_0 and T_{op} vs. time.

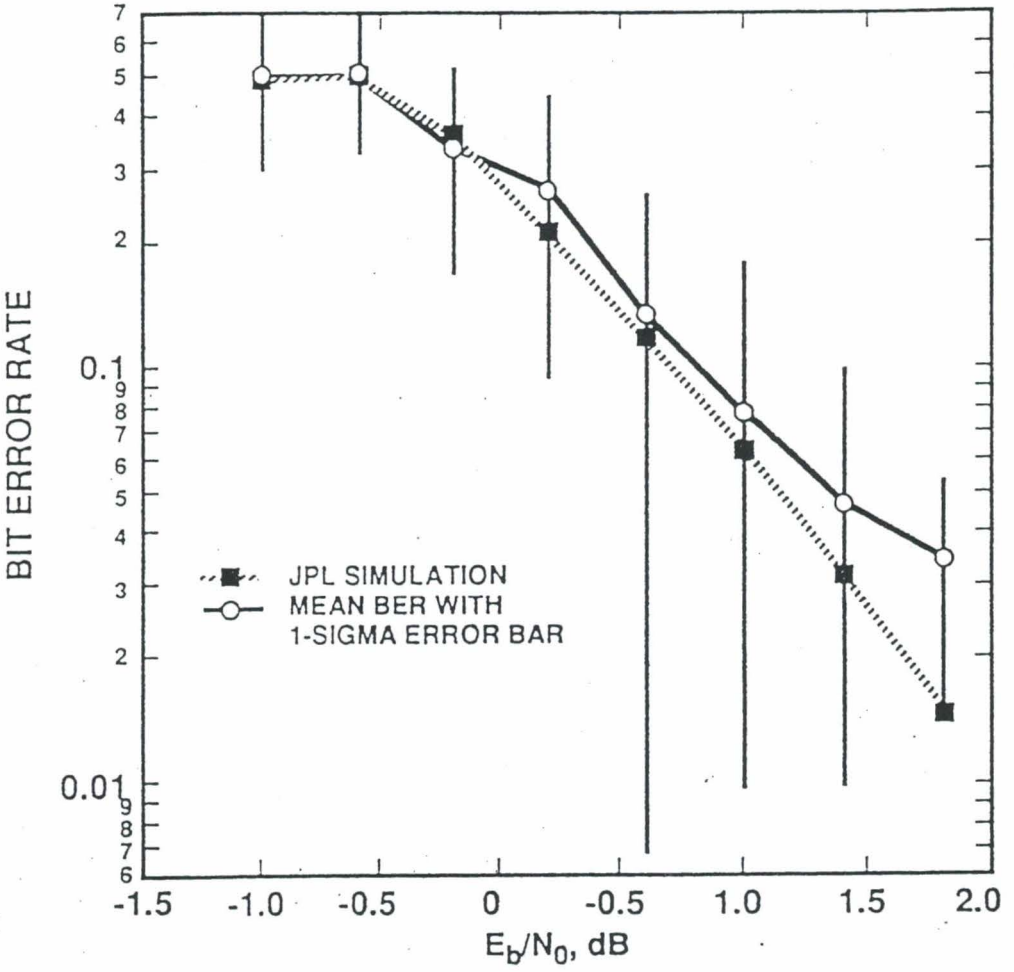

NOTE: SYSTEMATIC ERRORS IN THE E_b/N_0 AS WELL AS IN THE BER DATA HAVE BEEN REMOVED

Figure 13. Ka-band telemetry decoder performance.

[1] CCSDS Link Budget Weather Related Losses

Anil V. Kantak

National Aeronautics and Space Administration
Jet Propulsion Laboratory
California Institute of Technology
4800 Oak Grove Drive
Pasadena, California 91109

1.0 Abstract

The following paper describes the method used in computation of weather-related losses, namely the atmospheric attenuation and the system noise temperature increase due to weather. The method uses the model developed for the NASA/JPL/DSN tracking stations and is suggested as the first order approximation value to be entered into the Consultative Committee on Space Data Systems (CCSDS) link budget program to get a preliminary understanding of the link.

2.0 Introduction

The CCSDS is currently in the process of producing a CCSDS link budget program for use by the member agencies who are engaged in joint missions or missions with cross support to provide the link parameter values, either computed or assumed, to all the involved agencies. This CCSDS link budget is an excellent tool to compute link performance efficiently with minimum user effort in terms of gathering necessary parameter values. However, to compute the output values, the link naturally needs the pertinent input values. Most input values pertain to the satellite receive/transmit system or the ground transmit/receive system and once the design of the satellite has reached a certain stage, these values are known with a reasonable degree of confidence and can be used for the link budget. There are some input parameters that do not fall under the categories of the transmit/receive

[1] The research described in this paper was performed at the Jet Propulsion Laboratory, California Institute of Technology, under a contract with the National Aeronautics and Space Administration.

satellite or ground segments of the link; these belong to the weather- and path-related parameters category. CCSDS calls these "Earth-to-Space Path Parameters" and "Space-to-Earth Path Parameters" of the link. These parameter values are not readily available and are dependent upon the weather, elevation angles of the antennas, frequency used, etc., and may even be affected by the diurnal changes.

This paper gives some already-existing models that can be used to obtain the values of these weather related losses to be entered into the CCSDS link budget program so that the link performance can be computed. It should be noted that the loss values predicted by the models given below may not be quite applicable to the user's particular situation, but they are intended to help the user to provide reasonable estimates of the losses in the link. In what follows, the presentation is done in terms of the CCSDS link budget, however, the parameter values generated by using the models can be used in any other link budgets.

3.0 Theory

The CCSDS link budget has eight pages. The first page is file-keeping information. The second, third and fourth pages are the input pages for the Earth-to-Space uplink and Space-to-Earth downlink. The fifth and sixth pages are the uplink and downlink performance parameters, respectively, and pages seven and eight are the notes about the link. The user is supposed to supply the values of parameters contained in the first four pages and the results are computed and shown in the fifth and sixth pages. This paper discusses the atmospheric losses and the weather related temperature-increase.

4.0 Atmospheric Losses and Weather-Related System Noise Temperature Increase

The total noise density associated with the ground receiving station is a function of the weather around the ground station antenna along with the other usual sources of the noise temperature. The weather around the receiving station, basically, the physical temperature of the weather, adds a temperature increase to the temperature of the receiver. To estimate this temperature increase, the weather statistics have to be compiled at the specific receiving station and documented. From this statistical data, one can obtain a cumulative weather distribution (CD) at

the station or the antenna site. As an example, CD = 0.9 implies that 90% of the time the temperature increase is less than a given value. The temperature increase is a function of the physical temperature, T_p, at the antenna site, the atmospheric attenuation to the propagating wave, and the antenna elevation angle. It should be noted that all these parameters are station location dependent making the resulting empirical model station location dependent.

As an example, the empirical model developed for the NASA/JPL/DSN stations will be explained (reference 1) here. The physical temperature, T_p is related to the CD by the following empirical equation:

$$T_p = 265 + 15\,CD \quad \text{(Kelvins)} \tag{1}$$

where $0 < T_p < 1$, which implies that $265 < T_p < 280$ (K). A database exists for providing the attenuation at zenith at S-band, X-band, and Ka-band frequencies. Using this attenuation at zenith, say z_f dB (it should be remembered that according to the CCSDS recommendations, the losses should be in negative dB), the attenuation at an antenna elevation angle of α, denoted by $z_{f\alpha}$ is calculated by

$$z_{f\alpha} = \frac{z_f}{\mathrm{Sin}(\alpha)} \tag{2}$$

The system noise temperature increase is then computed using the physical temperature around the antenna site and the attenuation computed at the elevation angle α using the following formula:

$$\text{System Noise Temp Increase} = T_p\left[1 - 10^{\left(\frac{Z_{f\alpha}}{10}\right)}\right] \quad \text{(K)} \tag{3}$$

As an example of the empirical model, the temperature increase for CD=0.998 and α = 20 degrees, from the database, $z_{f\alpha}$= -0.0355 dB and the quantity $z_{f\alpha}$ is computed to be 0.104 dB and T_p is computed to be 280 (K) and finally the system noise temperature increase is calculated to be 6.6 (K). It should be noted that the system noise temperature calculated using the above formula is the increase over

the system noise temperature at zenith and should be added to the zenith system noise temperature.

It can be seen that as CD becomes closer to 1, i.e., if the link has to be operative regardless of the weather, the degradation to be considered in the link is large. The value of CD = 0.95, or 95%, seems to be sufficient for the link.

It should be clear that the model described above is valid only for the NASA/JPL/DSN stations around the world. The zenith attenuation is a function of the latitude and longitude of the station. As an example, the zenith attenuation of the NASA/JPL/DSN Goldstone stations is different from NASA/JPL/DSN Madrid or Canberra. This is so because the weather statistics at each of these stations is different. This in turn makes the system noise temperature increase different for the different stations. The ground station the user is associated with, will have its own zenith attenuation and physical temperature calculation empirical formulas and may be significantly different than described above and hence the user should use considerable caution in using the model described above. In any case, the model is given to provide an estimate of the atmospheric attenuation and the system noise temperature increase.

The following figures plot the above equations. All the figures are plotted for the JPL/DSN tracking stations at Goldstone, California. Figure 1 shows the zenith attenuation as a function of the cumulative weather distribution. The cumulative weather distribution is varied from 80% to 99.8% and the graphs are plotted for the S-band, X-band and K-band frequencies shown on the plot. The values of the zenith attenuation are measured and are not generated using a theoretical model. Alternately, the zenith attenuation may be obtained by using the already existing CCIR models and the weather regions map. Once the zenith attenuation is obtained, the atmospheric attenuation and the system noise temperature increase is obtained using the above models. Figure 2 shows a plot of the variation of the atmospheric attenuation as a function of the receiving antenna elevation angle. The atmospheric attenuation is described by equation (2). Figure 3 plots the system noise temperature increase as a function of the antenna elevation angle. Again, it should be remembered that these values and plots are only for the JPL/DSN tracking station at Goldstone, California and similar procedures have to be followed to obtain the atmospheric attenuation and the system noise temperature

increase for different tracking stations around the world. The actual value of attenuation and the system noise temperature increase depends upon the frequency used and the moisture content of the atmosphere in the region.

5.0 Conclusion

The paper presented a method used to calculate the system noise temperature increase and atmospheric attenuation due to weather at the NASA/JPL/DSN tracking stations at different frequencies. The non-DSN user may use the loss numbers generated by these curves only as a first approximation. Users should generate their own loss curves similar to those shown in this paper by using their own database of loss numbers.

REFERENCE

1. "Deep Space Network / Flight Project Interface Design Handbook," Volume 1: Existing DSN Capabilities, JPL 810-5, internal document, Section TCI-40 (Telecommunications Interfaces, Atmospherics), Jet Propulsion Laboratory, Pasadena, California, May 1, 1992.

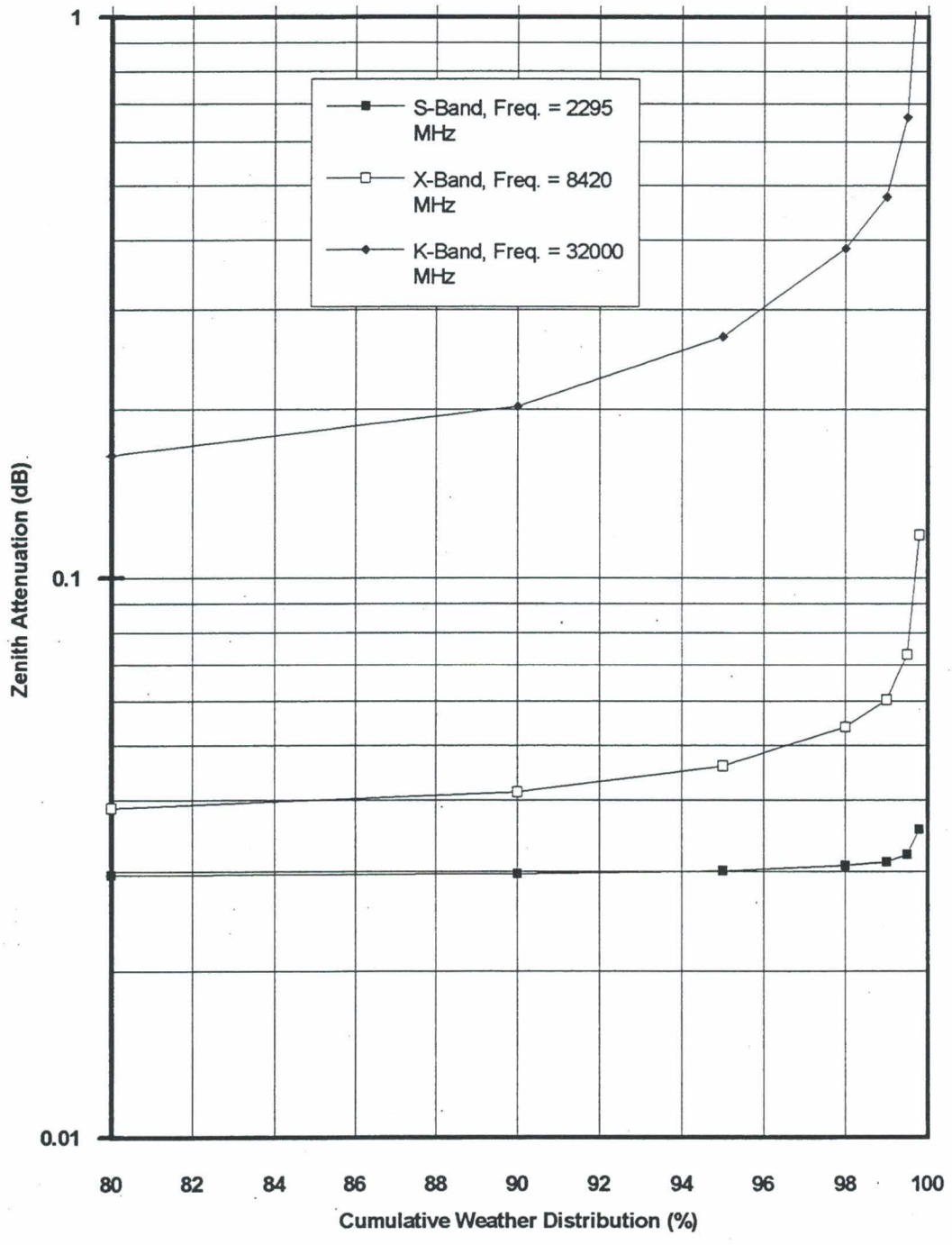

Figure 1. Zenith Attenuation as a Function of Cumulative Weather Distribution

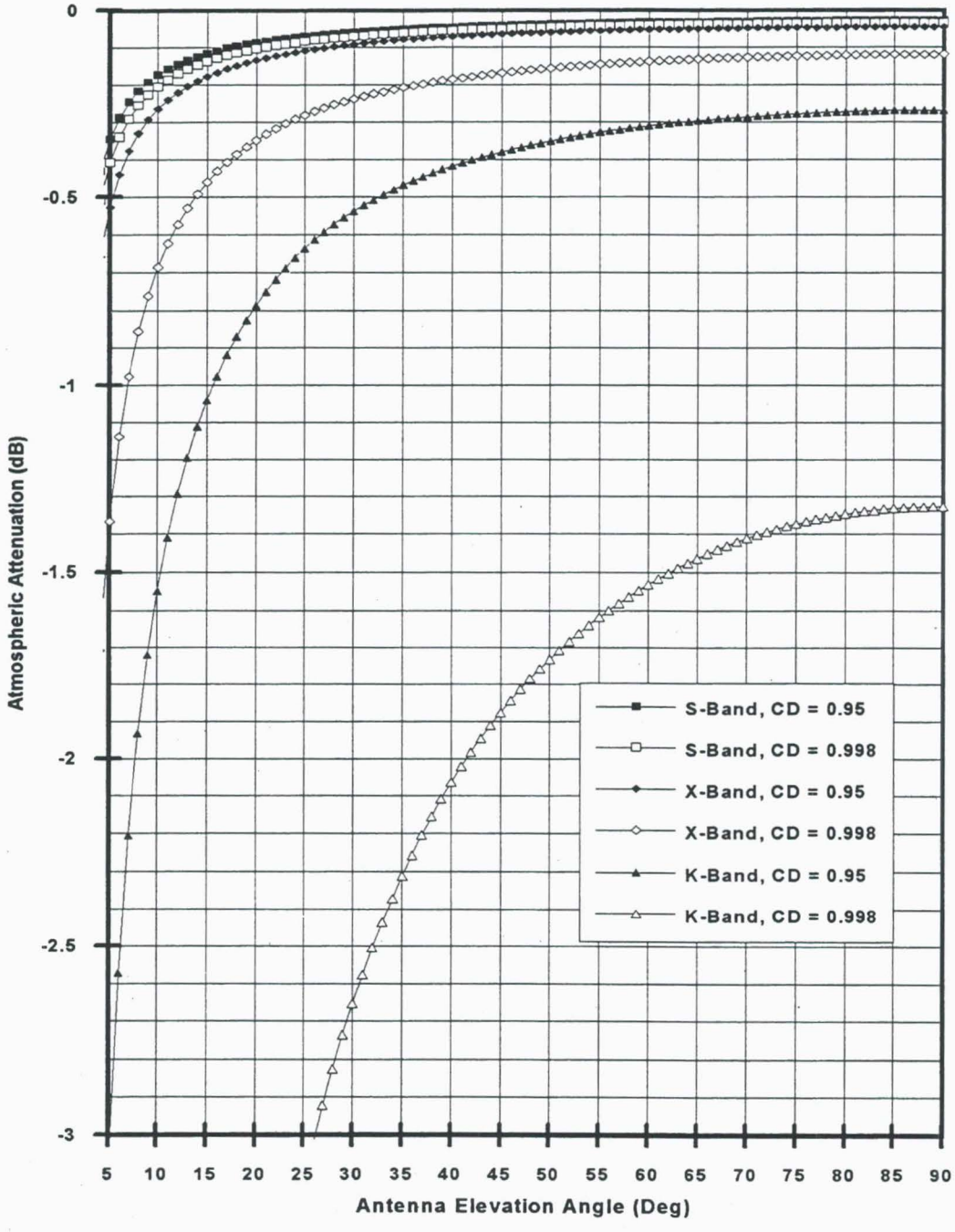

Figure 2. Atmospheric Attenuation as a Function of Antenna Elevation Angle

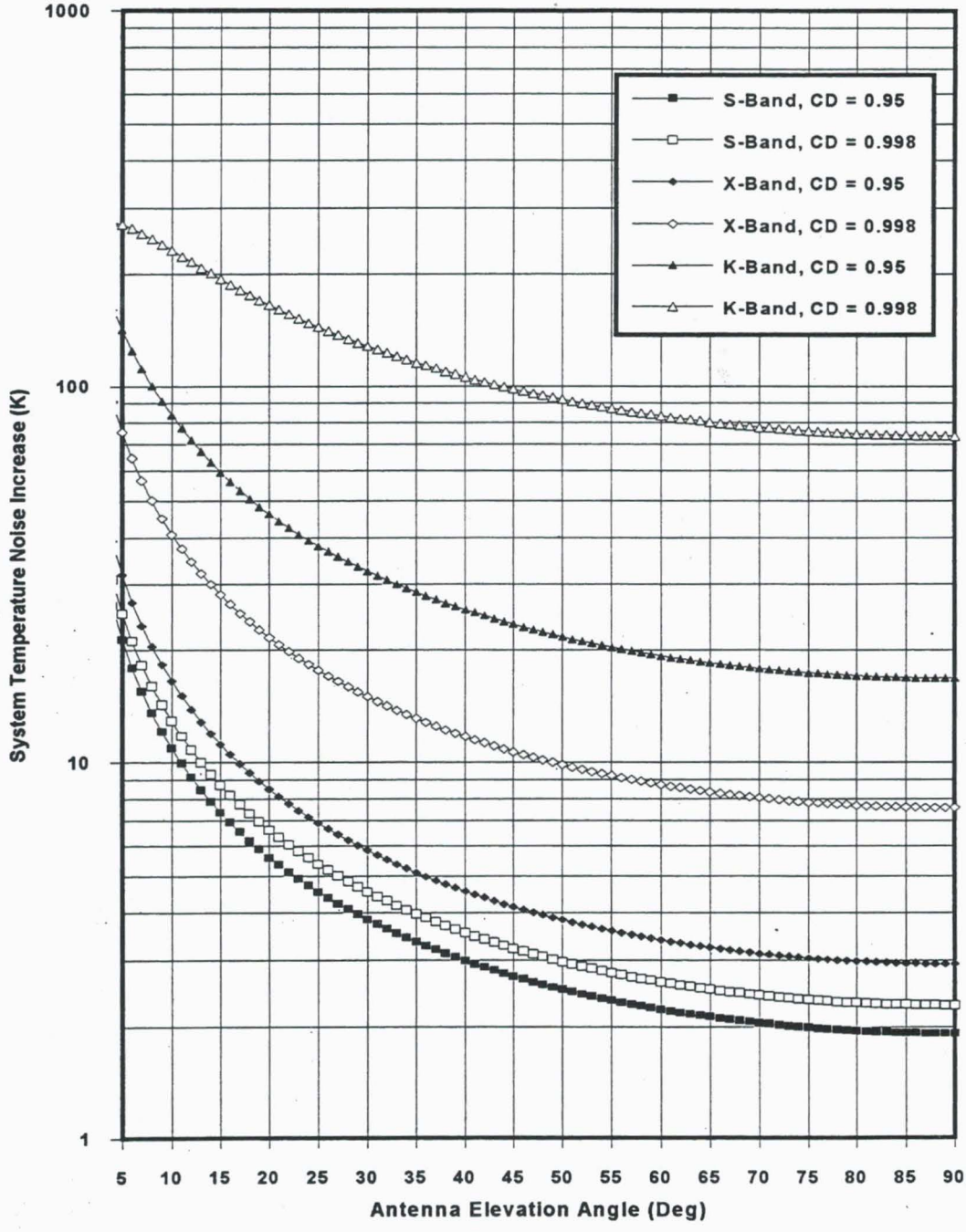

Figure 3. System Noise Temperature Increase as a Function of Antenna Elevation Angle